MEETING ON GROUND WIND LOAD PROBLEMS IN RELATION TO LAUNCH VEHICLES

Compilation of Papers Presented at the

NASA Langley Research Center

June 7-8, 1966

TM-X-57779

PREFACE

An unclassified technical meeting on ground wind load problems in relation to launch vehicles was held at the Langley Research Center on June 7 and 8, 1966. The meeting covered several sessions having the following topics: Specific Vehicle Results; Definition of Atmospheric Inputs; Experimental and Analytical Simulation Techniques; Basic Studies of Cylindrical Bodies; and Where Do We Go From Here? - The Designer's Viewpoint. The purpose of the meeting was to provide a forum for direct exchange of information and ideas between government, industry, and university personnel who are actively engaged in this area of work. In addition to focusing attention on current research and development information, the meeting also attempted to offer useful guidance on existing programs and on planning future efforts. The size of the meeting was kept small in order to encourage informal across-the-conference-table discussions among the attendees. In order to promote timely distribution of the papers presented at the meeting, this document has been printed using copy provided by the authors without the customary NASA editing.

CONTENTS

SESSION I - SPECIFIC VEHICLE RESULTS

Chairman - A. Gerald Rainey, NASA Langley Research Center

HIGHLIGHTS OF GROUND-WIND TESTS AT AMES

by Donald A. Buell

Ground-wind loads research at Ames Research Center has primarily involved specific configurations of launch vehicles. Since the models were three-dimensional with various stage configurations and protuberances, they did not present a convenient tool for generalizations. However, they exhibited a number of characteristics which help to define the scope of the problem of estimating ground-wind loads. In particular, the tests pointed up the magnitude of configuration effects such as payload shape, roughness of the cylindrical surface, conduits, and umbilical towers. Measurements included dynamic and steady-state bending moments, steady-state forces, and fluctuating and steady-state pressures. The results were reported in detail in NASA TN D-1893 and TN D-2889.

The intention of this presentation is to discuss a few typical results in the light of data that has been subsequently acquired by other researchers. Only the oscillatory loads perpendicular to the airstream will be considered. This is probably the least predictable part of the wind loads which can be studied in the conventional wind tunnel. Definition of symbols is the same as in the previously mentioned publications.

SIMULATION

Reynolds number and reduced frequency, based on the first mode cantilever frequency, have been assumed to be the most important factors in the vehicle simulation. Representative full-scale

Reynolds numbers have been obtained in the model tests by operating at abnormally high air densities and velocities. The Reynolds numbers obtained with representative models are shown in figure 1. They range from 0.1 to 10 million. The figure also indicates the Reynolds numbers where response measurements were made at a reduced frequency of 0.2. When the response at this frequency was large, this is so noted. A reduced frequency of 0.2 is of interest because other investigators have observed large responses at this frequency at both subcritical and supercritical Reynolds numbers. In addition, this frequency has been predicted in numerical studies of vortex shedding.

Figure 1 shows that the Ames models had only a few cases of large response at $fD/V = 0.2$. But the figure also shows that most of the response measurements at this frequency were made at Reynolds numbers between 0.5 and 2 million. It appears, therefore, that this range of supercritical Reynolds numbers involves a transitional type of flow which inhibits vortex shedding at the usual frequency. The idea of a broad transitional range of Reynolds numbers was suggested by Roshko for two-dimensional cylinders, although he was considering somewhat different characteristics of the flow.

SLENDER NOSE MODELS

Another factor which had a pronounced influence on the results was nose shape. For example, the large responses referred to in figure 1 occurred only on models with a "slender" nose, such as are shown in the model sketches. Most of the slender nose

models tested at Ames were not prone to oscillate at any frequency or Reynolds number, but there were exceptions which produced quite violent responses. Examples are shown in figure 2, which presents the variation of a response coefficient with reduced velocity. A Reynolds number scale is also included. The response coefficient has been obtained from the maximum dynamic bending moment occurring in approximately 1000 cycles. The low values of response coefficient in figure 2 represent a random motion. The larger responses were of the narrow-band periodic type, such as can be produced by a negative aerodynamic damping. More precisely, an increase in model motion above some minimum amplitude increased the excitation until a nonlinearity limited the amplitude.

There are many factors which can alter the results with this type of phenomenon. In the case of the model on the left side of figure 2, roughness decreased the random response, an effect which was observed generally on slender nose models. This reduction was apparently sufficient to eliminate the motion-coupled excitation. Other models with similar shapes but with higher structural damping and stiffness showed little evidence of the narrow band response at any Reynolds number. Pressure measurements on a relatively stiff model failed to reveal a narrow band excitation over a wide range of frequency and Reynolds number.

In contrast, the model on the right oscillated under a variety of test conditions, smooth or rough, despite having a higher structural damping. This may have been caused by the fact that it had somewhat less stiffness, in proportion to volume, than the first model and had only half the relative density ratio. It was thus

more readily accelerated to large motions by a random excitation. The addition of a horizontal plate under the nose greatly reduced the response for this model, which may indicate that the flow around the nose is important to the motion-coupled excitation. However, the response peaks for this model occurred at such low Reynolds numbers that one must be cautious of generalizations. It is presumed that the model would have had a large response at a V/fD of 5 if the Reynolds number had been higher. This conclusion is strengthened by the fact that roughness moved one of the peaks closer to that speed.

BLUNT NOSE MODELS

The situation was less complicated when the model had a blunt nose, provided that the nose diameter was a significant proportion of the maximum diameter. In such configurations the nose controlled the pressure fluctuations over a length several diameters below the nose, and there was no motion coupling. Typical responses for models with hemisphere noses are shown in figure 3. The data are for the same configuration, but the curves on the right represent a larger vehicle than those on the left. Without roughness, the response coefficient tended to increase with speed, and the slope became steeper as vehicle size increased. With roughness, a narrow-band random response peak was observed, which occurred at lower reduced speeds as vehicle size increased. When the simulated vehicle reached sufficiently large proportions, the response peak became fixed at a V/fD of 10, and the smooth-model response curve merged with that for the rough model.

In order to show something of the flow mechanism involved, pictures were taken of the models with oil on the surface. Figures 4 and 5 are photographs with and without a spoiler at the tip of the nose. The spoiler is of interest because it was very effective in reducing the pressure fluctuations caused by the blunt nose. It can be seen that the separation line in figure 4 terminated some distance from the tip, and that air was flowing smoothly over the nose and into the wake. Figure 5 shows that the spoiler caused the separation line to continue over the nose, thus isolating the wake from the free stream. Presumably, this broke up the line of communication between the approaching air and the shedding vortices so that the coherence of the pressure fluctuations was destroyed. Slender noses are believed to produce an effect similar to the spoiler.

CONDUIT EFFECTS

The last factor to be considered is perturbations from the circular cross section. Figure 6 shows data for one of the smaller models with circular rods, representing conduits, extending the length of the upper stage. An upstream conduit produced very large responses that were motion coupled. The flow mechanism in which the conduit acts as a trigger, sending vorticity around each side alternately, appears reasonably straightforward. Unfortunately, the Reynolds number is again too near the transition range to be sure that the same effect would be observed at higher Reynolds numbers. It can be seen that a second conduit near the normal separation point nearly eliminated the effect of the upstream

conduit. As a consequence, multiple conduits were generally favorable (on this model) in holding vortex shedding loads to a minimum.

CONCLUDING REMARKS

In summary, the data acquired at Ames are not in conflict with the expectation of a response at a reduced frequency of 0.2, if the Reynolds number is sufficiently removed from transition. However, factors such as roughness, damping, stiffness, and relative density ratio may profoundly affect the amplitude of the response. It was also found that blunt nose shapes can have a controlling influence on model excitation, if the nose is relatively large. It appears that conduits can increase or decrease the excitation depending on their location relative to the wind and to each other.

The effects of umbilical towers have been omitted, not because they are unimportant, but because the tests at Ames did not in many cases adequately define them.

REYNOLDS-NUMBER RANGE OF TESTS

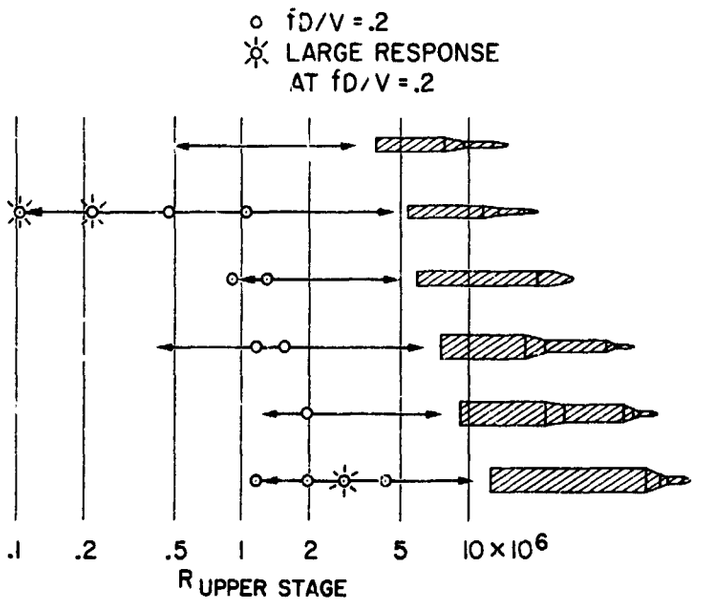

Figure 1.

RESPONSE OF SLENDER NOSE MODELS

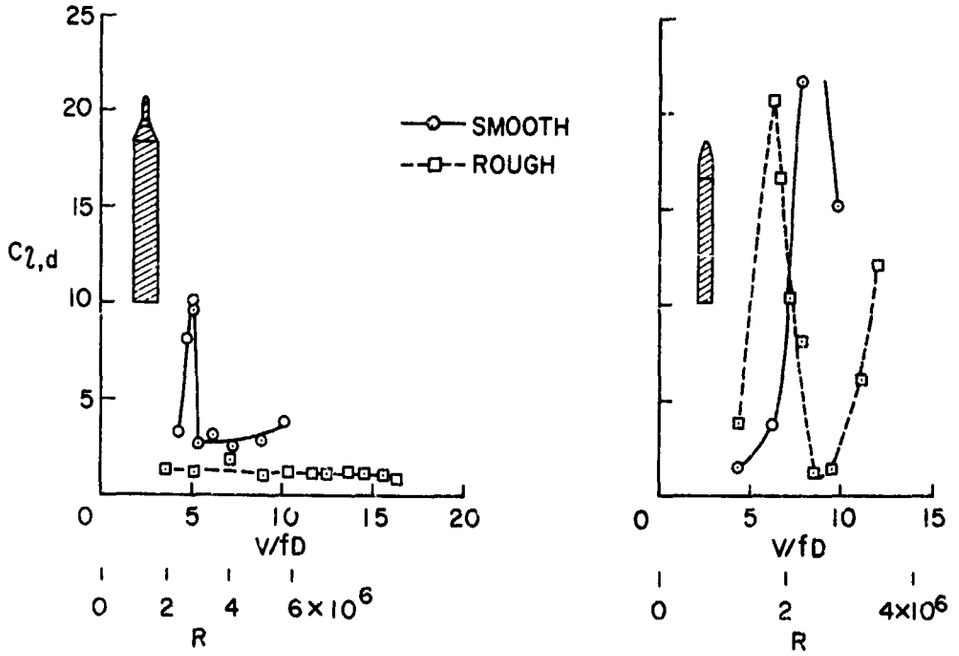

Figure 2.

RESPONSE CF BLUNT NOSE MODELS

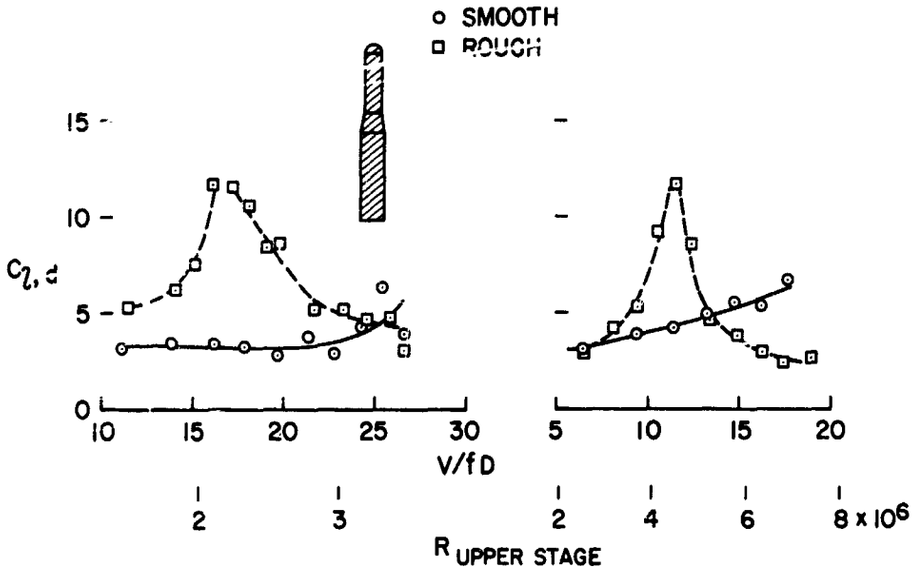

Figure 3.

BLUNT-NOSE MODEL WITH OIL

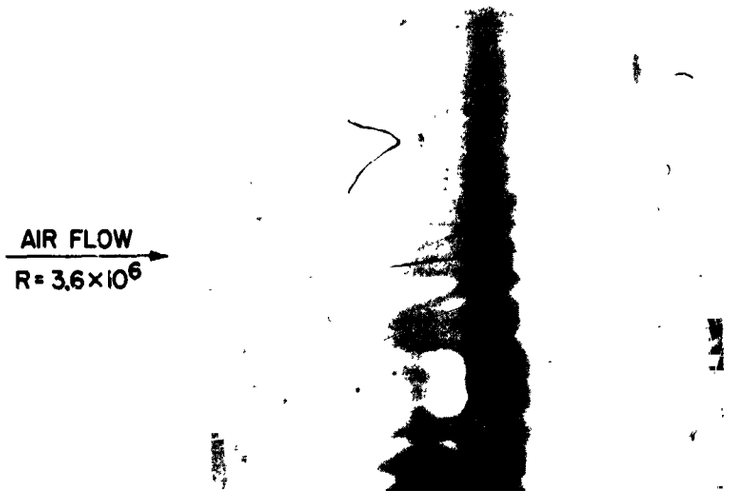

Figure 4.

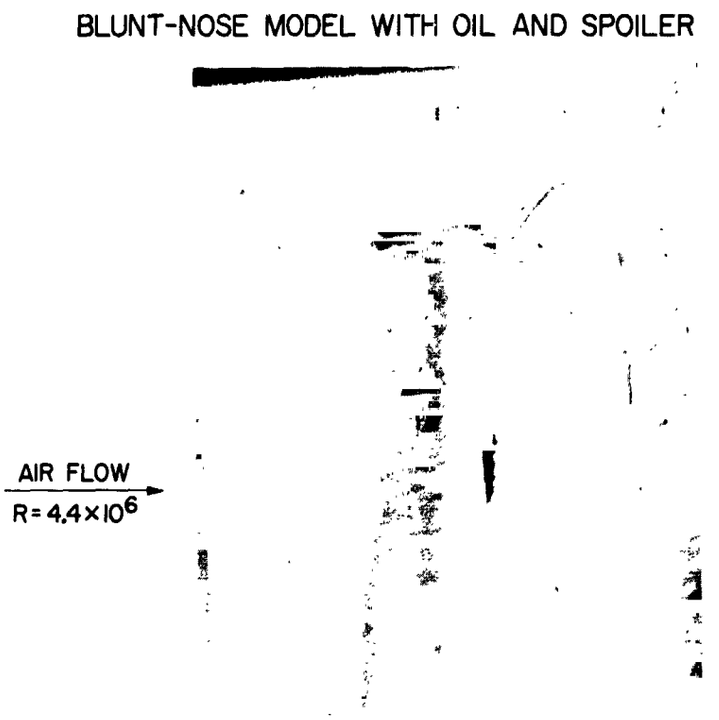

Figure 5.

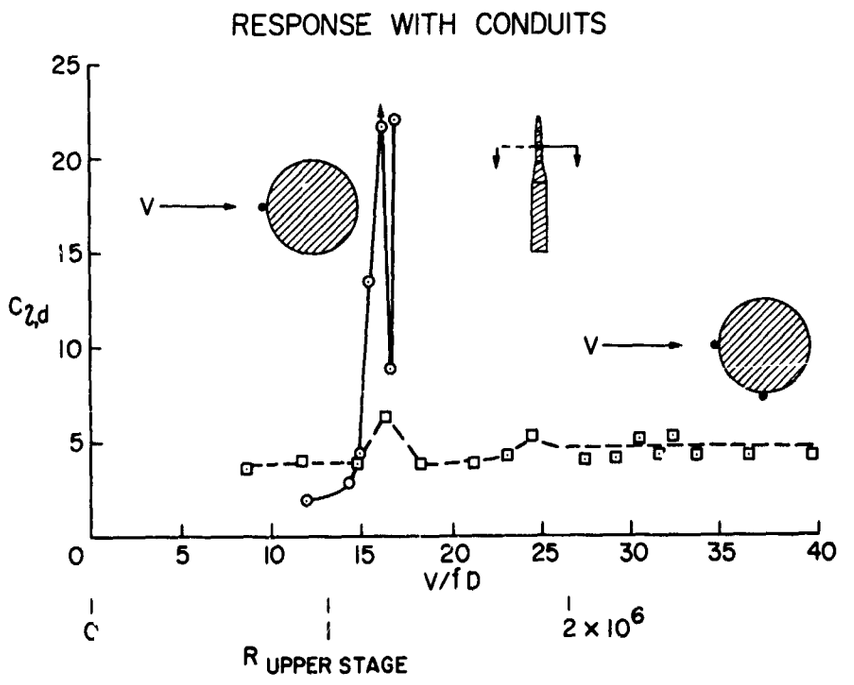

Figure 6.

SUMMARY OF LANGLEY WIND-TUNNEL STUDIES OF GROUND WIND LOADS ON LAUNCH VEHICLES

By

Moses G. Farmer and George W. Jones, Jr.

National Aeronautics and Space Administration

Langley Research Center

SUMMARY

Ground wind loads have been investigated for a large number of specific launch vehicle configurations in the Langley transonic dynamics wind tunnel. An examination of typical results obtained for the Saturn V vehicle has indicated several interesting features. When the structural damping is moderately low $\left(\frac{c}{c_c} \cong 0.01\right)$ lateral dynamic response apparently associated with vortex shedding from the lower two stages of the vehicle produces loads in excess of the design loads for the vehicle. These large responses occurred at conditions corresponding to a Strouhal number $\frac{fd}{v}$ of about 0.2 where d is the diameter of the lower stages and f is the frequency of the fundamental bending mode. The response had characteristics similar to a single-degree-of-freedom flutter and it was found that moderate increases of the structural damping $\left(\frac{c}{c_c} \cong 0.03\right)$ reduced the response to acceptable levels and changed its character to that of a lightly damped system responding to a random input. To take advantage of these beneficial effects of increased damping, a viscous damper has been incorporated in the full-scale vehicle launch complex.

INTRODUCTION

Ground winds blowing over erected launch vehicles can create problems in structural strength, guidance alignment, and clearance with adjacent structures. Usually ground-wind-loads data are needed before completion of the full-scale vehicle. Wind-tunnel studies using aeroelastic models are believed to provide the most direct and reliable means of predicting the response of launch vehicles to a steady wind. The two major ground wind loads are the vortex-shedding loads (which cannot be calculated at present) and the steady drag loads. Both types of loads are simulated by the wind tunnel.

Wind-tunnel studies of the effects of ground wind loads on a number of specific launch vehicles have been made in the Langley transonic dynamics wind tunnel. Some of this work has been reported in reference 1. The purpose of this paper is to summarize the work which has been done to date and to indicate future plans for ground-wind-load studies on launch vehicles.

APPARATUS

Models.- The models tested in the Langley transonic dynamics wind tunnel are listed in table I. The models ranged from small launch vehicles such as Scout to the Saturn V. The length scale factors in table I reflect that the models were scaled in size to be as large as possible and still fit in the wind-tunnel test section (approximately 16 feet square). Various weight configurations were simulated, depending upon the particular vehicle prelaunch fuel operational procedures. The models were aeroelastically scaled; that is, simulation was attempted for major aerodynamic and structural dynamic parameters such as Reynolds number, reduced velocity, detailed exterior geometry,

mass ratio, and generalized mass. Photographs of two typical models, the Saturn I Block II and Saturn IB mounted in the wind tunnel, are shown in figure 1. If umbilical towers are nearby during full-scale launch, they were modeled such as shown in figure 1. Generally, these tower models were only approximately geometrically scaled, but in the Titan III Phase II and Titan-Gemini investigations, dynamically similar umbilical towers were tested (see refs. 2-4).

The models were mounted on the tunnel test section floor on a massive turntable which could be remotely rotated so as to simulate any desired wind azimuth angle. This turntable, shown in figure 1, was held down by a vacuum while acquiring data, and lifted on a cushion of air for rotation. A variable-stiffness base tie-down support connected the model base to the turntable. This tie-down support, shown in figure 1(a), had a central column and eight peripheral pretensioned columns. By changing the number or size of the peripheral columns, the tie-down stiffeners may be varied.

Dampers.- On earlier models such as the Scout or Jupiter, damping of the model was not variable, and it was hoped that the model construction gave a structural damping representative of the full-scale vehicle. For later tests, however, the models were designed to have very low structural damping and internally mounted dampers were developed which could be used to increase the model damping. Two types of viscous dampers used are shown in figure 2. The fixed viscous damper was a closed cylinder filled with silicone oil in which a number of slightly concave trays were mounted. Each tray supported a lead slug which tended to stay in the center of the concave tray. This damper was mounted vertically inside the model and as the model vibrated, the relative motion between the slug and the oil provided a damping force. Damping could

be varied by changing the numbers of slugs or the viscosity of the oil. The tuned viscous damper in figure 2 was essentially a single slug suspended in oil except the cylinder was mounted in the model from a long rod like a pendulum. By varying the length of the rod, the frequency of the damper could be tuned to the model frequency for maximum damping or detuned for lower values of damping.

The viscous dampers had the disadvantage of requiring a tunnel entry and model change to vary the damping. A damper which allows the damping to be remotely controlled has recently been developed by Chang of Lockheed Corporation/Huntsville, and was successfully used in the Saturn V investigation at the Langley transonic dynamics tunnel. This damper system is shown schematically in figure 3. Two electromagnetic shakers were mounted on a low frequency vertical column which was fastened on its base to the turntable inside the model. The shakers were aligned to produce forces in two perpendicular planes and attached to the model. The shaker attachment rods had bearings at either end to allow the rods to pivot horizontally so as to minimize coupling forces between the shakers. Two accelerometers mounted inside the model in perpendicular planes sense accelerations in the direction of action of each shaker. The accelerometer outputs were integrated and the integrated signal proportional to the velocity was used in a feedback circuit to drive the shakers. In this way, a damping force (force in phase with velocity) was generated. By varying the gain of the feedback, the model damping could be varied.

TEST PROCEDURES

Reynolds number simulation.- The Langley transonic dynamics wind tunnel can use either air or Freon 12 as a test medium. In order to obtain high Reynolds number flows, Freon 12 was used. The kinematic viscosity of Freon 12 is about one-fifth that of air.

As shown in table I, it was not possible to obtain full-scale Reynolds numbers on the models of Saturn IB and Saturn V, even using Freon 12. Because of this lack of Reynolds numbers simulation, an investigation of high Reynolds number flows about a two-dimensional cylinder at Reynolds numbers up to full-scale Saturn V values was made in the Langley transonic dynamics wind tunnel (ref. 5). This investigation showed that the Reynolds numbers obtained in the model tests were sufficiently high so that no significant changes occurred in aerodynamic force parameters in the Reynolds number range from model test to full-scale values.

Response measurements.- The primary sources of model response data for these investigations were strain gages located near the model base and oriented to read static and dynamic bending moments in two perpendicular planes. Additional response measurements were made by accelerometers mounted near the nose of the models and oriented to read accelerations in the same two planes. Although time histories of these quantities are recorded, the most useful method of examining the data during tunnel operations employs a two-axis oscilloscope and a time exposure polaroid camera photograph as shown in figure 4. In this figure, a top view of a model is shown with the wind coming from an arbitrary azimuth angle and with the strain gages sensing responses in the X and Y directions. The strain-gage outputs are fed to the $M_{B,X}$ and

$M_{B,Y}$ axes of the oscilloscope and the sensitivities of the two channels are made equal. The origin represents a no-wind condition. As the model is exposed to a wind, a time exposure photograph of the oscilloscope screen produces a rough ellipse which defines the envelope of maximum bending moment oscillations during the data sampling period (equivalent to full-scale wind exposure time of the order of 1 hour). The vector from the wind-off point to the center of the ellipse represents the static drag and the longest vector which can be drawn from the origin to some point on the ellipse represents the maximum resultant bending moment. Also, this technique accounts for correlation effects without the requirement for direct measurement of correlation coefficients.

Test techniques.- In testing a given model configuration, the procedure is to take a time exposure oscilloscope photograph while slowly varying the velocity from a low value (very little response) up to a maximum. This maximum is either a simulated design wind velocity or a tunnel Mach number of 0.4, whichever is first reached. Since in the actual atmosphere the design wind values are all at velocities where compressibility effects are negligible, the test Mach number is restricted to an arbitrary upper limit of 0.4 where compressibility effects are assumed to be small. This procedure is repeated for a full range of azimuth angles in about 15° increments. When these "velocity sweeps" are completed, the azimuth angle at which the maximum responses occurred are selected and time exposure photographs at constant velocities are made at these critical azimuth angles.

RESULTS AND DISCUSSION

Although a large number of vehicles have been studied in the Langley transonic dynamics tunnel, typical interesting results have been obtained in the investigation of the Saturn V vehicle and the remainder of the discussion will be confined to these results.

Effect of damping.- In figure 5, the dynamic response of the unfueled Saturn V model is presented for two different values of structural damping. The data presented are scaled to full-scale conditions by using scaling laws outlined in reference 6. The steady drag bending moment, as shown by the dotted line, was essentially proportional to the square of the wind velocity. These data were obtained when the umbilical tower was downstream of the model.

Data obtained with a damping value $\frac{c}{c_c} = 0.019$ indicated a peak in the dynamic response at a wind speed of 57 knots. When this peak dynamic response was added vectorially to the steady drag bending moment, the resultant obtained was equal to the vehicle design bending moment. This minimum allowable damping was established by taking data with several different values of damping.

At all values of damping tested, the maximum dynamic response was perpendicular to the wind direction and was predominantly in the fundamental mode. For moderately low values of vehicle damping, the lateral dynamic response can be appreciably greater than the steady drag loads. For the minimum allowable damping condition, $\frac{c}{c_c} = 0.019$, the response at this peak occurred in long bursts of almost sinusoidal oscillation. Decreasing the damping below $\frac{c}{c_c} = 0.019$ gave a response peak at this velocity which exceeded the vehicle design bending moment and the character of the response was a nearly constant

amplitude oscillation - essentially a single-degree-of-freedom flutter. For both these cases, the response at velocities not in this peak was a random amplitude response in the fundamental mode, typical of the response of a lightly damped mechanical system to a random input. When the damping was increased to $\frac{c}{c_c} = 0.028$, the peak in the response was practically eliminated.

It is not possible to estimate with any degree of certainty what the damping of the Saturn V vehicle will be. On the basis of past experience, a $\frac{c}{c_c}$ greater than 0.02 would not be expected. Because of these wind-tunnel results, the Saturn V facility checkout vehicle (500-F) has been equipped with a viscous damper which increased the total vehicle damping to $\frac{c}{c_c} \approx 0.045$ (see ref. 7). Consideration is being given to the design of a similar damper system for subsequent Saturn V flight vehicles.

Effect of fuel condition.- The dynamic response of the Saturn V vehicle for three different simulated fuel conditions is shown in figure 6. The data for the unfueled condition are the same as presented in figure 5. Since the individual fuel tanks of the vehicle will be either completely full or empty, even for the fuel condition designated "intermediate," it was not necessary to consider fuel sloshing effects. The fuel was simulated by lead weights bolted rigidly to the structure.

For each fuel condition, the dynamic response showed a definite peak which is believed to be associated with vortex shedding on the lower two stages of the model. For each condition a Strouhal number $\frac{fd}{v}$ associated with the velocity of peak response was approximately 0.2 where d is the base diameter and f the model fundamental bending frequency. It should be pointed out that these data were obtained at Reynolds numbers of about 6.5 million for the unfueled condition - well above the Reynolds number range usually associated

with a periodic Karman vortex street. Further evidence that the primary aerodynamic excitation force occurred on the lower stages was obtained during attempts to reduce the response with aerodynamic devices. This work will be discussed in a later section.

The peak for the fueled condition is at such a low wind velocity that it presents no problem insofar as vehicle loads are concerned. This has also been found to be true for other models in the fueled condition.

Effects of nearby structures.- The response of the Saturn V was found to be significantly affected by the presence of nearby tower structures. Figure 7 shows the model in the wind tunnel with the umbilical tower alone, and also with the Mobile Service Structure. Some effects of these nearby structures are illustrated in figure 8. In figure 8, the shaded areas represent azimuth angles where the peak dynamic loads discussed in the previous two sections exceeded the vehicle design loads for values of $\frac{c}{c_c} \geq 0.01$. These critical regions pertain to both the unfueled and intermediate configurations. In general, some evidence of a peak in the dynamic response was observed whenever the flow was not completely obstructed by a tower structure. An exception occurred with the umbilical tower alone at azimuth near 45° and 315° in that no peaks were observed and the dynamic response was less than obtained in preliminary tests without the umbilical tower.

Within the shaded areas shown in figure 8, the critical azimuths could vary slightly between data runs. For instance, in the region near 0° with umbilical tower alone, one run might show large response for 345°, 0°, and 15°. A later run might indicate a shift of the critical region with large response occurring, for example, at 0°, 15°, and 30° with the azimuth of most severe response being shifted from 0° to 15°.

For azimuths where the flow was partially obstructed by the umbilical tower (150° and 240°), the high response occurred at a slightly greater wind velocity. In other ways these regions were similar to other critical regions with the response tending to become sinusoidal for low values of damping. The umbilical tower appeared to be acting as a partial shield to reduce the effective local wind velocity at the model. There is a possibility, however, that flow behind the umbilical tower was actually exciting the model. For example, in the Saturn IB and Titan III investigations (refs. 1 and 8), it was found that flow behind an umbilical tower could cause large model response.

The presence of the Mobile Service Structure was not sufficient to eliminate high response for flow between the two towers. The absence of a shaded area at 225° should not be construed as a positive effect of the MSS as the high response observed for this azimuth angle for the umbilical tower alone was not always repeatable. In an attempt to find means of further alleviating loads on the vehicle in the presence of the service structure, solid plates were bolted to the MSS over the surfaces shown by the dotted lines in figure 8. These plates, which extended to the top of the second stage, were found to eliminate the high response for all azimuth angles.

Aerodynamic load alleviation devices.- Previous experience in ground wind loads work has shown that dynamic loads can be reduced by spoiling the flow around critical sections of a structure (ref. 9). For example, in the Langley Jupiter investigation, dynamic loads were reduced by more than 50 percent by placing small spoilers on the payload section (ref. 10).

As part of the Saturn V investigation, several devices were tested - three of which are shown in figure 9. A splitter plate was rigidly attached to the umbilical tower and extended to within about 1/2 inch of the model.

For azimuths near 0° where the plate was downstream of the model, all trace of the large peak response was eliminated. For other azimuths such as 90°, however, the response was not affected. The helical strake concept was obtained from work by Scruton (ref. 11). Both the helical-strake and circular-disk configurations were found to diminish the level of the peaks but did not eliminate them.

In addition to these devices, long sheets of cloth were attached to the model and allowed to trail downstream in the wake. Also, a wire mesh screen mounted on the umbilical tower extended around the second stage without touching it. Both of these devices were found to be ineffective.

Previous studies (refs. 6 and 9) have indicated several cases where the occurrence of large dynamic response was sensitive to small configuration changes near the nose of the vehicle. This was not found to be true for the Saturn V vehicle. During the course of the investigation, several relatively large configuration variations were made (such as removing the launch escape rocket or placing spoilers on the payload cone) which had a negligible effect on the model response. In addition, it was found that changes in protuberances such as conduits, fins, and ullage rockets on the lower stages did not significantly alter the response. Thus, while nose geometry and protuberances may have had secondary effects, they are not believed to be the primary cause of the large dynamic response.

FUTURE PLANS FOR WIND PROFILE VARIATION

The work done at Langley has been conducted in a relatively smooth flow which does not simulate atmospheric turbulence. Also, because the flow velocity is essentially constant throughout the test section, the models are

not subjected to the variations of wind speed with height which would be found in atmospheric winds. At present, a method of varying the velocity profile in the wind tunnel is being developed. Some preliminary tests have been conducted in a 1/8-scale model of the Langley transonic dynamics tunnel test section as shown in figure 10. A series of 48 horizontal circular bars was installed across the upstream end of the test section. The spacing of the bars was chosen on the basis of a procedure developed in reference 12 for developing linear shear flow in a wind tunnel. In the present application, the design wind profile for Cape Kennedy, which varies as the one-fifth power of the height, was approximated by two such segments of linear shear flow. A comparison of the design wind profile and the simulated wind profile is shown in figure 10. On the basis of these rather encouraging results, plans are underway to install a similar system for shaping a wind profile in the Langley transonic dynamics tunnel.

CONCLUDING REMARKS

Ground wind loads have been investigated for a large number of specific launch vehicle configurations in the Langley transonic dynamics wind tunnel. An examination of typical results obtained for the Saturn V vehicle has indicated several interesting features. When the structural damping is moderately low $\left(\frac{c}{c_c} \cong 0.01\right)$ lateral dynamic response apparently associated with vortex shedding from the lower two stages of the vehicle produces loads in excess of the design loads for the vehicle. These large responses occurred at conditions corresponding to a Strouhal number $\frac{fd}{v}$ of about 0.2 where d is the the diameter of the lower stages and f is the frequency of the fundamental

bending mode. The response had characteristics similar to a single-degree-of-freedom flutter, and it was found that moderate increases of the structural damping $\left(\frac{c}{c_c} \cong 0.03\right)$ reduced the response to acceptable levels and changed its character to that of a lightly damped system responding to a random input.

To take advantage of these beneficial effects of increased damping, a viscous damper has been incorporated in the full-scale vehicle launch complex.

REFERENCES

1. Jones, George W., Jr.; and Farmer, Moses G.: Wind Tunnel Studies of Ground-Wind Loads on Saturn Launch Vehicles. Proceedings of AIAA/ASME Seventh Structures and Materials Conference, pp. 377-381, April 1966.

2. Lambert, W. H.; Cokonis, T. J.; and Riggen, C. L.: Wind Tunnel Investigation of Ground Wind Effects on the Gemini Launch Vehicle and Complete Vehicle Erector. The Martin Company, Contract No. LV281-5, August 1964.

3. Kosmal, D.; and Schultz, R.: Dynamic Response of the Full Scale Gemini Launch Vehicle and the Complete Vehicle Erector Under Actual Ground Wind Conditions. The Martin Company, Contract No. LV-387-IV, November 1965.

4. Lyons, J. M.; and Lum A. J.: Ground Wind Induced Oscillation of the Titan III ITL Transporter. Proceedings of Langley Ground-Wind Loads Meeting, Paper No. 5, June 1966.

5. Cincotta, Joseph J.; Jones, George W.; and Walker, Robert: Experimental Investigation of Wind Induced Oscillation Effects on Cylinders in Two-Dimensional Flow at High Reynold Numbers. Proceeding of Langley Ground Wind Loads Meeting, Paper No. 20, June 1966.

6. Buell, Donald A.; McCullough, George B.; and Steinmetz, William J.: A Wind-Tunnel Investigation of Ground-Wind Loads on Axisymmetric Launch Vehicles. NASA TN D-1893, October 1963.

7. Hunt, Robert M.: Saturn V Ground Wind Program. Proceedings of Langley Ground-Wind Loads Meeting, Paper No. 3, June 1966.

8. Lambert, W. H.; and Cincotta, J. J.: Investigation of Wind Induced Oscillations and Steady Ground Wind Forces on a 7.5 percent Dynamically Scaled Model of the 624A Vehicle. The Martin Company, Contract No. ER 13022, May 1963.

9. Buell, Donald A.: Highlights of Ground-Wind Tests at Ames. Proceedings of Langley Ground-Wind Loads Meeting, Paper No. 1, June 1966.

10. Killough, Thomas L.: Wind Induced Loads on a Dynamic 1/5 Scale Unfueled SM-78 Jupiter in the Launch Position. Army Ordnance Missile Command Report No. RG-TM-62-65, July 1962.

11. Scruton, C.: On the Wind-Excited Oscillations of Stacks, Towers, and Masts. Paper 16, Brit. Natl. Phys. Lab., June 1963.

12. Owen, P. R.; and Zienkiewicz, H. K.: The Production of Uniform Shear Flow in a Wind Tunnel. Journal of Fluid Mechanics. Vol. 2, Pt. 6, pp. 521-531, August 1957.

TABLE 1.– MODELS TESTED

VEHICLE SIMULATED	LENGTH SCALE FACTOR	REYNOLDS NUMBER SCALE FACTOR	WEIGHT CONFIGURATIONS SIMULATED
SCOUT	.15	1.00	FUELED
JUPITER	.20	1.00	UNFUELED
SATURN I-BLOCK I	.075	1.00	FUELED
TITAN III	.075	1.00	FUELED AND UNFUELED
TITAN III-PHASE II	.075	0.45	FUELED
TITAN GEMINI	.075	1.00	FUELED
SATURN I-BLOCK II	.070	1.00	FUELED AND UNFUELED
SATURN IB	.055	0.85	FUELED AND UNFUELED
SATURN V	.030	0.31	FUELED, INTERMEDIATE, AND UNFUELED

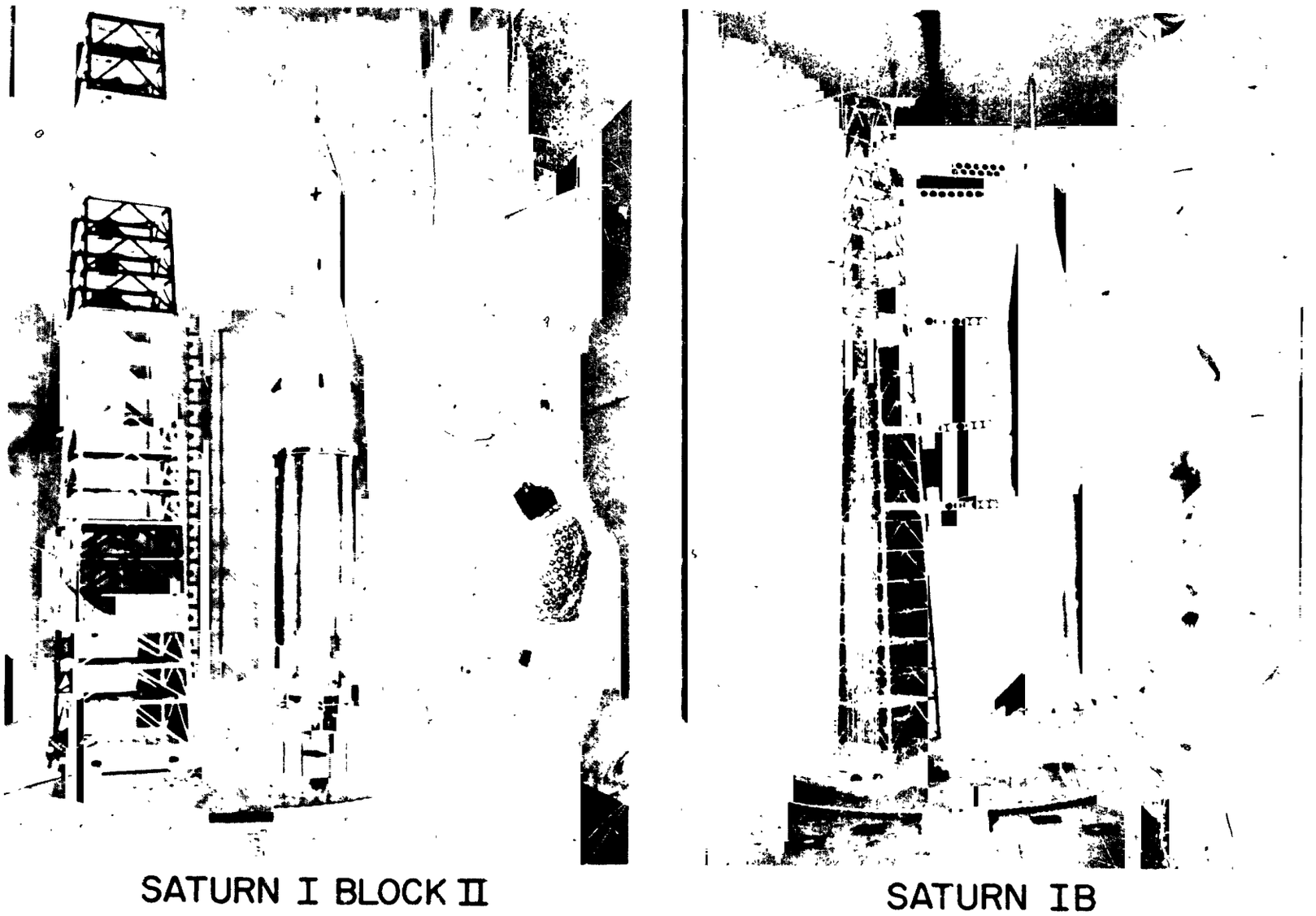

Figure 1.- Models in wind tunnel.

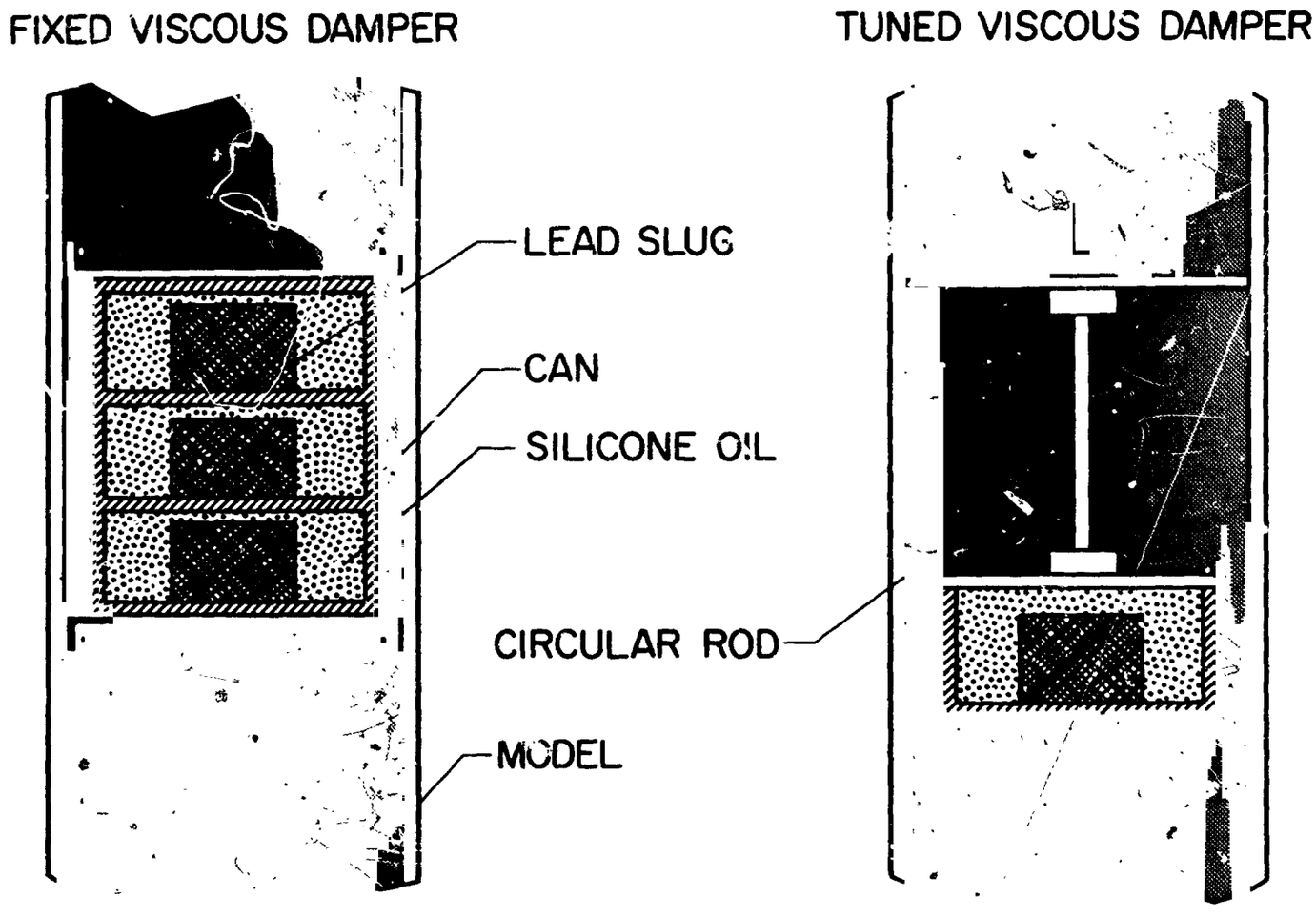

Figure 2.- Auxiliary dampers.

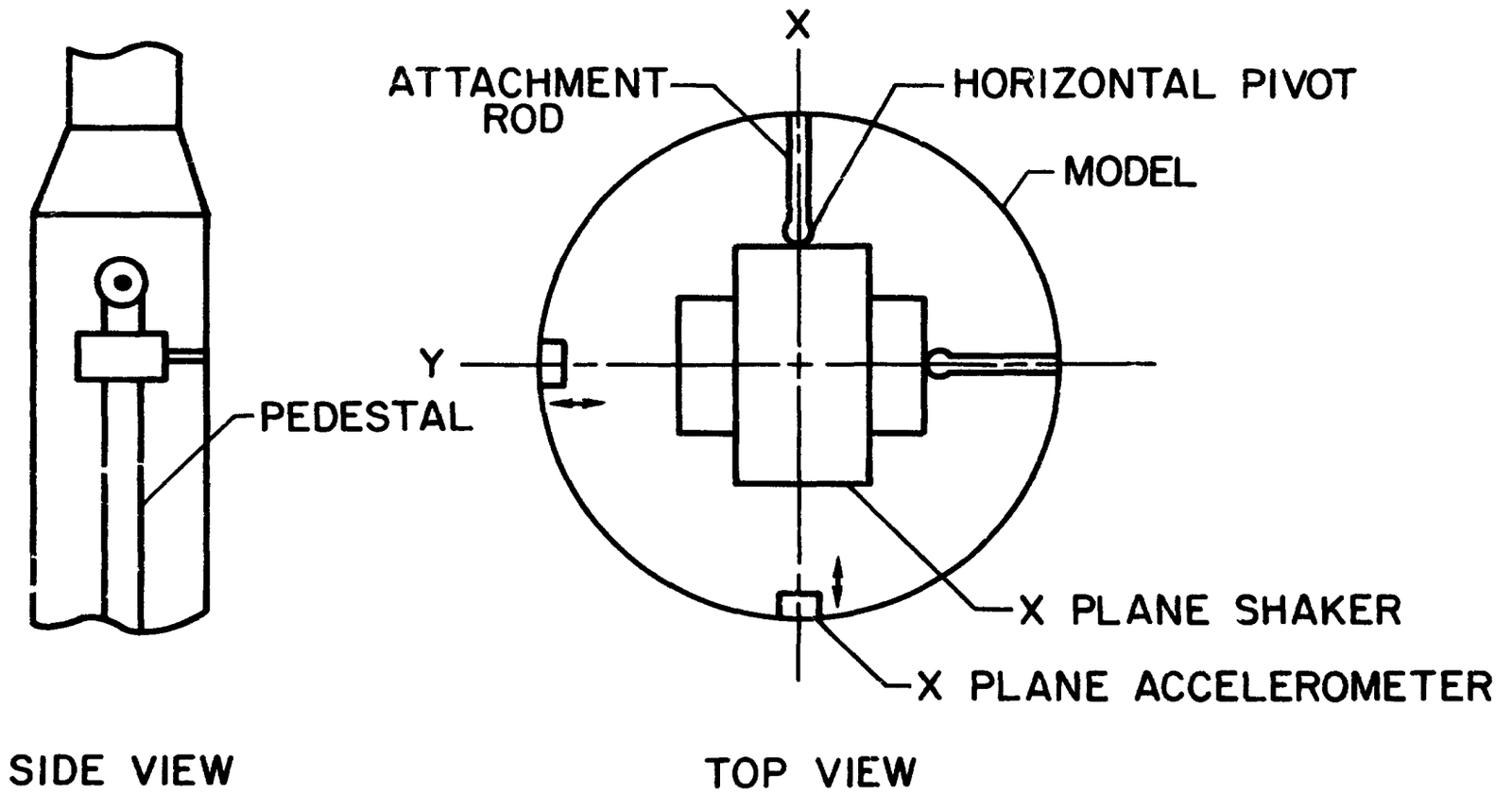

Figure 3.- Electromagnetic dampers.

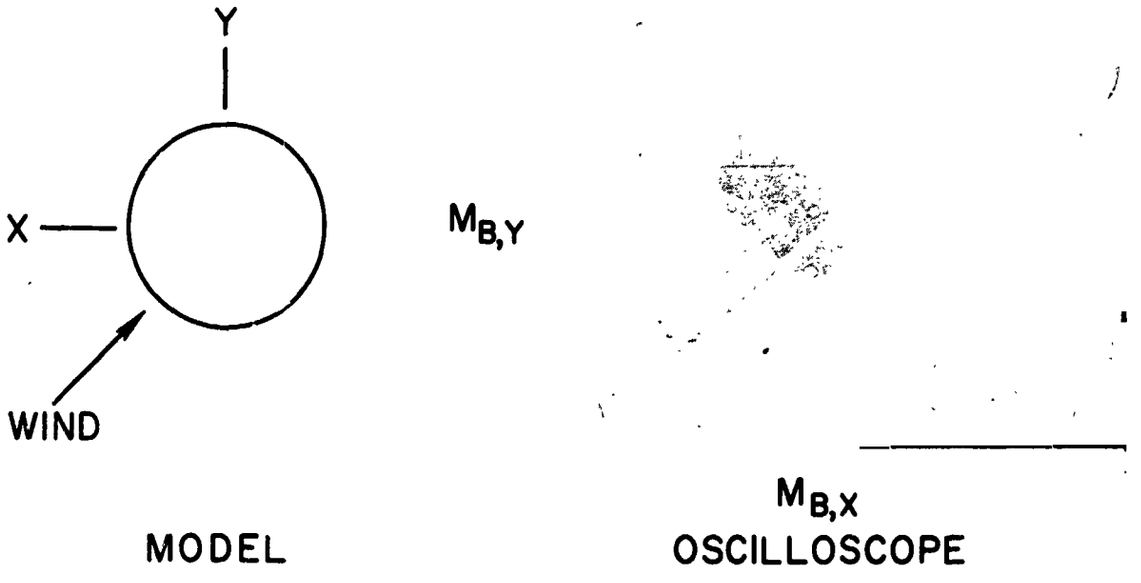

Figure 4.- Time exposure of bending moments.

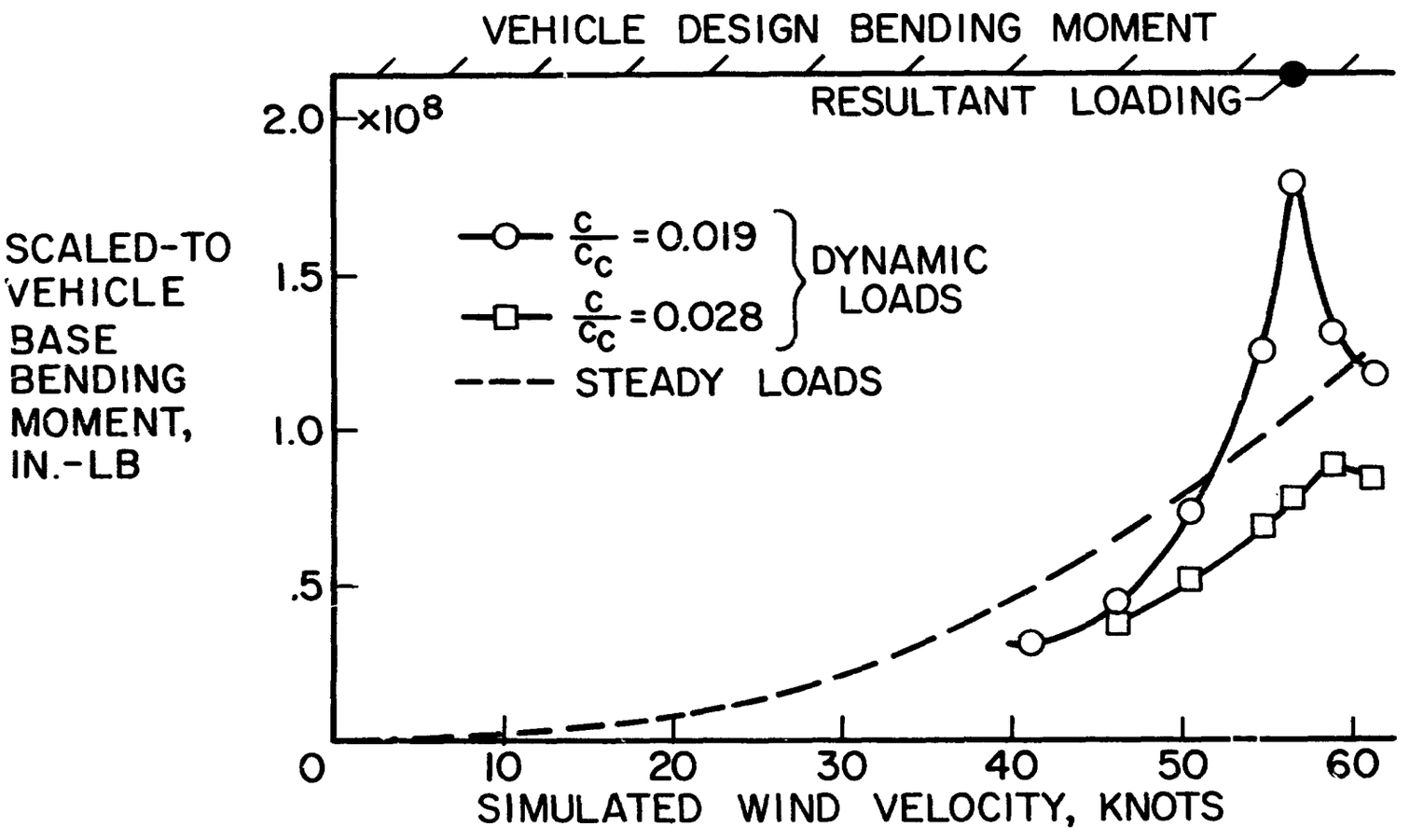

Figure 5.- Effects of structural damping on Saturn V vehicle response.

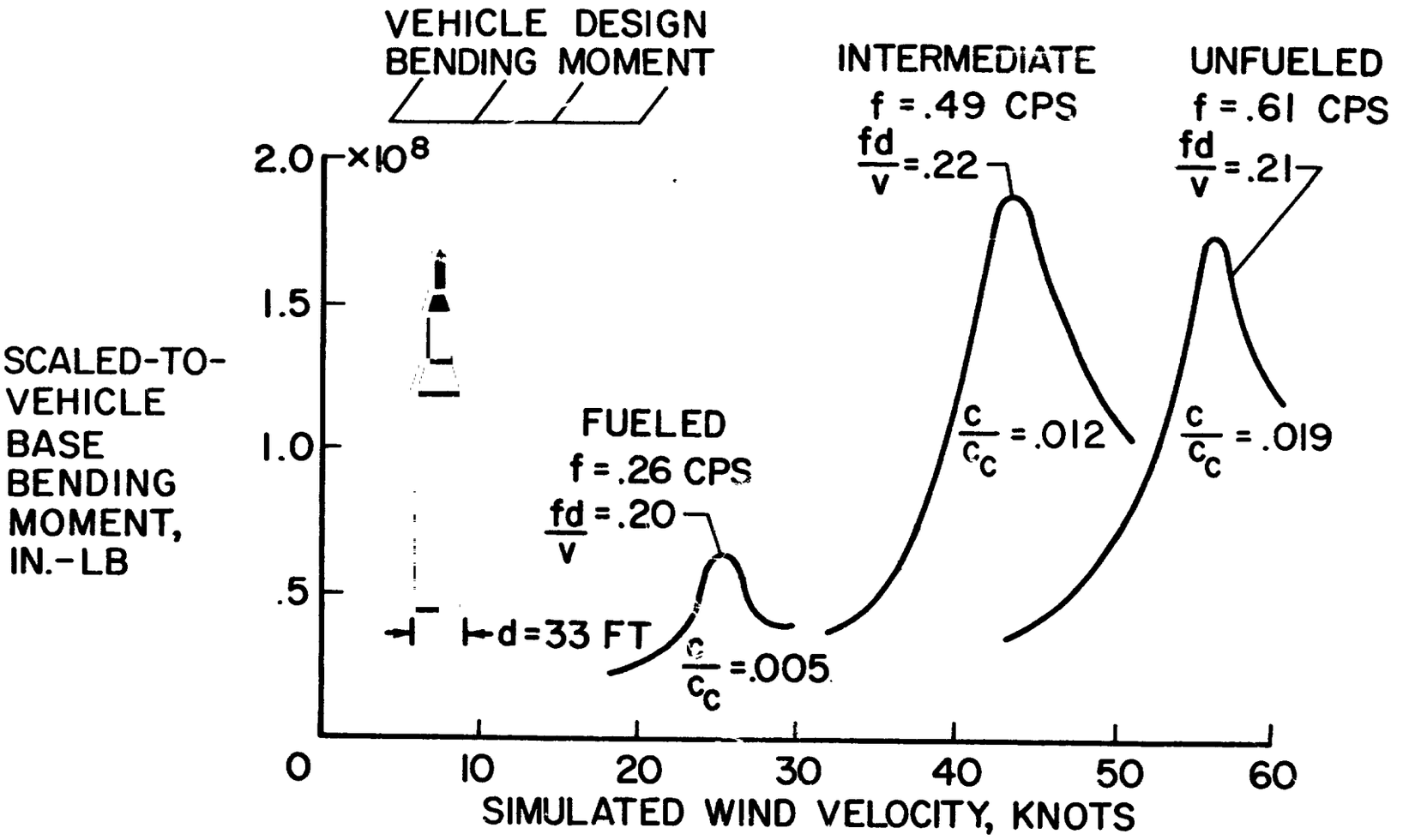

Figure 6.- Effect of fuel condition on Saturn V vehicle response.

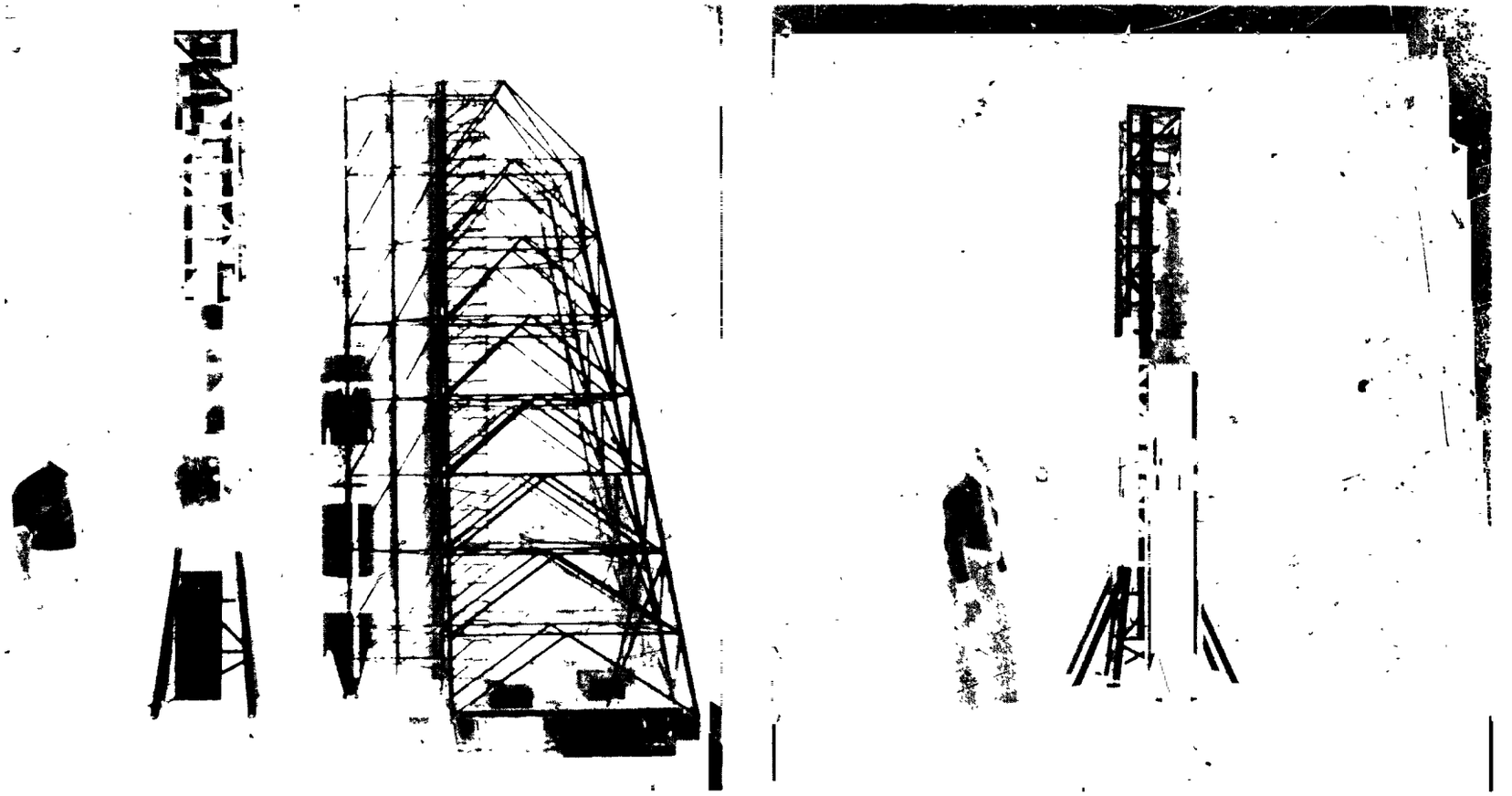

Figure 7.- Saturn V model.

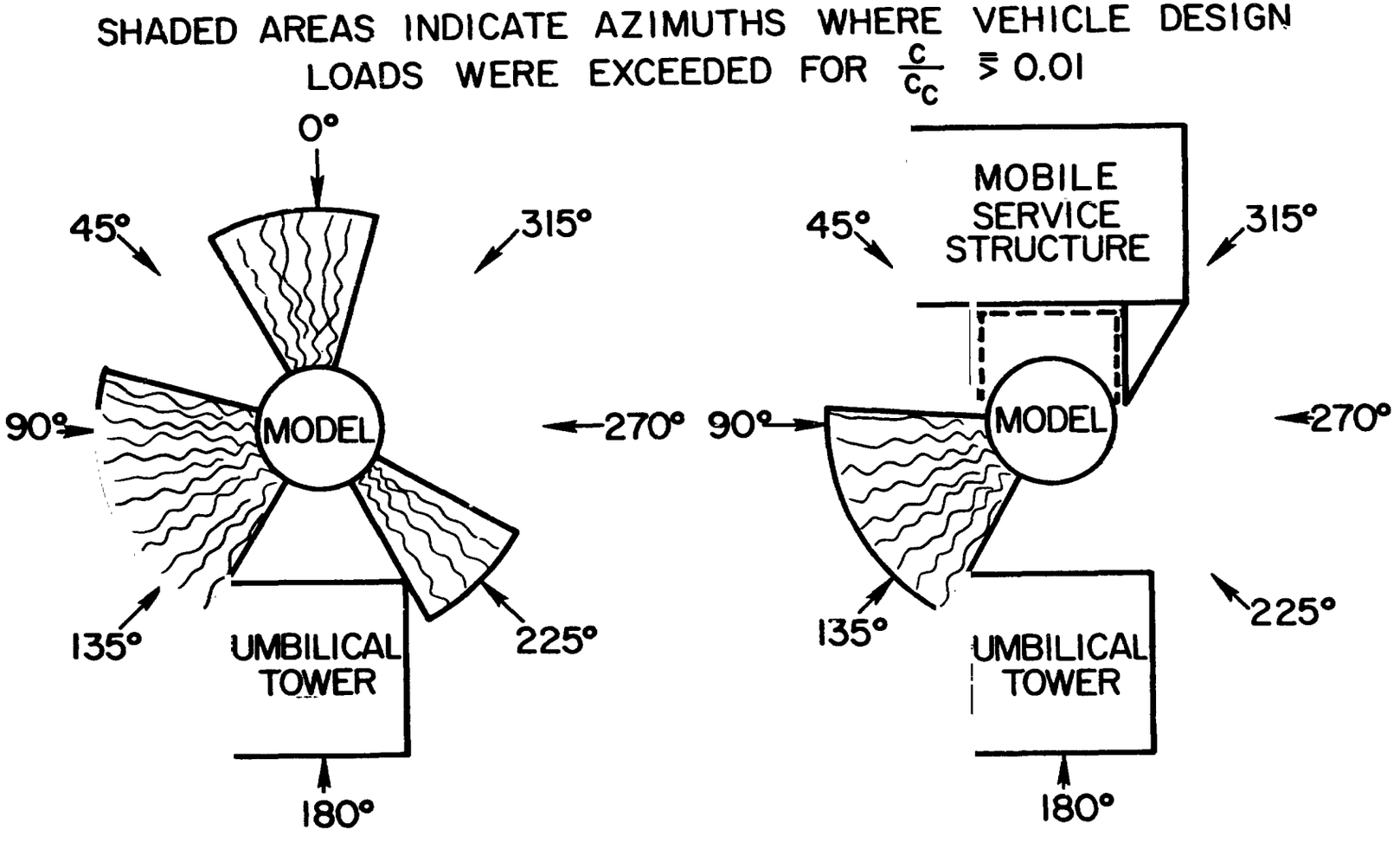

Figure 8.- Effects of nearby structures on Saturn V vehicle response.

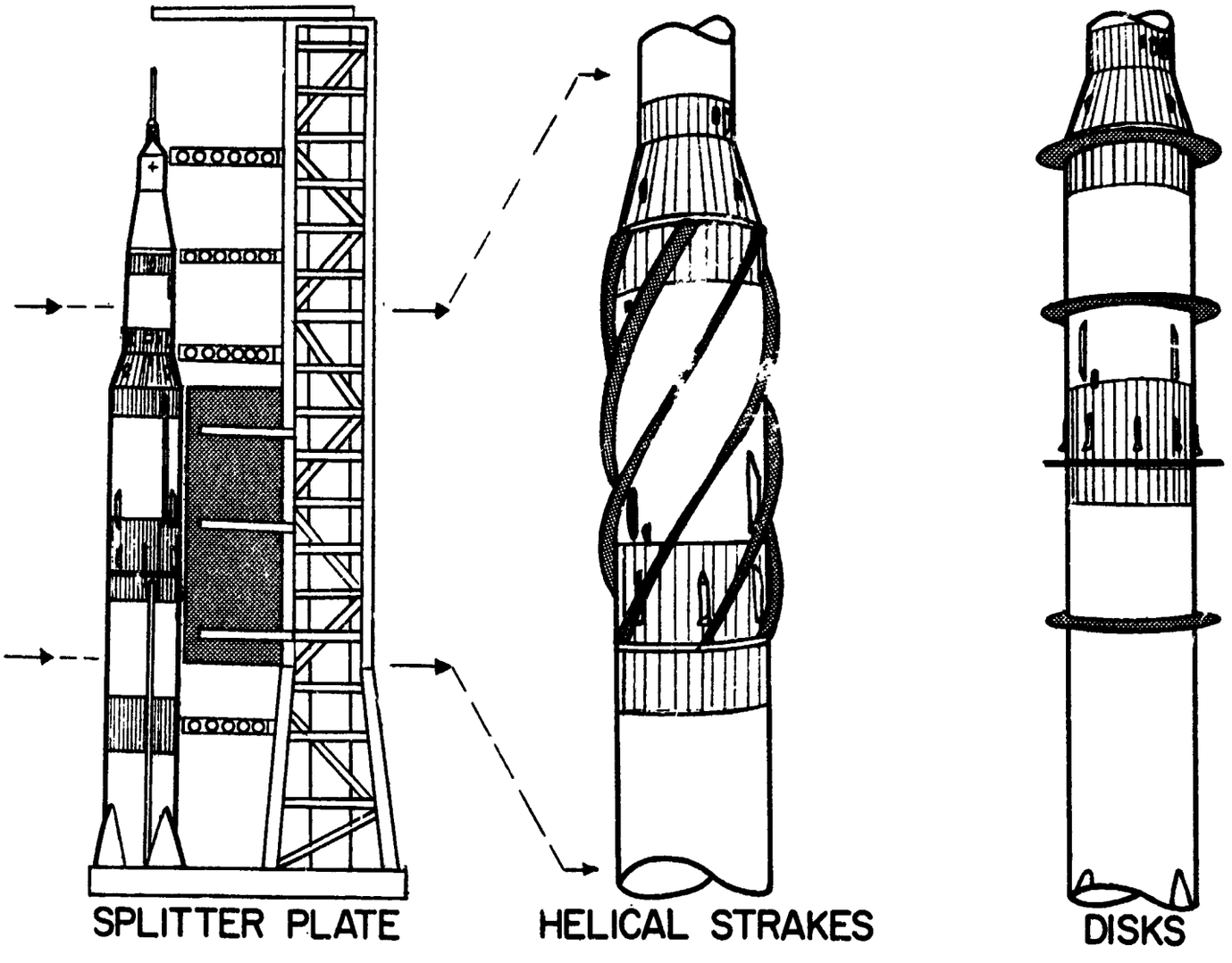

Figure 9.- Attempted load-alleviation devices.

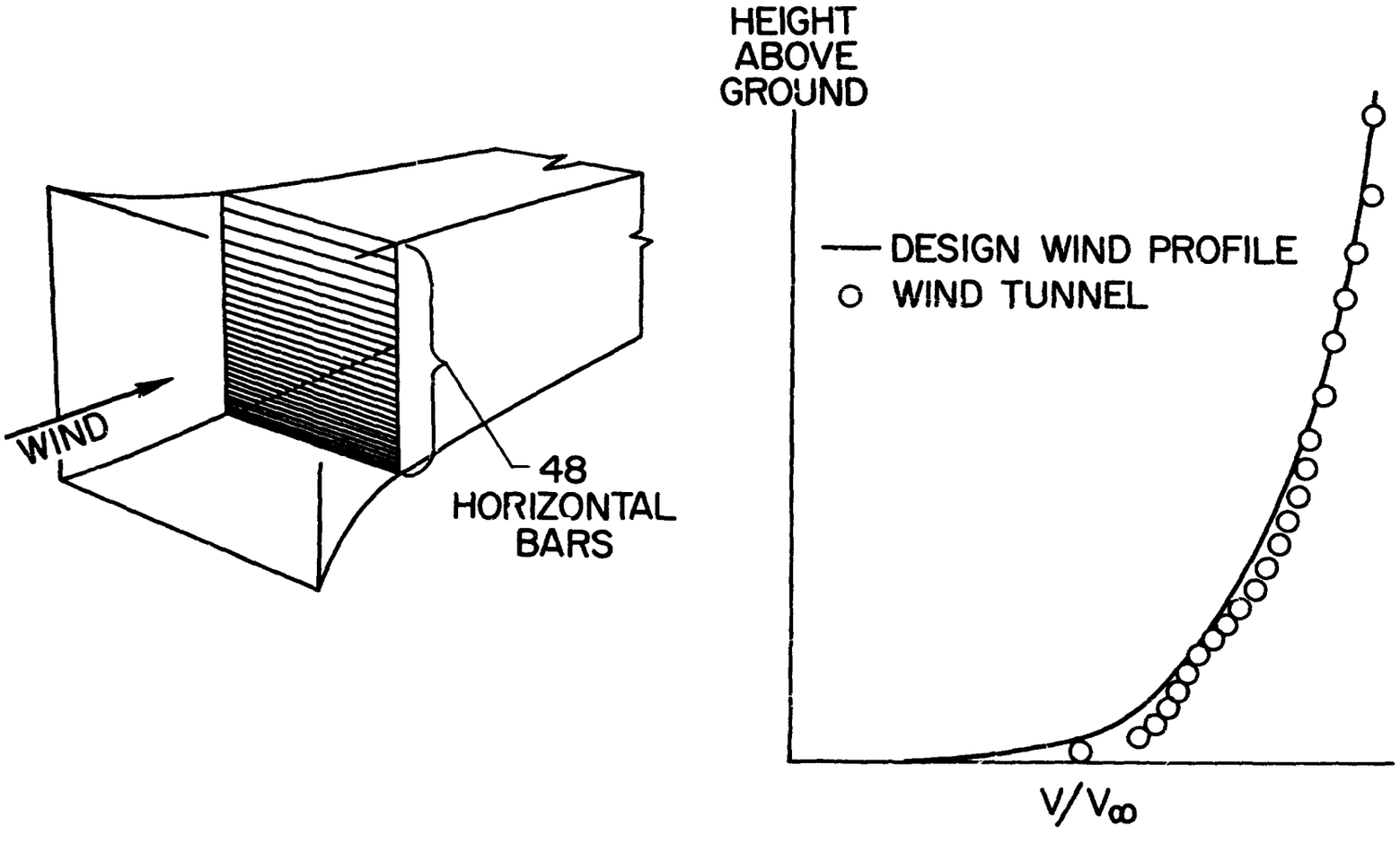

Figure 10.- Wind-tunnel simulation of wind profile.

May 6, 1966

SATURN V GROUND WINDS PROGRAM

BY

ROBERT M. HUNT

GEORGE C. MARSHALL SPACE FLIGHT CENTER

A B S T R A C T

The concept on SATURN V was to "budget" an amount for the dynamic portion of the wind load as a factor on the steady state drag. Wind tunnel tests paralleled the development and fabrication phases. The results indicated that the system was unable to withstand the design winds; thus, a decision was made to implement a viscous damper "fix" on the facility vehicle at the Kennedy Space Center. Damping tests in the Vertical Assembly Building (VAB) will have been completed and response tests on the pad will be in progress at the time of this symposium. This paper will present the history and status of this program to date.

NASA

GEORGE C. MARSHALL SPACE FLIGHT CENTER

Figure 1 shows the basic design criteria for Saturn V. There is no attempt here to predict response but 50% of the drag load is budgeted for this phenomenon .

Figure 2 shows how these vectors combine and that the dynamics portion in fact is given more consideration than the drag load.

Figure 3 shows the wind tunnel results superimposed on the design criteria. This graph indicates that the design limit was reached at a lower velocity than the design winds.

Figure 4 shows the Alternatives considered as possible solutions to the problem.

Waiving the wind criteria was never really given any serious consideration. The aerodynamic fixes will be given detailed treatment in a later paper at this symposium.

The mechanical fix was accepted but it evolved into two possible solutions. The first was to add an external support to the vehicle; thus, to add effective stiffness and increase the natural frequency of the system. This introduced large loads into the vehicle.

The second mechanical method was to add a viscous damper. This reduced the dynamic response to winds; thus, allowing the vehicle to traverse its critical response range without exceeding the design loads.

These approaches are shown in Figure 5.

The damper was begun 90 days before roll out of AS-500F and an unbelievable story on design, fabrication, testing, scheduling, transportation and erection followed. Figure 6 is an artist's conception of it installed at station 2560. Three hard points are provided in the vehicle and the rest is umbilical arm and tower equipment. Since AS-500F is a facility checkout and ground wind vehicle no provision is made for removing the arms except manually in the VAB. Figure 7 shows the vehicle during roll out. Note the umbilical arms and the damper arm.

The AS-500 Ground Winds Program consists of taking wind data simultaneously with vehicle response data. The wind data will be recorded both at the vehicle and at a remote tower some 4 miles away. The data obtained will be velocity and direction for the 60, 250, and 500 foot level.

The vehicle response will be measured by 2 horizontal mutually perpendicular accelerometers at 5 stations along the vehicle length and 3 mutually perpendicular accelerometers at the base of the vehicle. Strain readings will be taken at five stations. Three stations have 16 gages each located 22-1/2° apart and the other two stations have 16 gages per station with each of 2 gages located on the same hat section stringer every 45° circumferentially. One of these gages is on the crown, the other on the side of the hat. The third mode of data acquisition for vehicle response is optical. Four cameras approximately 90° apart will photograph targets at the same vehicle station in the payload area.

Attempts will be made to establish the vehicle response curve as a function of both wind direction and velocity. This in turn will be compared with the wind tunnel results. The damper was designed with variable orifices; thus, data may be acquired that shows response as a function of damping. Damping tests were run in the Vertical Assembly Building both before and after the dampers were installed. The values before ranged from 1.2 to 1.6% of critical and after the damper was installed they ranged around 4.5% of critical.

Pull tests were also run in the VAB in order to equate strain readings to bending moments.

The taking of data will continue on during the summer and end about August 25. These results will be collected and reported.

Bibliography

1. NASA SP-8008, NASA Space Vehicle Design Criteria - Prelaunch Ground Wind Loads - November, 1965.

2. Saturn V Ground Wind Loads Test Project Plan. MSFC I-V-TD No. 4, August 20, 1965, Rev March 31, 1966.

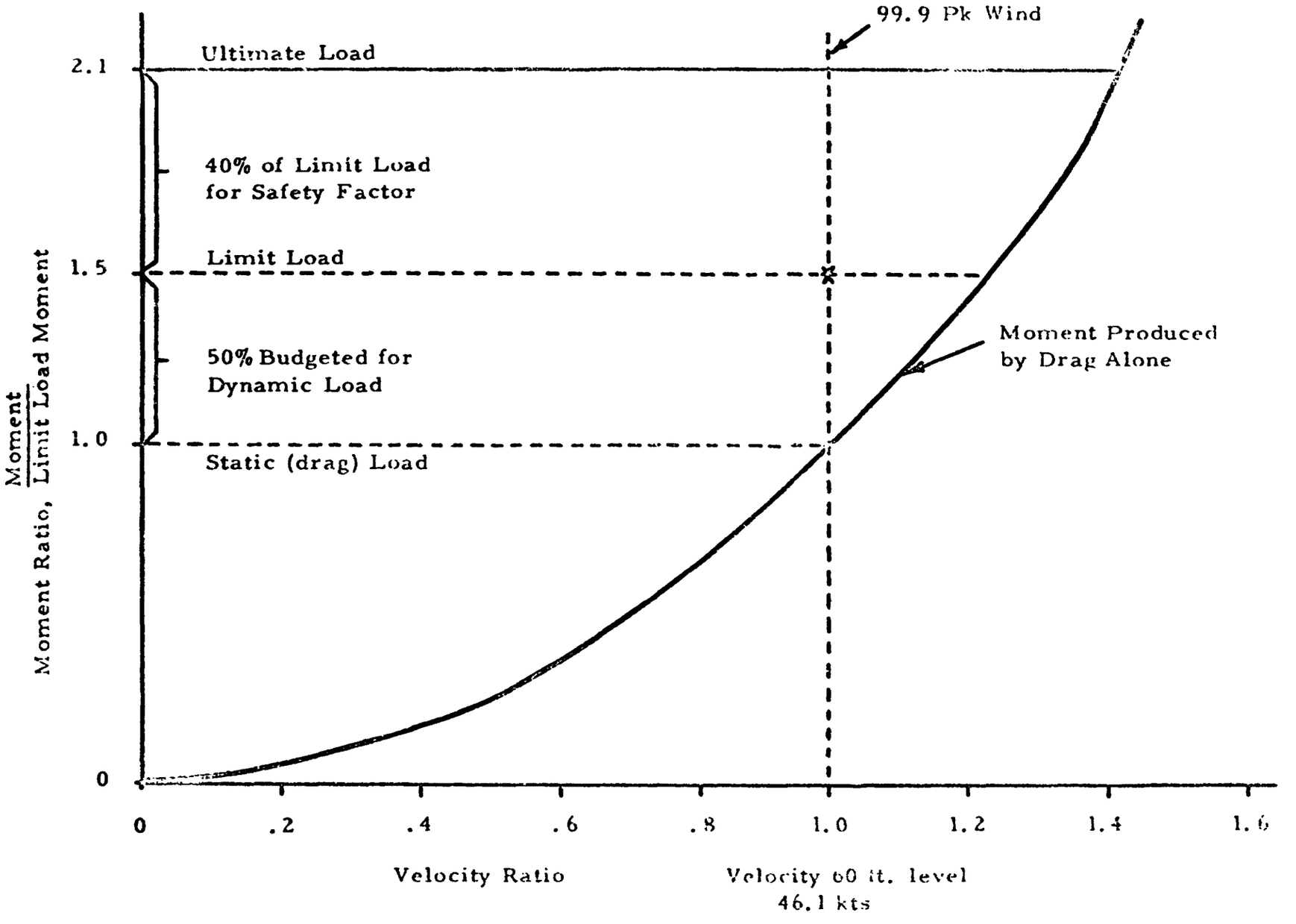

Figure 1. Schematic of Basic Structural Design Criteria Followed for Saturn V Related to Ground Wind Conditions

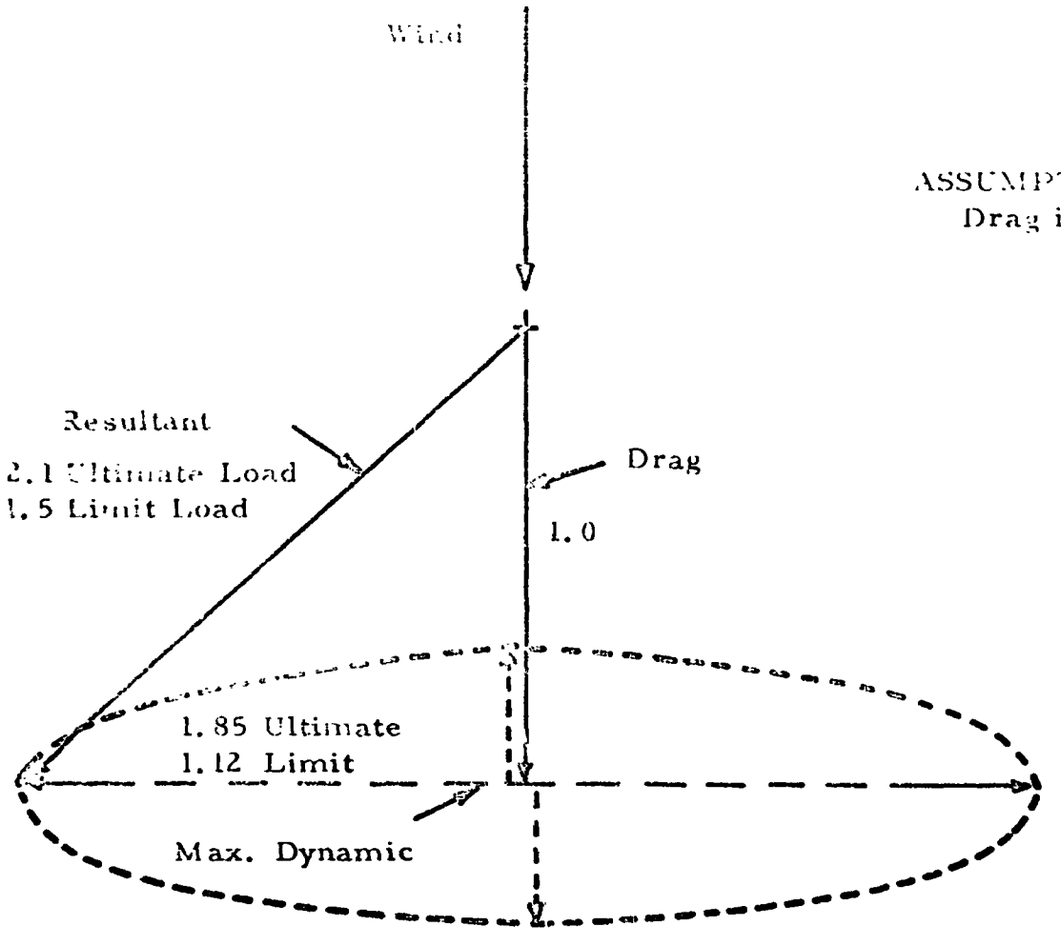

ASSUMPTIONS:
Drag is well defined load.

Figure 2. Schematic of Loads at Any Given Vehicle Station

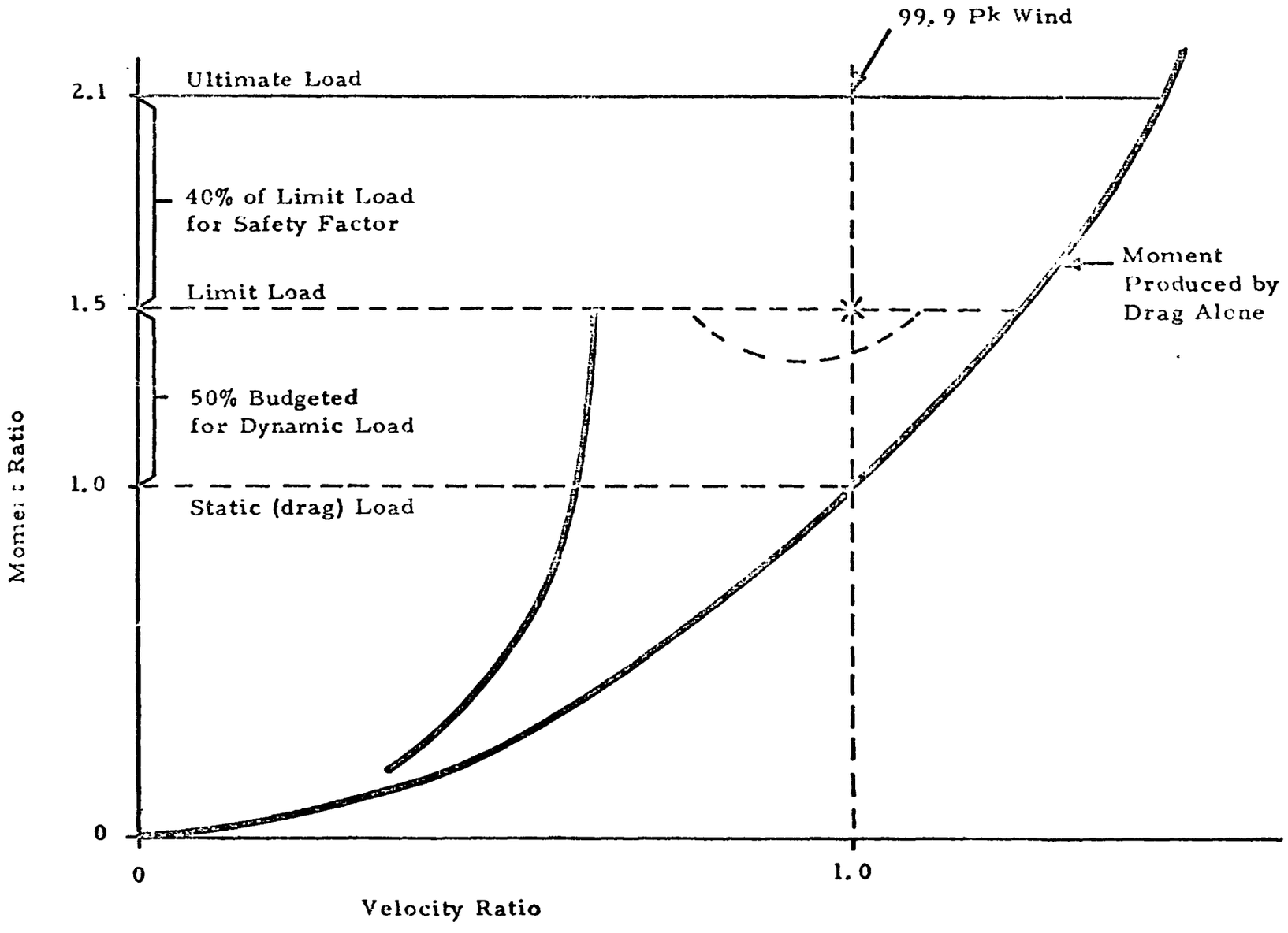

Figure 3. Schematic of Wind Tunnel Results

FIGURE 4

ALTERNATIVES CONSIDERED AS POSSIBLE SOLUTIONS TO FAILURE IN MEETING DESIGN CRITERIA:

WAIVE WIND CRITERIA THUS ACCEPT HIGHER RISK OF LOOSING VEHICLE ON PAD

DEVELOP AERODYNAMIC FIX

CRITERIA: (1) STABILIZE VEHICLE WITHIN DESIGN LIMITS AT ALL VELOCITIES BELOW DESIGN WIND CONDITIONS.

(2) OPERATIONALLY COMPATIBLE WITH LAUNCH AND FLIGHT FUNCTIONS.

DEVELOP MECHANICAL FIX

CRITERIA: (1) STABILIZE VEHICLE WITHIN DESIGN LIMITS AT ALL VELOCITIES BELOW DESIGN WIND CONDITIONS.

(2) OPERATIONALLY COMPATIBLE WITH LAUNCH AND FLIGHT FUNCTIONS.

(3) GROUND EQUIPMENT PREDOMINANTLY.

MAKE VEHICLE CAPABLE OF WITHSTANDING THE HIGHER LOADS

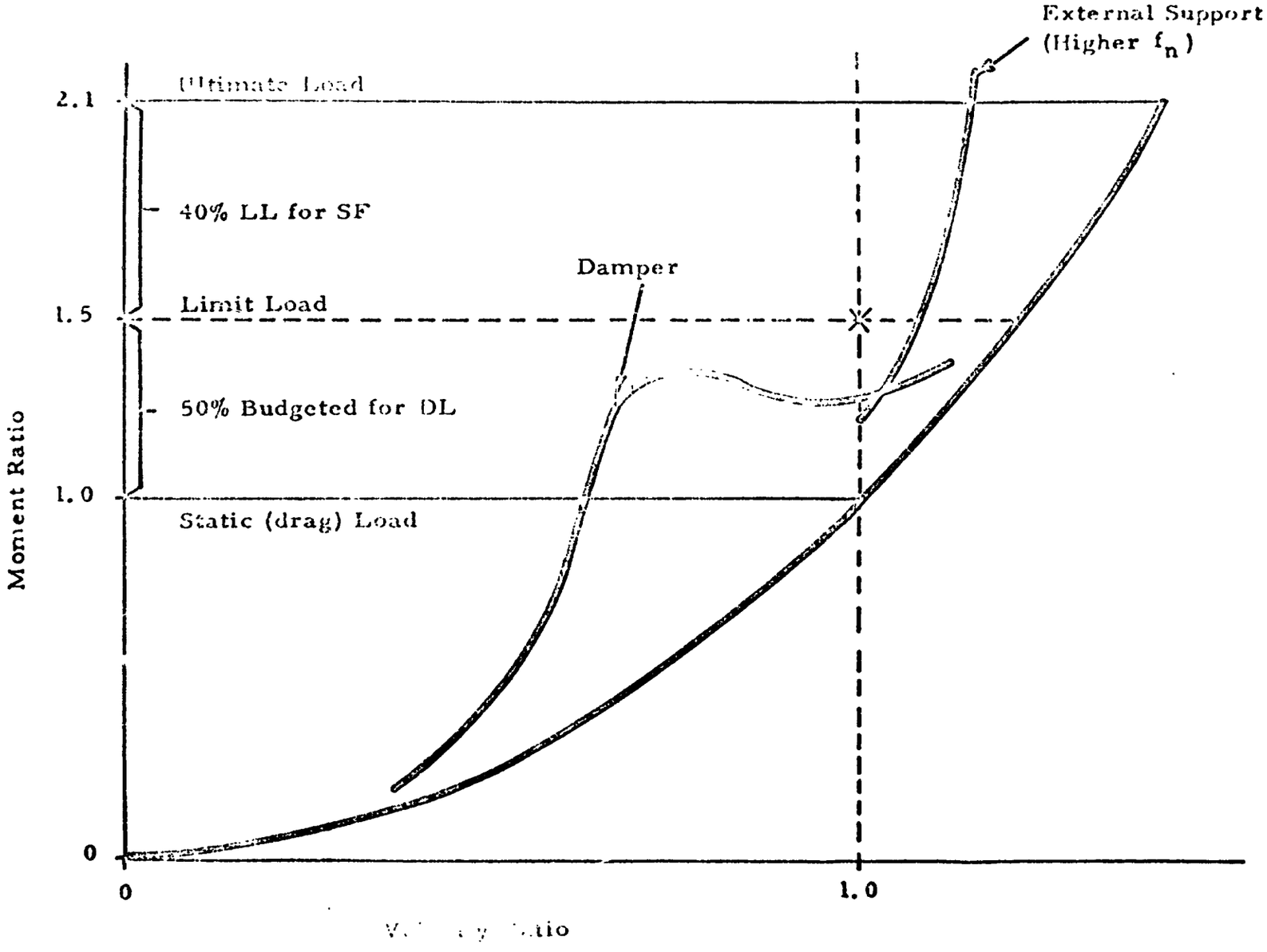

Figure 5. Comparison of Predicted Response Characteristics of Both the Damper and the External Support

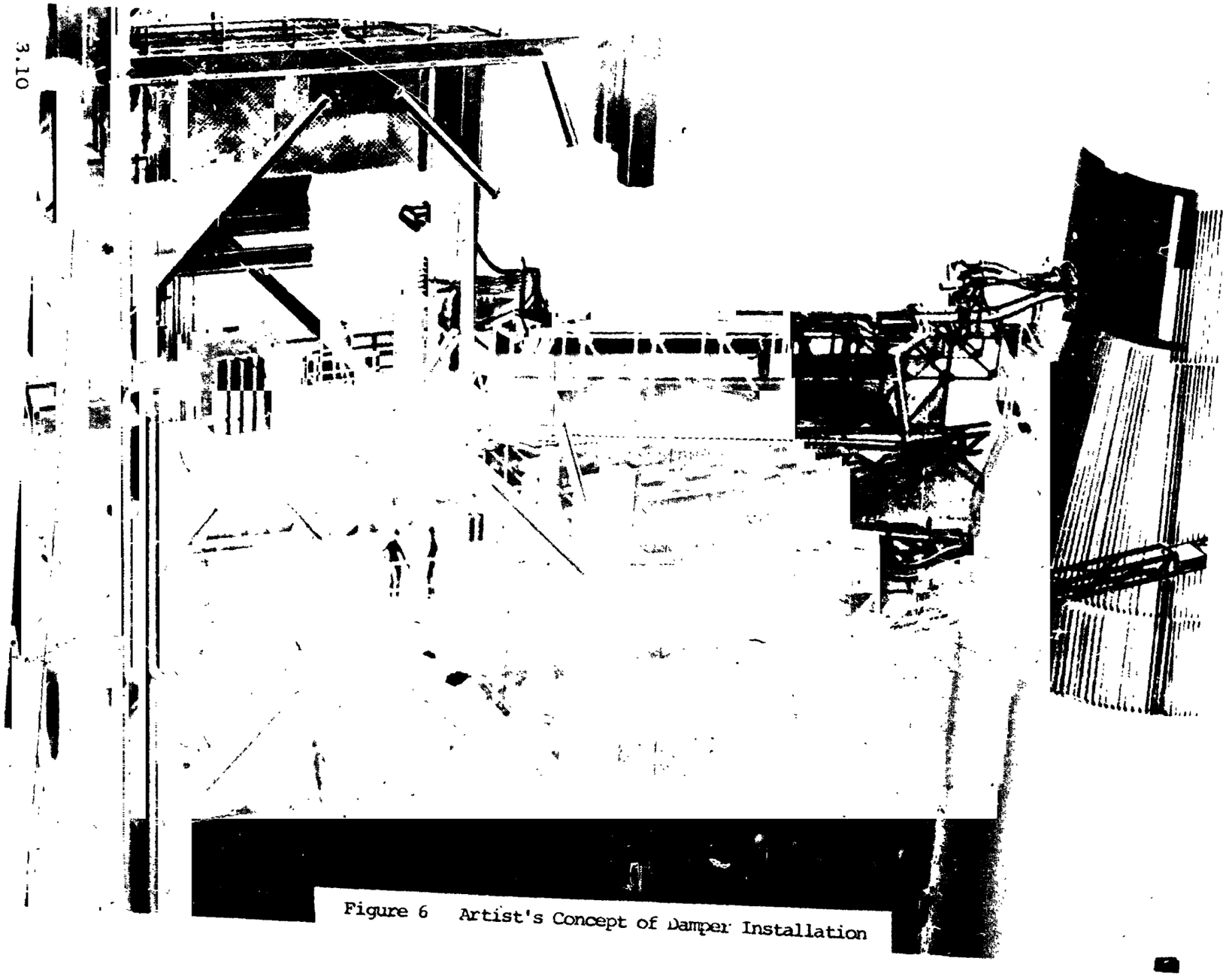

Figure 6 Artist's Concept of Damper Installation

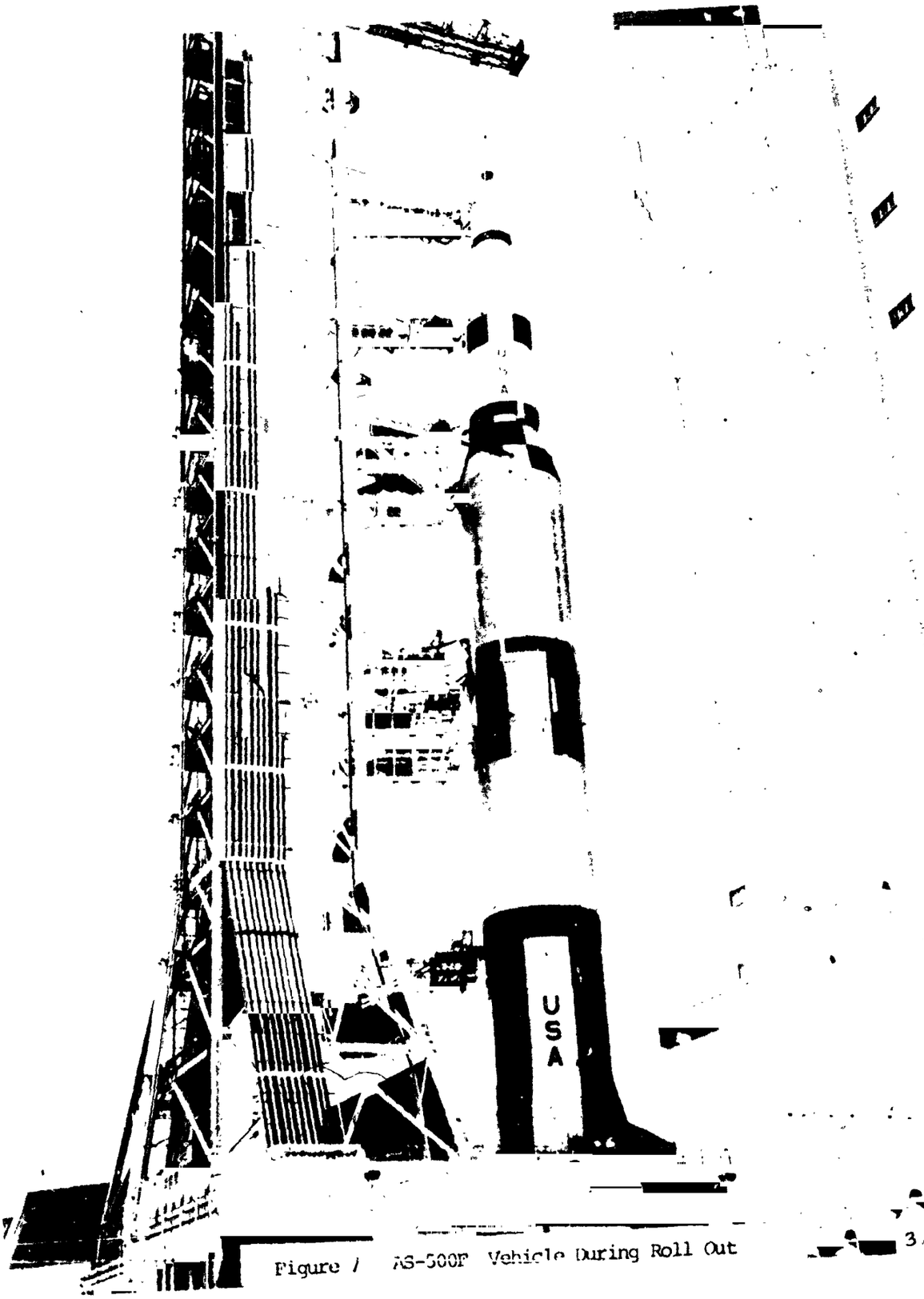

Figure / AS-500F Vehicle During Roll Out

A FULL-SCALE GROUND WIND LOAD PROGRAM

by

Jerome T. Foughner, Jr. and Rodney L. Duncan

National Aeronautics and Space Administration

Langley Research Center

SUMMARY

The NASA Langley Research Center is currently utilizing two surplus launch vehicles for the purpose of research on ground wind loads. The vehicles, a Jupiter and a Thor, have been erected at Wallops Island. The paper indicates program objectives and presents initial results in the form of drag and lateral dynamic response on each vehicle. A response power spectrum for the Thor vehicle is discussed. A preliminary comparison of the dynamic bending moment response of the Jupiter vehicle with available wind tunnel model data combined with theoretical predictions of response due to turbulence indicates poor agreement.

INTRODUCTION

The response of launch vehicles to ground wind loads is presently simulated by means of models. Physical models in wind tunnels to determine vortex shedding loads are discussed in references 1 and 2 and mathematical models to predict response due to

atmospheric turbulence are discussed in references 3, 4, and 5. It has not been established that these models are the intended analogs of their full-scale counterparts. This is primarily due to a lack of full-scale response data for correlation with similar model data. Due to launch schedules and other considerations, it is difficult to obtain response data on an active vehicle. In light of this, a research program has been initiated utilizing surplus launch vehicles, a Jupiter and a Thor, for the purpose of providing full-scale vehicle response to ground wind loads. The physical and mathematical models may then be evaluated by comparison with measured response. In addition the program will provide experimental data on ground wind turbulence through the use of fast response drag sphere anemometers (reference 6). The paper briefly describes the experimental set-up at Wallops Island and presents initial results of the program which is currently in progress. Data are presented in the form of drag and lateral dynamic loads on each vehicle. A response power spectrum for the Thor vehicle is discussed. The dynamic bending moment response of the Jupiter vehicle is compared with available wind tunnel data combined with theoretical predictions of response due to turbulence.

EXPERIMENTAL ARRANGEMENT

The Jupiter and the Thor vehicles were erected at Wallops Island, Virginia. Two views of the test area are presented in figures 1 and 2. Wallops Island is located on the Atlantic Coast of the Delmarva Peninsula. It is sparsely wooded, sandy, and comparatively flat. The coast line in figure 1 runs northeast

to southwest. Prominent structures shown in figure 1 and in figure 2 include the Thor vehicle, the Jupiter vehicle, drag sphere wind sensor pole on south side of Jupiter vehicle, Bendix-Friez anemometer on top on an observation tower, the instrumentation van, an emergency power generating van and the Wallops Island 250-foot meteorological tower. Maximum diameter of the Jupiter is 8.75-feet and its height on launcher is 66.0-feet above the ground. Maximum diameter of the Thor is 8.00-feet and its height on launcher is 76.0-feet. Drag sphere wind sensor heights above ground are 13-feet and 53-feet. Height of the Bendix-Friez anemometer is 66-feet above ground. Wind sensors on the 250-foot meteorological tower are located at 50-foot intervals.

Typical lateral separation distances are 235-feet between Thor and Jupiter vehicle, 48.5-feet between Jupiter vehicle and drag sphere pole, 200-feet between Jupiter vehicle and reference Bendix-Friez wind sensor tower, and 800-feet between Jupiter vehicle and the 250-foot meteorological tower.

INSTRUMENTATION

Vehicle response is determined from strain gages bonded to the outer skin of each vehicle and accelerometers located in the vehicle instrument compartments. Strain gages at base and mid-section stations together with accelerometers near the nose are oriented to measure perpendicular components.

Vehicle response and wind input data are amplified and recorded simultaneously on magnetic tape in the instrumentation

van. An automatic programmer actuates the recording system for 15 minutes at preset time intervals or when the wind exceeds a preselected value.

RESULTS AND DISCUSSION

Thor Dynamic Response

Full-scale lateral and drag dynamic bending moment response is presented in figure 3. The maximum dynamic bending moment is plotted as a function of mean wind speed. The data is for the unfueled vehicle and was obtained from strain gages located near the vehicle base. Mean wind was determined from an aerovane strip chart averaged over a 15-minute period. Each point in the dynamic bending moment data is the peak value that occurred in a 15-minute period. The readout system, a two-axis oscilloscope and camera, to determine the maximum dynamic bending moment is the same as discussed in reference 7. Essentially a time exposure photograph of the oscilloscope screen produces a pattern which defines the envelope of maximum bending moment oscillations encountered during the data sampling period. In figure 3 the lateral dynamic response for the Thor is consistently higher than the drag dynamic response.

A response spectra for a mean wind of 38 miles per hour is presented in figure 4. The spectrum for the base bending moment is plotted as a function of frequency in cycles per second. The response spectrum is presented for both the drag and the lateral directions. Figure 4 indicates the response is due primarily to

vortex shedding loads as the vehicle is responding in the lateral direction at a frequency of about 1.7 cycles per second. This frequency is the vehicle first cantilever mode frequency. Response due to turbulence is indicated by the high level near zero frequency in the drag direction. Thus, figure 4 indicates that predominant power due to turbulence occurs at low frequencies. It is seen in figure 4 that the standard deviation in the lateral direction is twice that of the drag direction. The lateral time history for the data point is shown in the upper right hand corner of figure 4. Response is more or less typical of a lightly damped single-degree-of-freedom system subjected to a random input. An unusual characteristic of the time history is shown in the lower figure with an expanded time scale. The vehicle hold-down system consists of three threaded studs capable of resisting overturning moments. From the squaring off of the amplitude response it is apparent that the hold-down system was not functioning properly for the period of this record and that the system was behaving nonlinearly. This nonlinear behavior may be causing the sub-harmonic response at a frequency of about one-half that of the main response peak.

Jupiter Dynamic Response

The measured lateral and drag dynamic bending moment response for the Jupiter vehicle is presented in figure 5. The data are for the unfueled vehicle and were obtained from strain gages located near the vehicle base. In figure 5 the maximum dynamic bending moment is plotted as a function of mean wind speed with

parameters as defined for the data of figure 3. Figure 5 shows that the Jupiter lateral loads are consistently higher than the drag loads just as they were for the Thor vehicle.

Comparison of Predicted Jupiter Dynamic Response With Measured Values

One of the main objectives of this research program is to determine the adequacy of existing simulation techniques by correlation of response measurements being obtained on the Jupiter and Thor full-scale vehicles with those predicted by models. Thus a preliminary set of predicted response data have been obtained by the method outlined in figure 6. Figure 6 indicates schematically how a total dynamic response was obtained by combining calculated loads due to turbulence with scaled vortex shedding loads from a wind tunnel model. As indicated in figure 6 the response due to turbulence is a function of the intensity of turbulence, scale of turbulence, and the frequency response function. A value of 0.17 was assumed for the intensity of turbulence, 300-feet for the scale of turbulence and a uniform one-dimensional gust input for the frequency function. Figure 6 also indicates that response due to vortex shedding loads is determined from wind tunnel studies scaled to full scale. Data from reference 8 was utilized to determine vortex shedding loads on the full-scale Jupiter vehicle. The 20-percent scale Jupiter model of reference 8 is shown in figure 7. As indicated in figure 6, the model data has to be scaled to full scale. The dynamic bending moment data of reference 8 was modified to account

for differences in structural damping and generalized mass between model and full-scale vehicle. A correction factor based on an equation for a linear system to a random input, equation 10 of reference 9, was applied to the model data. The maximum dynamic bending moments in reference 8 were obtained from the greatest peak response in a one-minute time interval. This corresponds to 5 minutes on the full-scale vehicle. The calculated response due to turbulence and the response due to vortex shedding loads were combined as indicated in figure 6. In the equation for the combined response shown at the right of figure 6 the maximum vortex shedding load M_{VS} is assumed to be a 3 sigma value. Thus the combined load is also considered to be a 3 sigma value. The combined response is compared with the measured Jupiter data in figure 8. The maximum dynamic bending moment is plotted as a function of mean wind speed in the lateral and drag directions. The predicted data are indicated by the solid curve. Levels of the vortex shedding loads and the loads due to turbulence are indicated in each direction by the cross-hatched areas in figure 8. As indicated, the gust loads near 50 miles per hour are 0.671 x 10^6 inch-pounds in the drag direction and 0.336 x 10^6 inch-pounds in the lateral direction. Vortex shedding loads near 50 miles per hour are 0.300 x 10^6 inch-pounds in the drag direction and 0.660 x 10^6 inch-pounds in the lateral direction. Thus gust load is predominant in the drag direction and vortex shedding load is predominant in the lateral direction. Figure 8 indicates that this preliminary prediction is not very good, and unfortunately falls on the unconservative side. Since precise

measurements of the wind are not now available and the wind tunnel data had to be modified appreciably, the correlation presented in figure 8 is not considered to be a final answer but only an initial comparison.

CURRENT STATUS OF PROGRAM AND CONCLUDING REMARKS

Figure 9 indicates that winds can, in fact, destroy a launch vehicle and points up the need for continued research into the ground wind load problem. Figure 9 shows the condition of the Thor vehicle after a wind storm on Sunday, January 23, 1966. Winds were from the west with gusts up to sixty miles per hour. Upon investigation it was found that two of the three threaded studs that serve as hold-down bolts capable of resisting overturning moments had completely backed out after "safety wires" had broken. Thus the only restraint against overturning wind moments was the empty vehicle weight. The Jupiter vehicle survived the storm and measurements are continuing with this vehicle.

Initial results of a full-scale ground wind load program which is currently in progress have been presented. The initial results indicate poor agreement between predicted and measured loads. Future work will include study of gust spectra, response spectra, and gust frequency response functions. Wind tunnel models more closely matching full-scale properties are being designed to provide accurate data on the effects of vortex shedding loads. The effectiveness of current simulation techniques

may then be evaluated more carefully through correlation of full-scale response measurements with those predicted by models.

REFERENCES

1. Buell, Donald A.: Highlights of Ground Wind Tests in the Ames 12-Foot Tunnel. Meeting on Ground Wind Load Problems in Relation to Launch Vehicles, Langley Research Center, Hampton, Va., June 7-8, 1966.
2. Farmer, Moses G., and Jones, George W., Jr.: Summary of Langley Wind Tunnel Studies of Ground Wind Loads on Launch Vehicles. Meeting on Ground Wind Load Problems in Relation to Launch Vehicles, Langley Research Center, Hampton, Va., June 7-8, 1966.
3. Reed, Wilmer H., III: Models for Obtaining Effects of Ground Winds on Space Vehicles Erected on the Launch Pad. Conference on the Role of Simulation in Space Technology, Virginia Polytechnic Institute, Engineering Extension Series, Circular No. 4, Part C, August 17-21, 1964.
4. Etkin, B.: Studies of Cylinder Aerodynamics at the University of Toronto Institute for Aerospace Studies. Meeting on Ground Wind Load Problems in Relation to Launch Vehicles, Langley Research Center, Hampton, Va., June 7-8, 1966.
5. Bohne, Q. R.: Power Spectral Considerations on the Launch Pad. USAF Geophysics Res. Dir. A.F. Surveys in Geophysics, No. 140, Proc. of National Symposium on Winds for Aerospace Vehicle Design, Vol. 1, AFCRL-62-273(I), March 1962.

6. Duncan, Rodney L., and Foughner, Jerome T., Jr.: Wind Measurements Using a Vertical Array of Fast Response Anemometers. Meeting on Ground Wind Load Problems in Relation to Launch Vehicles, Langley Research Center, Hampton, Virginia, June 7-8, 1966.

7. Jones, George W., Jr., and Farmer, Moses G.: Wind-Tunnel Studies of Ground Wind Loads on Saturn Launch Vehicles. AIAA/ASME 7th Structures and Materials Conference, Cocoa Beach, Florida, April 18-20, 1966.

8. Killough, T. L.: Wind-Induced Loads on a Dynamic 1/5-Scale Unfueled SM-78 Jupiter in the Launch Position. U.S. Army Ordance Missile Command, Report No. R.G.-TM-62-65, July 10, 1962.

9. Buell, Donald A., McCullough, George B., and Steinmetz, William J.: A Wind-Tunnel Investigation of Ground-Wind Loads on Axisymmetric Launch Vehicles. NASA TN D-1893, October 1963.

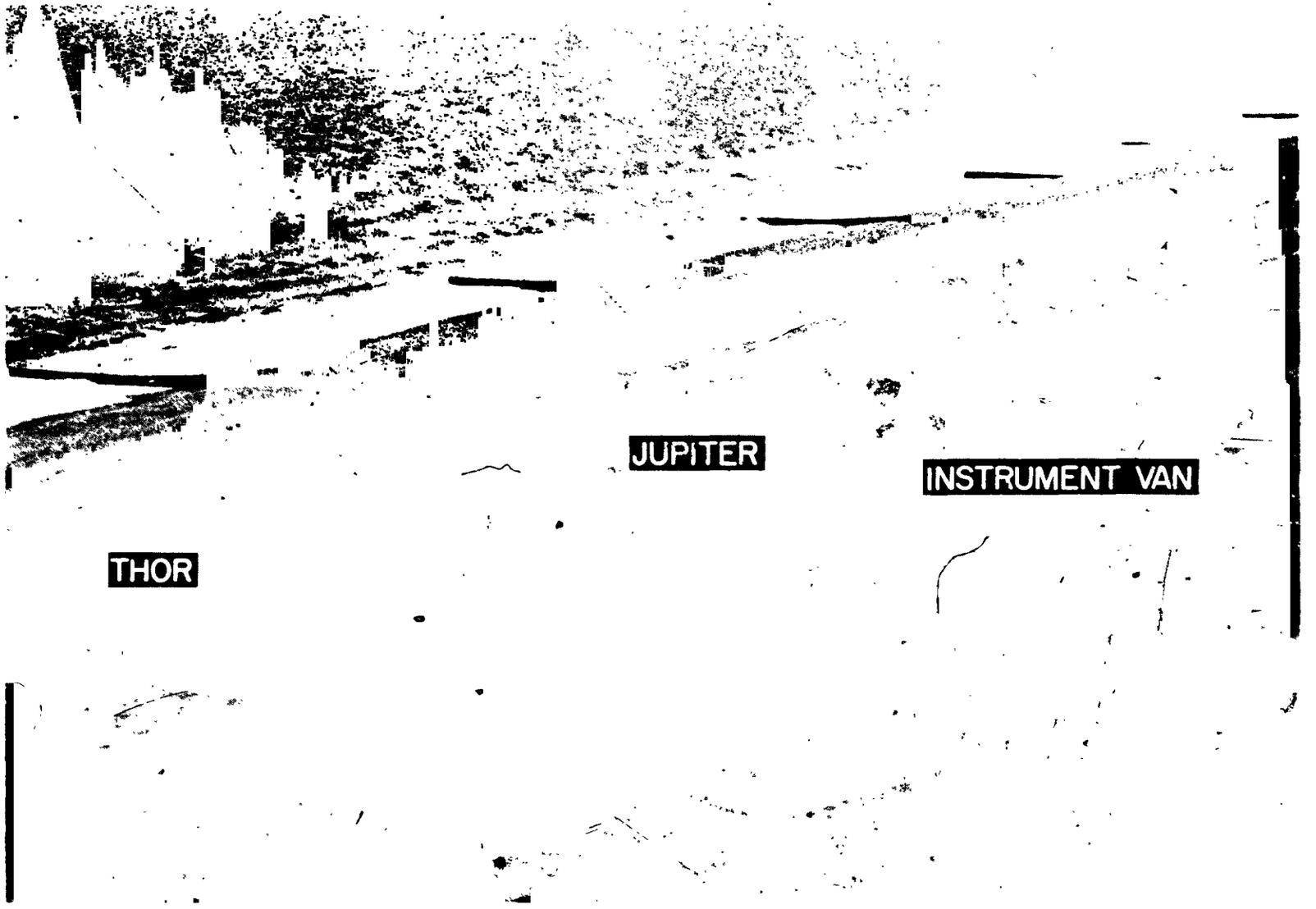

Figure 1.- Wallops Island test area view looking south.

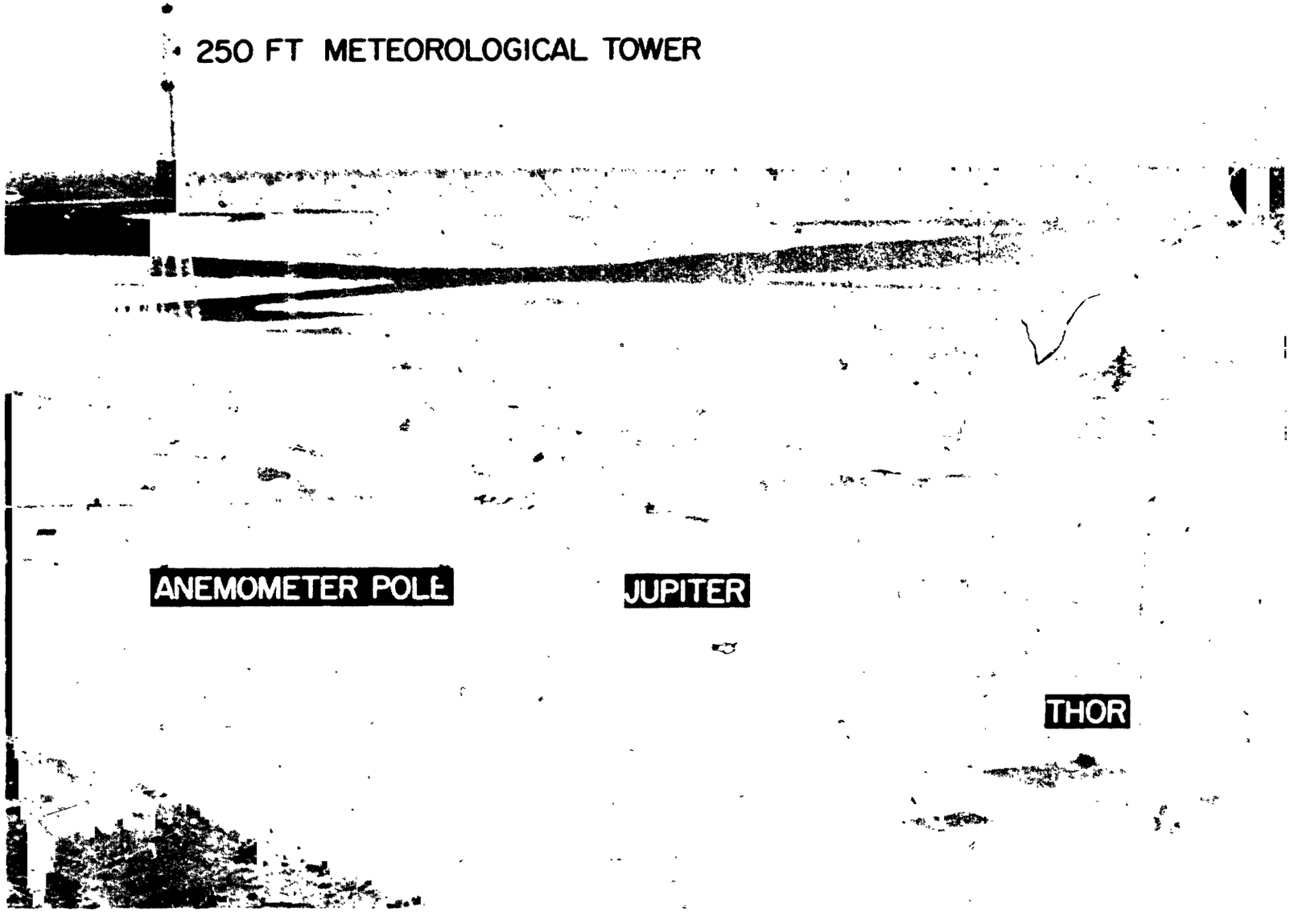

Figure 2.- Wallops Island test area view looking west.

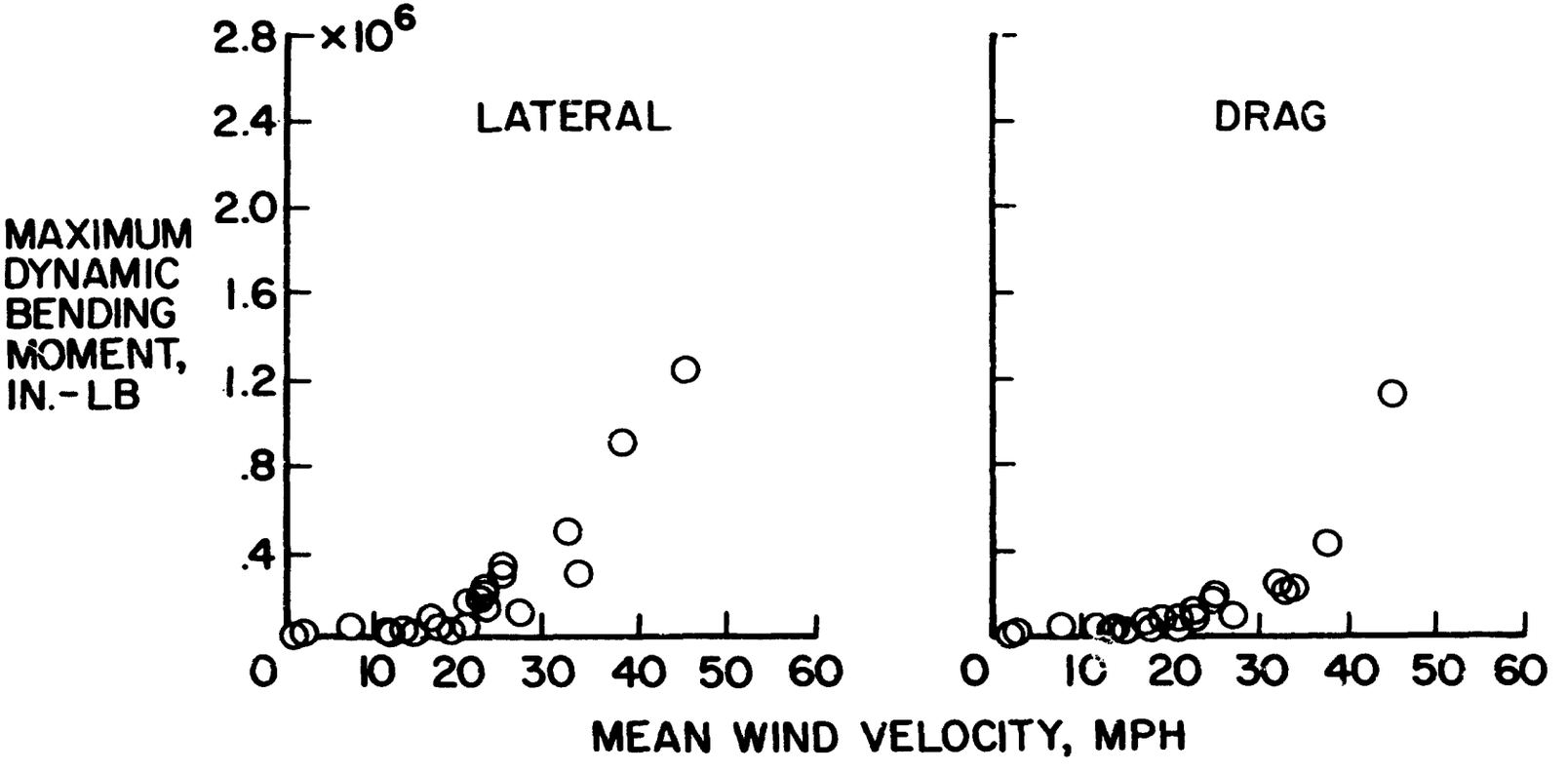

Figure 3.- Thor dynamic response, base bending moment.

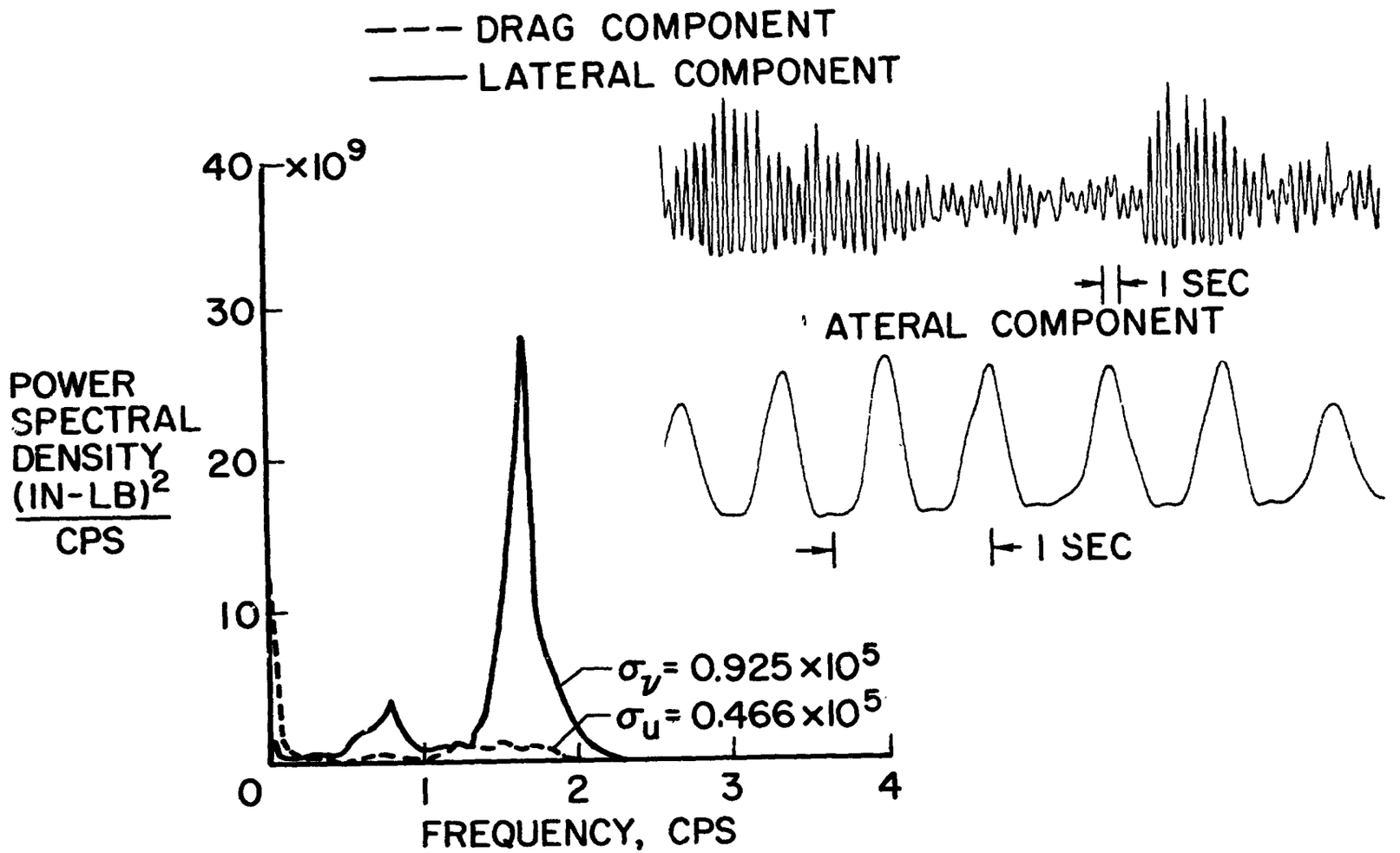

Figure 4.- Thor bending-moment response spectra.

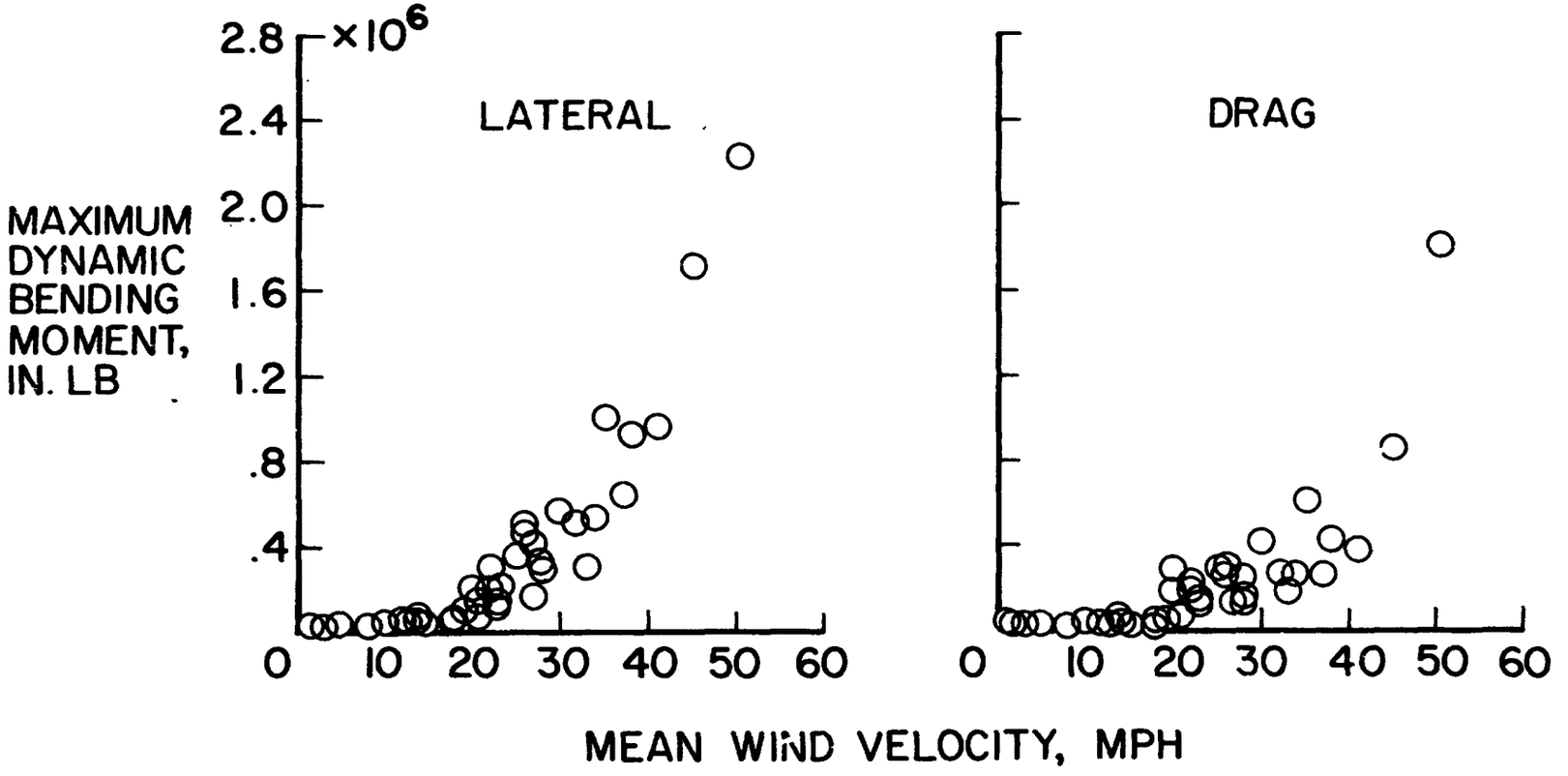

Figure 5.- Jupiter dynamic response, base bending moment.

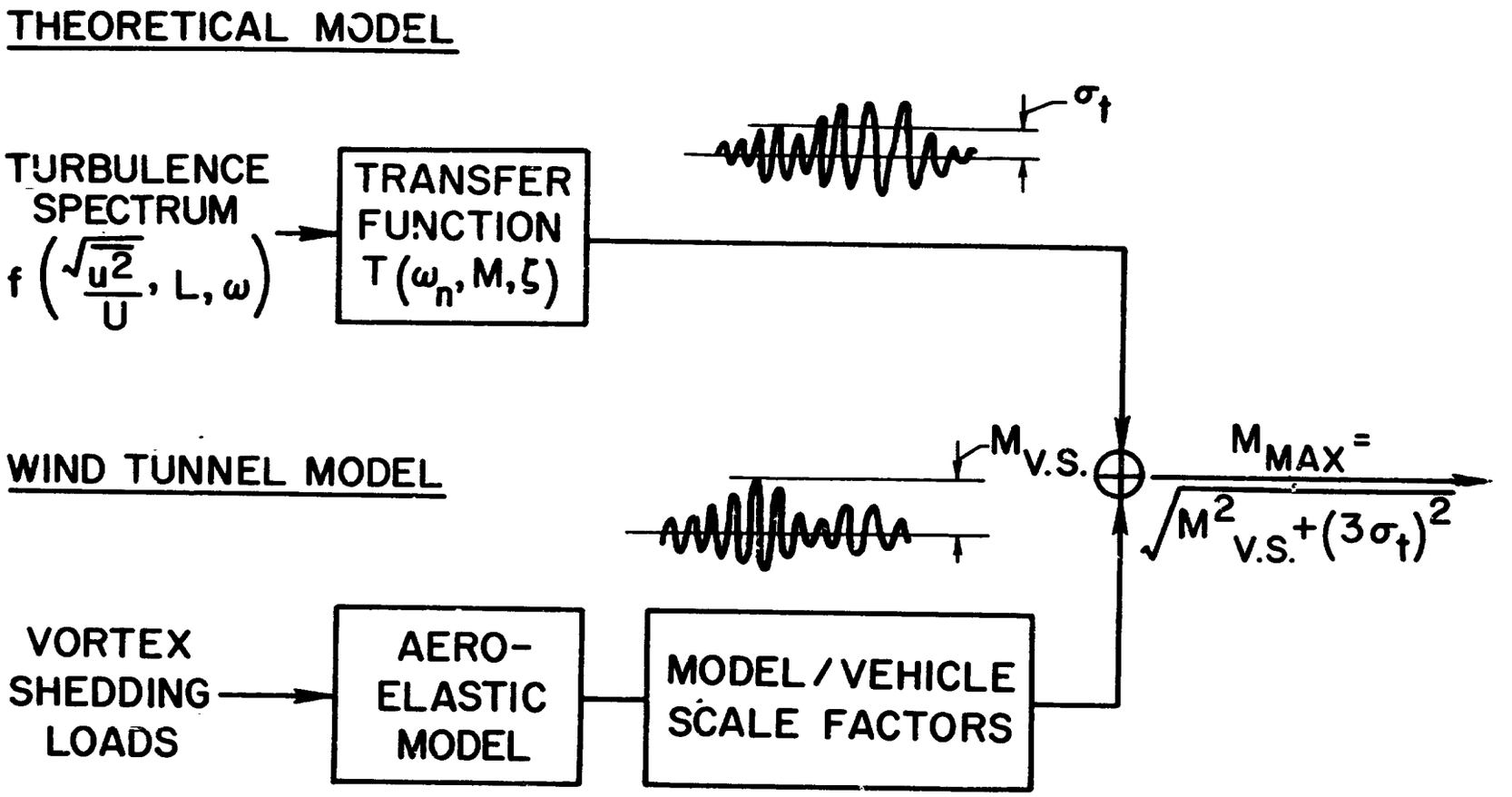

Figure 6.- Combined dynamic loads Jupiter response prediction.

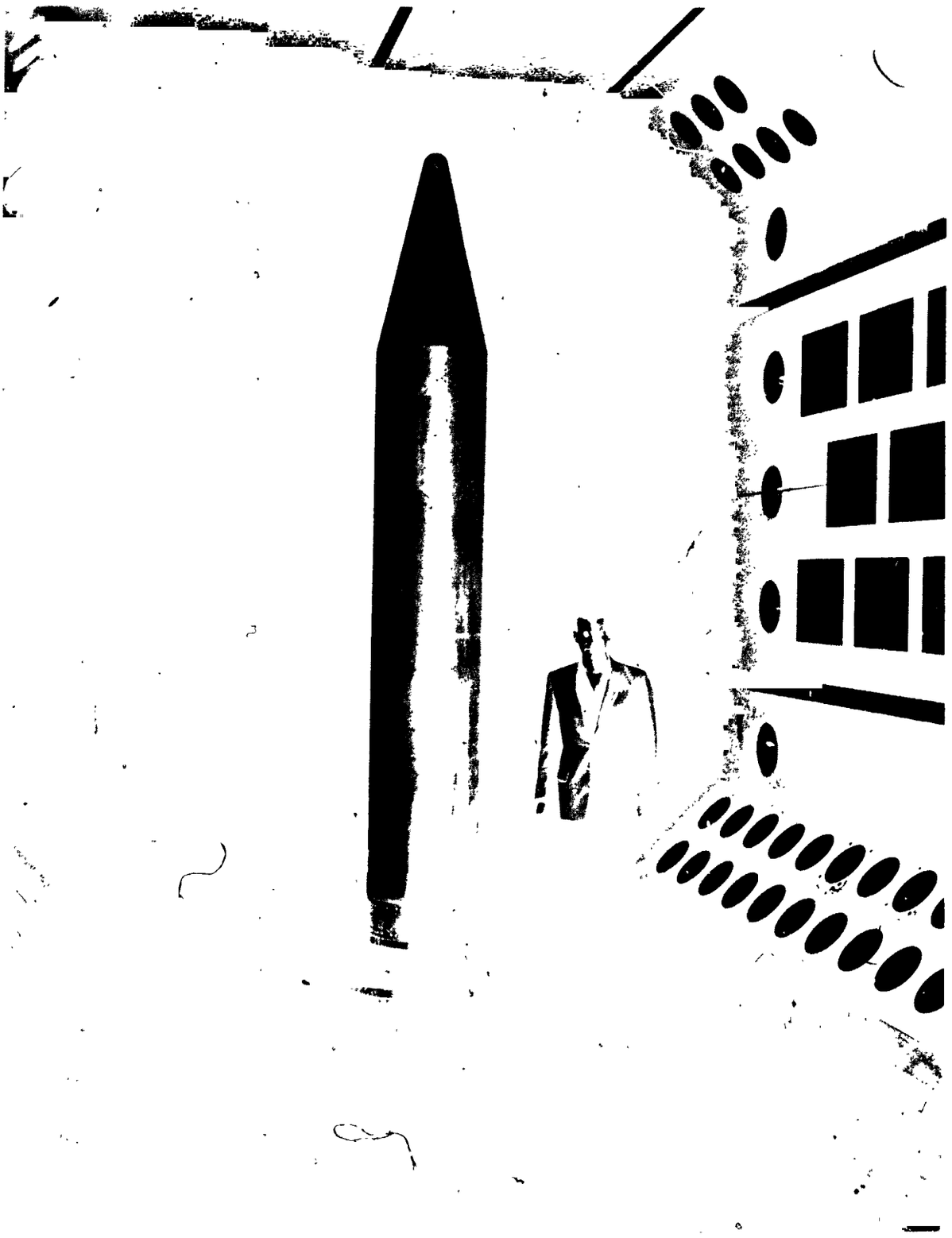

Figure 7.- Jupiter wind-tunnel model 20-percent scale.

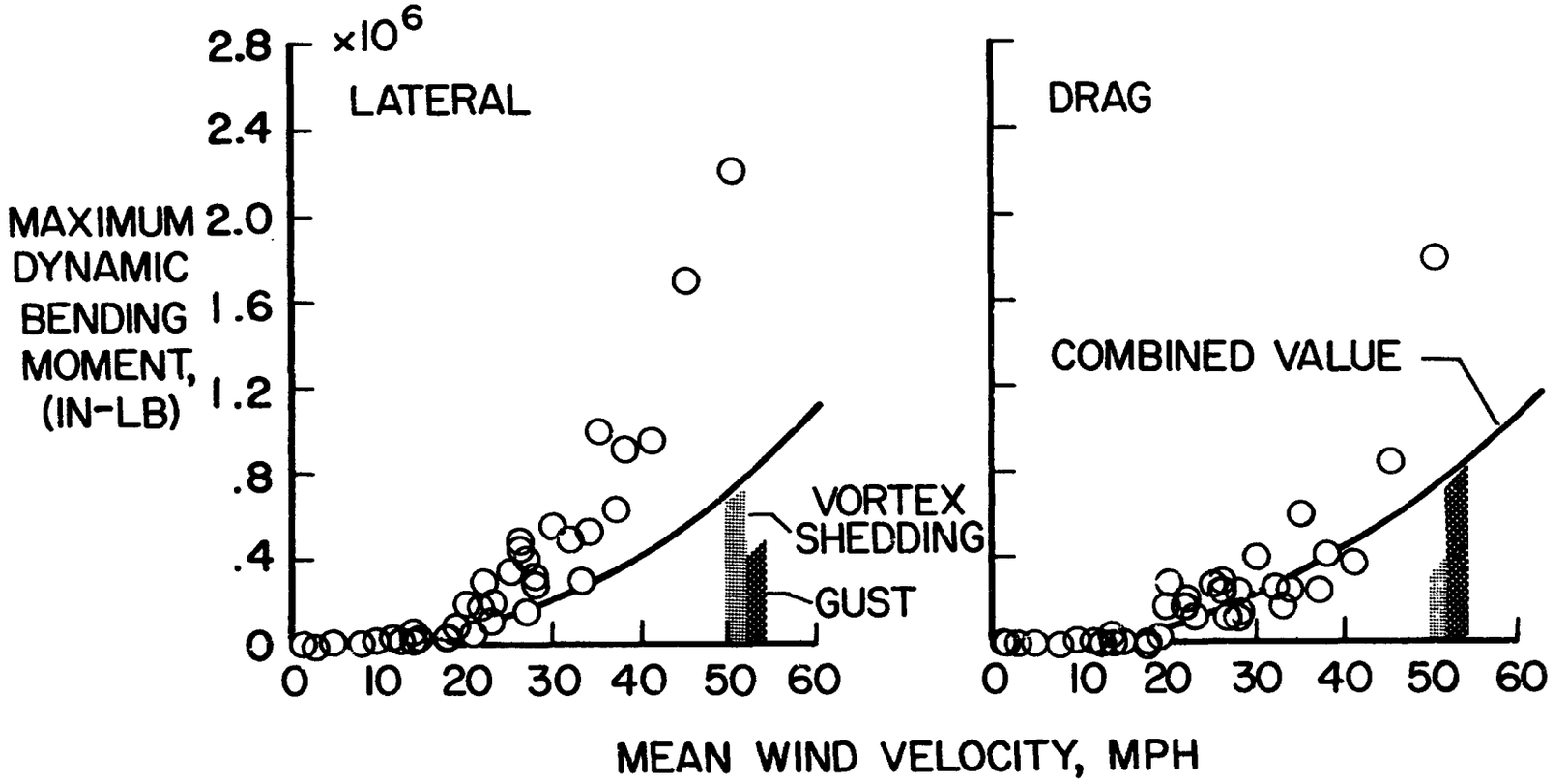

Figure 8.- Predicted and measured Jupiter dynamic response.

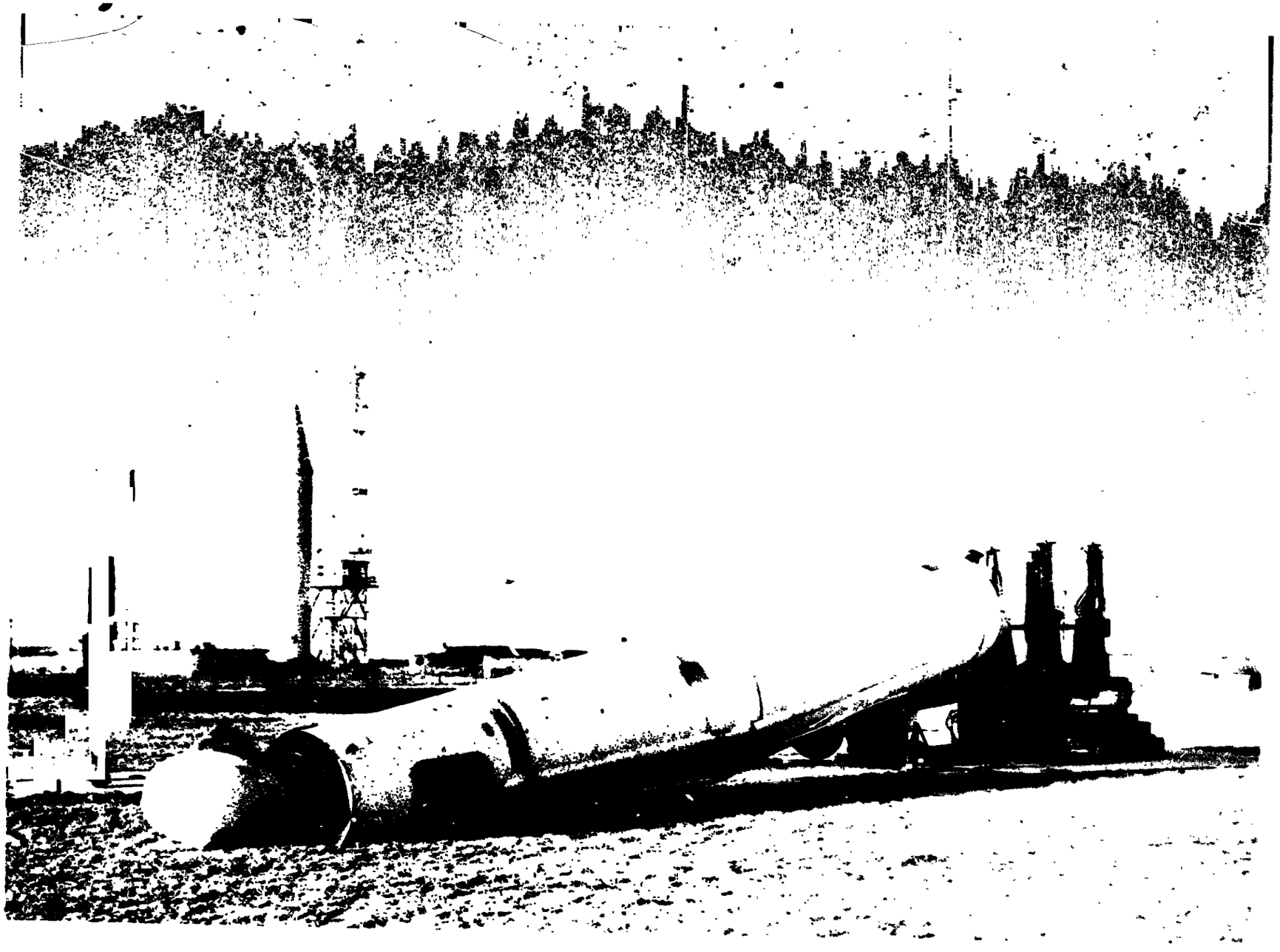

Figure 9.- Thor vehicle after wind storm.

GROUND WIND INDUCED OSCILLATIONS OF THE TITAN III ITL TRANSPORTER

Prepared by

J. M. Lyons and A. J. Lum

Aerospace Corporation

SUMMARY

The Air Force Titan IIIC launch vehicle is transferred from the assembly areas to the launch pad at Cape Kennedy by the Integrate-Transfer-Launch (ITL) transporter. On four occasions during the fall of 1964, the empty transporter was observed to oscillate in both moderate and high winds. In two instances the structure was damaged.

To understand and solve the problem, theoretical flow models of the aerodynamic phenomena were postulated, and a series of aerodynamic and mechanical fixes were designed to reduce or eliminate the ground wind induced oscillations of the transporter. A wind tunnel test was then conducted with dynamically scaled models of both the transporter and launch vehicle to (1) reproduce the phenomena; (2) define the problem; and (3) determine suitable fixes to eliminate the transporter problem without inducing any oscillation problems with the launch vehicle. A suitable fix was determined and the transporter is now being modified accordingly.

The results of the wind tunnel test are presented and compared with the pretest estimates. The significant aerodynamic phenomena are discussed.

1.0 INTRODUCTION

The isolated ITL transporter has experienced large amplitude ground wind induced oscillations at wind speeds below the design specifications. A wind tunnel test was conducted with 7.5 percent aeroelastic models of both the mast and the vehicle to define the problem explicitly and determine a mast "fix" to eliminate the oscillations or reduce them to acceptable levels without inducing a vehicle problem.

The object of this paper is to emphasize the importance of aeroelastic considerations in the design of high aspect ratio lightly damped structures such as the transporter mast and launch vehicles, and to

present some indication of the present state of the art by this particular example. Therefore, a comparison is presented between the full scale observations, the predicted wind induced oscillation phenomena postulated during the pretest period, and the actual wind tunnel test results. In addition, the most significant aerodynamic phenomena discovered during the test are discussed and possible explanations are proposed for some of the anomalous results.

2.0 FACILITY DESCRIPTION

2.1 Launch Complex

The Titan IIIC Standard Space Launch Vehicle (SSLV) is a three-body system consisting of a three-stage liquid engine core and two Solid Rocket Motor strap-on boosters. To achieve a rapid launch rate capability, the Titan IIIC utilizes the integrate, transfer, and launch concept rather than the conventional vehicle build-up on the pad. This means that the vehicle is assembled at remote locations and the complete vehicle, including all electrical auxiliary systems, is then transported to the launch pad on one of three transporters at the launch complex (Figure 1).

The transporter consists of the launch platform, the umbilical mast, and undercarriage system. One undercarriage is located under each corner of the launch platform. The system of undercarriages travels on two sets of standard gage railroad tracks spaced 27.8 ft apart and the total assembly is pushed by two diesel locomotives. The umbilical mast supports checkout and launch control umbilical cables connecting the vehicle to equipment installed in rail mounted vans.

The core and payload are assembled and checked out on the transporter mounted on pier supports in the Vertical Integration Building (VIB). The transporter assembly is then jacked off the pier supports onto the undercarriages, lowered onto the rails, and transferred with the equipment vans approximately 1 mile to the Solid Motor Assembly Building (SMAB). Here the SRM's are installed on a transporter and mated to the core vehicle. The transporter and vans are then transferred 1.5 to 2.5 miles to one of the launch pads where the transporter is jacked onto piers in a launch-ready position over the flame duct and adjacent to the Umbilical Tower (UT). When not in use, the transporter with its umbilical mast is stored on piers in the refurbish area south of the VIB.

2.2 Transporter

The transporter platform is approximately 42 ft wide, 52 ft long, and is of welded plate girder construction. The 148-ft tall electrical umbilical mast is located on the west side of the transporter platform (Figure 2). The total weight of the transporter platform and mast is 553,000 lb. Parallel to the yaw plane of the vehicle, the profile of the mast consists of two pylons, 6.8 ft in width for the full height with a 15.4 ft separation. In the pitch plane, the pylons taper from 11.1 ft at the base to 4.22 ft at the top. The entire front (facing vehicle) and sides of the mast are covered with steel plates and

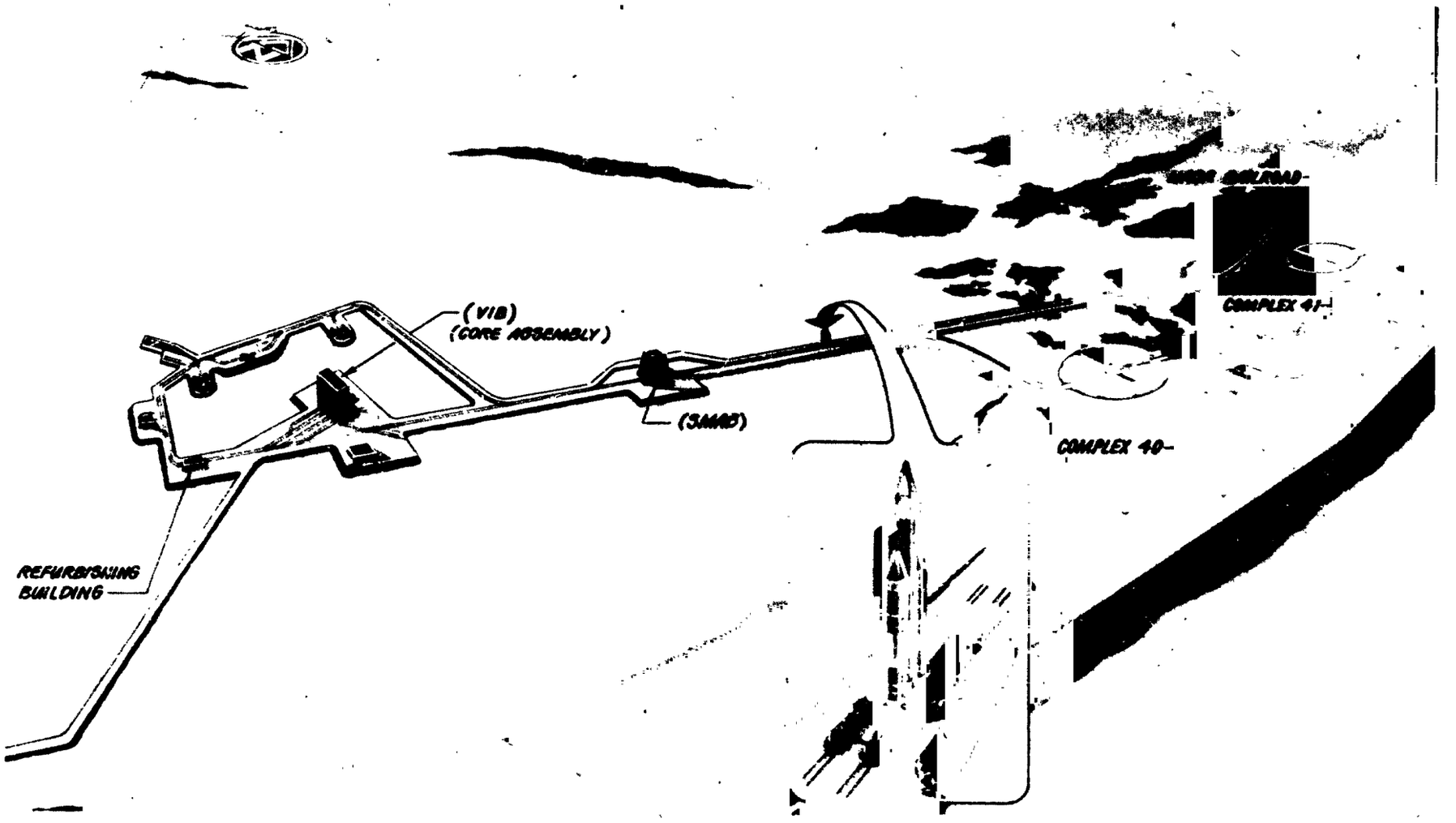

Figure 1. Titan III Launch Facilities.

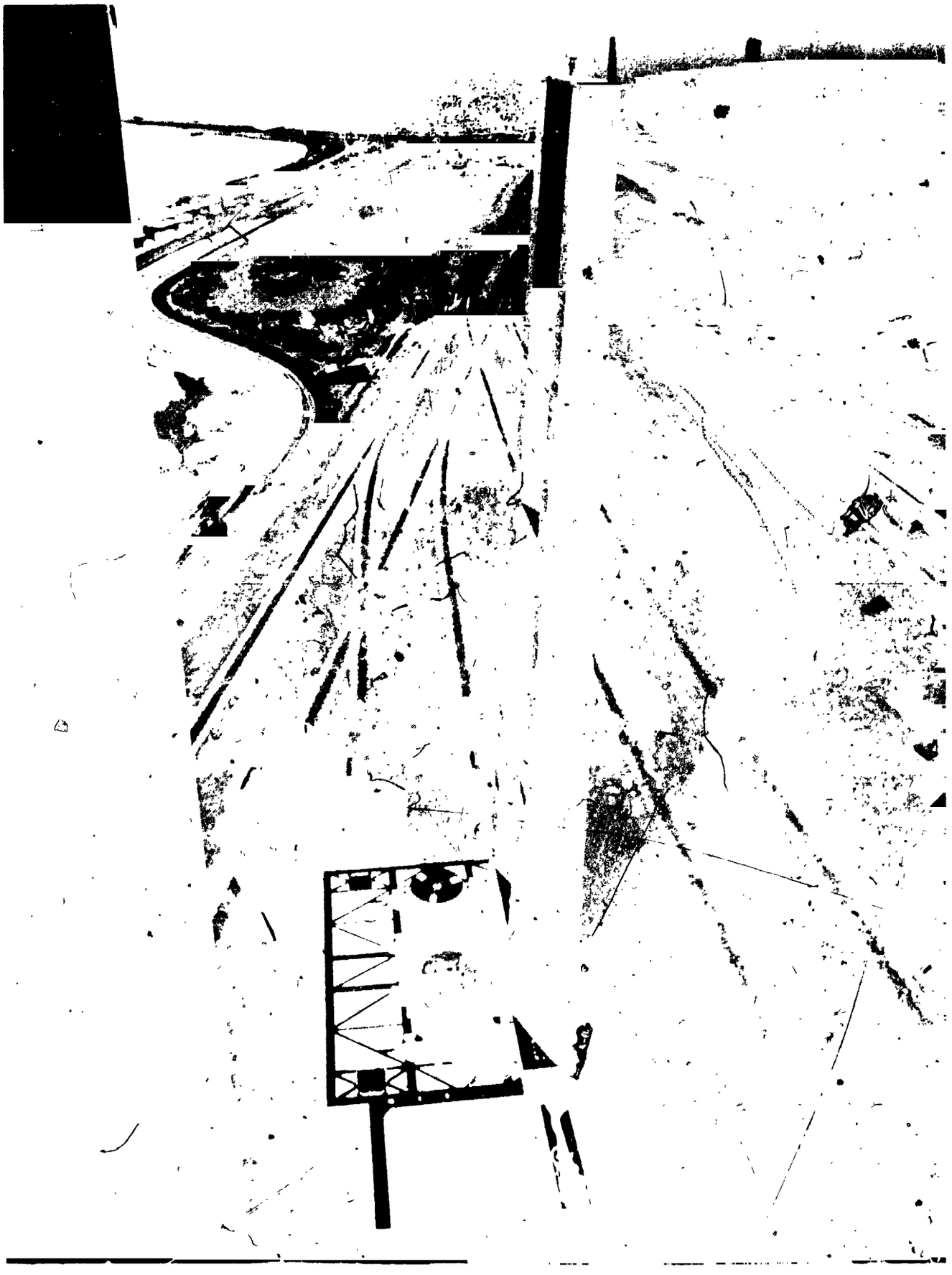

Figure 2. iTL Transporter.

coated with Martite, a flame resistant material, to protect the electrical umbilicals from exhaust flame damage. The rear face is left uncovered for access.

2.3 Design Specifications

The design specification for the transporter mast defines the required ground wind capability in terms of the various mast configurations. The specified peak wind speeds as measured at the top of the mast are summarized below.

Immobile on piers without launch vehicle - 77 mph.

Mobile on undercarriages without launch vehicle - 65 mph.

Immobile on piers with launch vehicle - 65 mph.

Mobile on undercarriages with launch vehicle - 65 mph.

3.0 PRETEST PROBLEM EVALUATION

3.1 Observed Phenomena

Oscillations of two transporters were observed on several occasions at both moderate and high wind speeds (Hurricanes Cleo and Dora) during and immediately after the construction of the three transporters in the fall of 1964. The two transporters were mounted either upon the railroad type undercarriages or on concrete piers in the refurbishing area. The vehicle was never present and the transporter masts were not sheltered by adjacent structures. During all observations, the wind direction was in or very close to the plane of the two pylons (yaw plane) and the oscillations always appeared in the pitch direction normal to this plane. When the wind direction changed, the oscillations ceased. The observed oscillations and pertinent characteristics of the transporter mast are summarized in Figure 3. It should be mentioned that the reported oscillations were never documented by the observers and the data consists of third or fourth hand hearsay evidence. It can only be regarded as qualitative and does not represent a scientific investigation.

Transporter No. 1, located on the launch pad, was never observed to oscillate under any wind conditions. The winds varied from 0 to at least 60 mph from various directions. In all probability the mast was sheltered by the large permanent umbilical tower (Figure 1) which dominates the flow field.

The wind speeds were recorded at remote stations of uncertain elevation with instruments which averaged the wind speed over a period of time and it can be concluded that the quoted wind speeds may be very poor estimates of the peak quasi-steady wind at the top of the mast.

Figure 3. Observed Full Scale Oscillations of the Isolated Transporter.

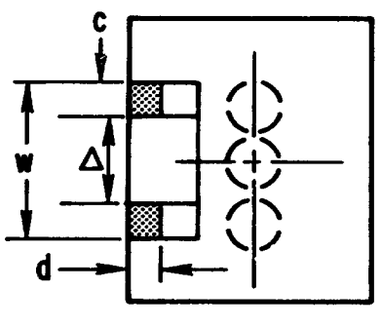

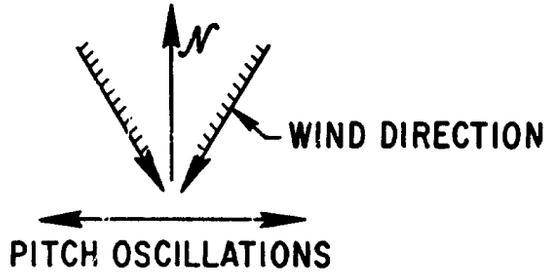

d = 4.22 ft
c = 6.8 ft
Δ = 15.4 ft
w = 29 ft

Reported Wind Speed V, (mph)	Location & Condition	Mode	Frequency, f (cps)	Comments
1. 60	Refurbish area, piers (Hurricane Cleo)	Unknown	Unknown	Mast No. 2 was damaged and platform was displaced 2 ft relative to piers. No one observed motion.
2. (a) 60	Refurbish area, piers (Hurricane Dora)	Unknown	Unknown	Platform No. 2 tied down. Mast was observed to oscillate but nature of motion was not identified.
(b) 60	Refurbish area, piers (Hurricane Dora)	Unknown	Unknown	Mast No. 3 oscillated with estimated double ampliture of 18 in. at tip. Platform was alternately lifted from and dropped onto the piers, and translated 3 in. westward along piers. Platform motion was eliminated by addition of weights.
3. 20-30	Refurbish area, piers	Pitch	0.7+ (0.97)	Mast No. 3, 4 in. double amplitude measured at tip with a transit, platform motion was not reported.
4. 25	Refurbish area, undercarriage	Pitch	1.0+ (0.75)	Transporter No 3 weighted with 125,000 lb of ballast. Platform oscillated in horizontal plane with a measured double amplitude of 15/16 in.

NOTE: +Frequency reported by observers during event.
( )First pitch mode frequency measured during full scale vibration test (Table 2) without ballast.

3.2 Proposed Explanations

The low speed oscillations were of the greatest concern because the wind speed was within the normal operating range of the transporter. The oscillation appeared to be a classic case of a resonant response to a periodic forcing function, the periodic forcing function being the oscillating lift on the mast produced by the periodic discharge of vortices from the pylons of rectangular cross-section at a constant Strouhal number (S). Resonance would occur for the wind speeds at which the natural frequencies of the structure (f) coincide with the frequency of vortex discharge (n).

The lowest frequency of the vortex discharge from tapered cantilever structures is determined by the dimensions at the top of the mast. Furthermore the Strouhal number relating the frequency of vortex discharge and wind speed is independent of Reynolds number because the sharp edges of the rectangular cross-section fix the separation point. Therefore, the data for stationary two-dimensional rectangular sections at low Reynolds numbers in Reference (1) was used to predict the Strouhal number as a function of c/d for the top of the windward pylon.

$$c/d = \frac{6.8}{4.22} = 1.612 \tag{1}$$

$$S = \frac{nd}{V} = .11 \tag{2}$$

The wind speed at which resonances occur would be:

$$V_R = 26.2 \ f \ \text{mph}$$

The resonant wind speeds for the transporter on piers and in the transport mode, using the measured frequencies of Figure 3, would then be 25.4 and 19.6 mph, respectively. Since these wind speeds correspond closely to the observations, it appeared that the nature of the low speed oscillation was defined. On this basis suitable modifications were selected to alleviate the problem.

The nature of the high speed oscillations was not readily apparent. The approximate natural frequencies were only known for the first pitch mode and the full scale observations were not accurate. Various explanations considered included gust response, periodic vortex shedding with resonance, and galloping.

The author was particularly concerned that "galloping" may have occurred. Galloping is a self-excited instability caused by a negative slope of normal force coefficient and its existence can be predicted by criteria of Reference 2. In the one-degree-of-freedom system being considered it appears as a negative viscous damping term in the equation of motion. The experimental work done at the University of British Columbia (References 3 and 4) indicates that rectangular sections with $0.75 < c/d < 4.0$ are unstable and galloping would occur for the speed at which the negative aerodynamic

damping exceeds the structural damping of the system. The chord-to-span ratio (c/d) of the mast varies from c/d = 1.61 at the top to c/d_B = 0.61 at the bottom and is within the unstable region.

The test results presented in Figure 5 indicate that galloping did not produce the large oscillation.

4.0 TEST OBJECTIVES AND SCALING PROCEDURE

A wind tunnel test was conducted to (1) reproduce the observed phenomena, (2) define the problem, and (3) determine suitable fixes to eliminate the transporter problem without inducing any oscillation problems with the launch vehicle. Also, it was desired that the mast fix would eliminate the resonant forced oscillations of a vehicle with a bulbous payload fairing when mounted on the transporter. This latter wind-induced oscillation problem was discovered in a previous Titan III test program, Reference 5, and is discussed in detail in Reference 6.

The wind tunnel test was conducted by the Martin Company* (Denver Division) under the technical direction of the Aerospace Corporation. The test took place in the 16-ft transonic dynamics tunnel at the Langley Research Center with freon as a test medium. Aeroelastic models of 7.5 percent scale were constructed for both the launch vehicle and the ITL transporter mast with variable base stiffness to simulate the undercarriage and pier base constraints. The characteristics of the prototype mast were obtained from a full scale vibration test (Reference 7). Photographs of the basic model installed in the wind tunnel plus three of the aerodynamic fixes are shown in Figure 4.

With one exception, the models were designed to satisfy all usual aeroelastic simulation parameters:

$\frac{Md}{EI}$, the bending moment parameter; ζ_S, the equivalent viscous damping ratio of structure; $\frac{fd}{V}$, the reduced frequency; $\frac{m}{\rho d^2}$, relative density; $\frac{(EI)}{mf^2d^4}$.

It was not possible to simulate both the relative density ($m/\rho d^2$) and the full scale Reynolds number ($Re = \rho vd/\mu$) for the empty launch vehicle.

*Unless noted, all wind tunnel data was obtained from the Martin wind tunnel report (Reference 8).

(a) Basic Configuration Pier Constraint

(b) Open Lattice Configuration Undercarriage Constraint

(c) Spoiler Configuration Pier Constraint

(d) Modified Cross-section Configurat Pier Constraint

Figure 4. Transporter Models.

Therefore, the relative density was simulated and the test was conducted at 45 percent of the full scale Reynolds number for all configurations. The lack of simulation was not important for the transporter mast. The Strouhal number and the aerodynamic force on cylinders with rectangular cross-sections are not dependent on the Reynolds number because the separation point is fixed by the sharp edges. The error in the Reynolds number may be significant for the launch vehicle with a circular cross-section. For most velocities of interest the model will be in the supercritical Re range where vortex shedding is random. However, the prototype will be in the trans-critical range, discussed in Reference 9, where there is evidence of periodic vortex shedding.

The desired scaling relationships between the model and prototype are summarized below.

Table 1. Scaling For Wind Tunnel Model

Reynolds Number, $Re_m = 0.45\ Re$	Bending Moment, $M_m = \frac{M}{425}$
Velocity, $V_m = 1.228\ V$	Length, $d_m = 0.075\ d$
Frequency, $f_m = 16.368\ f$	Dynamic Pressure, $q_m = 5.576\ q$

The comparison of the actual natural frequencies for model and prototype configurations presented in Table 2 indicates that the scaling relationships would not be applicable for all test conditions due to poor simulation of the yaw and torsion modes. It may be seen that the frequencies in the pitch mode, where the observed response seemed to occur, were accurately scaled. In addition to the full scale vibration test reported in Reference 7, there was a preliminary hand shake test in which the damping values obtained were generally lower. The selections presented in Table 2 were judged to be the most reasonable.

5.0 TEST RESULTS AND DISCUSSION - BASIC CONFIGURATION

5.1 Test Results

The basic configuration was tested with the full scale structural damping of $\zeta_S = 0.5$ percent for all wind directions and wind speeds from zero to at least the full scale equivalent of the specification requirement, which is 76 mph. The components of the static and dynamic bending moments in both the pitch and yaw planes were measured near the base of each pylon by means of strain gages.

Table 2. Comparison of Prototype and Model Dynamic Properties of the ITL Transporter Mast

Configuration	Property	Full Scale	Desired Model	Actual Model
Mast on piers	Pitch bending			
	f_p (cps)	0.97	15.9	15.6
	$\zeta_s (\% \frac{c}{c_{cr}})$	0.5	0.5	0.5[a]
	Yaw bending			
	f_y	1.59	26.0	16.4
	ζ_s	0.5	0.5	0.7
	Torsion			
	f_t	2.96	48.4	33.7
	ζ_s	1.2	1.2	--
Mast on Undercarriage	Pitch bending			
	f_p(cps)	0.75	12.3	12.4
	$\zeta_s (\% \frac{c}{c_{cr}})$	2.0	1.0[b]	--
	Yaw bending			
	f_y	1.33	21.8	16.1
	ζ_s	1.65	1.65	--
	Torsion			
	f_t	2.91	47.6	32.6
	ζ_s	--	--	

(a) The damping could be increased by use of a tuned viscous damper and values up to ζ_s = 4% were utilized during the test.

(b) Conservative value arbitrarily assigned for analyses

The maximum loads and largest oscillations occurred at relatively low wind speeds for the $\phi = 90^{\circ}$ direction in which the wind was in the plane of the pylons (i.e., yaw plane). The transporter oscillated in the pitch direction normal to the wind. The response was quite sensitive to wind direction and only reached large amplitudes when the wind direction was within 15° ($\phi = 90^{\circ} \pm 15^{\circ}$) of the yaw plane. This directional phenomenon is almost identical to the recorded observations for the full scale mast which were described in Section 3.

Plots of the bending moment as a function of wind tunnel dynamic pressure and equivalent full scale velocity are presented in Figure 5 for the critical wind direction* with the mast supported both on piers and undercarriages.

The static loads acted almost entirely in the drag direction and it may be seen that large oscillations occurred at both low and high speeds. Those oscillations were normal to the wind direction.

The equivalent full scale wind speed corresponds to the wind at the top of the mast. No corrections have been applied to the static moments to account for the ground wind profile.

5.2 Discussion of Results

5.2.1 Low Speed Response

The low speed oscillations of the prototype (Figure 3) were reported to have occurred between 20 and 30 mph and the preliminary predictions for the resonant speeds (V_R) were 25 mph for the pier, and 20 mph for the undercarriage constraints. Figure 5 indicates that the peak response in the wind tunnel occurred at equivalent full scale speeds of 32.5 mph and 26.5 mph for the mast on piers and undercarriages, respectively. It may be also seen that the loads approached the allowable limits. In fact, the allowable bending moment may have been exceeded because it was difficult to define a peak response accurately and the wind tunnel model was damaged during this phase of the test.

It is not surprising that the peak responses in the wind tunnel occurred at higher speeds than those reported for the prototype. The wind tunnel speed represents a peak or quasi-steady speed whereas the reported full scale values probably represent a mean wind speed averaged over a five minute interval. Averaging the wind over a period such as this would not measure low frequency gusts which could excite vortex shedding response. The quasi-steady speed could be 10 or 20 percent greater than the recorded mean wind speed. Furthermore, the recorded speed may have been

*The negligible response that was measured at $\phi = 0^{\circ}$ poses a very interesting aerodynamic problem. An analysis of this particular phenomenon is presented in the more comprehensive Aerospace report (Reference 10) dealing with this subject.

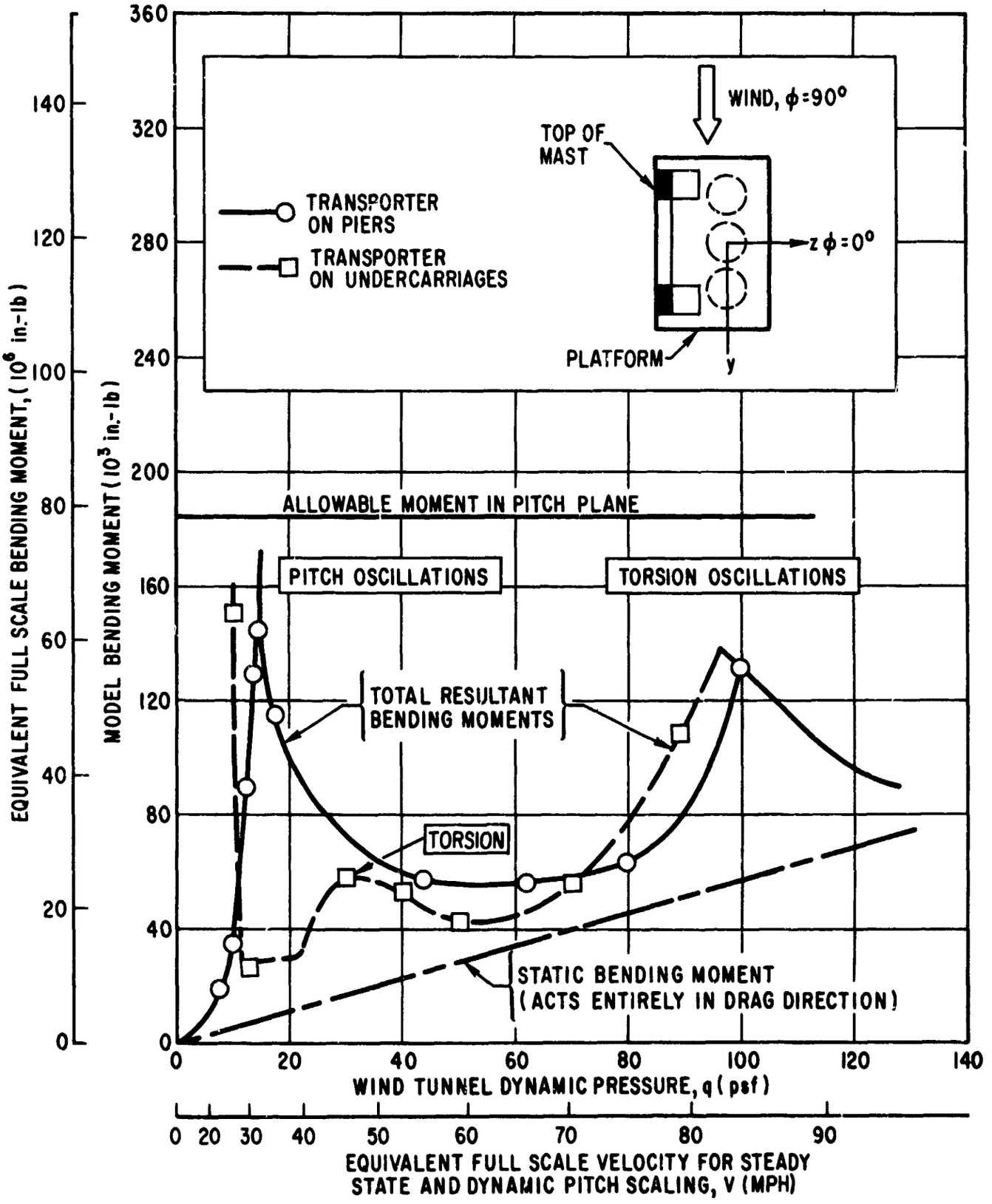

Figure 5. Isolated ITL Transporter - Measured Bending Moments at Base of Leeward Pylon for the Basic Configuration at the Critical Wind Direction.

measured at an elevation below the top of the mast. Thus it can be concluded that the low speed oscillations of the transporter mast were reproduced in the wind tunnel test.

The reduced frequencies (fd/V) of the low speed responses were approximately equal for the pier and undercarriage base simulations with $fd/V_R = 0.0845$ and 0.0822, respectively. These values were 25 percent lower than the Strouhal number ($S = 0.11$) that had been predicted to describe the periodic vortex shedding from the windward pylon. This large error in the prediction resulted since no attempt had been made to account for the interference effects of the leeward pylon.

If the leeward pylon in the wake is fairly close to the windward pylon, it will force the vortices to form further outboard. Since the Karman vortex trail is only stable for a definite longitudinal and lateral spacing of the vortices ($\ell/h \doteq 5.56$, Reference 11), the longitudinal spacing will also be increased. Consequently the frequency of periodic vortex discharge and Strouhal number will be reduced. No experimental data has been found for rectangular cylinders, but Roshko (Reference 12) has tested a splitter plate at varying distances downstream of both a circular cylinder in laminar flow and a flat plate. These data indicate that the Strouhal number would be reduced by approximately 30 percent and the wake width would be increased 25 percent for splitter plate locations corresponding to the approximate distance between the pylons expressed in terms of span (d), chord (c) or wake widths (h). The effect of this interference is summarized in Table 3.

Table 3. Comparison Of The Predicted And Measured Strouhal Numbers For Periodic Vortex Shedding And Reduced Velocity At Resonance

	Reported for Prototype	Predicted for One Pylon	Predicted with Interference	Measured
$S = \frac{nd}{V}$	--	0.11	0.077	--
$\frac{V_R}{fd}$	7.2 - 13.9	9.1	13	11.9

Thus it may be seen that the measured value for the resonant wind speed agrees quite well with the values predicted for a forced response due to periodic vortex shedding with interference.

The oscillograph traces at the resonant speed differed from the usual response of a mechanical system at resonance. The frequency was constant and equal to the natural frequency of the model but the amplitude of this resonant oscillation was random. This indicates that the exciting lift force also included random energy. These measurements are not inconsistent with the known characteristics of periodic vortex shedding at large Reynolds numbers and were not unexpected. The periodic vortex shedding from the

pylons is analogous to that for circular cylinders at subcritical Reynolds numbers where several authors have observed random amplitudes. Humphreys' data (Reference 13) indicate that the response of a two-dimensional cylinder is random in this periodic vortex shedding range. He implies that the periodic lift forces (S = 0.2) have random amplitudes and notes that the phenomenon is closely related to the three-dimensional effects that exist on two-dimensional models of constant cross-section. Roshko (Reference 11) measured the power spectral density of the velocity fluctuation in the wake of circular cylinders at very low subcritical Reynolds numbers and noted that there is a considerable amount of random energy distributed over all frequencies in addition to the energy concentrated in the spike at S = 0.2.

Therefore, it has been demonstrated that the large oscillations at low wind speeds were the result of the resonant response of the first cantilever pitch bending mode of the mast to the alternating lift force produced by periodic vortex shedding. It also has been shown that the resonant velocity is predictable with fair accuracy from the known Strouhal numbers for stationary two-dimensional cylinders.

5.2.2 Comparison With Other Experimental Data

Several instances of vortex-induced resonance have been observed in other experiments. Large amplitude oscillations for models of both the Atlas/Agena vehicles at PALC 1 and a Titan III with a bulbous payload located in the wake of an umbilical mast have been observed when the frequency of vortex discharge from the mast coincided with the natural frequency of the vehicle (Reference 6). The values of reduced frequency at resonance measured in these experiments were comparable to the present measurements.

Scruton (Reference 14) tested a suspension bridge tower very similar to the ITL transport and found results almost identical to the present ones. Vortex-induced resonance occurred for winds in the plane of the pylons and the resonant speed was within 10 percent of the value which would have been predicted by the methods described previously.

The "capture" phenomenon which Parkinson (Reference 1) has associated with vortex-induced resonance does not seem to have occurred. "Capture" is supposedly caused by coupling between the motion of the structure and the flow field so that the frequency of vortex discharge remains fixed at the natural frequency of the structure for a finite speed range above V_R. Thus, there would be a broad hump rather than a sharp peak in the response curve. Figure 5 indicates that the low speed resonance was characterized by a very sharp peak.

5.2.3 High Speed Response

Large oscillations were measured in the torsion mode with the peak at q = 100 psf (Figure 5). This corresponds to V_m = 151 fps. The torsion frequency of the model is f_T = 33.7 cps and correspondingly, the reduced frequency would be $f_T d/V_R$ = 0.070, which is within 15 percent of the

reduced frequency for the low speed resonance, $f_p d/V_R = 0.0840$. This close correspondence indicates that the high speed oscillations were probably caused by periodic vortex shedding with resonance occurring at q = 100 psf. Since the peak was sharp and the response fell off at higher speeds, galloping can be eliminated as a cause. In fact, there is no evidence that galloping occurred at any wind speed.

If the model had been accurately scaled in the torsion mode, Table 2 indicates the model frequencies should have been 47.6 cps and 48.4 cps for the undercarriage and pier base restraints instead of 32.6 and 33.7 cps. The corresponding full scale velocities for resonance would be 118 to 120 mph. These speeds are twice as high as the reported value of 60 mph and therefore do not represent the reported high speed response.

The power spectral densities presented in the Martin wind tunnel report (Reference 8) indicate that the model response at q = 30 psf was also in the torsion mode. Figure 5 indicates the response was most pronounced for the undercarriage restraint. If the torsion mode had been properly scaled, the oscillations would have occurred at q = 66 psf, a full scale velocity of 68 mph. The resulting bending moment would have been on the order of 60×10^6 in-lb per pylon which is below the structural allowable of 105×10^6 in-lb. However, it would be large enough to lift part of the flexible platform from the piers because the total gravity moment about the western edge is only 80×10^6 in-lb.

Thus it appears that the reported oscillations of the prototype at 60 mph may have occurred in the torsion mode and were reproduced in the wind tunnel test at an incorrect speed due to scaling errors. It is not known why the observers were able to estimate the deflection of the prototype mast without identifying the torsion mode.

6.0 TEST RESULTS AND DISCUSSION - MODIFICATIONS

6.1 Configuration Selection

A series of aerodynamic fixes were designed during the pretest period either to alter the frequency of, or to eliminate, the periodic vortex shedding that has been postulated as the cause of the large mast response at low wind speeds. These aerodynamic fixes are listed below in order of their anticipated efficiency in solving the mast problem.

a. Drop curtain

b. Open lattice

c. Spoilers

d. Modified cross-section (rounded leading and trailing edges in plane of pylons)

Photographs of the three latter fixes are presented in Figure 4. It may be seen that all consisted in changing the shape of the upper quarter of the mast above the splice line. The drop curtain fix consisted of covering the gap between the pylons for the top quarter of the mast with a panel on the side facing the vehicle.

Theoretical analyses and previous wind tunnel tests of launch vehicles (Reference 15) and towers (Reference 14) have indicated that increased structural damping was a very effective method of reducing the oscillations of these high aspect ratio structures. Therefore, a tuned viscous damper was designed by Mr. W. H. Reed of the Langley Research Center to simulate various levels of structural damping. It had been anticipated that doubling the critical damping ratio would solve the oscillation problem for the transporter mast. However, it was not certain that it would be feasible to incorporate this mechanical fix in the full-scale transporter.

All the fixes were then tested throughout the required speed range for all wind directions with the base constraint simulating the transporter on piers. The most feasible fix was then selected by considering performance, cost, and ground system feasibility, and this particular fix was then tested with the undercarriage base constraint and various launch vehicle configurations to insure that all wind-induced oscillation problems had been eliminated.

6.2 Test Results

A summary of the test results and comparison with pretest predictions is presented in Table 4. With the exception of increased damping, it may be seen that all the fixes reduced the loads more than 20 percent and could be considered partially or totally successful. Details of the most significant results are discussed in the following sections.

6.3 Discussion of Results

6.3.1 Aerodynamic Fixes

A comparison of the total resultant bending moment (M) for all the aerodynamic fixes is presented in Figure 6. It is obvious that the modified cross-section was the most successful fix. A greater insight of the non-steady aerodynamic forces may be obtained from Table 5 which presents the measured response in terms of peak dynamic pitch moment (MD_p) data at resonance.

Although Table 4 indicates that the aerodynamic fixes reduced the total moments by 24 to 86 percent, Table 5 indicates that the normalized forcing functions were reduced by 40 to 94 percent. Furthermore, the table indicates that the resonant speed could be predicted with existing two-dimensional data for stationary cylinders within 20 percent of the measured value for all configurations except the open lattice fix.

a. Drop Curtain Fix

This fix had been inspired by the experiment of Scruton with the tower of the Severn River Suspension Bridge. This experiment has been

Table 4. Summary of Critical Loads on Transporter Mast, and Comparison of Predicted and Measured Efficiency of the Fixes (Mast on Piers)

Fix	Pretest Predictions		Test Results				Comments
	Confidence in Fix	Expected Response	Critical Orientation ϕ	Critical Speed, V_R (Equivalent Full Scale, mph)	Bending Moment (Equivalent Full Scale) 10^6 in-lbs at V_R or 32.5 mph	Percent Reduction β	
Basic Configuration $\zeta_s = 0.5\%$	--	--	90°	32.5	73.4(a)	--	
Drop Curtain	Very High	Eliminate resonant peak in the manner of Ref. 14	95°	32.5	49	33%	Not Successful. Results did not agree with Scruton's data. Resonance occurred at same speed but critical wind direction shifted 5° from plane of pylons toward open side of mast.
Open Lattice	Very High	Large reduction in response and shift of resonant speed to 41 mph	90°	No Peak	17.5	77.5%	Evidence of peak response for $\frac{V}{fd} < 10$, $q < 12$ psf. Does not correlate with dimensions of solid portion of mast.
Spoilers	Moderate	Low peaks at 41 & 83 mph corresponding to pitch oscillations	90°	No Peak 53 $V_R \geq 75$mph	18.6 55.5 $M \geq 44.8$	75% 24.4% $\beta \leq 39\%$	Partially Successful. Fair Agreement with predictions.
Modified Cross Section	Low	Low response with V_R = 9 mph	90°	No Peak	9.82	86.5%	Best Fix could not verify predicted resonance because q was too low.
Doubled Structural Damping $\zeta_s = 1.0\%$	High	50% reduction of dynamic component	90°	33.5	64.8	11.6%	Not Successful, Predictions order of magnitude too high.
Quadrupled Structural Damping $\zeta_s = 4\%$	Very High	88% reduction of dynamic component	90°	30.5	32	56.5%	Partially Successful. Full Scale dampers not feasible. Large error in predictions.

(a) Estimate, the peak was never determined exactly.

Table 5. Isolated Transporter on Piers

Comparison of Non-Dimensional Forcing Functions at Resonance for Various Aerodynamic Fixes

ζ_s = 0.5% in pitch

$\phi = 90°$

Configuration	Reduced Velocity at Resonance (V_R/fd)		Dynamic Pressure at Resonance (q_R, psf)	Model Dynamic Pitch Moment (MD_p, in.-lb)	$\frac{MD_p/q_R}{(MD_p/q_R)_{Basic}}$	Net Reduction Percent
	Estimated	Measured				
Basic	9 - 13	11.9	15	172,00 [b]	1.0	--
	--	8.03	30 (torsion Under-carriage)	50,000	0.144	86
	--	14.2	100 (torsion)	90,000	0.079	92
Drop Curtain	--	11.9	15	95,800	0.56	44
Open Lattice	14.6	$V_R/fd < 10$	$q_R < 12$	$MD_p > 30,000$		
Spoilers	14.6	16.8	30	54,000	0.157	84
	29.6	27.4	80	50,000	0.0545	94
Modified Cross Section	3.3	$V_R/fd < 12$	$q_R < 15$ [a]	18,000 [a]	--	

[a] Does not represent a resonant condition, corresponds to q = 15 psf

[b] Estimate, the peak was never determined exactly

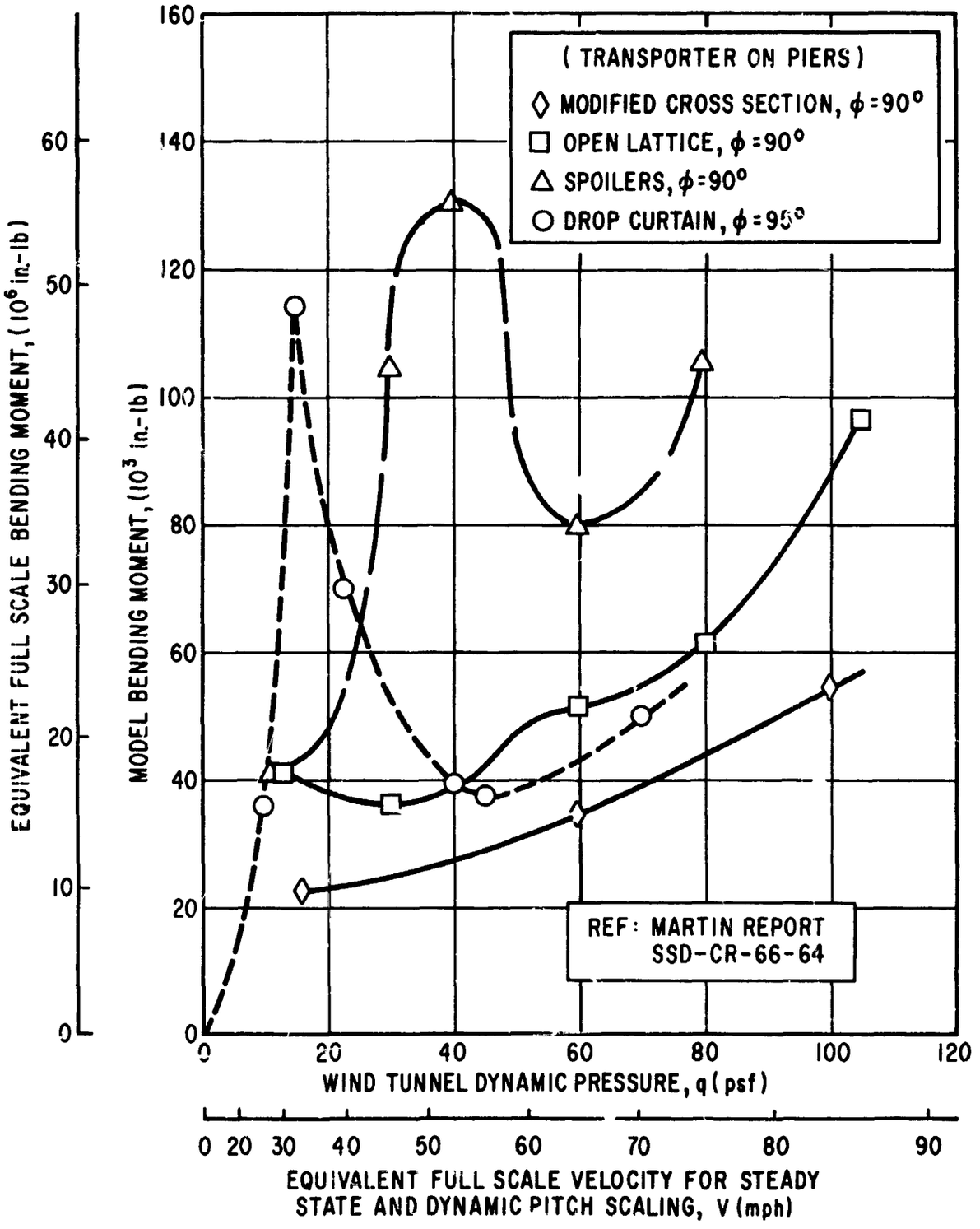

Figure 6. Isolated ITL Transporter - Resultant Bending Moment at Base of Leeward Pylon for Various Aerodynamic Fixes at the Critical Wind Direction.

discussed previously in Section 5.2.2. A high degree of confidence existed for this particular fix because the previous investigation indicated that a curtain on one side of the tower covering the top quarter eliminated all resonance and reduced the loads by an order of magnitude (Reference 14).

These results were not confirmed by the present experiments, the resonant speed was not changed, remaining at $V_R/fd = 12$, but the most critical wind direction shifted 5° away from the face with the curtain. The total bending moment was reduced 33 percent, the reduction in the dynamic pitch moment was 44 percent.

b. Open Lattice Fix (Figure 4b)

A high degree of confidence existed that this fix would reduce the critical oscillations because it was known that the periodic forcing function acted near the top of the mast. It was expected that a small resonant peak would occur at the reduced velocity of $V_R/fd = 14.6$ which would correspond to an estimated Strouhal number of $S = 0.098$ and the pylon width of 6 ft at the top of the solid faces. The data indicate that the peak actually occurred for $q < 12$ psf and $V_R/fd < 10$. This indicates that the frequency of vortex discharge was determined by an intermediate width between the top of the pylon and the top of the solid faces.

The 78 percent reduction in total load due to the very low resonant speed was much greater than expected. There was no significant change in the static loads because the drag of the open lattice is as great as that of the closed rectangular section.

c. Spoilers (Figure 4c)

The spoilers on top of a mast had proved to be very effective in reducing the response of the Atlas vehicle in the wake of the rectangular umbilical mast at PALC 1 (References 6, 15, and 16) if the spoiler width was at least 2.5 times the width of the mast or the diameter of the vehicle in the wake. These tests also indicated that the large resonant peak would be replaced by two much smaller ones corresponding to the periodic vortex shedding from the spoiler and the basic mast below the spoiler.

These expectations were confirmed, the reduced velocities for resonance agreed with predicted values within 13 percent, and Table 5 indicates that the non-dimensional periodic forcing functions were reduced by 84 and 94 percent. The 84 percent reduction in the low speed response was identical to the corresponding PALC 1 results shown in Figure 11 of Reference 6. The maximum dynamic response occurred at $q = 30$ psf and was associated with the vortex shedding from the pylon beneath the spoiler. However, Figure 6 and Table 4 indicate that large static drag loads shifted the maximum total load to $q = 40$ psf, which corresponds to 53 mph for the prototype on piers. The total load was only reduced 24 percent from that of the basic mast and the fix was not deemed to be completely satisfactory.

d. Modified Cross-section

Both pylons were streamlined by adding half conical fustums to both the leading and trailing edges in the yaw plane (Figure 4d). This was done to prevent separation at the leading edge, narrow the wake, and increase the Strouhal number so that the resonant speed would be reduced to a very low value. The two-dimensional data of Delany and Sorenson (Reference 17) for a two-dimensional cylinder similar to the cross-section of one pylon gave assurance that this modification would eliminate the problem for the critical wind direction of $\phi = 90^{o}$. The data indicated that (1) the lack of Reynolds number simulation would not be a significant effect, (2) the static drag would be reduced 70 percent, and (3) $S \doteq 0.3$ with mast interference effects included. The equivalent full-scale speed for pitch resonance would have been $V_R \doteq 9$ mph and the corresponding wind-tunnel dynamic pressure would have been $q \doteq 1.2$ psf.

Tables 4 and 5 indicate that the loads were reduced approximately 90 percent and no problems were encountered at other wind directions. Resonance in torsion would also have been expected at $S \doteq 0.3$ and the corresponding wind-tunnel dynamic pressure would have been $q \doteq 5.5$ psf. The plot of bending moment in Figure 9 indicates that a peak response probably occurred at a dynamic pressure less than the first data point at $q = 15$ psf. Therefore, it is reasonable to assume that the predicted resonant peak may have occurred at a low wind speed.

It was feared that this particular fix might induce a forced oscillation of the launch vehicle because the gap distance between the pylons would be reduced to 11.2 ft. The diameter of the vehicle is 10 ft and the previous wind-tunnel test of a 15-ft bulbous payload had indicated that a critical situation exists when the payload diameter is approximately the same size as the gap.

A detailed explanation of the phenomena is presented in Reference 6. Briefly, it may be said that the payload produces sufficient interference to convert the two pylons and the vehicle into an equivalent aerodynamic body. There would be a main sequence of low frequency vortex shedding from the extremities of the mast and high frequency vortex shedding in the gap. This situation is very similar to the effects described in Figure 6 of Reference 10. The periodic vortex shedding then oscillates the vehicle and resonance would occur at a particular wind speed.

It should be mentioned that the vehicle was tested in the presence of the basic mast and this type of resonant condition was observed with a 10-ft diameter payload downstream of the mast ($\phi = 180^{o}$, Reference 8, Figure 69). The resonant speed occurred at reduced frequencies of $f_V c/V_R = .082$ or $f_V w/V_R = .035$. This reduced frequency corresponds to the Strouhal number measured for the mast at $\phi = 90^{o}$ without the vehicle and is considerably less than the expected value of $S = 0.135$ for $\phi = 180^{o}$ without the vehicle.

Thus, it is not clear if vehicle interference is significant at $\Delta = 15.4$ ft. However, it is definite that it would be significant for the modified cross-section fix with a 10-ft payload.

6.3.2 Damper Fixes

The small decrease in mast response shown in Table 4 with large increase in structural damping was surprising because the resonant response of a linear system to a periodic forcing function is inversely proportional to the damping in the system. It was tacitly assumed that total damping of the system would be approximately equal to or slightly less than the measured value of structural damping (i.e., $\zeta_{net} \leq 0.5$ percent of critical). This was the case for the Severn River Suspension Bridge Tower tested by Scruton (Reference 14). The reported amplitude variation with damping (Figure 7) indicates that the bridge responded as if the net damping in the system were slightly less than the measured structural damping.

Table 6 and Figure 7 indicate that the dynamic response of the ITL mast did not vary in this manner with structural damping. In fact, the system responded as if it contained an additional increment of damping (ζ_A) equivalent to approximately 3 percent of the critical value. This additional damping must be of an aerodynamic origin but the nature of the phenomena is not obvious.

At resonance the damping force is equal and opposite to the applied force (180° out of phase with the applied force). Thus, it might be reasonable to suppose the additional damping was associated with the phase difference between the forces applied to the windward and leeward pylons. If this were the case, Figure 7 implies that the phase angle for the ITL mast should approach 180°, and that of the suspension bridge should be approximately zero. This information cannot be obtained directly from the test data because response was measured rather than aerodynamic force.

However, the frequency of vortex discharge (n) is equal to the natural frequency of the structure (f) at resonance and the resonant wind speed (V_R) was measured. It is known that the translation velocity of the vortices (v) is 85 percent of the free stream velocity for both bluff and streamlined bodies (experimental measurements from Reference 18 can be substantiated by use of a Von Karman's drag formula, wake characteristics, and measured Strouhal number). The time lag and phase angle may then be determined from Figure 3, Table 6, and Reference 14, as shown below.

The phase angle for the transporter mast and suspension bridge are of the same order, so that the differences in response for various levels of structural damping cannot be attributed to the time lag between the forces applied to the windward and leeward pylons.

Table 6. Effect of Structural Damping upon Transporter Response at Resonance ($\phi = 90°$, Model on Piers)

Configuration	Mode	ζ_s	q_R (psf)	$\frac{V_R}{fd}$	Resultant Moment $M \times 10^{-3}$ (in.-lb)	Dynamic Moment $MD \times 10^{-3}$ (in.-lb)	$\frac{MD/q_R}{(MD/q_R)\zeta_s = 1.0\%}$
Basic	Pitch	0.5%	15	11.9	172	172	1.13
	Torsion	*	100	14.2	131	90	--
Moderate Damping	Pitch	1%	16	12.2	152	152	1.0
	Torsion	*	*	*	*	*	*
High Damping	Pitch	4%	13.2	11.03	75	70	0.566
	Torsion	*	100	12.3	108	68	--

*Data not available

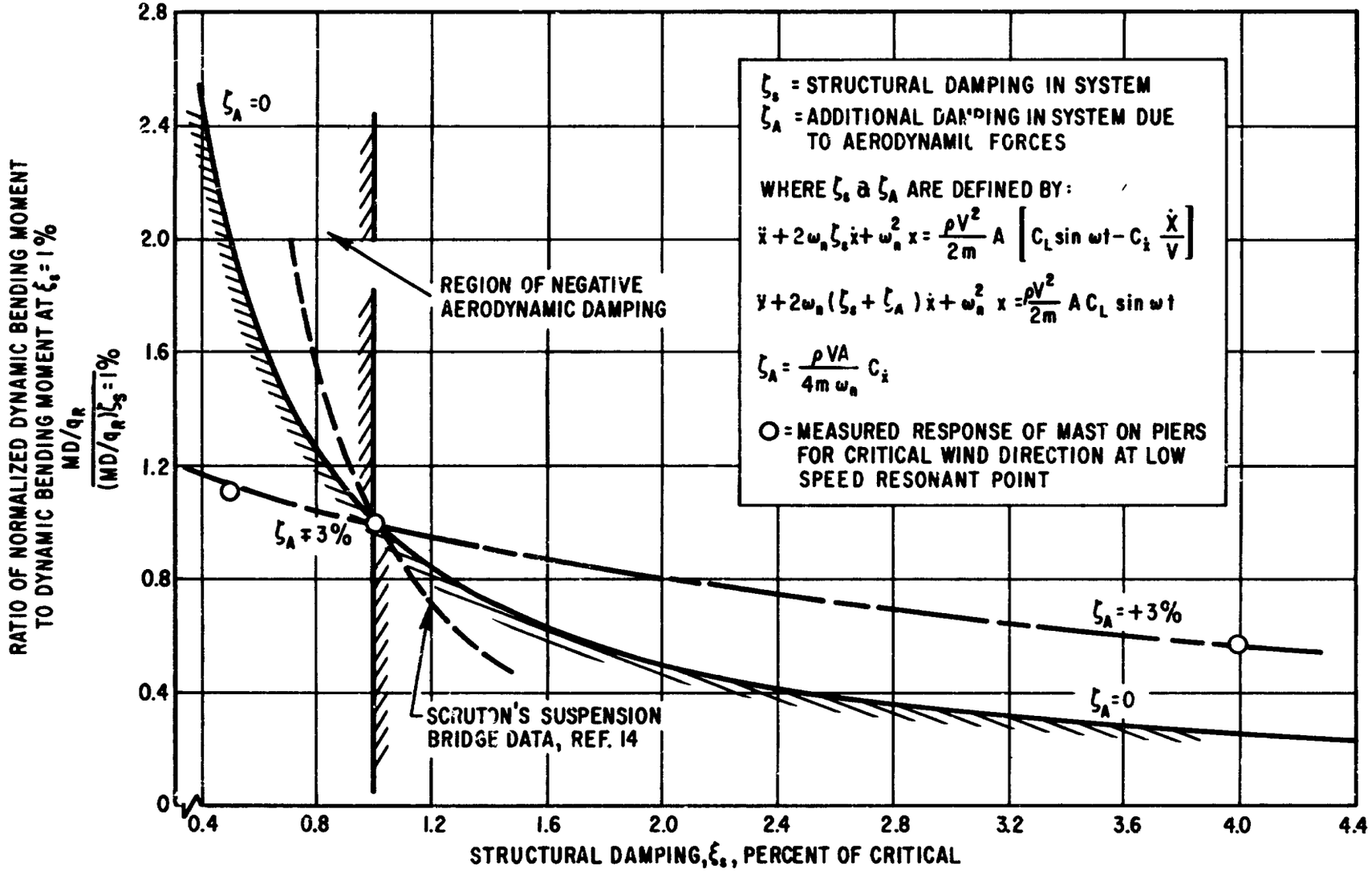

Figure 7. Comparison of the Measured Effect of Structural Damping With Response of an Equivalent Linear System at Resonance.

	Transporter Mast (Model)	Suspension Bridge (Full Scale)
V_R/fd	11.1 - 12.2	9
V_R (ft/sec)	54.8 - 60.4	49.4
v (ft/sec)	46.6 - 51.3	42
f (cps)	15.6	0.33
Δ (ft)	1.156	42 - 57*
$\frac{\Delta \cdot f}{v}$	0.387 - 0.363	0.33 - 0.45
$\theta = 360^\circ \frac{\Delta \cdot f}{v}$ (deg)	139° - 127°	119° - 162°

7.0 FINAL FIX

The open lattice fix was selected as the most feasible one for the following reasons:

a. It would eliminate the resonant oscillations of a bulbous payload launch vehicle located in the wake of the mast during the transportation phase.

b. Simplicity of required modifications with minimum interference to work platforms.

The suitability of the open lattice fix was then confirmed by testing the transporter on undercarriages with and without the various launch vehicle configurations.

8.0 CONCLUSIONS

The low speed wind induced oscillations of the prototype transporter mast were reproduced in a wind tunnel test. The nature of the problem was defined explicitly as a forced response due to periodic vortex shedding and this confirmed the pretest predictions.

*Reference 14 did not provide this dimension; values represent measurements scaled from a photograph.

The oscillations of the prototype observed at 60 mph were probably in the torsion mode and were reproduced in the wind tunnel. However, the nature of the forcing function was not defined explicitly.

Several of the aerodynamic modifications (fixes) were found to be satisfactory and performed as predicted. The most effective fix consisted in rounding the faces of the pylons.

The addition of increased structural damping to the system is not a feasible solution.

The open lattice fix was selected as the most desirable because it eliminated the wind induced oscillation problem of the bulbous payload vehicle on the transporter.

Many of the pretest predictions were confirmed by the wind tunnel test results. Some unexpected phenomena were observed and a few of the pretest predictions were found to be completely erroneous.

The wind induced oscillation phenomena was understood well enough to have predicted the resonant condition for the transporter if aeroelastic effects had been considered during the design phase.

9.0 RECOMMENDATIONS

Aeroelastic analyses should be performed during the preliminary design of all high aspect ratio lightly damped structures such as the transporter mast, towers, or launch vehicles.

The aeroelastic design of all unusual structures should then be confirmed by wind tunnel tests of aeroelastic models.

SYMBOLS

c	Viscous damping coefficient
c	Chord length of structure in nominal streamwise direction (ft)
c_L	Sectional lift coefficient
d	Reference diameter or width of object normal to the nominal wind direction (ft)
EI	Nominal bending stiffness ($lb\text{-}ft^2$)
f	Natural frequency of first bending mode of mast or vehicle (cps)
h	Width of wake defined as lateral distance between rows of vortex centers (ft)

ℓ	Longitudinal spacing of vortices (ft)
M	Total resultant bending moment (in-lb)
MD	Dynamic bending moment (in-lb)
$\frac{MD}{q}$	Normalized dynamic bending moment (in^3)
MS	Static bending moment (in-lb)
m	Nominal mass per unit length (slug-ft)
n	Frequency of vortex discharge (cps)
q	Dynamic pressure in wind tunnel (PSF)
S	Strouhal number, non-dimensional frequency of vortex discharge $S = n\frac{d}{V}$
t	time (sec)
V	Free stream velocity (fps unless noted)
$\frac{V}{fd}$	Reduced velocity of structure
v	Velocity of vortices (fps)
w	Total width of mast (ft)
Δ	Distance between pylons (ft)
ζ_A	Fraction of critical damping of system attributed to aerodynamic forces
ζ_S	Fraction of critical damping in system due to transporter structure
θ	Phase angle (deg)
μ	Absolute viscosity of air or Freon test medium $\left(\frac{slug}{ft\text{-}sec}\right)$
ρ	Mass density of air or the Freon test medium $\left(\frac{slug}{ft^3}\right)$
ϕ	Wind direction corresponding to wind tunnel coordinates (deg)

SUBSCRIPTS

m	model
p	pitch
R	resonance
y	yaw
v	vehicle

ACKNOWLEDGEMENT

Many personnel from the Martin Company, Langley Research Center, and Aerospace Corporation made significant contributions to the wind tunnel program. The authors would particularly like to recognize the efforts of the following individuals:

D. Olson and F. Peters of the Martin Company

T. Birdsong, R. Duncan, and W. Reed of the Langley Research Center

G. Fox, E. Lenk, B. Pershing, and G. Young of the Aerospace Corporation

REFERENCES

1. Parkinson, G. V., "Aspects of the Aeroelastic Behavior of Bluff Cylinders," Paper No. 58 presented Engineering Institute of Canada Annual Meeting, 1962.

2. Den Hartog, J. P., Mechanical Vibrations, 4th Edition, McGraw-Hill Book Co., Inc., New York (1956), Chap. 7.

3. Brooks, P. N., Experimental Investigation of the Aeroelastic Instability of Bluff Two Dimensional Cylinders, M. A. Sc. Thesis Univ. of British Columbia (1960).

4. Smith, J. D., An Experimental Study of the Aeroelastic Instability of Rectangular Cylinders, M. A. Sc. Thesis Univ. of British Columbia (1962).

5. Cincotta, J. J. and Lambert, W. H., Investigation of Wind Induced Oscillations and Steady Ground Wind Forces on a 7.5% Dynamically Scaled Model of the 624A Vehicle, SSD-CR-63-118, Martin Company, Denver, Colorado (August 1963) (Contract AF04(695-150) (C)

6. Ordway, D. E. and Lyons, J. M., Ground Wind Induced Resonance of Launch Vehicles, SSD-TDR-63-207, Aerospace Corp., El Segundo, Calif. (1963) (Contract No. AF04(695-269) (C)

or Ordway, D. E., Lyons, J. M., and Ward, B. D., Ground Wind Induced Resonance of Launch Vehicles, Transactions of the Eighth Symposium on Ballistic Missile and Space Technology, Vol. VI, Air Force Systems Command and Aerospace Corporation (October 1963, pp. 92-116) (S).

7. Newgent, J., ITL Mast-Frame Full Scale Vibration Test Report, SSD-CR-65-149, Martin Company, Denver, Colorado (July 1965) (Contract AF04(695)-150).

8. Olson, D. W. and Peters, F. W., Titan III 7.5% Scale Wind Induced Oscillations Test Phase II Final Report, SSD-CR-66-64, Martin Company, Denver, Colorado (April 1964) (Contract AF04(695)-150).

9. Roshko, A., "Experiments on the Flow Past a Circular Cylinder at Very High Reynolds Number," Journal of Fluid Mechanics 10 pp. 345-356 (1961).

10. Lyons, J. M., Ground Wind Induced Oscillations of the Titan III ITL Transporter, TR-669(6116-40)-3 Aerospace Corp., El Segundo, Calif. (July 1966).

11. Roshko, A., On the Development of Turbulent Wakes from Vortex Streets, NACA TR-1191, Washington, D. C. (1954).

12. Roshko, A., On the Drag and Shedding Frequency of Two-Dimensional Bluff Bodies, NACA TN 3169, Washington, D. C. (July 1954).

13. Humphreys, J. S., "On a Circular Cylinder in a Steady Wind at Transition Reynolds Numbers," Journal of Fluid Mechanics 9, pp. 603-612 (1960).

14. Scruton, C., "On the Wind Excited Oscillations of Stacks, Towers, and Masts," Paper 16 presented at International Conference on the Wind Effects on Buildings and Structures, National Physics Lab., Teddington, England (June 1963).

15. Gaffney, E. F., Ground Wind Loads Wind Tunnel Test on Atlas Vehicles, GD/A 63-0999, General Dynamics/Convair, San Diego, California (April 1964) (Contract AF04(647)-699).

16. McCullough, G. and Steinmetz, W., A Wind Tunnel Study of Ground-Wind Loads on Launch Vehicles Including the Effects of Conduits and Adjacent Structures, NASA TN D-2889, Washington, D. C. (July 1965).

17. Delaney, N. K. and Sorensen, N. E., Low Speed Drag of Cylinders of Various Shapes, NACA TN 3038, Washington, D. C. (November 1953).

18. Brown, F. N. M., "The Organized Boundary Layer," Transactions of the Sixth Mid-Western Conference on Fluid Mechanics, University of Texas, Austin, Texas (1959), pp. 331-349.

AERODYNAMIC EXCITATION OF STRUCTURES BY WIND - A REVIEW OF RECENT WORK AT THE NPL

by R. E. Whitbread

Aerodynamics Division, National Physical Laboratory,
Teddington, Middlesex, England

Presented at a Meeting on Ground Wind Load Problems in relation to Launch Vehicles held at the National Aeronautics and Space Administration, Langley Research Center, Hampton, Virginia, U.S.A., June 7-8, 1966.

AERODYNAMIC EXCITATION OF STRUCTURES BY WIND - A REVIEW OF RECENT WORK AT THE NPL

by R. E. Whitbread

INTRODUCTION

The National Physical Laboratory first became involved in the study of aerodynamic excitation of structures by wind in 1946 when Fraser and Scruton, who until then had been concerned with aircraft flutter research, were requested to investigate the problem of wind-excited oscillation of suspension bridges. Later chimneys, towers, and tall buildings were included within the general scope of the research programme but as yet, we have not come into direct contact with the particular problems of launch vehicles.

The approach that has been adopted to these problems to date has been to carry out wind-tunnel investigations using models scaled aeroelastically to give as close a dynamic representation of the full-scale prototype as materials and methods for model construction will allow. Some work has also been carried out to obtain basic aerodynamic data of general applicability and a little, but increasing amount directed towards a fundamental understanding of unsteady air flows. Until recently most of these investigations were carried out in smooth uniform flow conditions but more recent work at NPL and elsewhere, in which attempts have been made to introduce more representative wind

structure in the form of turbulence and wind shear, has indicated the fundamental importance of this aspect of the general scaling problem.

In this paper it is possible to give only a very brief and superficial treatment to the work that has been carried out by the NPL. Consequently it was considered that a list of NPL reports on this topic of aerodynamic stability might usefully be circulated at this meeting. This list is included at the end of the paper.

Definition of aerodynamic excitation.- In our work at the NPL we have tended to follow aeronautical practice and represent the unsteady aerodynamic force F in derivative form,

$$F = H_a Z + K_a \dot{Z}$$

where H_a may be considered to be an aerodynamic stiffness and K_a an aerodynamic damping.

In practice it has been found that, for lightly damped structures, the frequency of oscillation is independent of wind speed and equal to the value observed in still air so that it is reasonable to assume that $H_a = 0$. The aerodynamic damping K_a may be expressed non-dimensionally as

$$k_a = \frac{K_a}{\rho D^2 N} = \frac{2M\delta_a}{\rho D^2}$$

where M is a mass per unit length and δ_a, a logarithmic decrement which may be measured directly. This departure from the concept of a sinusoidal forcing function has the advantage that it is completely general and values for k_a may be determined for all types of excitation whether it be vortex shedding, galloping, or

from any other cause. It may be noted that when the frequency of vortex shedding, as given by the Strouhol number coincides with a structural frequency then there is an equivalence between k_a and C_L (the so-called Karman lift coefficient) such that

$$C_L = - \frac{4\pi k_a \eta_o}{V_r^2}$$

The above representation has proved satisfactory for tests conducted in smooth uniform airflows where the random component of both the wind speed and the response amplitudes are small. In turbulent winds, however, we would now follow Reed and introduce a random component L(t) into the expression for the aerodynamic force, so that

$$F = K_a \dot{Z} + L(t)$$

Measurements of excitation.- Measurements of aerodynamic excitation ($-k_a$) have for the most part been made under two-dimensional flow conditions, with low levels of turbulence and with Reynolds number hardly exceeding 10^5. Within these limitations measurements of aerodynamic excitation have been made covering both variation in wind speed and amplitude. Figure 1 shows the variation of the excitation ($-k_a$) with wind speed for a particular amplitude with a sharp peak at the wind speed for which the vortex shedding frequency coincides with the structural frequency. For other wind speeds ($-k_a$) is small and for the most part negative, i.e., an aerodynamic damping. The variation of the ($-k_a$) peak with amplitude is shown in Figure 2 where a plot of ($-k_a$) versus $1/\eta_o$ illustrates the equivalence, for this particular wind speed,

between the two forms of expressing the aerodynamic force.

Work is in hand to investigate the variation of $(-k_a)$ with Reynolds number with a programme of measurement in the NPL Compressed Air Tunnel which should provide additional data up to and just beyond a Reynolds number of 10^6.

Aspect ratio has been found to have a very considerable effect in reducing excitation values. A series of measurements on a near-circular section covering the range of aspect ratio from 7 up to the two-dimensional flow condition gave values for $(-k_a)$ in the approximate ratio of ' to 100 respectively.

To date no direct attempt has been m[illegible] to measure excitation values in turbulent flows. Measurements of root-mean-square lift coefficients have however been made by Vickery at NPL using a square sectional shape with two-dimensional flow conditions. Tests in smooth uniform flow and in a flow with a turbulence intensity of 10-percent showed a 50-percent drop in the root-mean-square lift coefficient measured with the flow directed normal to a face. The peak values recorded in the spectrum, however, differed by a factor of 10.

Preventive devices.- Requirements for the preventive devices with which we at the NPL have been concerned are that they shall be equally effective for all wind directions and shall require no maintenance. One such device, which has been fairly widely used in the United Kingdom and elsewhere mainly for steel chimney stacks, is known as straking and consists of a series of three strips wound as helices around the circumference of a cylinder

with, in its optimum configuration, a pitch of five diameters and a strake height of one-tenth of a diameter. A typical installation is shown in Figure 3 together with some measurements of $(-k_a)$. The device originally suggested by Price of fitting an outer perforated cylinder, has been adapted for use with a multiflue chimney in which the several flues were enclosed within and supported by a reinforced concrete shroud. Model tests indicated that perforation of this shroud was very effective in reducing excitation.

Model investigations.- Using aeroelastic scaling techniques originally developed for aircraft flutter investigations, it has been possible to construct complete aeroelastic models of structures such as chimney stacks and simple towers. For the more complex structures, which involve intricate arrangements of shear walls and floor slabs, aeroelastic construction has been found to be impracticable and has been abandoned in favor of a simplified linear-mode representation. This is achieved by construction of a stiff light-weight model of the correct moment of inertia pivoted at the base in a low friction bearing. It has been found very convenient to extend part of the model through to the underside of the wind tunnel where coil springs are attached to provide the appropriate stiffness, and where additional structural damping is applied by electro-magnetic means.

Real wind effects, such as turbulence and wind shear, are not easily reproducible in the conventional aeronautical wind tunnels at the NPL. Attempts to introduce such effects have been confined

to the use of grids upstream of the test section, either graded in resistance to produce both wind shear and turbulence or in some cases just a uniform grid has been used.

Some wind-tunnel investigations.- I now propose to devote a short time to some of the investigations that have been carried out at the NPL and to discuss them very briefly under headings which I hope will be relevant to the general theme of this meeting.

The stability of multi-cylinder configurations.- Three different configurations for a group of four circular chimney flues are shown in Figure 4. (a) The flues in this configuration were grouped closely together and were supported by an external steel lattice tower 321-feet in height. Each flue was 10-feet in diameter with 14-feet between centers. Excitation due to vortex shedding was found to be weak and to occur for a very limited range of wind direction. The frequency of shedding appeared to be controlled by an equivalent over all diameter rather than the diameter of an individual flue. (b) In the second confuguration the flues were more widely spaced and were carried by an internal lattice structure. The diameters in this case were 8-feet, and at the top 280-feet above ground, the center-to-center spacing of opposite flues was approximately 24-feet. This configuration was found to be very much more unstable than that mentioned previously with excitation occurring over a wide range of wind direction. The frequency of vortex shedding was controlled by the diameter of the individual flues. Tests with strakes fitted to all four flues showed a considerable reduction

in excitation and this preventive measure was adopted in the final design. (c) The third configuration, in which the four flues were completely enclosed by a reinforced concrete shroud, has been referred to earlier. Tests on this quadrafoil sectional shape and a comparable circular section showed that the former was subject to the greater excitation. Further tests on the quadrafoil shape with the top section perforated indicated favorable stability but in the final design the circular shroud was preferred.

The stability of slender tapered structures.- Aeroelastic models of two slender tapered structures are shown in Figure 5. The first is a 400-foot chimney stack and the second a proposed 1000-foot T.V. tower. In both cases vortex excitations occurred in both the fundamental and the first harmonic modes of oscillation with the shedding appearing to lock-in, over the top section, to a frequency based on the minimum diameter. The presence of the small turret at the top of the T.V. tower increased the excitation in the first harmonic mode whilst the addition of a small part-lattice mast on top of this turret had the effect of markedly reducing the excitation particularly in this first harmonic mode. This confirmed some earlier tests on the Crystal Palace television tower which had indicated that a lattice structure always experiences positive aerodynamic damping.

The stability of similar structures in close proximity.- Linear-mode models of a pair of square-section towers are shown in Figure 6. Tests on a single tower in smooth uniform flow indicated strong vortex excitation for a limited range of wind

direction. The placement of the second tower down-stream, off-set somewhat to one side, proved to have a stabilizing influence on the first tower. However, the interference created by the upstream tower produced excitation of the second tower in excess of that which had been experienced by the single tower. Later tests in which both turbulence and wind shear were introduced, demonstrated that large intensities of turbulence could have a marked effect on the response of the towers. The sudden peak in amplitude experienced in smooth uniform flow was replaced by a steadily increasing maximum amplitude with wind speed; it is necessary to refer to maximum amplitudes because the response to turbulent flow, although sinusoidal, tended to be of random amplitude. It was, however, noted that the motion was predominantly transverse to the direction of the wind and that instability occurred for much the same range of wind direction as it had for the smooth uniform flow.

Future research.- The following is a list of those topics on which research is planned to take place in the near future.

1. Measurement of aerodynamic excitation of circular cylinders for a range of aspect ratio and for a range of Reynolds number up to and just beyond 10^6.

2. Measurement of the pressure distribution around circular cylinders of various aspect ratio with the addition of efflux.

3. Further studies to ascertain the nature of vortex shedding from tapered cylinders.

4. Studies of the effects of turbulence on the wind loading

of structures. This work is to be subdivided as follows:

(a) production of representative atmospheric wind structure in the wind tunnel,

(b) influence of turbulence on aerodynamic excitation,

(c) measurement of "aerodynamic admittance" for a range of structural shapes,

(d) prediction of the response of structures to turbulence.

Most of these topics can readily be studied using existing NPL wind tunnels. However, in some important areas a wind tunnel of large working area and long working length will be required and plans are in hand to build such a tunnel. It is proposed to adopt a dual working section configuration with one section of 20-feet x 10-feet and the other 12-feet x 7-feet; also a smaller 3-foot square tunnel is under construction for turbulence studies.

Supplementary list of NPL reports

1. Walshe, D.E. The investigation of the aeroelastic behaviour in steady winds of the pinnacles of the Metropolitan Cathedral, Liverpool. NPL Aero Report 1190, April 1966.

2. Walshe, D.E. The aerodynamic investigation for a gas turbine exhaust tower for the West Burton Power Station. NPL Aero Report 1187, April 1966.

3. Whitbread, R.E. and Scruton, C. An investigation of the aerodynamic stability of a model of the proposed tower blocks for the World Trade Center, New York. NPL Aero Report 1156, July 1965.

4. Walshe, D.E. An aerodynamic investigation for the proposed Kniebrüche, Dusseldorf. NPL Aero Report 1149, April 1965.

5. Vickery, B.J. Fluctuating lift and drag on a long cylinder of square cross section in a smooth and in a turbulent stream. NPL Aero Report 1146, April 1965.

6. Vickery, B.J. On the flow behind a coarse grid and its use as a model of atmospheric turbulence in studies related to wind loads on buildings. NPL Aero Report 1143, March 1965.

7. Vickery, B.J. and Walshe, D.E. An aerodynamic investigation for a proposed multi-flue smoke stack at Fawley Power Station. NPL Aero Report 1132, December 1964.

8. Smith, I.P. The response of flexible structures to atmospheric turbulence. NPL Aero Report 1122, October 1964.

9. Whitbread, R.E. and Vickery, B.J. An aerodynamic investigation for the proposed Birmingham Radio Tower, NPL Aero Report 1114, August 1964.

10. Packer, Miss M.A. A comparison of the aerodynamic stability of a twin cylinder configuration with that of a single cylinder. NPL Aero Report 1109, June 1964.

11. Walshe, D.E. The investigation of the aerodynamic stability of the River Severn suspension bridge platform at an erection stage. NPL Aero Report 1107, May 1964.

12. Walshe, D.E. An investigation of the aerodynamic stability of a decking unit of the Severn suspension bridge. NPL Aero Report 1106, May 1964.

13. Smith, I.P. The aeroelastic stability of the Severn suspension bridge. NPL Aero Report 1105, May 1964.

14. Smith, I.P. An investigation of the aeroelastic stability of a water tower NPL Aero Report 1104, May 1964.

15. Walshe, D.E. The aerodynamic investigation for a proposed gas turbine exhaust tower for the Ferrybridge "C" Power Station. NPL Aero Report 1099, April 1964.

16. Whitbread, R.E. An aerodynamic investigation of a model of a proposed 1,000 ft concrete television tower. NPL Aero Report 1080, October 1963.

17. Scruton, C. Note on a device for the suppression of the vortex-excited oscillations of flexible structures of circular or near circular section, with special reference to its application to tall stacks. NPL Aero Note 1012, April 1963.

18. Packer, Miss M.A. The effect of solid cross girders on the aerodynamic stability of an open truss-stiffened suspension bridge. NPL Aero Report 1062, April 1963.

19. Walshe, D.E. and Packer, Miss M.A. The investigation of the aerodynamic stability of the Forth suspension bridge at various stages of construction. NPL Aero Report 1058, January 1963.

20. Scruton, C. and Walshe, D.E. An investigation of the aerodynamic stability of the towers proposed for the River Severn suspension bridge. NPL Aero Report 1052. January 1963.

21. Walshe, D.E. The influence of wind inclination on the effectiveness of strakes in suppressing and excited oscillations of cylinders of circular section. NPL Aero Note 1007, December 1962.

22. Walshe, D.E. and Packer, Miss M.A. The aerodynamic investigation for the proposed cable-stayed bridge over the Lower Tamar River (Tasmania). NPL Aero Report 1048, December 1962.

23. Pugh, P.G. and Woodgate, L. Some experimental observations upon the flow around circular cylinders fitted with helical strakes. NPL Aero Report 1040, October 1962.

24. Whitbread, R.E., Scruton, C. and Charlton, T.M. An aerodynamic investigation for the 437 ft tower block proposed for the Albert Embankment, Vauxhall, London. NPL Aero Report 1032, August 1962.

25. Walshe, D.E. Some measurements of the excitation due to vortex shedding of a smooth cylinder of circular cross-section. NPL Aero Report 1016, April 1962.

26. Walshe, D.E. and Rayner, D.V. A further aerodynamic investigation for the proposed River Severn suspension bridge. NPL Aero Report 1010, March 1962.

27. Walshe, D.E. An aerodynamic investigation for the Dungeness guide tubes. NPL Aero Report 1007, March 1962.

28. Whitbread, R.E. and Packer, Miss M.A. An aerodynamic investigation of a model of the proposed radio and television tower for the Museum telephone exchange. NPL/Aero/433, October 1961.

29. Walshe, D.E. Aerodynamic stability measurements on a model of a section of the Jonskruten transmitting tower. NPL/Aero/432, October 1961.

30. Walshe, D.E. and Rayer, D.V. An aerodynamic investigation for a proposed long-span monocable suspension bridge. NPL/Aero/418, December 1960.

31. Scruton, C. The use of wind tunnels in Industrial Aerodynamic research. NPL/Aero/411, September 1960.

32. Woodgate, L. Aerodynamic stability tests on a model of a 250 ft steel stack. NPL/Aero/408, July 1960.

33. Walshe, D.E. and Whitbread, R.E. The aerodynamic investigation for a stack for the Canada-India reactor project. NPL/Aero/395, November 1959.

34. Cowdrey, C.F. and Lawes, J.A. Drag measurements at high Reynolds number of a circular cylinder fitted with three helical strakes. NPL/Aero/384, July 1959.

35. Woodgate, L. and Maybrey, J.F.M. Further experiments on the use of helical strakes for avoiding wind excited oscillations of structures with circular or near-circular section. NPL/Aero/381, June 1959.

36. Scruton, C., Walshe, D.E. and Woodgate, L. The aerodynamic investigation for the east chimney stack of the Rugeley Generating Station. NPL/Aero/352, March 1958.

37. Scruton, C. and Walshe, D.E. A means for avoiding wind-excited oscillations of structures with circular or nearly circular cross-sections. NPL/Aero/335, October 1957.

38. Walshe, D.E. Further tests of the aerodynamic stability of the Crystal Palace television tower. NPL/Aero/330, June 1957.

39. Scruton, C. and Harding, D.A. Measurement of the structural damping of a reinforced concrete chimney stack at the Ferrybridge "B" Power Station. NPL/Aero/323, April 1957.

40. Scruton, C. and Walshe, D.E. The aerodynamic investigation for the proposed Tamar suspension bridge. NPL/Aero/311, August 1956.

FIG.1. VARIATION OF THE AERODYNAMIC EXCITATION OF A CIRCULAR CYLINDER WITH V_r

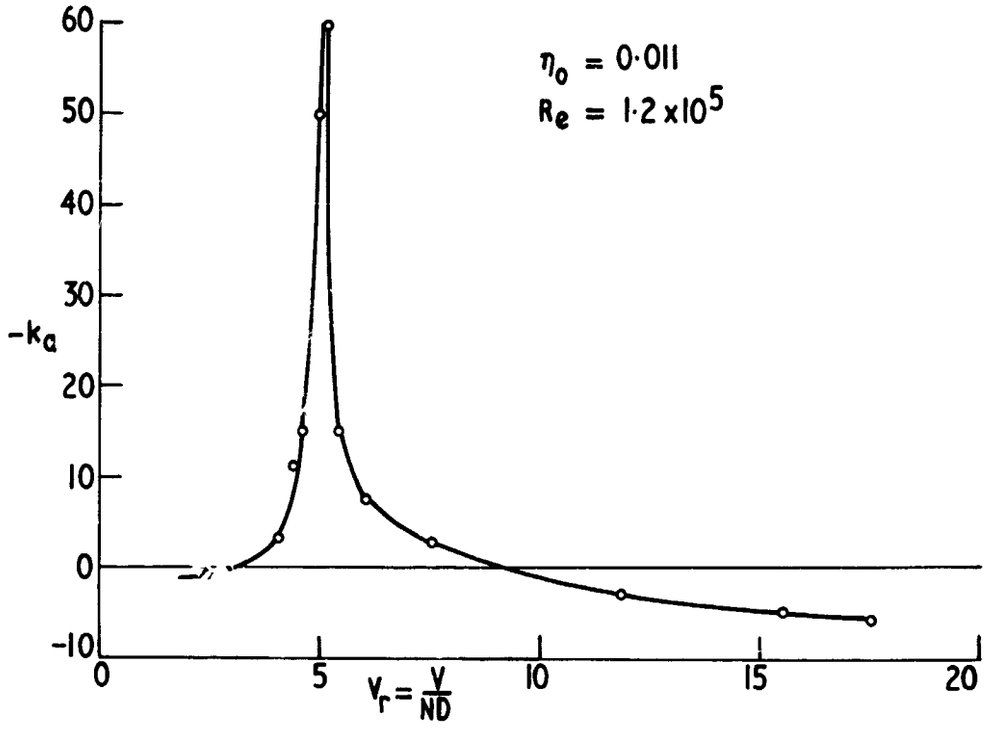

FIG. 2 VARIATION OF THE AERODYNAMIC EXCITATION OF A CIRCULAR CYLINDER WITH AMPLITUDE

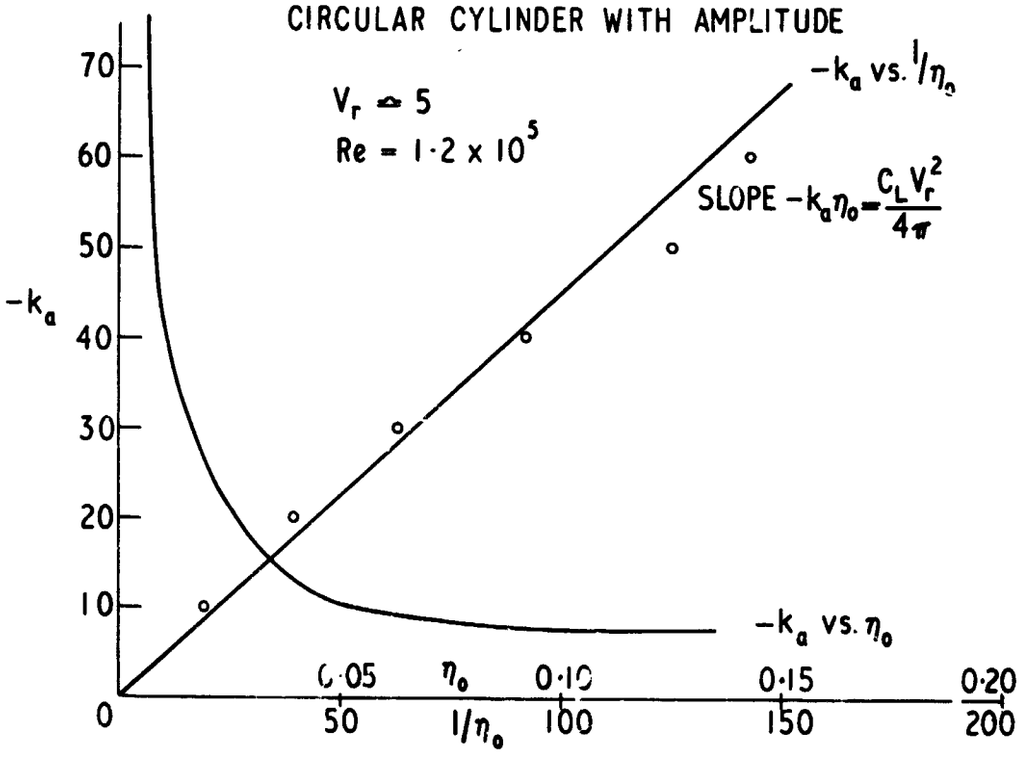

FIG. 3 HELICAL STRAKES AS A MEANS FOR INTRODUCING AERODYNAMIC DAMPING

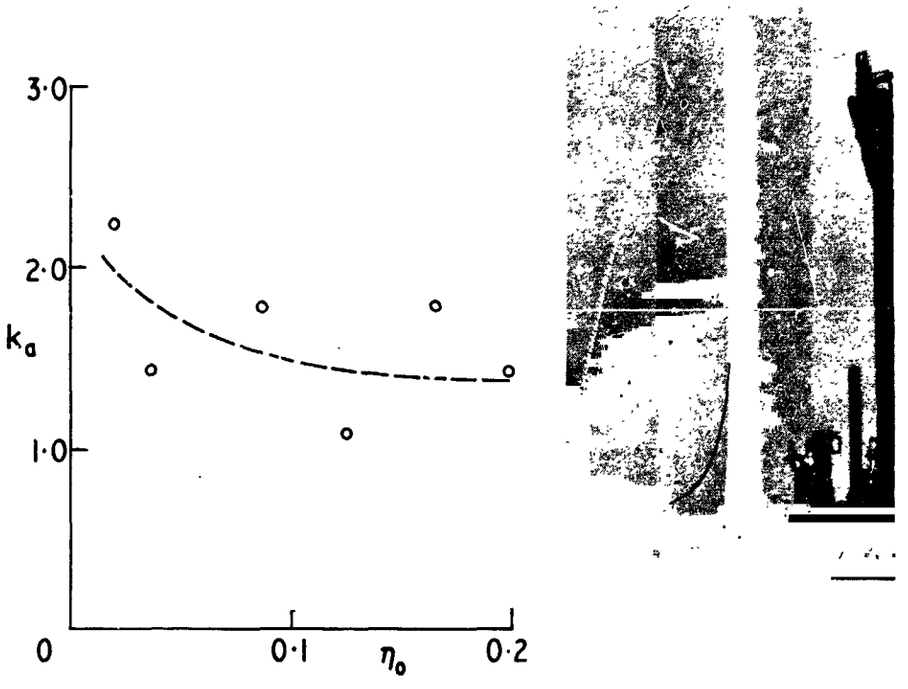

FIG. 4 SOME MULTI CYLINDER CONFIGURATIONS WHICH HAVE BEEN INVESTIGATED BY THE NPL

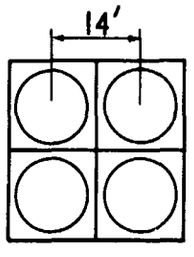

(a) 4 10 FT DIAMETER FLUES SUPPORTED WITHIN A STEEL LATTICE TOWER

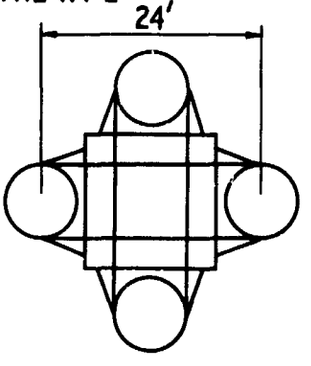

(b) 4 8 FT DIAMETER FLUES SUPPORTED EXTERNAL TO A STEEL LATTICE TOWER

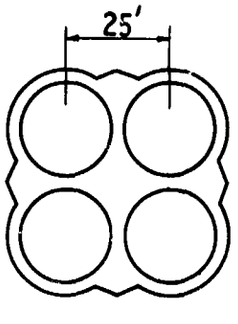

(c) 4 20 FT DIAMETER FLUES SUPPORTED BY AN EXTERNAL REINFORCED CONCRETE SHROUD

FIG. 5 WIND-TUNNEL MODELS OF TWO SLENDER TAPERED STRUCTURES

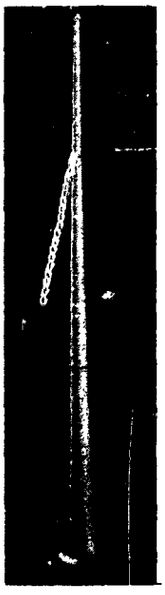

(a) A 400 FT CHIMNEY STACK

(b) A 1000 FT T.V. TOWER

DETAIL OF TURRET FITTED WITH PART LATTICE MAST

FIG. 6 WIND TUNNEL MODELS OF TWO SIMILAR SQUARE SECTION TOWERS IN CLOSE PROXIMITY

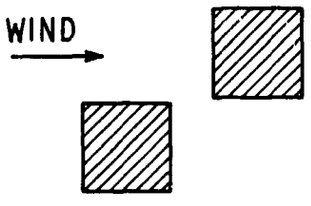

PLAN VIEW OF TOWERS

SESSION II - DEFINITION OF ATMOSPHERIC INPUTS

Chairman - Harold B. Tolefson, NASA Langley Research Center

CONSIDERATIONS AND PHILOSOPHY OF GROUND WINDS CRITERIA FORMULATION

By

William W. Vaughan

Aerospace Environment Division
Aero-Astrodynamics Laboratory
George C. Marshall Space Flight Center
Huntsville, Alabama

For presentation at the June 7-8, 1966 meeting on Ground Wind Load Problems in Relation to Launch Vehicles at Langley Research Center.

CONSIDERATIONS AND PHILOSOPHY OF GROUND WINDS CRITERIA FORMULATION

ABSTRACT

The various practical design and operational considerations involved in establishing ground winds criteria for aerospace vehicle developments are presented. The concept of exposure period probabilities in terms of risk to vehicles exposed to wind loading during operations is considered. Applications of extreme value statistics to wind design criteria and the use of spectral methods to represent the time-dependence structure of ground winds are discussed. Future needs for inputs in vehicle designs are outlined in the discussion.

INTRODUCTION

The principal purpose of all ground wind criteria is to provide a description of the ambient wind environment, such that, when employed with other inputs to space vehicle and supporting structural design problems, a design which will be acceptable for operational use is produced. The first thing that must be recognized is that the wind criteria, although important, are but one of the many inputs and considerations that must be taken into account in establishing, in the final analysis, the design strength of a structure, be it space vehicle or tool shed. It is, therefore, important that the users of these criteria work as a team with the developers of ambient ground wind models. Such a relationship helps to ensure both a physically realistic model and a practical and useable structural design.

This paper presents some considerations involved in establishing ground wind criteria, mainly from the atmospheric input viewpoint. From this presentation perhaps there will develop a basis for discussion of the subject which will promote an overall understanding of the current thinking and produce a consensus of direction for future activity.

Everyone concerned with this subject is well aware of the fact that ground winds ($\lesssim$ 150 meters) are a phenomenon which varies in both space and time. The following generalizations may be made: The longer term statistical analysis for most locations will show an increase in wind speed with height for a given risk level, the afternoon winds usually contain the high velocities relative to early morning hours, and the distribution

of obstacles (trees, buildings, etc.) contribute significantly to flow conditions at a specific place. However, even these relatively simple thoughts are overlooked in design or operational considerations.

In general, as many potential natural environmental problems as practical should be designed out. This broad remark needs to be qualified since, from a risk viewpoint, for every measured ambient extreme there exists a finite probability that it will be exceeded. So there is no such thing as being 100 per cent sure. Therefore, the ability or necessity to "design out" a potential natural environment problem depends on the trade-off between many things like cost, operational constraints, confidence in design approach, acceptable risks, etc. There is no single "right" answer to this problem. However, in some cases it appears to be controlled by one principal design input - money. This is illustrated by a case in which available money for a structure was equated to tons of steel which, in turn, was related to wind speed. Instead of deciding what risk would be acceptable and then selecting the wind speed, etc., the final design risk level was apparently arrived at by using the money available for the project.

Another aspect of this subject is the predictability of ground winds relative to design considerations. This question always arises whenever someone either has made a mistake in his design, and it is too late to change, or he finally realizes that a 0.1 per cent design risk does not mean he will not lose his vehicle tomorrow afternoon. This latter point is illustrated by a case where a design engineer stated that he wanted a 0.1 per cent risk wind criteria with a 150 per cent assurance that it would not be exceeded in an operational situation.

With the exception of a few rather well defined situations, it is impossible for present day weather forecasters (specialized or otherwise) to predict accurately peak ground winds. By accurately, it is meant that you would, with a high degree of confidence, leave a space vehicle known to be incapable of withstanding any wind above 25 knots, standing during an afternoon thunderstorm based on a weather forecaster's prediction of 24-knot peak winds. For certain well developed atmospheric situations, i.e., hurricanes, cold fronts, squall lines, and northeasters, the occurrence of these events can sometimes be predicted a few hours or a day in advance to permit protective action. But even here, no accurate prediction of the peak wind is possible in the sense mentioned earlier. The message intended is this: When one makes a design which is dependent on a wind prediction, consider carefully the element of increased risk.

DESIGN AND OPERATIONAL CONSIDERATIONS

Figure 1 provides a brief list of some considerations that should go into establishing ground wind criteria. It is rather obvious that the ground wind criteria immediately become an integral part of any design problem. They cannot be developed independently of the application. Before more is said, however, it should be understood that atmospheric physicists have been concerned with the behavior of ground winds for many decades. Volumes have been written on the subject, but there still is no universal model or criteria of ground wind behavior.

Most of the considerations itemized in Figure 1 are self-explanatory. Item No. 9, "Research Versus Project Requirements" should be stressed. Here, one should make a rather clear distinction between the needs of projects for consistent design inputs, often of a somewhat simple nature, and research studies endeavoring to relate complex vehicle responses to similarly complex forcing functions, as represented by wind inputs, for future application. The transition from the latter to the former should be made with due and deliberate considerations for the overall project impacts and consequences.

Wind loads criteria which have been established for buildings and other civil structures are used in the design of ordinary structures. The space program has unusual structures in terms of size, shape, and utility. The Vertical Assembly Building and the Saturn V space vehicle are prime examples. The established engineering building codes are not directly applicable for the design of these structures. Once the considerations in Figure 1 can be accommodated or reasonable estimates inferred, then wind criteria for initial analysis can be established. Design wind criteria cannot be established satisfactorily until the total engineering problem has been analyzed.

CURRENT DATA

Sufficient statistical records on ground winds exist, at best, only for some given height. These are the regular observations made by the U. S. Weather Bureau and other organizations with similar interests. Unfortunately, these measurements were not made for space vehicle design

use and, therefore, no special care has been exercised in producing the records beyond the normal weather forecasting and operation needs. Since it takes many unreplaceable years to acquire a useable record, we are forced to interpolate, extrapolate, theorize, and otherwise guess at sufficient additional information to establish even the simplest criteria relative to risk.

One of the older methods used to establish structural wind criteria was to take the largest wind speed (measured or assumed) for a location, and then in some cases double the value. Until rather recently, few, if any, vehicle designs considered anything other than a single wind speed for all heights regardless of location. Insofar as gust considerations are concerned, this appears to be a complicated input for design, even in the simplest form of description. Apparently most actual vehicle designs employ a peak wind as a steady force and then include a design allowance for dynamics, vortex shedding, etc. Use of various relatively sophisticated input models, such as power spectral relationships, still suffers from concern over spectral description representativeness, response characteristics of vehicle, and acceptable analytical models.

Two reports and the references thereto provide a relatively good background on what ground wind data are available relative to current-day use as criteria: NASA TM X-53328, "Terrestrial Environment (Climatic) Criteria Guidelines for Use in Space Vehicle Development, 1966 Revision," (Daniels, 1966) and the Air Force "Handbook of Geophysics and Space Environment, 1965 Revision" (Valley, 1965).

EXTREME VALUE WIND ANALYSIS FOR CRITERIA *

Statistical methods are acquiring an increasing role of importance in the physical sciences. The statistical analysis of wind is very difficult, because of the extreme variability of this atmospheric element in time and space.

The theory of extreme values proposed by E. J. Gumbel (Gumbel, 1958) is one of the most efficient methods presently available for the analysis of extreme winds and the resulting definition of design criteria for structures affected by strong winds.

The strongest wind a structure may encounter in its lifetime is very difficult to determine. Wind, more than any other atmospheric element, varies so widely in time and space that none of the many estimates of "design wind" have been found to be completely satisfactory. Classical statistical methods, which usually concern average values, are not adequate when the variable of interest is the largest (or smallest) in a set of observations. For many years engineers have used extreme values of wind speed in various forms to determine design wind pressures and loads. Often the design wind was defined simply as the highest speed ever recorded at a particular station. It was soon discovered that the value of this extreme depended on the length of record which varies from station to station. The variation of the single extreme is so large that

---

* This section was contributed by Mr. L. Falls, MSFC, R-AERO-YT.

it provides only an indication of what the design wind should be. It is at this point that the theory of extreme values developed by E. J. Gumbel may be introduced.

For a wind whose design return period*, T_d, is greater than 10 (so that the Poisson approximation is valid), the number of trials (desired lifetime), N, within which recurrence is likely, can be expressed, for various probabilities, in terms of percentages of the design return period, T_d, as

$$N = \frac{T_d}{R} \tag{1}$$

where R is any positive number; i.e., R is the percentage of the desired lifetime, N, which will give the design return period, T_d.

Now let

P = probability of the event not occurring in any of N trials.

P_1 = probability of the event occurring at least once in N trials.

We now introduce the concept of calculated risk, U, which is equal to P_1 above. Now,

$$P = (1 - \frac{1}{T_d})^N \tag{2}$$

and

$$U = P_1 = 1 - (1 - \frac{1}{T_d})^N. \tag{3}$$

---

* Average interval between recurrences of an event in a particular series of trials.

Substituting T_d/R for N from equation (1) into equation (3), we have

$$U = P_1 = 1 - (1 - \frac{1}{T_d})^{T_d/R} \xrightarrow[T_d \to \infty]{} 1 - e^{-1/R}. \qquad (4)$$

Thus, T_d may be obtained as a function of calculated risk. By plotting the range of U, $0 \leq U \leq 1$, versus various values of R, equation (4) gives us Figure 2 as a convenient method to obtain the value of R for any level of calculated risk, U.

Example:

Suppose we are given that a certain structure requires a desired lifetime of thirty days with a calculated risk of being destroyed by extreme winds of five per cent. We are required to find the average time interval between recurrence of a critical wind and the corresponding critical wind value.

The data sample used for this example is the serially complete peak wind speeds at the surface (10 meter reference height), Cape Kennedy, Florida for all months, February 1950 to December 1954. Figure 3 is the extreme value plot of these data with a sample size of N = 179 months.

Thus, given N = 30 days = desired lifetime

U = .05 = calculated risk.

Find: T_d = design return period

W* = critical wind.

From Figure 2, for U = .05, we have R = 19.5. Now from equation (1),

T_d = RN = 19.5 x 30 = 585 days = 19.5 months.

Entering the extreme-value graph, Figure 3, at a return period equal to 19.5 months, we read (on the least squares line AB) a corresponding critical wind speed of W* = 52.5 knots.

Following are several values of T_d (in months) and W* (in knots) corresponding to the indicated values of N for a calculated risk U = .05.

N	30 Days	60 Days	90 Days
T_d	19.5	39.0	58.5
W*	52.5	57.2	60.2

A combination of probability theory and Gumbel's recent theory of extreme values provides a theoretical method for analyzing and interpreting a random variable such as wind speed.

The basic theory of extreme values involves the development of a theoretical function for the probability that a given extreme value will not be exceeded by any of a large set of extremes. Observed extremes are fitted to this function by a least squares procedure, and the assumption is made that the sample of observed extremes is large so that limiting values can be used.

Several "calculated risks" were computed using the extreme value criteria. These calculated risks were compared to "exposure period probabilities" (Lifsey, 1964) which represent the empirical relative frequency of occurrence of the event, W*. The results were as follows for the indicated values of N = desired lifetime and W* = critical wind.

N	W* = 40.2 knots			W* = 59.2 knots		
	30 days	60 days	90 days	30 days	60 days	90 days
Calculated Risk	.240	.400	.550	.020	.039	.060
Exposure Period Probability	.245	.400	.520	.020	.043	.068

As shown by the above table, the agreement between the theory of extreme values and the empirical "exposure period probabilities" is very close for the selected sample. Thus, we may conclude, from a limited number of trials, that the "goodness of fit" between theory and observations is very good.

The derivation of the extreme value distribution is a theoretical procedure as opposed to empirical methods used by many engineers who believe that everything should be "normal" and whatever turns out not to be so can be made "normal" by a transformation. This is not true or practical in this situation.

No theory can explain all observations for which it is the proposed statistical model. The conditions for the use of the theory are not always fully satisfied by the observations. Therefore, certain areas of nonagreement must occur between theory and observation. This cannot be considered as a failure of the theory.

GROUND WIND PROFILE AND SPECTRAL REPRESENTATIONS *

During the design and fabrication stages of launch vehicles, the design engineer must be cognizant of the final weight of the launch configuration so that unnecessary weight penalties are avoided. Since the ground handling equipment will remain behind on the ground at launch, the present design philosophy, in the industry, is to design the auxiliary ground equipment to attenuate and alleviate some loads due to the ground winds. However, it is conceivable that ground handling equipment may have to be so sophisticated that to provide this capability will be impractical. Thus, it is imperative that the ground wind environment be defined in useable engineering terms as accurately and precisely as possible so that the engineer need not overdesign the ground handling equipment and the space vehicle structure. This is especially true if the space vehicle is required to withstand ground wind loads in the event the ground handling equipment cannot be designed to completely alleviate or attenuate the entire design ground wind loadings. Thus, the purpose of this section is to discuss the philosophy employed in the development of design criteria in the context of the ground winds problem.

The types of ground wind design criteria may be conveniently divided into two categories, mainly, the quasi-steady and unsteady properties. The quasi-steady characteristics produce steady drag forces which cause bending and an oscillatory lateral loading perpendicular to the wind direction which is a consequence of von Karman vortex shedding. Thus, it is important that the ground wind design criteria reflect the coupling

---

* This section was contributed by Mr. George H. Fichtl, MSFC, R-AERO-YE.

between these wind characteristics. The unsteady characteristics will cause the launch vehicle configuration to experience oscillatory bending in both the drag and lateral directions (Cardinale et al., 1964). However, one must bear in mind that the effects produced by these wind characteristics are coupled. For example, it appears that the mechanism for the vortex shedding produced by the steady-state wind is controlled by the unsteady characteristics (turbulence) which produce oscillatory deflections in both the drag and lateral directions. In the past, ground wind design criteria have been presented in the following forms: discrete profiles and spectra. In the remainder of this section, we will discuss these types of criteria in the context of defining the unsteady wind with a view toward determining the future needs for spectral type and related design inputs.

1. Wind Profiles Representation

One of the primary goals of atmospheric research concerning the atmospheric boundary layer is to establish an analytical representation of the wind profile. Researchers have found that the analytical form of the wind profile depends upon the stability configuration of the boundary layer as manifested by the Richardson number, the pressure gradient and Coriolis forces, and the vertical heat fluxes and Reynolds stresses that reside within and on the boundary of the atmospheric boundary layer. Accordingly, the literature abounds with profile equations which account for some or all of these effects. For example, in the surface boundary layer, the log profile is valid in neutral air (Sutton, 1953), the log-linear profile due to Monin and Obukhov is valid for near neutral

conditions (Panofsky et al., 1960), and the diabatic wind profiles due to Panofsky (1963) and Deacon (1949) are valid in unstable as well as in stable air. On the other hand, in the spiral layer where the Reynolds stresses are of the same order of magnitude as the pressure gradient and Coriolis forces, the theory first due to Ekman (Sutton, 1953) and recently expanded by Blackadar (1965) is applicable.

However, at the present time, it appears the empirically derived power law is the primary wind profile that is being employed for defining ground wind profile envelopes for design criteria application. It is given by

$$u = u_1 \left(\frac{z}{z}\right)^p, \tag{5}$$

where u is the wind speed at height z, u_1 is the wind speed at the reference height z_1, and p is a nondimensional quantity which depends upon the surface roughness, the wind speed, Richardson number, and perhaps other parameters. The exponent p is usually represented as a function of wind velocity at the reference level. Figure 4 shows p as a function of u_1 for the reference height z_1 based upon data obtained at Cape Kennedy, Florida, White Sands Missile Range, New Mexico, and Brookhaven National Laboratory, New York (Scoggins et al., 1960). The apparent reasons for the popularity of the power law as compared with the more theoretically acceptable profile equations mentioned above are twofold. First, the power law fits envelopes of wind data observations over a wide variety of meteorological conditions. Secondly, the power law may be applied to wind data with relative ease which one does not enjoy with the other profile formulas.

At most launch sites there are insufficient wind data in the vertical direction to perform statistical studies for constructing wind profile envelopes. Accordingly, a stable statistical sample must be constructed by supplementing the existing single height climatological sample with wind profile data from other observation sites. By employi g the power law profile, wind measurements at any height may be transformed to any other height so that the wind data may be combined consistently for design use. Upon establishing this sample, one may then determine the statistical distribution of u_1 at the reference level, and consequently construct the associated wind profile envelopes of the quasi-steady-state winds with the aid of equation (5). An obvious uncertainty in this procedure is that the resulting wind envelopes may not necessarily correspond to the true wind envelopes that would have resulted from using the actual wind data if they had existed.

In addition to providing wind profile envelopes of the quasi-steady wind field, it is equally important to define a design gust configuration for each envelope. At the present time, the philosophy for developing this type of criteria is to treat the gust as acting over the complete length of the vehicle. This supposedly provides the most detrimental gust loadings and reduces the problem of developing design criteria to providing gust factors and associated gust acceleration times. The gust factor G is defined as follows:

$$G = \frac{u_{max}}{\bar{u}} ,$$

where $\bar{u}$ is the mean wind and u_{max} is the wind speed associated with the peak gust. It is known that the gust factor is a function of the steady-state (mean) wind speed, the length of time used to obtain the mean wind, the prevailing stability conditions, terrain features, and height. The design gust factor adopted by Marshall Space Flight Center is 1.4 and the associated time for the wind to accelerate from the quasi-steady state to the peak wind condition is 2 sec. These criteria appear to be in agreement with the results of Mitsuta (1962).

2. Spectral Type Representation

a. Atmospheric Turbulence

As discussed previously, gust loading data are currently defined in terms of a steady-state wind profile, a gust factor, and the time it takes for the gust to obtain its maximum amplitude. However, in order to account for the interaction of the atmosphere with the launch vehicle in a more comprehensive manner, power spectral methods may be employed. In this case, design gust load inputs must be defined in terms of spectra. Spectral methods are not new in the aerospace industry, for one needs only to glance at the literature concerning aircraft gust response to see that spectral methods have enjoyed wide populatiry. Particularly noteworthy is the work of Press (1957), Lappe (1965) and Pritchard et al. (1965) with regard to defining spectral gust inputs for aircraft design. Bohne (Sissenwine and Kasten, 1962) has shown that the spectral methods which are frequently employed in the determination of aircraft flight gust loads are useful in the analysis of the nonlinear ground wind drag problem.

Wind spectra are obtained from both tower and low flying aircraft measurements. The aircraft observations yield spectra for various horizontal directions along the flight path of the plane, while tower measurements give Eulerian spectra that are represented as space spectra by using the Taylor hypothesis. In recent years, this hypothesis has been the cause of much discussion; however, Lumley and Panofsky (1964) have concluded from a survey of the available information that it appears that the Taylor hypothesis is generally applicable except for the low wave number components associated with vertical velocity fluctuations.

At the present time, only a limited amount of low level turbulence spectra exists. Thus, researchers have been able only to fix the general shape of the longitudinal spectrum, while the shape of the lateral spectrum appears to be even more elusive than that of the former. However, in the limit of small wave lengths or high frequencies, the spectrum of the lateral and longitudinal components varies approximately to the -5/3 power of frequency. The present method employed for determining the analytical forms of spectra from turbulence data is essentially trial-and-error fitting of assumed analytical forms to data, with intuition and theory to serve as a guide. In general, the analytical forms of the spectra are chosen so that for large frequencies they possess the -5/3 behavior which is characteristic of the inertial subrange first predicted by Kolmogorov (Panofsky 1963). However, it appears that the major effort toward defining spectra for vehicle response studies has been expended in the area of defining a longitudinal design spectrum. This apparently is

due to the fact that, only until very recently, there has been little need for lateral spectra in vehicle response problems. In the case of longitudinal spectra, the normalizing parameters that occur in the analytical representation are based upon similarity considerations.

Henry (1959), who has examined wind spectra associated with a range of stability conditions, has found an altitude dependence as indicated by the similarity theory. However, it appears that the present state of the art of the methods employed in spectral response studies of vertically erect launch vehicles does not have the degree of sophistication necessary for using design spectra which depend upon altitude. Thus, the analytical representation of the longitudinal spectrum due to Panofsky (Lumley and Panofsky, 1964) and based upon the strong wind spectra compiled by Davenport (1961) may develop to be an appropriate type spectral input for response calculations. His analytical representation is independent of z and is given by

$$\omega S(\omega) = 4u^{*2} \frac{900\Omega}{1 + (900\Omega)^{5/3}} \qquad (6)$$

where $\Omega = \omega/u_{10}$, u_{10} being the steady state wind speed at 10 m. The MKS system of units is being employed and ω has the units of cycles sec^{-1}. Figure 5 shows $\omega S(\omega)/u^{*2}$ as a function of Ω. Two wind profile parameters, namely, u^* and u_{10}, occur in this representation of the longitudinal spectra.

These parameters serve to couple the spectrum of turbulence and the wind profile, thus permitting the atmospheric scientist to define the steady state wind profile and the associated spectra consistently. Even though this seems to be a logical development, it should be verified for a specific location.

b. Isotropic Turbulence

It is common practice in launch vehicle response studies to use the longitudinal spectra of isotropic turbulence due to Dryden (1943) and von Karman (Pritchard et al., 1965) as a representation of atmospheric turbulence. In the case of the Dryden spectrum it is given by

$$\phi(\omega) = 2\sigma^2 \frac{L}{\pi} \frac{1}{1 + L^2\Omega^2}, \qquad (7)$$

where σ^2 is the variance of the longitudinal component of the turbulent fluctuations, L is the scale of turbulence, and Ω is now equal to ω/u_o, u_o being a quasi-steady characteristic wind speed. Figure 6 shows a plot of this spectrum in dimensionless variables. Usually the variance σ^2 is determined by integrating the above expression over all frequencies and comparing the resulting relationship with the corresponding integral of experimentally determined spectra. The major difficulty with using the isotropic turbulence model is the specification of the scale of turbulence, which in reality varies, as noted previously, with height in the atmospheric boundary layer and thus takes on a variety of values ranging from approximately

10 to 350 m. For example, Webb (1955), who has analyzed correlation functions of atmospheric turbulence, suggests that the scale of longitudinal turbulence is proportioned to the square root of the height, while Panofsky and Singer (1965) have recently suggested a two-thirds power dependence upon height.

Frequently in response calculations, the turbulent portion of the velocity field is assumed to vary randomly in time but uniformly over the complete length of the vehicle. It is possible that such a procedure could yield extremely conservative estimates of the vehicle's response. However, this simplification reduces the problem of specifying a spectral ground wind input to only defining a longitudinal power spectrum as discussed previously. Recently, there has been some interest in expanding response calculations to include the correlation between horizontal wind gusts in the vertical. The procedure is to assume that atmospheric turbulence is locally homogeneous and isotropic so that the cross spectra between like components of the wind depend only upon the distance between the correlated velocity components. In view of the assumption of isotropy, the cross correlations between unlike velocity components vanish and the quad-power of the spectrum associated with the correlation between the like components of velocity is zero for all frequencies. Particularly noteworthy is the extension of Houbolt's work (1957) by Reed (1964). Reed developed analytical expressions for the cross correlation functions for the horizontal, lateral and longitudinal components of turbulence by assuming that the patterns of turbulence are frozen into the fluid and convected at the rate of the mean wind speed for the case of isotropic turbulence as observed in a wind tunnel.

The popularity that the isotropic turbulence model has experienced in the aerospace industry may be attributed to its relatively simple mathematical form, as well as to the philosophy contained in the phrase "since so little is known about atmospheric turbulence, why not use the isotropic turbulence model which has proven itself in the aircraft industry." Although this philosophy may have been acceptable in the past, it may not be justified in the future when response calculations become more sophisticated, especially in view of the knowledge that has already been accumulated concerning atmospheric turbulence.

FUTURE OUTLOOK

In coming years, we may reasonably expect that design loading calculations with regard to ground wind inputs will become more sophisticated as experience is gained. It is thus imperative that the atmospheric scientist anticipate the future requirements for ground wind design inputs on the part of the design engineer. Currently, this calls for no less than a complete description of (1) the time dependent structure of the wind field, (2) the quasi-static wind field, and (3) the interactions and interrelationships of these two portions of the wind field. Clearly, the atmospheric scientist will have to work in close coordination with the design engineer so that the appropriate decisions can be made regarding the processing of wind data.

In addition to considering loads upon vertically erect vehicles, consideration must also be given to the possibility of other modes of launch. For example, horizontally launched vehicle configurations are

being considered. This type of configuration is envisioned as being launched with the aid of a launching sled. Before the launch vehicle initiates flight, it may experience severe loadings due to horizontal gusts while attached to the sled. Upon initiation of flight, the vehicle will experience a combination of wind loads due to vertical and horizontal gusts, as well as loads due to the mean wind profile while penetrating the atmospheric boundary layer. Accordingly, information will be needed about the horizontal as well as the vertical distribution of turbulence. Fortunately, a body of information exists concerning aircraft wind gust loading.

Another future problem area concerns vehicle booster recovery. As vehicle boosters increase in size, the cost of one-shot booster operations could become prohibitive, and it is conceivable that booster recovery operations will become common practice. Accordingly, the engineer will have to consider the problem of structural fatigue. This means that, in addition to spectral type ground wind inputs, there could be future need for exceedance probability models of atmospheric turbulence for space vehicle applications.

In developing any type of wind input for vehicle response and loading calculations, the ideal situation would be to have available a large body of existing data which will yield statistically stable results. However, in the case of wind spectra, one does not have available a statistical sample of spectra which a statistician would call stable. Thus, the atmospheric scientist must turn to other sources of data and develop design spectra in an indirect manner. At the present time, the only

ground wind data that exist in large quantities are the surface wind records obtained for given heights at U. S. Weather Bureau and military weather stations. Through our present knowledge of the wind profile, these data may be extrapolated into design wind profile envelopes. Thus, the question that remains is how do we specify spectral type inputs based upon wind profile statistics? It is apparent that the atmospheric scientist must establish the intimate relationships that exist between the wind profile and atmospheric turbulence by performing extensive field experiments. Hopefully, upon establishing these relationships, design spectra could then be prescribed, based upon a statistically stable sample of hourly wind observations. At the present time, this procedure is being followed on a very limited scale.

In addition to specifying spectral type inputs, it appears that there will also be requirements for wind inputs that depend explicitly upon the time. Recently, it has been suggested that the undulatory characteristics of the wind profile, both in magnitude and more so in direction, could significantly affect the von Karman vortex shedding mechanism. Thus, it is likely that information about the unsteadiness of the so-called "steady-state" wind profile will be needed in the very near future. It will be equally important to give some consideration to the development of a comprehensive discrete gust model. Such a model is envisioned to give statistical information about the shapes of discrete gusts both in the vertical and in time, in addition to information about gust exceedance probabilities.

A continued need will exist for better and more representative expressions of risk relative to ground wind exposure problems. In particular, the need to establish theoretical statistical models which may be employed without risk of change in the design values established therefrom, when another year or two of measurements become available, is apparent. Since the ground wind loads problem is, from a natural environment viewpoint, only one of many interrelated problems, it is likely that in the future we will see more emphasis on the "total" design problem of a space vehicle incorporating the multitude of interrelationships to formulate a design relative to an overall system risk.

BIBLIOGRAPHY

Anon., 1966, "Prelaunch Ground Wind Loads," NASA Space Vehicle Design Criteria Monograph, NASA - Office of Advanced Research and Technology, Washington, D. C.

Blackadar, A. K., 1965, "A Single Layer Theory of the Vertical Distribution of Wind in a Baroclinic Neutral Atmospheric Boundary Layer," Flux of Heat and Momentum in the Planetary Boundary Layer of the Atmosphere, Final Report, Contract No. AF9604)-6641. The Mineral Industries Experiment Station, Pennsylvania State University.

Camp, Dennis W. and John W. Kaufman, 1962, "The Use of Filtering and Smoothing Functions in the Analysis of Atmospheric Data," NASA MTP-AERO-62-54, George C. Marshall Space Flight Center, June 27, 1962.

Cardinale, S. V., F. G. England and M. M Kahudo, 1964, "Loads Requirements for Aerospace Vehicle Structures," Air Force Systems Command Technical Report #FDL-TDR-64-5, Wright-Patterson AFB, Ohio, November 1964.

Court, A., 1952, "Some New Statistical Techniques in Geophysics," Advances in Geophysics, I, edited by H. E. Landsberg, New York, Academic Press, pp. 45-85.

Court, A., 1953, "Wind Extremes as Design Factors," Journal of the Franklin Institute, Vol. 256, I, pp. 39-56.

Daniel, Glenn E., James R. Scoggins and Orvel E. Smith, 1966, "Terrestrial Environment (Climatic) Criteria Guidelines for Use in Space Vehicle Development, 1966 Revision," NASA - Marshall Space Flight Center Report #TM X-53728, Huntsville, Alabama, May 1966.

Davenport, A. G., 1961, "The Spectrum of Horizontal Gustiness Near the Ground in High Winds," Quarterly Journal of the Royal Meteorological Society, 87, p. 194.

Deacon, E. L., 1949, "Vertical Diffusion in the Lowest Layers of the Atmosphere," Quarterly Journal of the Royal Meteorological Society, 75, p. 89.

Dryden, Hugh L., 1943, "A Review of the Statistical Theory of Turbulence," Quart. Appl. Math., 1, p. 7.

Gumbel, E. J., 1958, Statistics of Extremes, Columbia University Press, New York, 1958.

BIBLIOGRAPHY (Continued)

Gleeson, T. A., 1964, "Risk and Extreme Value Statistics Applied to Design Criteria," Department of Meteorology, Florida State University, December 1964.

Henry, Robert M., 1959, "A Study of Effects of Wind Speed, Lapse Rate and Altitude on the Spectrum of Atmospheric Turbulence at Low Altitudes," Inst. Aero. Sci., Report No. 59-43.

Houbolt, John C., 1957, "On the Response of Structures Having Multiple Random Inputs," Jahr. 1957 der WGL, Frieds. Vieweg and Sohn (Braunshwlig), pp. 296-305.

Lappe, Oscar V., 1965, "A Low Altitude Turbulence Model for Estimating Gust Loads on Aircraft," AIAA 2nd Aerospace Sciences Meeting, New York, N. Y., January 25-27, 1965.

Lieblein, J., 1954, "A New Method of Analyzing Extreme Value Data," National Advisory Committee for Aeronautics, Technical Note 3053, Washington.

Lifsey, David J., 1964, "An Empirical Analysis of Daily Peak Surface Wind at Cape Kennedy, Florida for Project Apollo," NASA - Marshall Space Flight Center, TM X-53116, Huntsville, Alabama, August 1964.

Lumley, J. L. and H. A. Panofsky, 1964, "The Structure of Atmospheric Turbulence, Interscience Publishers, New York.

Mitsuta, Y., 1962, "Gust Factor and Analysis Time of Gust," Journ. Met. Soc., Japan, 40, p. 242.

Panofsky, H. A., A. K. Blackadar and G. E. McVehil, "The Diabatic Wind Profile," Quarterly Journal of the Royal Meteorological Society, 86, p. 390.

Panofsky, H. A., 1963, "Determination of Stress from Wind and Temperature Measurements," Quarterly Journal of the Royal Meteorological Society, 89, p. 85.

Panofsky, H. A. and I. A. Singer, 1965, "Vertical Structure of Turbulence," Quarterly Journal of the Royal Meteorological Society, 9, p. 339.

Press, Harry, 1957, "Atmospheric Turbulence Environment with Spherical Reference to Continuous Turbulence," Advisory Group for Aeronautical Research and Development, Report 115. North Atlantic Treaty Organization, Polais De Chaillat, Paris 16, April-May 1957.

BIBLIOGRAPHY (Continued)

Pritchard, F. E., et al., 1965, "Spectral and Exceedance Probability Models of Atmospheric Turbulence for Use in Aircraft Design and Operation," AF Flight Dynamics Laboratory, Research and Technology Division, Air Force Systems Command, Wright-Patterson Air Force Base, Ohio, November 1965.

Reed, Wilmer H., III, 1964, "Models for Obtaining Effects of Ground Winds on Space Vehicles Errected on the Launch Pad," NASA - Langley Research Center, presented at Conference on Role of Simulation in Space Technology, Blacksburg, Virginia, August 17-21, 1964.

Reed, Thomas, C., 1965, "Ground Winds and Space Vehicles," Astronautics and Aeronautics, December 1965.

Scoggins, J. R., W. W. Vaughan and O. E. Smith, 1960, "Low Level Wind Profiles Applicable in the Study of Vertically Rising Vehicle Performance between 3 Meters and 120 Meters, Cape Canaveral (Atlantic Missile Range), Florida," NASA MTP-AERO-60-23, George C. Marshall Space Flight Center, December 29, 1960.

Scoggins, J. R., O. E. Smith and W. W. Vaughan, 1962, "Role of Applied Meteorology in the Development of Large Space Vehicles," NASA - Marshall Space Flight Center. Presented at Fourth AMS Conference on Applied Meteorology, Hampton Virginia, September 10-14, 1962.

Sissenwine, N. and H. G. Kasten, Co-Chairman, 1962. Proceedings of the National Symposium on Winds for Aerospace Vehicle Design, Air Force Survey in Geophysics, No. 140, AFCRL-62-273(I), March 1962.

Smith, J. W. and O. E. Smith, 1961, "Surface Wind Statistics for Patrick AFB (Cape Canaveral), Florida," NASA - Marshall Space Flight Center, MTP-AERO-61-78, Huntsville, Alabama, October 1961.

Sutton, O. G., 1953, Micrometeorology, McGraw-Hill Book Company, Inc., New York.

Valley, Shea L., 1965, Handbook of Geophysics and Space Environments, Air Force Cambridge Research Laboratories, Bedford, Mass.

Webl, E. K., 1955, "Autocorrelations and Spectra of Atmospheric Turbulence," C.S.I.R.O. Div. Met. Phys., Tech. Paper No. 5, Melbourne.

SOME PRACTICAL CONSIDERATIONS INVOLVED IN ESTABLISHING CRITERIA

1. OPERATIONAL CONDITIONS (LOCATION, UTILITY, ETC.) OF STRUCTURE
2. ACCEPTABLE RISK LEVEL - DESIRED LIFETIME
3. RELATIVE UNCERTAINTIES IN OTHER DESIGN INPUTS AND ANALYTICAL PROCEDURES
4. ABILITY OF DESIGN PROCEDURE TO ACCEPT WIND CRITERIA MODELS
5. DESIGN DATA REFERENCE PERIOD
6. AVAILABLE BASIC WIND STATISTICS
7. PHYSICAL REPRESENTATIVENESS OF MODEL(S)
8. WIND CRITERIA - INTEGRAL OR SEPARATE PART OF DESIGN PICTURE
9. RESEARCH VERSUS PROJECT REQUIREMENTS
10. COMPOUNDING OF SAFETY FACTORS
11. STRUCTURAL CHARACTERISTICS OF VEHICLE
12. CONSEQUENCE OF A FAILURE

FIGURE 1

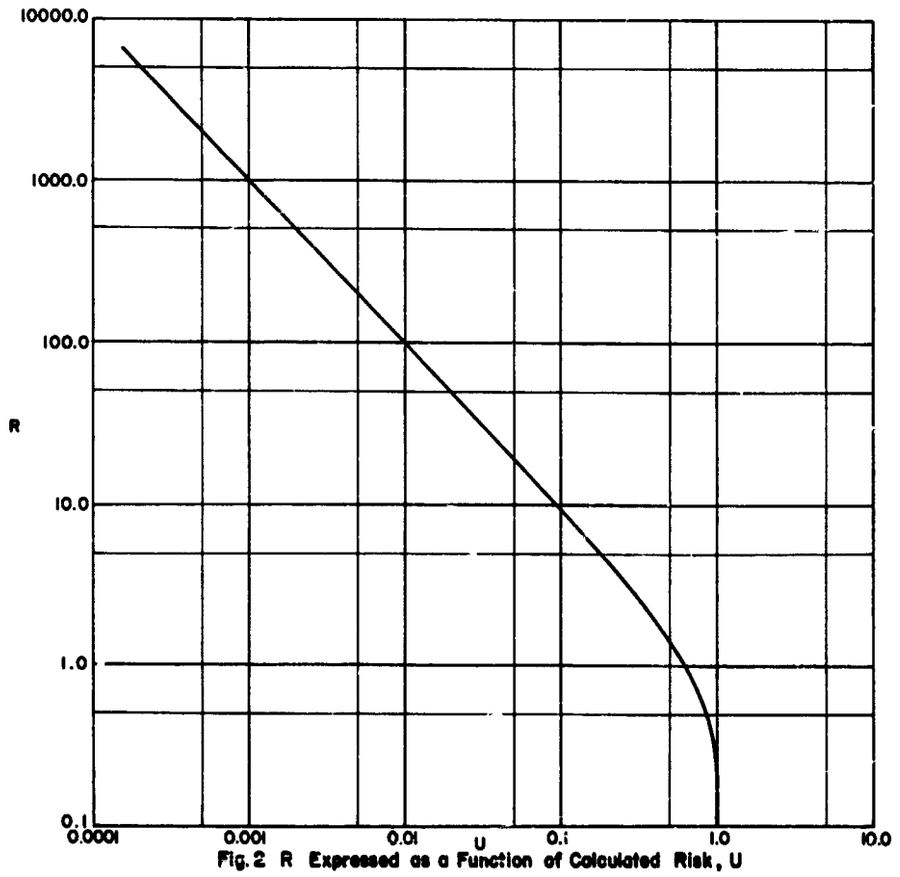

Fig. 2 R Expressed as a Function of Calculated Risk, U

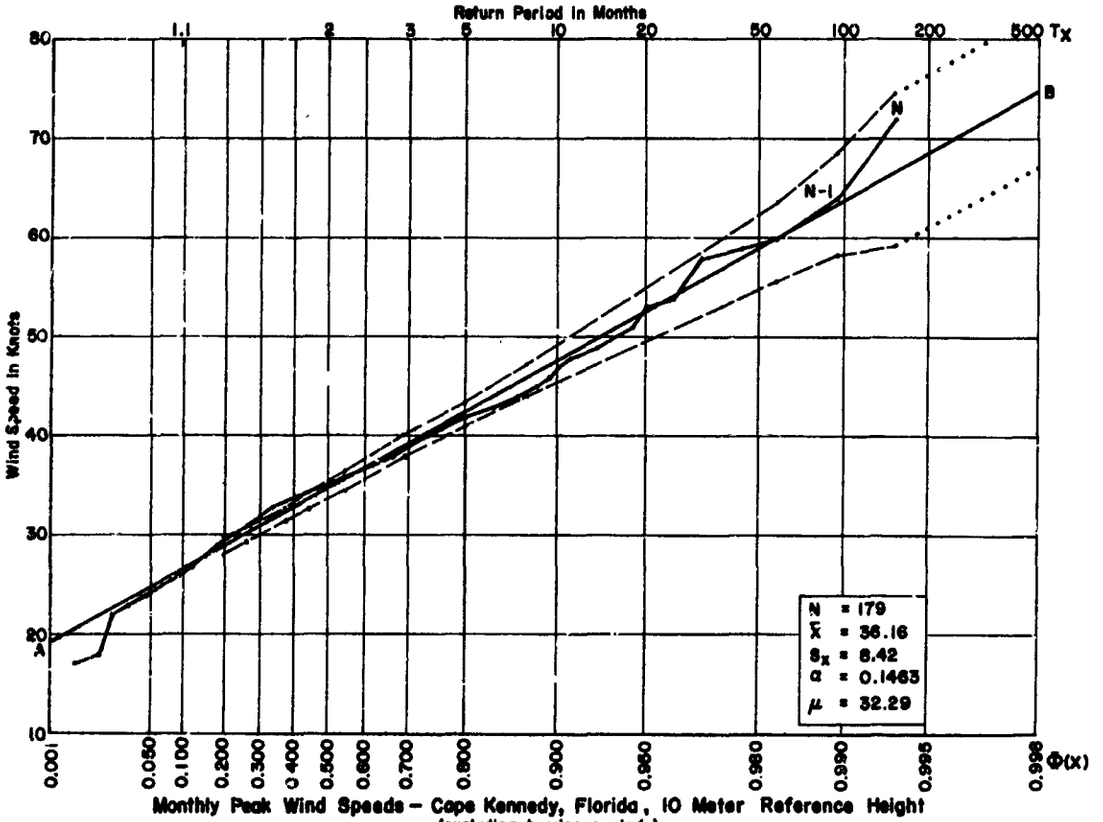

Monthly Peak Wind Speeds – Cape Kennedy, Florida, 10 Meter Reference Height
(excluding hurricane winds)
Fig. 3

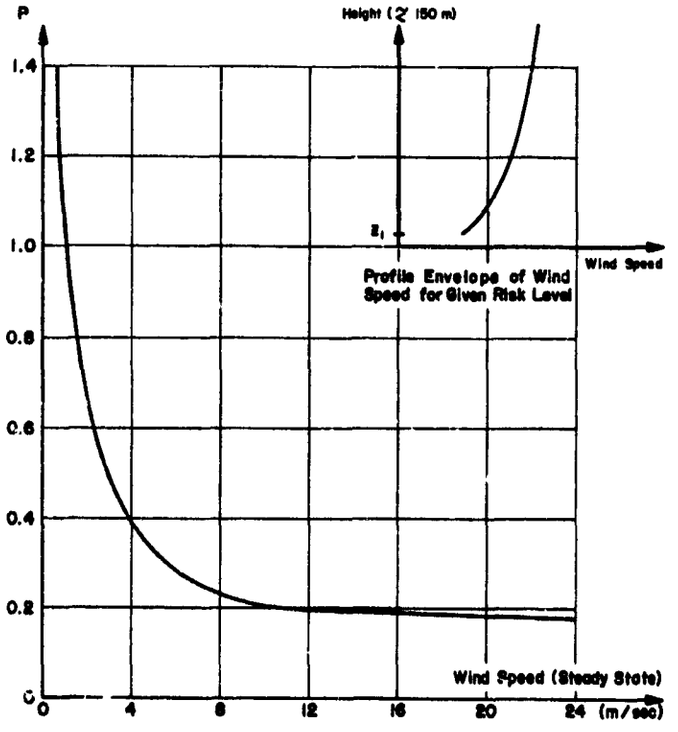

Variation of P with Wind Speed (Steady State) at Reference Level Z_1
Fig. 4

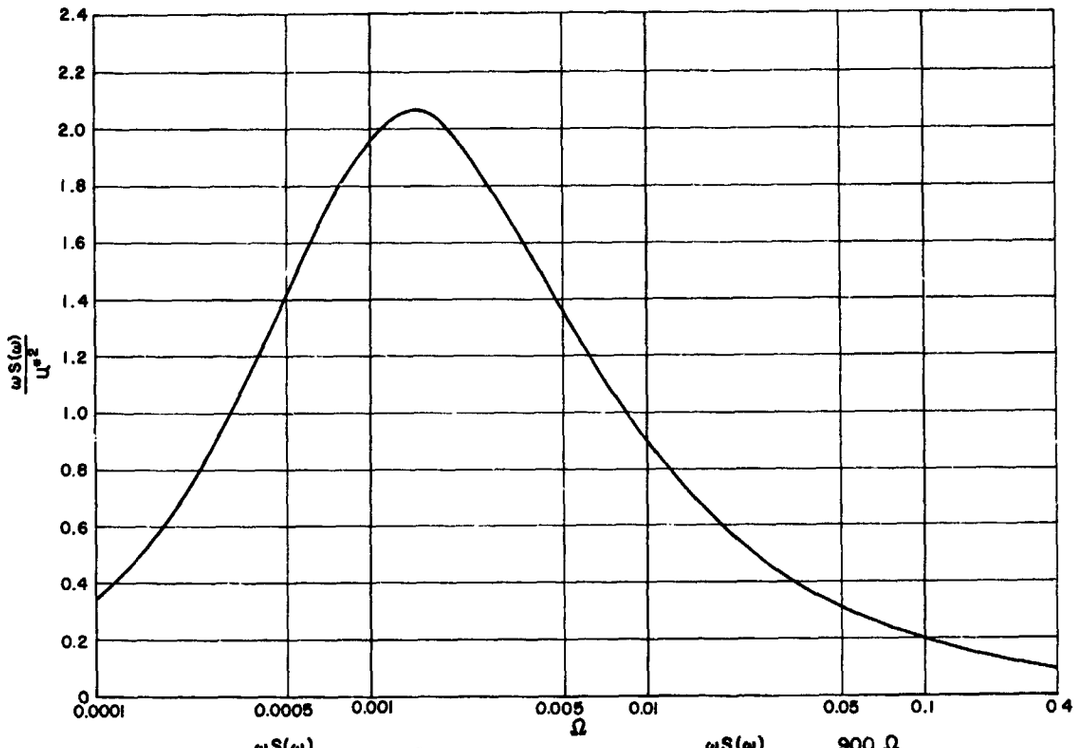

Fig. 5 $\frac{\omega S(\omega)}{u^{*2}}$ versus Ω According to the Equation $\frac{\omega S(\omega)}{u^{*2}} = 4\,\frac{900\,\Omega}{1+(900\,\Omega)^{5/3}}$

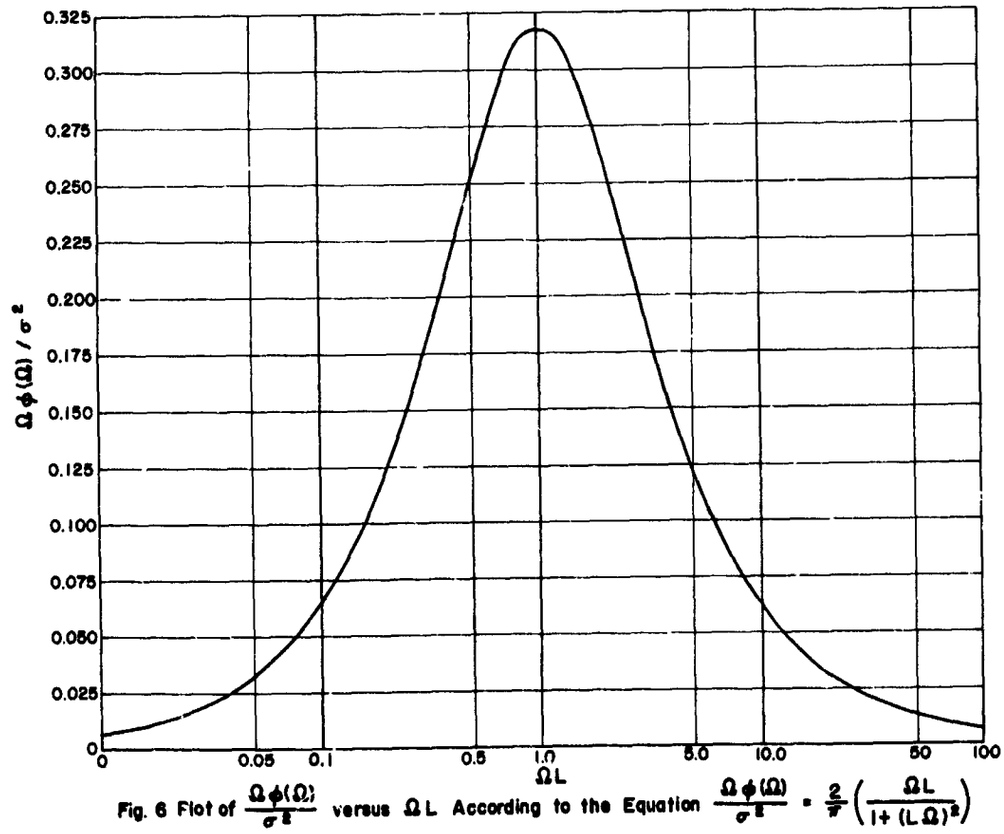

Fig. 6 Plot of $\frac{\Omega\phi(\Omega)}{\sigma^2}$ versus ΩL According to the Equation $\frac{\Omega\phi(\Omega)}{\sigma^2} = \frac{2}{\pi}\left(\frac{\Omega L}{1+(L\Omega)^2}\right)$

GROUND WIND MEASUREMENTS AND ANEMOMETER RESPONSE

By

James R. Scoggins

Aerospace Environment Division
Aero-Astrodynamics Laboratory
NASA - Marshall Space Flight Center
Huntsville, Alabama
June 2, 1966

ABSTRACT

The theoretical response of inertia-type anemometers is presented. The determination of response parameters using theory and wind tunnel data is explained and examples given. A comparison of simultaneous anemometer measurements in a real wind environment is made from which inferences are drawn regarding the validity of response parameters determined in a wind tunnel. Finally, the ground (Sfc. to 150 m) wind measurement program being conducted at the Eastern Test Range is discussed, and some practical problems in measuring ground winds outlined.

(For presentation at the June 7-8, 1966, meeting on Current Wind Load Problems in Relation to Launch Vehicles at Langley Research Center.)

GROUND WIND MEASUREMENTS AND ANEMOMETER RESPONSE

By

James R. Scoggins

Aerospace Environment Division
Aero-Astrodynamics Laboratory
NASA - Marshall Space Flight Center
Huntsville, Alabama

June 2, 1966

SECTION I. INTRODUCTION

The measurement of wind speeds in a turbulent environment can be quite difficult depending upon the accuracy and resolution required. Reasonably accurate measurements of wind speeds averaged over time periods in excess of approximately one minute are easy to make. Such measurements are made routinely by government weather services and other organizations throughout the world. These measurements are considered adequate for general meteorological uses where gust structure is not considered important. The time averaging filters out the gust structure regardless of how faithfully it may be reproduced by the instrument itself.

The accuracy and frequency resolution of wind measurements is determined by the response characteristics of the anemometer system. When measuring winds averaged over a few tens of seconds or longer, most conventional type anemometers probably provide adequate measurements (see Section IV); however, if measurements of the gust structure are desired, conventional anemometers are, in general, not adequate (see Sections II-IV).

The correct interpretation of measurements obtained by any anemometer is, in general, quite difficult but absolutely necessary if one is to draw correct conclusions. Think of how many "scientists" have drawn conclusions from data they

themselves didn't understand!

It is the intent of this paper to review response theory as usually applied to inertia-type anemometers, present results obtained in wind tunnels and in the free atmosphere, describe the measurement program for ground winds at KSC, and discuss some practical problems in measuring ground winds in general. The ultimate intent of this paper is to improve the overall understanding of measured ground winds, their interpretation, and to improve the understanding of the characteristics of anemometers commonly used to measure winds.

SECTION II. ANEMOMETER RESPONSE THEORY

The response of an anemometer is usually determined by assuming a linear relationship between input and output. This implies the relationship $O(t) = kI(t)$ where $O(t)$ is the output, $I(t)$ is the input, both a function of time, and k is constant for all time. In the general case, this relationship assumes the form of an ordinary linear differential equation of the form (Ferris 1962)

$$\sum_{k=0}^{n} A_k \frac{d^k}{dt^k} O(t) = I(t) \qquad (1)$$

where the coefficients A_k are constant, and $I(t)$ is the forcing function. Equation 1 is a linear differential equation; however, $I(t)$ may contain non-linear terms.

There are very few physical processes which are truly linear and, therefore, may be accurately represented by equation 1. Why, then, is linearity so often

assumed? In most cases, the primary reason is that the equations can be solved in closed form and well-defined and interpretable results obtained. The justification for assuming a linear system is that the solution approximates the true solution over a limited range of the variable. The range over which the solution is approximately valid depends upon the degree of nonlinearity of the system. A system is nonlinear if the A_k's are a function of $O(t)$ or if the derivatives in equation 1 are raised to a power greater than one.

The observed response of inertia-type anemometers may be approximated mathematically by the first order linear differential equation (MacCready and Jex 1963)

$$\dot{U} + \left(\frac{1}{T}\right) U = I(t) \qquad (2)$$

where U represents wind speed, I(t) the forcing function, and T the response time. This equation is a special form of equation 1 with 1/T replacing the ratio A_1/A_0. The solution of equation 2, where I(t) represents a step input function, is

$$U = \Delta U(1 - e^{-t/T}) \qquad (3)$$

where ΔU is the magnitude of the step input. From equation 3 it is obvious that the response time is the time required for the variable to reach 63% of the final value of the step function. For example, if an anemometer experiences a sudden increase in wind speed of 5 m/sec, 63% of this sudden increase of wind will be indicated by the anemometer in a time equal to T. Obviously, the smaller T, the quicker the response of the anemometer. Now, if we define a response distance by the equation

$$L = U_o T \qquad (4)$$

where U_o is the steady-state wind speed and L is the response distance, and letting X be the distance of wind flow past the anemometer given

$$X = U_o t \tag{5}$$

then by substitution of equations 4 and 5, into equation 3 gives

$$U = \Delta U \left(1 - e^{-\frac{X}{L}}\right) \tag{6}$$

The parameters T and L may be used to define the response characteristics of an anemometer to a step input. The distance constant L is usually employed rather than T; the smaller the distance constant, the more rapid the response of the anemometer. From equations 3 or 6 we see that the wind speed as indicated by the anemometer approaches the true wind speed exponentially in time. During the time period equal to the response time the anemometer will indicate 63% of the final value; during the next response time it will indicate 63% of the remaining difference, etc. A graphical solution of equations 3 and 6 is shown in Figure 1.

A more realistic assumption regarding the forcing function, yet still grossly inadequate, is to assume

$$I(t) = C \sin \omega t \tag{7}$$

where C is the amplitude of the sinusoidal input. The solution of equation 2 for this case is given by

$$U = C \left[\frac{1}{(1 + \omega^2 T^2)^{\frac{1}{2}}}\right] \sin (\omega t + \varphi) \tag{8}$$

in terms of time, and by

$$U = C\left[\frac{1}{\left(1 + \frac{\omega^2 L^2}{U^2}\right)^{\frac{1}{2}}}\right] \sin\left(\frac{a\omega}{U} + \varphi\right) \qquad (9)$$

in terms of distance. In equations 8 and 9, φ represents the phase angle, ω is circular frequency and is given by $2\pi f$, where f is frequency in cycles per second, and the terms in brackets represent the amplitude ratio of the output to input. These equations show that the output differs from the input only by phase and a change in amplitude. A plot of the amplitude ratio in either equation 8 or 9 as a function of frequency is called the response function or transfer function of the anemometer. It tells what percentage of the amplitude as a function of frequency is measured by the system. A schematic representation of the transfer function and the phase angle is shown in Figure 2. It must be kept in mind that the solutions of the equations shown in Figures 1 and 2 are highly idealized by the assumption of linearity.

The mathematical treatment given above does not consider electronic filtering problems associated with most anemometers. Even if, say, a cup-type anemometer is determined to have a certain response capability defined by equation 2, its effective response may be much less because of signal conditioning and inadequate response of the data recording mechanism. Also, aerodynamics associated with the flow of air around the cups or the housing may produce additional uncertainties. Thus, the response of the system must be considered in the interpretation of data and not just the response of the sensor alone. Camp (1965) gives a discussion regarding the effects of filtering on measured wind data.

In the mathematical treatment of wind sensors given above, only wind speed sensors were considered. For wind direction sensors (vanes) a second order equation is required to represent the system mathematically. For purposes of this paper it is sufficient to say that the solution to the second order differential equation is in the form of exponentials. For those interested in the response of vanes, additional information may be found in reports by Camp (1965), Adams (1954), and Mazzarella (1954).

A number of anemometers, which will not be discussed in detail in this paper, are available but are not in general use. These include sonics, hot wires, drag spheres, vector vanes, etc. An attempt was made to perform comparison tests (see Section IV) using these anemometers, but because of calibration, threshold speeds, drifts in calibration, head vibration of sonics, and other similar problems, it has not been possible to date to get satisfactory results. In general, these so-called faster response anemometers require constant personal attention during the period of operation and, even then, the accuracy and quality of the data are not adequately known.

SECTION III. WIND TUNNEL RESULTS OF ANEMOMETER RESPONSE

Camp (1965) investigated the response of the Beckman and Whitley Series 50 and the Climet Model C1-14 anemometers in the White Sands Missile Range wind tunnel. Both of these anemometers are cup types. The Beckman and Whitley Series 50 employs six cups and is referred to as the "staggered six," while the Climet instrument employs only three cups.

The procedure for determining the distance constant in a wind tunnel for an anemometer is to prevent the cups from rotating in the presence of a steady-state flow, then release the cups suddenly and note the acceleration. The

position of the cups at the moment of release, especially for three-cup anemometers, influences the value of the response parameters determined. The initial cup orientation used by Camp in his work is shown in Figure 3. Figures 4 and 5 show typical wind speed traces at wind speeds of 4.47 and 8.94 meters per second, respectively, obtained in the wind tunnel. The time constant is obtained by noting the time required for the anemometer to indicate 63% of the wind tunnel speed if one starts counting at the initial moment of release. The time constant may also be obtained by starting at any arbitrary point and determining the length of time required for the anemometer to indicate 63% of the remaining difference between the indicated velocity and the tunnel velocity. Thus, one can obtain several estimates of the time constant for an anemometer for a given wind tunnel run.

Table I shows results taken from Camp's report for the Beckman and Whitley Series 50 and Climet Model C1-14 for three wind tunnel speeds, 4.47, 8.94, and 13.41 meters per second. As indicated in the table, a number of wind tunnel runs were made to establish the distance constant for each speed category. The results obtained are believed to be highly accurate for the stated conditions of the tests and the filters used to condition the output signal. In all cases the Climet Model C1-14 three-cup anemometer had a smaller distance constant than did the Beckman and Whitley Series 50 six-cup anemometer. This means the Climet instrument has a faster response than the Beckman and Whitley Series 50 and, therefore, if nonlinearities are insignificant this may be interpreted as meaning that the Climet has a better frequency response resolution than does the Beckman and Whitley Series 50. However, for a different initial cup orientation for the Climet instrument the response distance may be somewhat larger.

Frequency response curves for the Climet wind sensor are shown in Figure 6 for the three wind speeds employed in the wind tunnel tests. Similar curves could be drawn for the Beckman and Whitley Series 50. As shown in the figure, frequencies up to about 3 cps can be measured with reasonable amplitude resolution during high wind speed conditions. Even during low wind speed conditions (4.47 m/sec), one cps can be measured reasonably well. These are highly idealized results which must not be taken to represent the true response characteristics of the anemometer (see Section IV).

One of the most difficult problems to solve when acquiring high resolution output from the cup anemometers discussed in this report is that of signal conditioning. The output from these anemometers is in the form of pulses. The Beckman and Whitley Series 50 gives forty pulses per revolution, while the Climet instrument gives 100 pulses per revolution. It turns out that the filtering problem is easier to handle and produces better results for the higher pulse rate. Referring to Figure 4, it may be seen that the Beckman and Whitley Series 50 trace contains rather large amplitudes associated with each pulse and these are superimposed on the average change of wind speed as a function of time. The trace from the Climet instrument also contains superimposed small amplitude oscillations; however, the amplitude is much smaller and of a higher frequency than for the Beckman and Whitley instrument. The Beckman and Whitley output signal had to be filtered more in order to reduce the amplitudes of the high frequency ripple to within acceptable limits, whereas the output from the Climet instrument could be filtered less and still achieve acceptable results. In principle, the six-cup anemometer should have a shorter distance constant than the three-cup anemometer if one considers only the sensor

response, but when one considers the system response the three-cup anemometer, in this case at least, has the best response.

The turbulence level in wind tunnels is usually very low compared to the atmosphere. The extent of variation in drag on the anemometer cups caused by turbulent flow is not known; however, it is known from space vehicle wind tunnel tests that the turbulence level does influence the vortex shedding and thereby changes the response of the vehicle to winds. It is reasonable to expect that a similar phenomenon occurs in relation to cup-type anemometers. Thus, the distance constants determined in wind tunnel tests may not be directly applicable to measurements made in the free atmosphere. This subject is considered further in Section IV.

SECTION IV. COMPARISON OF ANEMOMETERS IN THE REAL ENVIRONMENT

The theoretical response of anemometers was developed in Section II and applied in Section III above using wind tunnel results to establish the response characteristics of two anemometer systems. As pointed out in Section II, the theoretical results may not be applicable in the real atmosphere because of non-linearities. Applicability of theoretical and wind tunnel results was investigated by exposing several anemometers simultaneously to the real environment, then analyzing the results on a comparative basis. This section presents the results of those studies.

Four commonly used anemometers, the Beckman and Whitley Series 50 and Series 101, the Climet Model CI-14, and the Aerovane, were mounted on a crossarm perpendicular to the wind direction (Camp 1966). Time correlated measurements from all anemometers were recorded on magnetic tape simultaneously. When facing into

the wind, the anemometers were oriented on the crossarm in the following order reading from left to right: B&W Series 50, B&W Series 101, Aerovane, and Climet. These sensors were located approximately three feet apart. In order to eliminate a possible bias due to the separation of the instruments, only statistics of the measured wind speeds were analyzed.

Table II, taken from Camp's report, summarizes the statistical results from five anemometer comparison tests. Presented in the table are mean wind speeds for each anemometer, the variances about the mean, and the percent of the total variance for periods equal to or greater than five seconds. The means and variances were computed for a five-minute time period. Considering tests 1, 2, and 3, the mean wind speeds differed by as much as 25 percent while the variances differed by more than 50 percent. Variances associated with the Aerovane measurements are smaller than those associated with measurements of the other anemometers. This was expected since the Aerovane has a slower response than the other anemometers. However, one would not expect, based on the theoretical and wind tunnel results presented in Sections I and II, the Beckman and Whitley and Climet anemometers to provide significantly different results. Three cups were used with the Beckman and Whitley Series 50 for these tests since the staggered-six cup assembly was not available. This may have had some influence on the values obtained for this anemometer. Results from tests 4 and 5 presented in Table II compare the Aerovane with Meteorology Research, Inc.'s (MRI) Velocity Vane. As shown in the table, there is no significant difference between these two anemometers.

Spectrum techniques were employed to examine the distribution of the total variance over frequency in an effort to account for the large differences in

variances, and also to compare the results with theoretical and wind tunnel results presented above. Spectra associated with the five tests presented in Table II are shown in Figure 7. Aliasing was not considered and trend, if any was present, was not removed. These spectra must be considered tentative until more comprehensive results are available.

In test 1 the spectra are quite different over all frequencies, but in all other tests rather good agreement is shown for all frequencies. However, there is a divergence in the curves for periods greater than 5 to 10 seconds with no noticeable consistency in tests 1 through 3. The normalized spectra were integrated to obtain the percent of variance accounted for by periods 5 seconds and longer. These results are presented in Table II. Tests 4 and 5 are quite consistent and not very different over all frequencies. With the exception of the aerovane, which filters out the higher frequencies rather effectively, differences in the measured variances are distributed over all frequencies rather than being confined to a particular region of the spectrum. This implies that gusts with periods of several seconds or longer may not be measured accurately. The spectrum curves were drawn by eye to best represent the calculated spectral estimates. A considerable amount of smoothing was done, and if even more had been done, significant differences in the spectra would still have resulted. Another important conclusion which can be reached from these spectra is that the theoretical and wind tunnel results presented in Sections II and III above are not verified for the real environment. According to Figure 6, the Beckman and Whitley and Climet instruments should be capable of measuring gusts with periods on the order of one second or less with a reasonable amplitude resolution. Thus, the logical conclusion seems to be that nonlinearities occur which are not accounted for by the theory.

Results from tests 4 and 5 show that the Aerovane and the MRI velocity vane have very similar characteristics, measuring the same winds and variances, and have the same statistical distribution of the variances over frequency. From the results presented here, it does not appear that the higher frequencies (periods less than about 5 seconds) can be measured with confidence using any of the anemometers tested.

SECTION V. THE MEASUREMENT OF LOW ALTITUDE (SURFACE TO 150 METERS) WIND AT THE KENNEDY SPACE CENTER (KSC)

There exists a need for improved low altitude wind measurements at KSC for use in such programs as the response of space vehicles to ground winds, atmospheric diffusion, launch operations, vehicle design studies, etc. Most wind measurements collected to date have been made at a single location near the ground or on structures with poor exposure. None of these measurements have provided adequate details of the gust structure. A 500-foot (150 meters) meteorological tower has been built by NASA at Kennedy Space Center for the purpose of measuring low altitude winds for use in various programs. Figure 8 shows a schematic of the tower facility and the location of wind, temperature, and humidity sensors. The tower facility is located on Merritt Island approximately 3 miles from launch complex 39 and about the same distance from the coastline.

The main tower is triangular in shape, eight feet on a side, and contains instrumentation as shown in Figure 8. A small tower is located 18 meters to the northeast of the major tower for collecting data near the ground where the exposure on the big tower is poor. Anemometers are dual mounted on the northeast and southwest side of the big tower on twelve foot booms, but only on the

northeast side of the small tower. Humidity measurements are made at two locations, 3 and 120 meters. The absolute value of temperatures is measured at the three-meter level with temperature differences being measured between 3 and 18 meters on both the large and small towers, 3 and 60, 3 and 120, and 3 and 150 meters. The temperature nor humidity elements are dual mounted.

Paper strip chart recorders are used to record all wind, temperature, and humidity data inside a building located near the base of the tower. In addition, a 14 channel magnetic tape can be used to record wind data with high resolution and accuracy. Wind data are recorded from either the northeast or southwest side of the tower at all levels, but not from both sides simultaneously. An automatic switching device is included in the facility for selecting the best exposed bank of instruments. The tape recorder may be used automatically to record wind data once each hour or at other predetermined time periods, or it may be operated in a manual mode for collecting data upon command. The magnetic tape is used only to collect data for gust and turbulence studies.

The humidity is measured by the Foxboro dewcell, temperature by Climet aspirated thermocouples, and wind by the Beckman and Whitley Series 50 staggered six anemometer. Because of the undesirable filtering problems associated with the Beckman and Whitley Series 50 (see Section III) and maintenance difficulties which have been experienced since the tower became semi-operational the latter part of 1965, it is now planned to install Climet Model C1-14 anemometers within the next few weeks. When this change is made and the tape recorder checked out, the tower facility will be considered fully operational.

SECTION VI. SOME PRACTICAL PROBLEMS IN MEASURING SURFACE WINDS

Accurate high resolution wind measurements are difficult to make and, as pointed out above, the commonly used anemometers are not adequate for this purpose. When such measurements are attempted, there are several problem areas which must be considered. Some of these are discussed in this section, but there will no doubt be many others associated with specific installations.

One of the first problems which must be considered in the measurement of low altitude winds is that of establishing the need for and applications of the wind measurements. If one needs only five-minute averaged winds, the instrumentation required may be different, and in some cases much simpler, from the instrumentation required for measuring high frequency fluctuations. Also, data recording requirements may be a function of the intended application of the measurements. The next problem is the selection and testing of instrumentation. It is important to select a reliable instrument with the desired operational characteristics. The importance of experimentally evaluating the instrumentation is quite clear from the results presented above.

Regardless of how good the sensor responds to the wind, the degree of signal conditioning (filtering) required to eliminate undesirable output signals is of primary importance. The output signal from most anemometers is in the form of pulses and must be smoothed or filtered in order to get an output which can be properly interpreted. As pointed out in Section III, the effectiveness of the electronic filters is a function of the pulse rate. For a low pulse rate a high degree of filtering may be required to eliminate undesirable output signals (see Figure 4). A high degree of filtering may eliminate signals

representing wind variations, especially the higher frequencies. Also related to the signal conditioning (filtering) problem is that of adequate data recording facilities. The accuracy and resolution of the data recording equipment should be slightly better than any other component of the system. Paper strip chart recorders commonly used have some maximum frequency response beyond which they are incapable of recording fluctuations in the output signal. In most cases, these recorders act as a filter for high frequency signal variations and, therefore, may in effect reduce the capability of the anemometer system even though the sensor may have a far greater frequency response. This leads into perhaps the most important problem of all - the total system response characteristics. The old addage that, "A chain is no stronger than its weakest link," might be paraphrased to, "The response of an anemometer system is no better than the response of any one of its components."

The last problem area discussed here is that of instrument exposure. While this had nothing to do with the capability of the instrumentation itself, it does influence the validity of the measurements Because of structure interference, a dual system of anemometers was mounted on NASA's 150-m meteorological tower at KSC (see Section V). With two sets of instrumentation, it is possible to eliminate some of the structure interference by recording wind data from the best exposed bank of anemometers; however, the problem is still not completely eliminated. Another important consideration in the exposure of anemometers is the interference due to the surrounding area. If instruments are mounted in the vicinity of man-made structures or in the wake of natural obstacles, the measured wind conditions would not be representative of the free atmosphere. The exposure problem is quite important when considering the response of space vehicles to winds.

In this case, a free atmosphere exposure may not be the most desirable since there are usually structures located in the vicinity of the vehicle.

SECTION VII. COMMENTS AND CONCLUSIONS

The response characteristics of anemometers determined from wind tunnel results and based on first order response theory are not consistent with results obtained from comparison tests of anemometers made in the real environment. A logical conclusion is that the linear response theory is not adequate or the aerodynamics associated with flow around the cups introduce unsteady torques which produce error in the measured wind speeds. One possible solution to the aerodynamics problem, as suggested recently to several instrument manufacturers, would be to perform flow visualization tests using smoke or some other tracer in a wind tunnel. Such tests might serve to pinpoint aerodynamics problems or cup interference.

There are many problems to consider when designing a wind measuring facility. Briefly stated, some of these are: (1) establish need for and application of wind measurements, (2) selection and testing of instruments (sensors), (3) signal conditioning (filtering), (4) adequacy of data recording equipment, (5) system response characteristics, and (6) instrument exposure (structure interference and surrounding area).

All of the problem areas presented above were carefully considered in the planning and construction of NASA's 150-m meteorological tower at KSC. The primary purpose of this facility is research and development relating to turbulence and, therefore, the measurement of gust structure is of primary importance. Dual anemometer systems were installed, and strip chart recorders and

anemometers are being replaced on the basis of the problem areas noted above. Provisions have been made to install high response anemometers on the tower, which will be done as soon as a high response system is proven to be reliable and accurate. Tower motions may prove to be a problem when high response anemometers are installed. This problem remains to be investigated. With the exception of the high response anemometers, the 150-m meteorological tower facility at KSC should become fully operational during the summer of 1966 and hopefully will be one of the best facilities in the United States.

REFERENCES

1. Adams, Gerald H., 1954: Wind Equipment Evaluation, NBS Report 3316, National Bureau of Standards, Washington, D. C.

2. Camp, Dennis W., 1965: Analysis of Wind Tunnel Data for Several Beckman and Whitley Series 50 and Climet Model C1-14 Anemometers, NASA TM X-53271, NASA, Marshall Space Flight Center, Huntsville, Alabama.

3. Camp, Dennis W., 1966: Preliminary Results of Anemometer Comparison Tests, NASA TM X-53451, NASA, Marshall Space Flight Center, Huntsville, Alabama.

4. Ferris, Clifford D., 1962: Linear Network Theory, Charles E. Merrill Books, Inc., Columbus, Ohio.

5. MacCready, Paul B., Jr., 1963: Response Characteristics and Application Techniques of Some Meteorological Sensors, MRI 63 Pa-86, Meteorology Research, Inc., Altadena, California.

6. Mazzarella, Daniel A., 1954: Wind Tunnel Tests on Seven Aerovanes, Review of Scientific Instruments, Vol. 25, No. 1.

TABLE I

MEAN DISTANCE CONSTANT VALUES FOR THE BECKMAN & WHITLEY SERIES 50 AND CLIMET MODEL C1-14 WIND SPEED SENSORS OBTAINED FROM WIND TUNNEL TESTING OF THE ANEMOMETERS

INSTRUMENTS	TUNNEL WIND SPEED					
	4.47 (m/sec)		8.94 (m/sec)		13.41 (m/sec)	
	Distance Constant (m)	Number of Observations	Distance Constant (m)	Number of Observations	Distance Constant (m)	Number of Observations
Beckman & Whitley Series 50	1.22	42	1.12	35	1.09	38
Climet Model C1-14	0.72	31	0.72	31	0.77	38

TABLE II

STATISTICS FOR FIVE ANEMOMETER COMPARISON TESTS

ANEMOMETERS	MEAN WIND SPEED (M/SEC)	VARIANCE ABOUT MEAN (M^2/SEC^2)	PERCENT VARIANCE FOR P ≥ 5 SEC
		TEST 1	
B&W 50	6.73	1.66	0.89
CLIMET C1-14	7.77	1.14	0.91
B&W 101	7.97	2.26	0.93
AEROVANE	6.16	0.99	0.99
		TEST 2	
B&W 50	3.51	0.89	0.90
CLIMET C1-14	3.31	1.53	0.92
B&W 101	2.94	1.03	0.92
AEROVANE	3.52	0.86	0.98
		TEST 3	
B&W 50	3.88	1.48	0.85
CLIMET C1-14	3.76	2.12	0.87
B&W 101	3.42	1.77	0.86
AEROVANE	3.74	1.38	0.93
		TEST 4	
AEROVANE	4.23	0.79	0.98
MRI VELOCITY VANE	4.67	1.03	0.98
		TEST 5	
AEROVANE	4.28	0.39	0.98
MRI VELOCITY VANE	4.47	0.54	0.97

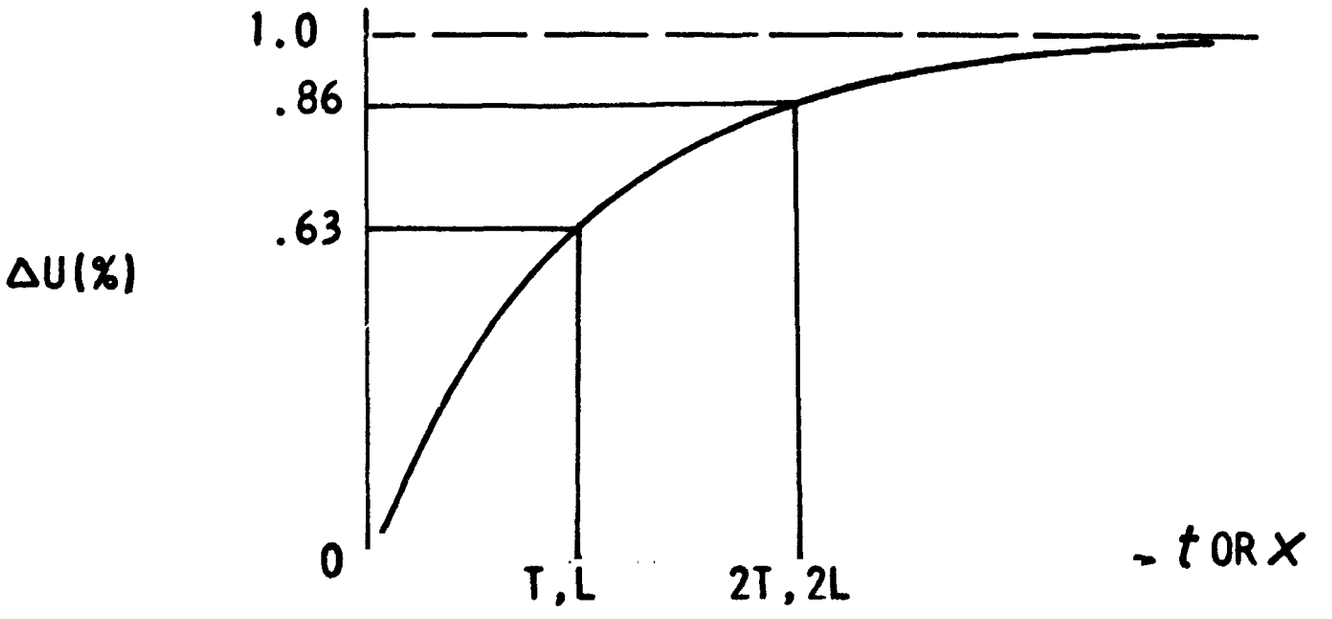

FIRST ORDER RESPONSE TO STEP INPUT

FIGURE 1

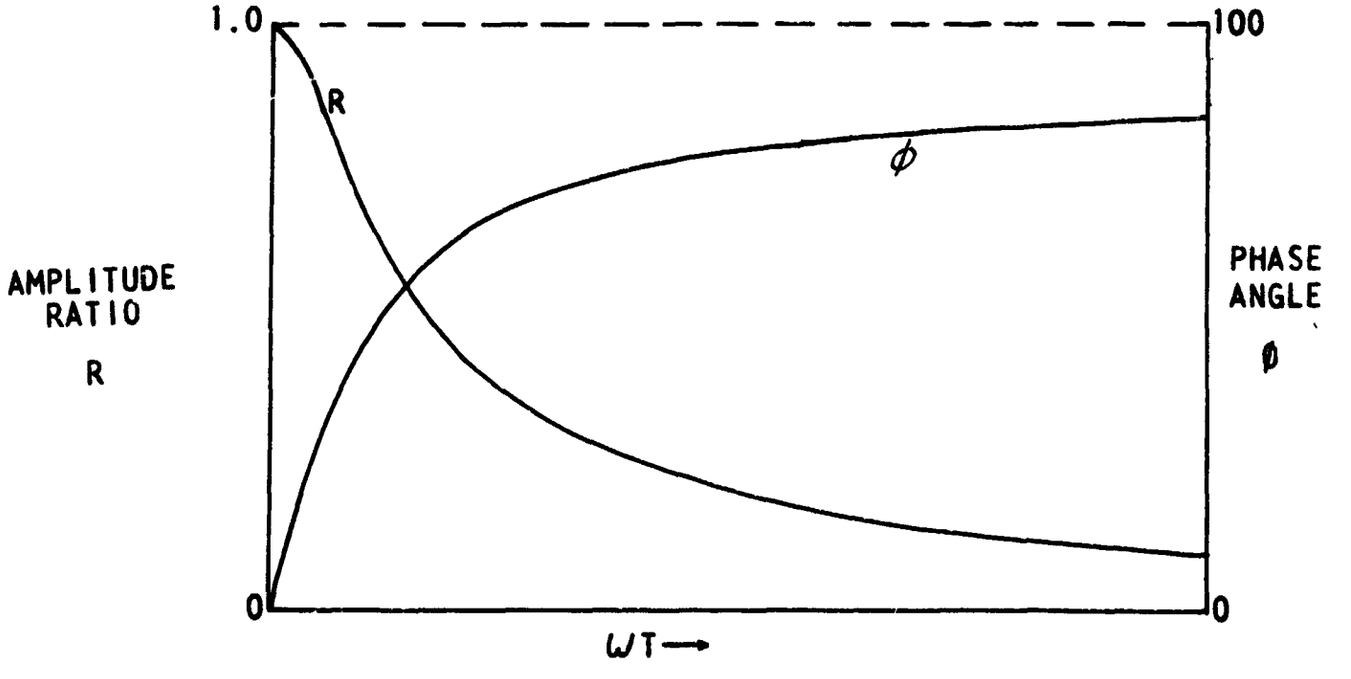

FIRST ORDER RESPONSE TO SINUSOIDAL INPUT

FIGURE 2

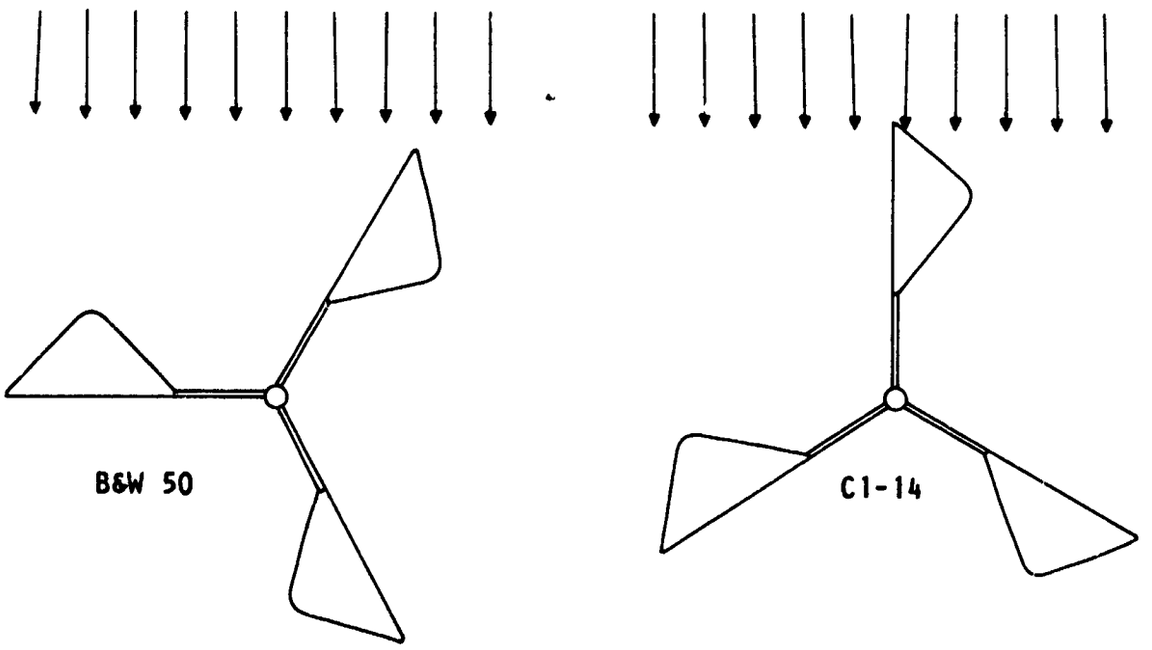

CUP ORIENTATION WITH REFERENCE TO WIND FLOW FOR BECKMAN & WHITLEY SERIES 50 AND CLIMET MODEL C1-14 PRIOR TO RELEASE OF CUPS DURING WIND TUNNEL TESTS

FIGURE 3

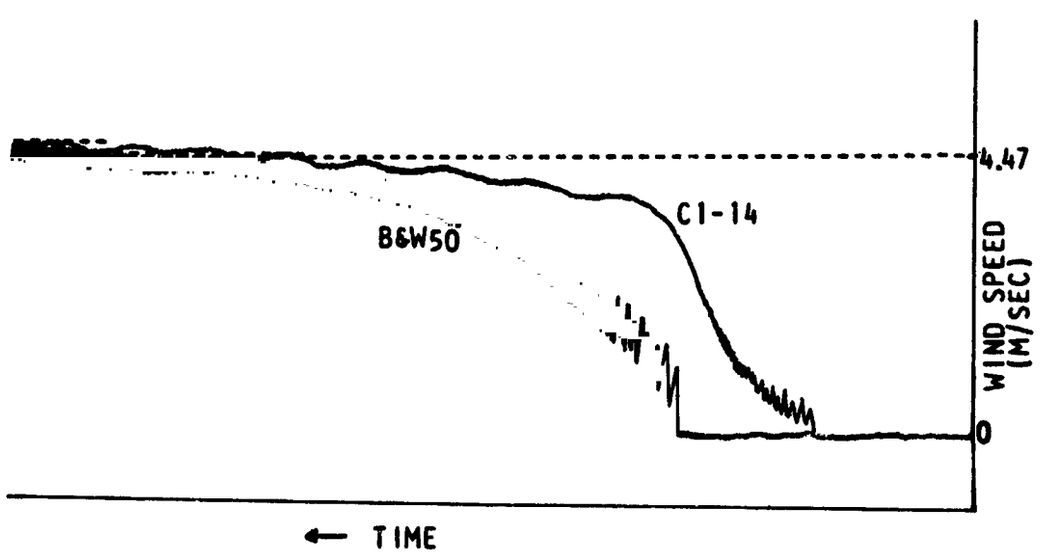

WIND SPEED TRACE FOR BECKMAN & WHITLEY SERIES 50 AND CLIMET MODEL C1-14 FOR A TUNNEL WIND SPEED OF 4.47 M/SEC

FIGURE 4

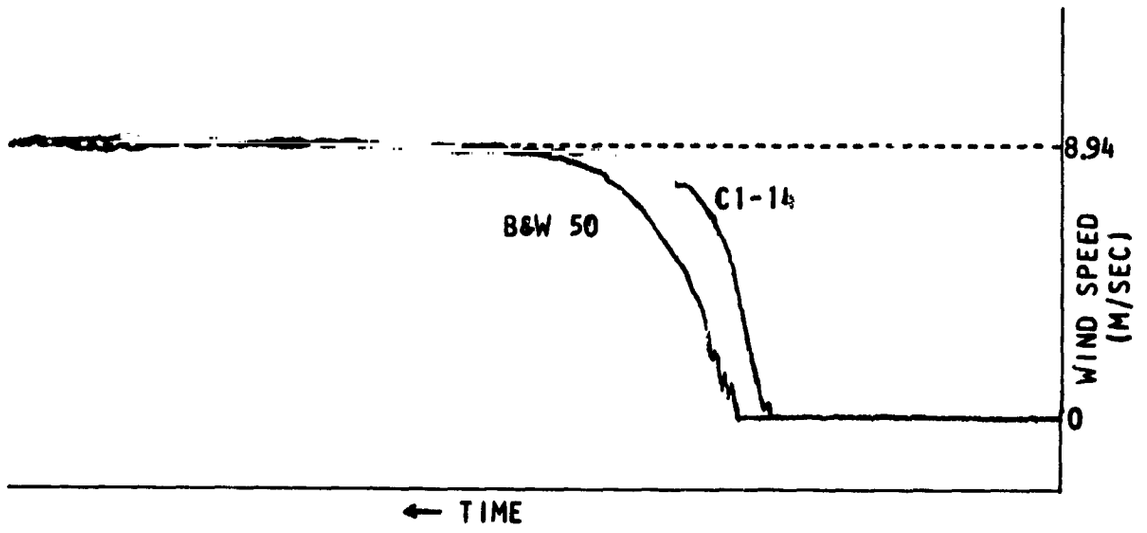

WIND SPEED TRACE FOR BECKMAN & WHITLEY SERIES 50 AND CLIMET MODEL C1-14 FOR A TUNNEL WIND SPEED OF 8.94 M/SEC

FIGURE 5

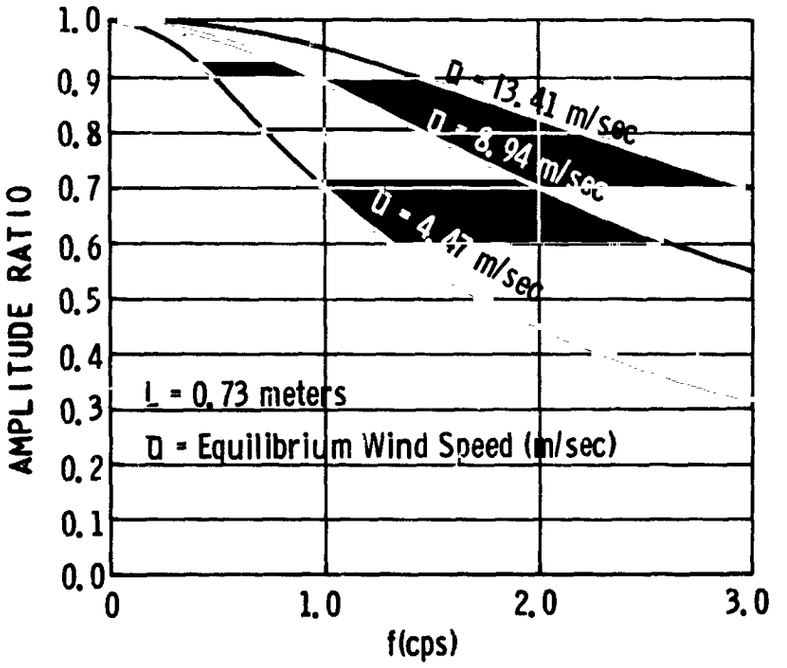

FREQUENCY RESPONSE CURVES FOR THE CLIMET WIND SPEED SENSOR

FIGURE 6

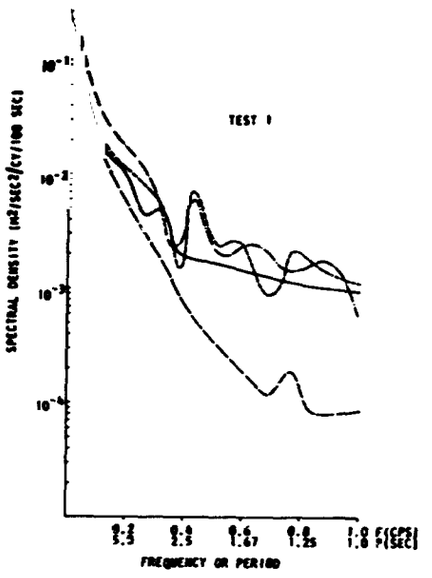

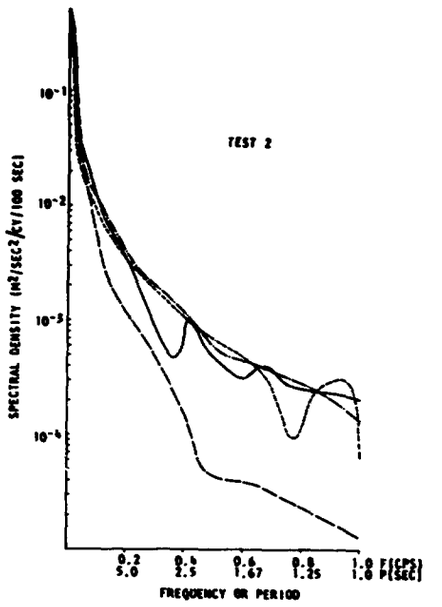

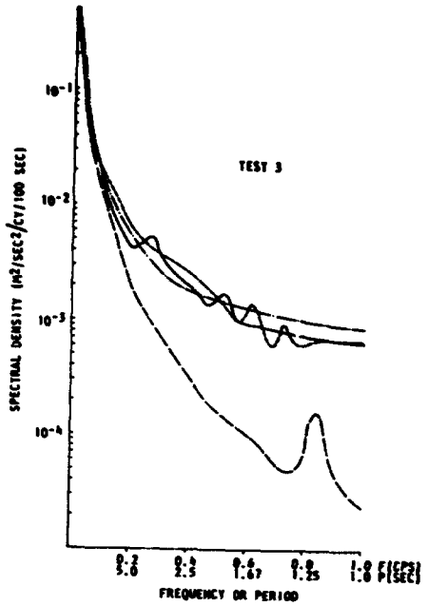

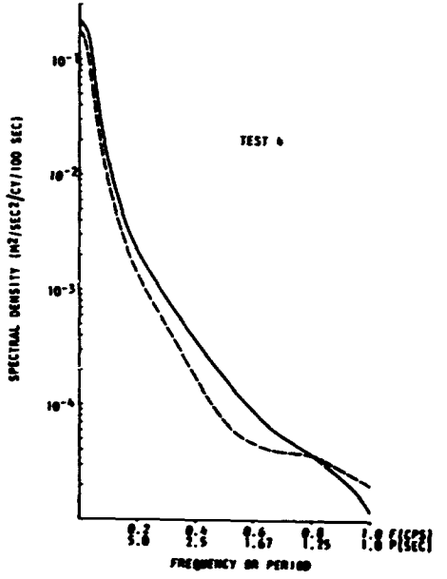

LEGEND FOR TESTS 1, 2 AND 3

CURVE	ANEMOMETER
- - - - -	AEROVANE MODEL 120
----------	BECKMAN & WHITLEY SERIES 50
-·-·-·-	BECKMAN & WHITLEY SERIES 10
———	CLIMET MODEL CI-14

LEGEND FOR TESTS 4 AND 5

CURVE	ANEMOMETER
- - - - -	AEROVANE MODEL 120
———	MRI VELOCITY VANE MODEL 1570

SPECTRA OF WIND SPEEDS FOR ANEMOMETER COMPARISON TESTS

FIGURE 7

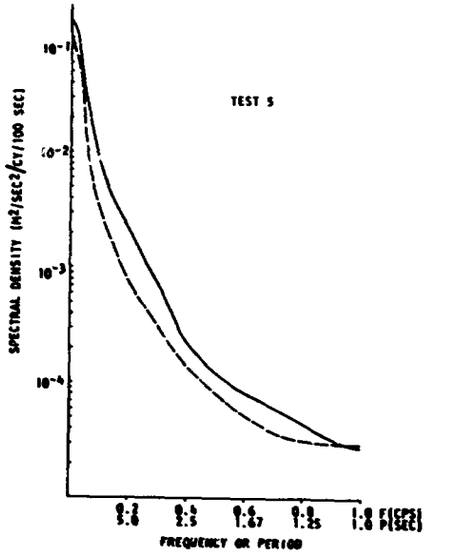

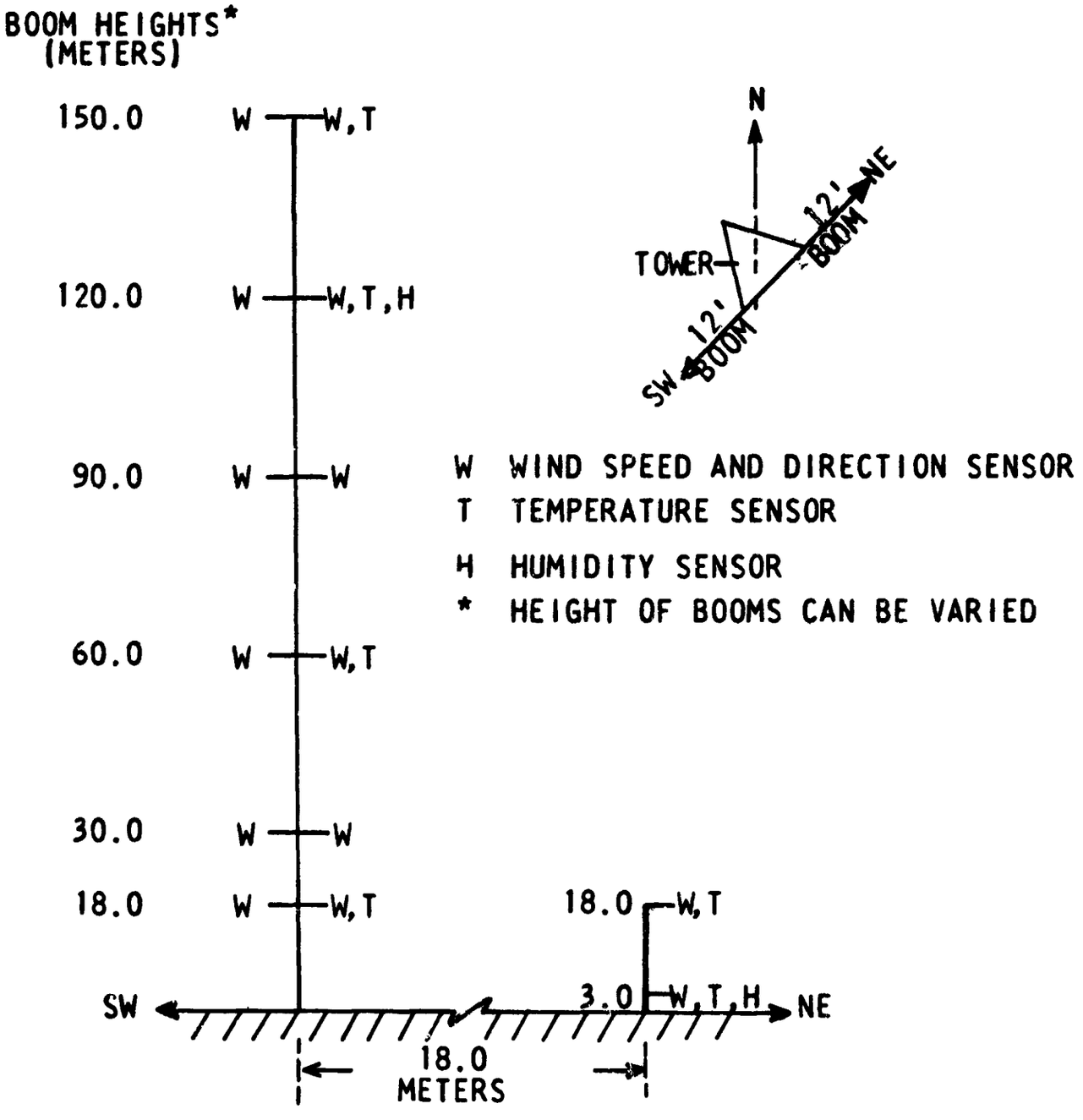

SCHEMATIC OF NASA'S 150-M METEOROLOGICAL TOWER AT CAPE KENNEDY, FLORIDA

FIGURE 8

WIND MEASUREMENTS USING A VERTICAL ARRAY OF FAST RESPONSE ANEMOMETERS

by

Rodney L. Duncan and Jerome T. Foughner, Jr.

National Aeronautics and Space Administration

Langley Research Center

SUMMARY

Orthogonal horizontal wind components are measured using a vertical array of 5 fast response anemometers mounted at vertical separation distances of 50 feet on the Wallops Island 250-foot meteorological tower. The transducer, a drag sphere type anemometer, and the test area are briefly described. Initial data in the form of power spectra up to 5 cps and the coherency between similar components at two measuring stations are presented for the 200 and 250 foot level. The spatial correlation of gusts is discussed in terms of gust loads on launch vehicles. Plans for future work on wind measurements using an additional array of fast response anemometers up to 53 feet and a program to experimentally test the validity of Taylor's hypothesis are described.

INTRODUCTION

An important part of the response of launch vehicles to ground wind loads is the response of the vehicle to turbulence. Initial

dynamic response data for Jupiter and Thor vehicles from the Wallops Island full-scale ground wind loads program are presented in reference 1. A comparison is made between measured full-scale response and predicted response using wind-tunnel vortex shedding response scaled to full-scale conditions added to the calculated response due to turbulence. The agreement is not good and most of the discrepancy is believed to be in the calculated response due to turbulence. For an accurate prediction of gust loads on launch vehicles, information is needed on the statistical properties of low level turbulence. Data on the correlation of gust velocities is particularly of interest. Not only is it important to study the correlation of these random fluctuations of atmospheric wind with time, it is also important to study the correlation of these fluctuations in space. The degree of correlation of turbulent fluctuations of the wind along the length of a vehicle has a significant effect on the response of the vehicle to turbulence.

A program to obtain data on the statistical characteristics of low level turbulence is currently in progress at Wallops Island, Virginia. This paper presents initial data from this program.

SPATIAL CORRELATION OF GUSTS

Unsteady atmospheric winds near the ground are typically as illustrated in figure 1. The profile patterns shown are instantaneous distributions of horizontal wind at different times as a field of turbulence is blown past an erected vehicle. The dashed line represents the mean wind profile while the arrows are rapid

fluctuations of the wind about the mean. These random fluctuations vary in both time and space. Reed in reference 2 has shown that for the fundamental cantilever frequency of Saturn V class vehicles, approximately 0.5 cps, the gust velocities along the length of the vehicle are essentially uncorrelated for separation distances greater than two maximum vehicle diameters. Reference 2 also states that when this degree of uncorrelated gusts is considered, calculations indicate that the response is significantly lower than that calculated assuming perfect correlation of gusts with vehicle length. This is evident in figure 17 of reference 2 part of which is reproduced here as figure 2. Figure 2 presents the calculated power spectral density of the response of a Saturn launch vehicle to the mean wind component of the turbulent fluctuations of the wind. The dynamic deflections have been normalized to the static deflection associated with the mean wind speed. The solid line represents the calculated response assuming perfect correlation of gusts along the length of the structure, and the dashed line refers to the response calculated for the degree of correlation previously described. The area under the dashed curve, the variance, ($\sigma^2 = 0.110$) is less than half that under the solid line ($\sigma^2 = 0.261$). The square root of the area under the curve is the rms level of response; thus, the rms response is reduced by approximately 35 percent when a representative correlation of gust velocities is considered.

Data on the spatial correlation of gusts are available in references 3 and 4 for various vertical separation distances and

at low fluctuation frequencies. Although the fundamental mode frequencies of Saturn V class vehicles are within this low frequency range, there are other vehicles whose frequencies are somewhat higher. Two such vehicl s are the Jupiter and Thor whose unfueled fundamental mode frequencies are 2.2 and 1.7 cps, respectively. The wind measurements discussed in this paper extend this frequency range to 5 cps using fast response drag sphere type anemometers.

DRAG SPHERE ANEMOMETERS AND TEST AREA

A cut-away view of the fast response drag sphere anemometer is shown in figure 3. The instrument consists of a 7-inch-diameter perforated sphere mounted on a two-component force balance that senses two orthogonal horizontal components of the wind. The counterweight shown in figure 3 aids in cancelling the effects of inertia loads. The instrument system is assumed to be capable of accurate measurements of wind fluctuations at frequencies at least as high as 5 cps although a precise dynamic calibration of the system has not been made. The only uncertainty in dynamic characteristics of the system is associated with the aerodynamic behavior of the perforated sphere itself; all other components having known frequency response flat to frequencies well above 5 cps.

Views of the test area and the installation of the drag sphere anemometers on the Wallops Island 250-foot meteorological tower are shown in figures 4 and 5. There are five drag sphere

anemometers located at equal vertical separation distances of 50 feet on the tower. The instruments are oriented so that their orthogonal sensing axes are coincidental with the north-south and east-west axes. Figure 5 shows the south face of the tower with the booms for the drag sphere mounts extending perpendicularly from this face on the southwest corner. Conventional aerovane type anemometers are mounted on the southeast corner of the tower and are visible in figure 5. The wind direction for the data presented in this paper is from east to west - or parallel to the south face of the tower.

PRESENTATION AND DISCUSSION OF DATA

Statistical analysis of limited data from the 200-and 250-foot level stations has been performed and samples of such an analysis are presented.

A sample power spectrum of the mean wind component of atmospheric turbulence is given in figure 6. The spectrum is for the horizontal fluctuations of the dynamic pressure, as sensed by the drag forces on the sphere, due to turbulence in the wind. For small fluctuations of the wind compared to the mean wind speed, this power spectrum of pressure is simply related to the power spectrum of velocity by a constant involving the density and the mean wind. The spectrum presented is from the 200-foot level instrument, the mean wind speed was 18 mph, and the intensity of turbulence ($\sqrt{\overline{u^2}}/U$) was 0.14. The data fit very well with the $-5/3$ slope law, shown by the dashed line, up to 1 cps which agrees

with the velocity spectra presented in references 3 and 4. The curve in the range from 1 to 5 cps deviates from the - 5/3 slope and is of very low intensity - perhaps even in the noise level of the instrumentation. No noise level check on these anemometers and the instrumentation has been conducted to date.

Initial data on the spatial correlation of turbulent gust velocities are presented in figure 7 which is a comparison of turbulent coherence functions. The ordinate is the square root of the coherence function defined as the absolute value o the cross spectral density between similar gust components at different heights normalized to the product of their individual power spectra. The abscissa is a non-dimensional frequency defined by a vertical separation distance, Δz, frequency, f, and the mean wind speed, U. The coherence for both the mean wind component, u(t), and the lateral component, v(t), of turbulent fluctuations are presented in figure 7. The solid symbols are the experimental data obtained at the Wallops Island test facility, while the open symbols are data taken at other locations (refs. 3 and 4). The solid line represents theoretical considerations from reference 2 assuming locally homogeneous and isotropic turbulence and the validity of Taylor's hypothesis. All data tend to scatter about this theory with the Wallops Island data consistently higher than the others throughout the range presented. One possible explanation for the high values from the present results may be the fact that the vertical separation distance for the Wallops data is less than that for any of the other data. Information on the lateral

component of turbulent fluctuations is shown in the lower plot of figure 7. There are no experimental data on the lateral gust component for comparison but the limited Wallops data presented compares well with theory.

It appears from these curves that the gust velocities are essentially uncorrelated for values of this non-dimensional frequency greater than 0.3 for the mean wind component and 0.5 for the lateral component. Using the Jupiter fundamental mode frequency of 2.2 cps, a wind velocity of 50 mph, and the limit value of 0.3 for this non-dimensional frequency, the curve and data indicate that the correlation of gust components is very small for vertical separation distances greater than 10 feet, or approximately one maximum vehicle diameter.

CURRENT STATUS OF PROGRAM AND CONCLUDING REMARKS

The Wallops Island full-scale ground wind loads program discussed in reference 1 utilizes Jupiter and Thor vehicles which are of heights considerably lower than that of the data presented from the 250-foot meteorological tower. A vertical array of the fast response drag sphere anemometers has been mounted on a pole at the Wallops test site (fig. 8) in an effort to obtain data in the heights covered by these vehicles - up to approximately 65 feet. These instruments are mounted at equal vertical separation distances up to 53 feet and are also oriented so that their sensing axes are north-south and east-west. Further insight into the correlation of gusts with vertical separation distances in this

range of heights near the ground is hoped to be gained using this array. Future efforts will be concentrated on analyzing the data from this array in the same manner as that employed for the data just presented.

Another facet of this program will be an experimental test of Taylor's hypothesis up to 5 cps. Taylor's hypothesis states that a fixed field of turbulence is transported by the mean wind with no change in its statistical characteristics as it is being convected. This investigation will be conducted using the four sensors on the stationary array shown in figure 8 and a portable tower arrangement as shown in the schematic in figure 9. The correlation of gust velocities with horizontal instead of vertical separation distances will be of concern. By moving the portable tower, the two measuring stations can be aligned with the mean wind direction and the horizontal separation distance may be varied. A similar investigation is being conducted by Harris (ref. 5) in the United Kingdom. Harris will utilize a stationary horizontal array of six 1 1/2-inch-diameter sphere gust anemometers mounted in a rather interesting pattern and aligned with the prevailing wind direction. This array is illustrated on the right of figure 9. By using different combinations of the six sensors, data may be obtained on the correlation of gusts for horizontal separation distances from 45 to 765 feet in increments of 45 feet. In other words, for one data period, information is available for separation distances of 45, 90, 135, etc., up to 765 feet.

In conclusion, this paper has presented an indication of the

meteorological information obtained from the 250-foot tower and discussed future work in conjunction with the Wallops Island full-scale ground wind loads program. Data are just beginning to be reduced from these programs and those presented have been initial results. It is felt that these programs will provide valuable information on the contribution of gust loads on launch vehicles.

REFERENCES

1. Foughner, Jerome T., Jr., and Duncan, Rodney L.: A Full-Scale Ground Wind Load Research Program. Presented at the Meeting on Ground Wind Load Problems in Relation to Launch Vehicles, Langley Research Center, Hampton, Virginia, June 7-8, 1966.
2. Reed, Wilmer H., III: Models for Obtaining Effects of Ground Winds on Space Vehicles Erected on the Launch Pad. Presented at the Conference on the Role of Simulation in Space Technology, Virginia Polytechnic Institute, Engineering Extension Series, Circular No. 4, Part C, August 17-21, 1964.
3. Davenport, A. G.: The Spectrum of Horizontal Gustiness Near the Ground in High Winds. Quarterl, Jour. Royal Met. Soc., Vol. 87, 1961.
4. Singer, Irving A., and Nagle, Constance M.: A Study of the Wind Profile in the Lowest 400 Feet of the Atmosphere. Final Report, Brookhaven National Laboratory, March 31, 1962.
5. Harris, R. I.: An Experimental Test of Taylor's Hypothesis. Electrical Research Association report in preparation.

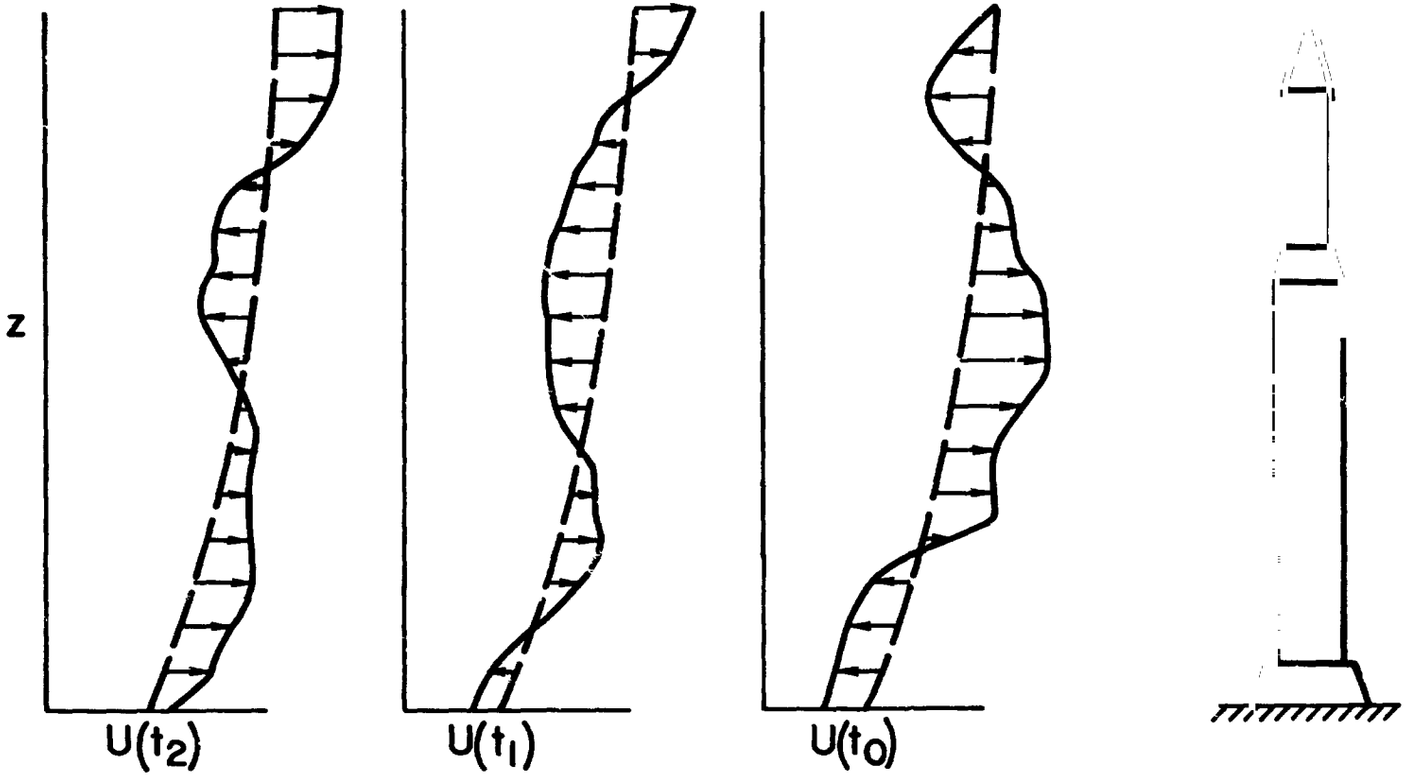

Figure 1.- Typical variations of unsteady wind with height.

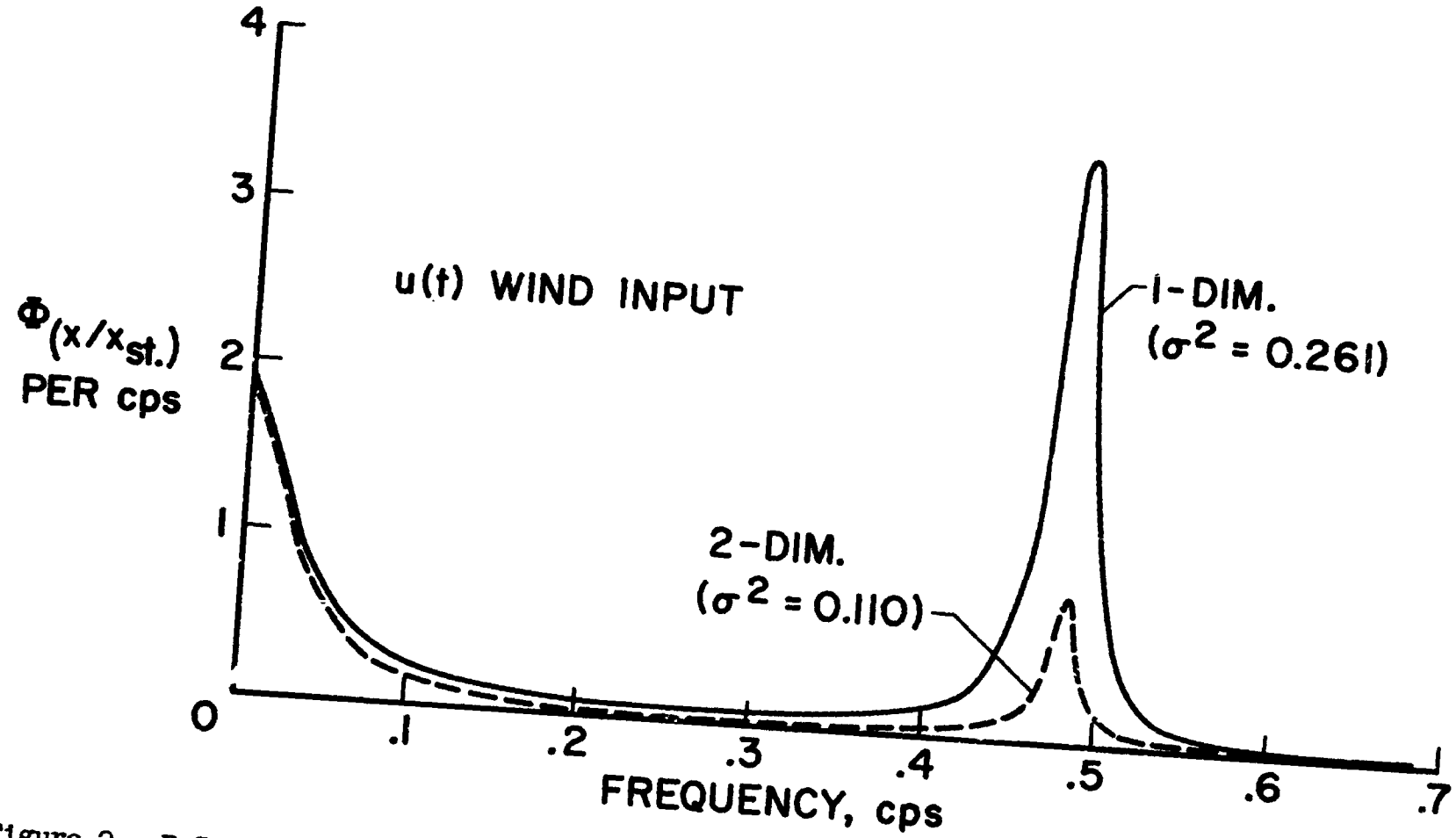

Figure 2.- P.S.D. of vehicle response to the mean wind component of atmospheric turbulence.

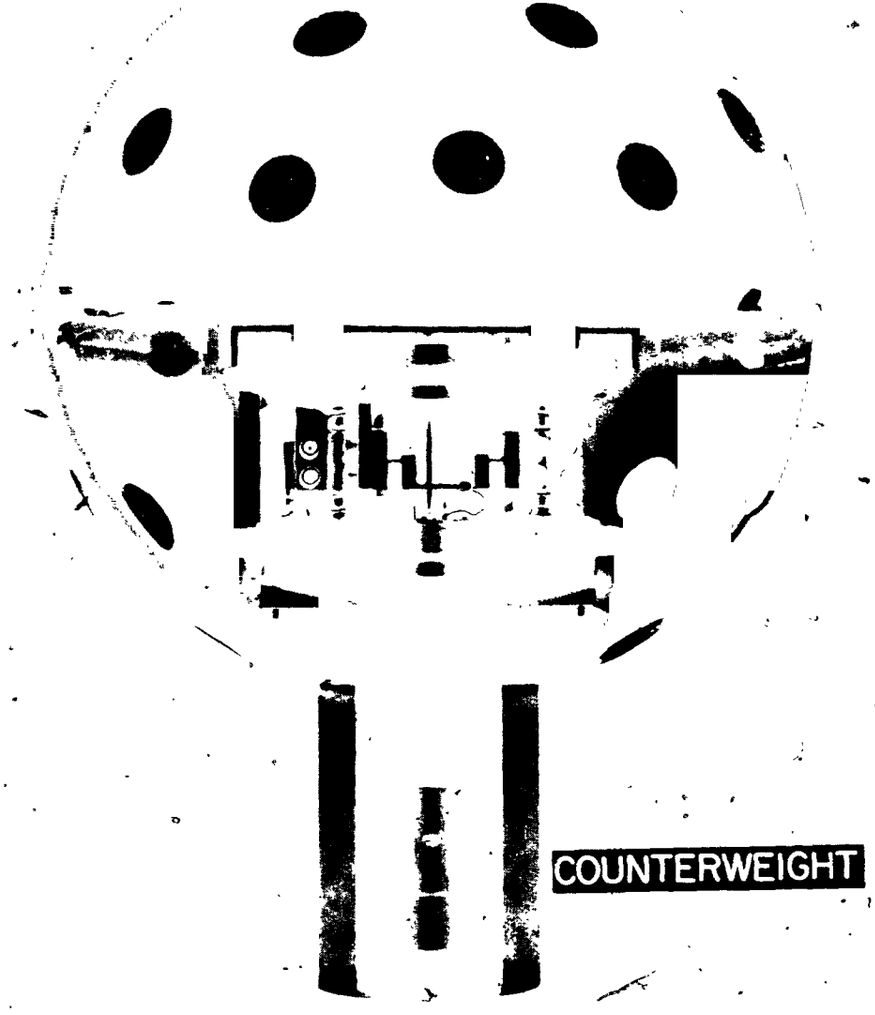

Figure 3.- Cutaway view of fast response drag sphere anemometer.

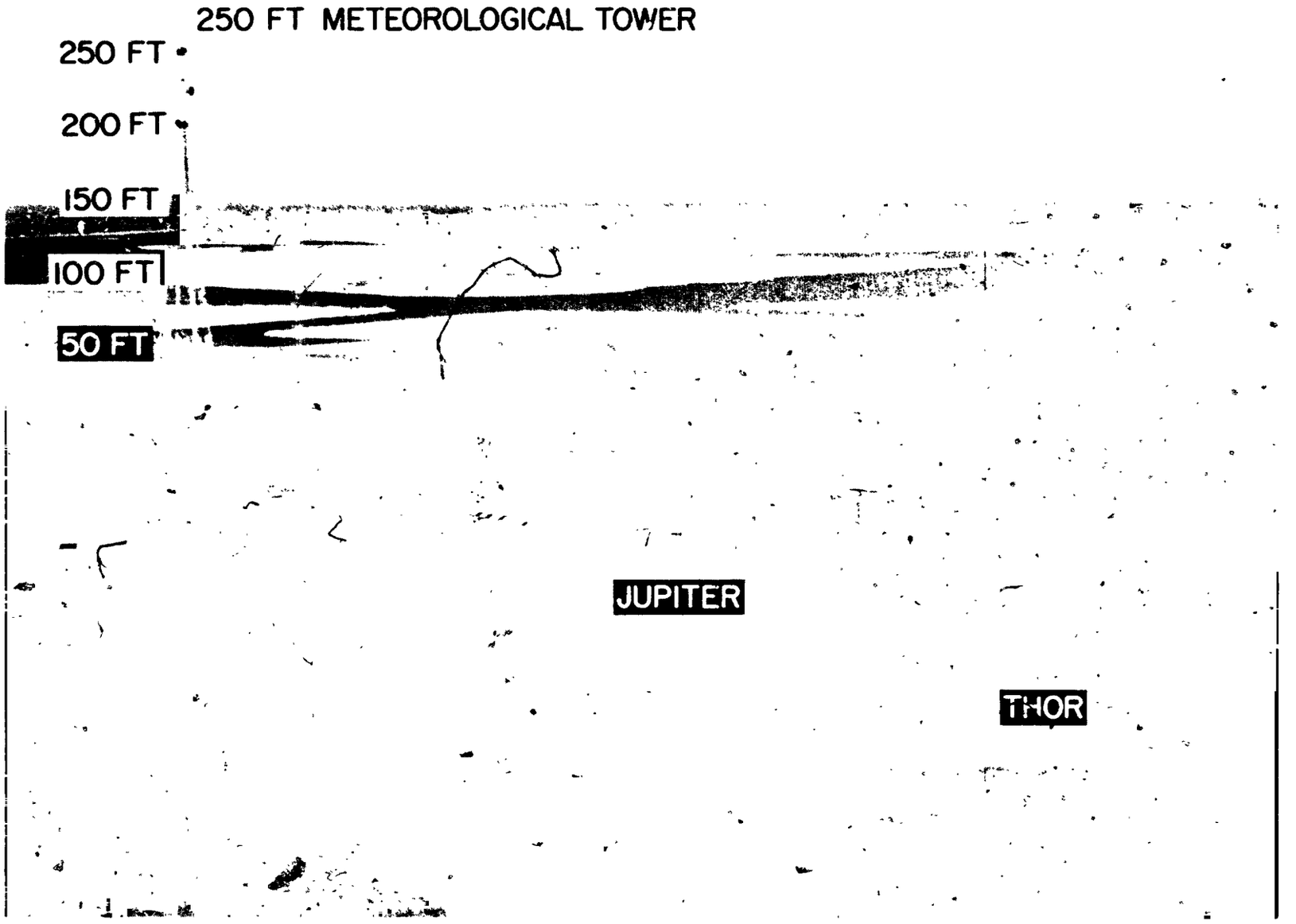

Figure 4.- Wallops Island test facility.

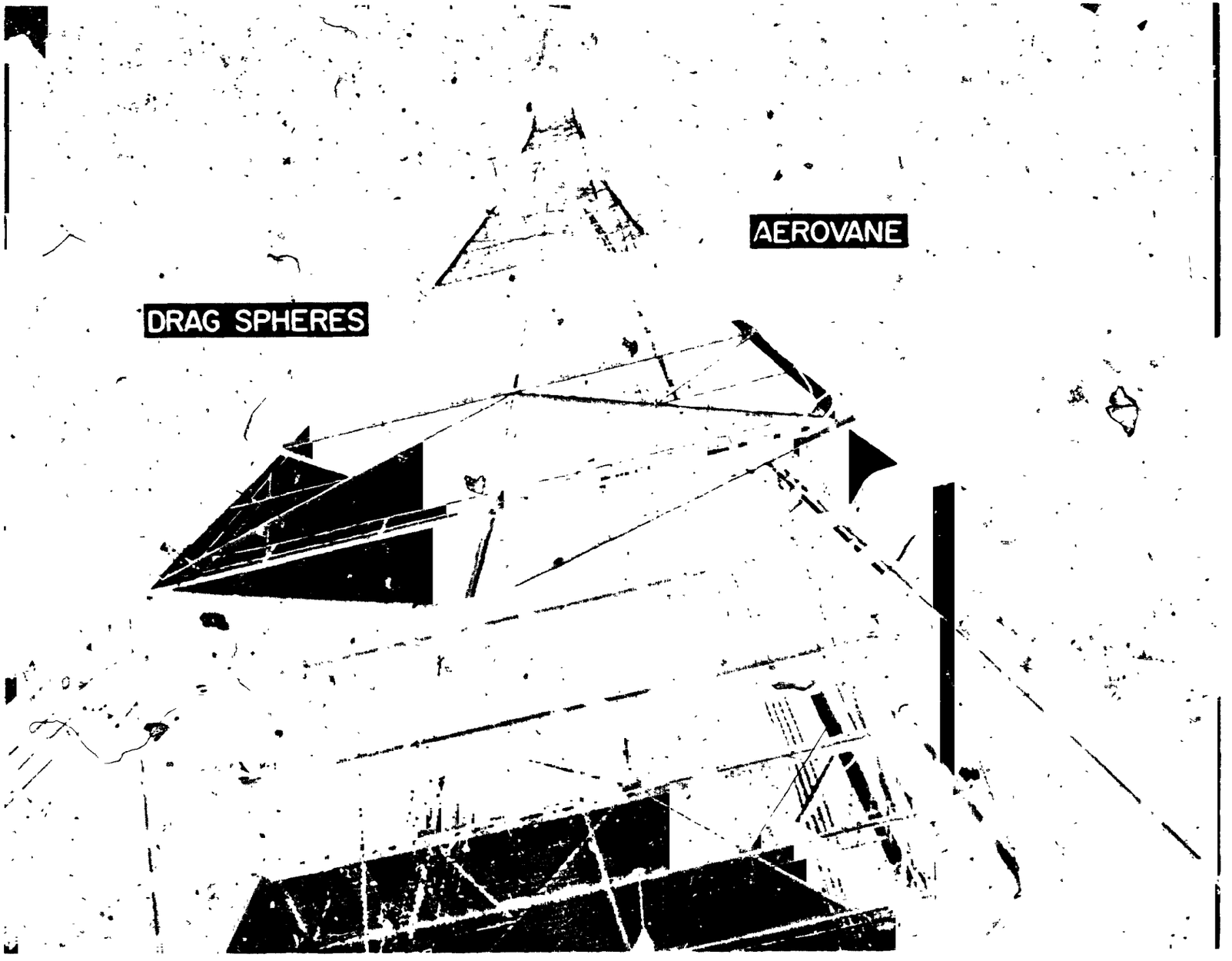

Figure 5.- Wallops Island 250-foot meteorological tower.

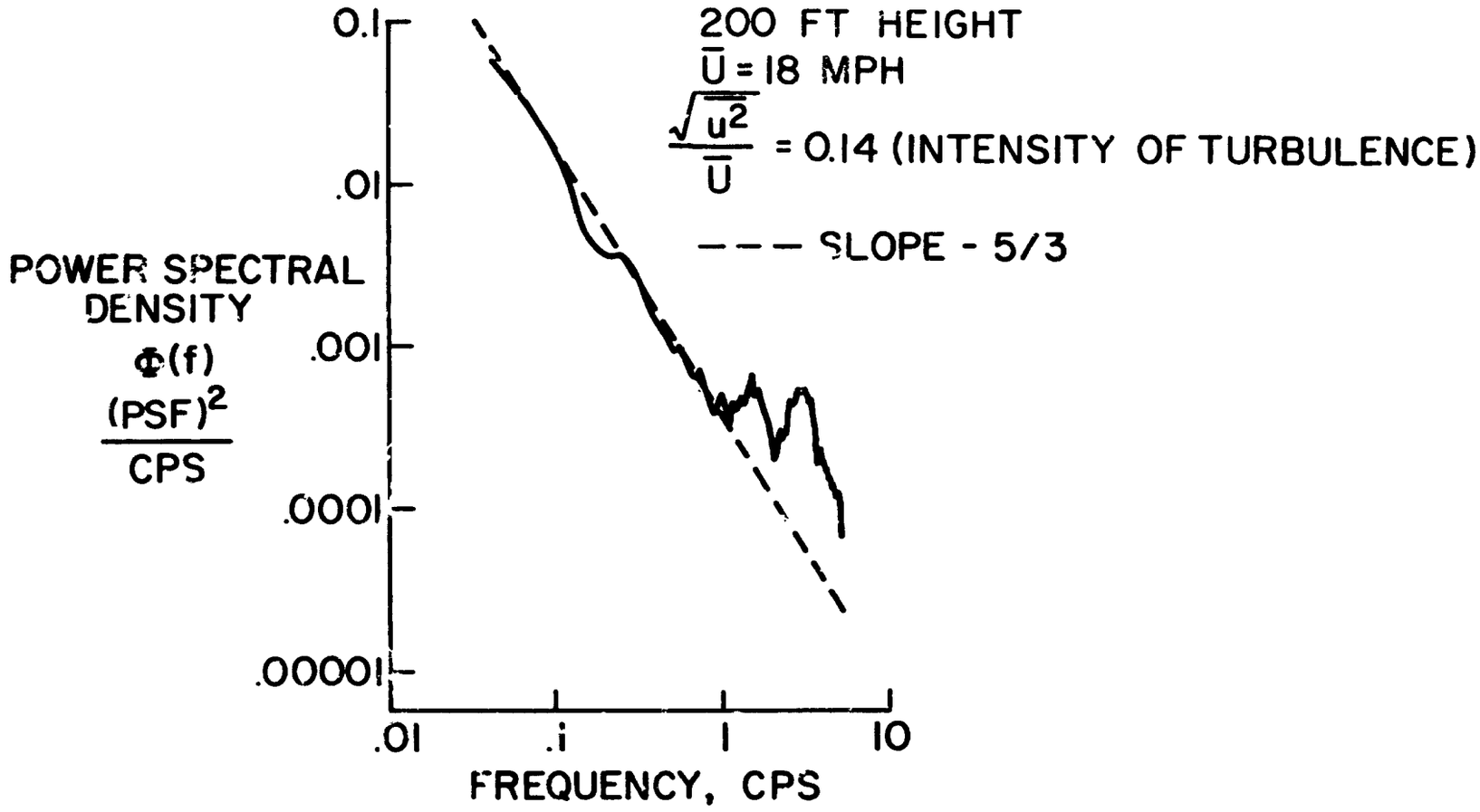

Figure 6.- Sample power spectra of mean wind component of turbulence.

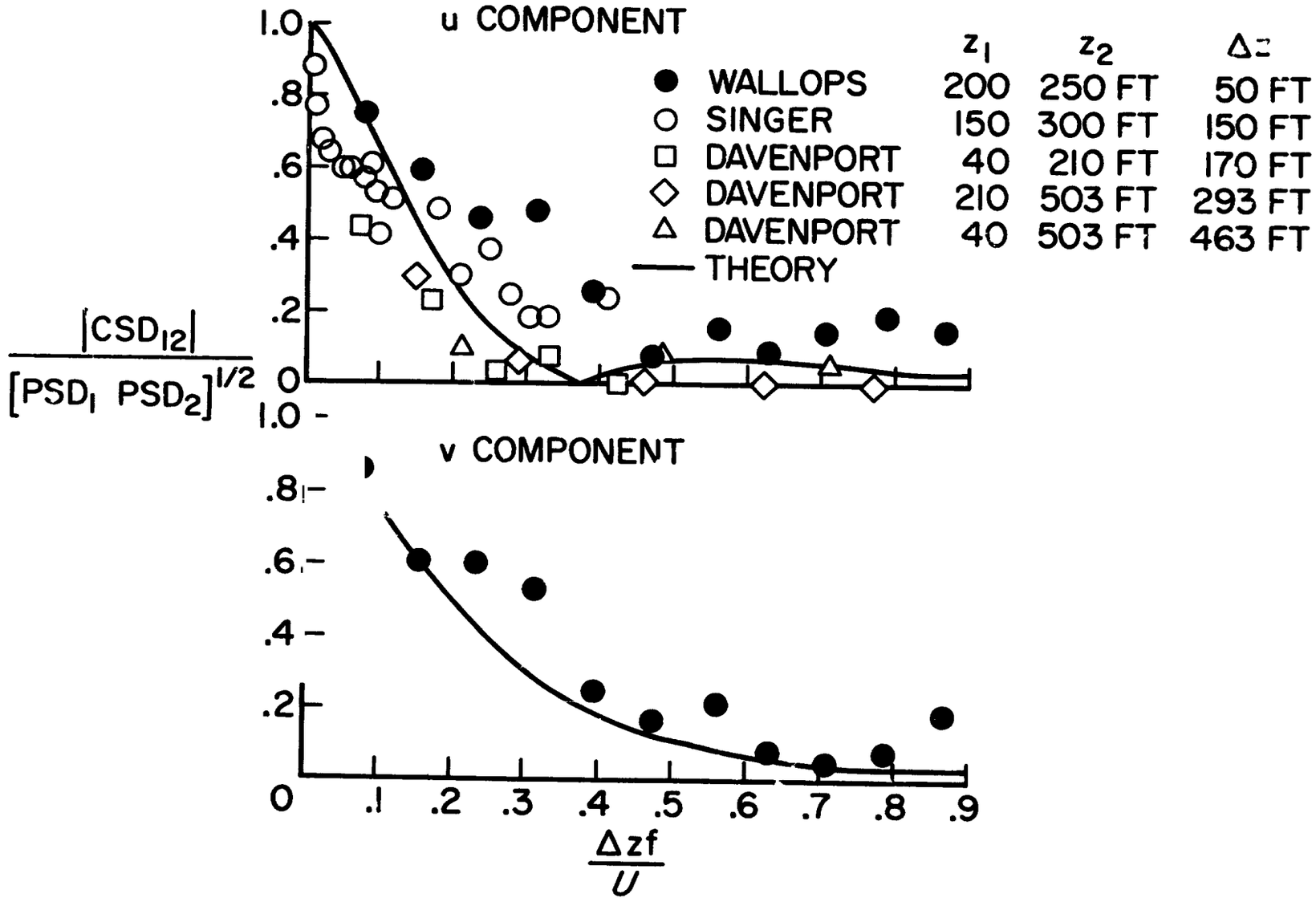

Figure 7.- Comparison of turbulent coherence functions.

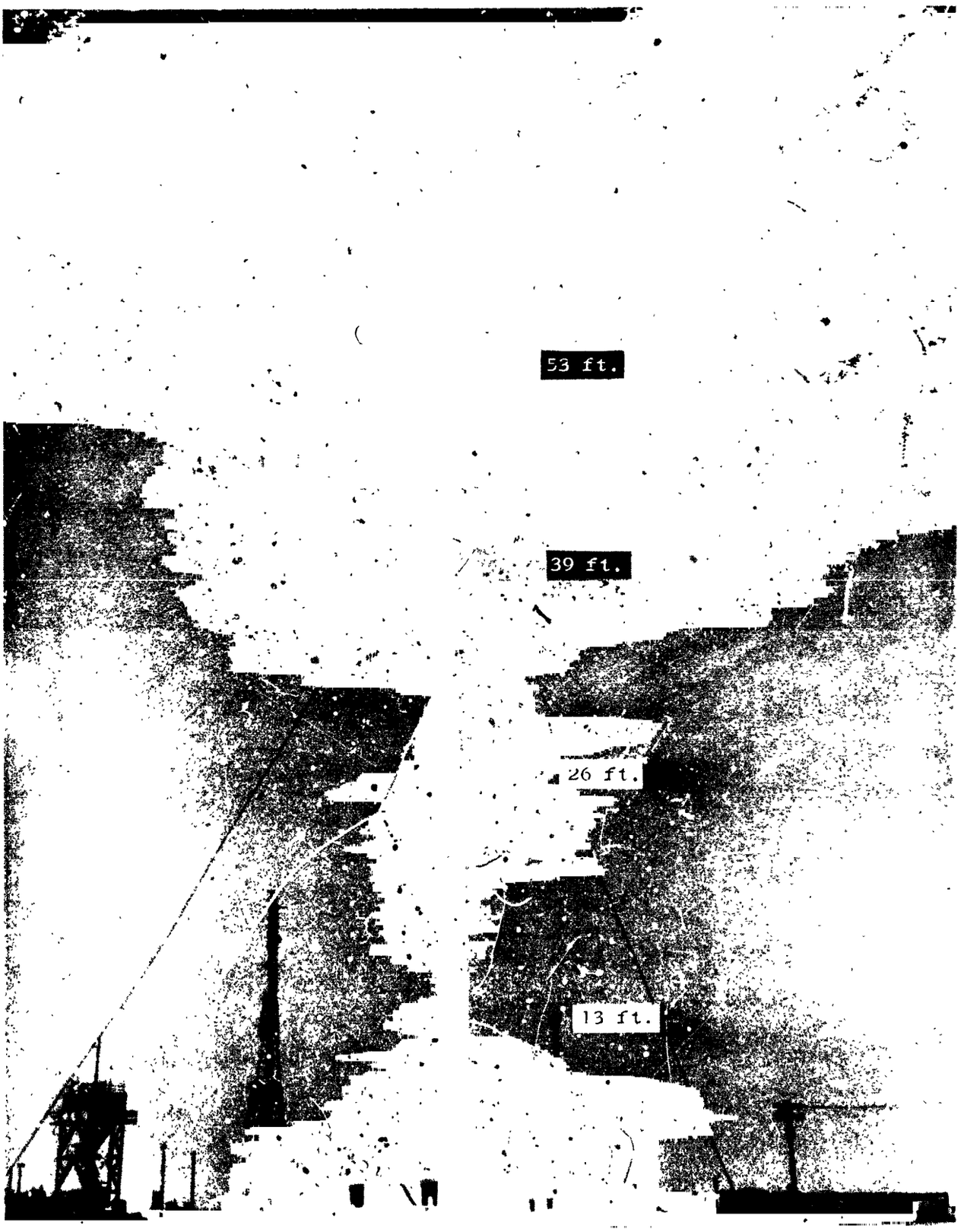

Figure 8.- Low elevation vertical array of fast response drag sphere anemometers.

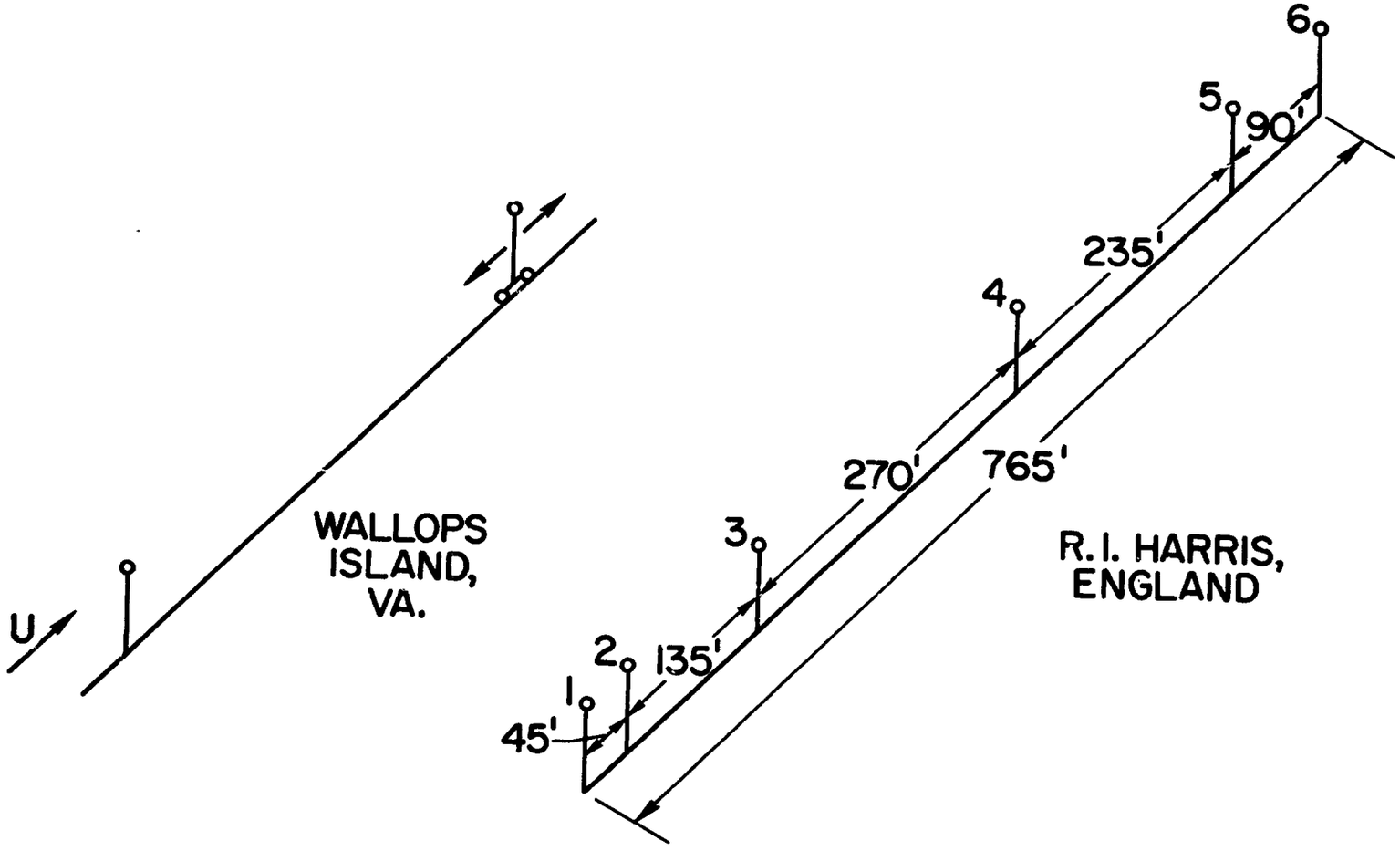

Figure 9.- Verification of Taylor's hypothesis.

THE RELATIONSHIP OF WIND STRUCTURE TO WIND LOADING

By A. G. Davenport
Professor of Engineering Science

University of Western Ontario
London, Canada

INTRODUCTION

If one studies the response of structures in the wind over a fairly long period of time one finds that its behaviour can tidily be considered in two parts, a steady component and a dynamic component. It is found from the aerodynamics that the steady component of response can be directly related to the action of the mean wind: the fluctuating part is related either to the fluctuating component of the wind or to the mean wind itself, through the mechanism of vortex shedding or some form of aerodynamic instability.

The design of the structure is basically concerned with answering such questions as what are the maximum stresses and deflexions or alternatively how many cycles of given stress amplitude likely to occur? The latter is possibly a more sophisticated question than the former yet, it is nevertheless a significant question from the design standpoint as the large number of fatigue induced wind failures bears testimony.

The purpose of this paper is to consider some of the meteorological factors influencing the answers to these questions.

The convenience of considering the steady and dynamic components of the response of a structure has been referred to. The same convenience also applies when discussing the wind itself. The wind however is a perpetually restless phenomenon and the distinction between the steady and the fluctuating part is

basically pragmatic. Fortunately it appears the distinction can be made on reasonable physical foundations.

If we determined the spectrum of windspeed near the ground over a period of time comparable to the lifetime of a structure, we might find the general form shown in Fig. 1. This spectrum is taken mainly from actual records analysed by van der Hoven.

The spectrum shows a number of significant peaks and gaps. A fairly broad gap occurs between fluctuations having periods lying between roughly a few minutes and several hours. This gap is particularly noticeable in stronger winds when the right-hand peak, due to mechanical turbulence, is very pronounced. This gap has been observed to exist quite generally and has been attributed to the lack of physical processes which are capable of producing fluctuations in this range.

This gap separates what might be termed gust fluctuations, due mainly to mechanical turbulence, from the much slower fluctuations which for present purposes will be termed fluctuations in the mean velocity. The presence of the gap also indicates that fairly stable estimates of the mean windspeed can be made when the windspeed is averaged over a period in the range ten minutes to an hour.

This period for averaging the mean is also suitable for the structural analysis. Since this period is far longer than any natural period of structural vibration it assures that effects caused by the mean wind properly represent steady-state, non-transient effects.

This distinction between the mean velocity and gusts enables the two aspects of the wind to be treated separately.

THE MEAN WIND

In establishing the properties of the mean wind for structural design purposes two questions appear paramount. The first is the establishment of the mean wind climate at the site of a structure and the second is the variation of the mean flow in the atmospheric boundary layer.

One of the difficulties in trying to define the wind climate at a locality is to do so independent of the boundary layer characteristics themselves. Meteorological stations from whose long term records we should expect to be able to establish statistical properties of the wind climate are frequently distant from the structure. Unless the exposures at the structure and at the meteorological station are similar, very different wind conditions can often prevail even a few miles away. The comparison in Fig. 2 of the once-in-50 year wind speeds at city and airport stations in the United States illustrates this fact. Even though the anemometers in the city were significantly higher than at the airport, the windspeeds there are in all cases lower than at the airport.

BOUNDARY LAYER PROFILE

This difference is easily explained if we consider the retarding effect of the roughness of the terrain as shown in Fig. 3. It is noted that at 100 feet above ground the velocity in the city is approximately half that in open country for the same gradient wind blowing.

These curves were drawn from data collected several years ago from a wide range of sources and have been substantially confirmed by additional data collected since.

This difference in wind speeds which is due entirely to local exposure conditions, in particular the ground roughness, has obvious importance in

estimating the wind conditions at a particular site from the wind measured at some point distant. The different rate of increase of wind speed with height is also important.

In these curves the power law has been used to describe mean speed profiles. Two parameters define the profile, namely the power-law exponent and the gradient height, at which the gradient velocity is attained.

The use of the power law is of course empirical. It has nevertheless been used extensively in fluid mechanics to define the boundary layer profile both in the atmosphere and in the wind tunnel. Recently several slightly less empirical profiles have been proposed such as the KEYPS profile by Panofsky and others and the theoretical wind spiral by Lettau; at present there seems no obvious advantage over the power law profiles from the standpoint of wind loading.

It should perhaps be remarked that under general conditions the profile is considerably dependent on the thermal stability. Fortunately, however, in strong winds the stability of the atmosphere tends towards neutral conditions under the strong mixing action produced by mechanical turbulence which prevents thermal imbalance.

It is often found that a structure is situated near the boundary of two roughnesses and in these circumstances an estimate of the rate at which the boundary layer adapts itself from one roughness to the new roughness is important.

A recent theoretical development by Townsend and Panofsky seems useful in this respect. This theory suggests that on average the new boundary layer grows with a slope of about 1 in 10 downwind from the interface of the two roughnesses. This slope is approximately in the same ratio as the RMS vertical

velocity to the mean wind speed. This is reasonable since it is the vertical component of turbulence that is largely responsible for transmitting the new shear stress from the ground. The slope is found to be somewhat steeper when going from a smooth to rough surface than vice versa, which again is in accordance with the vertical turbulence intensities then prevailing.

Some recent exploratory experiments carried out in the University of Western Ontario Boundary Layer Wind Tunnel have tended to confirm this.

MEAN WIND CLIMATE

For structural design two different types of information appear to be relevant. First a description of the distribution of all mean wind speeds on a relative frequency basis and second a description of the distribution of the annual maximum mean wind speeds. Both types of statistical information can be assembled using Weather Bureau data. Several approaches are possible; the most advantageous being dictated by the nature of the structural calculations being made, the reliability of the information, the number of years of record available, the height of the structure above ground and the distance of the structure from the meteorological observing station.

Figs. 4, 5 and 6 show three types of analyses. Fig. 4 shows the distribution of Rawindsonde measurements at 500 meters from John F. Kennedy airport in New York. This represents approximately the distribution of all stronger wind speeds. It is seen to fit reasonably closely to a theoretical Rayleigh distribution which, it can be shown, is the distribution appropriate for a horizontally isotropic wind field. Because the wind at this height is relatively free of the surface influence it can be assumed that it is probably typical of a

fairly wide region. Surface wind distributions can be estimated using the mean wind profile given in Fig. 3 appropriate to the particular terrain.

If desired, extreme value theory can be used to estimate the annual maximum (or any other period) from this parent distribution of wind speeds. To establish this distribution, 2 or 3 years of record provide a very large sample and the reliability is therefore probably quite high. This type of analysis can be taken further to show directional effects.

Figs. 5 and 6 both show extreme value analyses of surface wind data. These data are less reliable. Since they are necessarily accumulated over several years of record during which period, the instruments have probably been changed, have been located at different places and heights, have sometimes been inoperative due to ice or improper maintenance, and their exposure may have been changed due to encroachment of buildings or may have been poor to begin with. Nevertheless these surface data can be assembled without difficulty, and they give an indication of the wind speeds that are likely to prevail.

In both Figs. 5 and 6 comparison is made with the theoretical extreme value distributions of the Fisher-Tippett type I. Reasonable agreement is apparent.

To accurately correlate the mean wind speeds at the site of a structure with those at a station for which long term records are available usually requires a minimal amount of field testing. Simultaneous records at the two locations over a period of one or two months is probably sufficient.

PROPERTIES OF TURBULENCE NEAR THE GROUND

The properties of turbulence near the ground can conveniently be defined in terms of statistical quantities. These quantities consist of the various correlations of the three velocity components in each of the three components spatial directions and also in the time domain. Alternatively these correlations can be transformed into the various spectra and cross-spectra of the turbulence.

For structural engineering design, one of the most important properties of turbulence is the spectrum of wind speed--or the longitudinal component of velocity. Fig. 7 shows a generalized spectrum of the wind speed from a number of different localities and normalized by the square of the friction velocity V_*^2. Reasonably good agreement is found for data from a wide variety of localities. The data is found also to conform approximately to the empirical expression

$$\frac{n\,S(n)}{V_*^2} = 4.0\,\frac{x^2}{(1+x^2)^{4/3}}$$

in which $x = \frac{nL}{\bar{V}}$

an $S(n)$ is the power spectral density at frequency n

$\bar{V}$ is the mean velocity

and L is a scale length.

The value of the scale length is in the neighbourhood of 4000 feet for the data shown. More recently the writer has found that larger values of the scale L are sometimes required to fit observed spectra.

The above form of the spectrum implies that there is no great variation in the variance of the velocity component with height. Although this is

approximately true, some improvement in the agreement can be obtained if the spectra are presented in the form

$$\frac{n\,S(n)}{\sigma^2} = 6\,\frac{x^2}{\left(1 + x^2\right)^{4/3}}$$

where σ^2 represents the variance at the particular level being considered. The latter has the tendency to increase with height and then to gradually fall off at greater heights.

The vertical and horizontal lateral spectra have been measured extensively by Panofsky, Singer and others. The energy in these directions appears to be approximately half that in the longitudinal. In these directions the scale of the turbulence tends to increase with height above ground.

The spatial correlations of velocity are a most important consideration when analyzing the loading of large structures.

These correlations can be used to define the "average size" of gusts. Figs. 8 and 9 show measures of these correlations (or coherence) in a wind tunnel and in the natural wind, respectively. If the "effective width" of these curves is defined as the scale (or in fact semi-scale) then it is found that the gusts of the longitudinal component in the vertical direction are approximately 1/3-1/4 the gust wavelength. In the lateral direction the width is appreciably smaller in strong winds--approximately 1/10th of the wavelength.

CONCLUSIONS

The following summarizes the principal observations made above.

1) For structural design purposes it is convenient to consider the characteristics of the mean wind and of the turbulence separately.

2) An averaging period in the range 10 minutes to an hour generally provides stable estimates of mean velocity and allows the processes during this period to be treated as stationary.

3) In strong winds the profile of the mean windspeed in the earth's boundary layer is mainly influenced by the roughness of the terrain. The profiles given in Fig. 3 appear to be in reasonable agreement with observation.

4) Surface roughness can cause significant local modification in the wind climate.

5) The transition in boundary layer characteristics downwind from a change in roughness appear to be well described by the Panofsky-Townsend profile. The slope of the new boundary layer is on average approximately 1/10th; a steeper slope is found when going from smooth to rough and a shallower slope from rough to smooth.

6) Two statistical distributions are useful in defining the wind climate, the distribution of all wind speeds and the distribution of the annual maximum wind speeds. Greater reliability can be expected from the distribution of all wind speeds than from the distribution of the annual maxima; extreme value theory may be used to predict the extreme wind speeds from the parent distribution of all wind speeds. Both types of distribution can be developed from routine U.S. Weather Bureau data.

7) The distributions of upper level winds as well as surface winds can be estimated. Upper level distributions will usually have application to a broader area since the magnitude of surface winds is significantly affected by exposure.

8) Distributions of all wind speeds can usually be represented theoretically by a distribution of the Weibull type of which the Rayleigh distribution is

a particular case and which is appropriate for an horizontally isotropic wind regime. Extreme values can be asymptotically represented by the Fisher-Tippett Type I distribution.

9) Turbulence in the atmospheric boundary layer generally exhibits a number of non-isotropic characteristics. For example, the relative distribution of energy is stronger in the longitudinal direction than in the transverse which is the reverse of isotropic turbulence.

10) Expressions for the spectrum of the wind speed have been given by Davenport, for the transverse components by Panofsky, Singer and others.

11) The spatial correlation of turbulence indicates that in strong wind the effective width of gusts in the vertical direction is approximately 1/3-1/5 of the wavelength. In the horizontal direction the width is closer to 1/10th of the wavelength.

BIBLIOGRAPHY

This paper is a condensed and updated version of a longer paper having the same title and presented at the 1963 Conference on Wind Effects on Structures held at the National Physical Laboratory, London, England. Readers are referred to this for a fuller discussion.

Additional references are given below:

Davenport, A. G. "The treatment of wind loading of tall buildings". Proc. of Symp. on Tall Bldgs., Univ. of Southampton, April 1966 to be published by Pergamon Press.

Lettau, H. H. "Theoretical wind spirals in the boundary layer of a barotropic atmosphere". Beitrage 2nd Physik der Atmosphäre 35 3/4 1962.

Lumley, John L., Panofsky, H. A. "The structure of atmospheric turbulence". Interscience monographs and texts in physics and astronomy. John Wiley, 1964.

Panofsky, H. A., Townsend, A. A. "Change of terrain roughness and the wind profile". Qu. Jul. Roy. Met. Society 90 1964, p. 147.

Singer, I. A. "Wind gust spectra". Proc. of Conference on Large Steerable radio antennas - climatological and aerodynamic considerations. Annals of the New York Academy of Sciences 116 pp. 116.

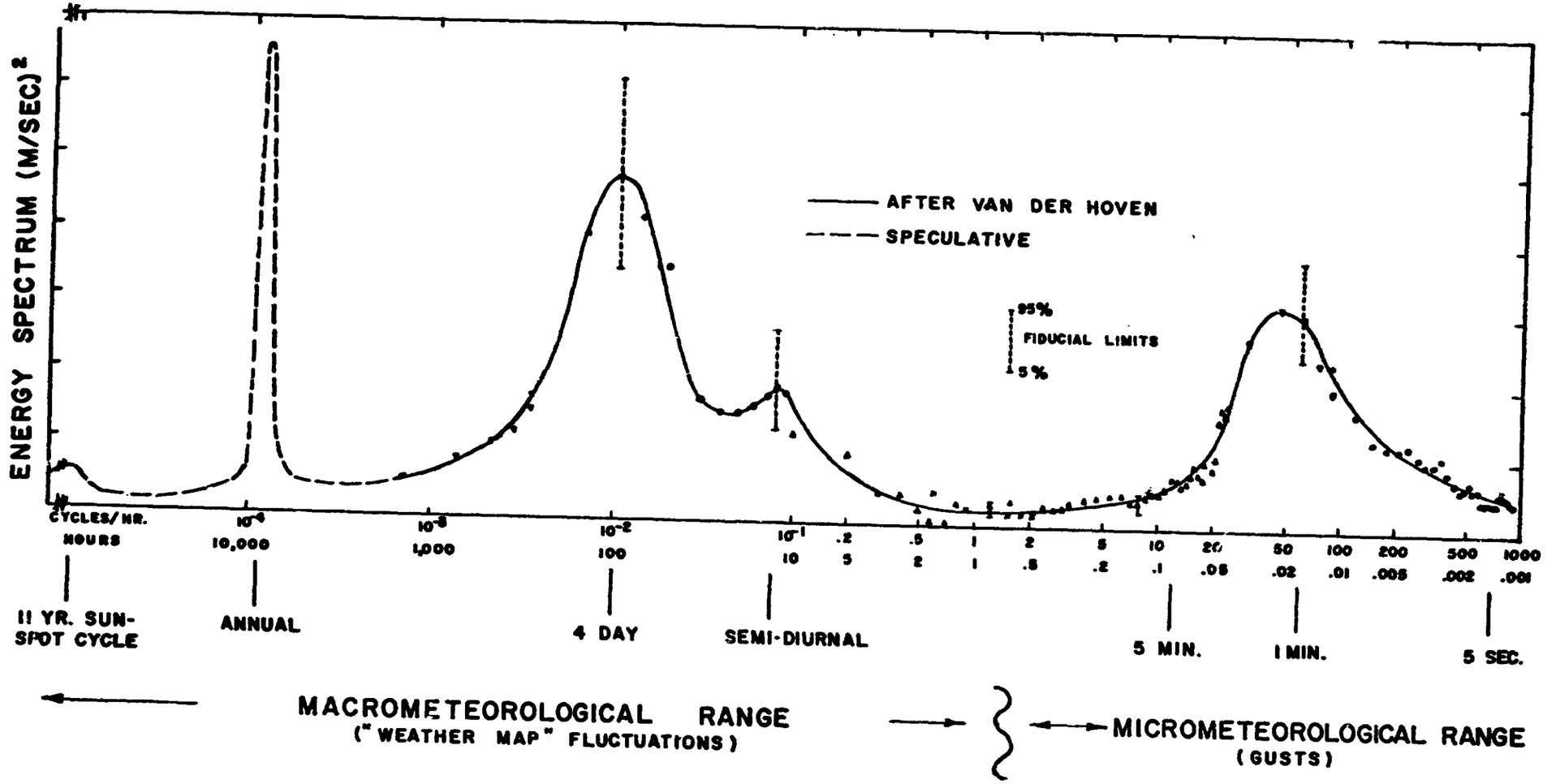

FIG. 1 SPECTRUM OF HORIZONTAL WIND SPEED NEAR THE GROUND FOR AN EXTENSIVE FREQUENCY RANGE (FROM MEASUREMENTS AT 100 METRE HEIGHT BY VAN DER HOVEN AT BROOKHAVEN, N.Y., U.S.A.)

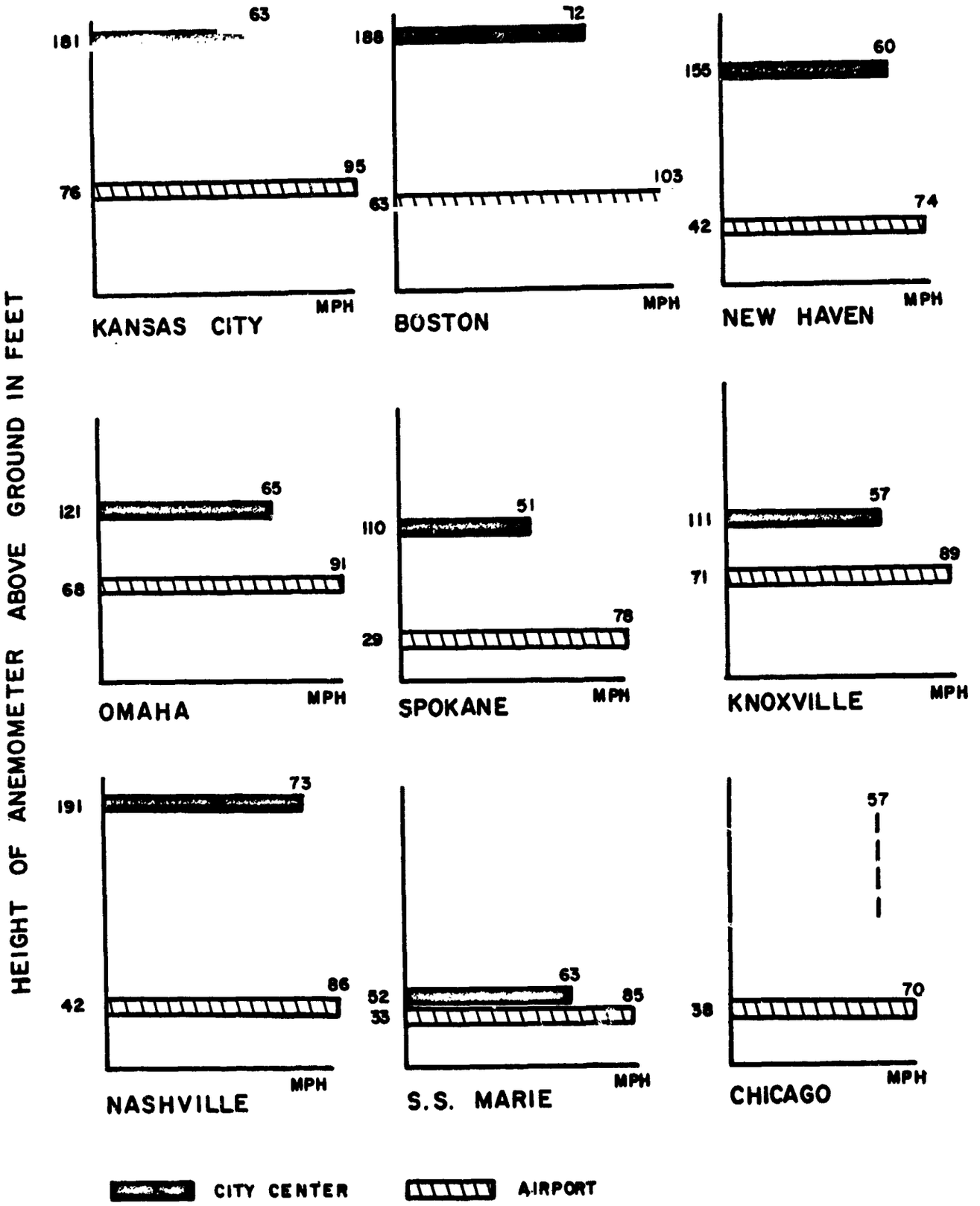

FIG. 2 COMPARISON OF ONCE-IN-50 YEAR WINDSPEEDS AT AIRPORTS AND CITY METEOROLOGICAL STATIONS IN UNITED STATES.

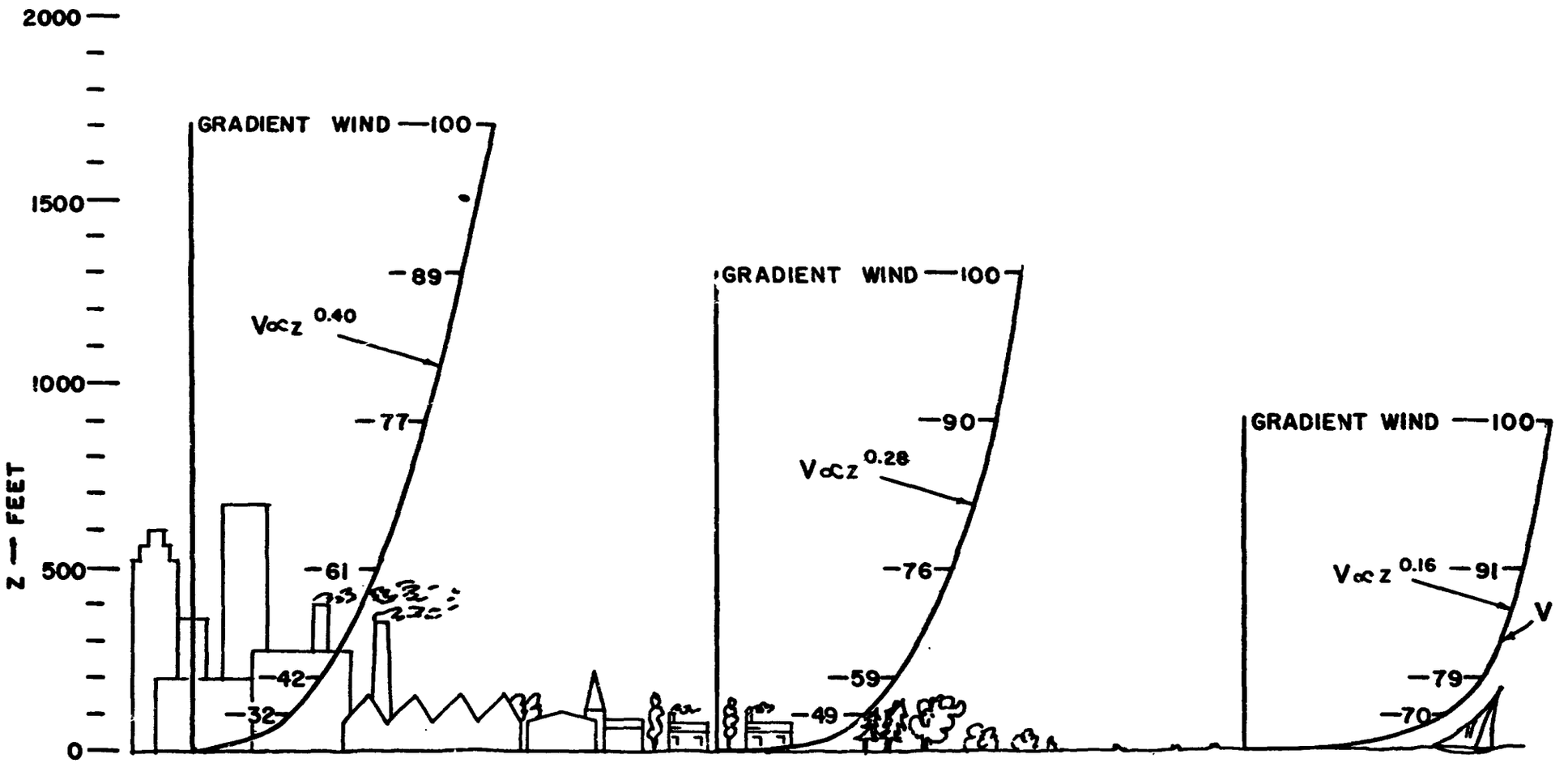

FIG. 3 PROFILES OF MEAN WIND VELOCITY OVER LEVEL TERRAINS OF DIFFERING ROUGHNESS

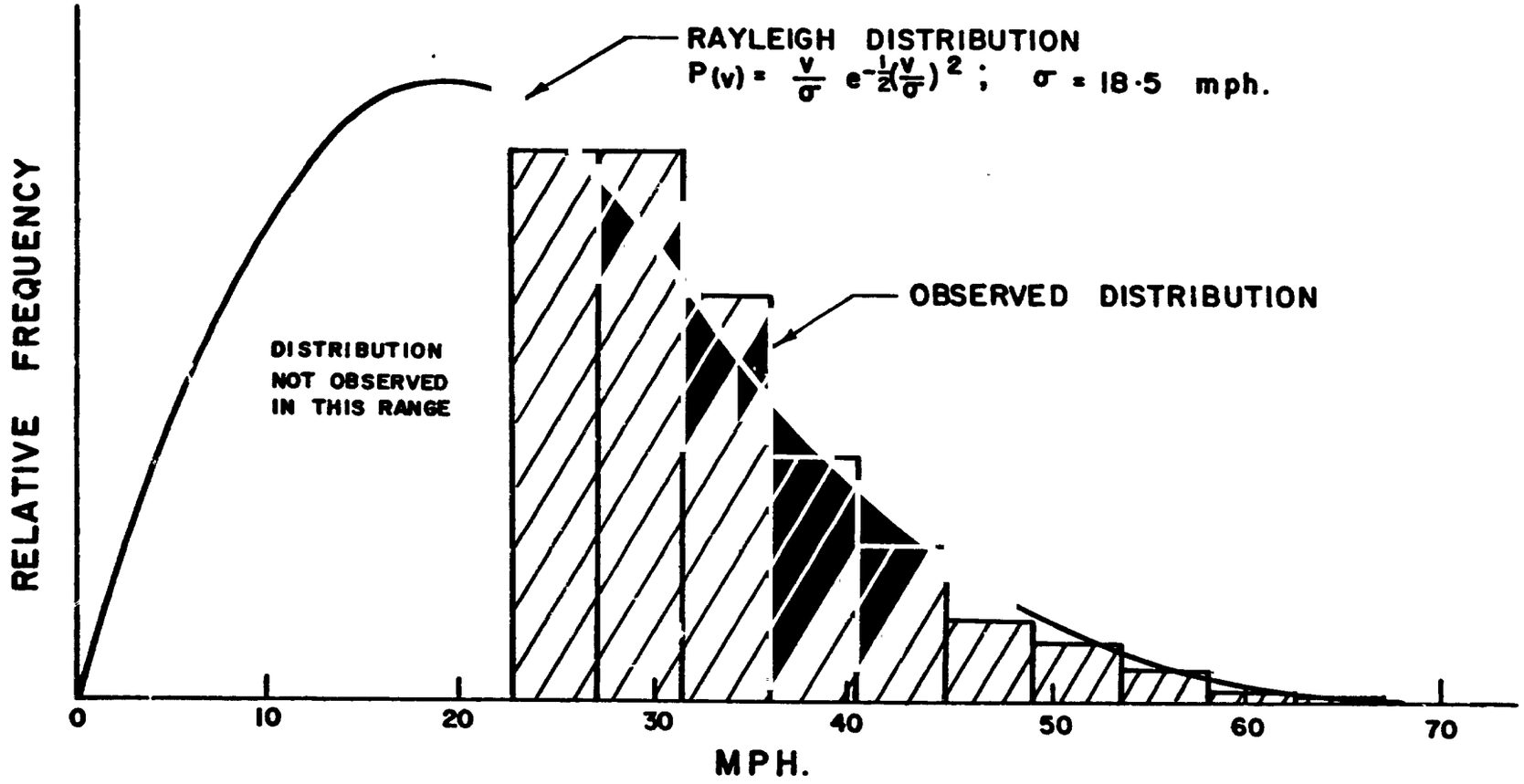

FIG. 4 RAYLEIGH DISTRIBUTION OF WIND SPEEDS AT 500 M AT JOHN F. KENNEDY AIRPORT , NEW YORK CITY

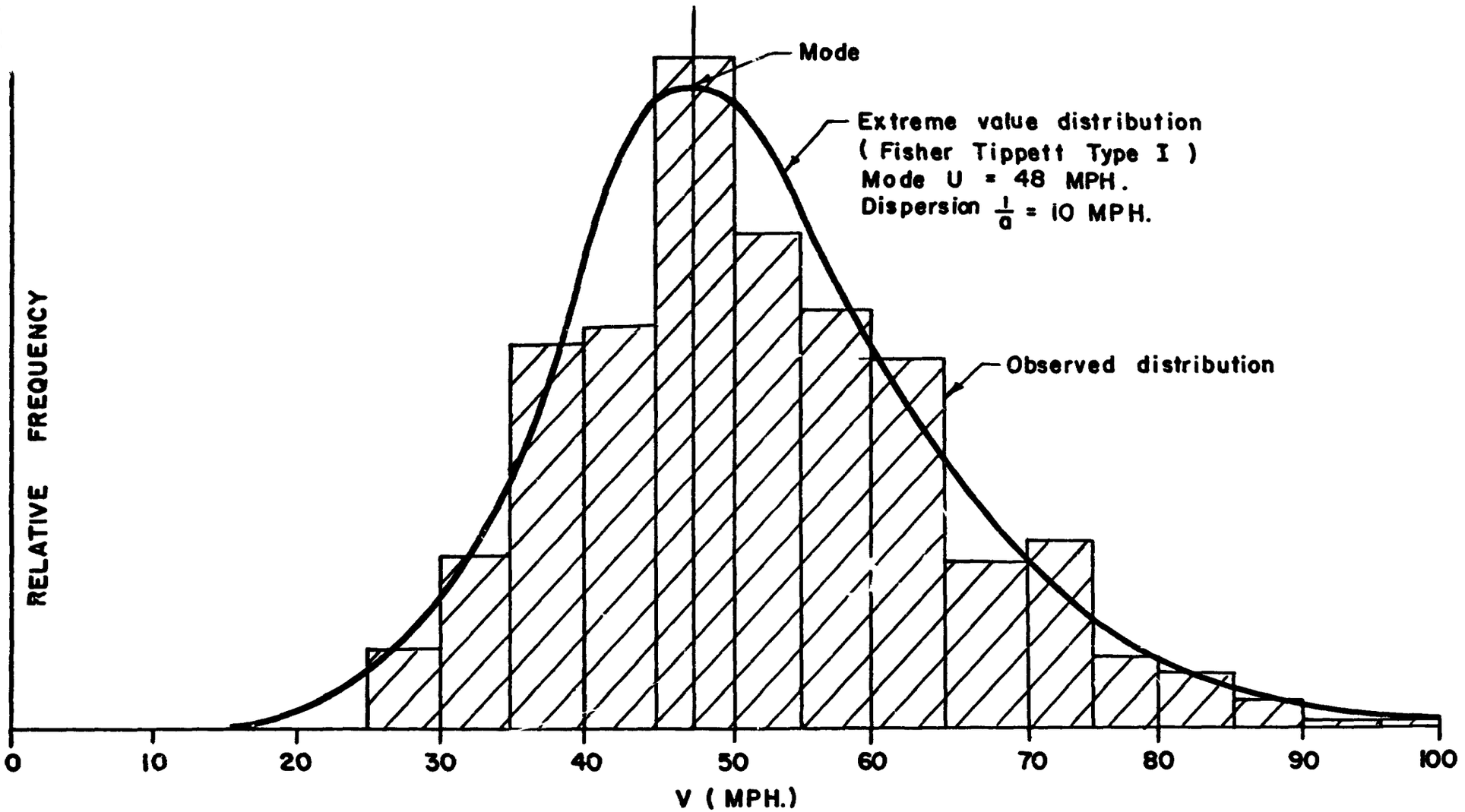

FIG. 5 COMPARISON OF OBSERVED DISTRIBUTION OF MAXIMUM MONTHLY 5-MINUTE WIND SPEED IN NEW YORK CITY AT 450 FT. (1884 - 1950) WITH TYPE I EXTREME VALUE DISTRIBUTION.

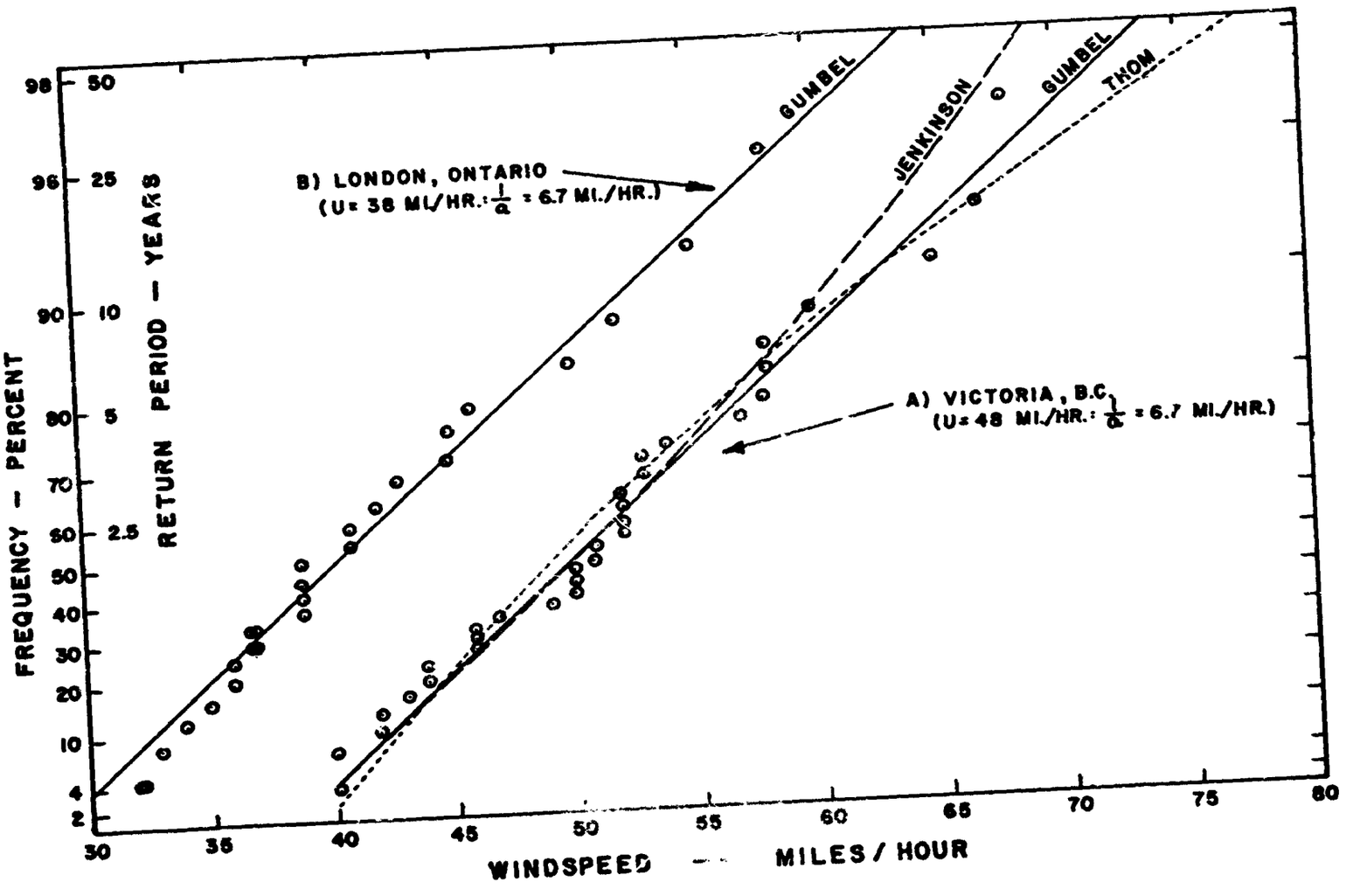

FIG. 6 COMPARISON OF ANNUAL MAXIMUM HOURLY WIND SPEEDS AT VICTORIA B.C. AND LONDON ONTARIO WITH THEORETICAL DISTRIBUTIONS OF EXTREME VALUES (AFTER BOYD AND KENDALL).

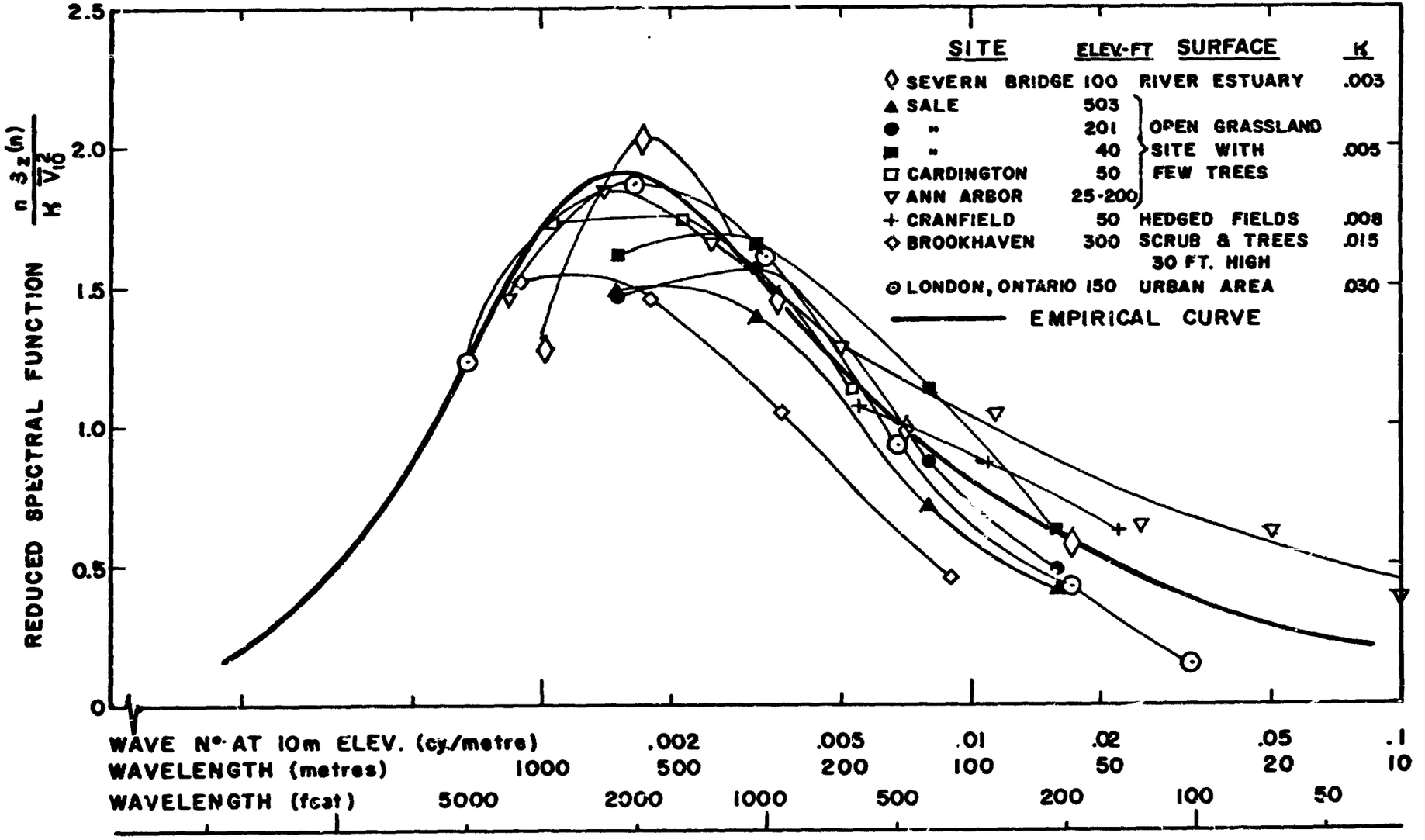

FIG. 7 SPECTRUM OF HORIZONTAL GUSTINESS IN HIGH WINDS

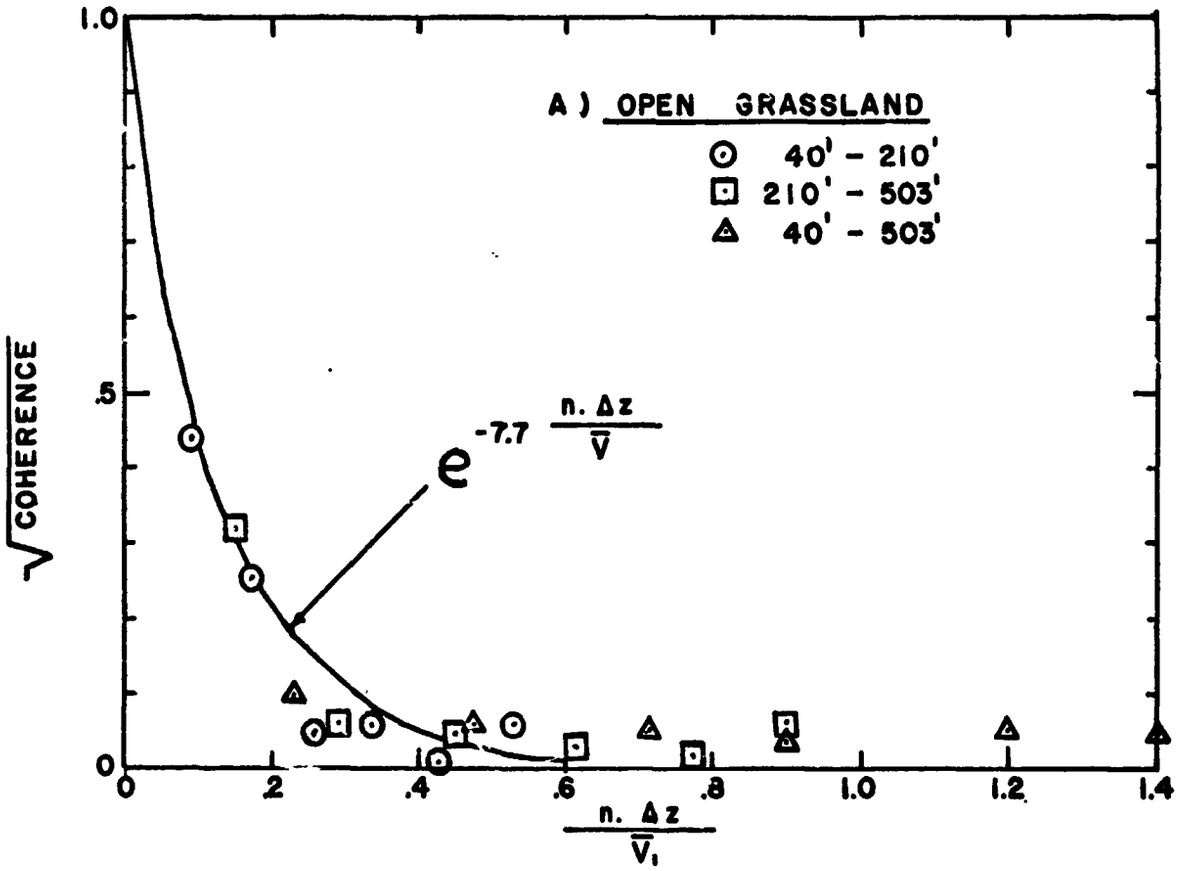

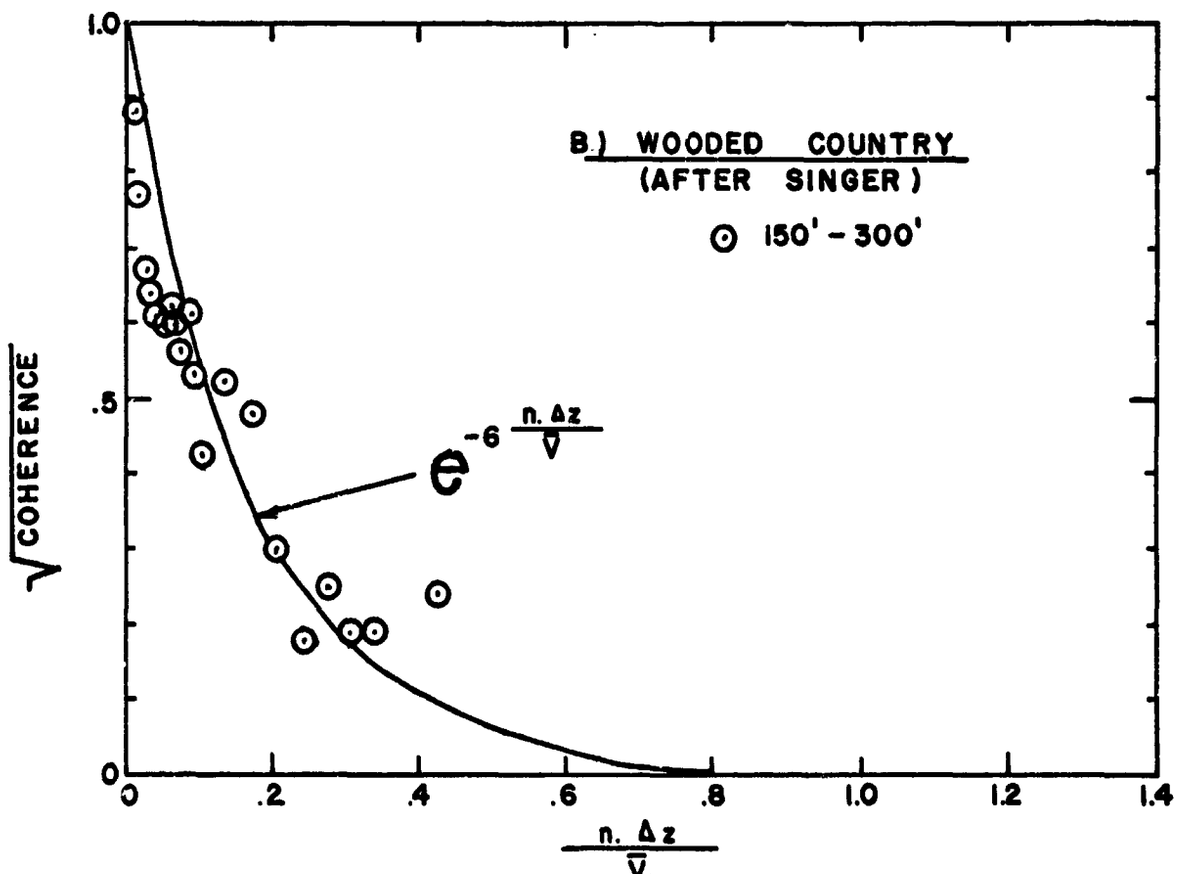

FIG. 8 ABSOLUTE VALUE OF CORRELATION ($\sqrt{\text{COHERENCE}}$) OF WINDSPEED IN VERTICAL DIRECTION AS FUNCTION OF SEPARATION TO WAVELENGTH RATIO

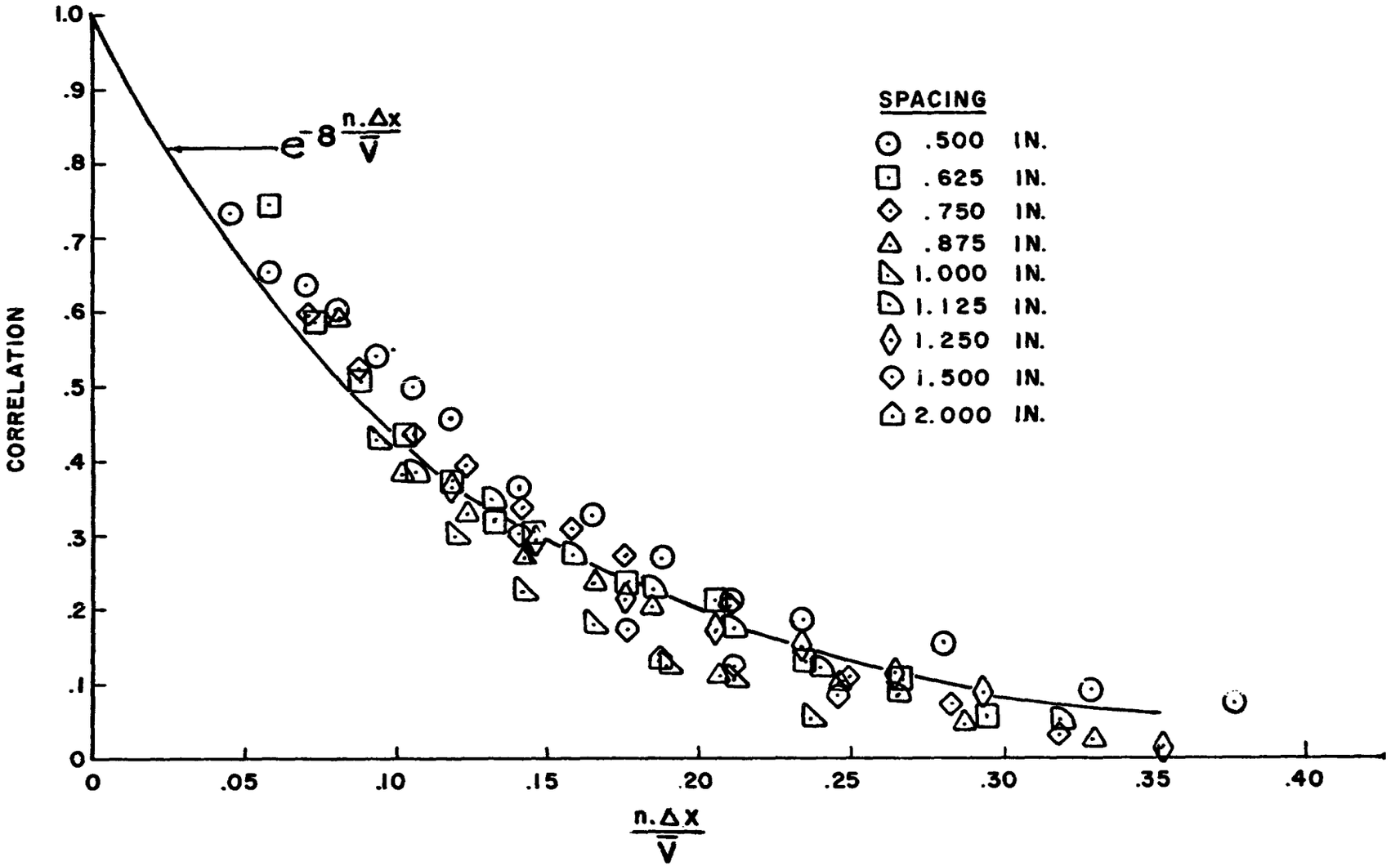

FIG. 9 LATERAL CORRELATION OF LONGITUDINAL VELOCITY IN STRONG TURBULENCE IN WIND TUNNEL.

SESSION III - EXPERIMENTAL AND ANALYTICAL SIMULATION TECHNIQUES

Chairman - Wilmer H. Reed, III, NASA Langley Research Center

LABORATORY SIMULATION OF ATMOSPHERIC MOTIONS IN THE LOWEST ONE HUNDRED METERS

by

J. E. Cermak
Professor-in-Charge, Fluid Mechanics Program
College of Engineering
Colorado State University
Fort Collins, Colorado

Paper presented at

Meeting on Ground Wind Load Problems
in Relation to Launch Vehicles
Langely Research Center
Hampton, Virginia
7-8 January, 1966

CER66JEC31

Summary

The simulation of motion in the atmospheric surface layer by low-speed, wind-tunnel flows is discussed. Similarity parameters and wind-tunnel characteristics required for simulation of small- and micro-scale atmospheric motions are stated. Comparisons of vertical distributions of mean velocity for different thermal conditions, turbulence power spectra, energy dissipation rates, and intensity of the vertical component of turbulence are made for wind-tunnel and atmospheric data -- data taken in the thick turbulent boundary layer (1 m) produced by flow over a long test-section floor (20 m) show good agreement with atmospheric data.

Time and length scaling factors for small and large scale turbulence are established through the use of similarity agreements utilizing the energy dissipation rate per unit of mass ϵ.

LABORATORY SIMULATION OF ATMOSPHERIC MOTIONS IN THE LOWEST ONE HUNDRED METERS

by

J. E. Cermak

Introduction

Simulation of atmospheric motions in the lowest one hundred meters by laboratory flows is desirable from several points of view. From a scientific perspective, laboratory flows which are faithful models of atmospheric prototypes can be systematically studied under controlled geometrical, dynamical and thermal conditions to produce new knowledge about geophysical systems. From an engineering or applied perspective, simulated atmospheric flows in the laboratory are of value in experimental efforts to establish the dynamic behavior of structures, to predict the diffusion of heat and mass for various environmental circumstances, to study the scattering of electromagnetic energy, and to explore many other interactions between atmospheric motions and man's activities on the surface of his planet.

The remarks in this paper are confined to what is commonly called small-scale and micro-scale atmospheric motions. A restriction to small-scale motions limits the distances for which simulation is considered to those giving large values of the Rossby number or, in other words, flows in which the Coriolis acceleration is a minor factor in determining the flow. Horizontal distances are thus limited to about 150 km. Micro-scale motions are defined to be the turbulent motions embedded in the small-scale mean motion.

Nonuniformity of the small-scale mean motion occurs both in horizontal and in vertical directions. Horizontal nonuniformity is influenced strongly by terrain nonuniformity while nonuniformity in the vertical direction is conditioned by surface shear stress and vertical heat flux. Simulation of these nonuniformities is discussed for steady flow of the surface layer.

Turbulence structure -- the micro-scale motion -- is characterized by numerous measures of which length scales, intensities, energy spectra, and turbulent energy dissipation are of primary importance. Comparisons of such quantities for laboratory and atmospheric data have been made in an exploratory sense at the Fluid Dynamics and Diffusion Laboratory of Colorado State University. These studies which are described in Ref. 1, reveal that much research remains to be accomplished before atmospheric turbulence structure can be simulated with a high degree of confidence; however, the special type of wind tunnel developed at Colorado State University produces turbulent boundary-layer flows having the desired characteristics.

Symbols

Symbol	Definition	Dimensions
g	gravitational acceleration	Lt^{-2}
h	reference height	L
k	Karman constant or wave number - or	L^{-1}
m	subscript designating model flow	-
p	subscript designating prototype flow	-
t	time	t
u	turbulent velocity fluctuation in mean flow direction	Lt^{-1}
$\overline{u^2}$	time mean of u^2	L^2t^{-2}
w	turbulent velocity fluctuation in vertical direction	Lt^{-1}
w'	$(\overline{w^2})^{1/2}$	Lt^{-1}
C	constant	-
C_p	Specific heat at constant pressure	$QL^{-3}T^{-1}$
E(k)	three-dimensional energy spectrum	L^3t^{-2}
$E_1(k)$	one-dimensional energy spectrum	L^3t^{-2}
F	force	F
H	turbulent heat flux	$QL^{-2}t^{-1}$
L	Monin-Obukov stability length	L
L_x	integral scale in direction of mean flow	L

Symbols - continued

Symbol	Definition	Dimensions
L_d	scale length for small scale turbulence	L
L_δ	scale length for large scale turbulence	L
Q	thermal energy	Q
Ri	Richardson number	-
T	mean absolute temperature	T
U	mean local wind speed	Lt^{-1}
U_a	mean ambient wind speed	Lt^{-1}
U_*	shear velocity	Lt^{-1}
V	mean reference wind speed	Lt^{-1}
Z	vertical distance above surface	L
Z_o	aerodynamic surface roughness	L
β	constant	-
δ	boundary-layer thickness	L
ϵ	turbulent energy dissipation rate per unit of mass	L^2t^{-3}
ν	kinematic viscosity of fluid	L^2t^{-1}
ρ	mass density of fluid	ML^{-3}
τ_o	surface shear stress	FL^{-2}

Army Meteorological Wind Tunnel

If the laboratory data referred to in this paper are to be fully appreciated, a brief comment on the wind tunnel in which they were obtained should be made. The motivating idea leading to the design of this unique facility was to provide a long test section so that a thick turbulent boundary layer can develop in a natural manner. Figure 1 shows this laboratory facility.

Gross operating conditions of the wind tunnel have the following characteristics:

Ambient wind speed U_a : 0.5-37 m/sec

Ambient turbulence intensity: 0.1 per cent

Max. temperature differences at 1.5 m/sec:

$T_{\text{cold floor}} - T_{\text{hot air}} = -65^{0}C$

$T_{\text{hot floor}} - T_{\text{cold air}} = 105^{0}C$

Most of the data referred to were taken at the downstream portion of the test-section approximately 24 m from the entrance and about 12 m from the beginning of the thermally controlled floor section. Reference 2 describes the wind tunnel in detail; however, the following flow characteristics at a wind speed of about 9 m/sec are useful to keep in mind:

Boundary-layer thickness δ : $70 < \delta < 110$ cm (depends on floor roughness)

Turbulence integral scale L_x: 11 cm at $Z = \delta/2$

Taylor's micro-scale : 0.9 cm at $Z = \delta/2$

Richardson number Ri : $-0.8 < Ri < 0.3$ at $Z = 3$ cm ($U_a = 1.5$ m/sec)

Requirements for Laboratory Simulation of the Atmospheric Surface Layer

An examination of the governing equations of motion and the equation for conservation of energy gives parameters which must be equal in both the laboratory and the field for similarity in the strict sense. The parameters and auxiliary condition which must be matched are shown in Fig. 2. In addition, the boundary conditions, including surface temperature and roughness variation with position and ambient turbulence intensity, must be similar.

Meeting all of these requirements simultaneously is generally impossible; therefore, a compromise with strict similarity is necessary. The important problem which must be faced is to determine the conditions under which equality of certain parameters can be relaxed without introducing serious error in the laboratory flow. By limiting the flow extent to under 150 km, equality of the Rossby numbers is no longer a necessity. If air is used for the laboratory flow the Prandtl numbers and specific heat ratios are automatically equal. Since the Froude number and Richardson number for thermally stratified flows are equivalent, the major parameters remaining to be matched are the Reynolds number and the Richardson number. By an adequately designed heating and cooling system an equality of Richardson numbers is possible. Therefore, the Reynolds number, because of the necessity to use length scale ratios up to about 1:1000, presents the major difficulty in achieving strict similarity.

Spatial Nonuniformity of the Mean Wind Field (small-scale motions)

A. Variation in the horizontal due to topographic features.

Topographic features and large structures may produce variation of the surface wind field. If these features are "sharp-edged",

models scaled to 1:1000 or even 1:5000 (Ref. 3) give good simulation of the mean wind field in spite of the Reynolds number differing by three orders of magnitude. The reason for successful flow simulation in these cases is that the basic flow pattern no longer is a function of Reynolds numbers (for sufficiently high values) but depends only on the geometry.

An example of such simulation is reported in Ref. 4 and is shown in Fig. 3. Comparison of the model flow with actual field data gave excellent agreement. The main lesson to be learned from these experiences is that strict equality of the Reynolds number for model and prototype flows is not necessary in order to achieve similarity of gross flow patterns over objects having sharp edges.

B. Variations in the vertical direction due to shear and thermal structure

Variation of wind speed in the vertical direction is in general complex; therefore, simulation has been studied primarily for the "ideal" case. By "ideal"is meant flows over level plane areas where topographic effects discussed in section A are negligible and buoyancy forces have no component parallel to the surface.

Mean velocity profiles under a variety of thermal stability conditions have been measured in the thick turbulent boundary layer at about 24 m from the test section entrance. These vertical distributions are compared with field data taken during project Prairie Grass in Fig. 4. The basis for comparison is the log-linear relationship

$$\frac{U}{U_*} = \frac{1}{k}\left(\ln\frac{Z}{|L|} + \beta\frac{Z}{L} + C\right)$$

in which the Monin-Obukov stability length $L = \dfrac{-U_*^3\, C_p \rho T}{k g H}$ is the reference length and the shear velocity $U_* = (\tau_o/\rho)^{\frac{1}{2}}$ is the reference

velocity. The agreement of the two sets of data reveals that the mean flows are similar over at least the lower one-third of the wind-tunnel boundary layer. The corresponding height in the atmosphere may vary from about 20 to 200 m.

Under neutral thermal conditions (adiabatic in the atmosphere) the corresponding vertical variation of wind speed becomes

$$\frac{U}{U_*} = \frac{1}{k} \ln \frac{Z - Z_o}{Z_o} .$$

Therefore, under such conditions where the object to be studied has a height h less than the boundary-layer thickness δ one arrives at the similitude criteria of Jensen (5). This criteria is merely that the ratio of roughness heights for model and prototype $(Z_o)_m / (Z_o)_p$ must equal the length scale ratio determined by the height ratio of model and prototype structure h_m/h_p; i.e.,

$$\frac{h_m}{h_p} = \frac{(Z_o)_m}{(Z_o)_p}$$

Similarity comparisons for the outer part of the boundary layer have not been made. When sufficient field data become available, a velocity defect form such as proposed by Hama (6)

$$\frac{U_a - U}{U_*} = 9.6 \left(1 - \frac{Z}{\delta}\right)^2$$

which correlates laboratory data well for $0.15 < Z/\delta < 1$ is expected to also correlate the field data. Since δ is an unknown in the atmosphere a more practical form of the velocity-defect relationship can be taken as

$$\frac{U_h - U}{U_*} = C \left(1 - \frac{Z}{h}\right)^2$$

where C is expected to depend upon h and the ambient turbulence.

Turbulence Structure (micro-scale motions)

Efforts to simulate turbulent structure of the atmospheric surface layer in the laboratory are closely associated with the problem

of producing a laboratory spectral energy distribution $E_1(k)$ which is similar to what is found in the atmosphere. If the one-dimensional energy spectra $E_1(k)$ are similar, then one can proceed to derive, on the basis of dimensional arguments, time and length scales relating the two flow fields.

Fortunately, close similarity of the one-dimensional energy spectra exists for boundary layer flows obtained in the downstream portion of the long meteorological wind tunnel. The data shown in Fig. 5 reveal close correspondence (including a significant inertial subrange where $E_1(k) \propto k^{-5/3}$ excepting at small relative wave numbers $k/k_d = \frac{k}{\epsilon^{1/4} \nu^{-3/4}}$ where the boundary-layer thickness of the wind-tunnel flow limits the large-scale turbulent motions to being of order δ. Apart from limitation on large-scale turbulent motions, the significant energy-spectrum features are present in the laboratory flow provided the boundary layer can develop over a sufficiently long fetch.

If the small-scale turbulence structure over the outer 90 percent of the boundary layer is acknowledged to closely approximate an isotropic turbulence field, dimensional arguments lead to a length scale relationship. Consider a field of turbulence in which the turbulence Reynolds number is moderately large. Should a volume of fluid moving downstream from a turbulence generating grid in a wind tunnel be followed, the turbulence structure (energy spectrum) is expected to depend only upon the energy dissipation per unit of mass ϵ, the kinematic viscosity ν and the time of travel t. As is indicated by Hinze (7, p. 187) these three quantities form a dimensionless group which must then be a constant; i.e.,

$$\frac{\epsilon t^2}{\nu} = \text{constant.}$$

In the boundary-layer flow under consideration the time t has little meaning in the sense of our model flow; therefore, we shall construct a time scale which depends on a characteristic velocity and length. Keeping in mind that the energy spectra are nearly similar for the two flows, a velocity derivable from this distribution should be selected for reference; therefore, the mean square longitudinal velocity fluctuation $\overline{u^2}$ becomes significant since it may be expressed as

$$\overline{u^2} = \int_0^\infty E_1(k)\, dk = \int_0^\infty E(k)\, dk$$

where $E(k)$ is the three-dimensional energy spectral function.

Defining a scale length as L_d, the dimensionless grouping obtained for the turbulence field may be expressed as

$$\frac{\epsilon L_d^2}{\overline{u^2}\,\nu} = \text{constant}.$$

Considering that ν is equal for both the laboratory and the atmospheric boundary layer, a statement relating the laboratory model length scale $(L_d)_m$ to the prototype atmospheric length scale $(L_d)_p$ can be made. This statement is

$$\frac{(L_d)_m}{(L_d)_p} = \left[\frac{(\epsilon/\overline{u^2})_p}{(\epsilon/\overline{u^2})_m}\right]^{1/2}$$

The length L_d defined is entirely dependent upon the turbulence energy spectrum because ϵ can be written as

$$\epsilon = 2\nu \int_0^\infty k^2 E(k)\, dk$$

therefore,

$$L_d^2 \propto \frac{\int_0^\infty E(k)\,dk}{2\int_0^\infty k^2 E(k)\,dk}$$

Exploratory data have been collected in the wind tunnel (Ref. 8) and in the atmosphere (Ref. 9) which permit calculation of the length scales. Distributions of $\epsilon/\overline{u^2}$ are shown in Fig. 6 for both the wind-tunnel flow and the atmosphere. The distributions appear to be of the same form. If the ratio $(\epsilon/\overline{u^2})_p / (\epsilon/\overline{u^2})_m$ is computed for the outer portion of these profiles, the prototype length scale $(L_d)_p$ is 16 times larger than the model length scale $(L_d)_m$. A corresponding ratio of time scales is given by $t_m/t_p = (\epsilon_p/\epsilon_m)^{1/2}$. For these flows $t_m/t_p = (260/9300)^{1/2} = 1/6$. The scale ratios obtained by these arguments give a measure of the relative small scale characteristics for the two flows. The importance of scaling these small-scale micro motions depends upon the problem under study -- for flow around objects, say a cylinder of diameter d, where d_m or d_p is large compared to $(L_d)_m$ or $(L_d)_p$, respectively, similitude at this scale is relatively unimportant compared to similitude for the large-scale micro motions which we discuss in the next paragraph.

To examine similarity of the large-scale turbulence consider that

$$\epsilon \propto \frac{(\Delta U)^3}{L_\delta}$$

where ΔU is a gross mean velocity difference. On this basis, the ratio of large scale lengths becomes

$$\frac{(L_\delta)_m}{(L_\delta)_p} = \left(\frac{\Delta U_m}{\Delta U_p}\right)^3 \frac{\epsilon_p}{\epsilon_m}$$

For the wind-tunnel flow over the rough boundary and the atmospheric flow referred to in Fig. 6, the quantities on the right-hand side of the previous equation are as follows:

	prototype	model
ϵ (cm^2/sec^3)	260	9300
ΔU (m/sec)	16	9.15

Here ΔU is taken as the velocity where the vertical velocity gradient vanishes in both cases. The length-scale ratio then becomes

$$\frac{(L_\delta)_m}{(L_\delta)_p} = \frac{1}{190}$$

Accordingly, if the mean turbulent dissipation rates are known and the wind-speeds at approximately zero vertical wind gradient are known for both a laboratory and an atmospheric flow, it becomes possible to establish the relationship between height in the model and the prototype. The corresponding time-scale ratio for the large-scale turbulent motion becomes

$$\frac{t_m}{t_p} = \left(\frac{(L_\delta)_m}{(L_\delta)_p}\right)^{2/3} \left(\frac{\epsilon_p}{\epsilon_m}\right)^{1/3} .$$

These scale ratios become particularly significant when it is desired to simulate flow around structures or other phenomena which are sensitive to the large-scale micro motions or turbulence. To simulate flow around a structure using the atmospheric flow and wind-tunnel flow referred to here, the appropriate model scale would be approximately 1:200. Of course, the wind-tunnel boundary layer must be sufficiently thick to submerge the model.

In Fig. 7 data are shown which compare the behavior of the intensity of the vertical velocity fluctuations at 3 cm above the smooth wind-tunnel floor and 1 and 2 m above the earth's surface as affected by thermal stratification. These data which are presented in Ref. 10 show that the effects of thermal stratification are similar for the two flows. In the region where these data were taken ($Z < 0.1\ \delta$) the actual average height ratio of 1/50 is estimated to be approximately equal to $(Z_o)_m / (Z_o)_p$ for the two flows. The wind-tunnel data taken at U = 150 cm/sec appears to be strongly influenced by viscous forces; i.e., the Reynolds number $\frac{UZ}{\nu}$ is too small compared to the prototype value.

Summary

Mean flow characteristics and turbulence characteristics in the lowest 100 m of the atmosphere can be simulated in the laboratory if adequate wind-tunnel facilities are available. The wind-tunnel should have a long test section which will permit development of a turbulent boundary layer having a thickness at least equal to the height of any object, scaled to a practical size for study, which is to be placed in the flow. At a test section length of 20-30 m the spectrum of turbulence is similar excepting at the smallest wave numbers. If the energy dissipation rate and the ambient wind speed are known for a laboratory flow and an atmospheric flow, the scaling ratio for vertical heights or the large-scale turbulent motions can be established.

Acknowledgments

The writer is indebted to Dr. H. Chuang and Professor V. A. Sandborn for their consent to use unpublished wind-tunnel data obtained in their studies as shown in Figs. 4 and 6, respectively. Support under Army Research Grant DA-AMC-28-043-65-G20 has made possible all of the wind-tunnel studies referred to in this paper.

References

1. Cermak, J. E.; Sandborn, V. A.; Plate, E. J.; Binder, G. H.; Chuang, H.; Meroney, R. N.; and Ito, S. Simulation of atmospheric motion by wind-tunnel flows. Fluid Mechanics Program, Colorado State University, May 1966, CER66JEC-VAS-EJP-GJB-HC-RNM-SI-17.

2. Plate, E. J. and Cermak, J. E. Micrometeorological wind-tunnel facility. Final Report, Contract No. DA-36-039-56-80371. Fluid Dynamics and Diffusion Laboratory Report No. CER63-EJP-JEC9. Colorado State University, February 1963.

3. Field, J. H. and Warden, R. A survey of air currents in the Bay of Gibralter, 1929-1930. Geophysical Memoirs, No. 59 (R and M 1563) published by Her Majesty's Stationery Office.

4. Cermak, J. E., Malhotra, R. C., and Plate, E. J. Investigations of the Candlestick Park wind problem, vol. II: wind-tunnel model study, Fluid Dynamics and Diffusion Laboratory. Report No. CER63JEC-RCM-EJP27, Colorado State University, July 1963.

5. Jensen, M. The model-law for phenomena in natural wind, Ingeniren (International Edition) 2, 121-128, 1958.

6. Hama, F. R. Boundary layer characteristics for smooth and rough surface, Soc. Naval Architects Marine Engrs. Trans. 62, 333, 1954.

7. Hinze, J. O. Turbulence, McGraw-Hill Book Co., 1959.

8. Plate, E. J. and Sandborn, V. A. Modeling of a thermally stratified boundary layer. Res. Memo. CEM66EJP-VAS8. Fluid Dynamics and Diffusion Laboratory (U.S. Army Grant DA-AMC-28-043-65-G20), April 1966.

9. Ivanov, V. N. On certain characteristics of turbulence of the wind field in the lower 300-m layer of the atmosphere. Izuchenie Pogranichnogo Cloya Atmosfery S 300-metrovoj Meteorologicheskoj Bashni, Acad. of Sci., USSR, Moscow, 1963.

References - continued

10. Cermak, J. E. and Chuang, H. Vertical-velocity fluctuations in thermally-stratified shear flows. Tech. Report CER65JEC-HC48. Fluid Dynamics and Diffusion Laboratory, Colorado State University, 1965.

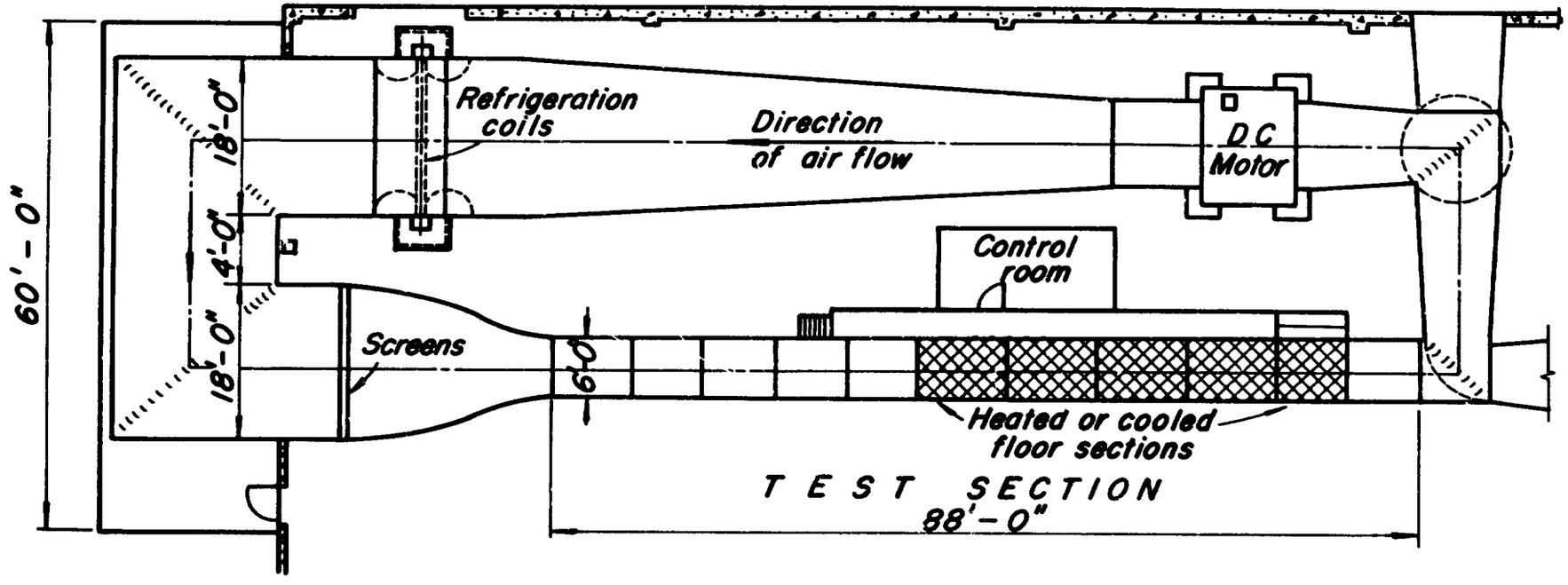

PLAN VIEW

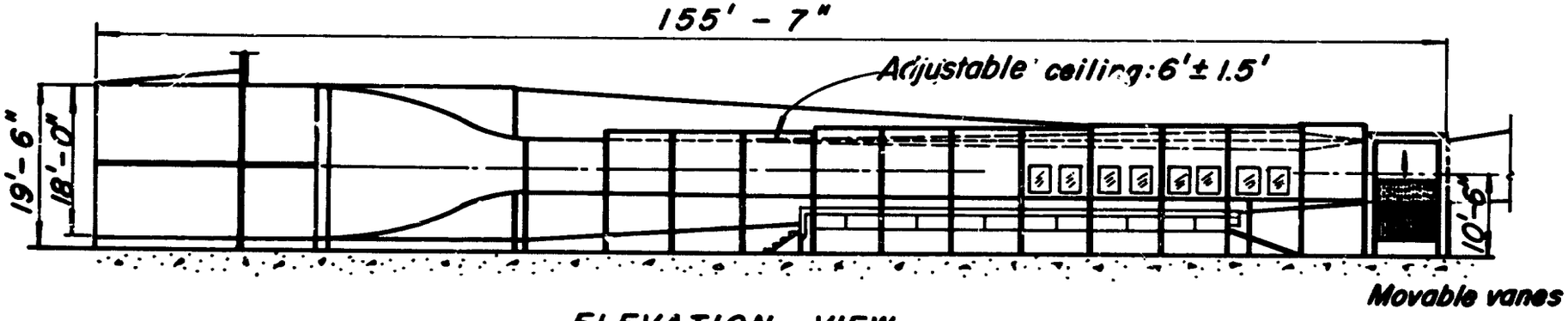

ELEVATION VIEW

FIG. 1

GEOMETRICAL SIMILARITY: Scale model

DYNAMIC SIMILARITY: Rossby number -- $\frac{V}{L\Omega_0}$

Froude number -- $\left(\frac{V^2}{g_0 L \frac{\Delta\gamma_0}{\gamma_0}}\right)^{\frac{1}{2}}$

Reynolds number -- $\frac{VL}{\upsilon}$

THERMAL SIMILARITY: Prandtl number -- $\frac{k}{c_p \mu}$

Specific heat ratio -- $\frac{c_p}{c_v}$

Richardson number -- $\frac{g_0}{T_0} \frac{\Delta T}{V^2} L$

BOUNDARY CONDITION SIMILARITY:

Surface temperature distribution
Surface roughness distribution
Ambient turbulence

FIG. 2 SIMILARITY PARAMETERS

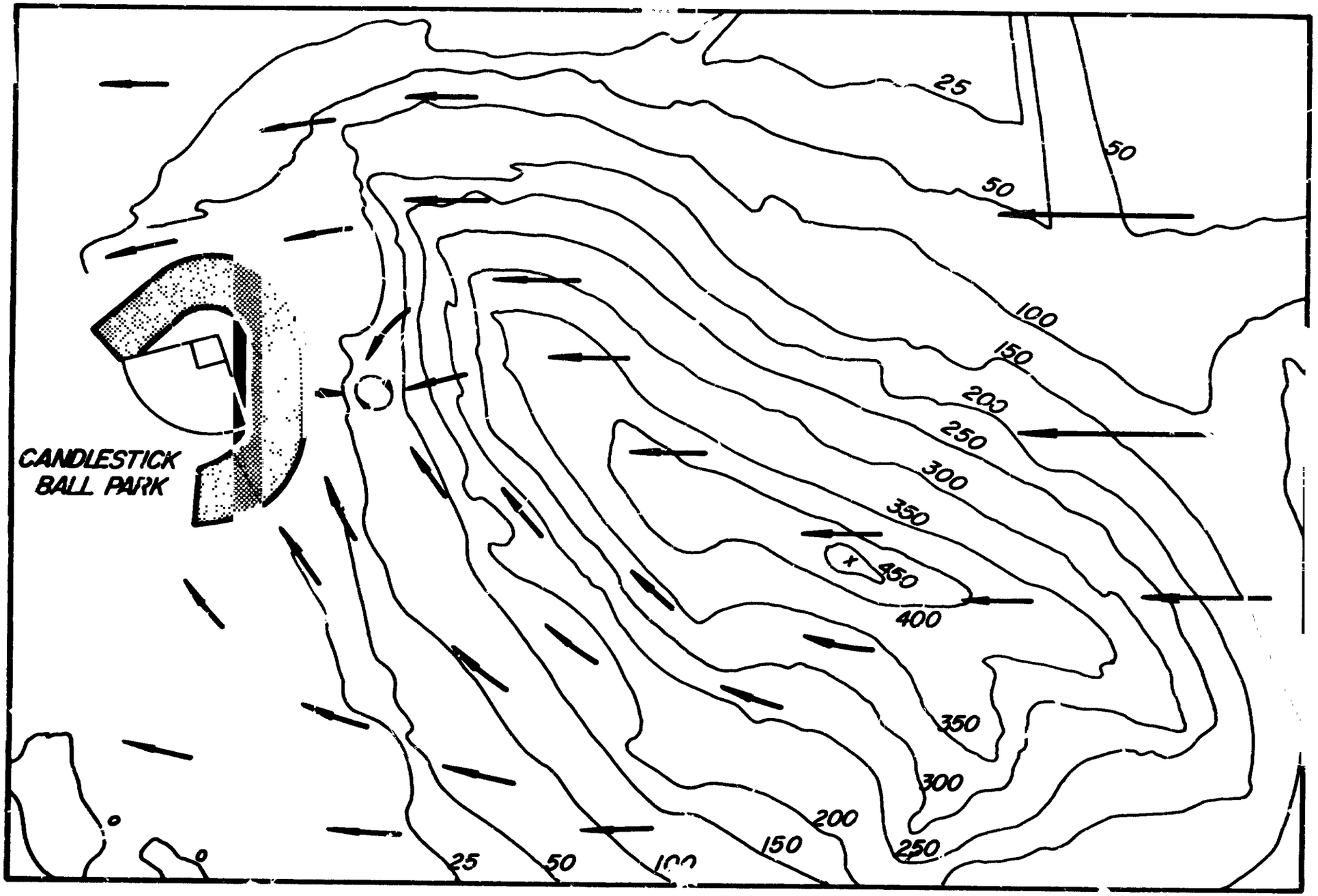

FIG. 3 SURFACE FLOW PATTERN -- 1:800 scale model

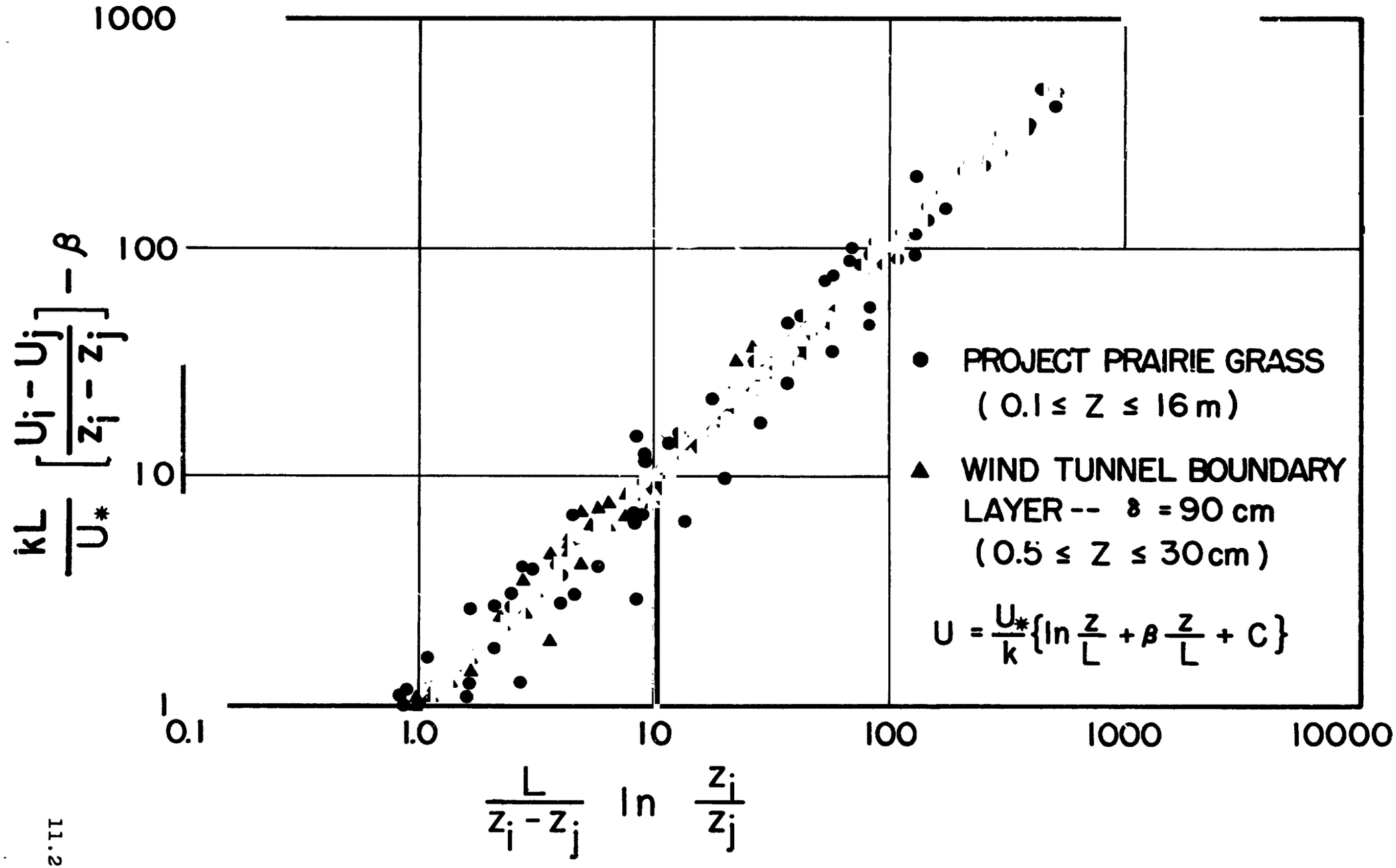

11.21

FIG. 4 COMPARISON OF WIND-TUNNEL AND FIELD WIND-SPEED DATA BASED ON LOG-LINEAR RELATION

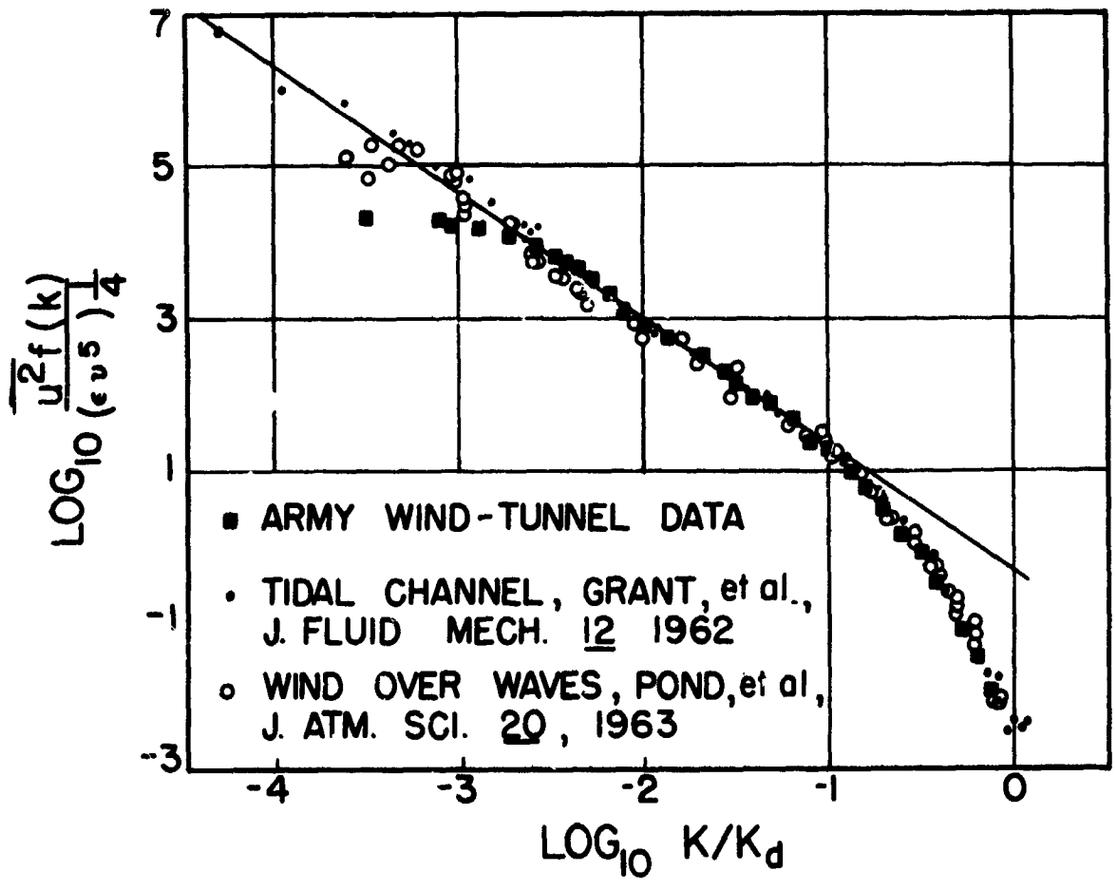

FIG. 5 COMPARISON OF SPECTRA MEASUREMENTS

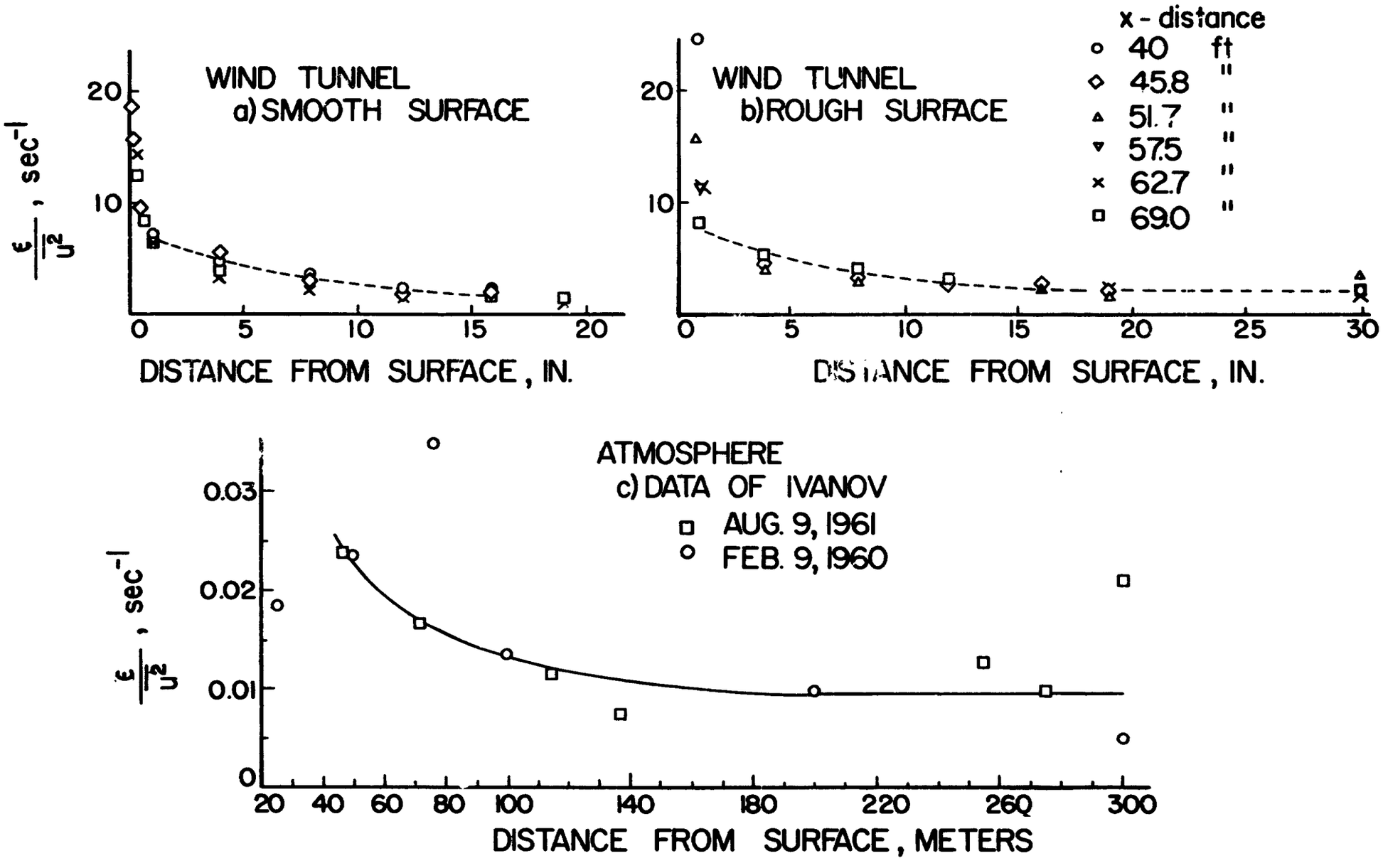

11.23

FIG. 6 VARIATION OF THE RATIO OF TURBULENT DISSIPATION TO THE MEAN SQUARE LONGITUDINAL TURBULENT VELOCITY

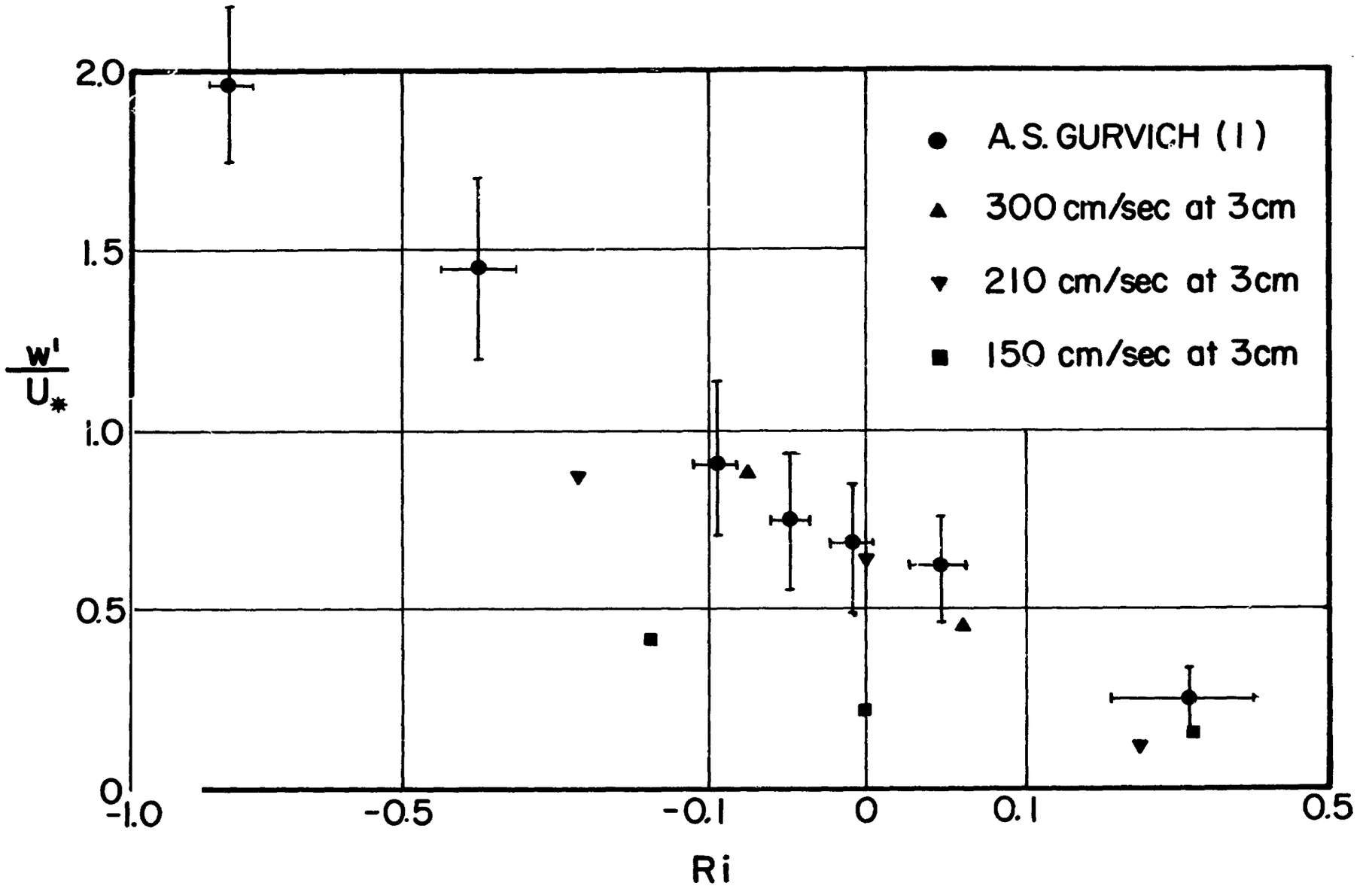

FIG. 7 DEPENDENCE OF DIMENSIONLESS TURBULENT INTENSITY OF THE VERTICAL COMPONENT UPON RICHARDSON NUMBER

AN APPROACH TO THE WIND-TUNNEL MODELLING OF THE RESPONSE OF STRUCTURES TO THE NATURAL WIND

By A. G. Davenport
Professor of Engineering Science

University of Western Ontario
London, Canada

INTRODUCTION

Historically, it has been traditional to design structures against the wind through the use of nominal static pressures of between 10 and 100 pounds per square foot applied to the horizontal projected area of the structure. These pressures have been derived, through a combination of some fairly approximate aerodynamic ideas, on the structure of the wind and how it acts on structures and from empirical observation and experience with the performance of full-scale structures.

Experiences such as the Tay Bridge disaster of 1879, in which the then longest bridge in the world plunged into the Firth of Tay with considerable loss of life, raised the values of design wind pressures from a figure less than 10 pounds per square foot to over 50 pounds per square foot. For a number of years the wind loads were derived largely on the basis of largest observed gust speeds and the drag coefficient of a flat plate. This gave birth to a generation of extremely stout and sturdy bridges and buildings.

Since that time most structures designed according to their static loading precepts have been comparatively immune to the effects of wind. However there have been a number of notable exceptions, amongst these were suspension bridges and stacks. Some of these structures, even though designed to resist thermal static loads, were known to show dangerous forms of oscillation which on

occasion led to failure. The failure of the Tacoma Narrows Bridge surprised the engineering profession into an awareness of problems due to wind loading which did not appear to respond to the traditional solutions. The diagnoses of some of these problems and their proper solutions are still being sought today.

HISTORICAL DEVELOPMENT OF THE APPLICATION OF WIND TUNNELS

The application of wind tunnels to structural engineering problems is at least as old as its application to aeronautical problems. Its impact and sophistication in development to meet its needs however has been far slower.

One of the earliest wind tunnels was built in the 1880's by Irminger, the manager of a gas works in Copenhagen. He used the facility in his factories to measure the forces on simple shapes. Later in his life he worked with Professor Nokkentred at the Technical University and did extensive work on the pressures on buildings. Gustof Eiffel, foremost a structural engineer, initiated wind-tunnel tests in Paris at the turn of the century.

From these beginnings, numerous wind-tunnel tests on building structures were undertaken during the first half of this century. In all cases the tests were carried out in the steady laminar flow of aeronautical wind tunnels. Only steady pressures and forces were considered.

There was some discussion on the proper modelling techniques that should be used; this mainly centered on the question of Reynold's number. It was generally conceded however that with sharp-edged structures duplication of Reynold's number was not important; only with curved structures was this likely to be significant and here devices, such as trip wires, could often be used to overcome what otherwise would have been a difficult problem of simulation on a wind-tunnel scale.

The existence of a mean velocity profile present in the natural wind was of course realized by meteorologists; it was not however a very well defined phenomenon, particularly in the urban environment of buildings which was far away from the meteorologists' customary fields of investigation which were mainly confined to grass fields and open water. This lack of firsthand experience offered no real encouragement to considering the effects of boundary layers in the wind tunnel. Besides most of the wind tunnels were used mainly for aeronautical purposes and had been deliberately designed to suppress the formation of boundary layers.

Only in one series of tests by Bailey and Vincent, which were carried out in the old Duplex wind tunnel at the National Physical Laboratory in England and having a uniform working section approximately 100 feet long, was the influence of boundary layers considered.

The pressures measured in these tests showed quite significant dissimilarities to previous tests. These tests were carried out at the beginning of the war however, and there were, perhaps, more pressing matters at hand which prevented these investigators pursuing the questions raised by the experiments and the possibilities opened up by this early, but unconventional, wind tunnel.

In the late 1950's Dr. Martin Jensen, working in the same laboratory as Irminger and Nokkentred in Copenhagen, carried out some most significant experiments on building shapes. The wind tunnel he used was a similar shape to the National Physical Laboratory Duplex wind tunnel and had a long parallel sided working section. The models he placed at the downstream end of the working section. On the floor of the tunnel he placed roughness mats, the texture of which ranged from the smooth floor of the tunnel to corrugated card board to small

stones. He measured the pressures on the models on the tunnel floor in the flows produced by these rough surfaces.

At the same time Jensen undertook experiments in the natural wind on larger scale versions of the same shapes. The results of his full-scale and model experiments are shown in Fig. 1.

As a result of these experiments Jensen published in 1958 a paper called "The Model-Law for Phenomena in Natural Wind". For the conclusions he drew I quote from the introduction to that paper.

> A great many technical circumstances depend on the wind in nature and cannot, or can only with great difficulty, be analysed except through model tests.
>
> As examples may be mentioned the wind load on buildings and structures, the contamination of the air from chimneys, and the various sheltering problems in agriculture and in living spaces between buildings.
>
> There is an unquestionable need of model tests, and as a matter of fact, a great many model tests have been carried out in the course of time within the said fields and similar fields in the aerodynamic laboratories.
>
> These investigations, however, are to some extent misleading, because the test procedure, especially the model-law, has been wrong. It may seem strange that within a vast research field incorrect model-laws have been applied, but the explanation is both simple and not very flattering: the model tests have practically never been checked by full-scale tests in nature.
>
> The natural wind is turbulent, and the phenomena dealt with in this paper take place in the boundary layer of the wind, and, as should be emphasized, are highly dependent on the nature of this boundary layer.
>
> Unfortunately, however, almost all previous tests have been carried out in wind-tunnels with as far as possible a smooth flow of air, and as for models of objects standing on the ground, it has moreover been tried earnestly to avoid the boundary layer of the wind tunnel.
>
> The correct model test for phenomena in the wind must be carried out in a turbulent boundary layer, and the model-law requires that this boundary layer be to scale as regards the velocity profile.

It should be noted that the few tests carried out on full scale structures generally indicated a lack of agreement with the laminar flow wind tunnel tests. Rathbun for example concluded that the pressures he measured on the Empire State Building did not resemble those determined by Dryden and Hill in the wind tunnel.

In Jensen's experiments in the wind tunnel he confined his interest to the steady pressures. In this sense while he attempted to model the flow correctly through shear stresses at the ground surface as in the atmospheric boundary layer, he did not attempt to model completely the structures themselves as well. To model any structure completely it is also necessary to model its dynamic characteristics.

Probably the first tests carried out on structures in which the correct dynamic properties are reproduced were those run after the failure of the Tacoma Narrows Bridge. Since then others have followed notably Scruton and his colleagues at the National Physical Laboratory in England. In the suspension bridge experiments at Washington open jet wind tunnels were used producing a laminar flow. They did not therefore reproduce the turbulence.

THE PRESENT APPROACH TO WIND TUNNEL MODELLING

Two years ago the writer was asked to direct a wind tunnel test programme in preparation for the design of The World Trade Center. These tests carried out at the Colorado State University in cooperation with Dr. Cermak may have constructed the first tests in which the dynamics of the structure and the turbulent boundary layer flow were both reproduced.

Some other tests on square prisms have since been carried out and Fig. 2 illustrates the influence of the boundary layer on the behaviour. These tests

in Fig. 2 were carried out on a rigid model pivoted at the base with springs. It is reasonable to conclude from this series of diagrams that aeroelastic tests which are not carried out with the correct boundary layer can be seriously misleading.

Colorado State University appears to have built the first tunnel in North America in which it is feasible to carry out tests of this nature. It will be described at this symposium by Dr. Cermak the Director.

Recently the writer has built a tunnel of similar dimensions at the University of Western Ontario. This is illustrated in Fig. 3. It shows the long working section of approximately 100 feet in length and 8 feet in width. The roof height is adjustable throughout to permit control over the longitudinal pressure gradient.

This tunnel was first put into use early this year. One of the first studies we have undertaken concerns the dynamic response of hyperbolic cooling towers. This followed the failure of a number of these structures in England. Fig. 4 shows a view of the dynamic model of the cooling towers. This model conforms to the full scale structure in geometry, damping, mass and stiffness.

One of the significant series of tests we ran with this cylindrical structure was to compare the interaction of Reynold's number, model size, surface roughness of the tower itself and scale and intensity of turbulence. (This has some significance from the point of view of the tests on space vehicles which we will be considering later this year.)

It was found that over the range of Reynold's numbers tested (.1 to .5 million) all of the variables produced some interaction. It was of some encouragement to note that turbulence in the flow tended to stabilize the response to Reynold's number and, it would appear, induced super-critical flow conditions.

This appears to be an area that should be considered further, and we will be doing so in the test programme on space vehicles.

Finally I would like to make reference to the degree of success that is likely to be achieved in simulating the atmosphere. First, one might observe, we are never likely to be completely successful. Even if we overlook the question of the thermal conditions as being of secondary significance in the wind-loading problem there are still features of the atmosphere such as the coriolis forces, which undeniably influence the earth's boundary layer yet cannot be simulated in a wind tunnel. Even the earth's boundary layer itself is a somewhat nebulous phenomenon when it comes to defining its limits. It would certainly not appear to have the tidy upper boundary possessed by a boundary layer in a wind tunnel.

The best that can be hoped for possibly is to measure the properties in the wind tunnel and in the earth's atmosphere and to match them as well as possible. For this reason we have over the past few years been studying the wind in the atmosphere quite intensively.

In some tunnels use is being made of graduated screens, primarily to produce the mean flow profile, but inevitably some turbulence as well. We are adopting the same technique in order to give the boundary layer a start at the upstream end of the tunnel and thereby develop a thicker boundary layer than would be developed by the roughness alone. The belief is that the flow will have "forgotten" what caused the boundary layer by the time it reaches the downstream test section.

There might be some doubt as to whether the screen alone will produce the same detailed flow structure as does shearing action at the surface. Fig. 5 possibly suggests the relationship of the flow structure near the floor as

suggested by Townsend. The formation of jets shown in this diagram agrees well with some characteristics observed in atmospheric turbulence as well as boundary layer turbulence in the wind tunnel. The same formation is unlikely to develop behind a screen.

I am ending this paper without drawing any particular conclusions concerning the approach described toward modelling the action of wind in the boundary layer. The conclusions we hope will follow in a few months time, in particular in relation to the study on space vehicles. In the meantime we have nothing to suggest we are on the wrong track.

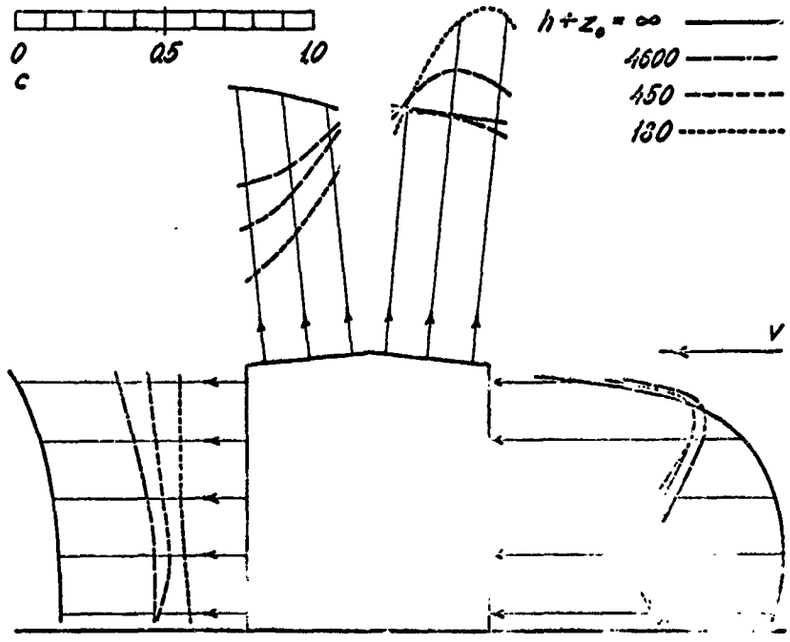

Smoothest Cases

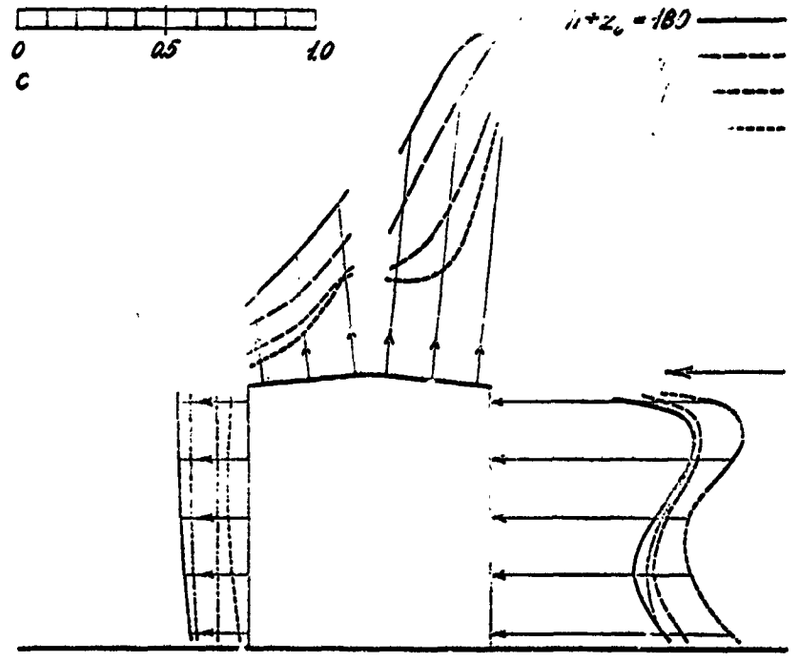

Roughest Cases

Fig. 1 Jensen's Measurements of Pressure on a Building in Boundary Layers of Differing Profile. (z_o = roughness length)

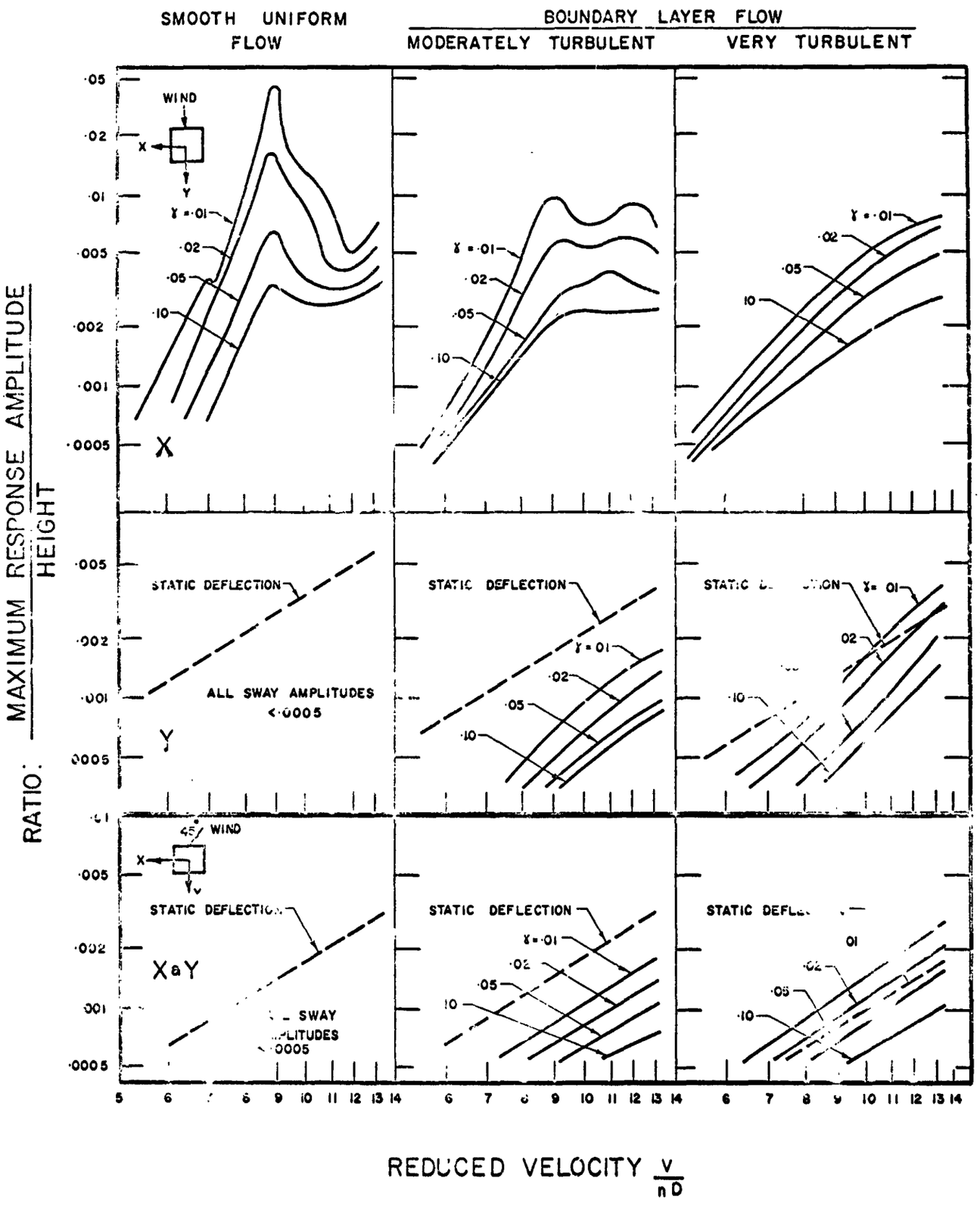

FIG. 2 COMPARISON OF DYNAMIC AND STATIC RESPONSE OF SQUARE TOWER (H = 6·5 D) TO UNIFORM STEADY FLOW AND TO TURBULENT BOUNDARY LAYER FLOW FOR VARIOUS CRITICAL DAMPING RATIOS γ

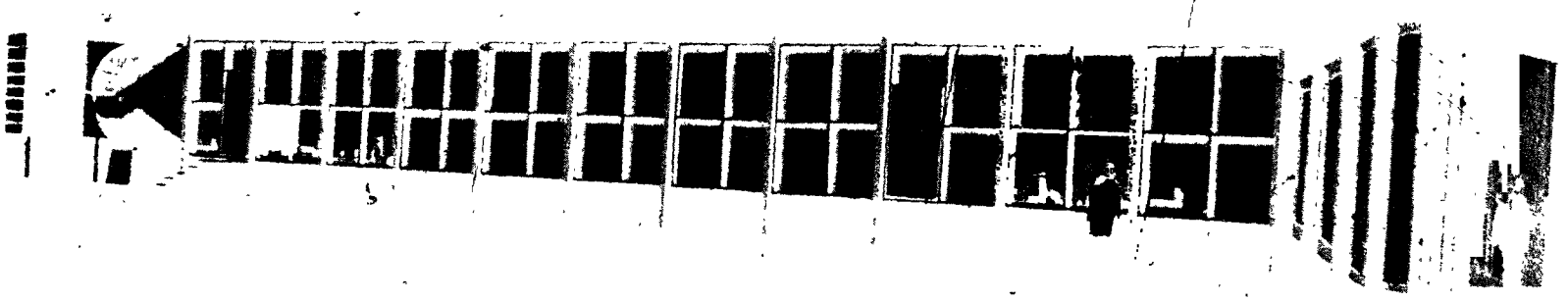

Fig. 3 The University of Western Ontario Boundary Layer Wind Tunnel

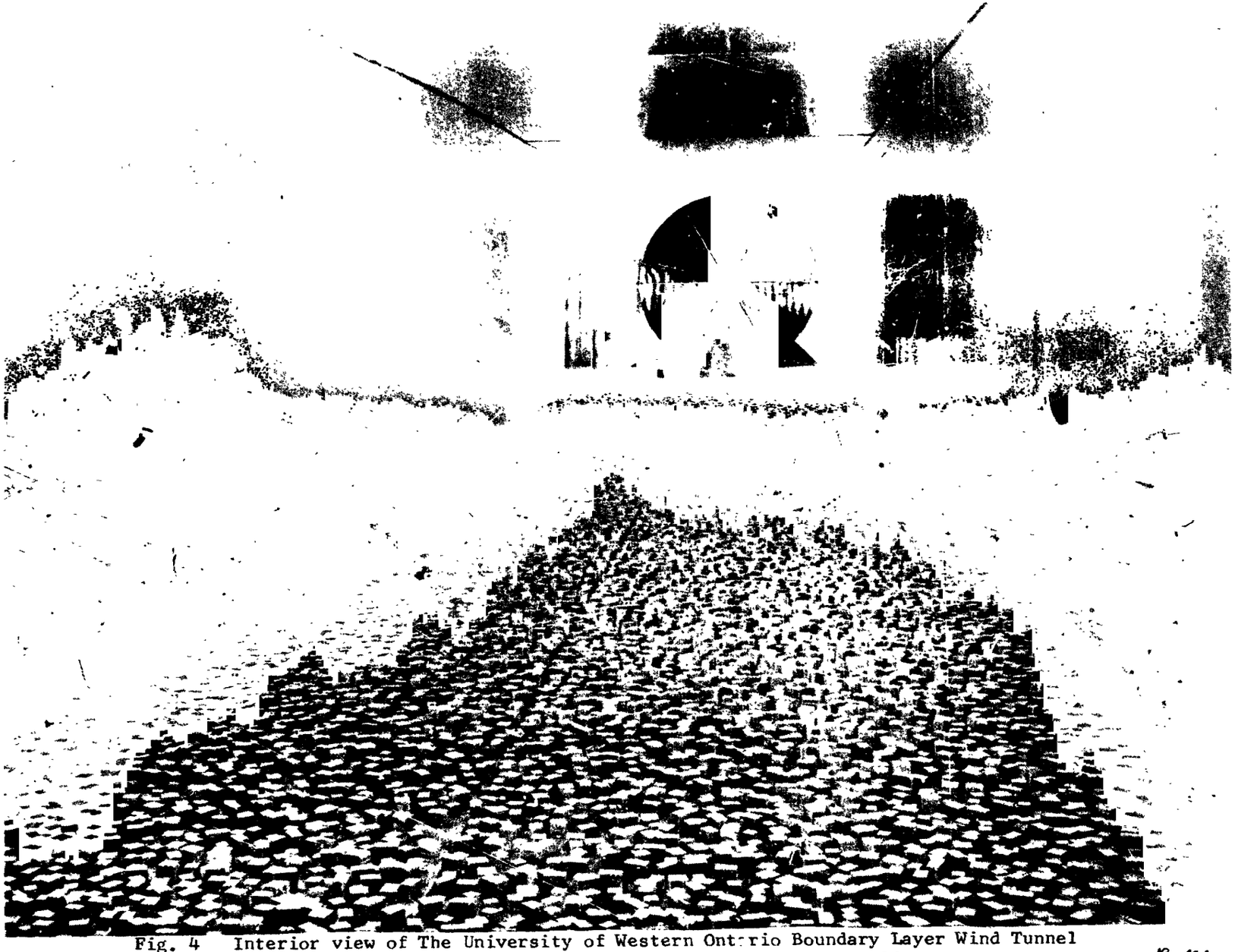

Fig. 4 Interior view of The University of Western Ontario Boundary Layer Wind Tunnel showing rough floor and aeroelastic model of hyperbolic cooling tower.

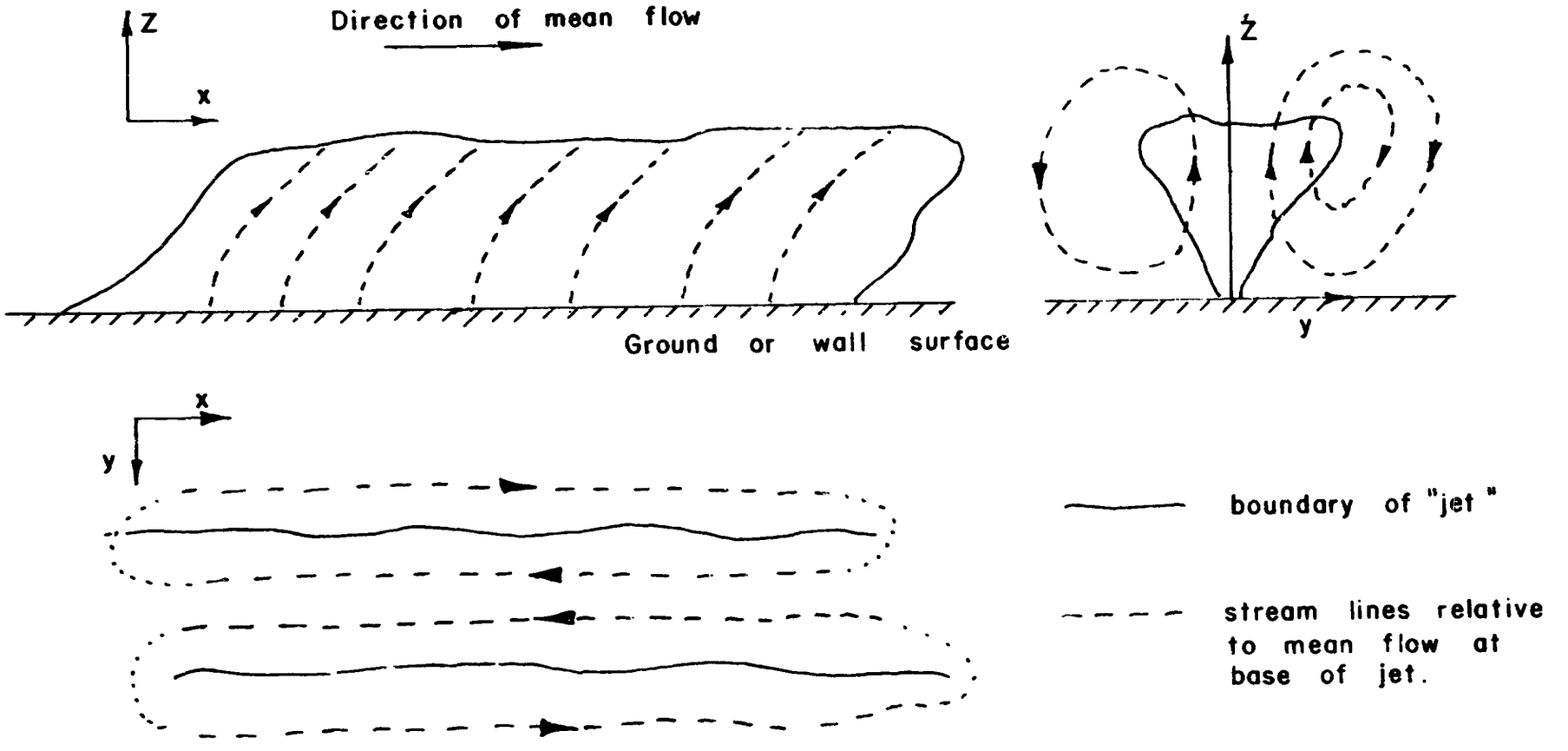

FIG. 5 STRUCTURE OF THE "TWO-DIMENSIONAL" JETS IN THE CONSTANT STRESS LAYER (AFTER TOWNSEND - 1957)

PREDICTIONS AND IMPLICATIONS OF THE FLOW FIELD PARAMETER ANALYSIS OF THE WIND INDUCED OSCILLATION PROBLEM*

By

Wayne E. Simon
Associate Research Scientist

Martin Company
Denver, Colorado

*This work was sponsored by NASA Marshall Space Flight Center Contract NAS 8-5322.

The fundamental ideas of the flow field parameter analysis and applications to the case of a vehicle standing alone are presented in Reference 1. Basically, the idea is to construct a good representation of the drag and pressure distribution on the vehicle. Then the spectrum of the local aerodynamic excitation is described by three characteristics: magnitude, shape factor, and the frequency (Strouhal) at which the peak excitation occurs. The magnitude is related to the steady drag, the shape factor to the separation angle, and the frequency to the curvature of the pressure distribution at the separation angle. Finally, the total aerodynamic excitation is made motion-dependent by assuming that the axial correlation length of the excitation is related in a specific way to the motion of the tip of the vehicle. Figures 1 through 18 are reproduced from Reference 1 and show how well the observed behavior of models can be duplicated with the analysis.

The next problem to be handled was the addition of tower effects to the analysis. The effects of the tower on the mean flow were approximated by superimposing a two-dimensional potential flow disturbance and a two-dimensional wake. The equivalent cylinder diameter for the potential flow and width and centerline velocity defect of the wake were then adjusted until the observed steady drag base bending moment on the model was duplicated. The model of the Saturn V tower is a truss-type structure with a cross-section approximately 14 inches square, and horizontal plates spaced vertically at 6 to 8 inches apart. For this model:

1) The equivalent two-dimensional potential flow disturbance was equal to the potential flow about a circular cylinder of 14.5 inch diameter;

2) The equivalent two-dimensional drag of the tower is equal to that of a circular cylinder whose (C_D . d) equals 26.5 inches;

3) The equivalent two-dimensional wake distribution of mean velocity is the same as that of the cylinder of 2), at a distance of 63.5 inches.

Figure 19 shows the steady drag base bending moment computed for these parameters compared with the data for the Saturn V model.

Thus the effect of the tower on the mean velocity at the model can be included in the computations. Now, if the response of the model is computed for the case of the model directly in the wake of the tower, it is found that the response is negligible. However, the observed response, although small, is not negligible. The conclusion drawn from this is that, in this case, it is necessary to include the effects of the high turbulence in the wake of the tower on the response of the model. In order to do this, the turbulence in the tower wake must be approximated.

The dynamic characteristics of the tower wake were represented by two parameters, turbulence scale and tower Strouhal number. In principle, a third parameter, the wake centerline turbulence intensity, should be used. However, the model response measurements determine only the combined effect of intensity and scale, so, based on Dryden's measurements

behind screens, the wake centerline turbulence intensity was assumed to be equal to the ratio of the turbulence scale to the distance between the tower and the vehicle. The values of the two parameters which were consistent with the data implied a turbulence scale of 5.66 inches (which compares favorably with the 6 to 8 inch spacing of the horizontal plates in the model of the tower) and a tower Strouhal number of 0.25, based on the 14.5 inch diameter implied by the potential flow disturbance.

Now, when the model is outside the wake of the tower, the only effect of the tower is through the potential flow disturbance. Thus the response of the model is affected only through the change in the local stream velocity at the model caused by the potential disturbance. Thus, the model response, as a function of local stream velocity, is unaffected by the tower for azimuth angles from 0° to $\pm$ 150° (outside the wake of the tower). Figure 20 shows model data plotted on this basis and compared with the computed response. Figure 21 presents data for the case of the model directly in the wake of the tower. Similar comparisons have been made for many configurations of the Saturn V models.

Now consider the implication of what has just been done. In order to match the data for the model in the wake of the tower, it was necessary to include the effect of the turbulence of the wake. Now to the model, turbulence is turbulence, and the source of the turbulence is immaterial. Thus it follows that the free stream turbulence should also be included in the response calculations. The point is academic for the wind tunnel models, since the turbulence in the wind tunnel is very

low, but it is important for the prototype response since the turbulence is typically two orders-of-magnitude higher than that in the wind tunnel. In order to make some calculations of this effect, an estimate of turbulence spectrum and scale was made as shown in Figure 22. Now the Reynolds number and Mach number for the prototype environment also differ from that of the model. Figure 23 shows the result of the changes in these three variables from model test values to prototype values on the computed response of the prototype. The most striking feature of Figure 23 is the dominant effect of the turbulence.

Now, a note of caution. These results are based on semi-empirical equations for drag, pressure distribution, and aerodynamic excitation. While the results are good representations of the observed response of wind tunnel models, the range of the variables in the wind tunnel is not large enough to provide a good test of the equations. For this reason, wind tunnel tests of cylinders have been conducted at Colorado State University during the last nine months to test some aspects of these equations. Approximately 600 runs have been made in which the variation of surface pressure, shearing stress, and rms unsteady pressure with azimuth angle has been measured. Blockage ratio was varied from 4% to 50%. Turbulence intensity from 0.1% to 11%, surface roughness from smooth to 0.01 x diameter, and Reynolds number from 2×10^4 to 4×10^6. Figure 24 presents a measured pressure distribution, the fitted curve, and the parameters computed from the fitted curve. Approximately 300 pressure distributions have been fitted and work is starting on the shearing

stress distributions (determined from heat transfer measurements). Comparison of the experimental results with the equations will be made as soon as the data reduction is complete.

REFERENCES

1. Simon, W. E., "Flow Field Parameter Analysis of the Wind Induced Oscillation of Launch Vehicles", AIAA Symposium on Structural Dynamics and Aeroelasticity, Boston, Mass., August 1965.

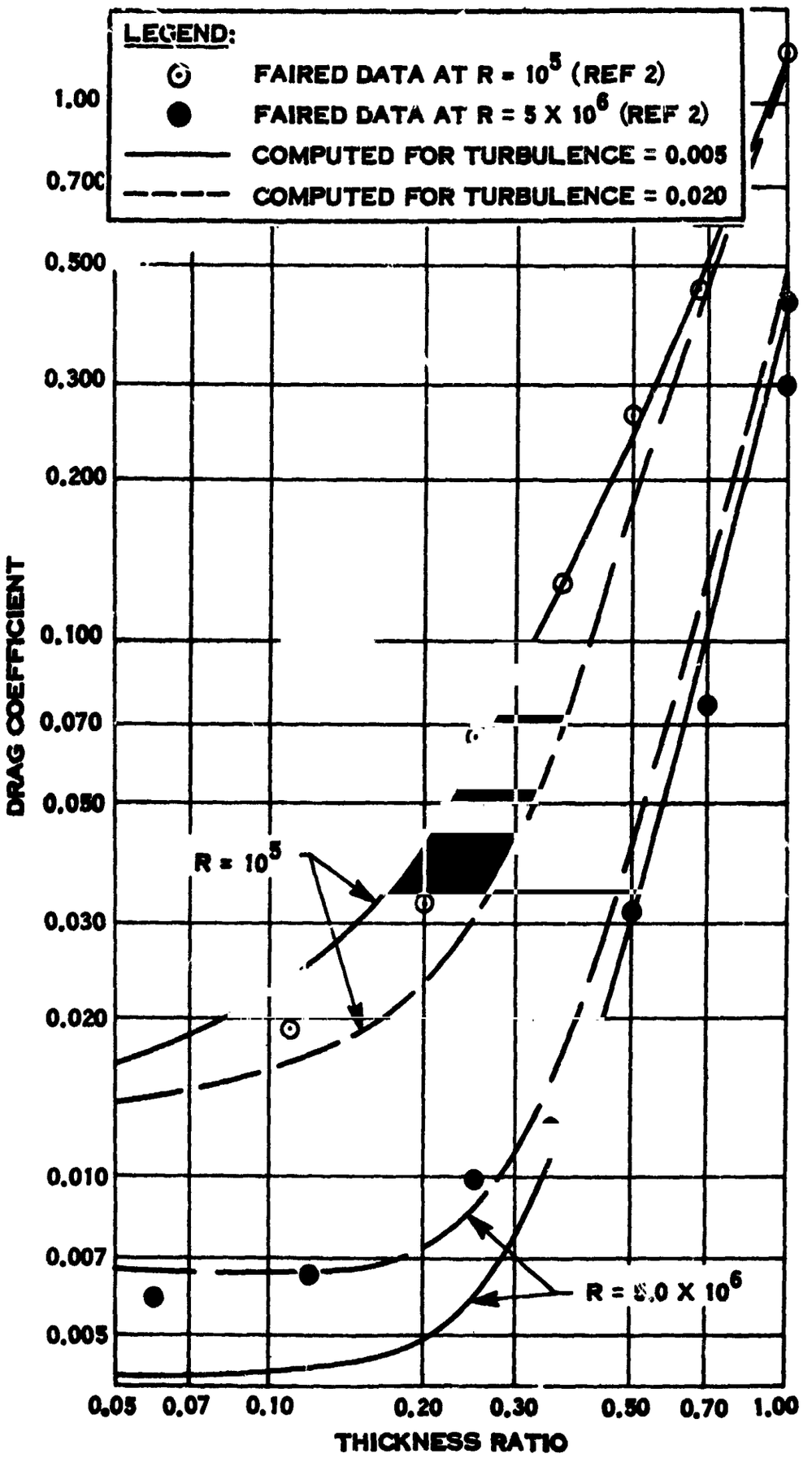

FIG. 1 DEPENDENCE OF INFINITE CYLINDER DRAG ON THICKNESS RATIO

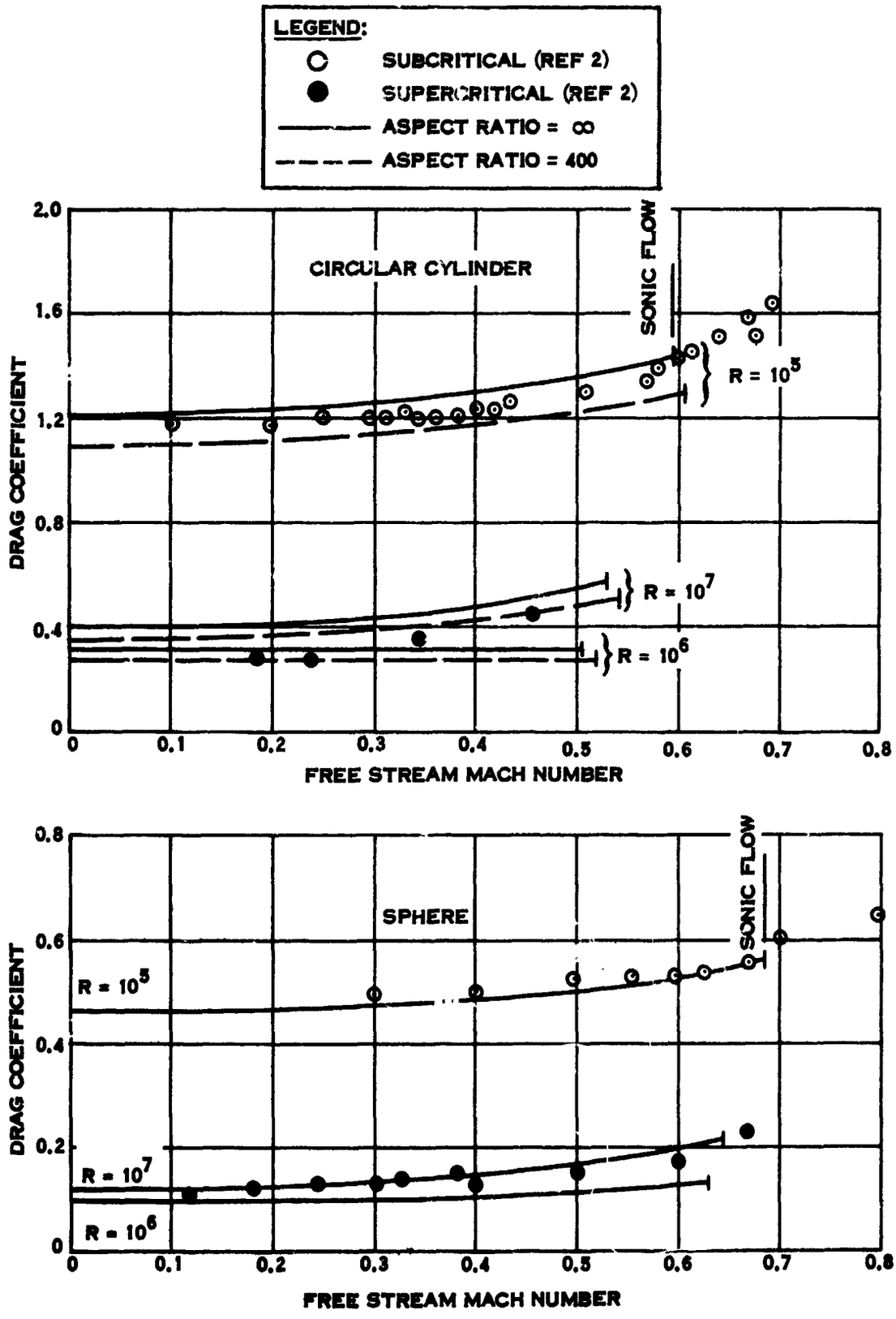

FIG. 2 DEPENDENCE OF CIRCULAR CYLINDER AND SPHERE DRAG ON MACH NUMBER

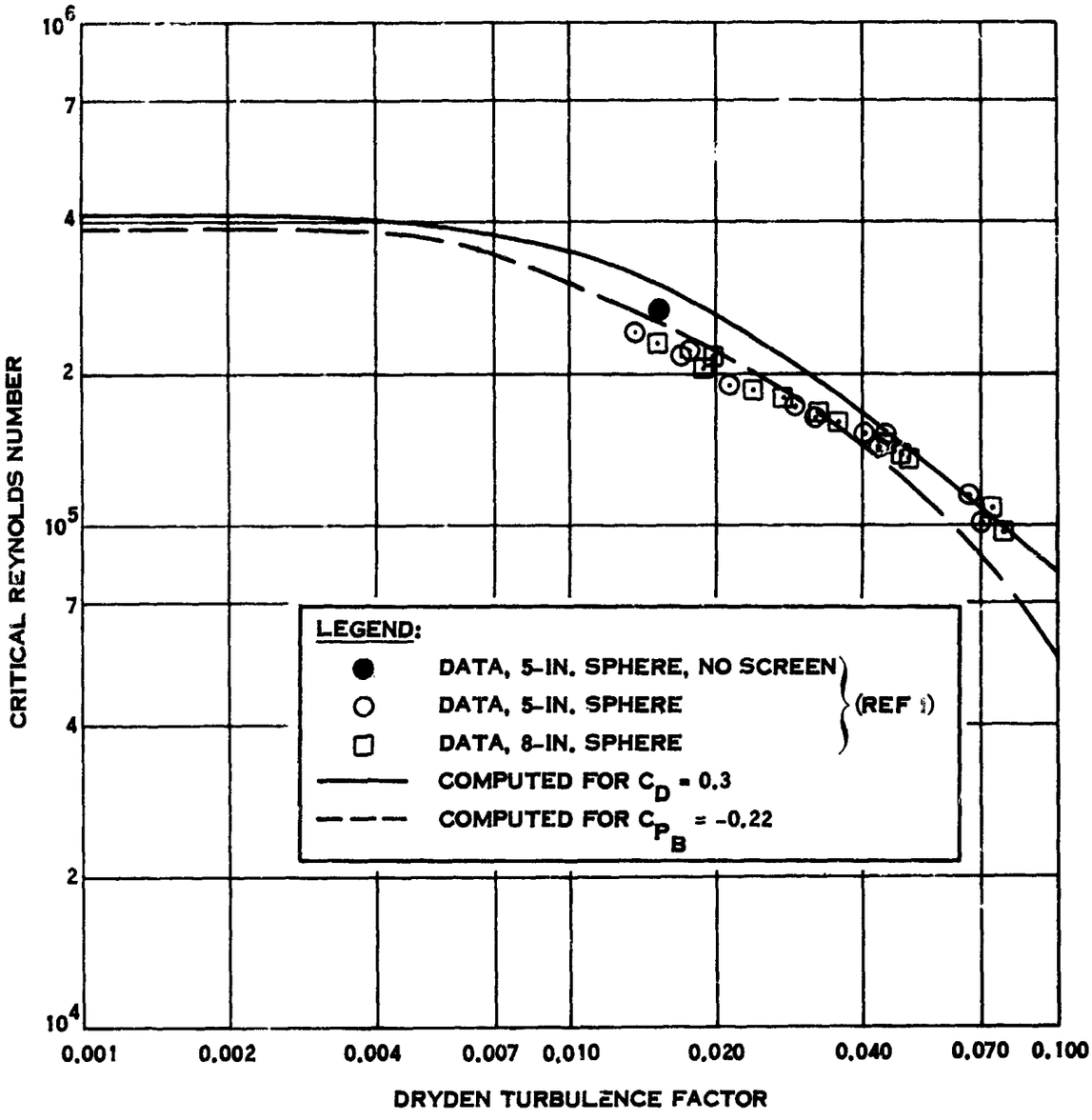

FIG. 3 DEPENDENCE OF SPHERE CRITICAL REYNOLDS NUMBER ON TURBULENCE

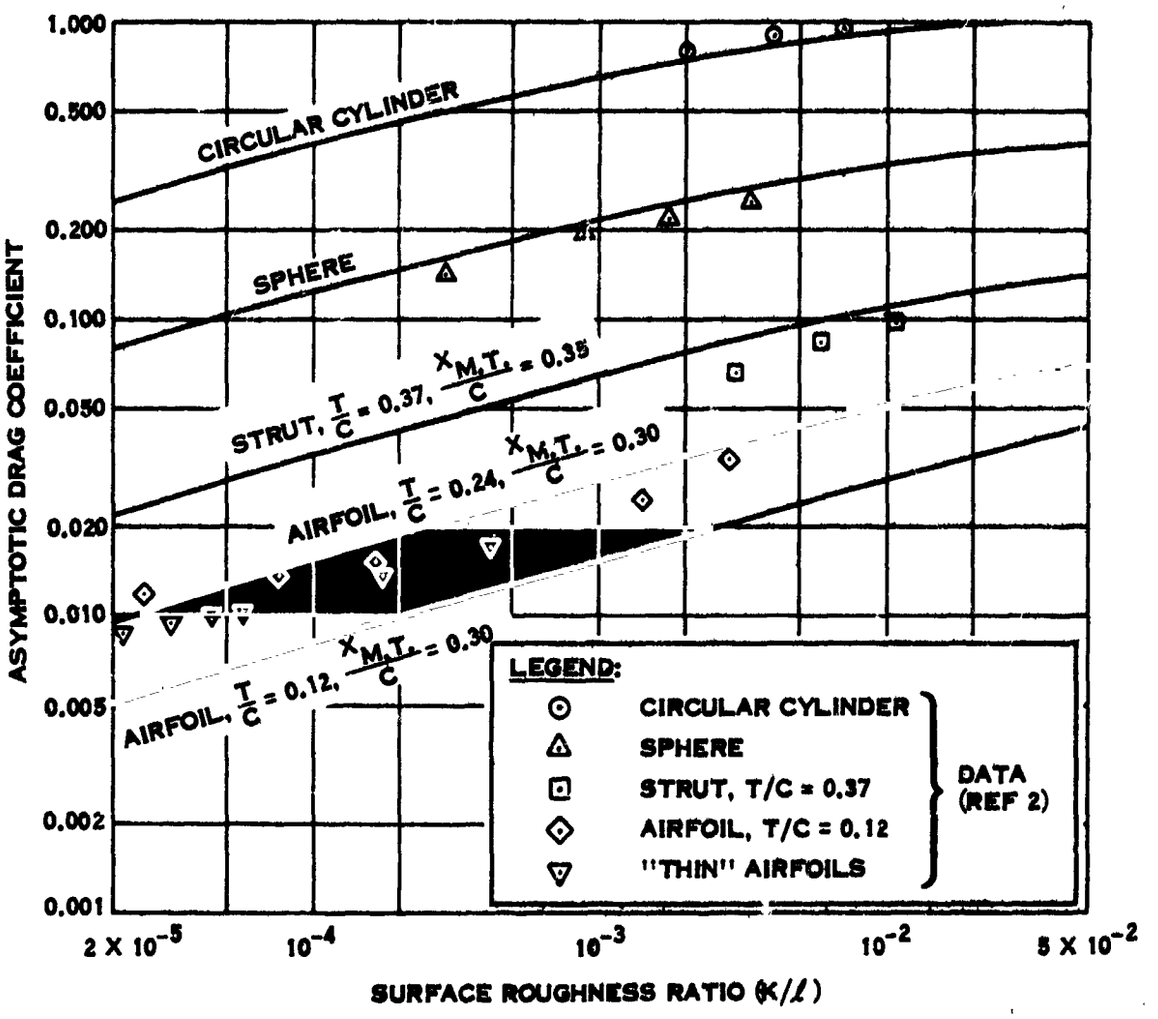

FIG. 4 DEPENDENCE OF ASYMPTOTIC DRAG ($R \to \infty$) ON SURFACE ROUGHNESS

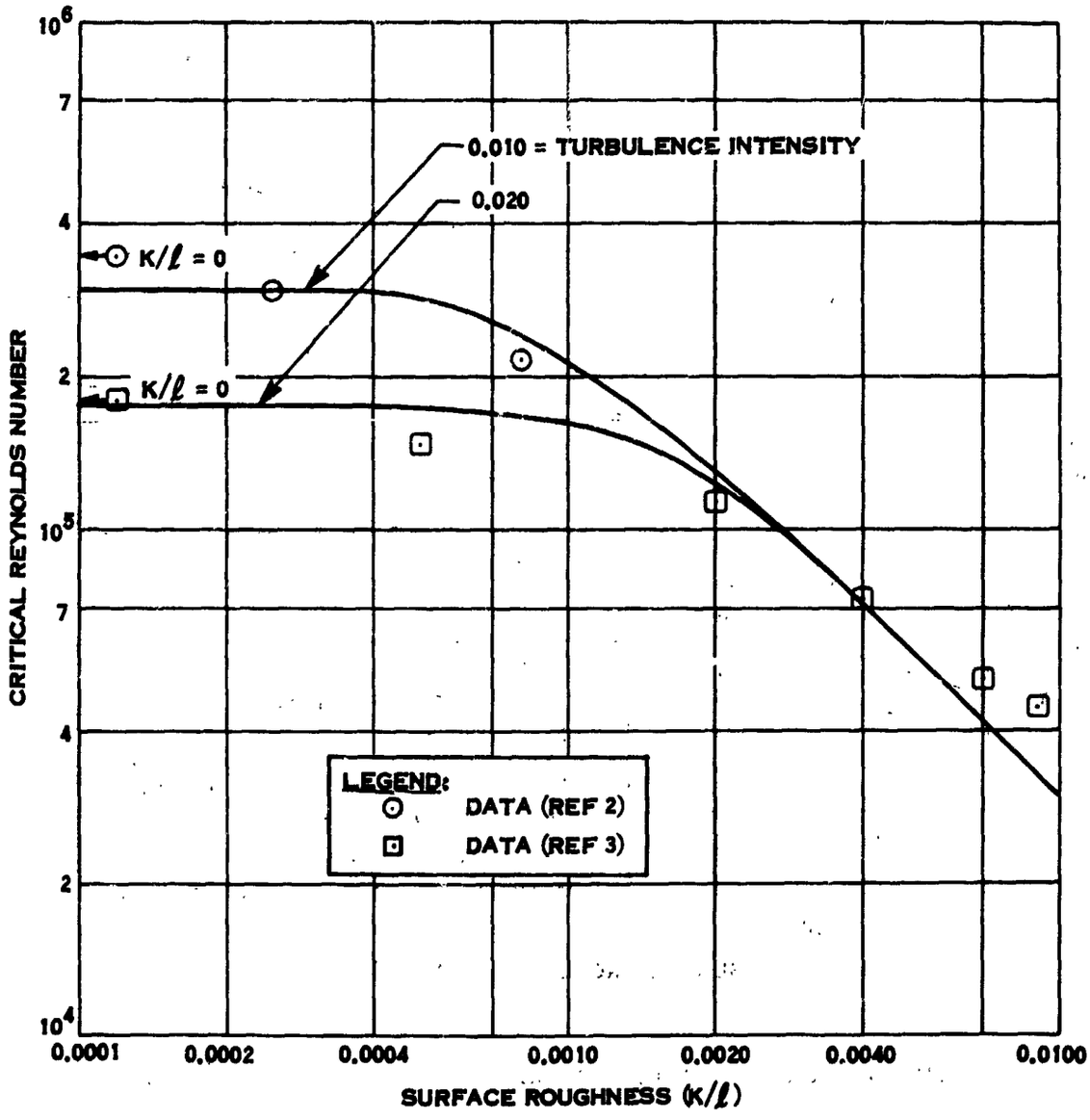

FIG. 5 DEPENDENCE OF CIRCULAR CYLINDER CRITICAL REYNOLDS NUMBER ON SURFACE ROUGHNESS

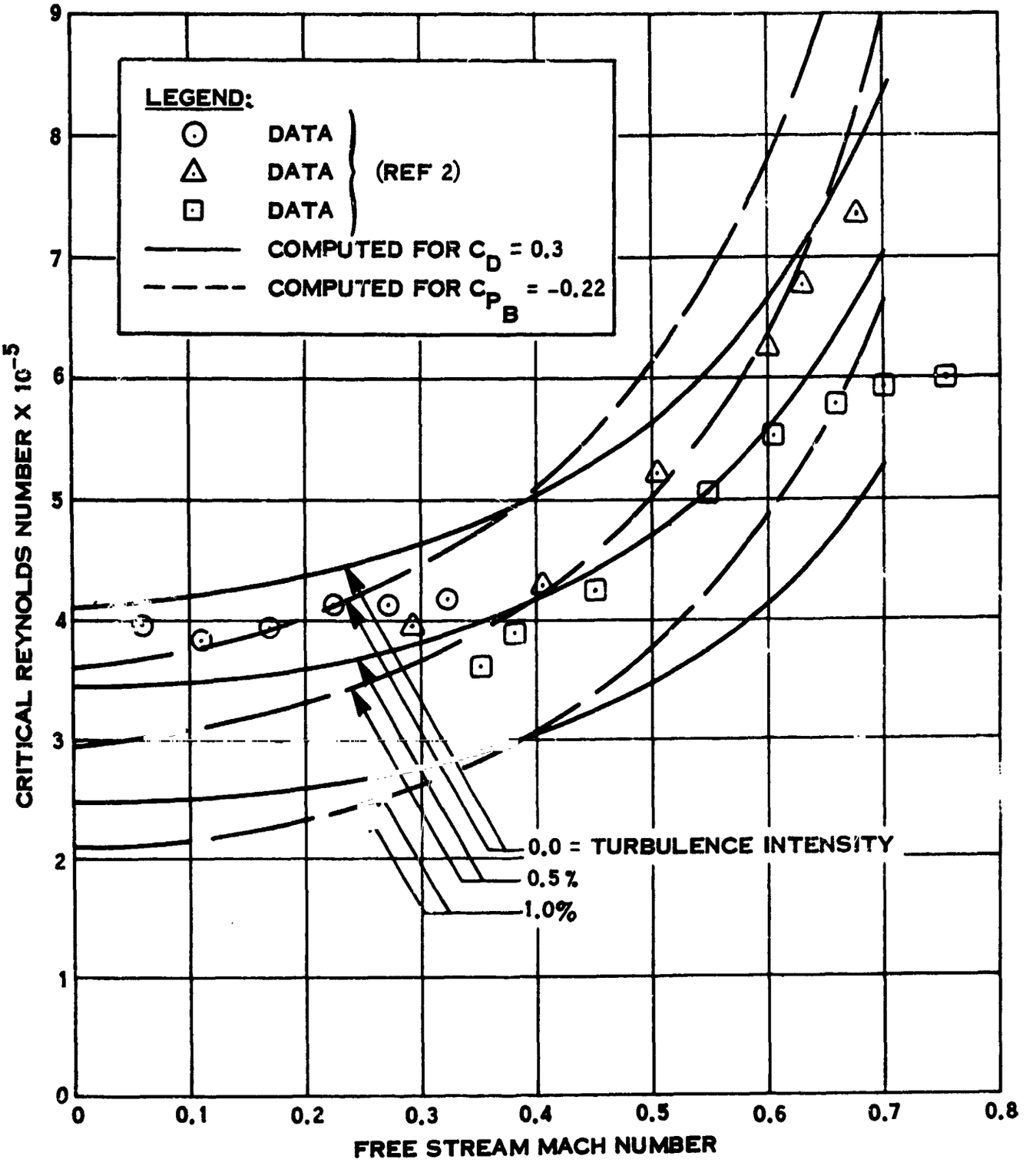

FIG. 6 DEPENDENCE OF SPHERE CRITICAL REYNOLDS NUMBER ON MACH NUMBER

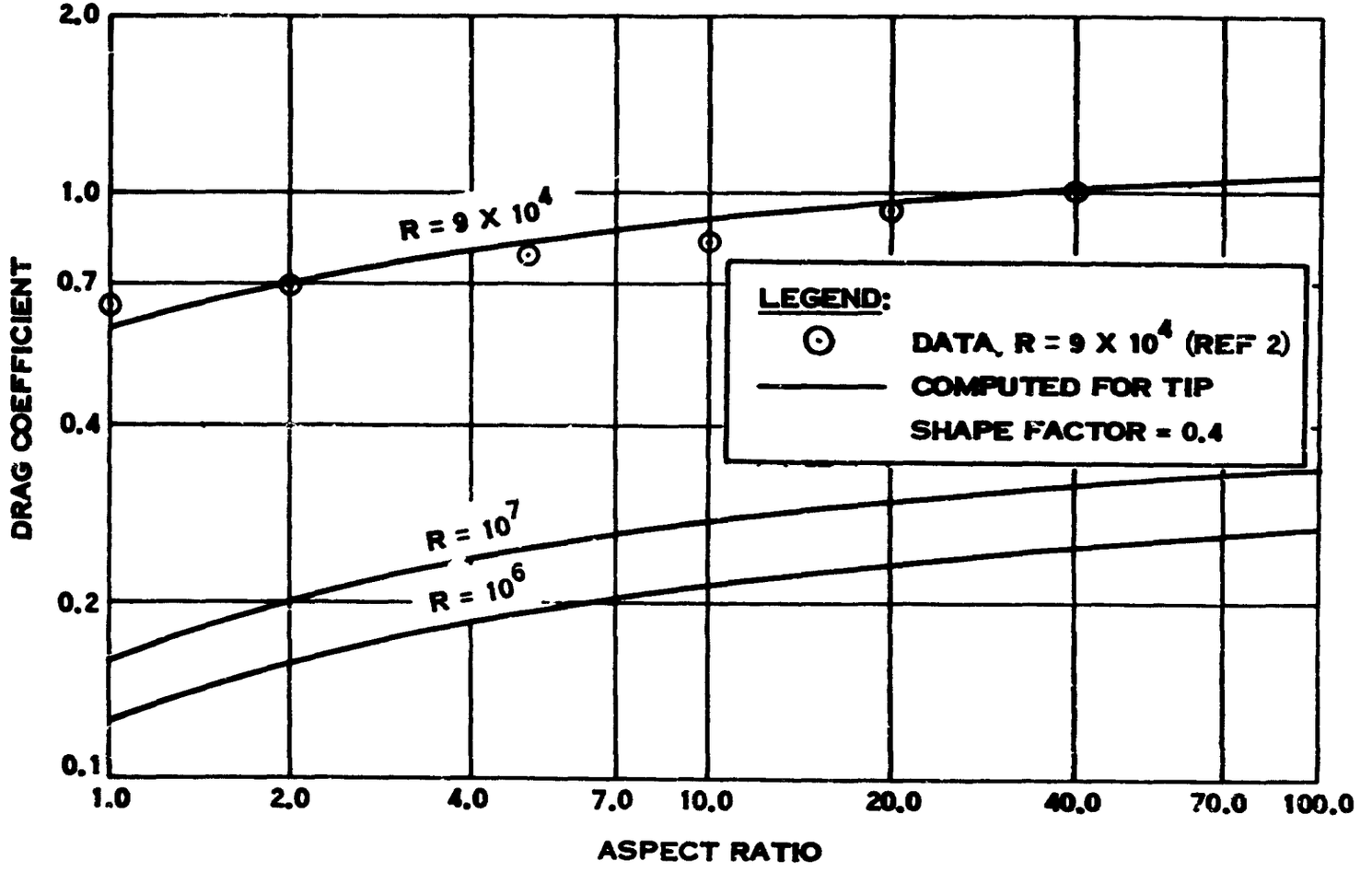

FIG. 7 DEPENDENCE OF DRAG OF CIRCULAR CYLINDER ON ASPECT RATIO

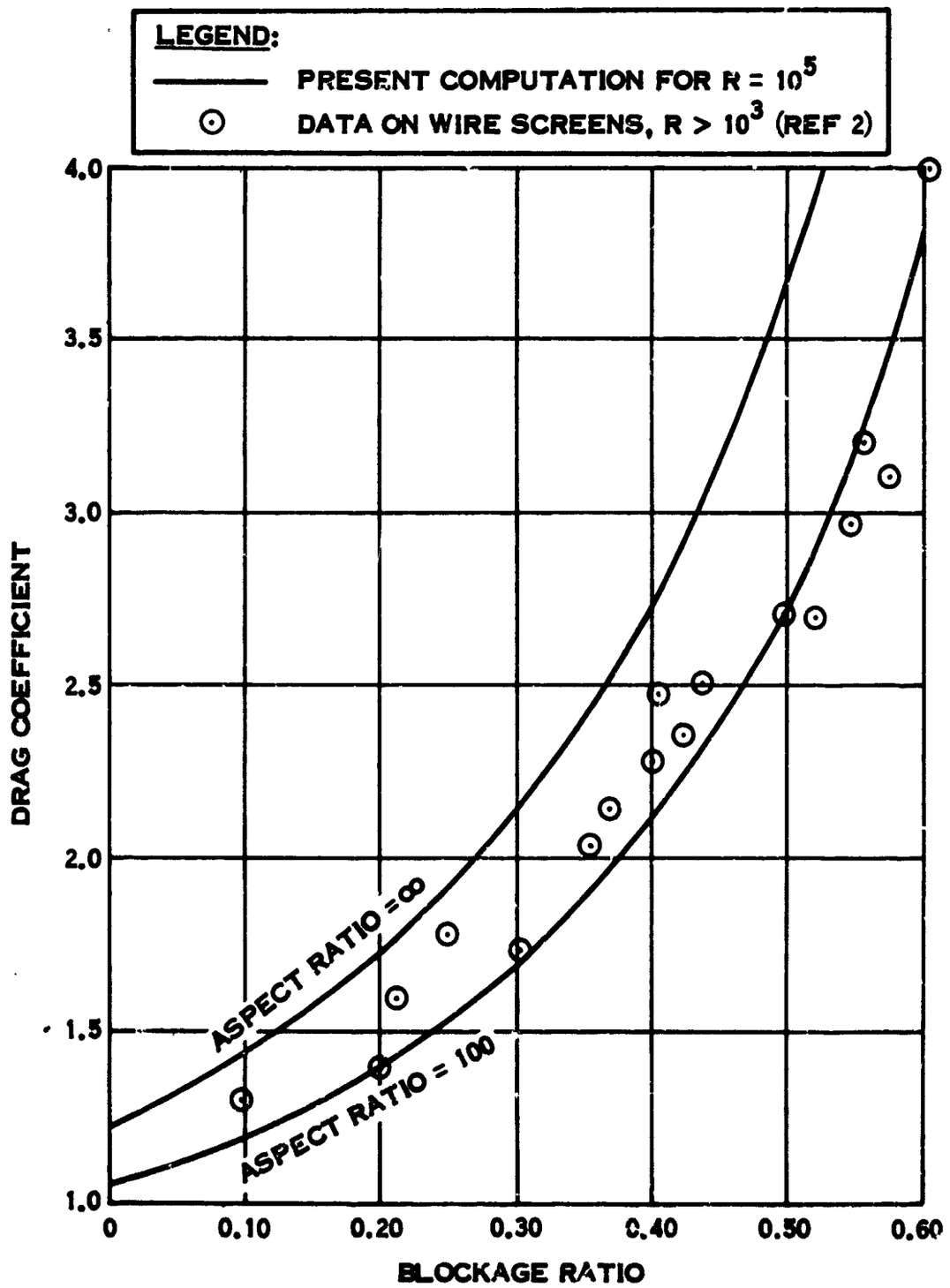

FIG. 8 EFFECT OF BLOCKAGE ON DRAG OF A CIRCULAR CYLINDER AT SUBCRITICAL REYNOLDS NUMBER

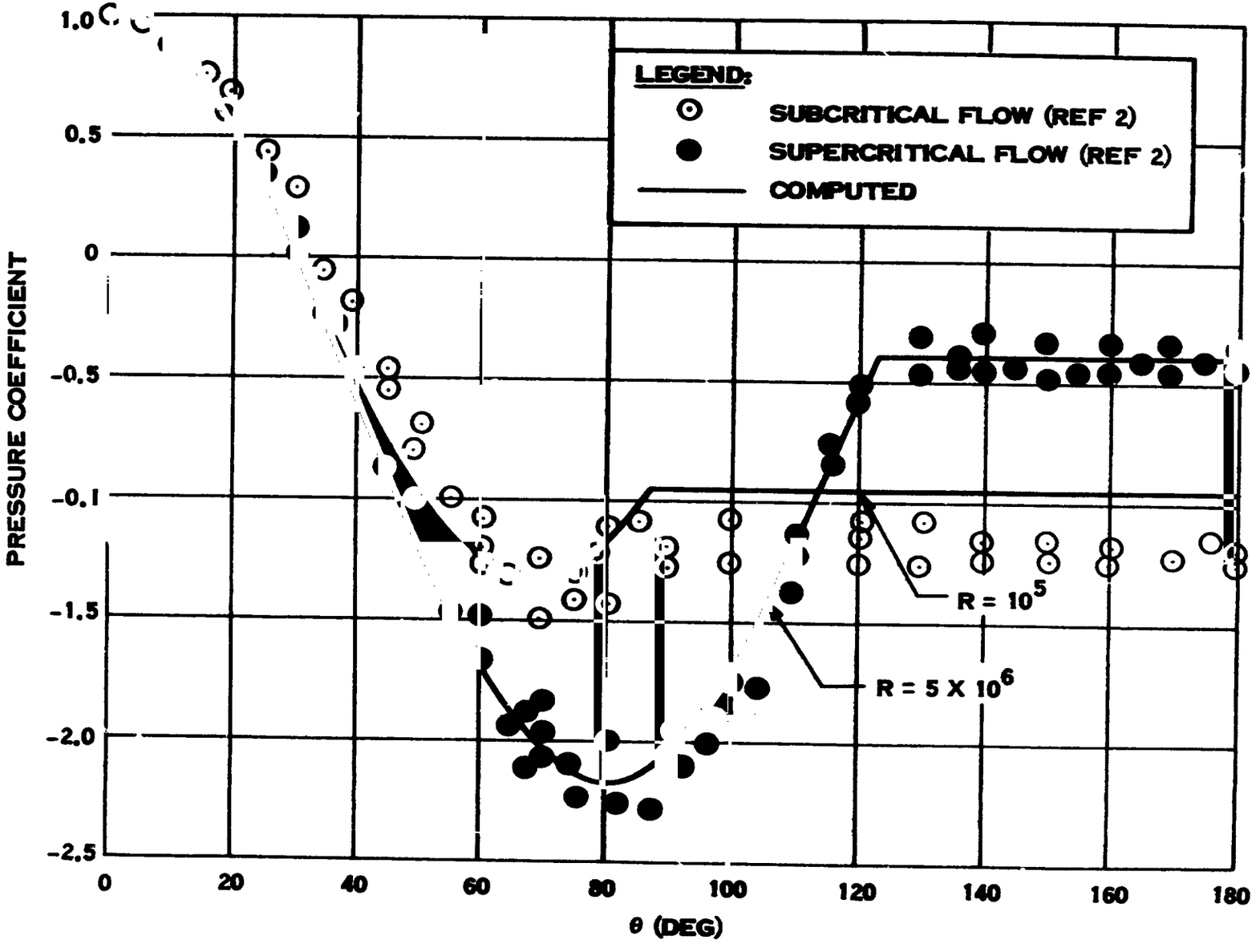

FIG. 9 PRESSURE DISTRIBUTION ON CIRCULAR CYLINDERS

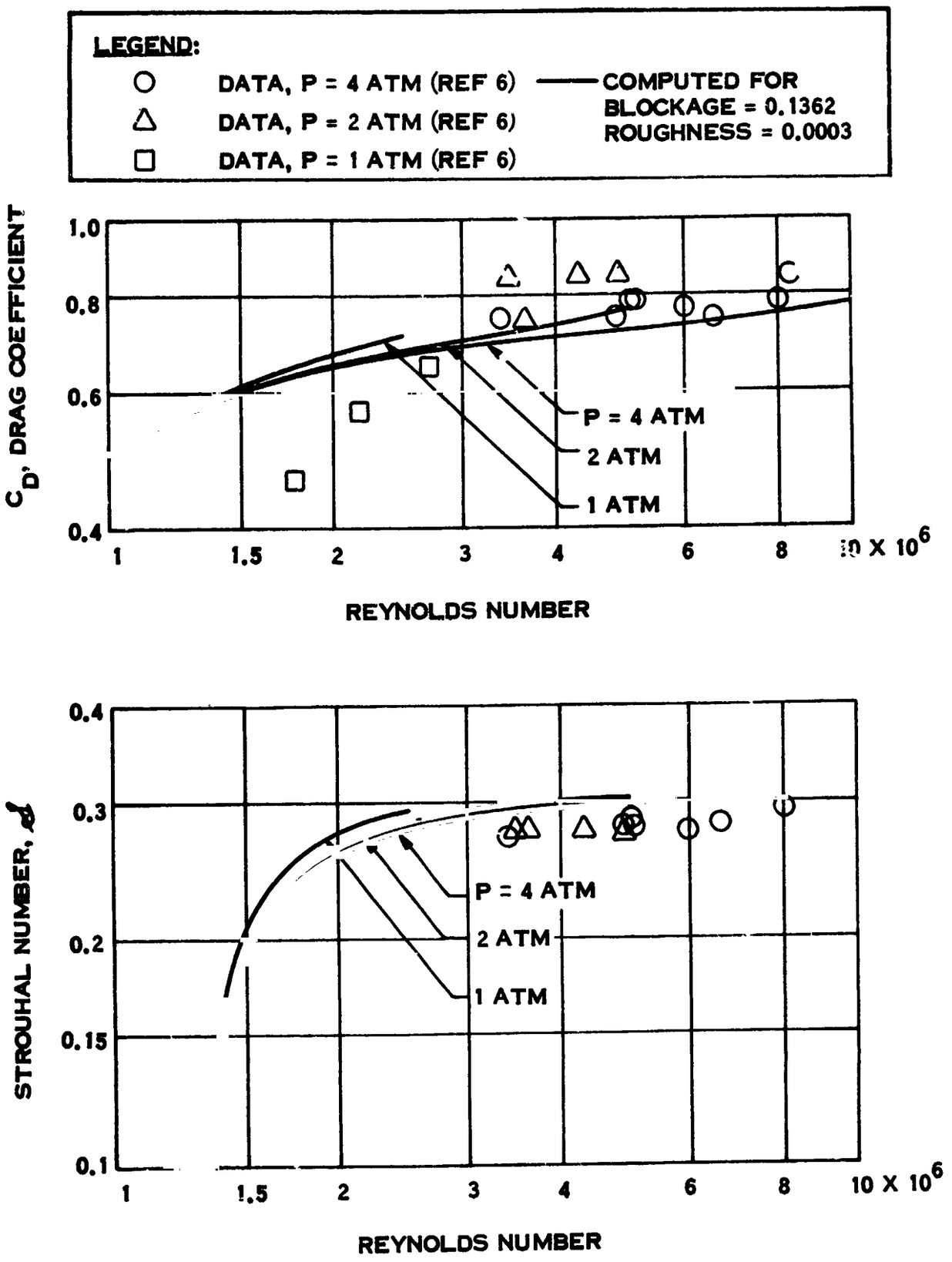

FIG. 10 DRAG AND STROUHAL NUMBER OF A CIRCULAR CYLINDER AT LARGE REYNOLDS NUMBER

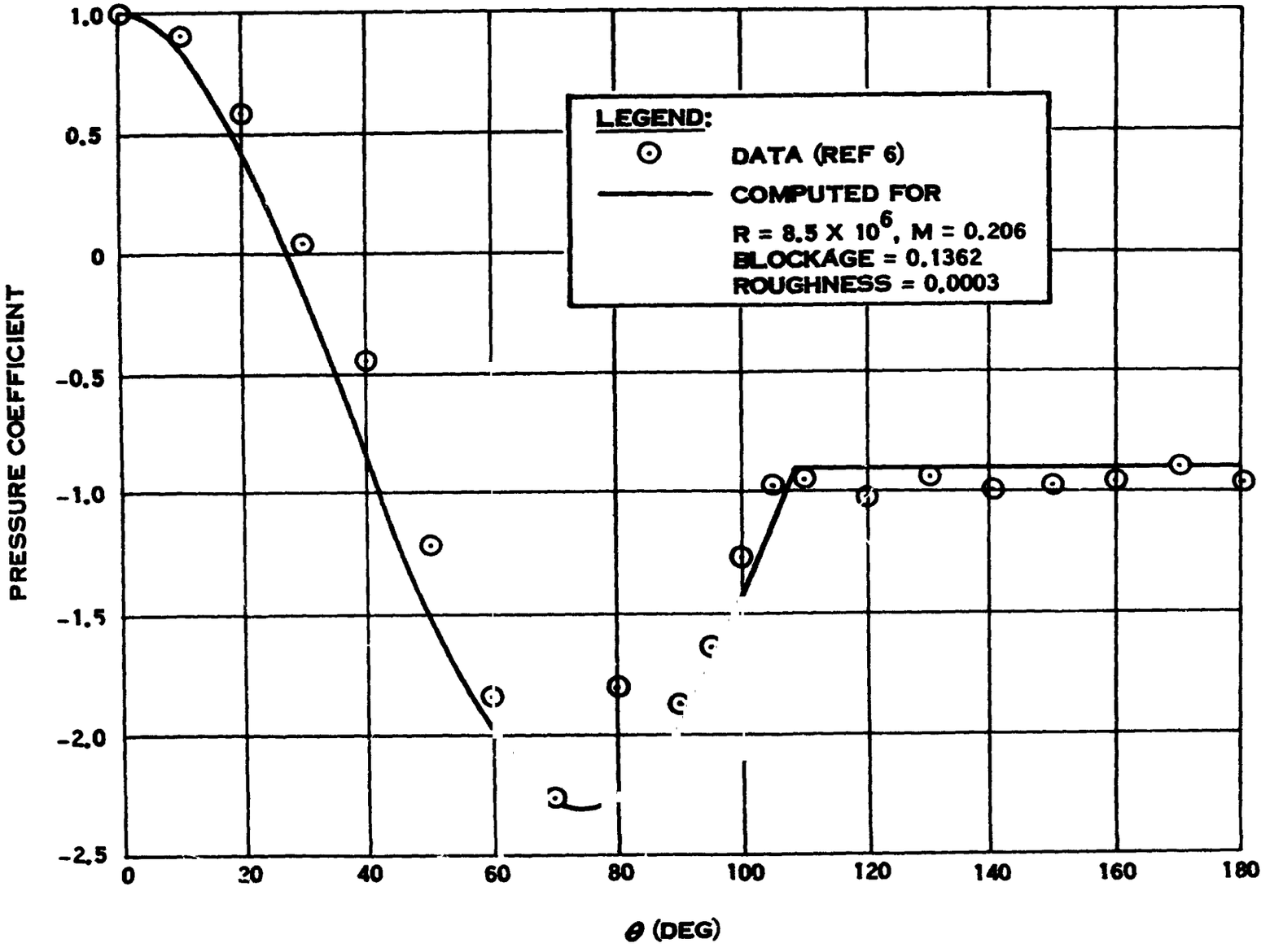

FIG. 11 PRESSURE DISTRIBUTION ON A CIRCULAR CYLINDER AT R = 8.4 X 10^6

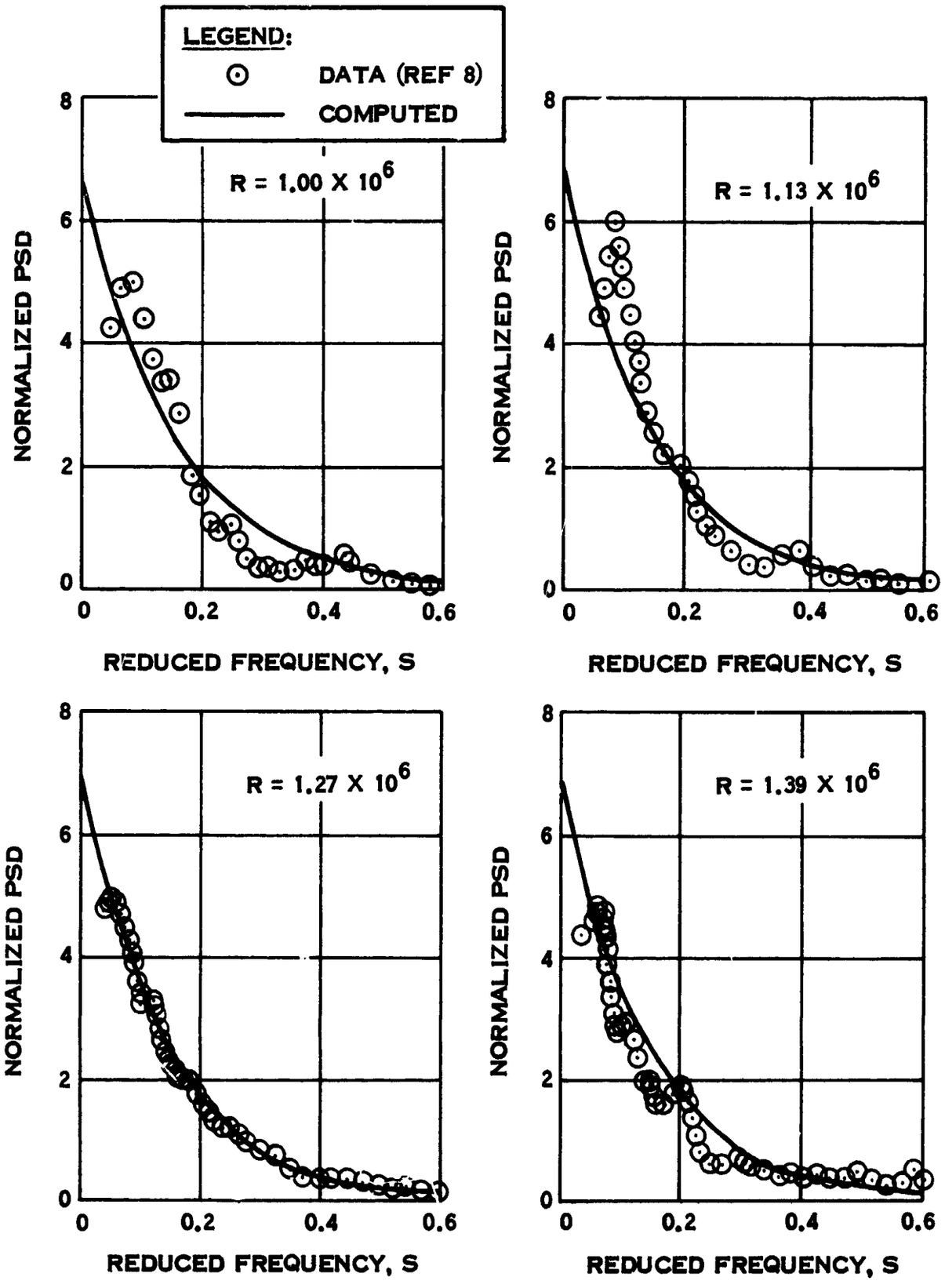

FIG. 12 NORMALIZED POWER SPECTRUM LIFT ON A CYLINDER

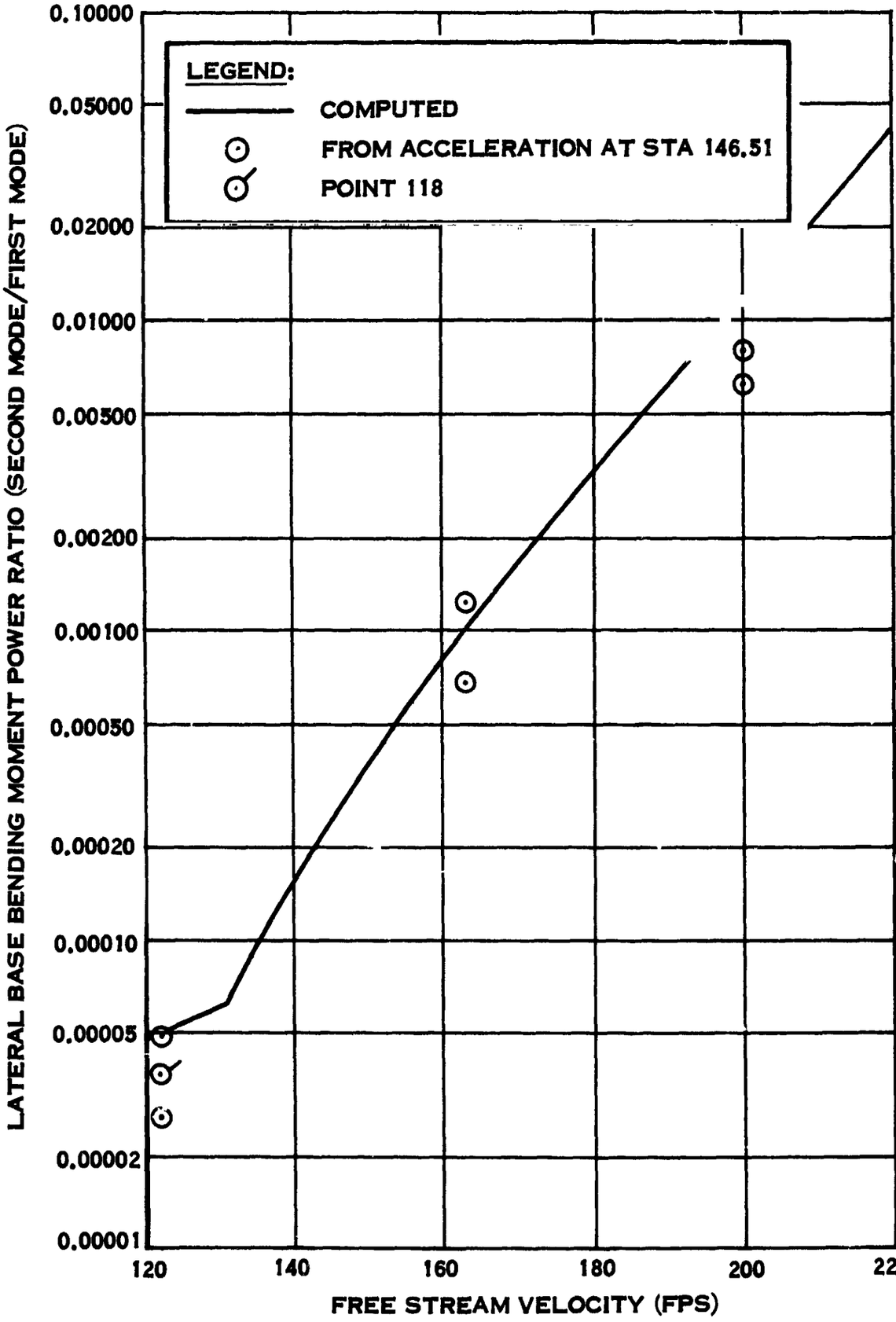

FIG. 13 SATURN IB MODEL, CONFIGURATION 1, LATERAL BASE BENDING MOMENT POWER RATIO (SECOND MODE/FIRST MODE)

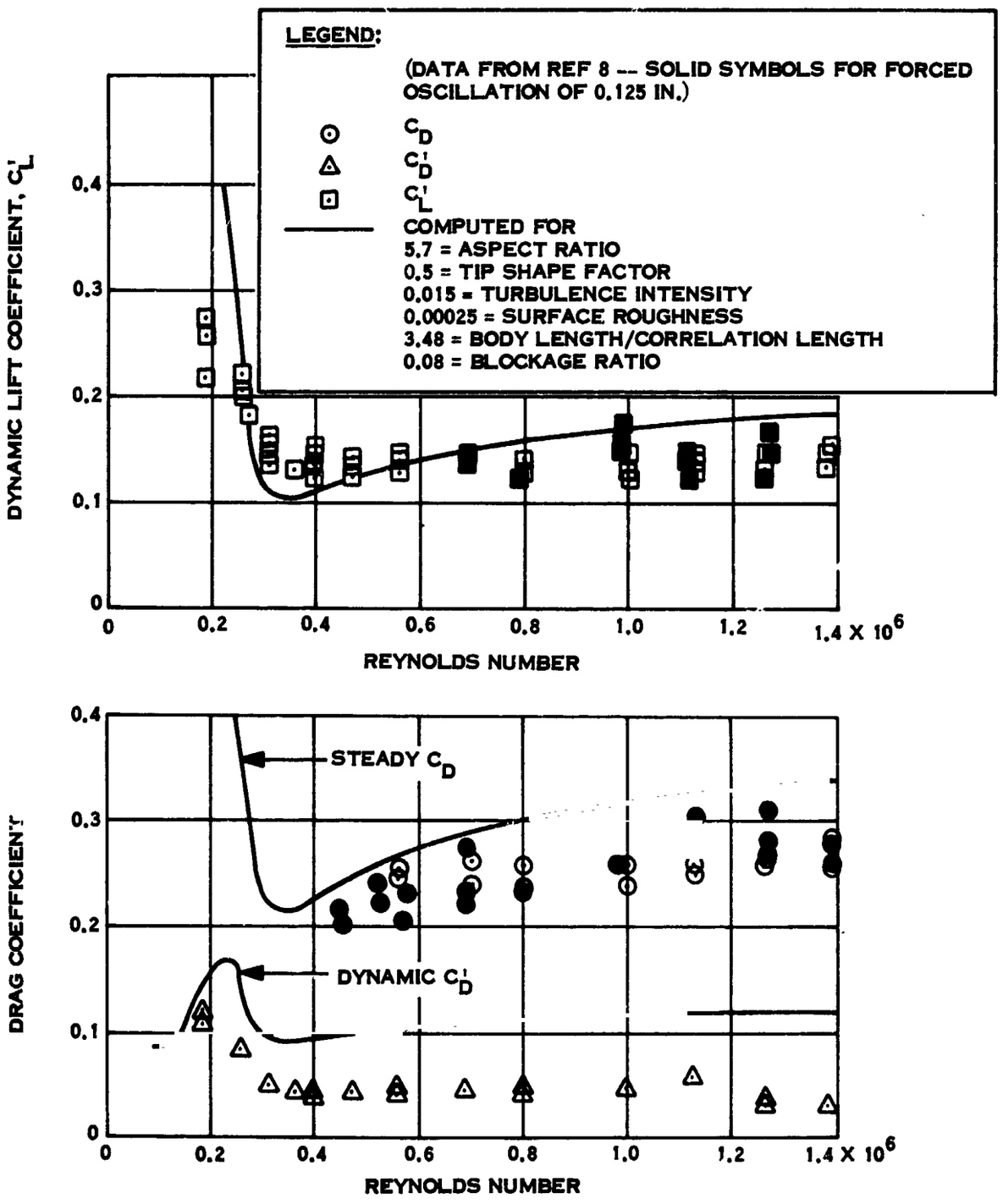

FIG. 14 LIFT AND DRAG ON A CYLINDER IN SUPERCRITICAL FLOW

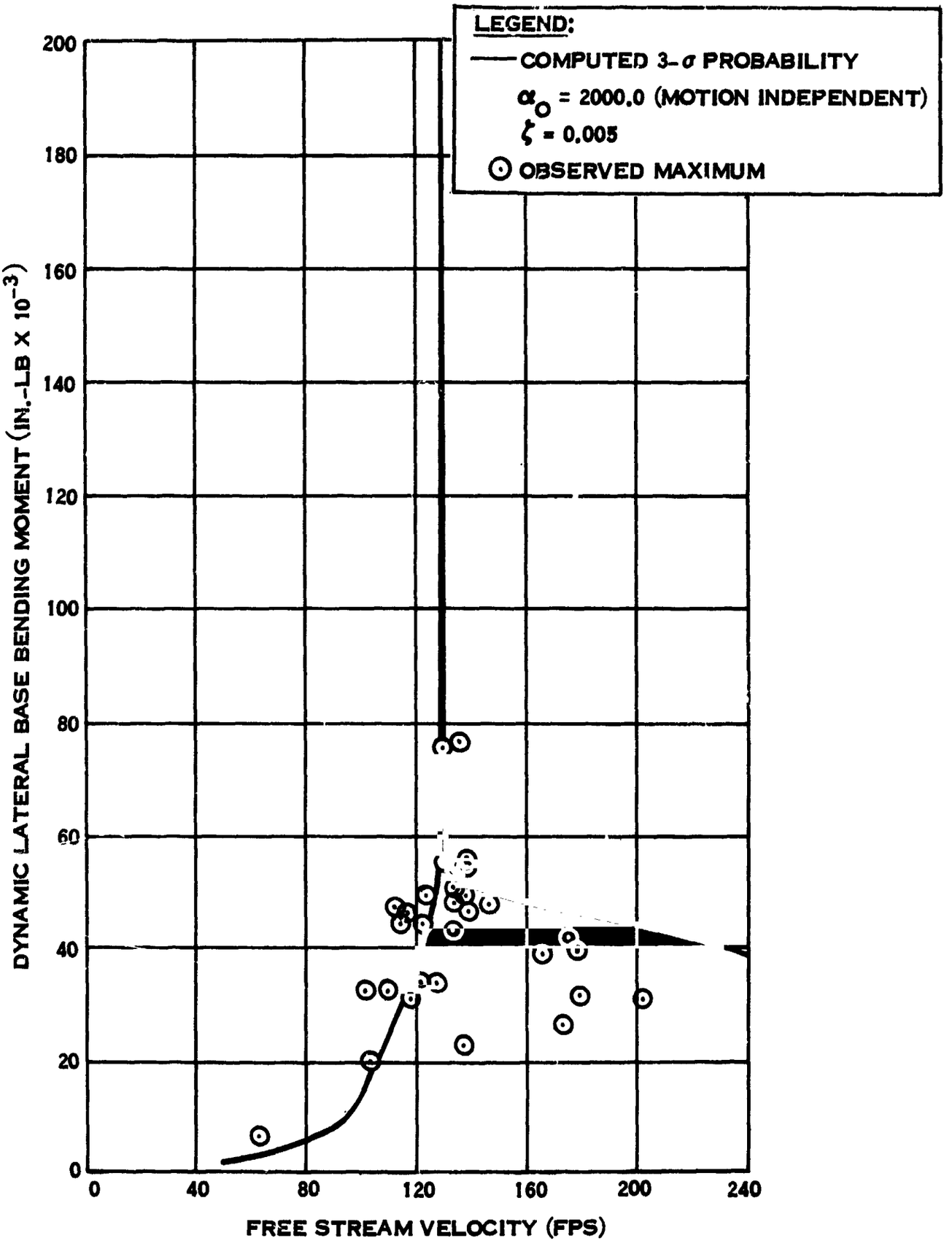

FIG. 15 SATURN IB MODEL, CONFIGURATION 1, DYNAMIC LATERAL BASE BENDING MOMENT

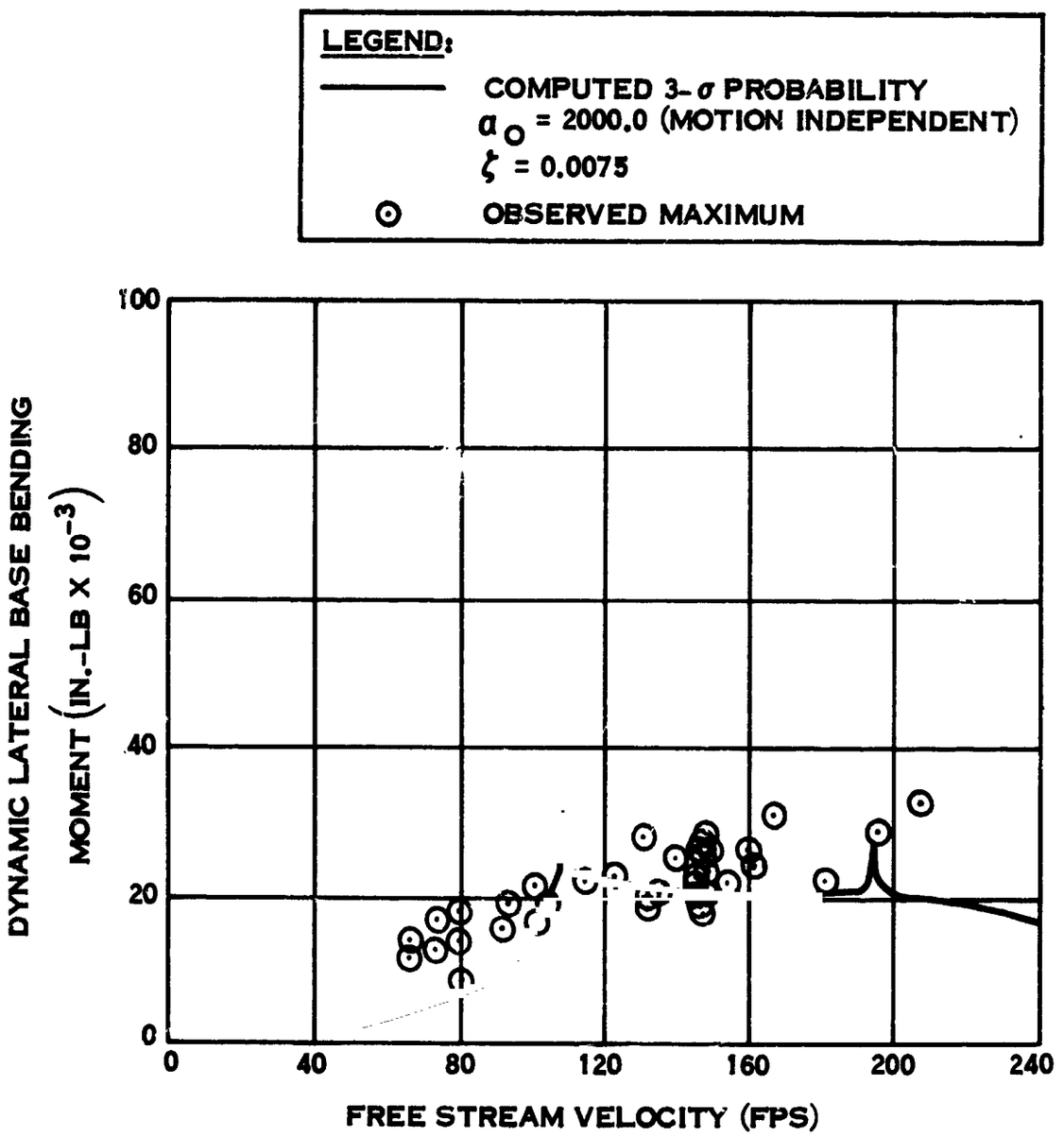

FIG. 16 SATURN IB MODEL, CONFIGURATION 6 DYNAMIC LATERAL BASE BENDING MOMENT

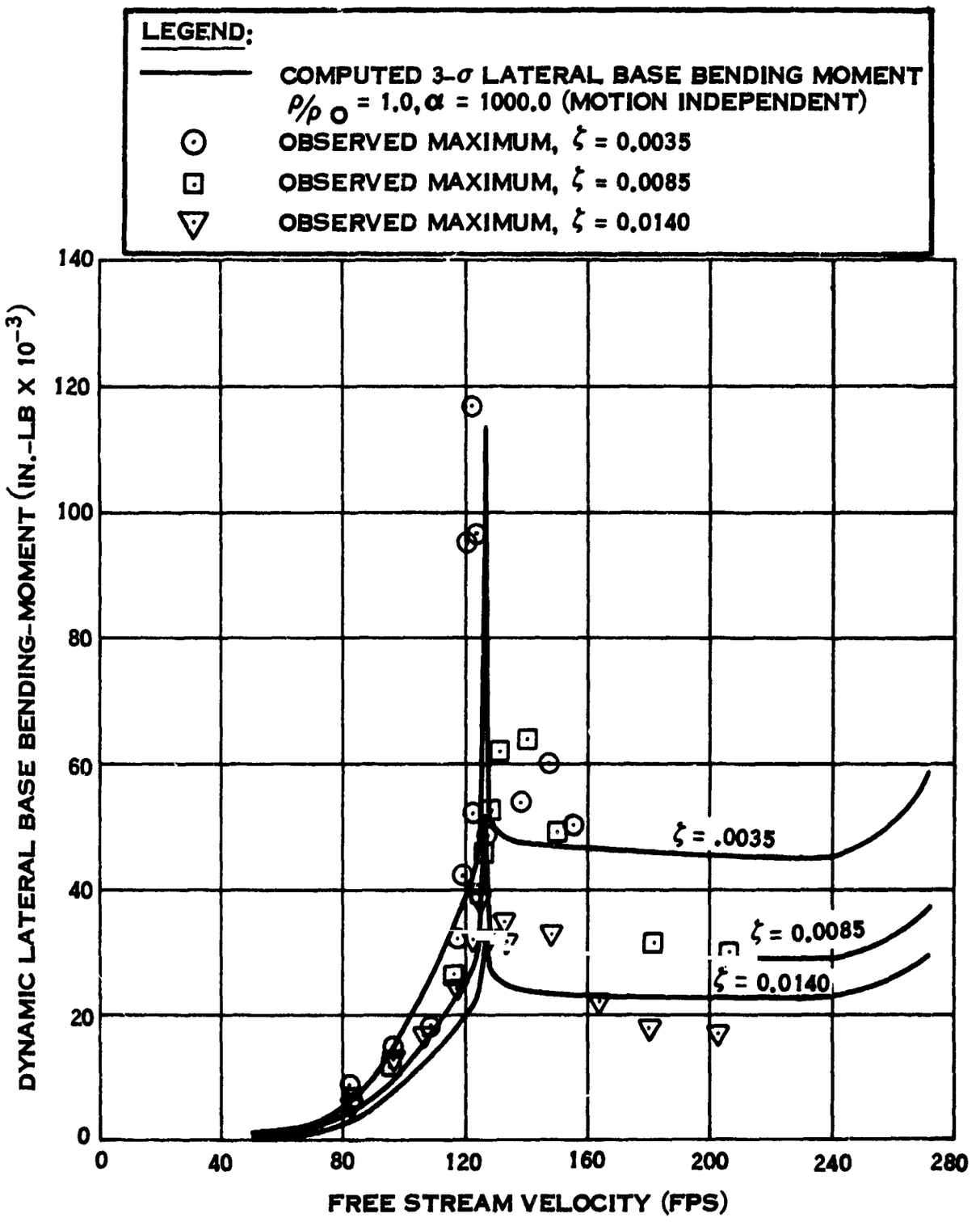

FIG. 17 SATURN V MODEL CONFIGURATION E-00 DYNAMIC LATERAL BASE BENDING MOMENT

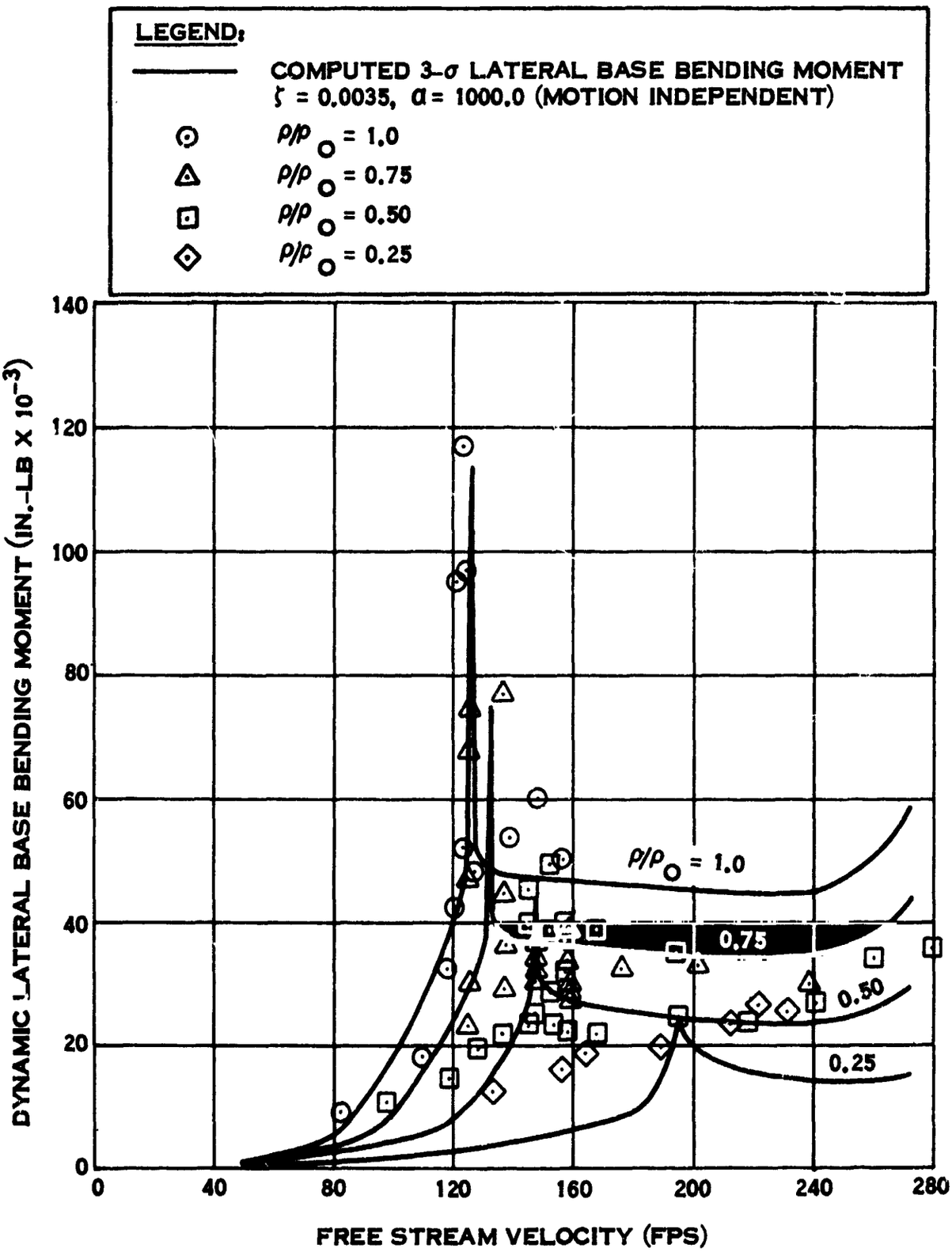

FIG. 18 SATURN V MODEL, CONFIGURATION E-00 DYNAMIC LATERAL BASE BENDING MOMENT

STEADY DRAG BASE B.M. FOR SATURN V MODEL WITH TOWER FOR 180 PSF DYN. PRES.

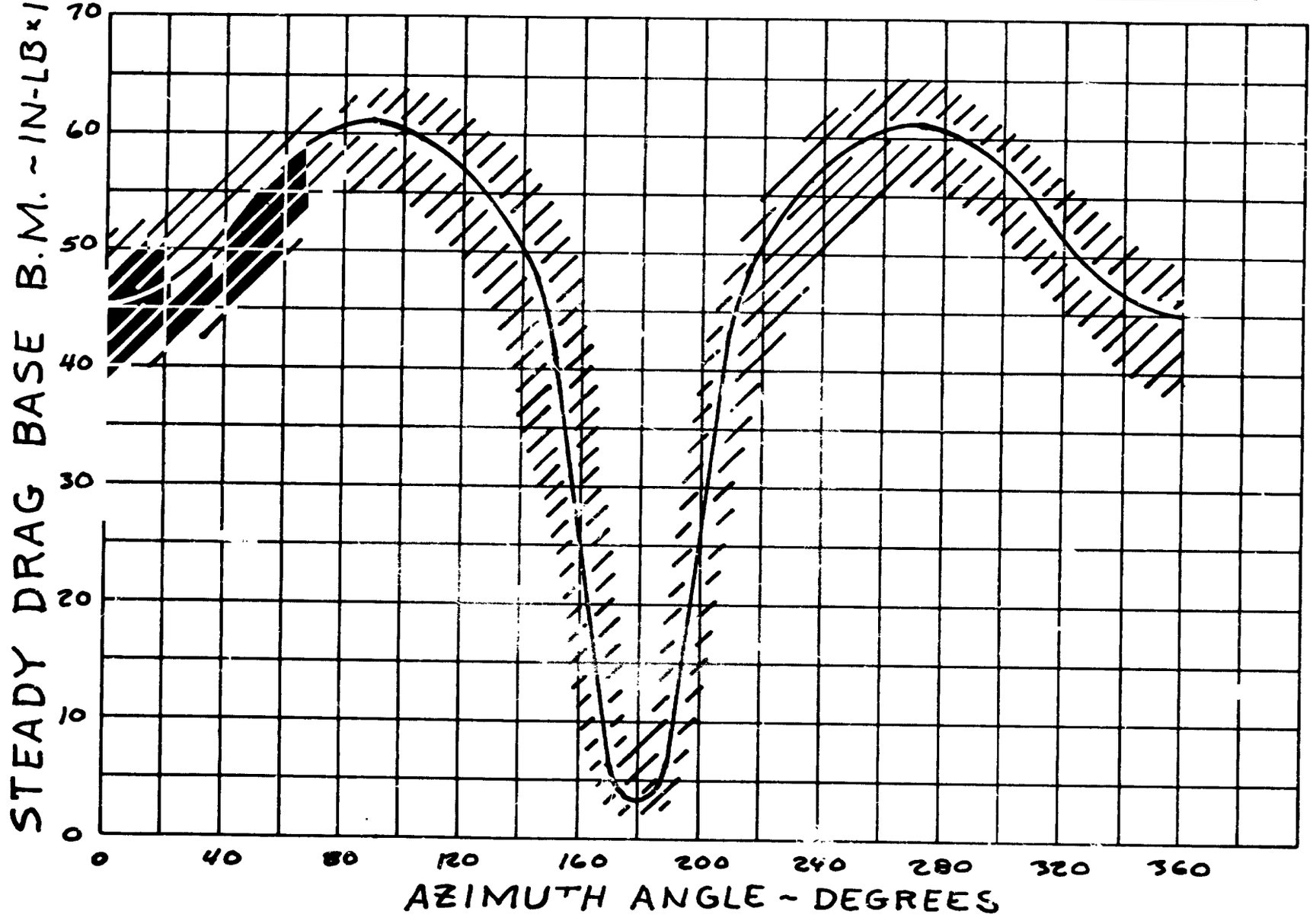

FIGURE 19

MAXIMUM DYN. LAT. B.B.M. FOR SATURN V MODEL WITH TOWER (EMP./CRAWLER), -150° < AZ. ANGLE < 150°

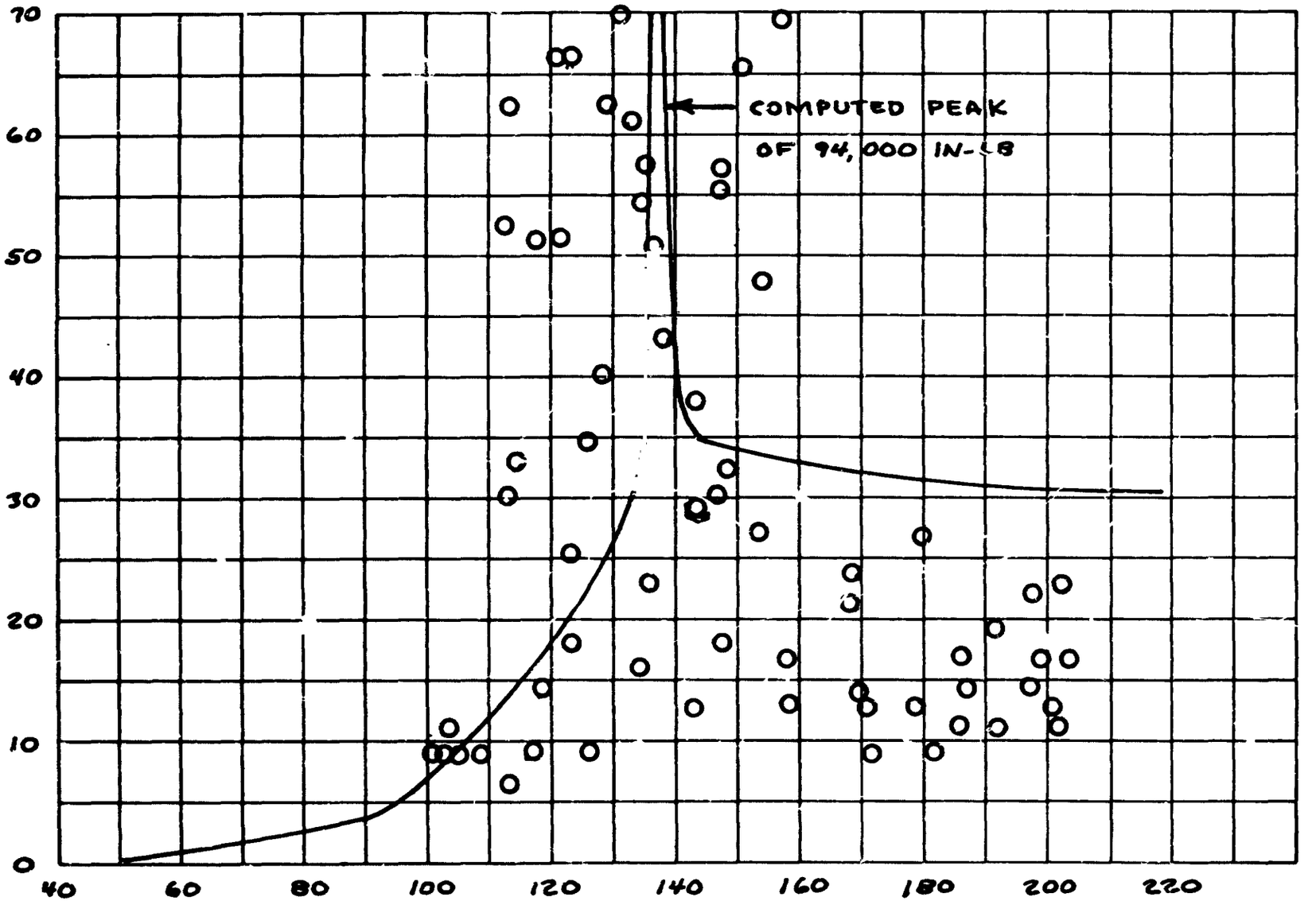

FIGURE 20

MAXIMUM DYN. LAT. B.B.M. FOR SATURN V MODEL WITH TOWER (EMP./CRAWLER), AZ. ANGLE = 180°

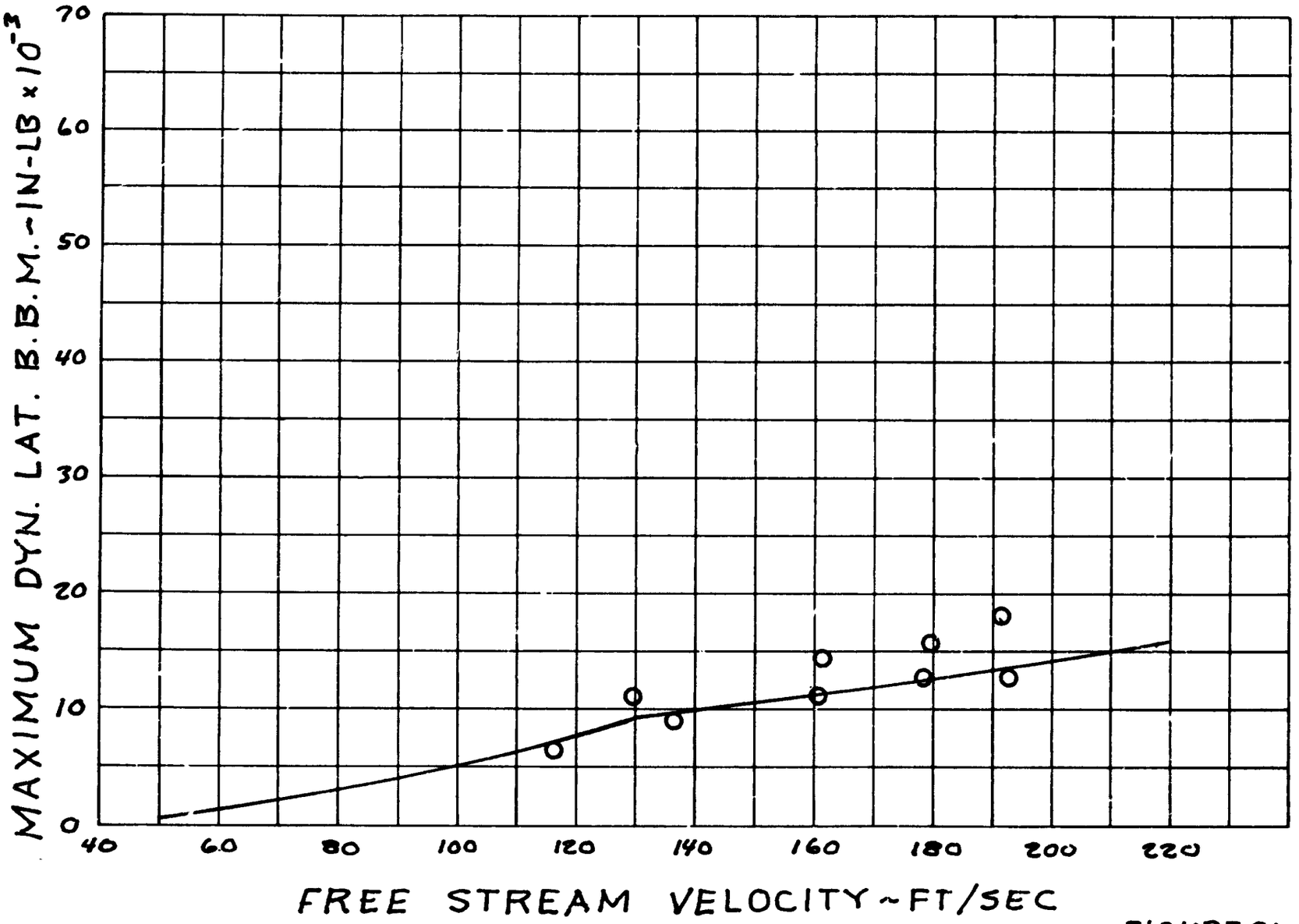

FIGURE 21

POWER SPECTRAL DENSITY OF FREE STREAM TURBULENCE

FIGURE 22

DATA FROM "ATMOSPHERIC DIFFUSION" BY PASQUILL, 1962

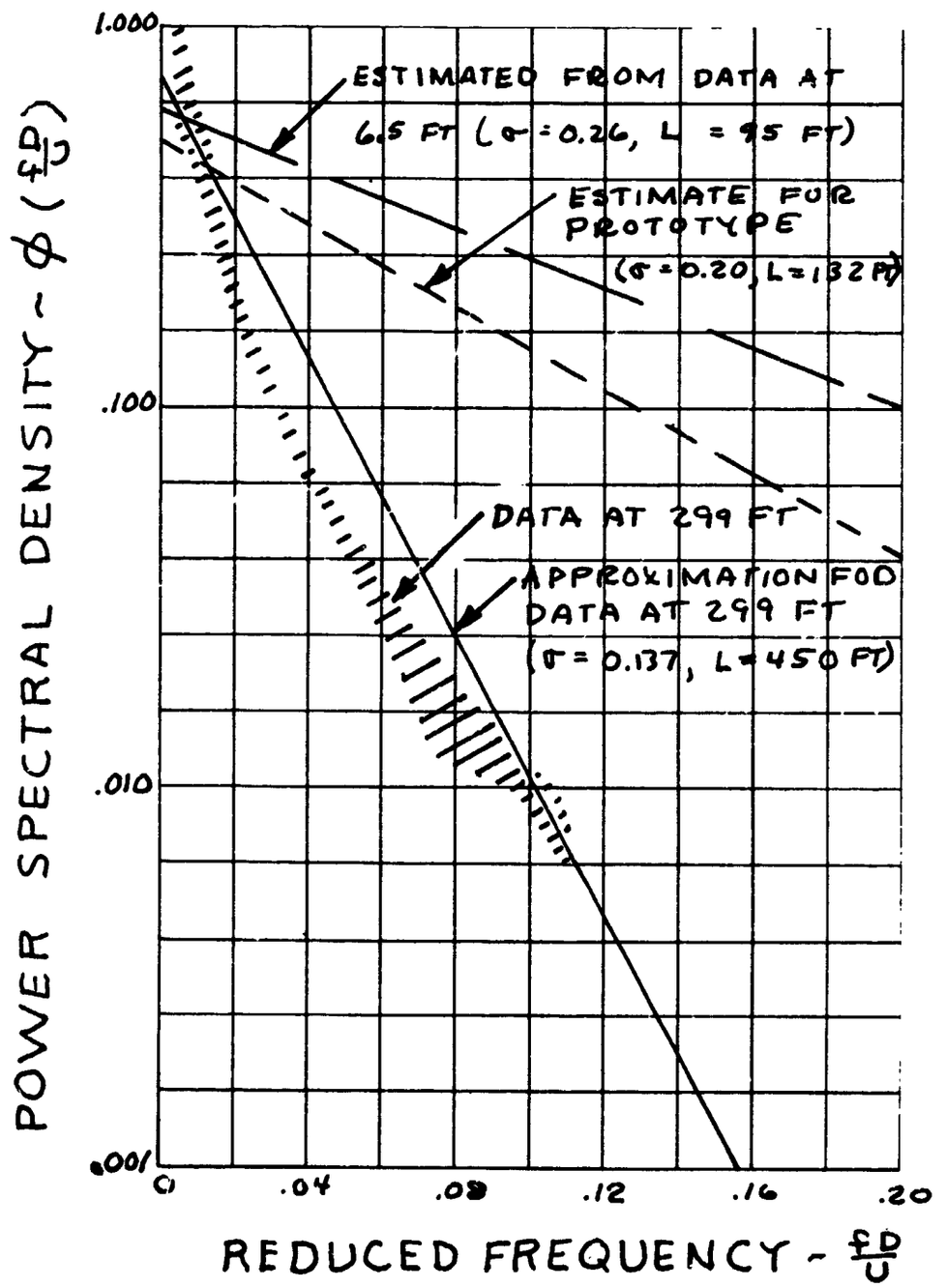

MAX. RESULTANT B.B.M. FOR SATURN V PROTOTYPE (EMPTY/CRAWLER) - 1% DAMPING - AZ. ANGLE = 45°

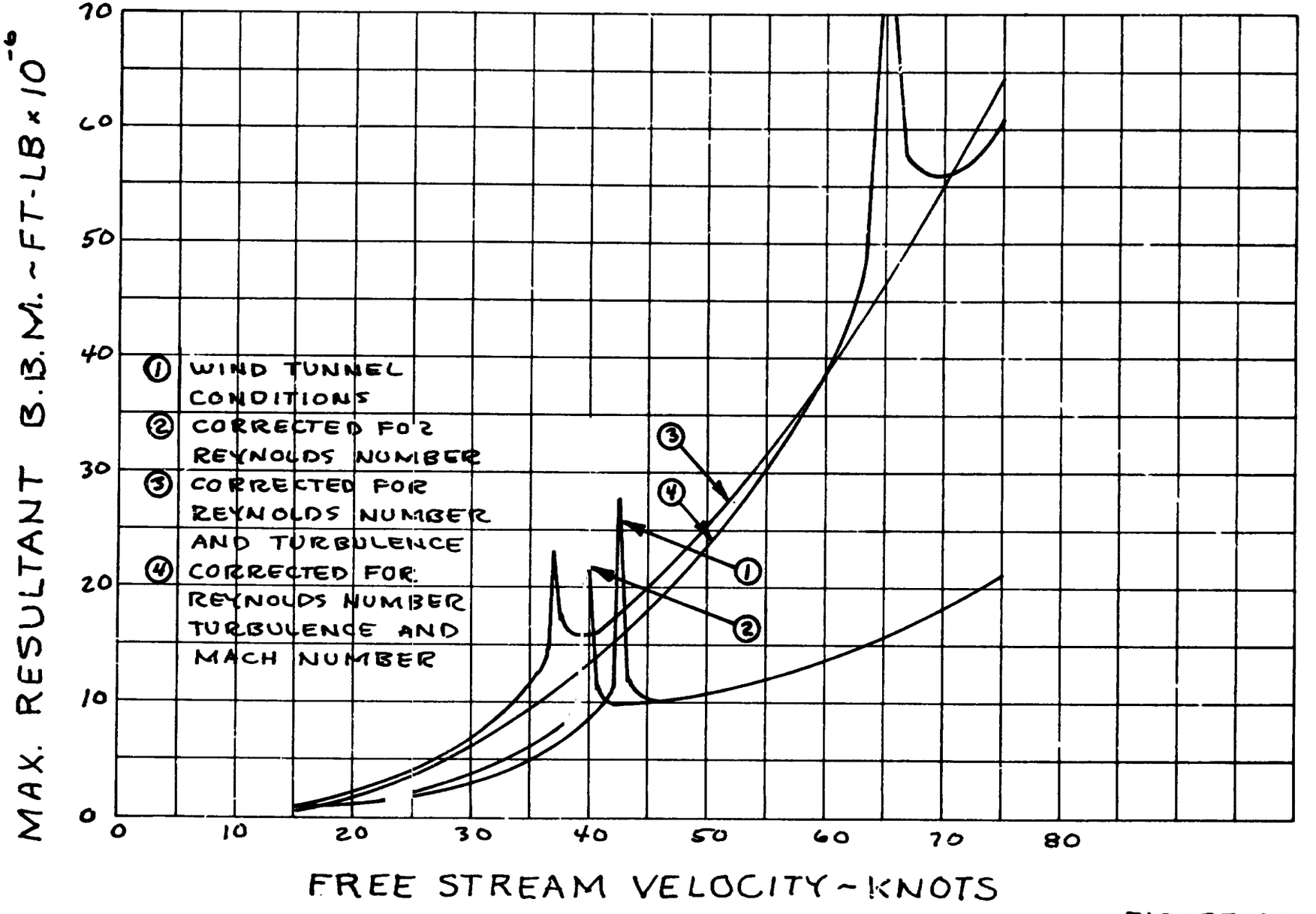

FIGURE 23

EXPERIMENTAL PRESSURE DISTRIBUTION

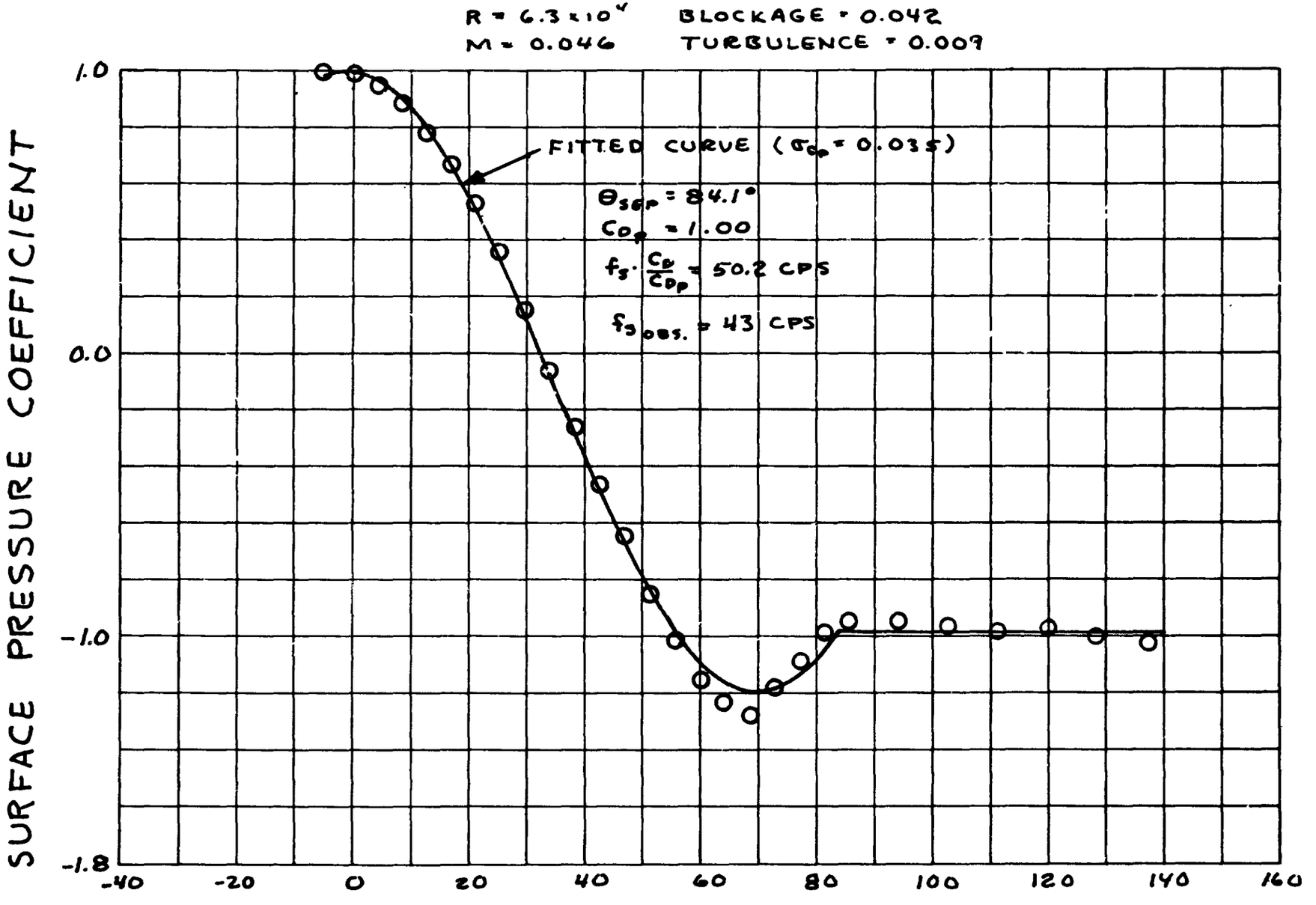

FIGURE 24

THE AMES WIND-TUNNEL GUST GENERATOR

by Donald A. Buell

The current research effort at Ames Research Center in the field of ground-wind loads is to develop a gust generator for use in a wind tunnel capable of high Reynolds numbers. A pilot model has been constructed with which to obtain data for design of the final version. This paper will be concerned only with the objectives of the research, since data have not yet been obtained.

The gust loads on a vehicle arise from the variation in magnitude and direction of the resultant wind velocity vector as indicated in figure 1. Unless the force is determined experimentally, it is necessary to assume that the force on a section of the vehicle is that due to a steady velocity equal in magnitude and direction to the actual instantaneous resultant velocity. It is implied that the flow field adjusts itself instantaneously to changes in velocity and that the resultant force is thus independent of the frequency of the gust.

Since two-dimensional cylinders have a tendency to shed vortices in a regular pattern, it is more reasonable to suppose that the shedding period is a sort of minimum adjustment time which must elapse after a velocity change, before the steady-state drag is representative of the force on the cylinder. Thus, one might expect gust load calculations to be uncertain for frequencies above the Strouhal frequency. This maximum frequency for valid gust load calculations could be even lower for three dimensional cylinders. In addition, one expects interactions between the gust forces and the vortex-shedding forces when the frequency of the two are close.

These considerations become of special concern at frequencies near the natural frequencies of the vehicle, where the vehicle is most responsive to an input.

One form of the frequency distribution of atmospheric turbulence is shown in figure 2, together with the portion to be simulated by the gust generator. The abscissa is reduced frequency, L being the scale of atmospheric turbulence. The spectrum of velocity in the ordinate has been nondimensionalized with the mean square of the velocity and has been multiplied by frequency, as suggested by Professor Davenport, to preserve the relation between areas under the curve when a log scale of frequency is used. The spectrum shown is for velocities parallel to the mean in isotropic turbulence. There are other expressions for the spectrum which may be more accurate, and another form of isotropic spectrum for the lateral direction, but the spectrum shown will serve to illustrate the point. The Strouhal frequency for a modern large vehicle corresponds to fL/U of about 2. This also corresponds approximately to the natural frequency of the vehicle at high wind velocities. Hence, it is desired to simulate the spectra in this area so as to experimentally determine the oscillatory forces that may be encountered.

The response spectrum of a vehicle might be as shown in figure 3 if it is cast in a form similar to the turbulence spectrum. There is a large area under the curve at low frequencies (resulting from the large input) where the assumption of instantaneous flow adjustment is adequate. However, the response at the natural frequency can be very large and is the uncertain part of the gust load. As

vehicles get larger, their natural frequencies will probably get smaller. More important, the fL/U for the Strouhal frequency will get smaller. These factors will decrease the range of fL/J which is amenable to calculation and make an experimental determination of gust loads more important.

As Professor Davenport and Mr. W. H. Reed have pointed out, the cross correlation of the velocities at various heights must also be properly accounted for. It is our intention to simulate insofar as possible representative values of both spectra and cross spectra. Isotropic turbulence will serve as the model for simulation in order to take advantage of its simplicity of expression. It is then planned to vary the simulated turbulence scale and intensity over a range of values to match those observed by various researchers.

The method for creating the gusts will be to place oscillating vanes upstream of the model as indicated schematically in figure 4. As the vanes move, they shed vorticity which distorts the airstream to give either lateral or longitudinal velocity increments, depending on the phase differences between vanes. In the pilot model, the vanes will oscillate sinusoidally, but in a final version, each vane will oscillate with a complex motion to produce approximately random gusts. There would also be provision for a sinusoidal input at the vehicle frequency to simulate model motion.

In the pilot model there can be a variation in the number of rows and columns of vanes and in the amplitude, mean deflection, and phase relation of the individual vanes. Hot wires will be used to measure velocity fluctuations throughout the wake. The

vanes have been designed for oscillation amplitudes up to ± 55 degrees at low frequencies and for frequencies up to 50 cycles per second at low amplitudes. Tests with the pilot model will take place in a low speed atmospheric wind tunnel.

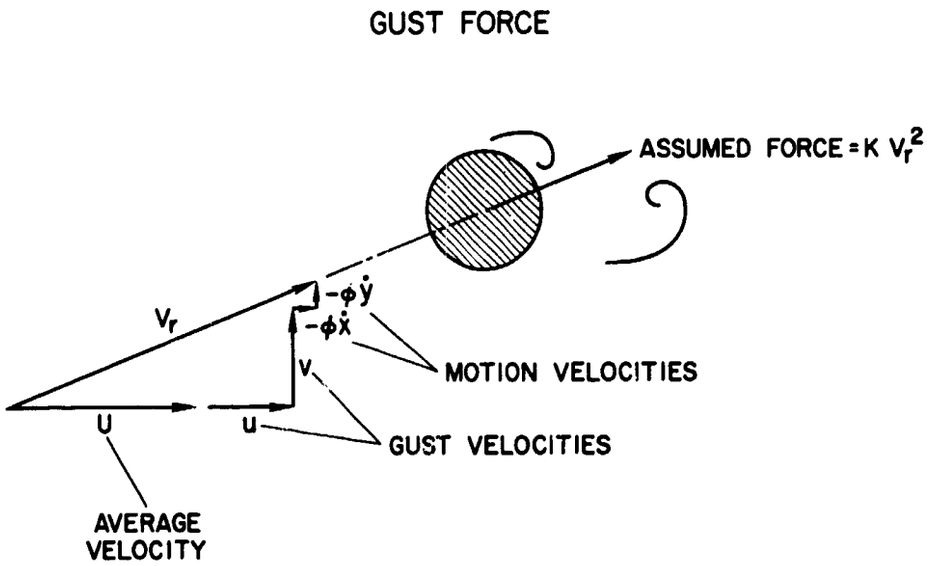

Figure 1.

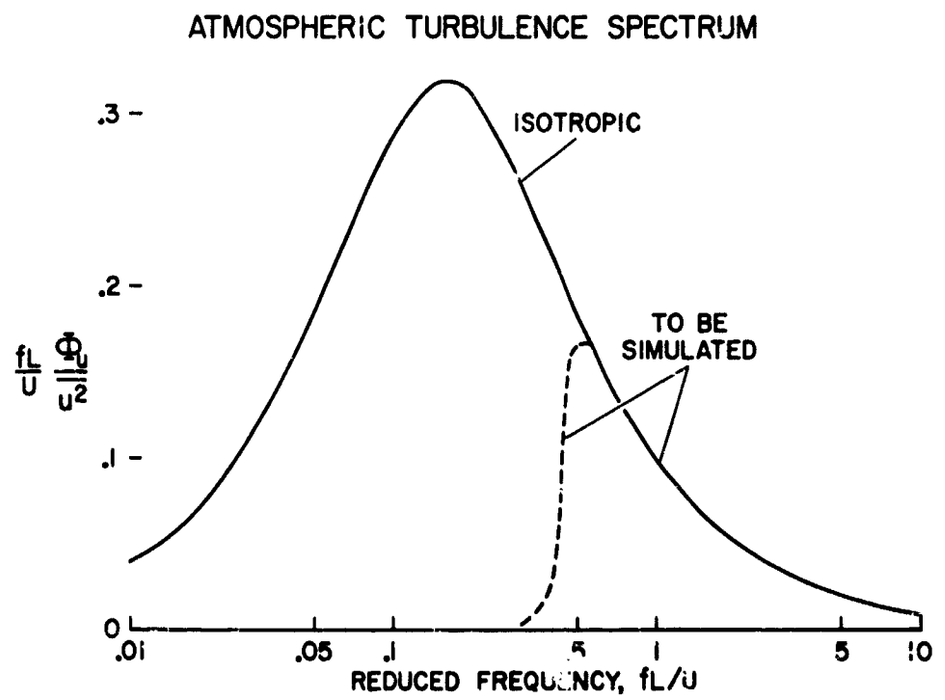

Figure 2.

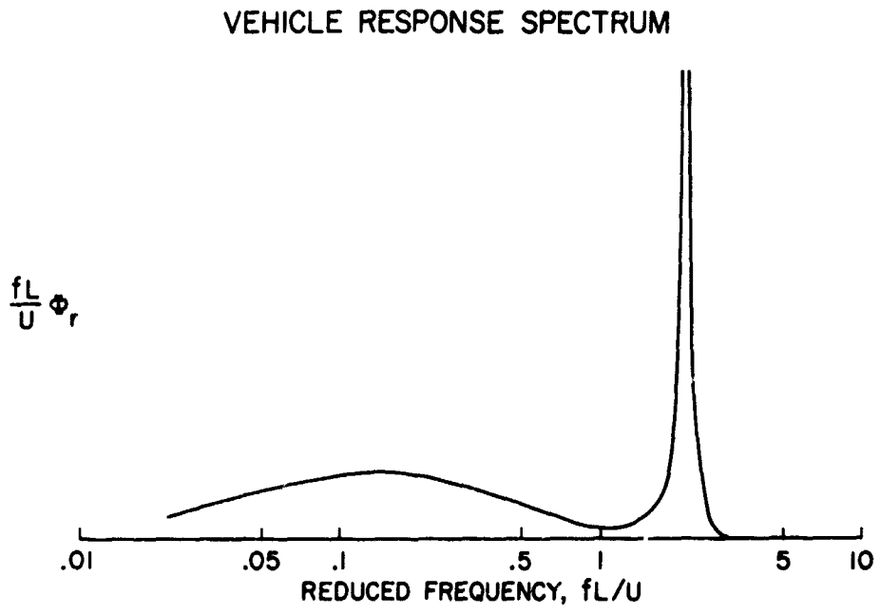

Figure 3.

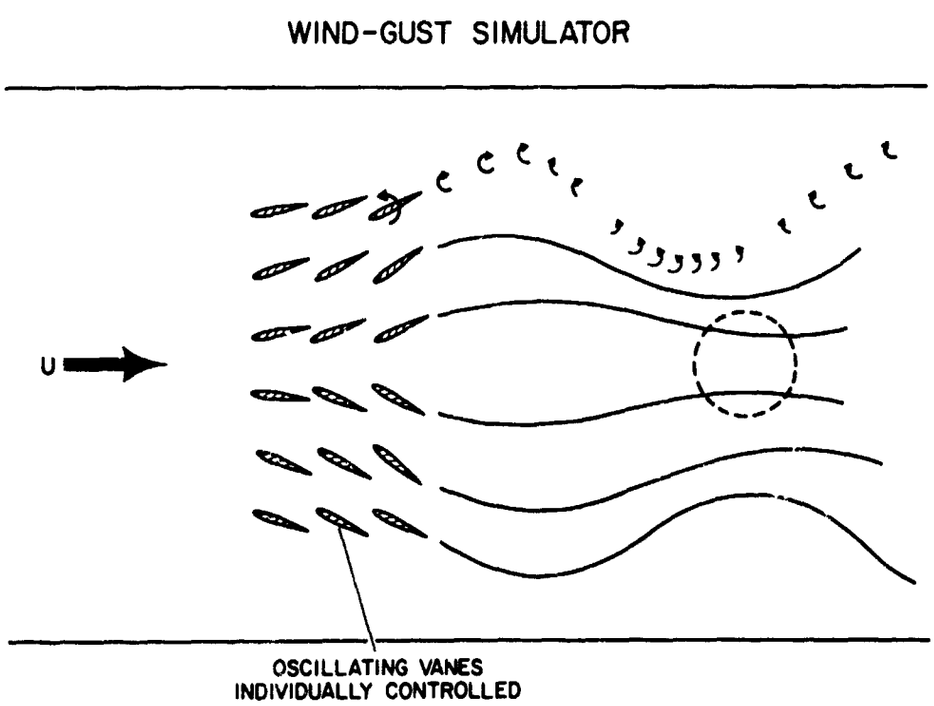

Figure 4.

Use of Air Injection in the Simulation of Atmospheric Processes

Richard E. Thomas
Department of Aerospace Engineering
Texas A&M University

Presented at the Meeting on
Ground Wind Load Problems in Relation to Launch Vehicles.
National Aeronautics and Space Administration
Langley Research Center

7-8 June 1966

The investigation currently proceeding at Texas A&M University has as its objective the study of the use of air injection to oscillate a wind tunnel stream and to otherwise simulate atmospheric processes in the wind tunnel.

The study has only recently begun and there are essentially no results to be presented now, therefore the discussion here will be limited to plans for the initial tests. The range of parameters, especially the Strouhal member, are based on use of a large wind tunnel such as the 7 foot by 10 foot Low Speed Wind Tunnel at Texas A&M. Postulating the use of a model of the order of 1 foot in diameter means that gust frequencies might range up to 50 c.p.s. Transverse velocities up to 10 ft. per second in a basic 100 ft./sec. stream are sought. Preliminary studies are being completed in the 2 foot by 3 foot Low Speed Wind Tunnel.

The general scheme is shown in Figure 1. Ejector nozzles are mounted at the downstream end of the test section. The air supply system includes a modulating valve which is rotated at a selected speed and "pulses" the ejectors. The induction action of the ejectors causes the tunnel stream to oscillate.

It appears possible to generate "sinusoidal" gusts by pulsing, for example, the top ejectors out of phase with the bottom ejectors. Longitudinal gusts can be obtained by pulsing all ejectors in phase. Random turbulence could be generated by pulsing the ejectors individually in a random fashion. Wind shears might be simulated by steady operation of the ejectors, but with the top ejectors operating at a higher pressure than the lower ones.

There are many questions to be answered by our study as shown in Figure 2.

(1) What is the configuration of the transverse gusts which can be simulated? Uniformity?

(2) Can relatively pure longitudinal gusts and wind shears be produced?

(3) What is the optimum ejector configuration? Air supply?

(4) What are the pertinent performance parameters which one can use to scale the system to a different wind tunnel?

(5) Others

(a) What type of instrumentation is optimum from the standpoints of sensitivity, ruggedness, reliability?

(b) What is the influence of ejector air in the tunnel stream?

To give some indication of what might be expected with this system some results of a rough preliminary study are presented. As shown in Figure 3, a six inch by six inch duct was mounted in the 2 foot by 3 foot Low Speed Wind Tunnel and a M = 1.5, 1 inch exit diameter nozzle was installed as shown. The steady state performance of the ejector is shown in Figure 4. The ejector was operated in both the downstream direction shown and in the upstream direction, that is, opposing the main stream flow.

The results show that for a given mass flow ratio the upstream facing ejector was more effective in changing the stream velocity as might be expected from the consideration of blockage versus induction effects.

The ejector air supply was pulsed at 10 c.p.s. and 30 c.p.s. and the modulation of the stream was influenced by the frequency response characteristics of the pneumatic system consisting of the modulating valve, the nozzle, and the interconnecting line.

The results must be regarded as preliminary because no dynamic calibration of the transducers was performed. However, in general, the results were consistent with those which would be expected based on the static performance of the ejector. Typically, the stream was oscillated at 10 c.p.s. from 83.1 f.p.s. to 103.4 f.p.s. by ejector pressures ranging from 17.5 psia to 30.3 psia with downstream ejection. For upstream ejection the stream velocity was varied from 59.0 f.p.s. to 74.8 f.p.s. by ejector pressures of from 14.58 psi to 21.76 psia. The performance at 30 c.p.s. with downstream ejection showed the stream velocity fluctuating between 63.4 f.p.s. and 74.6 f.p.s. with pressures ranging from 14.8 p.s.i.a. to 33.4 p.s.i.a. It is not possible to judge from these results the probability of success of the multiple nozzle arrangement in inducing transverse gusts. Such results must await our more detailed studies.

At the present time the first ejectors for the 2 foot by 3 foot wind tunnel are being made. They are Mach 2 nozzles with a 2 inch diameter exit. The modulating valve is expected shortly and will be modified. Instrumentation is on hand and will consist initially of hot wire and hot film gages. The airfoil probes developed at the University of Toronto are also going to be used.

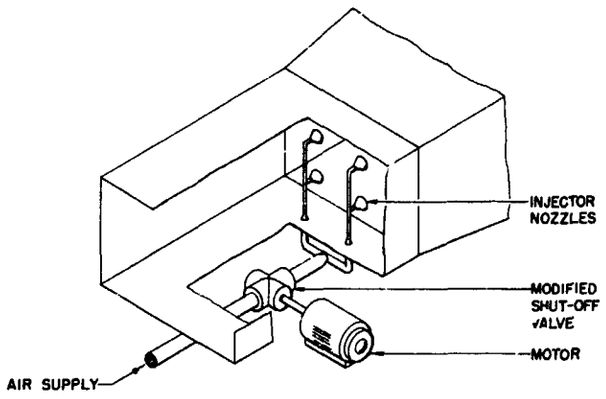

FIGURE 1
AN AIR INJECTOR CONFIGURATION

OBJECTIVES

1. GUST CONFIGURATION AND UNIFORMITY ?
2. PURITY OF LONGITUDINAL GUSTS ? WIND SHEARS ?
3. OPTIMUM EJECTOR CONFIGURATION ? AIR SUPPLY ?
4. SYSTEM SCALING PARAMETERS ?
5. OTHER
   (a) INSTRUMENTATION ?
   (b) TURBULENCE CAUSED BY INJECTED AIR IN CIRCUIT ?

FIGURE 2 - OBJECTIVES OF THE STUDY

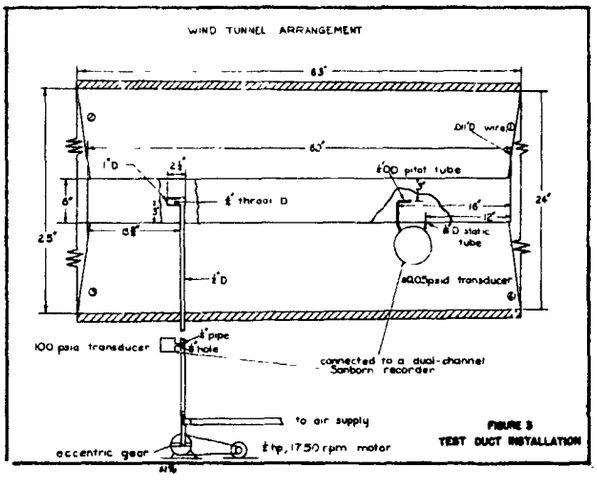

FIGURE 3
TEST DUCT INSTALLATION

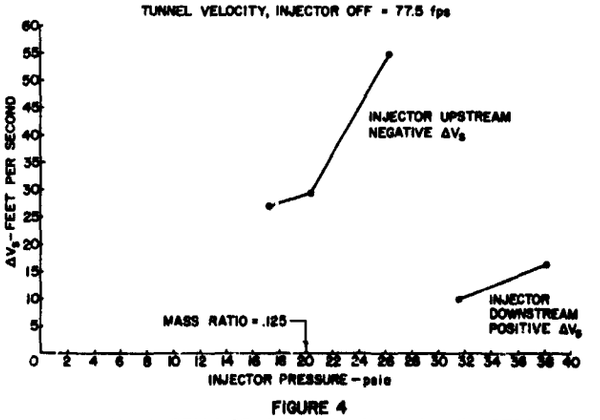

FIGURE 4
STEADY STATE PERFORMANCE OF SINGLE INJECTOR

NUMERICAL SOLUTION OF THE EQUATIONS OF CONTINUUM MOTION: VORTEX FORMATION AND SHEDDING IN A VISCOUS COMPRESSIBLE FLUID

By John G. Trulio

APPLIED THEORY, INC.

The work reported here consists of the numerical solution of the Navier-Stokes equation for the flow of a viscous compressible fluid around an infinite right circular cylinder. The calculations were performed for the Marshall Space Flight Center*, and have the ultimate two-fold objective of providing an understanding of the basic mechanisms involved in the growth and formation of vortices and turbulent wakes, and the development of theoretical tools with which to effect the practical solution of viscous compressible fluid flow problems.

In this program, recently developed numerical methods for the solution of continuum motion problems were adapted to the solution of aerodynamic problems. Previously these methods had been used mainly to solve ideal compressible fluid flow problems connected with nuclear weapons design and weapons effects; the specific numerical technique used in this program, and the computer code based on it, were developed under Air Force Contract to predict the motion of the ground as a result of a nuclear explosion. From a physical point of view, weapons problems differ considerably from those of vortex formation or turbulence. However, the equations of classical mechanics, on which the macroscopic theory of continuum motion is based, are the same in both cases, and indeed, for all the systems of continuum mechanics. The essential principle involved is that of momentum conservation, independently of whether the forces producing motion result from a gravitational field, shearing stresses in an elastic medium, or pressure in an ideal gas. Moreover, the other continuum mechanical

*Excerpted from NASA CR-430.

principles, conservation of mass, conservation of energy, and/or the first law of thermodynamics, take the same form irrespective of the nature of the materials, or their configuration, in a given system. Obviously, the solution of the equations of motion in any specific case will depend on the nature of the materials making up the system, their initial configuration, and subsequent boundary conditions. The point here is that the relation between the stress and the variables upon which it depends for a given material is beyond classical mechanics to determine, and must therefore be provided as part of the statement of any particular problem; to establish a constitutive relation is basically an experimental problem as far as classical mechanics is concerned. It is therefore reasonable to ask that schemes of integration of the equations of continuum motion be invariant to changes in the constitutive properties of materials or to applied external force fields, as well as the initial and boundary conditions for a properly posed mechanical problem. The great potential power of numerical approaches to the solution of the equations of continuum mechanics - and the refreshingly new aspect they present - is that these methods can be fashioned to apply once and for all to any system describable by classical mechanics. It is also theoretically satisfying that, in considering possible numerical approaches to the solution of continuum motion problems, it turns out to be at least as simple and natural to attack directly the job of integrating the equations of motion in general, rather than to limit oneself to numerical procedures valid only for special cases. To show this more clearly, we now give a brief description of a numerical method typical of those developed over a period of years at the nuclear weapons laboratories; our method is of the same kind.

First, every finite difference scheme for solving continuum mechanics problems replaces continuous space-time variables by a discrete set of points.

The schemes which have proven to be most generally useful in practice retain the time as an independent variable, as opposed, for example, to the use of characteristic coordinates as independent variables. The material of which a system consists is divided into finite elements, and Newton's Second Law is applied to these elements; i.e., each element is acted upon by stresses exerted across its boundaries by its neighbors, and perhaps by external forces such as gravity. Given the total stress field, the accelerations of the various elements are therefore known. It is then assumed that the stress field is constant for a short time interval, or time step, Δt. On this assumption, the impulse delivered to a given element can be found at once, and, by Newton's Second Law, its change in momentum is then known; hence, knowing the momentum of a material element at the start of the interval Δt, its momentum can be found directly at the end of the interval. The mass of each element being known and independent of time, its center of mass velocity at the end of the time interval is then found simply by dividing its new momentum by its mass. The new velocity so obtained, multiplied by Δt, is just the change in the position of the element's center of mass, so that if its center of mass coordinates are known at the start of the time step Δt, then they will now be known at the end of this time step. In general, the relative positions of the centers of mass will have changed over the time Δt, implying that each element has undergone some change in size and shape over this time. The precise description of the shape and size of each element amounts to the calculation of a general strain field and is fairly complicated; this is particularly true when the displacement field is known only at discrete points. For the present purpose, it should be noted that when the new strains are calculated, the changes in these strains in the time interval Δt will also be known. Thus, the calculation of strain rates,

which are an essential element of the Navier-Stokes equations, enters the numerical method in a straightforward way. In general, the stress of a material element will then be related to its internal energy, and to such quantities as the strain or instantaneous strain-rate of the element. The internal energy of the element appears for the first time at this point in the numerical calculation. Its value is also assumed known at the start of the time interval Δt, and must be found at the end of this interval. For this purpose, the First Law of thermodynamics is invoked, and the constitutive equation, taken with the First Law, provides a set of simultaneous equations whose solution yields both the internal energy and the components of stress for a given element at the end of the time interval. At this point, all the variables known at the start of the interval Δt will have been computed at the end of the interval, and the just-computed values of these variables can now serve as initial data for the next time step.

The numerical procedure, which is of the "time-marching" kind, has been sketched for the case in which we calculate directly the motions of specific material elements. This is the simplest case and is termed a "Lagrangian" description of motion. Alternatively, one might observe changes in the variables of the motion on fixed regions of space - a so-called Eulerian description of the motion. In either case, the principles employed in calculating the history of the system are conservation of momentum (Newton's Second Law), conservation of mass, and the First Law of thermodynamics. In the Lagrangian case, conservation of mass is automatic, although it must still be invoked to compute strains. In the Eulerian case, the calculation must take into account the additional processes of material flow across the boundaries of the spatial regions formed by connecting adjacent discrete points of the finite difference mesh with

straight lines. In general, as material crosses the boundary of a region, carrying with it its properties such as mass and internal energy, these properties - including mass - will change on the region. Such "transport" changes in the variables of the motion are taken into account in the computer program used to obtain the results presented below.

Since the practical aim of the program is to predict ground wind loading on vehicles or structures, interest centered on low Mach numbers; a Mach number of 0.2 was used in all our calculations. However, the air was treated throughout as compressible, the non-viscous part of its stress being that of a polytropic gas with a heat capacity ratio of 1.4. Also, in keeping with our previous remarks, the only portions of the computer code which had to be modified for these calculations were its stress and boundary subroutines. Prior to this program, the code had not been used to solve problems involving either Eulerian boundary conditions or viscous compressible materials. With regard to the place of the constitutive equations in these calculations, the same initial and boundary conditions could have been used to define a corresponding problem of motion for an elastic solid; only a small change in input would have been required to instruct the code to compute stresses for an elastic medium rather than for a compressible Stokesian fluid. At the present time, both constitutive equations, and some others as well, are contained in the stress subroutine of the computer code.

Since the motion is naturally described in a frame in which the cylinder is stationary, the coordinate systems used in the program were Eulerian; however the points of the finite difference mesh were not arrayed in straight lines, since these are not well suited to the description of flow in the neighborhood of a circular obstacle. The finite difference mesh used in most of our

calculations is shown in Figure 1. The direction of free stream flow is taken to be that of the Y axis, with lines normal to it corresponding to constant values of the coordinate X. The diameter of the cylinder was arbitrarily set equal to three units of length. Air entered the flow field across an upstream boundary at $Y = -7$ and exited across a downstream boundary at $Y = +15$. The lateral boundaries, which coincide with the lines $X = 10$ and $X = -10$, were treated as rigid surfaces of frictionless sliding. A no-slip condition was applied at the surface of the cylinder itself. The most extensive calculations were made in the program for a Reynolds number R of 100. The initial conditions for the problem were impulsive, with all the air in uniform motion in the Y direction at a Mach number of 0.2. Figure 2 shows the velocity field at the initial time. In this and succeeding figures, velocities appear as vectors centered on the various points of the finite difference mesh; also, time is measured in terms of the distance moved by a free stream particle.

A short time after the start of the problem, the flow field adjusts itself to the presence of the cylinder, as shown in Figure 3, to form a roughly streamlined flow. This adjustment takes place in part through a shock reflected from the cylinder at its upstream side; the shock appears plainly in the numerical output, although no plots were made for this phase of the flow. With the passage of time, sufficient circulation accumulates in the wake of the cylinder to make apparent the initial development of vortices, as shown in Figure 4. In Figure 5, these vortices have grown considerably and still appear perfectly symmetrical. The system itself was deliberately made slightly asymmetric with respect to reflection through the line $X = 0$, in that the three points of the cylinder closest to one of the lateral boundaries of the system lie on a straight line, while the points opposite these lie on a circle. This perturbation

to the symmetry of the system is evidently insufficient to cause vortex shedding in a time comparable to that observed experimentally; vortices continued to elongate in the downstream direction, becoming asymmetric only very slowly. Of course, since the initial condition asymmetries present in actual experiments were not known to us, the relatively slow growth of asymmetry predicted by the computer code says nothing about the accuracy of this prediction; a system built precisely to correspond to our initial conditions might indeed develop elongated vortices. Nevertheless, the slow growth of asymmetry was inconvenient in this program. The system was therefore perturbed by setting a group of velocities equal to zero near the cylinder at its downstream side; these velocities were subsequently allowed to change in accord with the equations of motion. The perturbation to the flow field is evident in Figure 6 and was sufficient to initiate the shedding of vortices, as shown in Figures 7 , 8 , and 9 .

The alternate shedding of vortices from the upper and lower portions of the cylinder at its downstream side is qualitatively very similar to that observed experimentally. A Reynolds number of 100 was used in these calculations mainly to provide an important quantitative check on the computed results in terms of the shedding frequency of the vortices. The Strouhal number, a dimensionless form of the shedding frequency, has been measured as a function of the Reynolds number and found to vary most rapidly with Reynolds number at $R = 100$. Its value at $R = 100$ is 0.17. Two estimates of the Strouhal number were made at different positions and times in the computed flow fields, and the values 0.16 and 0.18 were obtained.

Calculations were also made for Reynolds numbers of 1000 and 5000 in the early stages of vortex formation. The results are shown for $R = 1000$ in

Figure 10, at a time very nearly equal to that shown in Figure 4 for R = 1.00. It can be seen that the vortex is more fully developed for R = 1000. Similar calculations were made for a Reynolds number of 5000, and, as can be seen from Figure 11, no vortices formed at all. Experimentally, vortex streets are observed to develop at Reynolds number below about 2500, while turbulent wakes are observed above this Reynolds number; our results are in agreement with this experimental observation.

Perhaps the most interesting results of all relate to the drag on the cylinder. The time-averaged drag, normalized to the pressure head and to a cross-sectional area of the cylinder, has the experimental value 1.7, which is also the value predicted by the code. In Figure 12, which shows the pressure distribution around the cylinder for R = 1000, the computed and measured values do not agree this well. Moreover, more detailed plots of the pressure around the cylinder show some point-to-point fluctuations which are not apparent in Figure 12. These variations were even more striking when the calculation was repeated with a finer spatial mesh. The results are shown in Figure 13. At first it was suspected that these oscillations were of a non-physical kind often observed in numerical calculations of the sort described here; this is the price paid for replacing a continuum by a discrete set of points. However, non-physical spatial oscillations in the numerical results are almost always accompanied by similar oscillations in time, with a period of at most a few time-steps. Accordingly, pressure-time plots were made for several adjacent points at the back side of the cylinder, and, as shown in Figure 14, pressure oscillations were found with a period of about 100 time-steps. The amplitudes of these waves vary somewhat. However, their phases appear random, in keeping with the zone-by-zone pressure fluctuations of Figure 13. The period of

oscillation of the waves of Figure 14 greatly exceeds the time required for either a sound signal or a material particle to cross a zone. Thus, there is no obvious connection between the numerical parameters of the problem and these waves. On repeating the calculations with the mesh of Figure 1, they appeared again, but with smaller amplitudes; they are diminished still further by lowering the Reynolds number. We expect soon to carry out similar calculations with as fine meshes as are economically feasible in order to determine whether these oscillations persist, and perhaps approach a limiting pattern. If so, then the definitive test of their reality would lie in an experimental measurement of pressure as a function of time; resolution of at least 50-kilocycle signals would be required in such experiments, since this is the calculated frequency of the pressure fluctuations.

If the pressure fluctuations of Figure 14 are real, then they appear to us to have two main implications. First, with respect to turbulence, the conclusion strongly suggested is that at low Reynolds numbers, where there is relatively strong damping of the fluctuations, their amplitude is not so great as to disrupt the formation of vortices; however, the fluctuations grow in amplitude with increasing Reynolds number, until finally organized flow on a scale of distance comparable to the radius of the cylinder is not possible, and a turbulent wake results. We would then be left with the task of explaining why the Navier-Stokes equations have solutions of this kind at all, i.e., the problem of describing the physical processes which cause such solutions. For this task, computer calculations would probably be our main tool. Finally, if point-to-point pressure fluctuations - or even fluctuations in the spatial derivatives of the pressure - are really implied over finite regions in these flow fields by the principles of motion, then the Navier-Stokes equations in

their familiar differential form cannot govern this kind of motion; flow fields for which the derivatives appearing in these equations do not exist cannot satisfy the equations. However, the fundamental statements of the principles of continuum motion are relations among integrals, and not derivatives. Differential forms happen to be particularly fruitful when the available computational aids consist of pencil-and-paper; if the continuity of the solution implicitly assumed in writing differential equations does not exist, then classical pencil-and-paper methods for their solution will not work. On the other hand, it is natural to base numerical methods of solution of continuum motion problems on the more general integral statements of the principles of continuum mechanics. The interesting thought then arises that, far from being a substitute for insight, high-speed computers and numerical methods designed for them, might play a key role in understanding the basic mechanisms of such phenomena of viscous compressible fluid flow as vortex formation and turbulence.

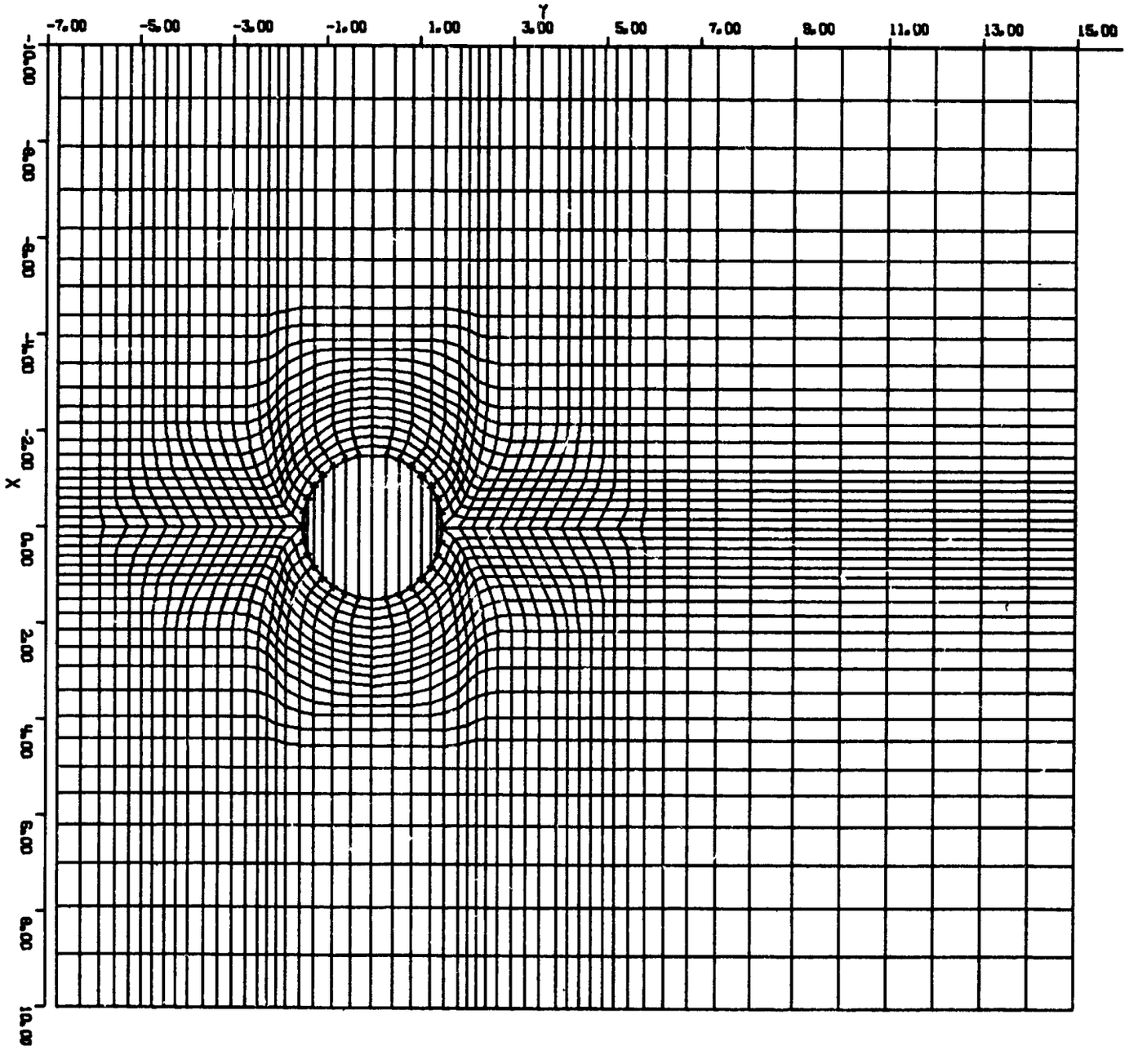

Fig. 1. Medium Mesh (43 x 48)

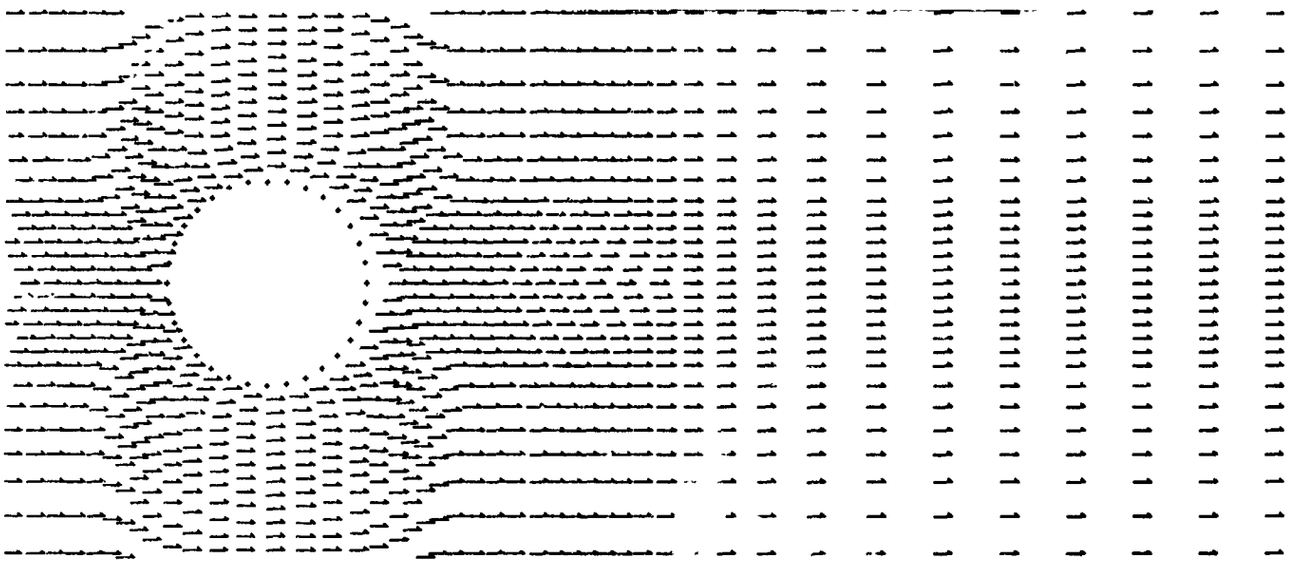

Fig. 2. Problem No. 211.3, $\kappa = 100$, Medium Mesh; Old boundary condition; Free stream particles have moved 0.0 cylinder diameters.

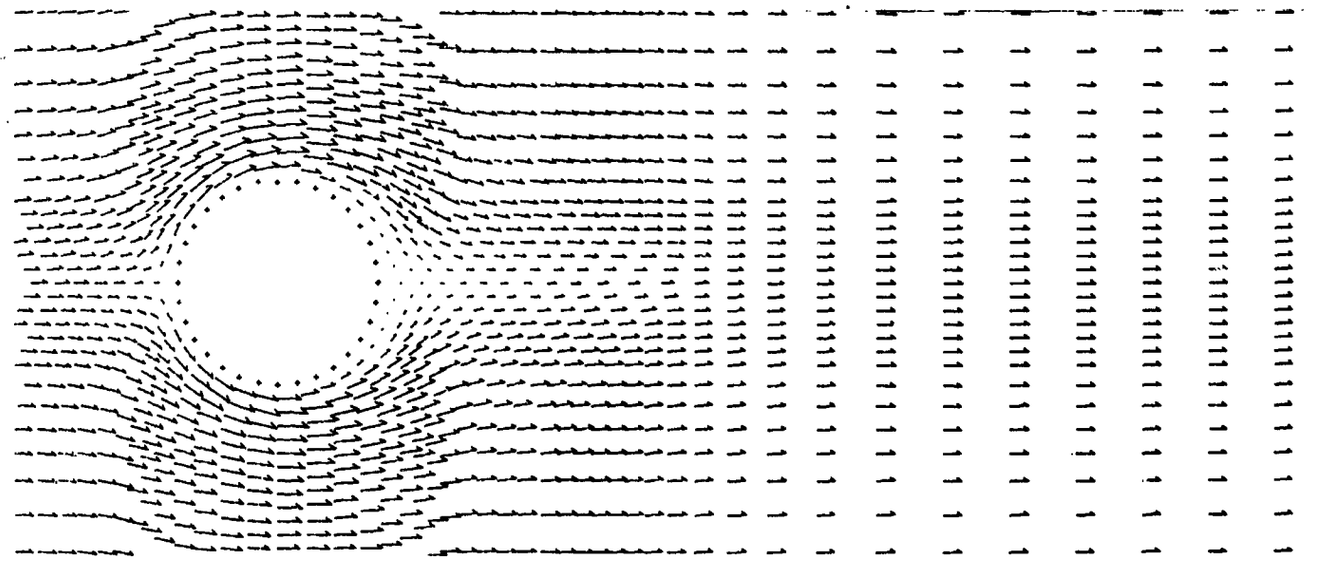

Fig. 3. Problem No. 211.3, R = 100, Medium Mesh; Old boundary condition; Free stream particles have moved 0.397 cylinder diameters.

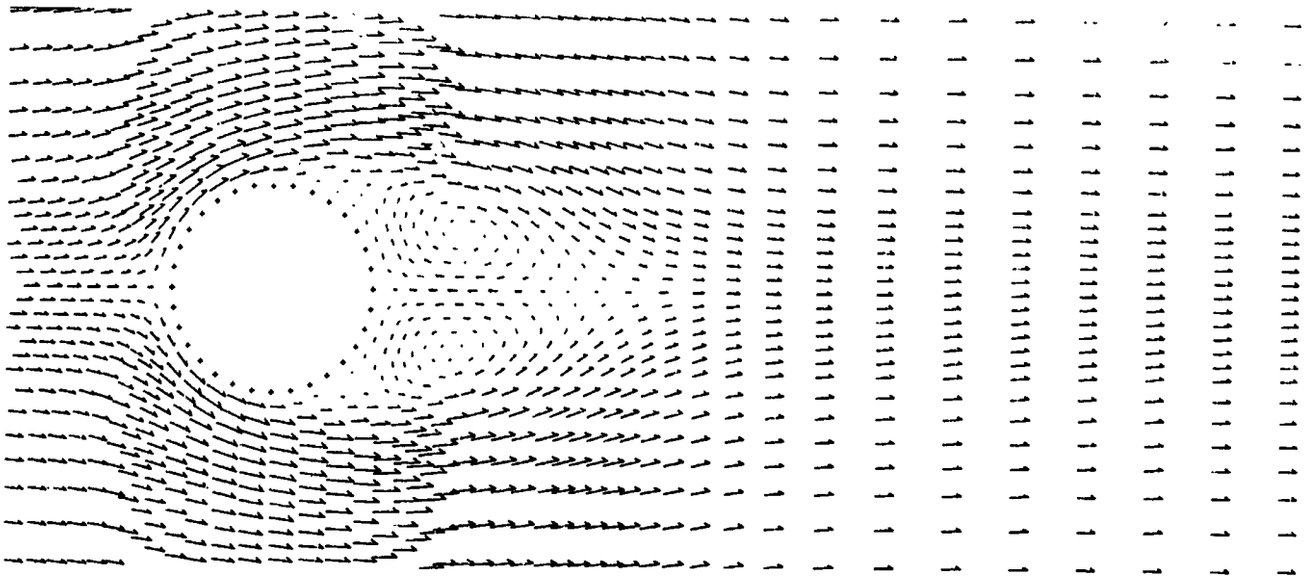

Fig. 4. Problem No. 211.3, R = 100, Medium Mesh; Old boundary condition; Free stream particles have moved 2.38 cylinder diameters.

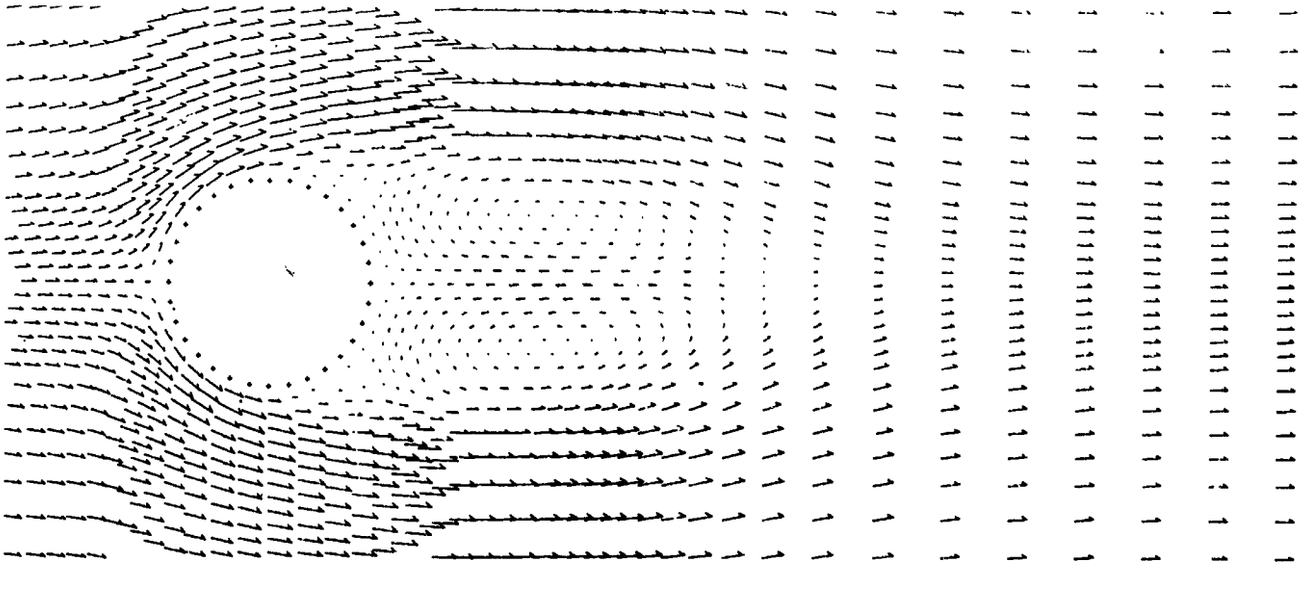

Fig. 5. Problem No. 211.3, R = 100, Medium Mesh; Old boundary condition; Free stream particles have moved 5.12 cylinder diameters.

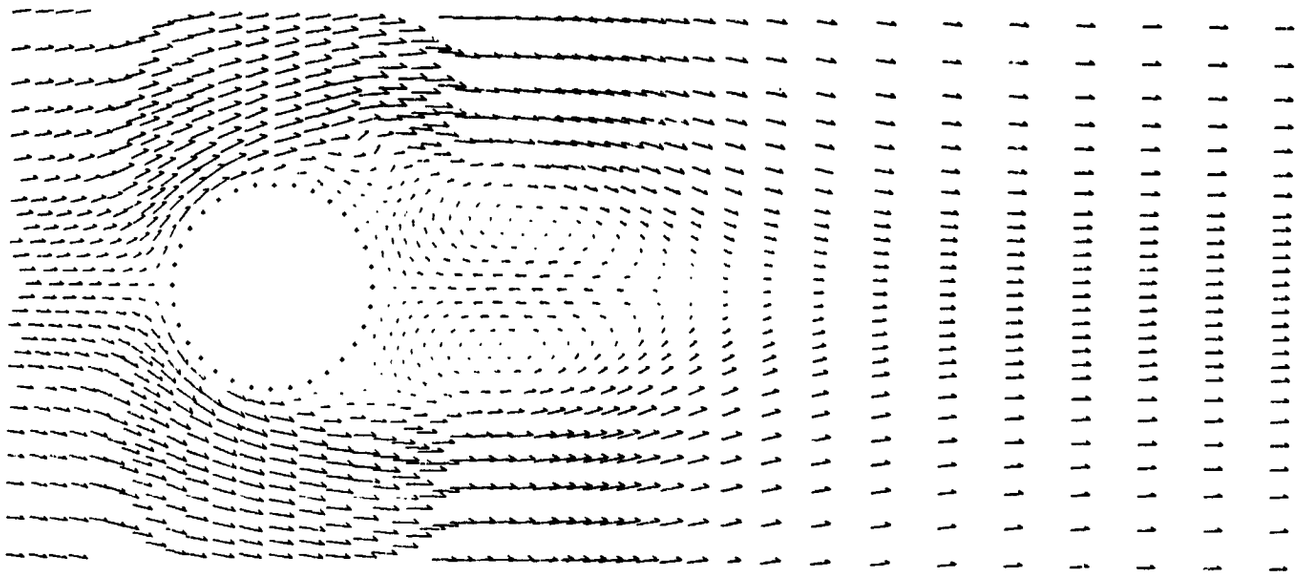

Fig. 6. Problem No. 211.4, R = 100, Medium Mesh; Old boundary condition; Free stream particles have moved 3.89 cylinder diameters.

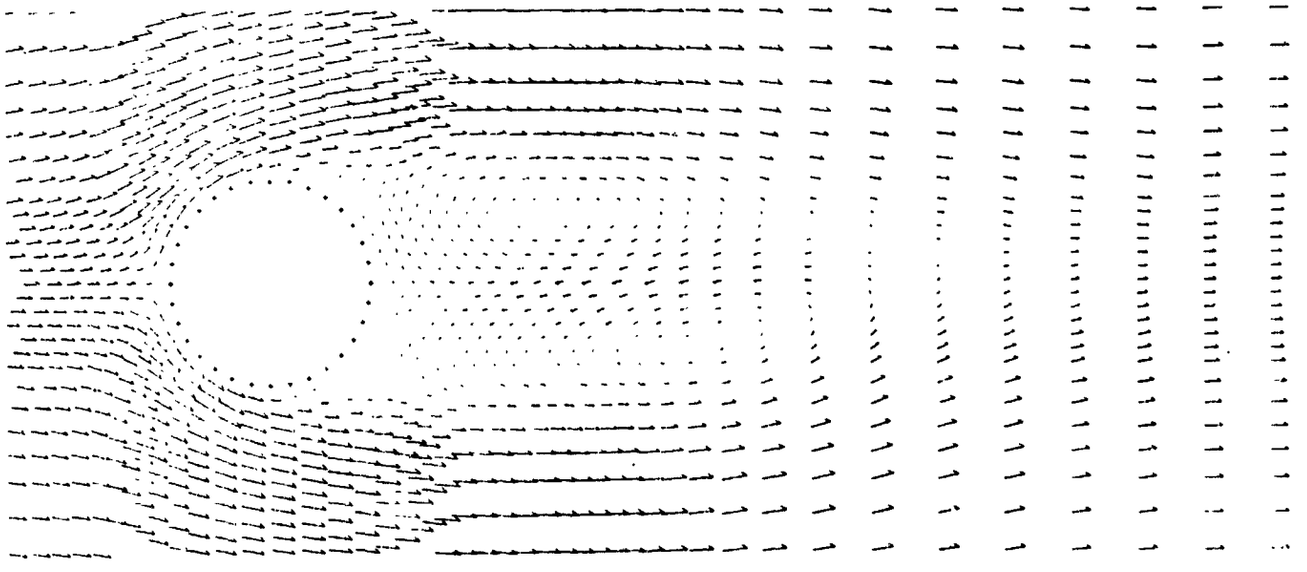

Fig. 7. Problem No. 211.4, R = 100, Medium Mesh; Old boundary condition; Free stream particles have moved 7.54 cylinder diameters.

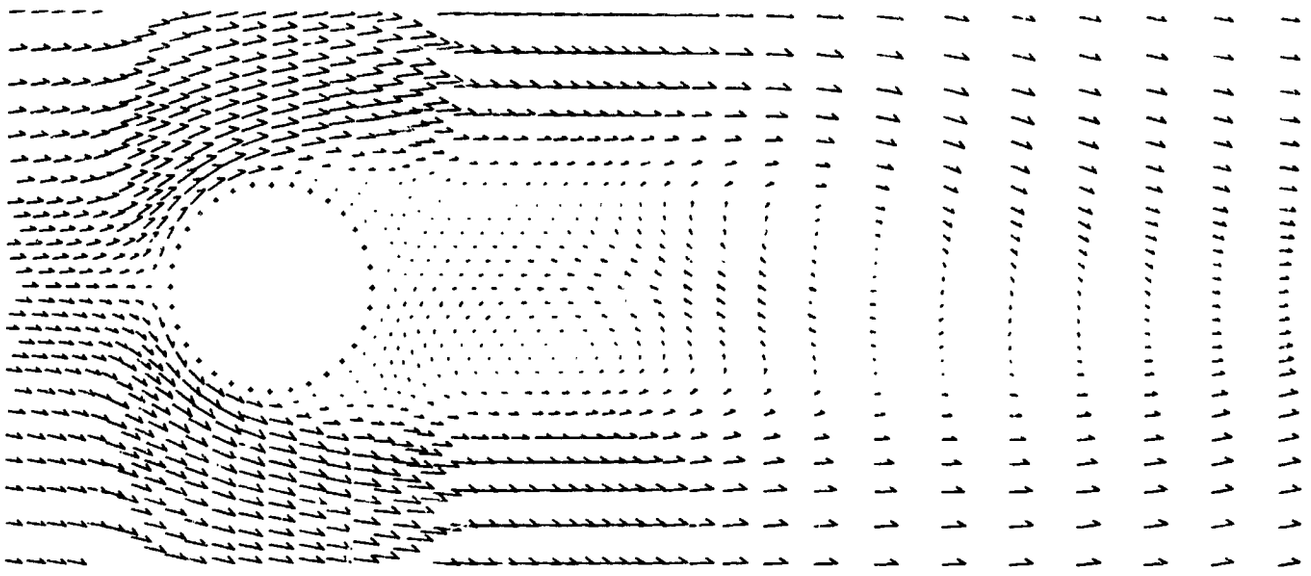

Fig. 8. Problem No. 211.41, R = 100, Medium Mesh; New boundary condition; Free stream particles have moved 11.1 cylinder diameters.

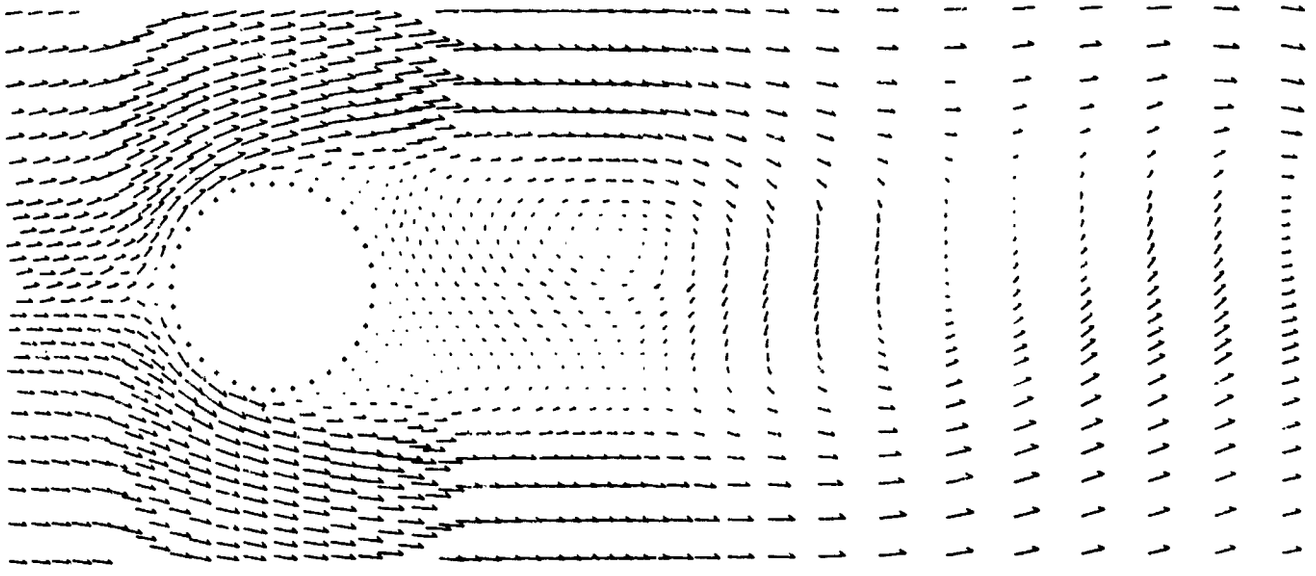

Fig. 9. Problem No. 211.41, R = 100, Medium Mesh, New boundary condition; Free stream particles have moved 14.7 cylinder diameters.

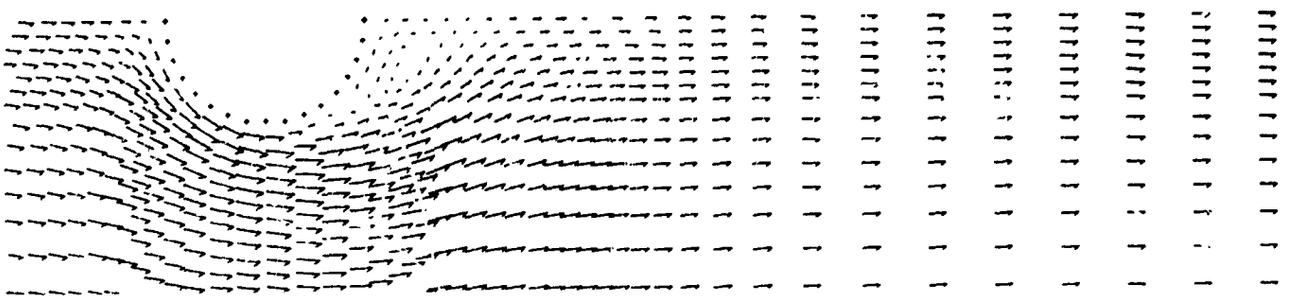

Fig.10. Problem No. 211.3, R = 1000, Medium Mesh; Free stream particles have moved 1.19 cylinder diameters.

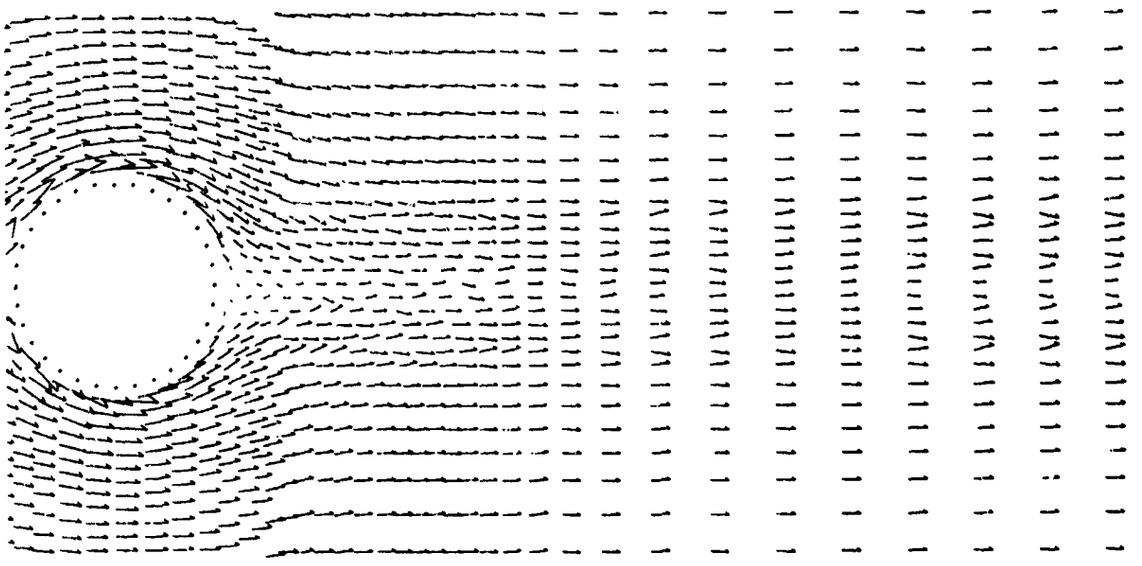

Fig. 11. Problem No. 211.2, R = 5000, Medium Mesh; Free stream particles have moved 4.77 cylinder diameters.

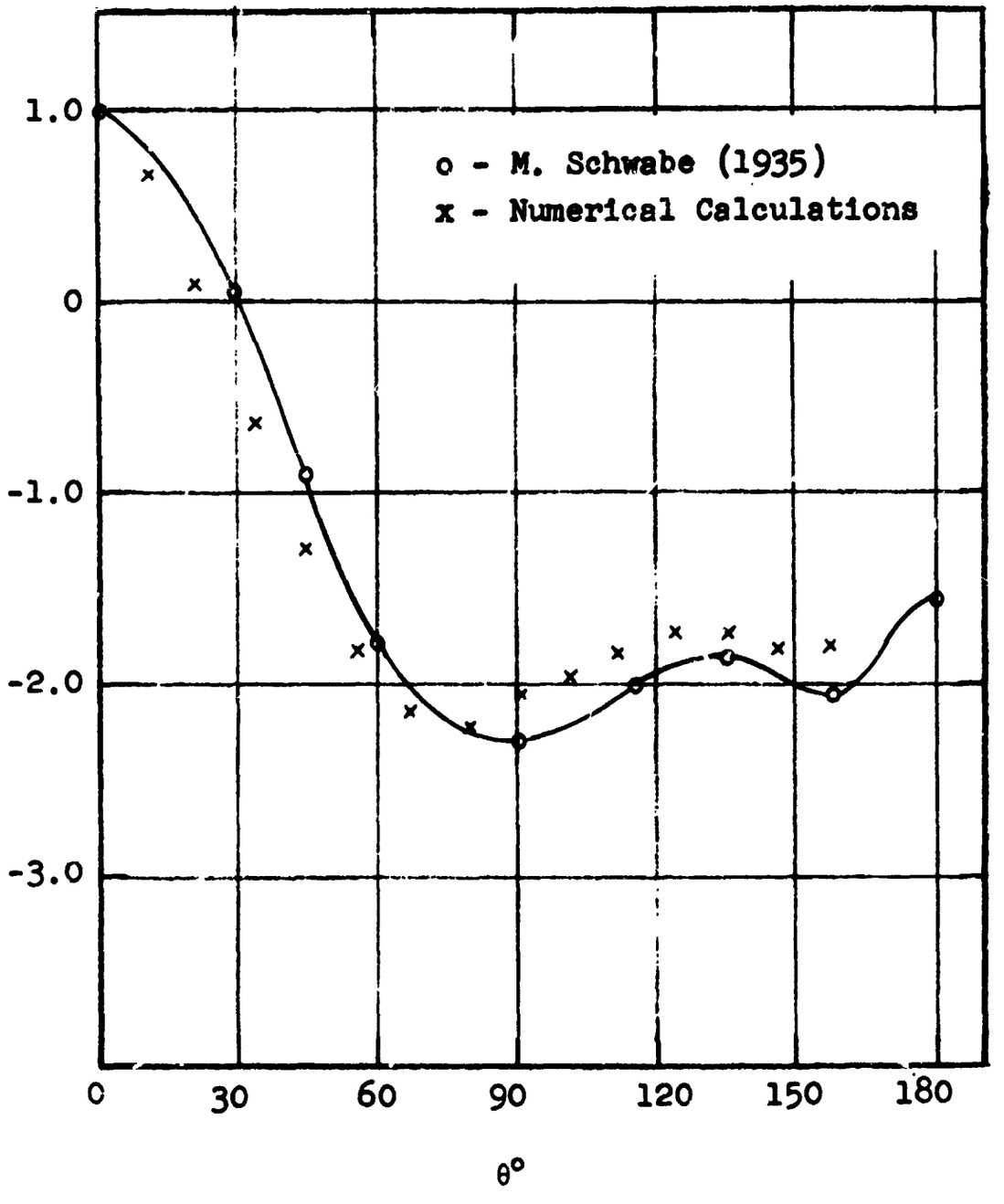

Figure 12

Calculated Pressure Distribution Around a Circular Cylinder During the Starting Process for R = 1000. Medium Mesh Used for the Numerical Calculations.

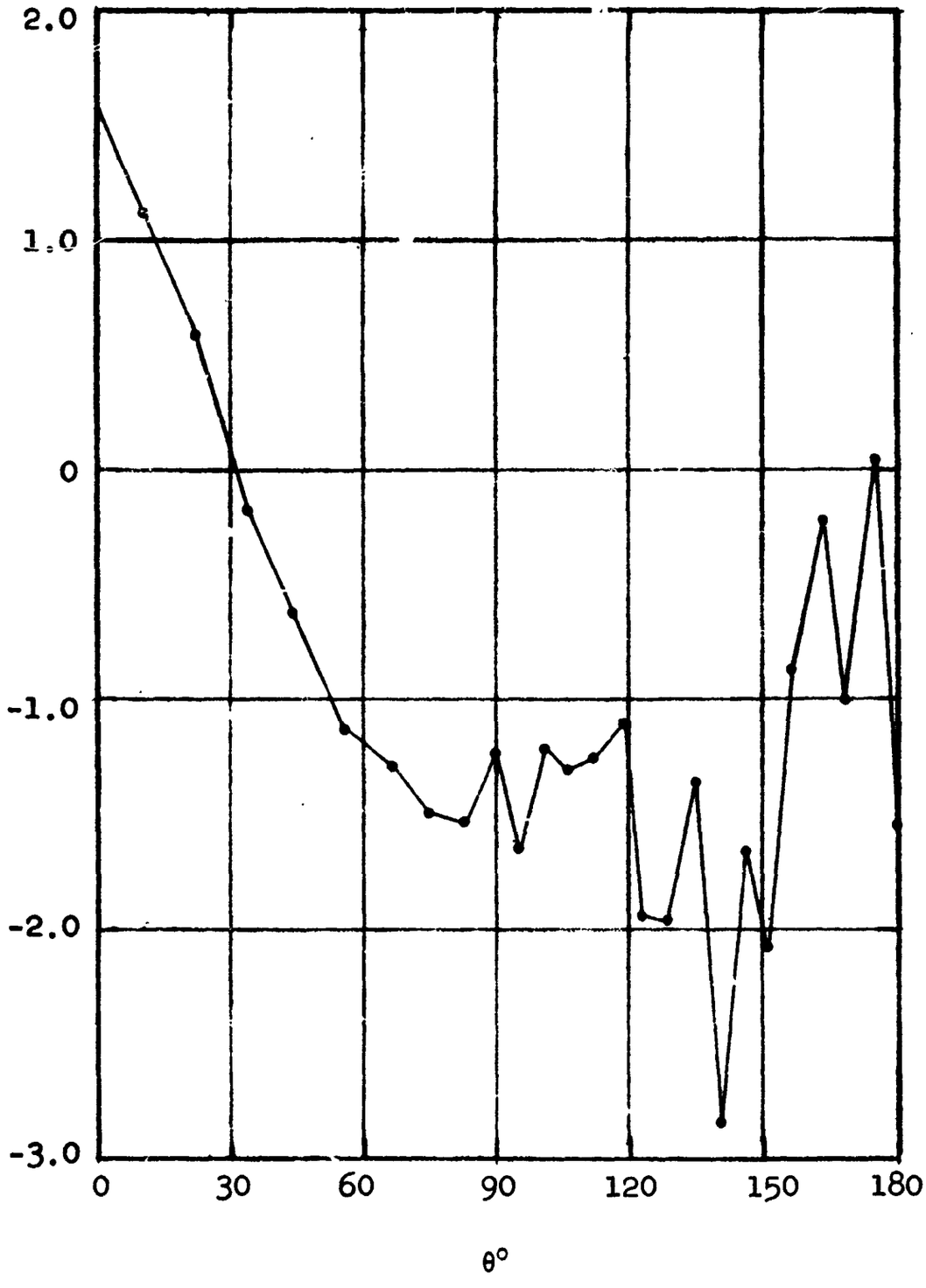

Figure 13

Calculated Pressure Distribution Around a Circular Cylinder During the Starting Process for R = 1000. Fine Mesh Used for the Numerical Calculations.

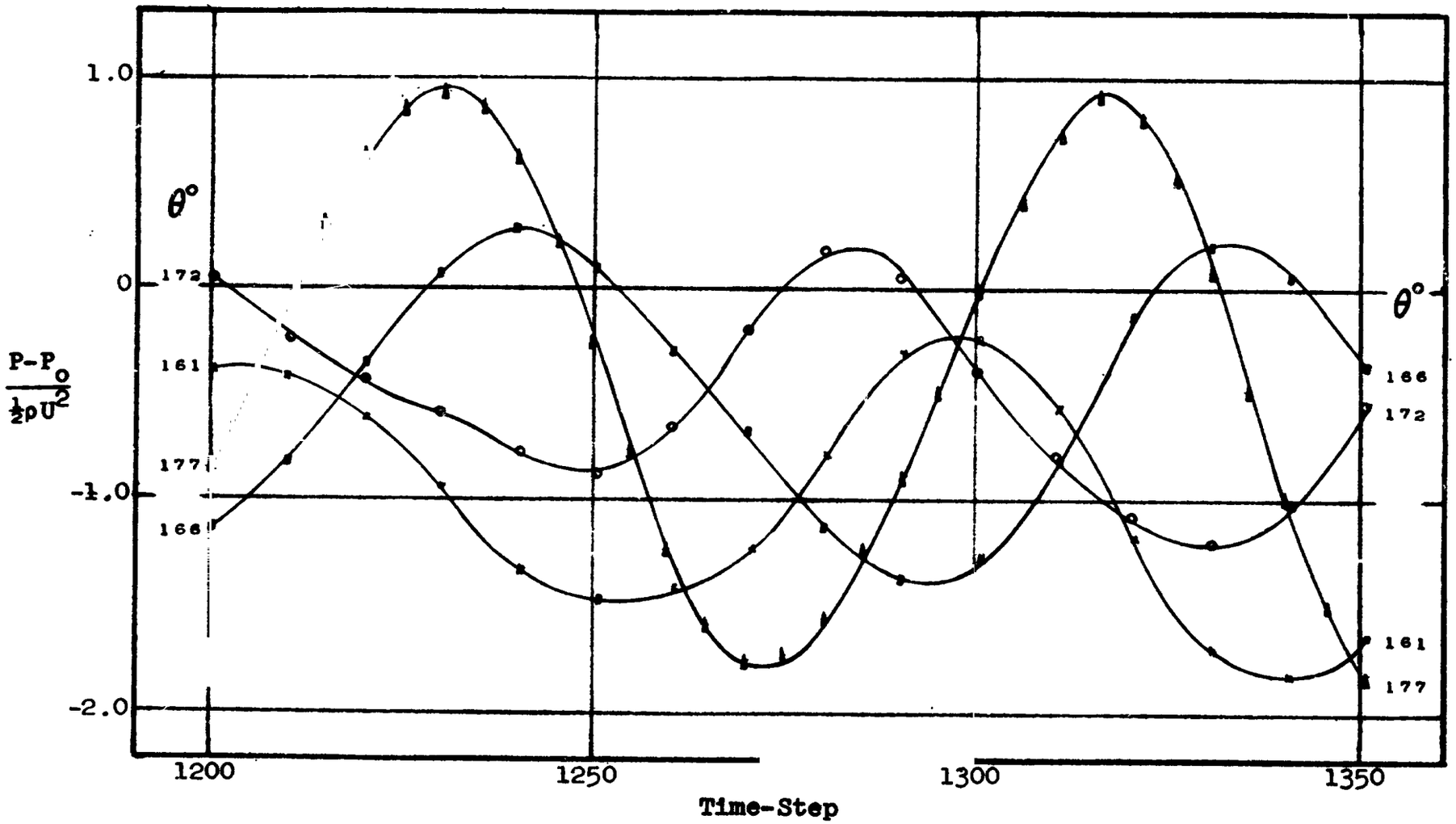

Figure 14

Pressure Variation as a Function of Time-Step for Each of Four Contiguous Zones Located Near the Most Downstream Part of the Cylindrical Surface; R = 1000, Fine Mesh Used for the Numerical Calculations.

SESSION IV - BASIC STUDIES OF CYLINDRICAL BODIES

Chairman - Y. C. Fung, California Institute of Technology

SOME WATER TABLE EXPERIMENTS ON OSCILLATING CYLINDERS*

Leon Schindel** and Garabed Zartarian**

Summary

This paper presents some preliminary results of forced and free oscillation tests on small cylinders in a water table flow, at Reynolds numbers of the order of 10^4. These simple, exploratory experiments consisted primarily of wake-visualization studies, and measurements of the phase angles between lateral displacements and lateral hydrodynamic forces at various amplitudes and reduced frequencies. It was found that negative hydrodynamic damping exists only at reduced frequencies within a few percent of the Strouhal number and for a limited range of amplitude. Using the hydrogen bubble technique, vortex trajectories behind stationary and oscillating cylinders were determined. Large lateral wake movements were noted, particularly for cases with large-amplitude oscillations.

Hopefully, these results will guide and test the formulation of a simple analytical model for the purpose of predicting adequately the aerodynamic forces on an oscillating cylinder. Two such models are suggested and briefly discussed.

The task is not completed; the presented results are subject to checks with some repeated tests which are in progress.

Introduction

A main objective of the study performed some thirty years ago by Meier-Windhorst (Ref. 1) was to answer the following important

* Study conducted for NASA, under Contract No. NAS8-20186.

** Research Aeronautical Engineers, Department of Aeronautics and Astronautics, Massachusetts Institute of Technology.

question:

What is the nature of the motion-dependent hydrodynamic forces on an oscillating cylinder in a water-channel flow, and how do these forces limit the oscillations initiated by the Strouhal forces (i.e., the periodic forces on the stationary cylinder)?

Meier-Windhorst observed the free oscillations of an elastically-mounted cylinder in an 18-cm deep water channel flow, at various combinations of cylinder mass, cylinder natural frequency and of built-in viscous damping. For each case he tried to establish the dependence of amplitude and frequency of oscillations on the free-stream velocity. Some features of his results of interest to the present study are:

(1) When the velocity was increased slowly, a critical velocity was reached where the amplitude rose sharply. This point corresponded to a motion frequency equal to the natural frequency of the system in still water, f_N, and also equal to the Strouhal frequency f_S ($= \frac{0.2V_0}{D}$, where V_0 is the free-stream velocity, and D the diameter).

(2) As the velocity was further increased by as much as 10%, the amplitudes of motion increased slowly. The motion frequency was found to be somewhere between the Strouhal frequency and the natural frequency, being closer to the latter for higher mass ratios. For still higher velocities, amplitudes dropped gradually.

(3) The mass ratio, ψ, defined as

$$\psi = \frac{\text{mass of the cylinder + reduced mass of oscillation arm}}{\text{mass of displaced fluid}} + 1,$$

varied from about 2.3 to 8.8*. With increasing ψ, the width of the amplitude vs. V_0 curve, the maximum amplitude, and the difference between motion frequency and natural frequency decreased.

---

* It should be realized that the mass ratios of practical interest are much greater. In the experiments to be described later, ψ was estimated to be around 300-400.

It is apparent from these results that the cylinder response to the hydrodynamic forces is not strictly speaking a resonance effect. Stated alternatively, the cylinder motion alters the flow field significantly, and the vortex shedding frequency is different from both f_N and f_S generally. One would also expect changes in the equivalent hydrodynamic damping force. For present purposes, it is adequate to express the total hydrodynamic force F_a as

$$F_a = -m_a \omega^2 x + c_a \dot{x} \qquad (1)$$

the two terms representing the parts in phase with acceleration $\ddot{x}$ and with velocity $\dot{x}$ respectively. Scruton (Ref. 2) has adopted this sort of division in his analysis and presentation of experimental results on aerodynamic derivatives. This sort of representation can be justified only when the amplitudes are large and the dominant forces are of the same frequency as the motion. At lower amplitudes, unless motion and Strouhal frequencies are very close, the force signal will contain both frequencies, and Eq. (1) is no longer useful. At reduced frequencies, sufficiently close to the Strouhal frequency, c_a will have a negative sign at low amplitudes. With increasing amplitude, c_a will increase and reverse in sign at some amplitude which will be denoted here by A_0. In the absence of structural damping forces in the system, A_0 would be the maximum attainable amplitude in free oscillations. A_0, as obtained from forced oscillation tests, will depend on the reduced frequency of motion.

An important first objective in the present investigation was to determine approximately the aerodynamic* zero-damping boundary as a function of reduced frequency, or equivalently the $c_a = 0$ - lines in an amplitude-reduced frequency plot. Having established the regions of negative c_a, the next task was to examine by flow visualization the wake pattern (the shedding process) in such cases. These results are now being used in an attempt to formulate a simple analytical model which will predict the aforementioned $c_a = 0$ - boundaries, as well as the magnitudes of the oscillatory forces.

---

* Hereafter the words aerodynamic and hydrodynamic will be used interchangeably.

Apparatus

Figure 1 shows the overall test set up. The cylinder model was mounted at the lower end of a "pendulum". The pendulum was flexure-supported at the other end. The natural frequency of the system could be varied from about 0.7 cps to 5.0 cps by changing the effective length of the flexure. For the forced oscillation tests, the system was excited by rotating an eccentric weight mounted at the center of percussion of the pendulum and driven by a small d-c motor. By varying the motor rpm, the pendulum could be tuned to get maximum amplitude. The hollow cylinder model, sealed at both ends, was partially immersed in a water stream the velocity of which could be varied from 0.5 to 1 ft/sec. The depth of the water changed from 0.4 to 0.6 in., with the larger depths occurring at the higher velocities. The height of the cylinder was always greater than the water depth. The clearance at the bottom was made small, but was not measured. Slightly different gap sizes did exist for tests carried out at different times.

Figure 2 shows the details of the model and its support. It consisted of two identical cylinders, about 1 1/2 " in diameter and connected by a 3/64" - thick aluminum bar on which strain gages were installed. One cylinder was in the flow, the other out of the flow and serving to remove the inertia force signal from the strain gage output. Thus the strain gage signals, without further modifications, represented forces due to the flow including the apparent mass forces.

In the flow visualization studies, the hydrogen bubble technique was used. A kinked piano wire of 0.006" diameter was placed just below the water surface, a little ahead of the cylinder. (This arrangement turned out to be satisfactory in previous experiments, see for example Ref. 3). The wire was energized with a 200 V, 300 ma, d-c power supply.

Test Procedures and Results

The phase angle measurements were taken from a display of the force and displacement signals on the same oscilloscope. The results were obtained for several amplitudes at various flow speeds and frequencies of motion. The relation between the phase angle ϕ and the

effective flow damping c_a is a simple one and can be derived once F_a is assumed to be of the form of Eq. (1). It is further assumed that m_a is equal to the virtual mass and is independent of amplitude. This is a reasonable approximation for present purposes. It was observed experimentally that the F_a-signal was a fairly clean sinusoid, when the cylinder was forced into the sinusoidal motion $x = A \sin \omega t$. Letting $F_a = \bar{Y}_a \sin(\omega t - \phi)$, one finds from Eq. (1) that

$$\phi = \tan^{-1} \left(\frac{c_a}{m_a \omega} \right) \qquad (2)$$

Thus ϕ is also a measure of the damping due to the flow. By estimating m_a, and knowing ω and ϕ, an approximate value of c_a may be calculated, if desired. As $|c_a|$ is appreciably smaller than $m_a\omega$, i.e. damping forces are small compared to forces due to the virtual mass for sizeable amplitudes, ϕ will be small. To improve the accuracy of measuring the amplitude where $c_a = \phi = 0$, i.e. A_0, one may artificially reduce m_a by placing a small mass in the dummy cylinder, a mass not exceeding m_a. Although the resultant phase angle vs. A curves will be different with different m_a's, the cross-over point ($\phi = 0$) will be the same. m_a's were reduced in this manner by 50% or more in arriving at the results shown in Figs. 3 and 4.

For these tests, the following procedure was followed: f_N and V_0 were fixed, thus fixing also the reduced natural frequency $f_N D/V_0$. The forced amplitude was varied, and the ϕ vs. A-data were taken. The excitation was shut-off. The motion would die out or would stabilize at some noticeable amplitude, depending on the closeness of the reduced natural frequency to the Strouhal number. The points marked with arrows in Figs. 3 and 4 are the free-oscillation points. In the tests with reduced natural frequencies between 0.2 and 0.22, it was possible for the motion to build up from zero amplitude, with the buildup being more rapid for reduced frequencies very near the Strouhal number. At lower frequencies, corresponding to $f_N D/V_0 \leq 0.19$, no free oscillations were noted.

The amplitudes of the free oscillations in these figures are of the order of 0.2D. In another test, at the lower frequency of 0.8 cps, with

a lower velocity to attain an $f_N D/V_0 \cong 0.21$, amplitudes of the order of 0.5D were encountered. This trend was inconsistent with the results of Meier-Windhorst (Ref. 1). The properties of the supporting flexure and hydrodynamic forces were examined more closely to explain this discrepancy. Three points were noted which served to explain partially this result.

(1) Changes in flexure length had apparently brought about sizeable variations in the effective structural damping coefficient.

(2) The water depth was found to increase in almost direct proportion with the velocity, (and also with the frequency f, since the reduced frequency was kept constant).

(3) Even more striking was the measured variation of the two-dimensional lift coefficient C_L vs. V_0 (or R.N.) on the stationary cylinder. C_L displayed a negative slope, almost in inverse proportion to the velocity. This again is not in accord with measurements of other investigators as summarized in Fig. 28 of Keefe's report (Ref. 4).

Recent repeatability tests have shown a marked influence by the gap at the bottom of the cylinder on the C_L of the stationary cylinder. This was also noted by Keefe. The tests will be repeated with a much closer monitoring of the gap and the water depth to obtain quantitatively meaningful results. The results presented thus far should be interpreted qualitatively only.

To understand the complex flow field behind the oscillating cylinder, it was deemed desirable to observe the vortex shedding process. Several short rolls of movies were taken of the wake patterns (the streaklines traced by the hydrogen bubbles) for a stationary cylinder, as well as for a cylinder with small, large, and very large amplitudes of oscillation.

The approximate "vortex positions" were measured from film frames for different times. The "vortex position" was taken to be the center of concentration of vorticity near the end of the shear layer separating from the cylinder. This position, which is shown in Fig. 5a, is somewhat vague because the true center may lie anywhere inside the curved tip of the streakline. The separation point, which is indicated in Fig. 5b, is defined for convenience to be that point closest to the wake in the bubble-saturated region.

Consider the stationary cylinder first, for which the vortex positions are indicated in Fig. 6 at 1/16 sec intervals. The vortex first appeared about one diameter behind the cylinder (a = D, where a is defined in Fig. 5a), and the separation points varied in the neighborhood of the points $\theta = \pm 90°$. The vortex was not strong enough before this point to be visible. Beyond this point, it moved towards the centerline. For the case shown, the period for vortex shedding was approximately 9/8 sec, and thus 10 consecutive points on this plot constituted a half period. After reaching the centerline, the vortex drifted a short distance and then separated from its feeding sheet. After that time, it seemed to move away from the centerline as it drifted downstream.

At higher velocities, the rate of bubble generation had to be increased; and since the vortices were stronger then, they were noted at distances "a" less than D. Their paths were very much like illustrated by Fig. 6.

As the vortex appeared and started its inward movement, the separation point began to move toward the back stagnation point ($\theta = 0$). After the vortex reached the center and drifted downstream, the separation point appeared stationary. When the vortex discharged from its feeding sheet, the separation point receded to its original position.

It would have been useful, also, to have a measurement of the relation of the vortex positions to the transverse forces on the cylinder, in particular, the vortex position at the time when the cylinder experienced maximum transverse force. Unfortunately, this information was not obtained.

Figure 7 presents selected frames from movies of the oscillating cylinder. In (a), the amplitude was small (about 0.2D), and the wake looked much like that of the stationary cylinder. In (b), the amplitude was about 0.5D, the frequency was 0.78 cps, and the velocity was approximately 5.7 ft/sec. This meant a transverse velocity of 3.5"/sec, which was comparable to the free-stream velocity. One notes in these photographs significant lateral movements of the vortex. In (c), the case a forced oscillation with a large amplitude (.7D) is depicted; it shows the continuation of the trend from (a) to (b). In each of the sets

above, the middle photograph corresponds to the median positions of the cylinder, while the two end photographs correspond to the extremities of cylinder travel.

Figure 8a presents the vortex position as a function of time, at intervals of 1/12 sec, for the high-amplitude case. The instantaneous cylinder lateral position is included. In each case, the location of the vortex is relative to the cylinder possessing the same index, i.e., vortex labeled 1 means it is to be considered with cylinder position 1, etc. Arrows at the center indicate directions of motion.

Position 5 corresponds nearly to the location of the clockwise vortex when it was first noted. The vortex had its origin at an earlier time, say at 1. It is interesting to note this position relative to the cylinder 5, considering the relative wind direction at that time. Instantaneously, the pattern looks like that of the stationary cylinder. At later times, the vortex moved towards the centerline, as in positions 6, 7, 8. The positions 9, 10, 11 were obtained from the observed locations 1a, 2a, etc. of the alternate (counterclockwise) vortex emanating from the other side of the cylinder Position 8 of the top vortex corresponds nearly to position 1a of the lower vortex.

Figure 8b shows the trajectory of the vortex shed from A. The cylinder is fixed in the stream direction in this case. The trajectory of the counterclockwise vortex from B can be drawn, as it is the image of that from A about the motion centerline. Both trajectories cross the centerline at a fixed downstream point but, of course, the two alternate vortices reach this point at different times (half a period apart). In comparing these trajectories with similar ones from Ref. 1, one finds disagreement for positions 6 and beyond. As far as can be determined from Ref. 1, Meier-Windhorst observed the vortex movement for times corresponding to early positions 1-5, and extrapolated on these results for late positions; it is felt that the intermediate portion of his trajectory is incorrect.

The movement of the separation point in these cases was as follows: Let t_1 denote the instant when the cylinder was at its median position and travelling downward as seen in Fig. 8a (near position 5); the cylinder crossed the same position travelling upward at time $t_1 + \tau/2$,

where τ was the period of oscillation. The separation point on the A-side moved from a position ahead of A ($\theta > 90°$) at time t_1 to a position nearer to the rear stagnation point ($\theta < 90°$) at time $t_1 + \tau/2$. This is as expected, if one considers the cylinder stationary at any instant but with the relative velocity as the free-stream velocity. The separation point indicated for position 5 in Fig. 8a illustrates this situation.

Proposed Simplified Analytical Models for the Flow Field

The wake visualization studies have been helpful in formulating two simple mathematical models of the flow field which are now described. It is assumed that the flow field is potential with singularities at vortex points and cuts along the feeding sheets. Previous investigators have successfully adopted potential flow models (cf. Refs. 5, 6) for the separated flow behind circular cylinders.

Figure 9a presents a model similar to that used by Bryson (Ref. 5). The vortices are shed antisymmetrically from the two sides of the cylinder, but are attached to the cylinder by feeding sheets from fixed stagnation points for one full period of shedding. Knowing the locations of the stagnation points, and imposing the assumed condition that the net force on the vortex plus its feeding sheet is zero, a set of equations with complex coefficients is obtained. These equations describe the positions and strengths of the two nearest vortices. Certain initial conditions must be assumed, such as initial vortex positions, and the period of shedding τ. At the ends of a half period, the positions of the vortices and strengths must be such that the flow field is completely antisymmetric with respect to the (streamwise) centerline of motion. Initial positions must be adjusted to fulfill this antisymmetry condition.

Figure 9b presents a second model which is related to one used by Ujihara (Ref. 6), but with the following added simplifying assumptions: (a) the vorticity is shed from two fixed feeding points on the cylinder at an equal and constant rate (b) the total vorticity is concentrated at the end of the sheet. The last model has the advantage of simplicity but may be an inadequate representation. The extensive and more elaborate calculations of Ujihara (Ref. 6) show appreciable periodic

changes in the location of the separation point and in the vorticity shedding rate.

Both of these models are in the trial stages and no conclusive results are available at this time.

Conclusion

These experiments, together with other available data, indicate no undamped aerodynamic forces on circular cylinders outside of a narrow range of reduced frequencies around the Strouhal number. The amplitude of Strouhal-driven oscillations is limited by the aerodynamic drag which increases with amplitude as well as by structural damping in the system.

Since the driving force arises from the alternate vortex shedding associated with the Strouhal oscillation, the force is closely related to the wake vortex pattern. Therefore attempts to understand and analyze the stationary and motion-dependent forces on an oscillating cylinder are concentrated on adequately describing the vortex development.

REFERENCES

1. Meier-Windhorst, A., Flatterschwingungen von Zylindern un gleichmassigen Flüssigkeitsstrom, Mitt. des Hydraulischen Institute der Technischen Hochschule München, Heft 9, Munich, 1939.

2. Scruton, C., On the Wind-Excited Oscillations of Stacks, Towers and Masts, NPL Paper No. 16, Teddington, England, 1963

3. Friberg, E.G., Measurement of Vortex Separation, Part I: Two-Dimensional Circular and Elliptic Bodies, M.I.T. Aerophysics Laboratory Report TR 114, August 1965.

4. Keefe, R.T., An Investigation of the Fluctuating Forces Acting on a Stationary Circular Cylinder in a Subsonic Stream and of the Associated Sound Field, University of Toronto, Institute of Aerophysics Report No. 76, (also AFOSR Report No. 2147), September 1961.

5. Bryson, A.E., Symmetric Vortex Separation on Circular Cylinders and Cones, Journal of Applied Mechanics, December 1959, pp. 643-648.

6. Ujihara, B.H., An Analytical Study of Separated Flow About a Circular Cylinder, North American Report SID 65-1730, under NASA Contract NAS8-20140, January 1966.

FIGURE 1

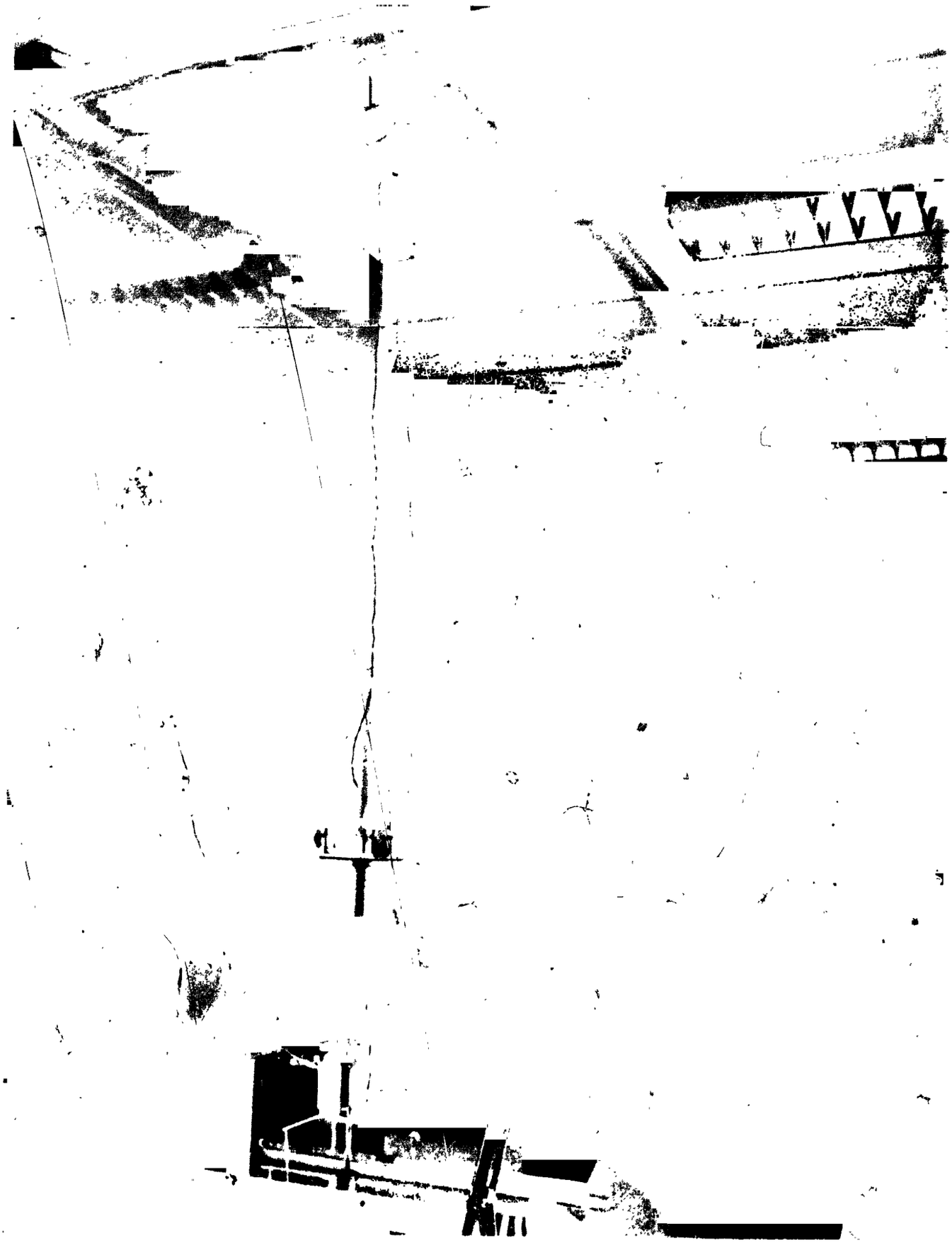

FIGURE 2

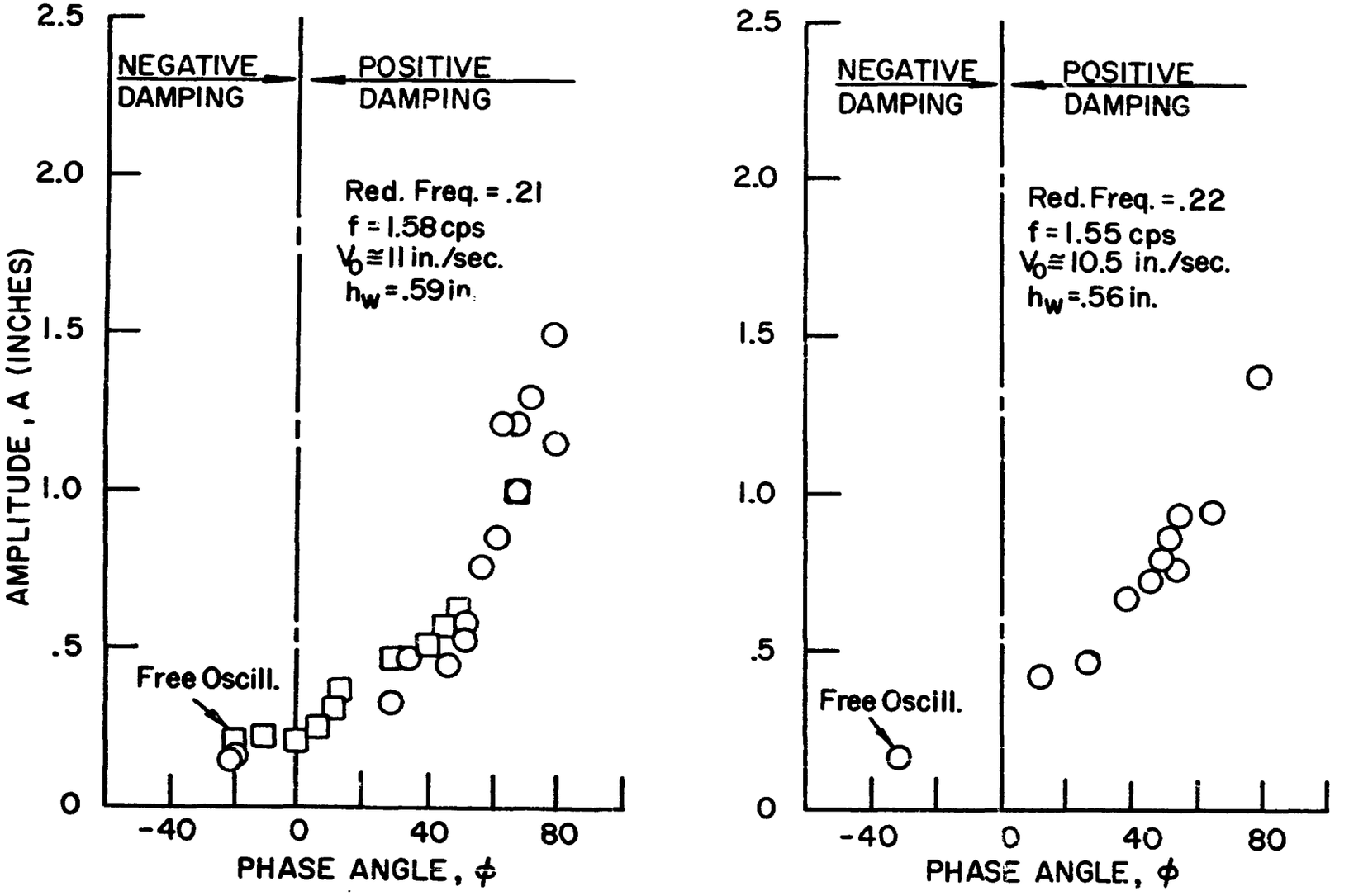
NEGATIVE DAMPING
POSITIVE DAMPING
Red. Freq. = .21
f = 1.58 cps
$V_0 \cong$ 11 in./sec.
h_w = .59 in.
Free Oscill.
AMPLITUDE, A (INCHES)
PHASE ANGLE, ϕ
2.5
2.0
1.5
1.0
.5
0
-40
0
40
80
NEGATIVE DAMPING
POSITIVE DAMPING
Red. Freq. = .22
f = 1.55 cps
$V_0 \cong$ 10.5 in./sec.
h_w = .56 in.
Free Oscill.
PHASE ANGLE, ϕ

Figure 3.

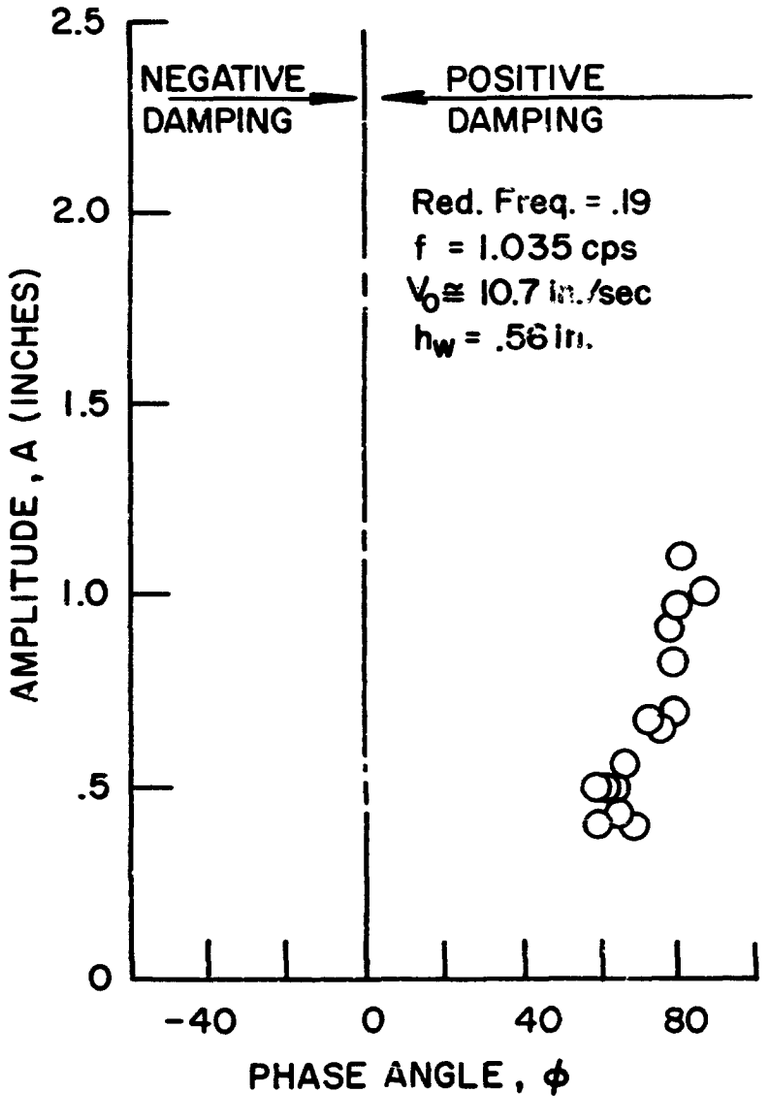
2.5
2.0
1.5
1.0
.5
0
NEGATIVE DAMPING
POSITIVE DAMPING
Red. Freq. = .19
f = 1.035 cps
$V_0 \cong$ 10.7 in./sec
h_w = .56 in.
AMPLITUDE, A (INCHES)
-40
0
40
80
PHASE ANGLE, ϕ

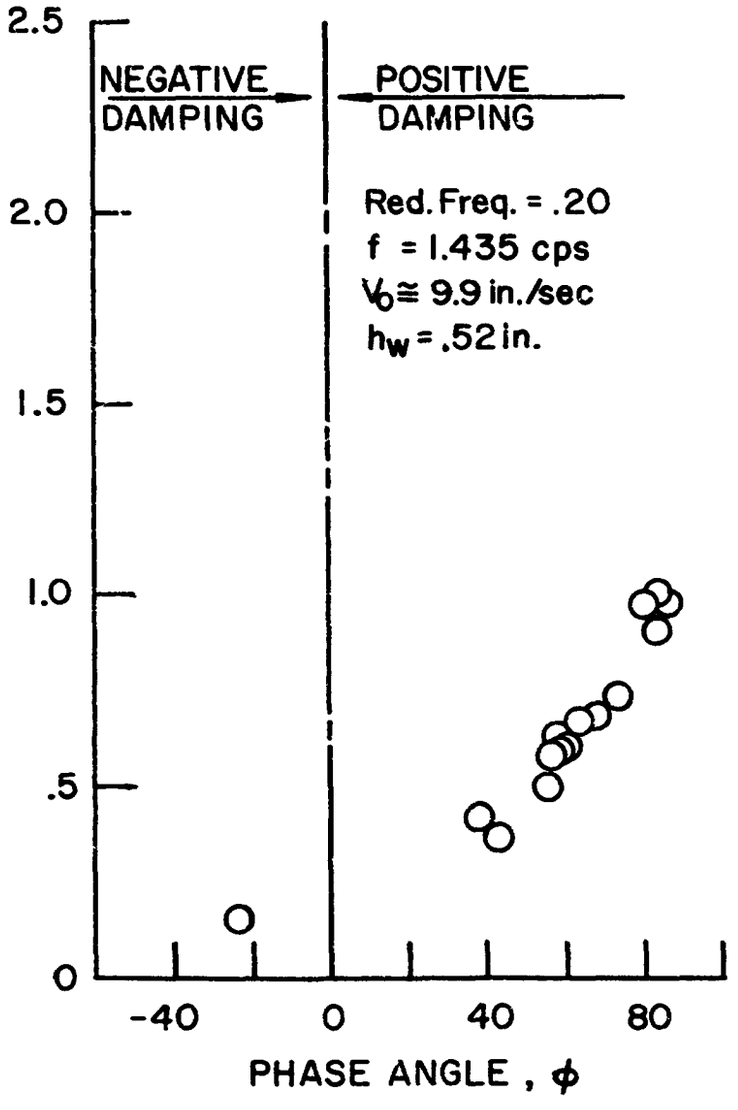
2.5
2.0
1.5
1.0
.5
0
NEGATIVE DAMPING
POSITIVE DAMPING
Red. Freq. = .20
f = 1.435 cps
$V_0 \cong$ 9.9 in./sec
h_w = .52 in.
-40
0
40
80
PHASE ANGLE, ϕ

Figure 4.

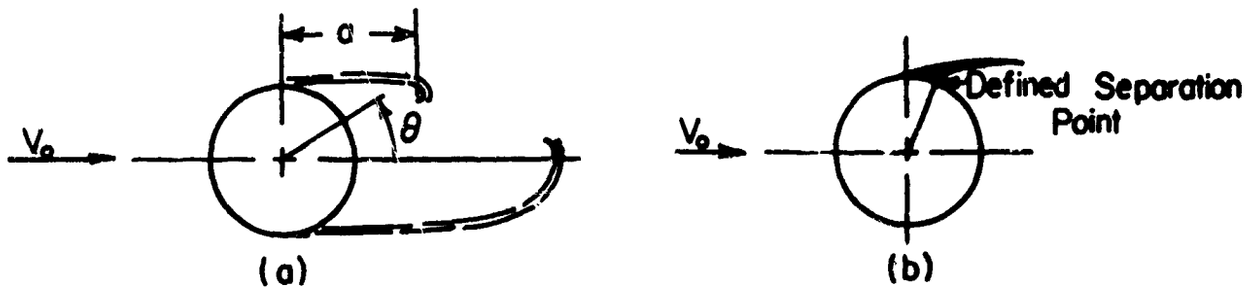

Figure 5.

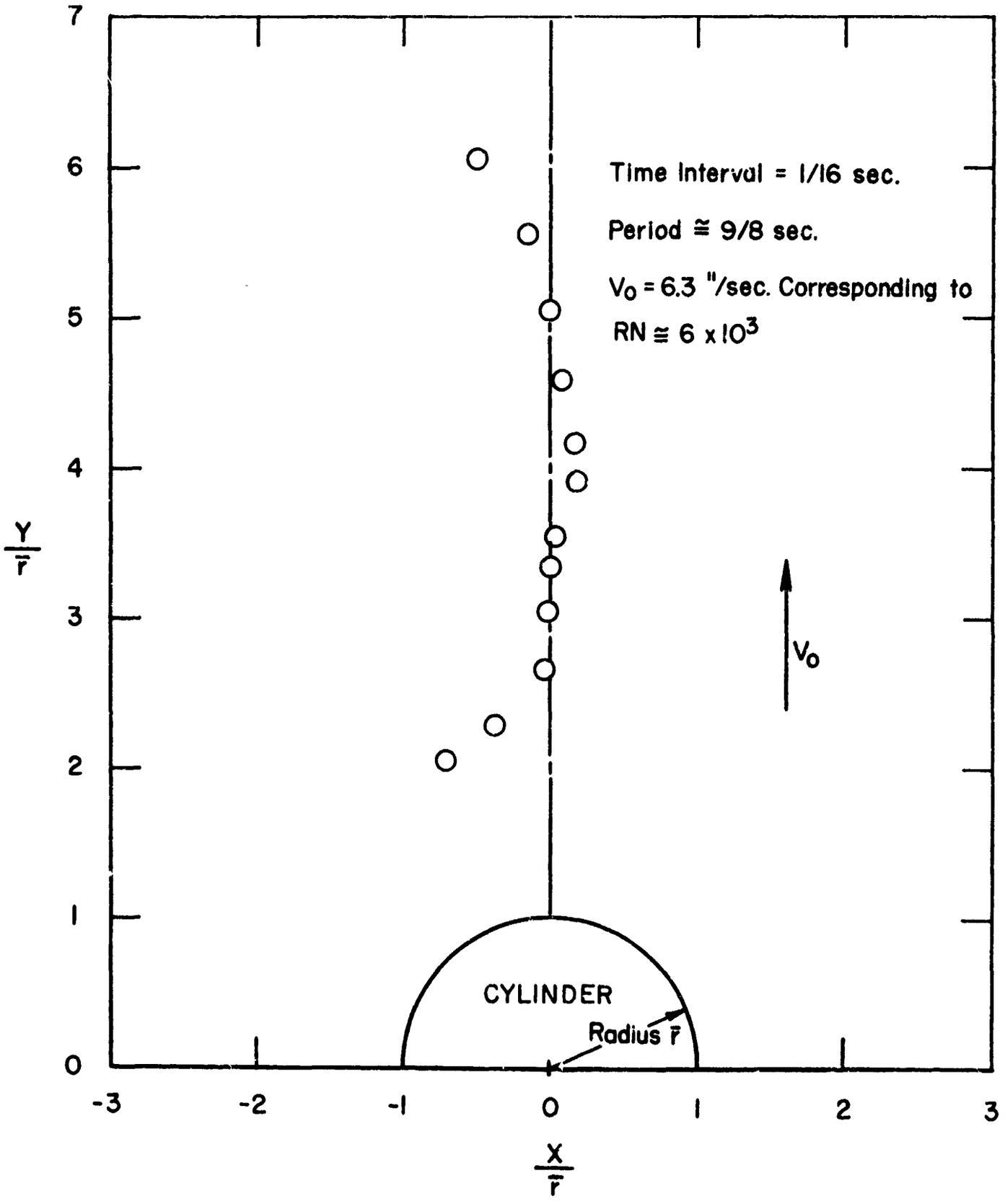
Time Interval = 1/16 sec.
Period ≅ 9/8 sec.
V_0 = 6.3 "/sec. Corresponding to
RN ≅ 6 x 10^3
V_0
CYLINDER
Radius $\bar{r}$
$\frac{Y}{\bar{r}}$
$\frac{X}{\bar{r}}$
7
6
5
4
3
2
1
0
-3
-2
-1
0
1
2
3

Figure 6.

(a) Small Amplitude (A ≅ .25 inch)

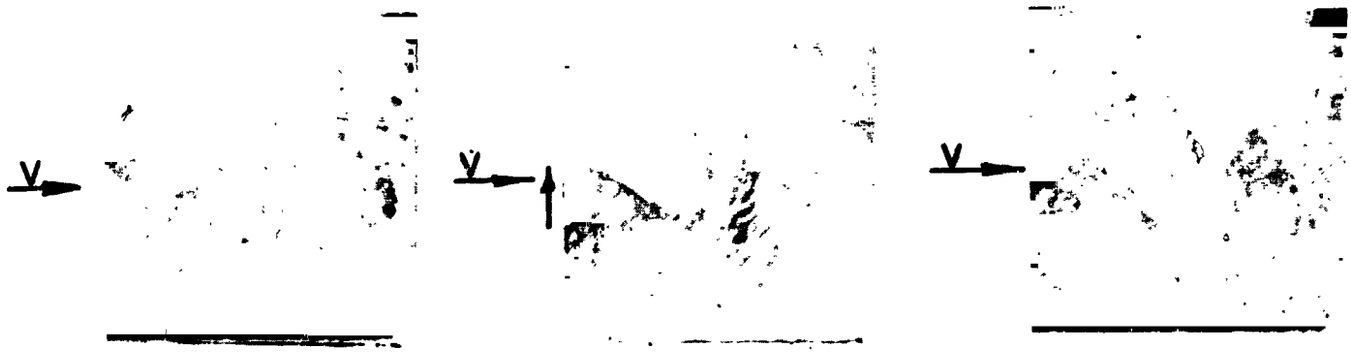

(b) Large Amplitude (A ≅ .7 inch)

(c) Very Large Amplitude (A ≅ 1.05 inch)

Figure 7.

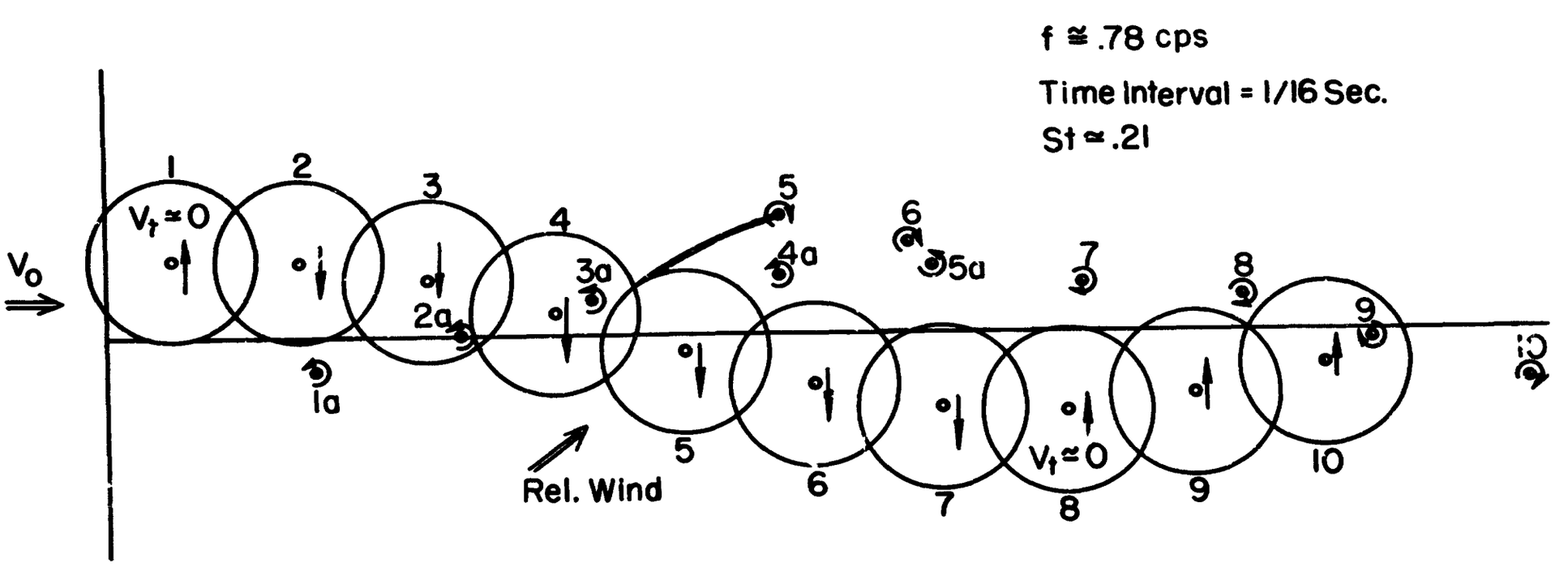

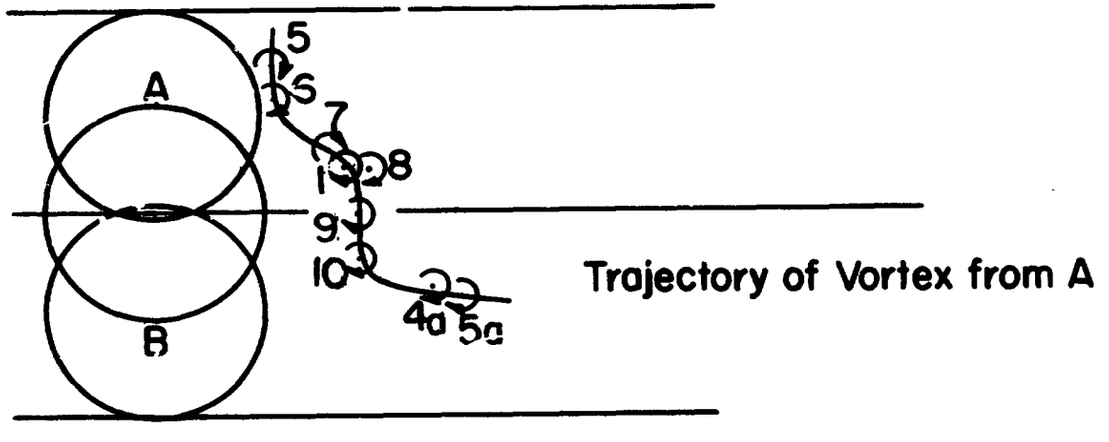

Trajectory of Vortex from A

Figure 8.

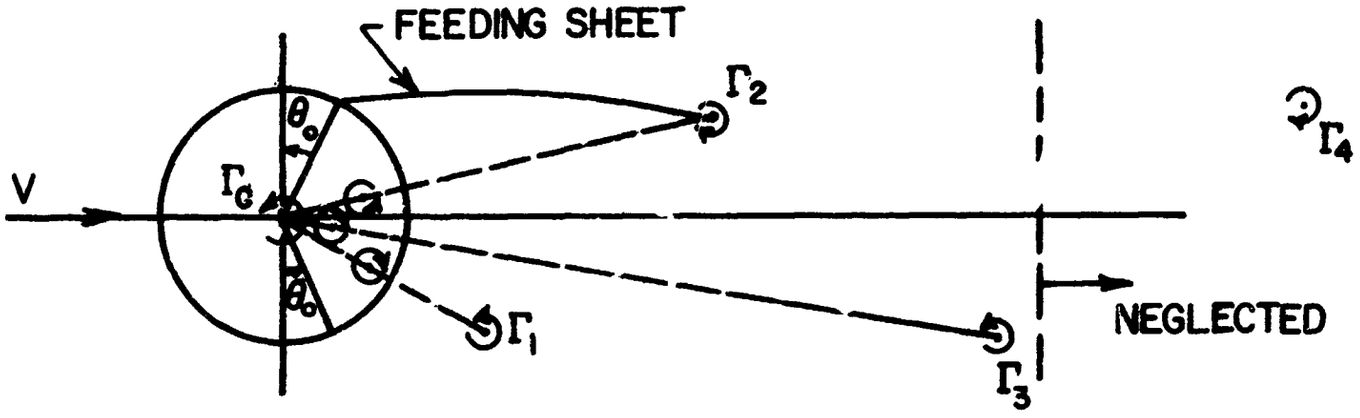

(a) BRYSON MODEL ($\Gamma_c = 1/2\,\Gamma_3$)

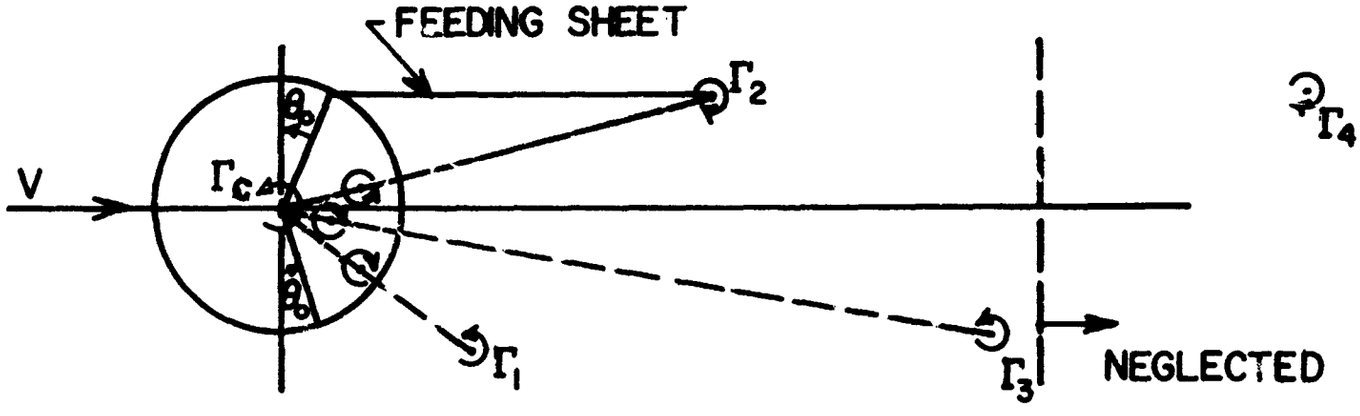

(b) SIMPLER MODEL WITH RATE OF VORTICITY GENERATION CONSTANT ($\Gamma_c = 1/2\,\Gamma_3$)

Figure 9.

*AMPLITUDE AND SURFACE PRESSURE MEASUREMENTS FOR A CIRCULAR CYLINDER IN VORTEX-EXCITED OSCILLATION AT SUBCRITICAL REYNOLDS NUMBERS

**G. V. Parkinson and +N. Ferguson

ABSTRACT

Measurements are presented of cylinder amplitude and frequency, wake vortex formation frequency, and phase angle between lateral force and displacement, as a function of wind speed, for a circular cylinder tested at subcritical Reynolds numbers in a wind tunnel. Oscilloscope photographs of cylinder displacement and surface pressure are shown, illustrating changes in relative amplitudes, and in amplitude modulation, with wind speed in the vortex-excited range.

---

* Presented at the 'Meeting on Ground Wind Load Problems in Relation to Launch Vehicles', Langley Research Center, Hampton, Virginia, U. S. A., June 7-8, 1966.

** Professor of Mechanical Engineering, University of British Columbia.

+ Department of Mechanical Engineering, Nova Scotia Technical College.

INTRODUCTION

Phenomena of aerodynamically-excited oscillations of bluff cylindrical bodies have been studied for several years in a continuing program at The University of British Columbia. Both galloping oscillations, arising from aerodynamic instability of the cross-section (1, 2, 3, 4, 5, 6), and vortex-excited oscillations (1, 7, 8), have been investigated under conditions approaching two-dimensionality as closely as possible. Cylinder cross-sections have included the circle, the D-section, various rectangles including the square, an ellipse, and an airfoil at high incidence. The models have spanned the vertical 27 in. dimension of the 27 in. by 36 in. tunnel test section, and their lateral dimensions have ranged from 0.5 in. to 3 in., so that boundary corrections have been small. Rigid models have been used, generally connected to external springs and restrained to lateral plunging oscillations by external low-friction air bearings. The models were constructed with smooth surfaces and sharp corners, and the tunnel air flow is very uniform and of less than 0.1% turbulence. Reynolds numbers based on the lateral section dimension have been in the range 10^4 to 10^5.

The present paper describes a few of the measurements made by the junior author in his graduate research. The work is reported in detail in Reference 8.

PHENOMENA OF VORTEX-EXCITED OSCILLATION

The model in which the measurements were made was a 3 in. diameter circular cylinder made from aluminum tubing of .022 in. wall thickness. The cylinder ends cleared the

tunnel floor and ceiling by about 1/16 in. and were connected to the external springs and sleeve air bearings by thin struts passing through narrow lateral slots in floor and ceiling. Cylinder lateral displacement was measured by a transducer in which an extension to the aluminum shaft of the upper air bearing system was made to interfere between the primary and secondary of an air-core transformer. The natural frequency of lateral oscillations was 9.10 cps, and the non-aerodynamic damping was about 0.1% of critical.

The cylinder surface had several flush pressure taps of .025 in. diameter. Each was connected to a 4 ft. length of .066 in. I.D. tubing which passed outside the tunnel through the lower end fitting. Each tube could be connected to a pressure transducer mounted outside the tunnel. In the transducer, the fluctuating pressure signal displaced a rubber diaphragm, causing a shutter to interfere with a light beam impinging on a light-dependent resistance, and a bridge circuit produced a voltage proportional to the pressure on the diaphragm.

The attenuation and phase lag experienced by the pressure signal in travelling from the cylinder surface tap to the transducer were determined as functions of frequency and initial amplitude by mechanical calibration, using a vibration generator and a tiny piston fitting the input end of the transmission tube. A dummy tube tied to the active tube communicated to the other side of the diaphragm, and this eliminated spurious signals due to motion of the tubes.

The output signals from the displacement and pressure transducers were displayed and photographed on the screen of a storage oscilloscope, and Figs. 1(a) to 1(e) show some of these photographs. In each photograph the upper trace is cylinder displacement and the lower is cylinder surface

pressure at a mid-span tap on the transverse diameter. Figs 1(b), 1(c), and 1(d) show both traces at a constant magnification of 50 mv/division. In Fig. 1(a) the displacement is amplified to 5 mv/div. and the pressure to 20 mv/div. In Fig. 1(e) the displacement is at 50 mv/div. but the pressure is amplified to 20 mv/div. Also the pressure signal displayed in Fig. 1(e) is at a higher frequency than the other pressure signals, and accordingly experienced more attenuation in the transmission tube. The fundamental frequency of the surface pressure fluctuation indicates the formation frequency of the cylinder wake vortices, and in Fig. 1(a), taken at a wind speed of 10.2 fps, this frequency is 8.0 cps, whereas the cylinder is oscillating with quite small amplitude, less than 0.02 diameter, at 9.0 cps. Both signals are seen to experience a regular beat modulation at about 1.0 cps.

When the wind speed was increased to 12.7 fps, the traces shown in Fig. 1(b) were obtained. The displacement amplitude modulation has disappeared and the modulation of the pressure signal has been significantly reduced. Both amplitudes have increased greatly, and both signals are at the same frequency, 9.0 cps. The peak cylinder amplitude of about 0.3 diameter was obtained at a wind speed of 13.7 fps, and the displacement and pressure traces are shown in Fig. 1(c). Both traces are almost unmodulated, and both are at the same frequency of 9.0 cps. The surface pressure amplitude is also at a maximum, corresponding to a fluctuating pressure coefficient $C'_p = \frac{\text{fluctuating pressure amplitude}}{\text{free stream dynamic pressure}}$ of about 0.8.

When the wind speed was increased only slightly to 14.4 fps, the rather dramatic change in the relative strength of the signals shown in Fig. 1(d) was obtained. The

displacement and pressure are still unmodulated and at 9.0 cps, and the displacement amplitude has decreased moderately from the previous peak, but the pressure amplitude has decreased to less than one third of its previous value.

For the final photograph, Fig. 1(e), the wind speed was increased to 16.5 fps, and the cylinder again oscillated at 9.0 cps without amplitude modulation, but with considerably reduced amplitude, about 0.08 diameter. The surface pressure, however, oscillated at a much higher fundamental frequency of 13.0 cps and displayed a strong random amplitude modulation.

The phenomena of Fig. 1 can be correlated and partly explained by considering Fig. 2, in which cylinder dimensionless amplitude $\bar{Y} = \frac{\text{cylinder amplitude}}{\text{cylinder diameter}}$ and frequency f_c, and surface pressure (or vortex) frequency f_v and phase angle ϕ are plotted as ordinates versus wind speed V as abscissa. ϕ is the phase angle by which the underpressure at the surface tap represented in Fig. 1 leads the displacement in the direction of that tap (this is equivalent to the phase angle between transverse force and displacement).

The solid straight line from the origin of Fig. 2 is the mean line of measured data points of f_v vs V for the cylinder held stationary, and it corresponds to a Strouhal number of 0.198. The horizontal dashed line gives the cylinder natural frequency $f_n = 9.10$ cps.

When the cylinder was free to exhibit transverse oscillations, none occurred at wind speeds below about 10 fps. Then small oscillations began with the surface pressure fluctuations at the same frequency f_v as for the stationary cylinder at that wind speed, and with the cylinder frequency f_c lying below the natural frequency f_n

but above the vortex frequency f_v. This is the region of the regular beat modulation of Fig. 1(a). At a slightly higher wind speed, about 11 fps, when $\bar{Y}$ reached about 0.03, f_v locked in to f_c, and both remained at 9.0 cps over a further 40% increase in wind speed. This is the region covered by Figs. 1(b), (c), (d). Since $f_c = f_v$, phase angle ϕ can be measured, and this was done from fast sweep oscilloscope photographs of the two traces. Individual measurements are not very accurate, so that the results show considerable scatter, but the trend is clear, with ϕ increasing rapidly, probably from near 0^o at the beginning of the wind speed range (measurements were difficult at the lower wind speeds) to about 180^o at the end of the range. Peak cylinder amplitude seemed to occur with ϕ near 90^o.

When V reached about 15 fps the frequency lock-in was suddenly lost, and f_v jumped to a value near that for the stationary cylinder at that wind speed, while f_c remained at 9.0 cps. The cylinder amplitude continued a smooth decrease with increasing wind speed, and continued to show no modulation, while the surface pressure at these wind speeds showed the random amplitude modulation and values of amplitude characteristic of pressures on the stationary cylinder. The value of f_v obtained in this wind speed range was very sensitive to test conditions, and considerable scatter is shown on Fig. 2. At wind speeds above about 18 fps, the cylinder did not oscillate.

CONCLUDING REMARKS

These results correlate well with measurements by Bishop and Hassan (9), in which cylinders were given mechanically forced transverse oscillations in a water channel. Although our tests were under more or less two-dimensional conditions, and at subcritical Reynolds numbers

$(1.5(10)^4 < N_R < 3.0(10)^4)$, the cylinder motions seem to have some relevance to observed motions at supercritical and transcritical Reynolds numbers of launch vehicle models, as for example in tests reported by Reed (10).

Funds for the research reported here were provided by the National Research Council of Canada, through Grant A586.

REFERENCES

1. Brooks, N. P. H. 'Experimental Investigation of the Aeroelastic Instability of Bluff Two-Dimensional Cylinders'. M.A.Sc. thesis, U. B. C., 1960.

2. Parkinson, G. V., and Brooks, N. P. H. 'On the Aeroelastic Instability of Bluff Cylinders'. JAM, 28, June, 1961, pp. 252-8.

3. Smith, J. D. 'An Experimental Study of the Aeroelastic Instability of Rectangular Cylinders'. M.A.Sc. thesis, U. B. C., 1962.

4. Parkinson, G. V., and Smith, J. D. 'The Square Prism as an Aeroelastic Nonlinear Oscillator'. QJMAM, XVII, May, 1964, pp. 225-239.

5. Parkinson, G. V. 'Aeroelastic Galloping in One Degree of Freedom'. Proc. Symp. Wind Effects on Buildings and Structures, N.P.L., 1965.

6. Santosham, T. V. 'Force Measurements on Bluff Cylinders and Aeroelastic Galloping of a Rectangular Cylinder'. M.A.Sc. thesis, U. B. C., 1966.

7. Heine, W. 'On the Experimental Investigation of Vortex Excited Pressure Fluctuations'. M.A.Sc. thesis, U. B. C., 1964.

8. Ferguson, N. 'The Measurement of Wake and Surface Effects in the Subcritical Flow past a Circular Cylinder at Rest and in Vortex-Excited Oscillation'. M.A.Sc. thesis, U. B. C., 1965.

9. Bishop, R. E. D., and Hassan, A. Y. 'The Lift and Drag Forces on a Circular Cylinder Oscillating in a Flowing Fluid'. Proc. Roy. Soc. A, 277, 1964, pp. 51-75.

10. Reed, W. H. 'Models for Obtaining Effects of Ground Winds on Space Vehicles Erected on the Launch Pad'. Conf. on Role of Simulation in Space Technology, Virg. Poly. Inst., 1964.

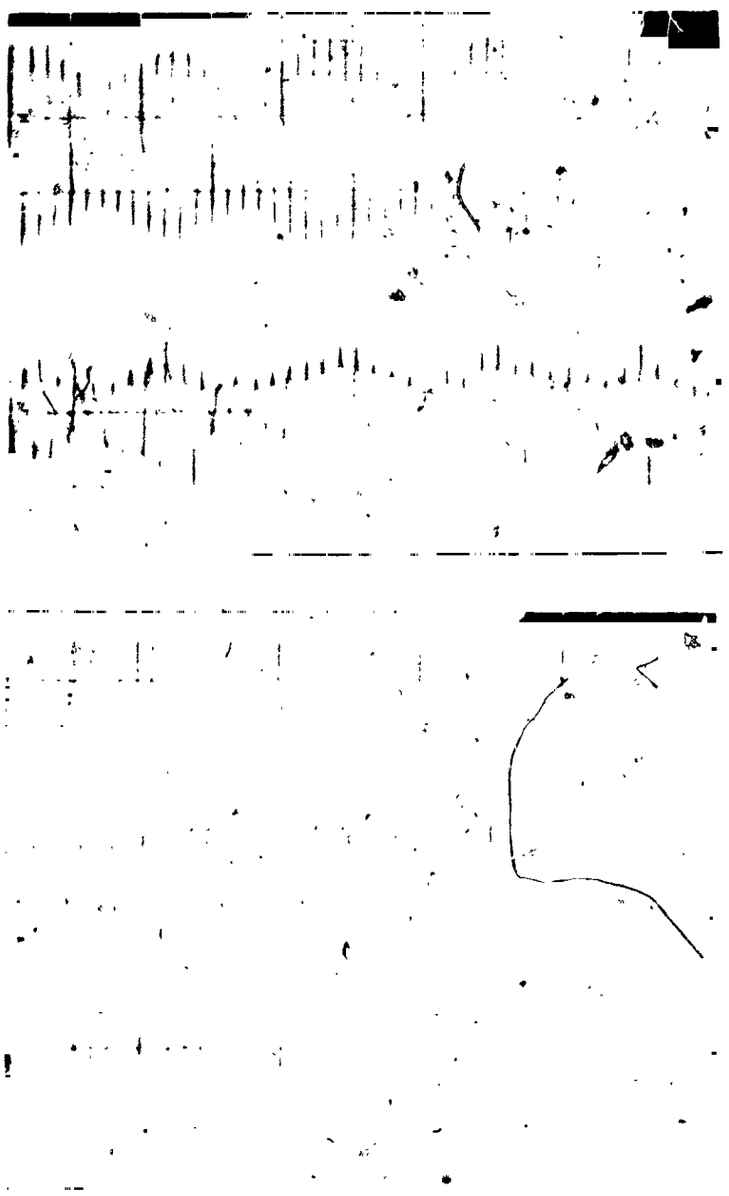

(a)

(b)

FIG 1

Cylinder Displacement & 90° Surface Pressure

(a) $V = 10.2$ fps
$f_c = 9.0$ cps
$f_v = 8.0$ cps

(b) $V = 12.7$ fps
$f_c = 9.0$ cps
$f_v = 9.0$ cps

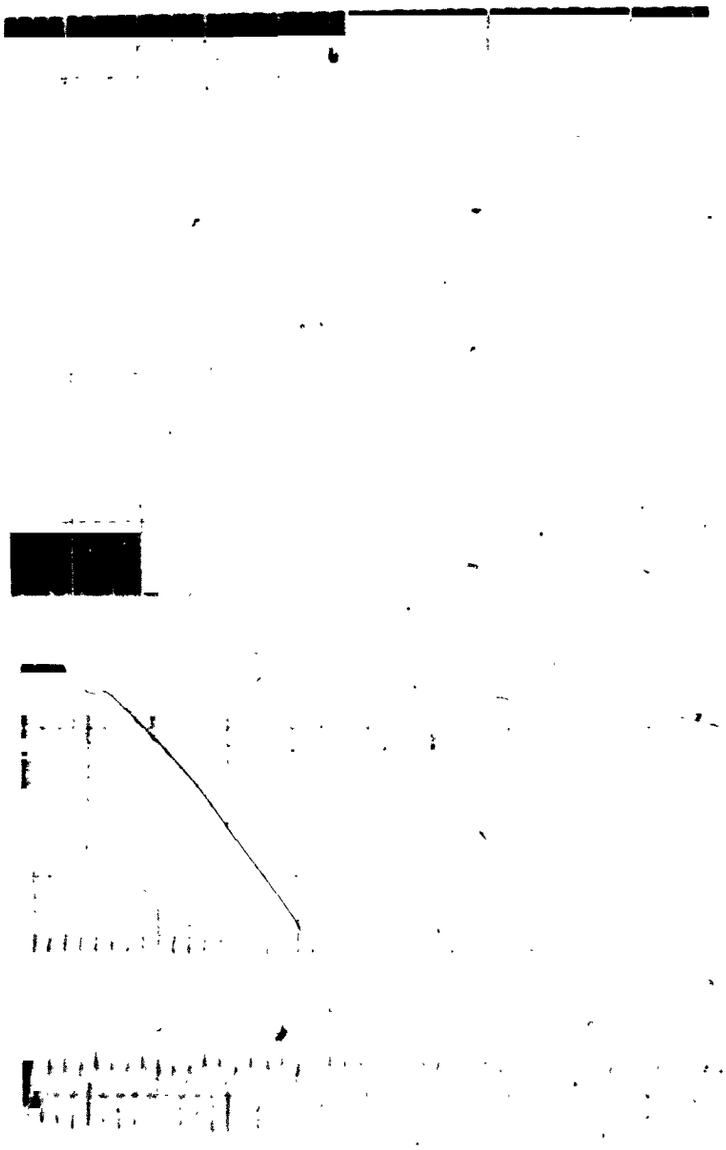

(c)

(d)

FIG 1

(c) $V = 13.7$ fps
$f_c = 9.0$ cps
$f_v = 9.0$ cps

(d) $V = 14.4$ fps
$f_c = 9.0$ cps
$f_v = 9.0$ cps

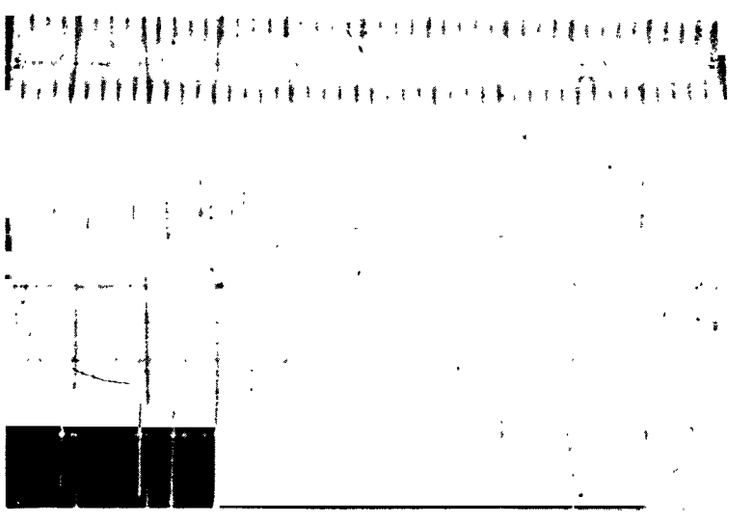

(e)

FIG 1

(e) $V = 16.5$ fps
$f_c = 9.0$ cps
$f_v = 13.0$ cps

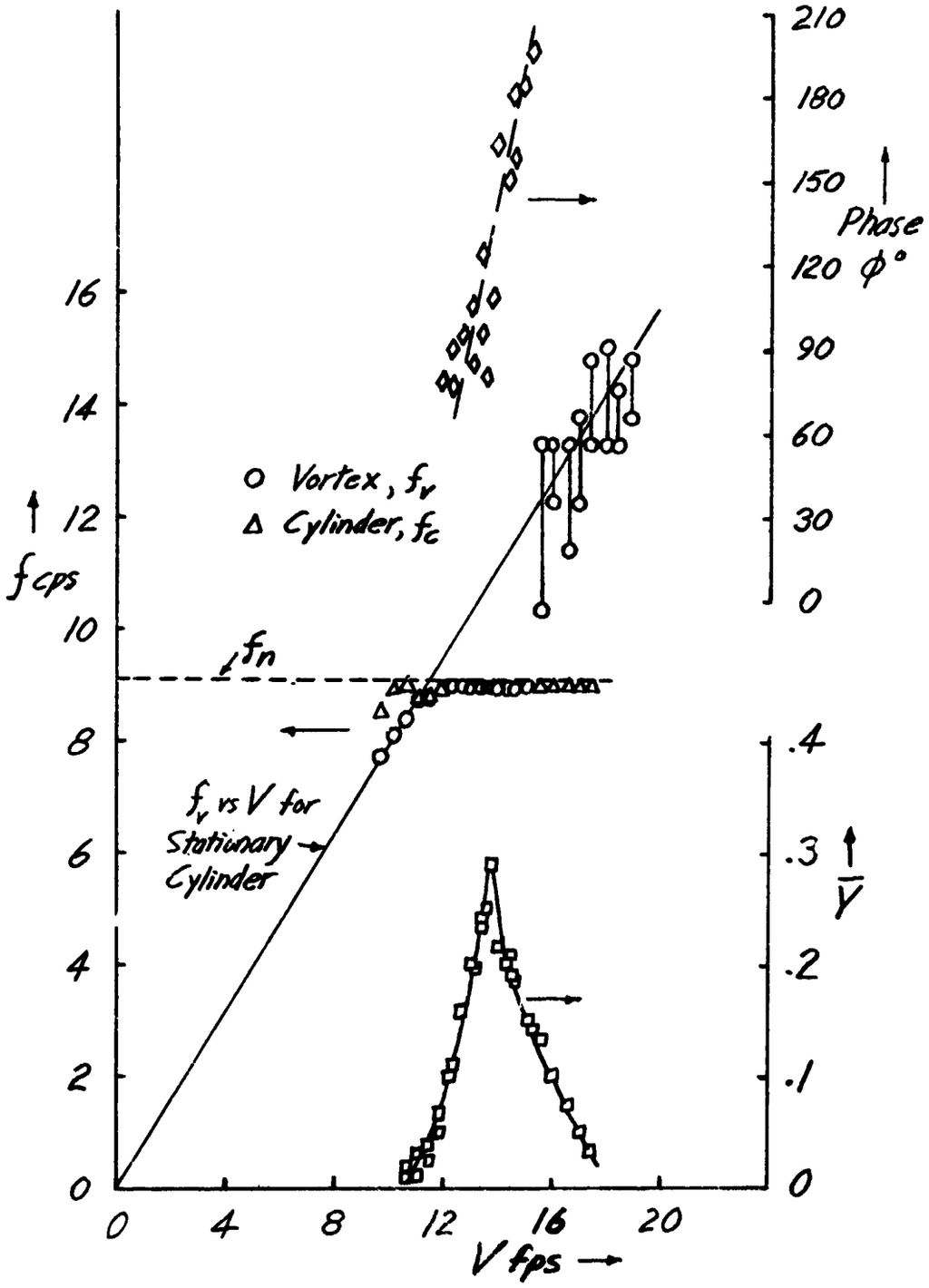

FIG. 2

$f_v, f_c, \varphi, \& \bar{Y}$ vs V for Oscillating Cylinder

FLUCTUATING FORCE MEASUREMENTS UPON A CIRCULAR CYLINDER AT REYNOLDS NUMBERS UP TO 5×10^6

By Louis V. Schmidt
Associate Professor of Aeronautics*

U.S. Naval Postgraduate School
Monterey, California

ABSTRACT

An approximate 8:1 aspect ratio circular cylinder has been extensively tested both at the GALCIT 10-foot Low-speed Circular wind tunnel and at the NASA Ames 12-foot Pressure Tunnel. The results of these tests provide a coverage in Reynolds number from approximately 3×10^5 to 5×10^6. Data obtained included the steady and fluctuating values of sectional lift and drag in addition to individual surface static pressures. Multiple data stations allowed the determination of the spatial traits of the random-type air loads.

The model, essentially rigid, had interchangeable tip sections. A clear demonstration of the effects of tip shape upon sectional air loads was obtained in addition to a definition of the scope of this influence.

Evaluation of the data is being made using an analog to digital conversion system in conjunction with a CDC 1604 digital computer located at the U.S. Naval Postgraduate School. Available results will be reported.

Studies of bluff body separation effects have been made upon square, rectangular, and circular cross sections using a simple single degree of freedom aeroelastic model. The results are not as definitive as those reported above

---

*Formerly: Research Fellow, GALCIT Flutter Group,
California Institute of Technology,
Pasadena, California

since these results pertain to model response measurements for varying model resonance frequencies, and estimates can be made only of the average random forcing function. Significant differences have been observed in the aerodynamic forcing function for various bluff bodies. This program has application to an antenna element vibration problem.

INTRODUCTION

The study of unsteady air loads about a circular cylinder described in this paper is the outgrowth of a program started at the GALCIT* by Fung[1,2] in 1958. His results were applicable to the supercritical Reynolds number range, and showed significant differences from the accepted air-load traits in the subcritical Reynolds number range. In particular, the unsteady lift coefficients were found to be reduced in magnitude from the estimates for the subcritical flow range, the loads appeared to be random in character, and there was evidence that the random loads had a spatial dependence.

A subsequent study was initiated in 1960 in an attempt to clarify and/or extend the previous work. The air loads were measured using an instantaneous summation of eighteen static pressures at an axial station on a cantilevered cylinder model. The initial results (Reference 3) confirmed the unsteady loads obtained by Fung, and in addition showed that the cross-correlation along the axis of the cylinder was small for spacings of two load packages beyond one cylinder diameter. The extreme sensitivity of the unsteady loads to small surface disturbances was noted, but in general their influence was not manifested beyond an axial distance of about a cylinder diameter.

---

*Graduate Aeronautical Laboratories, California Institute of Technology.

Blackiston[4] conducted a study of the influence of tip shape upon local load using the cantilevered cylinder model. His results confirmed the observations by Ezra and Birnbaum[5] as to the importance of tip shape, and in particular showed that a hemispherical configuration resulted in unsteady lift loads up to five times greater than would be obtained with a "smokestack" or conical nose shape. Again, the influence of nose shape was not evident beyond a distance of approximately a cylinder diameter from the tip.

As a consequence of these programs, Spitzer[6] mapped the fluctuating static pressures on the cantilevered cylinder model in supercritical flow and observed the random background pattern similar to atmospheric turbulence with the presence of an energy peak at a Strouhal number (S) of 0.24 on the forward portion of the cylinder, and spikes at $S = 0.24$, 0.36, and 0.48 on the aft portion of the cylinder. No energy peaks were observed near to the separation point.

All of these results were obtained at the GALCIT 10-Foot wind tunnel, and were limited to Reynolds numbers of 1×10^6 or less. Roshko[7] was able to extend the values of steady state drag coefficient up to a Reynolds number of 8×10^6 in the last experimental program conducted at the Cooperative Wind Tunnel, Pasadena, California. His results showed that the drag value rose again at Reynolds numbers beyond about 3×10^6 and approached a value of about $C_D = 0.7$ similar to results obtained in subcritical flow using a splitter plate. Also he noted the reappearance of periodicity in the wake. A similar extension of unsteady load results is the purpose of the work reported herein.

NOMENCLATURE

C_L = local lift force coefficient = (lift force/unit span)/qD

C_D = local drag force coefficient = (drag force/unit span)/qD

$C_{P_{(-)}}$ = static pressure coefficient = $\left(p_{(-)} - p_o\right)/q$

D = cylinder diameter

f = frequency, cps

q = dynamic pressure = $\frac{1}{2}\rho V^2$

t = time

R = Reynolds number of cylinder = VD/ν

S = Strouhal number = fD/V

V = velocity of undisturbed flow

x = axial coordinate along cylinder axis, x = 0 at base

y = lateral displacement at base of aeroelastic model

ρ = mass density of fluid

ν = kinematic viscosity of fluid

P = stagnation pressure

$p_{(-)}$ = static pressure, subscript (o) refers to freestream condition

ϕ = power spectral density

R( ) = cross-correlation coefficient, subscript denotes load station orientation

CIRCULAR CYLINDER PROGRAM AND RESULTS

The cantilevered cylinder model was installed in the NASA Ames 12-Foot wind tunnel upon a steel base plate as shown in Figure 1. The instrument packages were similar to those used at the GALCIT except that the pressure range was increased in order to allow measurement over a larger spread in operating conditions. Four relocatable instrument sections were employed in

order to provide a threefold increase in data gathering capability. In addition, a remote control drive system was incorporated so as to allow reorientation of the model from the lift to the drag mode without having to open the pressure shell. The aluminum sleeves were clamped together using a steel tie rod and strain gages at the model base were continually monitored for reasons of assuring model integrity. Otherwise the model was identical to that used at the GALCIT, and essentially may be considered as rigid in nature.

The test program extended the work of Schmidt[3], Blackiston[4], and Spitzer[6] to a Reynolds number of 5×10^6 (tunnel pressurized to four atmospheres). Included in the program were definitions of steady-state drag, fluctuating lift and drag, cross-correlations, tip effects, and pressure mapping. Time histories of the data were recorded on magnetic tape for subsequent data processing.

A partial evaluation of the data has been made using an analog to digital conversion system in conjunction with a Controls Data Corporation (CDC) 1604 digital computer located at the U.S. Naval Postgraduate School, Monterey, California.

The steady-state drag data, Figure 2, show a value of $C_D = 0.18$ for $R \cong 1 \times 10^6$ with a gradual rise to $C_D = 0.53$ as Reynolds number was increased to 5×10^6. Static pressures that were obtained using NASA supplied pressure transducers were integrated to obtain drag coefficient. Good agreement was obtained between the integrated results and the direct measurements of the instrumentation packages. The variation of C_D for R values of 1×10^5 to 8×10^6 are summarized on Figure 2 using the material of Delany and Sorensen[8] and Roshko[7]. It will be noted that the drag values obtained in the experiments described here are in general lower than those of references 7 and 8.

An interesting comparison can be made using the base pressures on the aft portion of the cylinder, since as pointed out by Roshko[7], base pressures have the same traits with respect to R as C_D. Figure 3 indicates that the static pressures at the model base are lower than those reported by Roshko, and the discrepancy in base pressures and drag coefficients are in direct correspondence.

A possible reason for the difference in results may be that the model surface conditions were not alike. The model used by Roshko had a sand-blasted finish while the cantilever model used here had a high polish. The importance of surface roughness at the higher values of Reynolds number is not clear at this time.

Unsteady load values were not as sensitive to Reynolds number change as the steady-state drag. Figure 4 presents a summary of unsteady lift range and the results of Fung[1,2] and Schmidt[3] in the low supercritical range. In general, the unsteady lift values were in the range of $\sqrt{\overline{C_L^2}} = 0.04$ to 0.10 although some values in excess of 0.15 were noted. A similar comparison made for unsteady drag, Figure 5, disclosed that the root mean square level of drag coefficient varied between 0.02 and 0.05. It will be noted that the data in the supercritical Reynolds number range are faired in a broad-brush manner indicating that the values are not well defined. These results pertain to measurements made in the model mid-span region and do not reflect any effects that are due to tip configuration.

The time history of air loads was processed using digital techniques and may be seen in the form of power spectral densities on Figures 6 and 7 at values of $R = 1.1 \times 10^6$ and 5.0×10^6 respectively. Only the unsteady lift data are shown since the unsteady drag data are quite similar. The results did

not differ significantly from data obtained at the GALCIT, and periodicity in the form of energy peaks was not found.

Spectral densities were estimated for frequencies up to 125 cps for the initial analyses. Several instances appear where it may be necessary to recalculate the spectral estimates to a higher value of frequency.

Cross-correlation calculations were made for both the lift and drag measurements, and are shown summarily on Figures 8 and 9. The rapid decrease in cross-correlation coefficient with axial spacing is evident and the results are quite similar to those obtained at the GALCIT. The degree of confidence in these calculations is about ±0.05 based upon consideration of inertia effects during data taking and accuracy of digitizing two channels of information to a common time base.

Cross-correlation coefficient, as used here, refers to the mean cross product of the two load time histories normalized with respect to the individual RMS values. The time lag was set at zero. The definition is:

$$R_{l2} = \frac{\frac{1}{T}\int_0^T l_1(t)\,l_2(t)\,dt}{\sqrt{\overline{l_1^2}}\sqrt{\overline{l_2^2}}}$$

For the calculations presented here, the time span, T, was eight seconds.

AEROELASTIC MODEL AND RESULTS

As a consequence of a vibration problem encountered in an element of a large antenna installation, a study was initiated of bluff-body separation effects using cross sections that are square, rectangular, and circular. A single degree of freedom aeroelastic model was constructed so as to allow

lateral response when the model vertically spanned the test section of the 3.5 x 5.0 foot wind tunnel located at the U.S.N. Postgraduate School. The results were not as definitive as those reported for direct load measurements upon the rigid circular cylinder since the quantity measured was model response, and the average random forcing function was estimated indirectly using a transfer function concept applied to the spectral density of the displacement.

Figure 10 presents a sketch of the installation of the aeroelastic model in the wind tunnel. The simple pivot was obtained using a flexure plate so that friction effects would be minimized. The spring constraint at the lower end of the aluminum beam was a variable, which made possible variations in model resonant frequency from 30 to 90 cps. The displacements, as measured at the lower end of the beam, were recorded onto magnetic tape, converted to digital form, and subsequently used for calculating auto-correlations and power spectral densities.

The model cross section reported herein may be seen in Figure 10 as corresponding to a square with rounded corners. This configuration was selected for a detailed analysis since its response was better behaved than a cross section such as sharp-edged square or rectangle. A systematic variation was made in both tunnel velocity and model resonant frequency. The amplitude responses were somewhat systematic in variation, but trends were not clear. However, after the fluctuating lift coefficient was estimated, a clear trend appeared (Figure 11). The quantity l_B denotes beam length for the spring constraint and the lower value implies a higher value of model resonant frequency.

In general, a transition appeared at a Reynolds number of about 3.4×10^5, similar to that observed for C_D of a circular cylinder. A bluff body with

this cross section has been described by Delany and Sorensen[8] with respect to C_D and the importance of the corner radii in controlling the drag transition has been demonstrated.

Another interesting item to note in Figure 11 is that as the resonant frequency of the model is increased, the estimated value of fluctuating lift decreased. The value of fluctuating lift has been replotted as a function of (normalized) lateral displacement for two Reynolds numbers, Figure 12. It may be readily seen that the value of fluctuating lift appears to be linearly dependent upon RMS amplitude of motion, and extrapolates to a rigid value not significantly different from that obtained for a circular cylinder. The aeroelastic feedback term appears remarkably powerful since for the subcritical case, an RMS amplitude of several thousandths of an inch doubled the amplitude of the estimated lift.

An attempt to estimate the aeroelastic feedback term by assuming that the lateral motion causes an effective angle of attack change with a subsequent rotation of the steady state drag vector yielded a dependence of fluctuating lift upon amplitude. However, this approach gave estimates that were approximately four orders of magnitude too low.

CONCLUDING REMARKS

Unsteady air loads have been measured upon a circular cylinder for Reynolds numbers up to 5.0×10^6. Initial analyses of the data do not disclose significant differences from measurements made in the low supercritical Reynolds number range ($R = 1 \times 10^6$). Final conclusions remain to be drawn following a complete evaluation of all the results.

A single degree of freedom aeroelastic model was applied to an antenna vibration problem. An analysis of one of the configurations disclosed a strong dependence of unsteady air load upon motion; however, further work remains in order to confirm or disprove these observations.

REFERENCES

1. Fung, Y. C., "Fluctuating lift and drag acting on a cylinder in a flow at supercritical Reynolds numbers," TR EM 8-5, Space Technology Labs, Inc. (May 1958).
2. Fung, Y. C., "Fluctuating lift and drag acting on a cylinder in a flow at supercritical Reynolds numbers," J. Aerospace Sci., Vol. 27, 801-814 (1960).
3. Schmidt, L. V., "Measurements of Fluctuating air loads on a circular cylinder," J. Aircraft, Vol. 2, No. 1, 49-55 (1965).
4. Blackiston, H. S., Jr., "Tip effects on fluctuating lift and drag forces acting on a circular cylinder perpendicular to an air flow," Engineering Degree Thesis, California Institute of Technology (1963).
5. Ezra, A. A., and Birnbaum, S., "Design criteria for space vehicles to resist wind induced oscillations," ARS Paper 1081-60 (April 1960).
6. Spitzer, R. E., "Measurements of unsteady pressures and wake fluctuations for flow over a cylinder at supercritical Reynolds number," Engineering Degree Thesis, California Institute of Technology (1965).
7. Roshko, A., "Experiments on the flow past a circular cylinder at very high Reynolds number," J. Fluid Mech., Vol. 10, 345-356 (1961).
8. Delany, N. K., and Sorensen, N. E., "Low-speed drag of cylinders of various shapes," NACA TN 3038 (1953).

9. Keefe, R. T., "An investigation of the fluctuating forces acting on a stationary circular cylinder in a subsonic stream and of the associated sound field," Univ. of Toronto, UTIA Rept. 76 (1961).

ACKNOWLEDGMENTS

The author is indebted to Prof. Y. C. Fung for the counsel and advice provided during the course of the program reported herein. Without the sponsorship of the National Science Foundation, the support of the NASA Ames laboratory, and the encouragement of the Office of Naval Research, this work could not have been undertaken.

Many members of the GALCIT wind tunnel and electronics group were invaluable in providing help and friendship under many situations and these acts are sincerely appreciated. Messrs. D. A. Buell, J. B. Dods, and J. R. Brownson of NASA, Ames were extremely helpful in supporting this effort and their assistance in making this program possible is acknowledged.

FIG. 1: SKETCH OF CYLINDER MODEL INSTALLATION

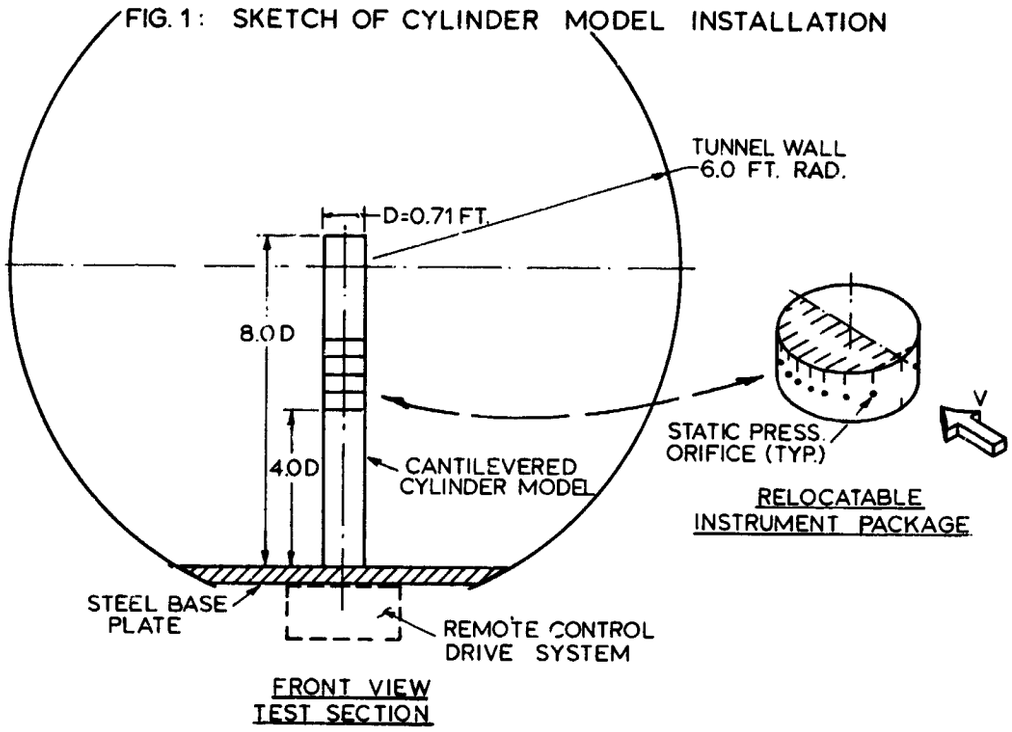

NASA AMES 12-FOOT WIND TUNNEL

FIG. 2: SUMMARY OF STEADY DRAG

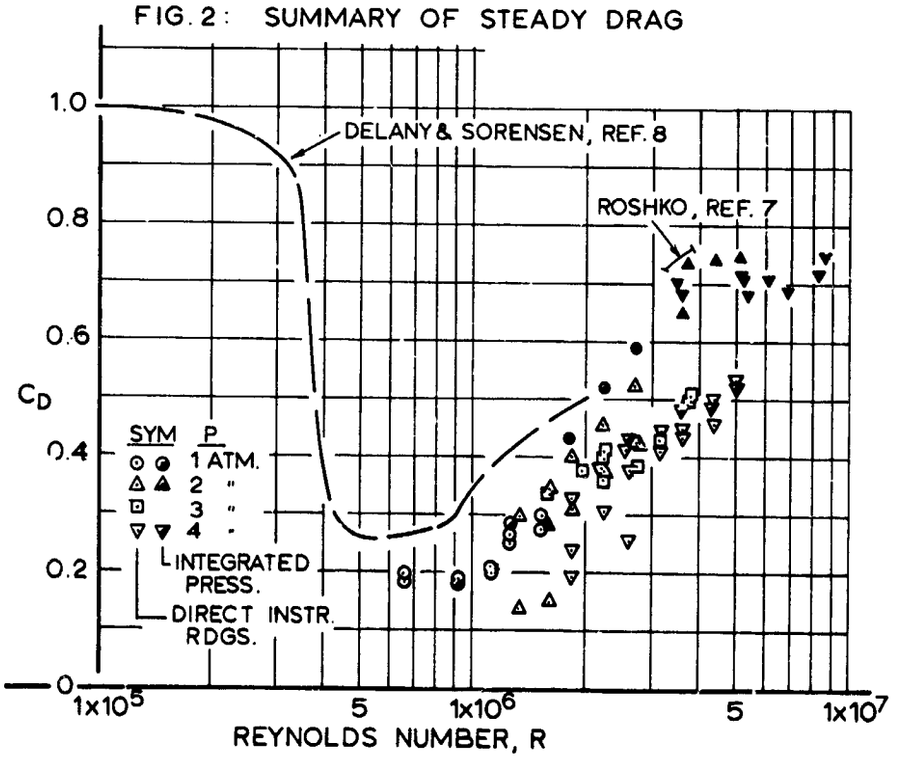

FIG.3: CYLINDER BASE PRESSURES

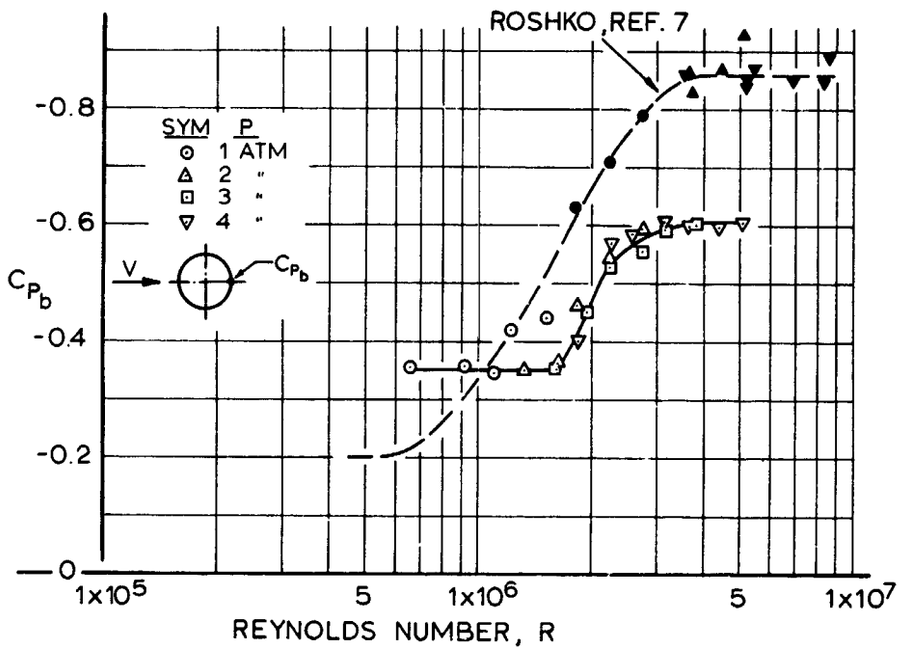

FIG.4: UNSTEADY LIFT RESULTS

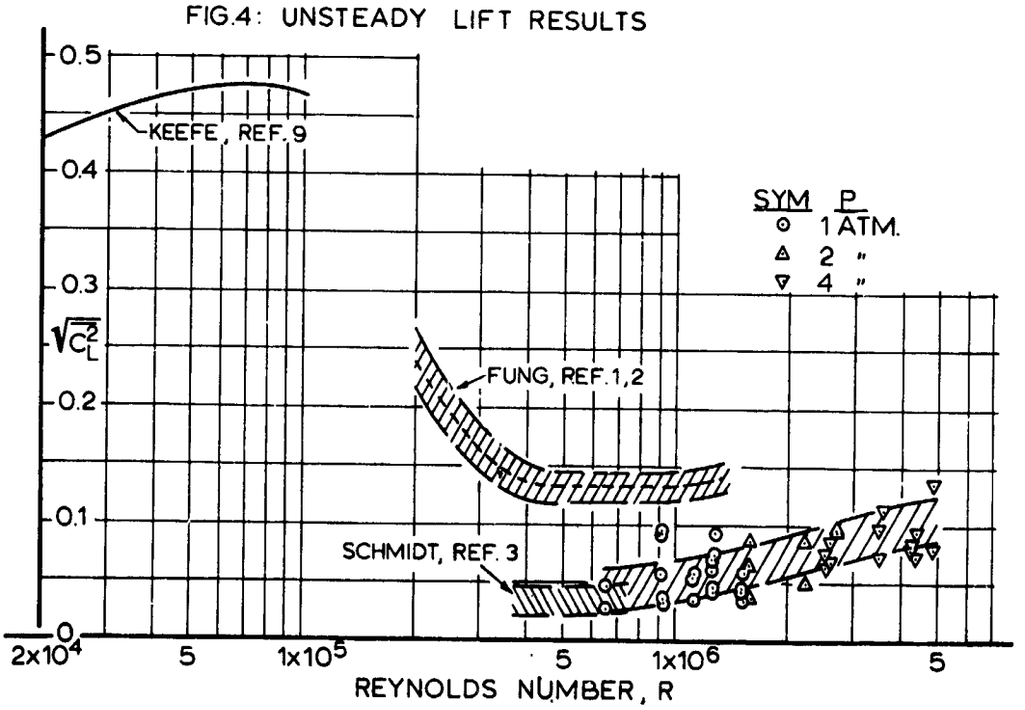

FIG. 5: UNSTEADY DRAG RESULTS

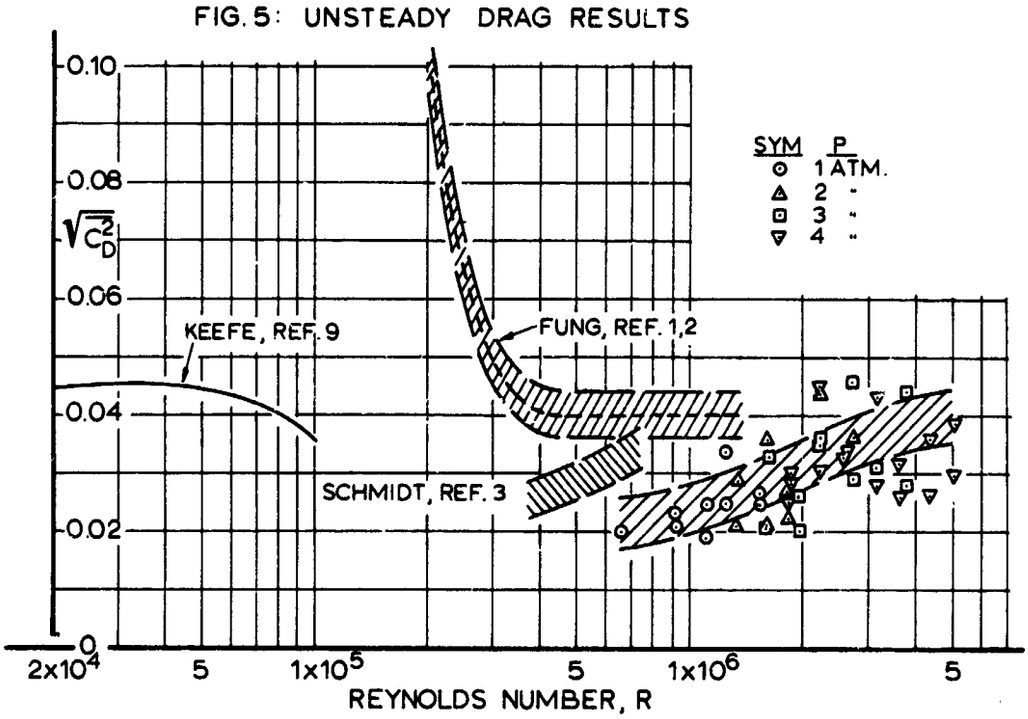

FIG. 6: POWER SPECTRUM FOR LIFT FORCE
$R = 1.1 \times 10^6$

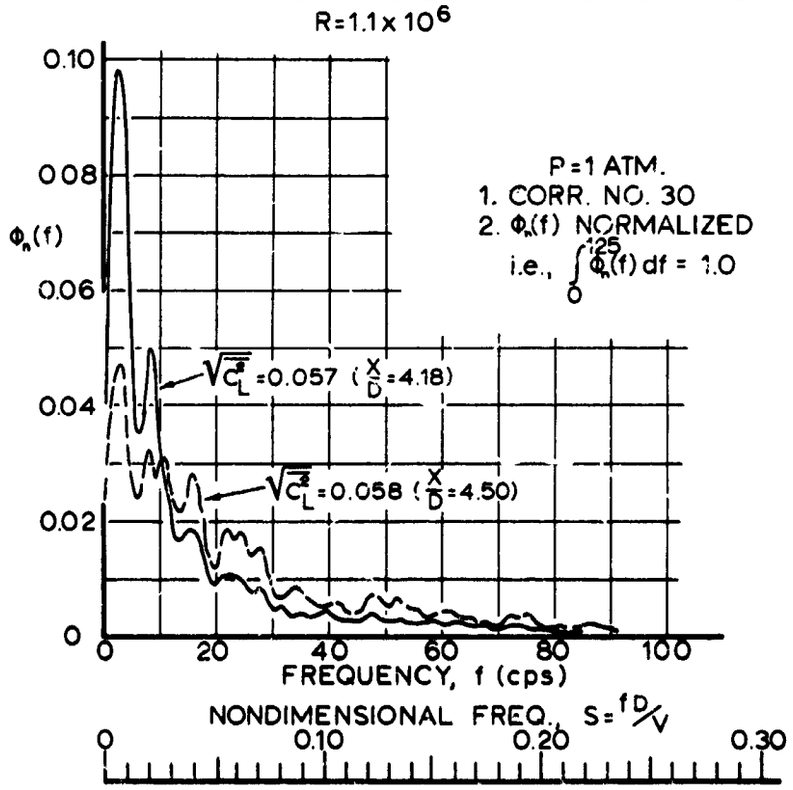

FIG. 7: POWER SPECTRUM FOR LIFT FORCE
$R = 5.0 \times 10^6$

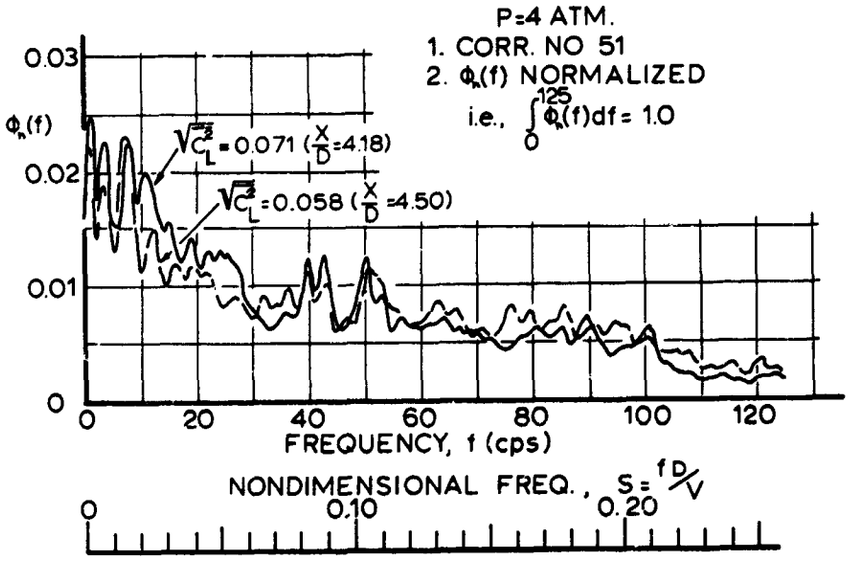

FIG. 8: CROSS CORRELATION
LIFT FORCE

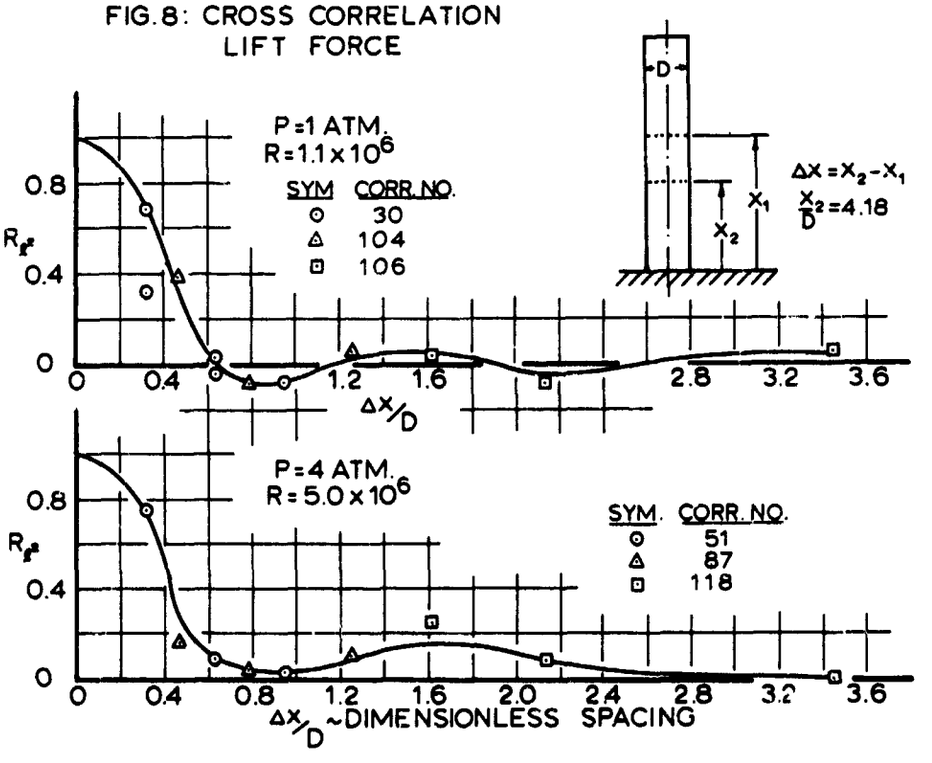

FIG. 9: CROSS CORRELATION DRAG FORCE

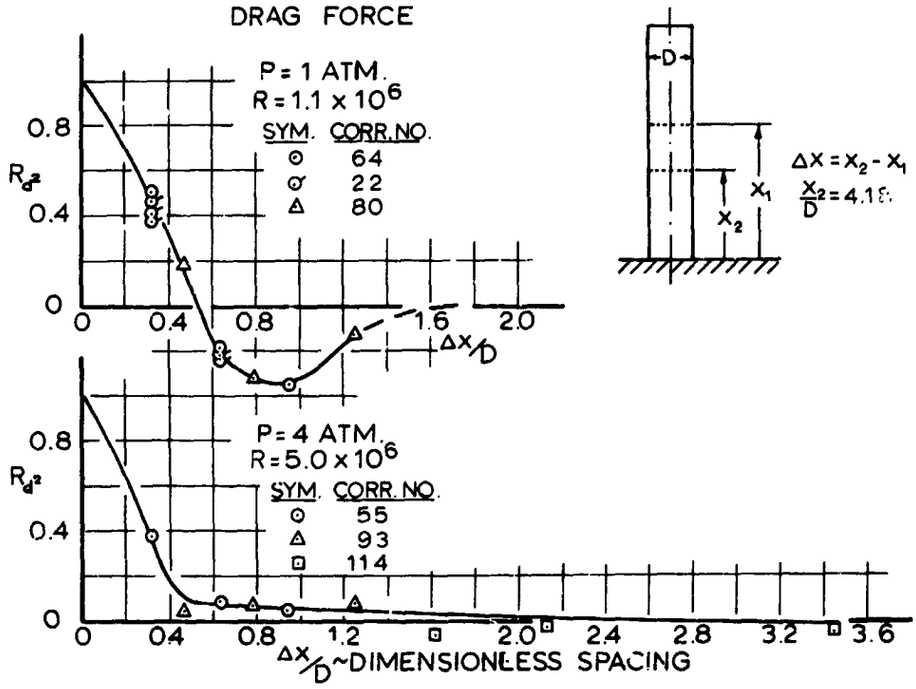

FIG. 10: SKETCH OF AEROELASTIC MODEL INSTALLATION

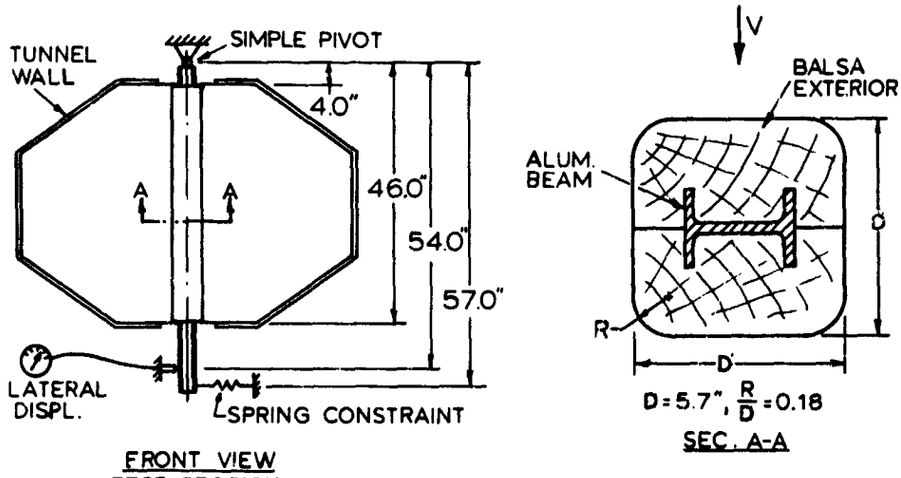

FRONT VIEW TEST SECTION

U.S.N. POSTGRADUATE SCHOOL
3.5 x 5.0 FOOT WIND TUNNEL

FIG. 11: ESTIMATED UNSTEADY LIFT, AEROELASTIC MODEL

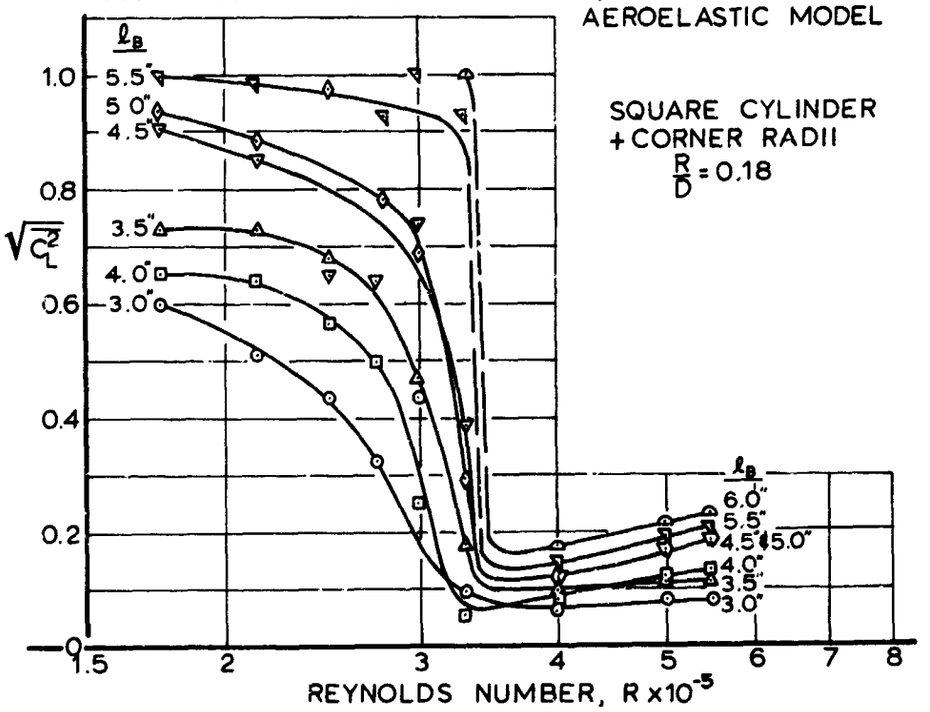

FIG. 12: AEROELASTIC EFFECTS ON UNSTEADY LIFT

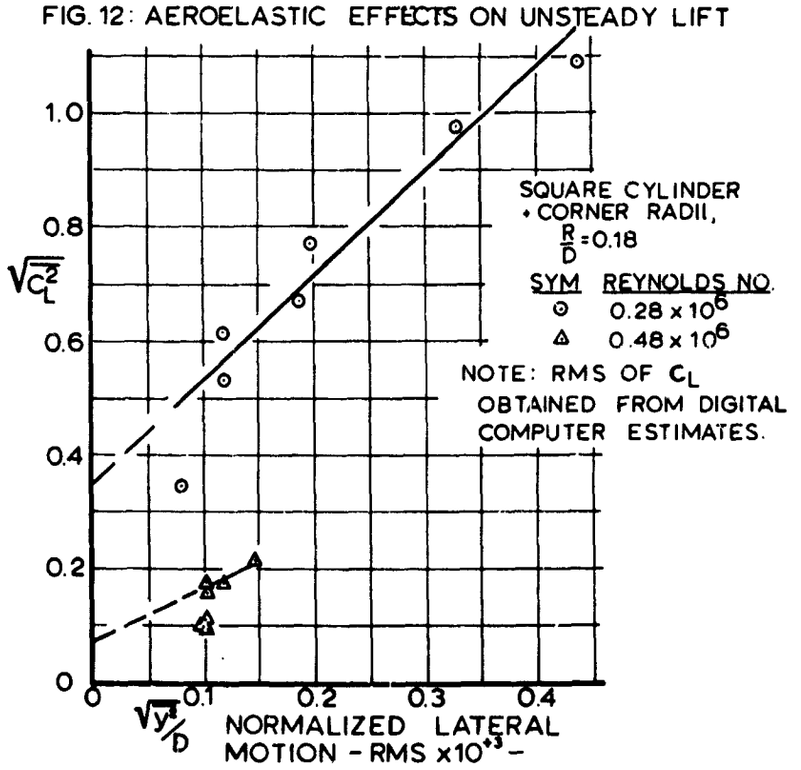

EXPERIMENTAL INVESTIGATION OF WIND INDUCED OSCILLATION EFFECTS ON CYLINDERS IN TWO-DIMENSIONAL FLOW AT HIGH REYNOLDS NUMBERS

by

Joseph J. Cincotta, Martin Company, (Baltimore)
George W. Jones, Jr., NASA Langley Research Center
Robert W. Walker, NASA Marshall Space Flight Center

SUMMARY

This paper presents the salient results of an experimental investigation of the steady drag and unsteady lift forces acting on a two-dimensional circular cylinder subjected to flow perpendicular to its axis. The study includes the affects of model motion, Strouhal Number and Mach Number over a range of Reynolds Number from 0.6×10^6 to 18.7×10^6. These tests were performed on a stationary and oscillating model for a model Strouhal Number range from 0.06 to 0.5.

It was found that with increasing Reynolds Number the unsteady lift force characteristic changes from wide band random to narrow band random to random plus periodic with these transitions occurring at approximately 3.5 million and 6 million Reynolds Number. The Strouhal Number of the unsteady aerodynamic force on the stationary model increased with increasing Reynolds Number to a constant value of 0.3 in the random plus periodic (Transcritical) Reynolds Number range.

In the transcritical regime, the unsteady lift forces were found to increase with amplitude of model oscillation, with the maximum amplification occurring when the model oscillating frequency was approximately equal to the aerodynamic Strouhal frequency. For model oscillation frequencies below the stationary model aerodynamic Strouhal frequency, the unsteady lift forces exhibited negative aerodynamic damping characteristics.

Mach Number was found to effect both the static drag and unsteady lift data for Mach Number greater than 0.2. For Reynolds Numbers above 3 million and Mach Number less than or equal to 0.2 the static drag coefficient was relatively constant at approximately 0.54.

INTRODUCTION

When launch vehicles are subjected to steady ground winds while in the vertical position, unsteady aerodynamic forces are exerted on them occurring primarily in a direction perpendicular to the wind. These unsteady forces are associated with vortices shedding from the sides of the vehicle and are generally influenced by vehicle geometry, Reynolds Number, oscillatory vehicle motion, Strouhal Number, surface conditions and non-uniformities of the stream. (See Humphreys[1], Fung[2], Schmidt[3], Roshko[4], Scruton[5].) These phenomena are not amenable to analysis at Reynolds Numbers of practical interest (See Morkovin Ref. 6)

As a start toward providing a better understanding of the unsteady aerodynamic forces and the most important parameters controlling them in the high Reynolds Number range, applicable to large launch vehicles, a wind tunnel investigation has been conducted for the simplest geometry of a smooth two-dimensional cylinder. The objectives of this program were to evaluate the unsteady aerodynamic forces acting on a segment of the cylinder, as influenced by cylinder motion, Strouhal Number and Reynolds Number, and to obtain and correlate visual observations with this quantitative information so as to clarify possible spanwise vortex formations. The supercritical Reynolds Number range, where limited data were available (Ref. Fung[2], Schmidt[3]), was investigated, but primary emphasis was placed on the Roshko transcritical Reynolds Number range where only mean cylinder pressure measurements and wake frequency measurements had been made.

EXPERIMENTAL CONSIDERATIONS

In Fig. 1, the Strouhal Number range, of the present model oscillation, as a function of Reynolds Number is compared with those of some previous investigations. The conditions obtained during this program extend from

0.6×10^6 to 18.7×10^6 Reynolds Number and from 0.06 to 0.5 oscillating model Strouhal Number. This boundary goes beyond previous investigations to higher Reynolds Numbers and incorporates the region of critical aerodynamic Strouhal Number (0.2 to 0.27) as previously observed in the Subcritical and Transcritical Reynolds Number Range.

The experiments were performed in the NASA Langley transonic dynamics wind tunnel, utilizing various densities of both air and freon as test media. The use of freon as a test medium, with a density of approximately 3.75 times the density of air, and kinematic viscosity approximately one-fifth that of air, provided the desired high Reynolds Number on the test cylinder. The choice of test media and the variation of their densities allowed limited separate variations of Mach Number and Reynolds Numbers effects aimed at the possible separation of the viscous and compressibility effects on the aerodynamic forces.

The model consisted of a 3 foot diameter cylinder which spanned the entire 16 foot test section of the wind tunnel. This cylinder was effectively rigid and derived its motion from a variable stiffness torque bar suspension system in conjunction with a hydraulic shaker system located at each end of the cylindrical model. The suspension-shaker systems were located in the floor and ceiling of the test section out of the air stream. A diagram of the model system is shown in Fig. 2 as it was assembled in the wind tunnel. The model structure was comprised of four basic parts: 1) inner support cylinder; 2) outer cylindrical sections; 3) variable stiffness suspension system, and 4) hydraulic shaker system.

The outer cylinders consisted of four cylindrical sections constructed of lightweight aluminum honeycomb sandwiched between two thin aluminum skins with an outer diameter of 36 inches. The lengths of these four sections were 3 feet, 7 feet, 3.6 inches and 5.7 feet, respectively, from top to bottom of the model. The two center sections, 7 foot length (2.33 diameters) and 3.6 inch length (0.1 diameter), were attached to the inner cylinder through force transducers in the lift and drag directions, while the end cylinders were attached directly to the inner cylinder. The uninstrumented end cylinders minimized wall effects from the aerodynamic force measurements while preserving the two-dimensional cylindrical shape. The inner cylinder consisted of a 19-inch diameter seamless aluminum tube, 17 feet long with a hydraulic shaker attachment point at each end. This inner cylinder provided the structural load carrying capability necessary to withstand the dynamic and static loads imposed on the model.

The model suspension system consisted of a set of tapered torque bars and remotely controlled clamping mechanisms whose position along the torque bar could be changed by means of a motor-chain drive. The lateral translation motion of the model was transferred to the torque bars by means of torque arms attached to the model and the torque bar as shown in Fig. 2.

The model tests were performed on the resonant system, formed by the cylinder on its suspension system. The resonant frequency was variable from 3 to 20 cps by changing the torque bar clamping position. The model driving forces were obtained from a set of hydraulic shakers, each capable of 1400 pounds force and 6 inches double amplitude displacement. The use of this resonant model system decreased the harmonic distortion of the model accelerations and substantially reduced the force required to drive the system.

The unsteady aerodynamic forces were measured directly with the Martin Inertia Compensated Balance (Ref. 7). This system combines the signals from a strain gage force transducer and a strategically located accelerometer in such a manner as to provide a direct measurement of the external unsteady aerodynamic forces acting on the model. A circuit schematic of a typical Inertia Compensated Balance measurement system is shown in Fig. 3. The model utilized three separate balance systems to measure: (1) unsteady aerodynamic lift forces on the 2.33 diameter length cylinder; (2) unsteady aerodynamic lift forces acting on the 0.1 diameter length cylinder; and (3) unsteady aerodynamic drag forces on the 0.1 diameter length cylinder. For the experiments reported herein the 0.03 inch gaps between cylinders were sealed at the surface of the cylinder with a silicone rubber compound in order to eliminate the aerodynamic discontinuity caused by these gaps. Because of some load carrythrough and the flexibilities of the small segment, the data for the 0.1 diameter lengths cylinder will not be presented.

The steady aerodynamic drag forces were measured by force transducers on the 2.33 diameter length cylinder. In addition, static pressure distributions were measured by a ring of 48 static pressure orifices, installed at one longitudinal station 1.14 diameters from the lower end of the model. Two methods of flow visualization were used; a tuft grid located 2 diameters downstream and illuminated by a stroboscope and a fluorescent oil film on the cylinder surface. The tuft grid observations were limited because the grid collapsed just before the narrow band lift response was achieved.

RESULTS OF INVESTIGATION

Flow Visualization Techniques

The observations of the tuft grid, limited to air at atmospheric pressure below a Reynolds Number of approximately 5 million disclosed no evidence of any cell or eddy structure larger than a cylinder diameter across the frequency range.

The oil film technique was used to observe the mean separation lines* on the model and consisted of a mixture of fluorescent powder mixed in oil and painted on the model. The resulting oil streaks caused by the air on the model were then photographed under ultra-violet light. The dual separation (laminar and turbulent) of the laminar bubble phenomena is shown in Fig. 4 at 1.7 million Reynolds Number. Mean venting of the bubble by a narrow turbulence wedge from a speck of dirt can be seen just above the upper gap. This essentially unvented laminar bubble separation pattern was observed to approximately 2.5 million Reynolds Number.

In addition, this flow visualization technique was used to investigate the gap effects. When the gaps were open, the mean separation line was generally disturbed by premature separation in the area of the gaps as seen in Fig. 5a. Sealing the gaps with the silicone rubber compounds decreased the aerodynamic discontinuity as shown in Fig. 5b.

Static Drag Data

The static drag data presented for the stationary model were determined from the 2.33 diameter length cylinder. A comparison of the open gap and closed gap static drag coefficient is presented in Fig. 6. The open gap data indicates a generally higher drag coefficient than the closed gap data(particularly in the low Reynolds Number range) as would be expected from the visualization results. This was also observed for the drag coefficient determined by integrating the measured pressure distribution.

Figure 7 presents the drag coefficient as a function of Reynolds Number for various Mach Numbers through Mach 0.4. There is a peak in the drag

*The presence of a thin oil film under a gaseous boundary layer influences the location of separation very little in steady flows (Ref. 8). The oil film virtually does not respond to the unsteady flow at the frequencies of interest so that the unsteady turbulent reattachment, closing the bubble, or its temporary venting cannot be discerned by this technique.

coefficient data in the Reynolds Number range of 3 million to 8 million, which becomes more predominant with increasing Mach Number to Mach 0.4. No scheme of separating the Mach Number and Reynolds Number contributions was successful. Hence the peak is considered to be associated with the combined effects of Mach Number and Reynolds Number. For the data obtained at Mach Numbers less than 0.2, which is the practical Mach limit for ground wind design loads, the hump essentially disappears. A larger scatter of data on the order of $\pm$ 8 percent which exists in the 3 to 5 million Reynolds Number range could as well be ascribed to the irregular transition of the new mode of more organized vorticity shedding (narrow band random). The drag coefficient for Mach Numbers less than 0.2 tends to level off at the value of approximately 0.54 at Reynolds Numbers above 3 million. A comparison of the static drag data for the oscillating and stationary model is given in Fig. 8. There appears to be little or no effect due to model motion on the static drag coefficient.

Aerodynamic Strouhal Number

The Aerodynamic Strouhal Number will be defined as the predominant frequency measured from the autocorrelation function (or the peak of the power spectral density) of the unsteady aerodynamic lift force acting on the stationary model (even in the case of the broad band spectra). In addition to determining the Aerodynamic Strouhal Number from the autocorrelation functions, the variation of the bandwidth of the unsteady aerodynamic force was quantitatively determined. The bandwidth variations of the autocorrelation functions were categorized as: (1) wide band random, characterized by an autocorrelation function of no more than one peak other than the peak at zero time displacement, (2) narrow band random having an autocorrelation function consisting of more than two consecutive peaks, decaying with increasing time

delay by greater than 10% per cycle, and (3) very narrow band or random plus periodic, in which the autocorrelation function is described by consistent peaks through the entire analyzed range of time displacement, with constant amplitude within 10% at the largest time displacement peak. The autocorrelation functions in the Reynolds Number range from 1.4 million to approximately 3.5 million were of the wide band category, while with increasing Reynolds Number in a range of from 3.5 million to 6 million, the unsteady aerodynamic force was characterized as narrow band random. In the Reynolds Number range from 6 million to 18.2 million, the unsteady aerodynamic force was generally random plus periodic. Figures 9, 10 and 11 show typical examples of these Reynolds Numbers ranges, in the form of their autocorrelation functions, power spectral densities, amplitude probability densities and sample time histories. The aerodynamic nature of the forces for the Transcritical Reynolds Number range (Fig. 11) are generally the same for the full range of Mach Numbers tested.

The effective bandwidth of the unsteady aerodynamic force is presented in terms of the Strouhal Number determined from the half power point of its power spectral density for Mach Numbers less than .3 in Fig. 12 (solid lines). The aerodynamic Strouhal Number determined from the autocorrelation function, which is essentially the center frequency or peaked frequency point of the Power Spectral Density, is shown in Fig. 12 as the dashed line. The characteristic narrowing of the Strouhal Number bandwidth with increasing Reynolds Number is evident. In Fig. 13, at Mach Numbers greater than .4, the effects of compressibility are shown by the narrow Aerodynamic Strouhal bandwidth throughout the entire Reynolds Number range.

The preceding results indicate that in the Transcritical Reynolds Number range (above 6 million), the unsteady aerodynamic force contains a periodicity

at a constant Strouhal Number of approximately .3, perhaps decreasing somewhat with increasing Mach Number above M = 0.4. Because of the relatively rough model utilized by Roshko[4], this emergence into the Transcritical Reynolds Number range occurred at a lower Reynolds Number (3.5 million).

Stationary Model Unsteady Aerodynamic Lift Coefficient (C_L)

The unsteady aerodynamic lift coefficient acting on the stationary model was determined from the 2.33 diameter cylinder using the sealed gap data. The wide band rms lift coefficients were obtained from the maximum value of the autocorrelation functions (zero time displacement) and verified by a time average, wide band, mean square measurement.

Upon reduction, the data appeared to congregate along two distinct curves in the lower Reynolds Number range and coalesced into a single band between approximately 6.0 to 8.0 million Reynolds Number. Figure 14 exhibits these dual data paths for two separate tunnel sweeps with freon at atmospheric pressure as the medium. Figures 15a and 15b are oil film photographs of the separation lines for atmospheric air data at approximately 5.7 million Reynolds Number corresponding to the upper path of data; Fig. 15c, which has a more uneven separation line, corresponds to the lower data path, again for 5.6 million Reynolds Number in atmospheric air.

From other observations such as mean pressure distributions, it appears that these dual data paths are associated with symmetric or asymmetric mean flow states around the cylinder. The upper data path appears to correspond to an asymmetric flow distribution and the lower data path associated with the symmetric distribution. Since the separation photographs were taken from only one side of the model, the visual observations of the symmetry conclusion is not possible.

A cross plot of the unsteady aerodynamic lift coefficient as a function of Reynolds Numbers for various fixed Mach Numbers is presented in Fig. 16. The dual data paths occur at Mach Numbers less than 0.3 up to 6 to 8 million Reynolds Number range. For Mach 0.4, where the data may be more organized by the stronger compressible pressure gradients, the lift coefficient is single valued for all Reynolds Numbers. The dual data paths at lower Mach Numbers coalesce with the onset of the Transcritical Reynolds Number range where the near wake is also more organized and the unsteady aerodynamic lift force becomes random plus periodic.

Oscillating Model Aerodynamic Lift Coefficient

At a given tunnel speed, the stationary characteristics were first established and then the model was oscillated at a series of fixed amplitudes up to a maximum of 6 inches double amplitude at forcing frequencies from 3 cps to 19 cps. In the following discussion, the model Strouhal Number (S_m) will be defined as the Strouhal Number, based on the model diameter of 3 feet, determined by the frequency of the model oscillation (shake frequency). The model Strouhal Number ranged from 0.06 to 0.5. The autocorrelation functions of the unsteady lift forces on the 2.33 diameter length cylinder were determined for all the oscillating model conditions.

The effects of model motion on the lift coefficient for the random plus periodic Reynolds Number range (6 million to 18.7 million) are depicted in Fig. 17. This information is given in terms of the lift amplification factor, C_{L_O}/C_{L_S}, (oscillating model lift coefficient to stationary model lift coefficient) as a function of the ratio of the Model Strouhal Number to the Aerodynamic Strouhal Number, (S_M/S_A). As model Strouhal Number first increases the lift amplification factor also increases and reaches its maximum amplification when the model Strouhal Number is approximately equal to the Aerodynamic

Strouhal Number. Increasing the model Strouhal Number to values greater than the Aerodynamic Strouhal Number decreases the lift amplification factor. Furthermore, increasing the model amplitude generally increases the amplification factor. Section plots at Strouhal ratios of .9, 1.0, and 1.1, shown in Fig. 17, indicate the dependence of the lift amplification factor on the amplitude of model oscillation.

In order to determine the effects of model motion on the nature of the aerodynamic lift forces, the components of the lift forces in phase with the model acceleration and in phase with the model velocity, were determined. These components of the aerodynamic lift force were determined from both Co and Quad spectra and cross correlation functions with respect to the model displacement. The approximate variation of the "mass" component (in phase with model acceleration) and the "damping" component (in phase with model velocity) of the unsteady aerodynamic lift forces are indicated in Fig. 18 as a function of the ratio of model to Aerodynamic Strouhal Number. The mass component increases with increasing model amplitude and Strouhal Ratio with the maximum occurring when the model Strouhal Number is approximately equal to the Aerodynamic Strouhal Number. The damping component, however, indicates an unstable, or negative aerodynamic damping, when the model to Aerodynamic Strouhal ratio is less than 1. The maximum negative aerodynamic damping is rather sharp and occurs when the Strouhal Ratio is approximately .95. Above the Strouhal ratio of 1., the damping component of the aerodynamic force has a stabilizing or positive damping effect.

The Aerodynamic Strouhal Number associated with the peak negative aerodynamic damping component is the Strouhal Number which would result in a maximum response of a dynamic system (the observed Strouhal Number when

measuring response of a structure). The maximum model response Strouhal Number has been defined in previous investigations as the Critical Strouhal Number. In this Transcritical Reynolds Number range, the results of this investigation indicate that the Critical Strouhal Number is approximately 0.28.

CONCLUSIONS

In summary, based on the data of this experimental investigation, the following conclusions can be made regarding the magnitudes and nature of the steady drag and unsteady aerodynamic lift forces acting on a two-dimensional cylinder.

(1) The static drag coefficient is constant at approximately 0.54 in the Reynolds Number range from 3.5 million to 10 million for Mach numbers less than or equal to .2. With increasing Mach Numbers the drag coefficient exhibits a peak in the Reynolds Number Range from 3 million to 8 million.

(2) The nature of the unsteady aerodynamic lift forces varied from wide band random to random plus periodic with increasing Reynolds Number as follows:

Reynolds Number Range	Nature
1.4 million to 3.5 million	Wide band random
3.5 million to 6 million	Narrow band random
6 million to 18.2 million	Random plus periodic

(3) At Mach Numbers less than 0.3 through the wide band and narrow band ranges of Reynolds Number, the Aerodynamic Strouhal Number determined from the autocorrelations function increases with increasing Reynolds Number from .15 to .3. It then remains constant at .3 into the random plus periodic range.

(4) The unsteady aerodynamic lift coefficient for the stationary cylinder in the wide band and narrow band ranges of Reynolds Number is double valued. These double valued lift coefficients are probably associated with a symmetric or asymmetric flow distribution around the cylinder.

(5) The effects of model motion on the aerodynamic lift coefficient indicates that the rms lift coefficient increases with model motion with a maximum lift coefficient occurring when the model oscillating frequency coincides with the aerodynamic frequency An unstable (negative) aerodynamic damping component of the unsteady lift force occurs when the model frequency is less than the aerodynamic frequency, while a stable damping component occurs when the model frequency is higher than the aerodynamic frequency.

Acknowledgements

This study was performed as part of the continuing development and research effort by Langley Research Center under A. G. Rainey and Marshall Space Flight Center under T. G. Reed to understand and provide for the environmental loads on launch vehicles.

References

(1) Humphreys, J. S., "On a Circular Cylinder in a Steady Wind at Transition Reynolds Numbers", Journal of Fluid Mechanics, Vol. 9, Part 4, December 1960.

(2) Fung, Y.C., "Fluctuating Lift and Drag Acting on a Cylinder in a Flow at Supercritical Reynolds Numbers", Presented at IAS 28th Annual Meeting, New York, IAS, Paper No. 60-6, January 1960.

(3) Schmidt, L.V. "Measurements of Fluctuating Air Loads on a Circular Cylinder", Journal of Aircraft, Vol. 2, No. 1, Jan-Feb 1965.

(4) Roshko, A. "Experiments on the Flow Past a Circular Cylinder at Very High Reynolds Numbers", Journal of Fluid Mechanics, Vol. 10, Part 3, May 1961.

(5) Scruton, C., "On the Wind Excited Oscillations of Stacks, Towers and Masts", National Physical Laboratory, Teddington Middlesex, England, June 1963.

(6) Morkovin, M. V., "Flow Around Circular Cylinder--A Kaleidoscope of Challenging Fluid Phenomena", Symposium of Fully Separated Flows, The American Society of Mechanical Engineers, May 1964.

(7) Stahle, C. V., Stouffer, C. G., and Silver, W., "A Simplified Inertia Compensated Balance Technique for Wind Tunnel Measurements of Launch Vehicle Random Buffet Excitation", IA-ASD Symposium on Aeroelastic and Dynamic Modeling Technology, September 1963.

(8) Squire, L. C., "On the Motion of a Thin Oil Sheet under the Steady Boundary-Layer of a Body", Journal of Fluid Mechanics, Vol. 11, Part 2, September 1961.

APPENDIX A

LIST OF SYMBOLS

A	unit frontal area (1 x d), ft^2
C_D	static drag coefficient on 7-foot instrumented section, D/qs
C_L	lift coefficient, F_L/qA
$C_{L,co}$	component of lift coefficient in phase with displacement ($C_L \cos \theta$)
$C_{L,quad}$	component of lift coefficient 90° out-of-phase with displacement ($-C_L \sin \theta$)
C_{L_O}	rms oscillating model lift coefficient
C_{L_S}	rms stationary model lift coefficient
d	model diameter (3 feet)
D	static drag force on 7-foot instrumented section, lbs
f_A	aerodynamic shedding frequency, determined from predominant frequency of the aerodynamic force autocorrelation function for stationary model, cps
f_M	oscillating model forcing frequency, cps
F_L	external aerodynamic force measured on model in lift direction, lbs
$F(s)$	non-dimensional power spectral density of lift force
M	Mach number
q	dynamic pressure, $\frac{\rho V^2}{2}$
R_N	Reynolds number, $\rho Vd/\mu$
s	frontal area of 7-foot instrumented section, ft^2
S_A	aerodynamic Strouhal number (stationary model), $f_A d/V$
S_M	model Strouhal number (oscillating model), $f_M d/V$
V	flow velocity, ft/sec

θ	phase angle between lift force vector and displacement vector (positive for force lagging displacement)
η	model shake amplitude (inches, double amplitude)
μ	dynamic viscosity of test medium, slugs/ft-sec
ρ	density of test medium, slugs/ft^3

PREVIOUS INVESTIGATION OF TWO-DIMENSIONAL WIND-INDUCED OSCILLATION EFFECTS ON CYLINDERS

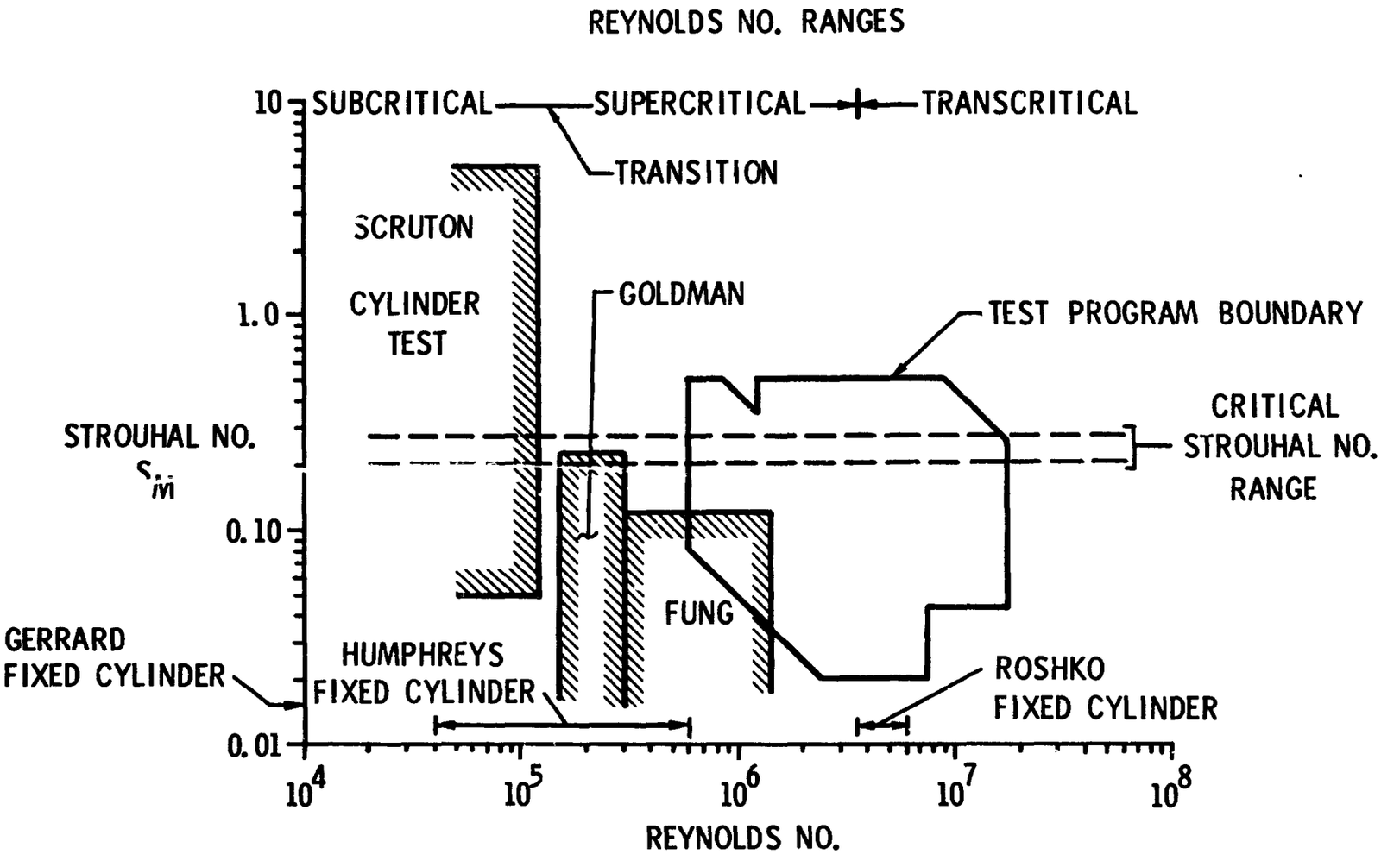

Fig. 1.

MODEL ARRANGEMENT IN WIND TUNNEL

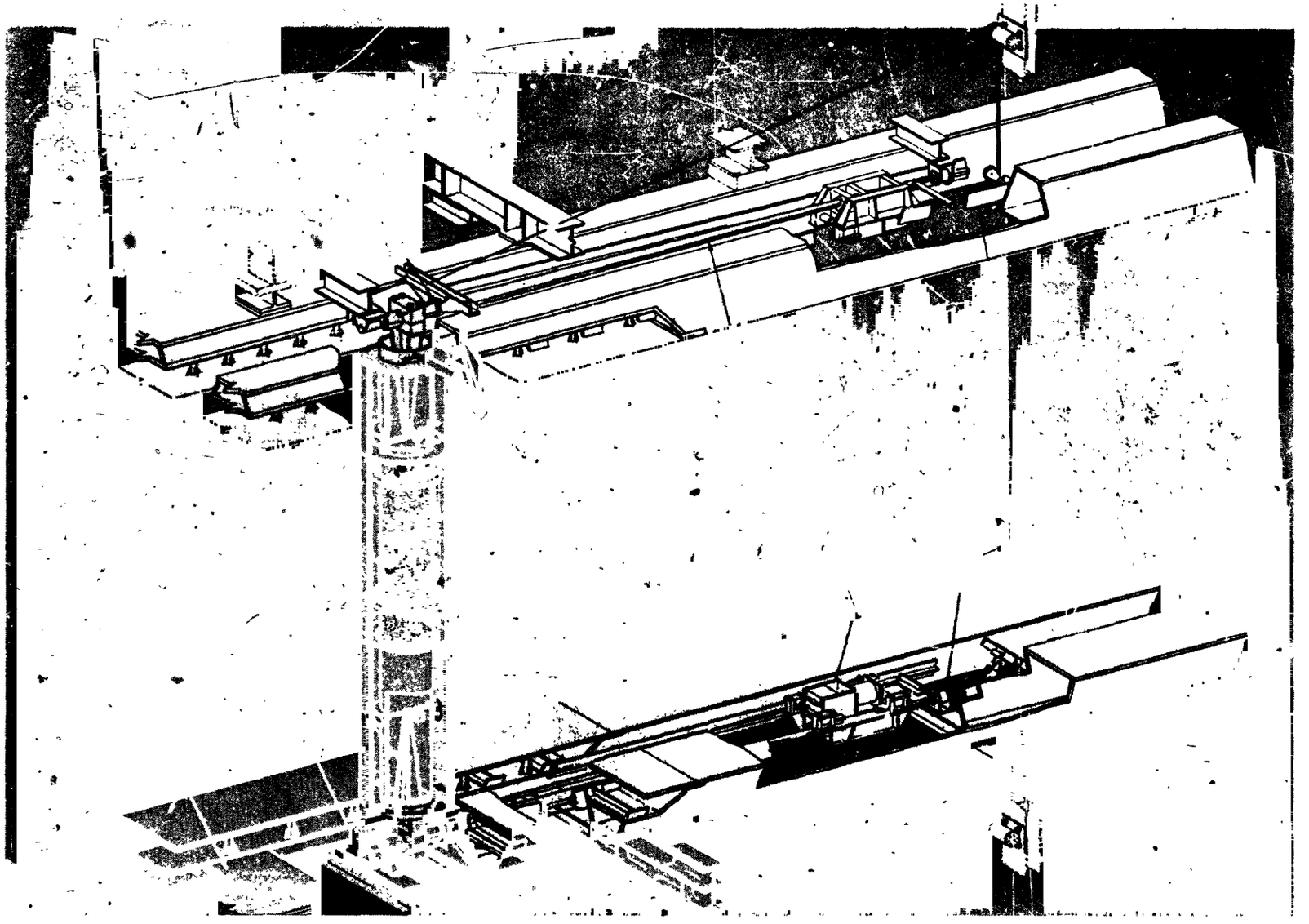

Fig. 2.

LARGE CYLINDER (2.33 DIA LENGTH) INSTRUMENTATION SYSTEM

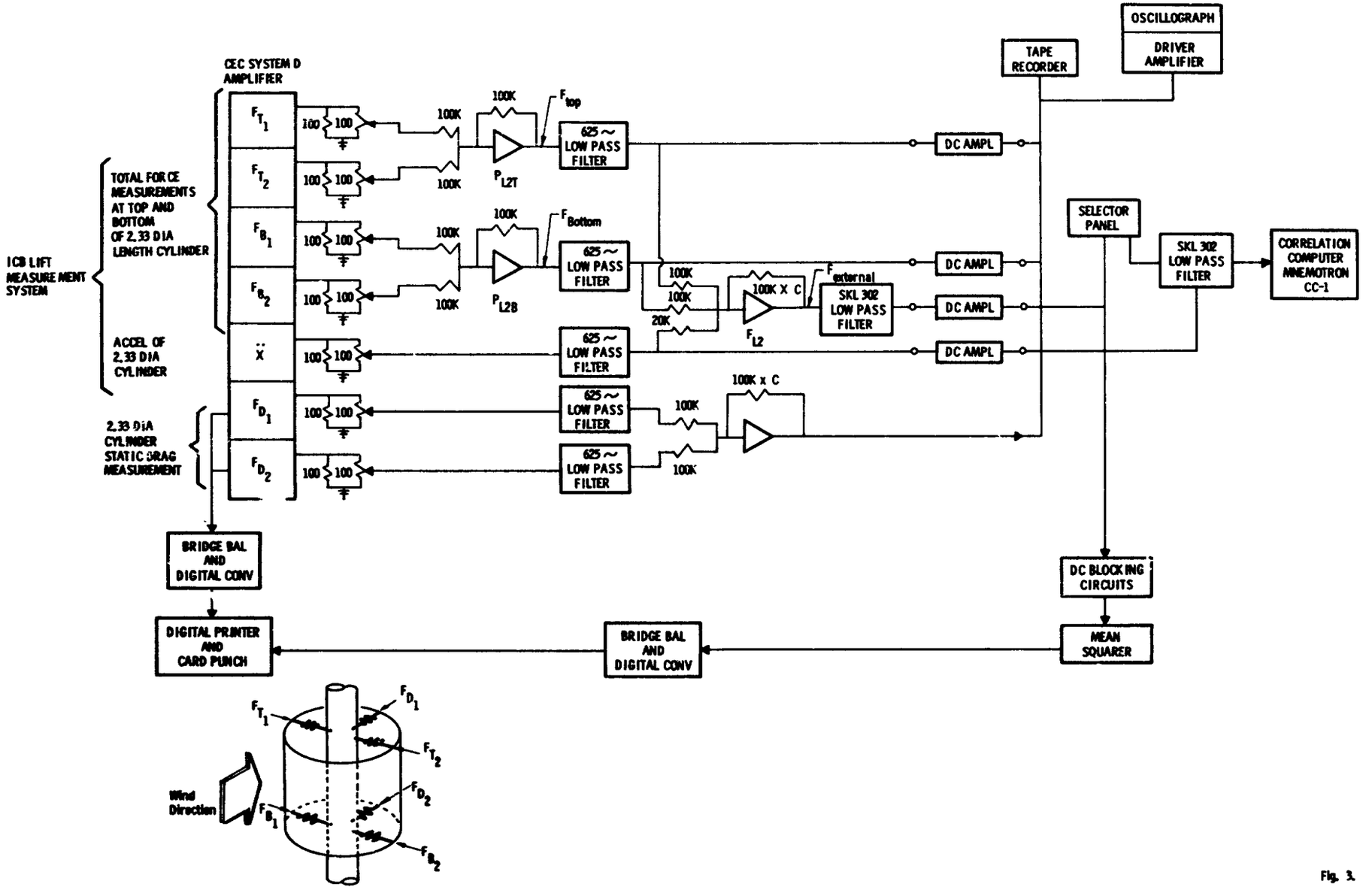

Fig. 3.

OIL FLOW PHOTOGRAPH SHOWING LAMINAR BUBBLE

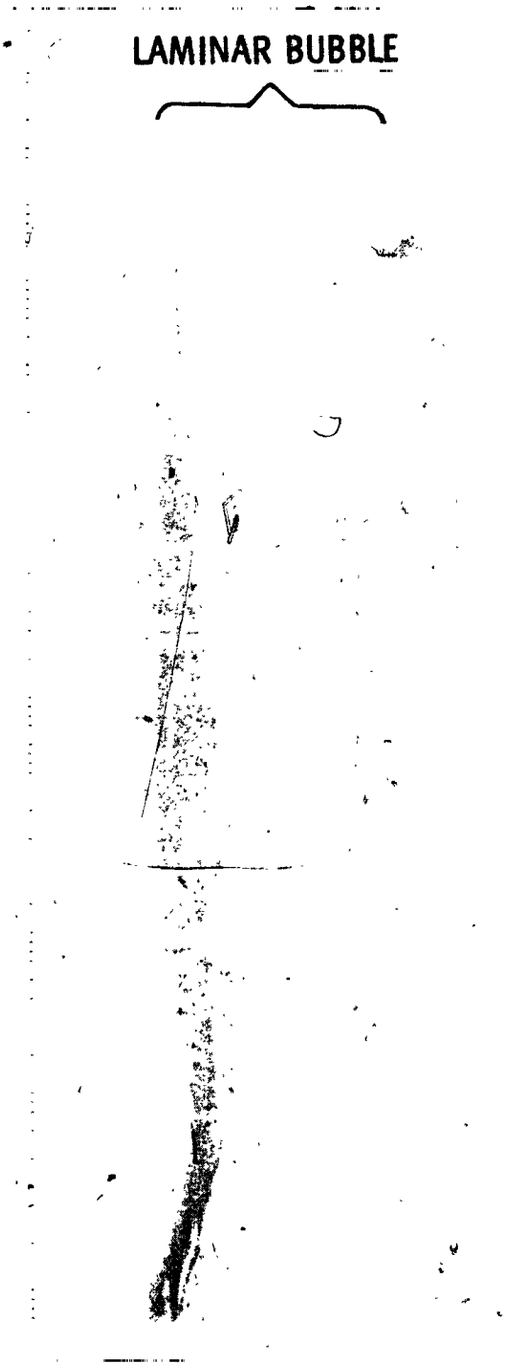

REYNOLDS NUMBER 1.73×10^6

Fig. 4

OIL FLOW PHOTOGRAPHS ILLUSTRATING FLOW ABOUT CYLINDER WITH GAPS OPEN, $R_N = 2.3 \times 10^6$

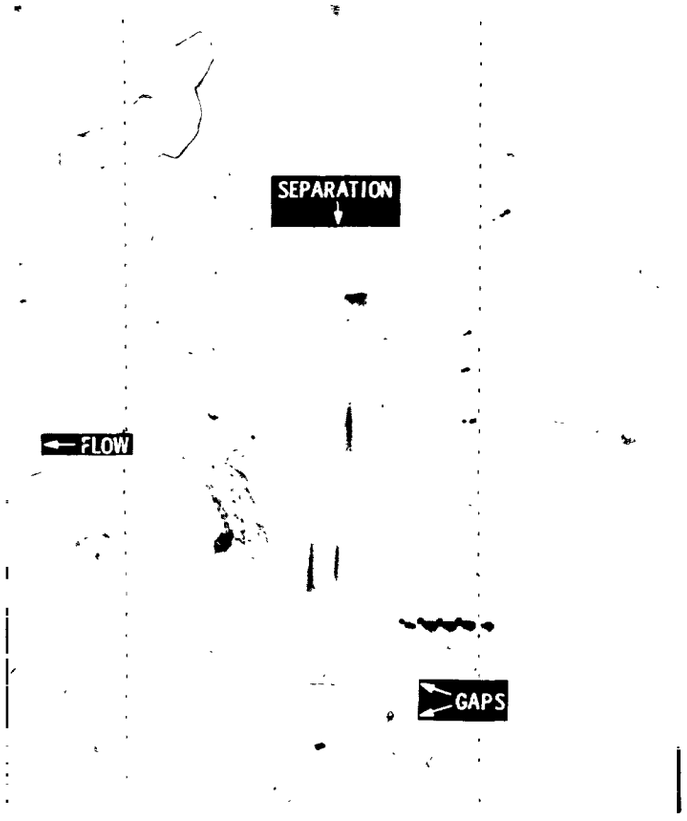

Fig. 5a.

OIL FLOW PHOTOGRAPHS ILLUSTRATING FLOW ABOUT CYLINDER WITH GAPS SEALED, $R_N = 2.9 \times 10^6$

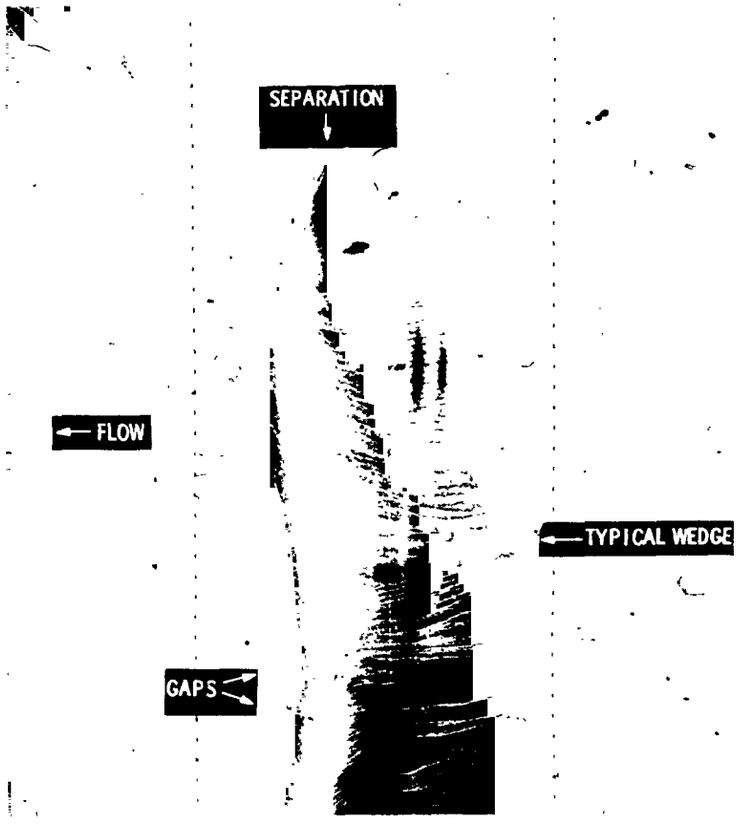

Fig. 5b.

COMPARISON OF GAP SEALED DRAG DATA WITH GAP OPEN DRAG DATA AND WITH STATIC PRESSURE ORIFICE DRAG DATA

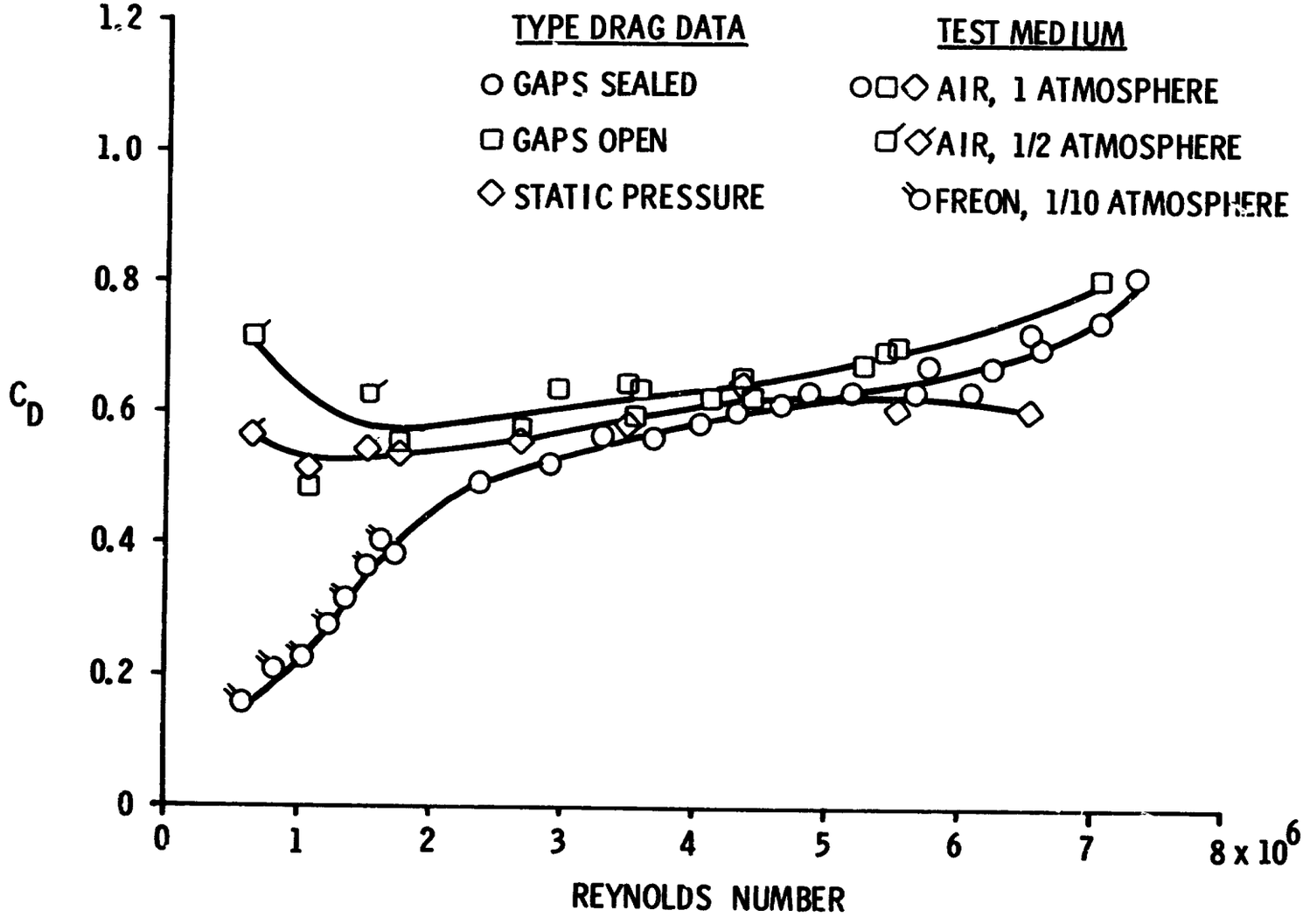

Fig. 6.

VARIATION OF DRAG COEFFICIENT WITH REYNOLDS NUMBER AT MACH NUMBERS ≤ 0.20

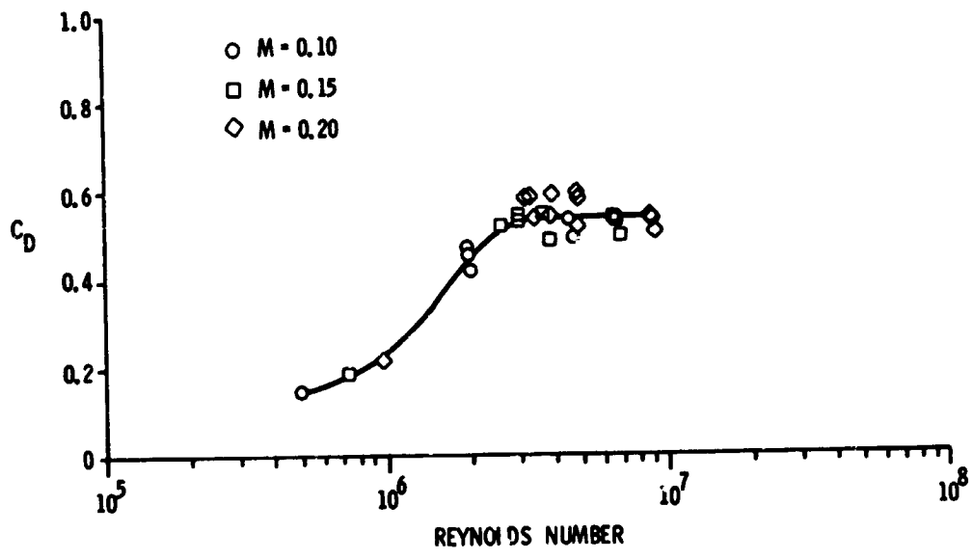

SUMMARY OF VARIATION OF DRAG COEFFICIENT WITH REYNOLDS NUMBER; PRESENTED AT CONSTANT MACH NUMBERS

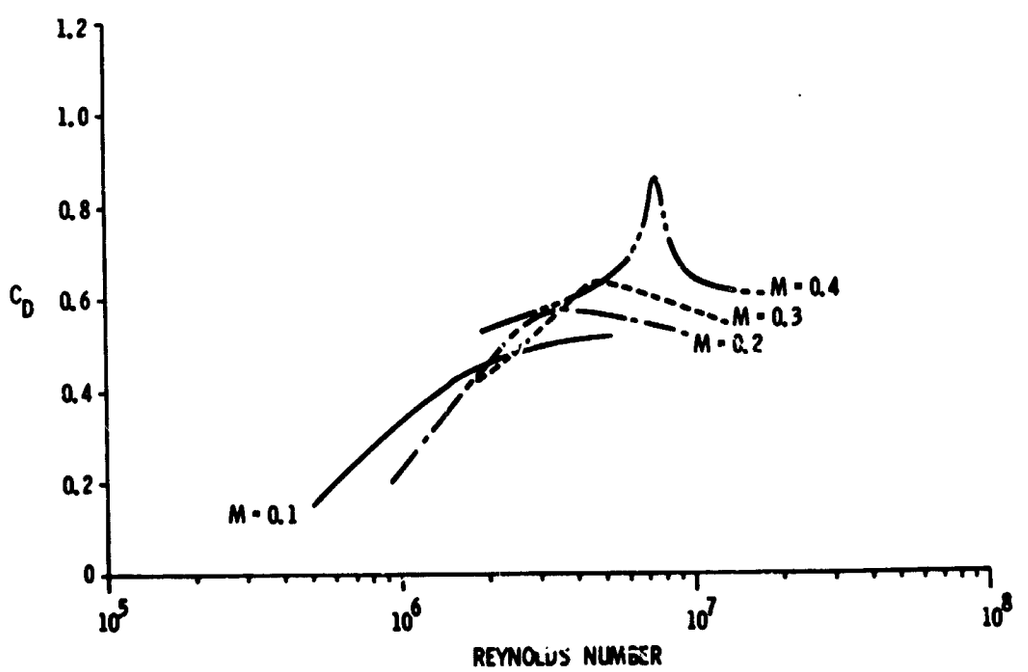

Fig. 7.

EFFE OF CYLINDER MOTION ON VARIATION OF
STATIC DRAG COEFFICIENT WITH REYNOLDS NUMBER

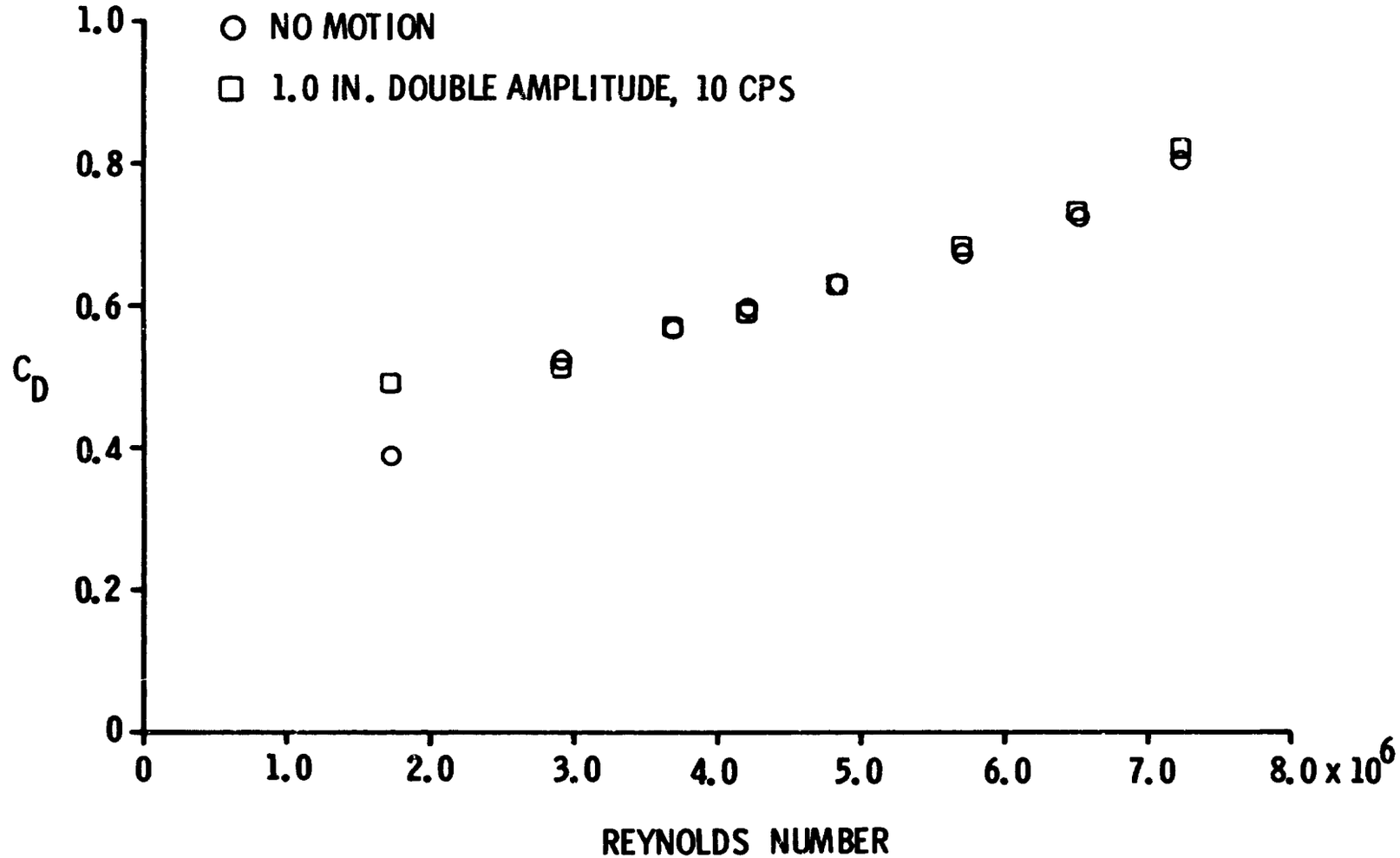

Fig. 8.

CHARACTERISTIC FUNCTIONS OF UNSTEADY AERODYNAMIC LIFT FORCE IN THE SUPERCRITICAL REYNOLDS NO. RANGE

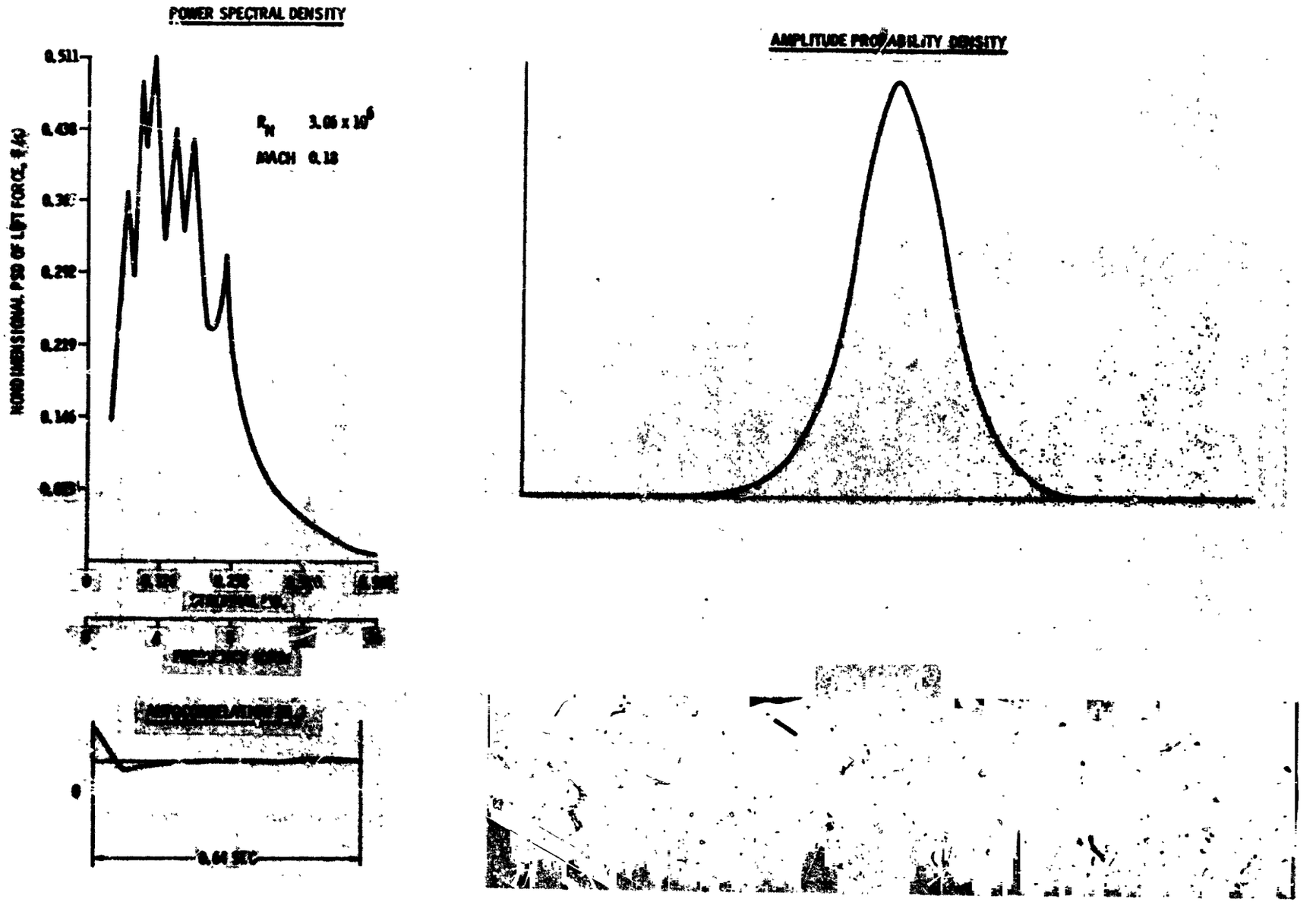

Fig. 9.

CHARACTERISTIC FUNCTIONS OF UNSTEADY AERODYNAMIC LIFT FORCE IN THE TRANSITION REYNOLDS NO. RANGE

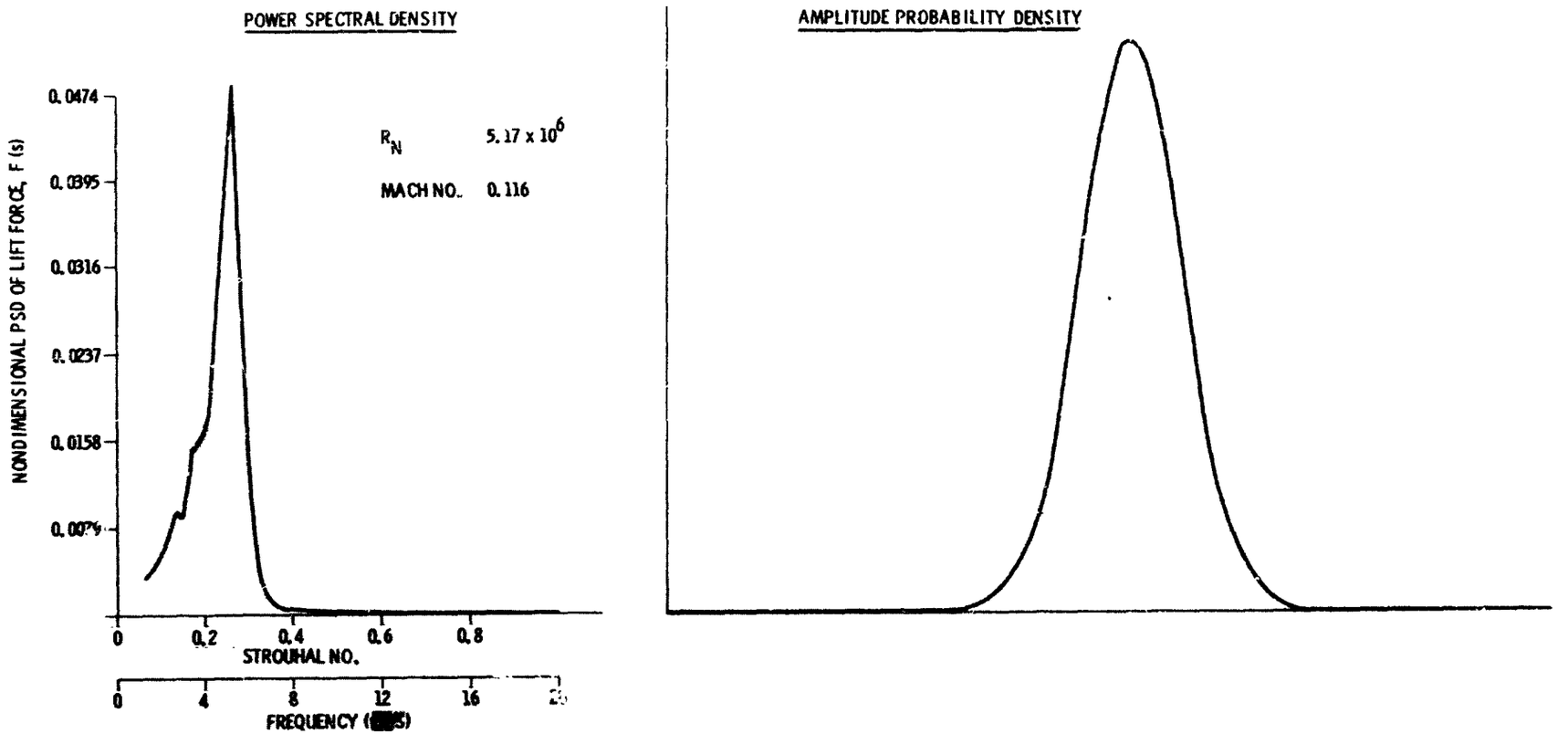

Fig. 10.

CHARACTERISTIC FUNCTIONS OF UNSTEADY AERODYNAMIC LIFT FORCE IN THE TRANSCRITICAL REYNOLDS NO. RANGE

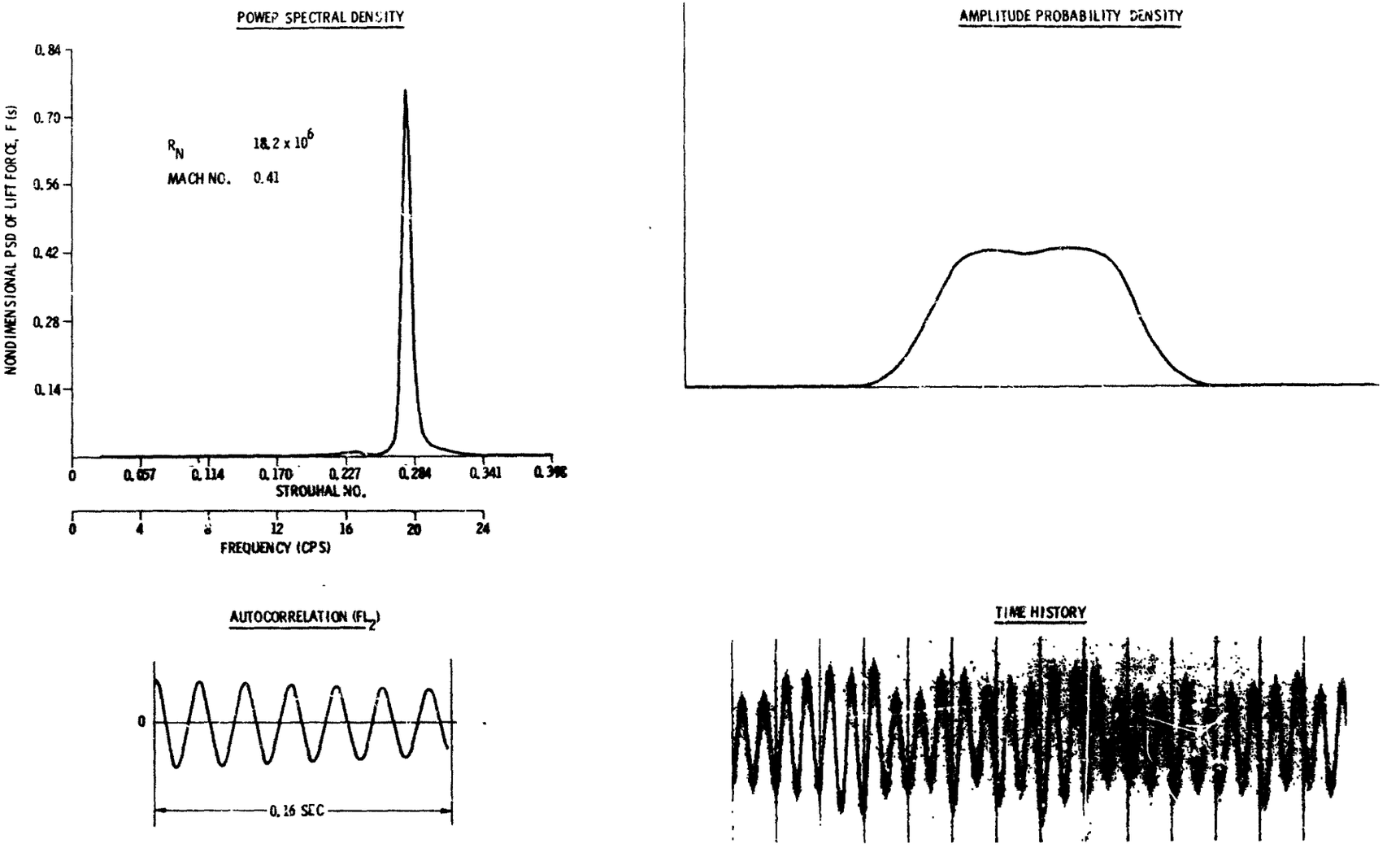

Fig. 12.

REYNOLDS NUMBER VARIATION OF THE AERODYNAMIC STROUHAL NUMBER BAND WIDTH AT THE HALF POWER POINTS OF THE P.S.D., MACH NO $\leq$ 0.3, STATIONARY MODEL

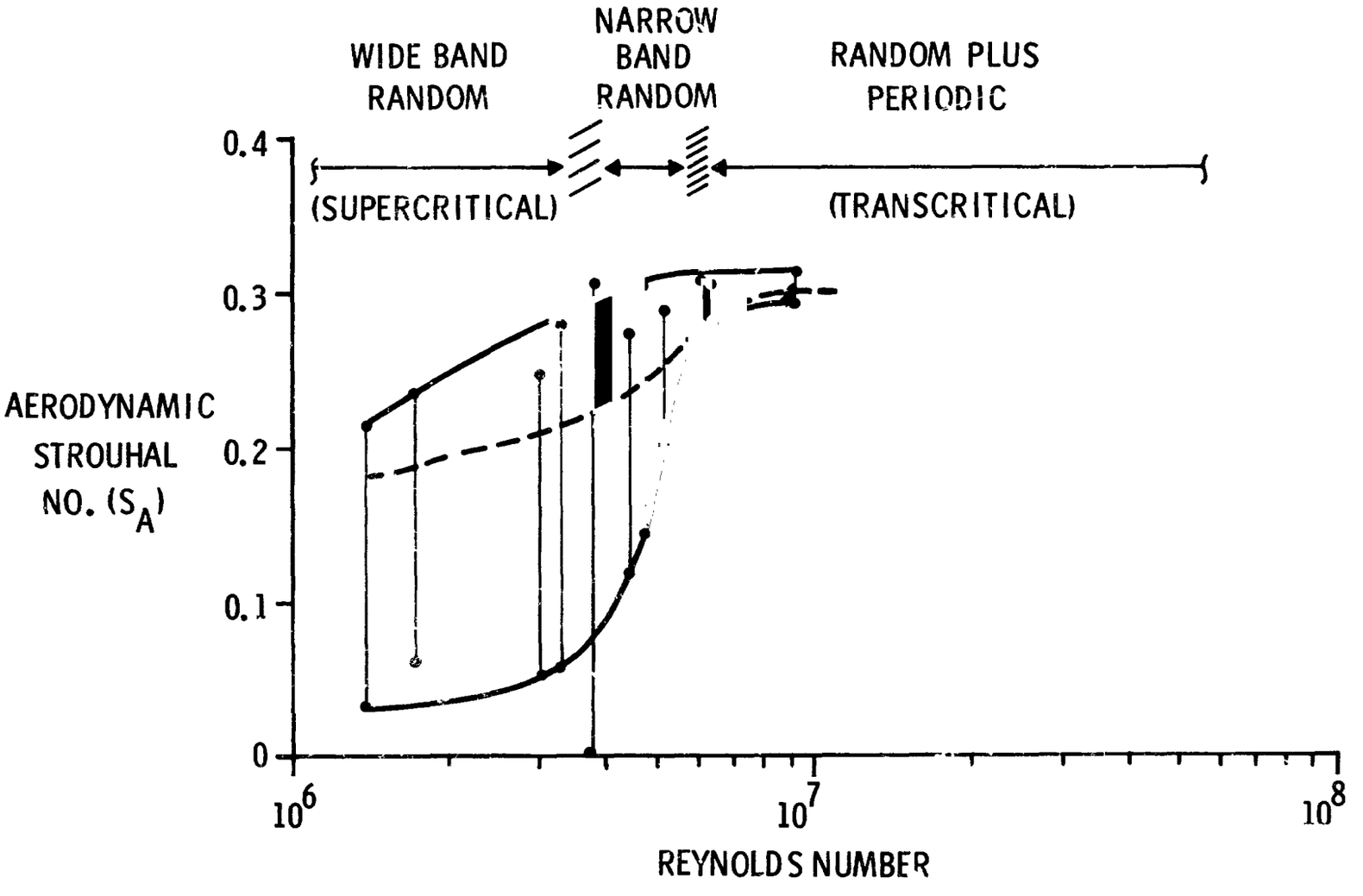

Fig. 12.

REYNOLDS NUMBER VARIATION OF THE AERODYNAMIC STROUHAL NUMBER BAND WIDTH AT THE HALF POWER POINTS OF THE PSD, STATIONARY MODEL

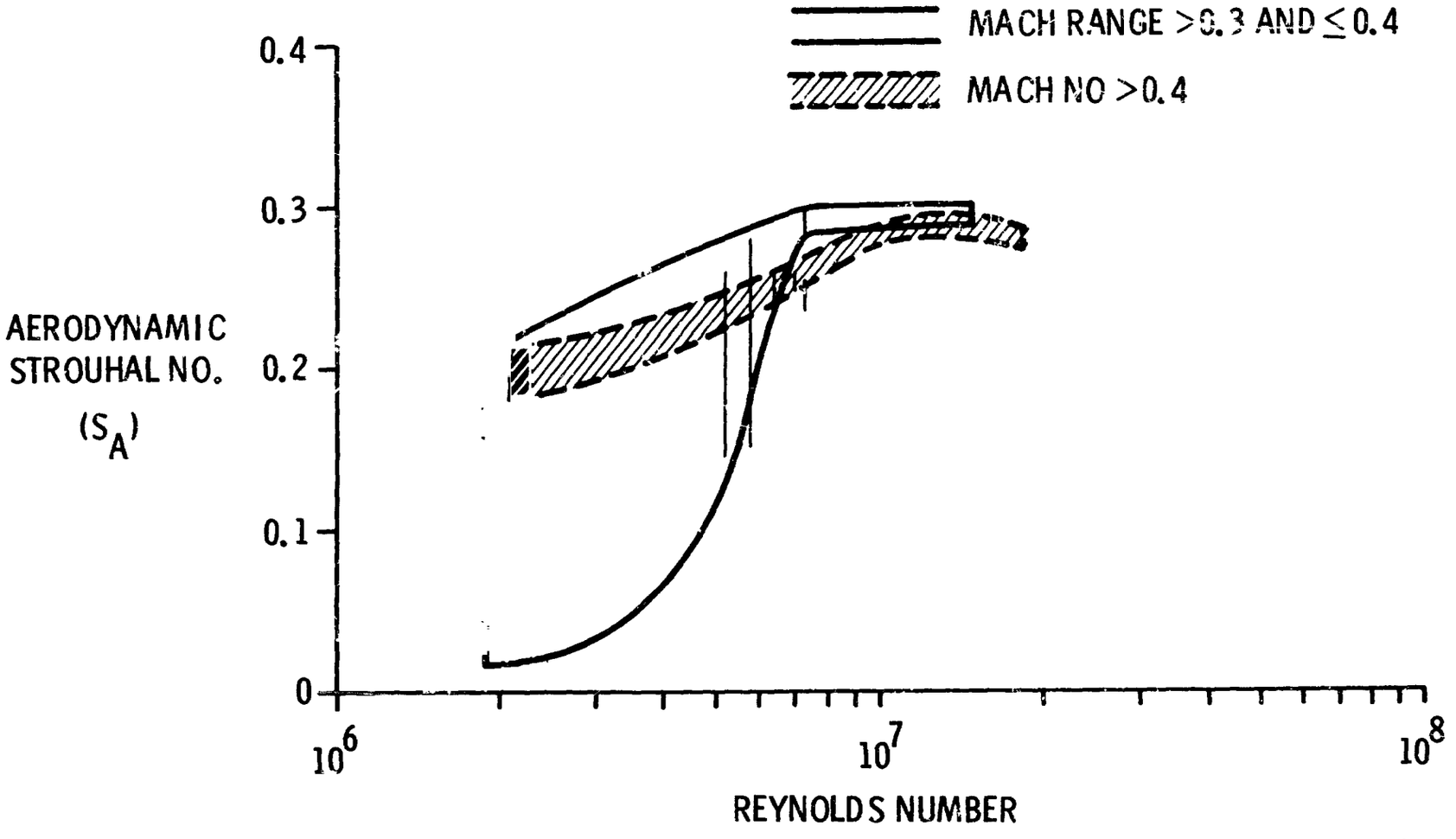

Fig. 13.

STATIONARY MODEL LIFT COEFFICIENT VARIATION AS A FUNCTION OF MACH NUMBER FOR ATMOSPHERIC FREON TEST MEDIA

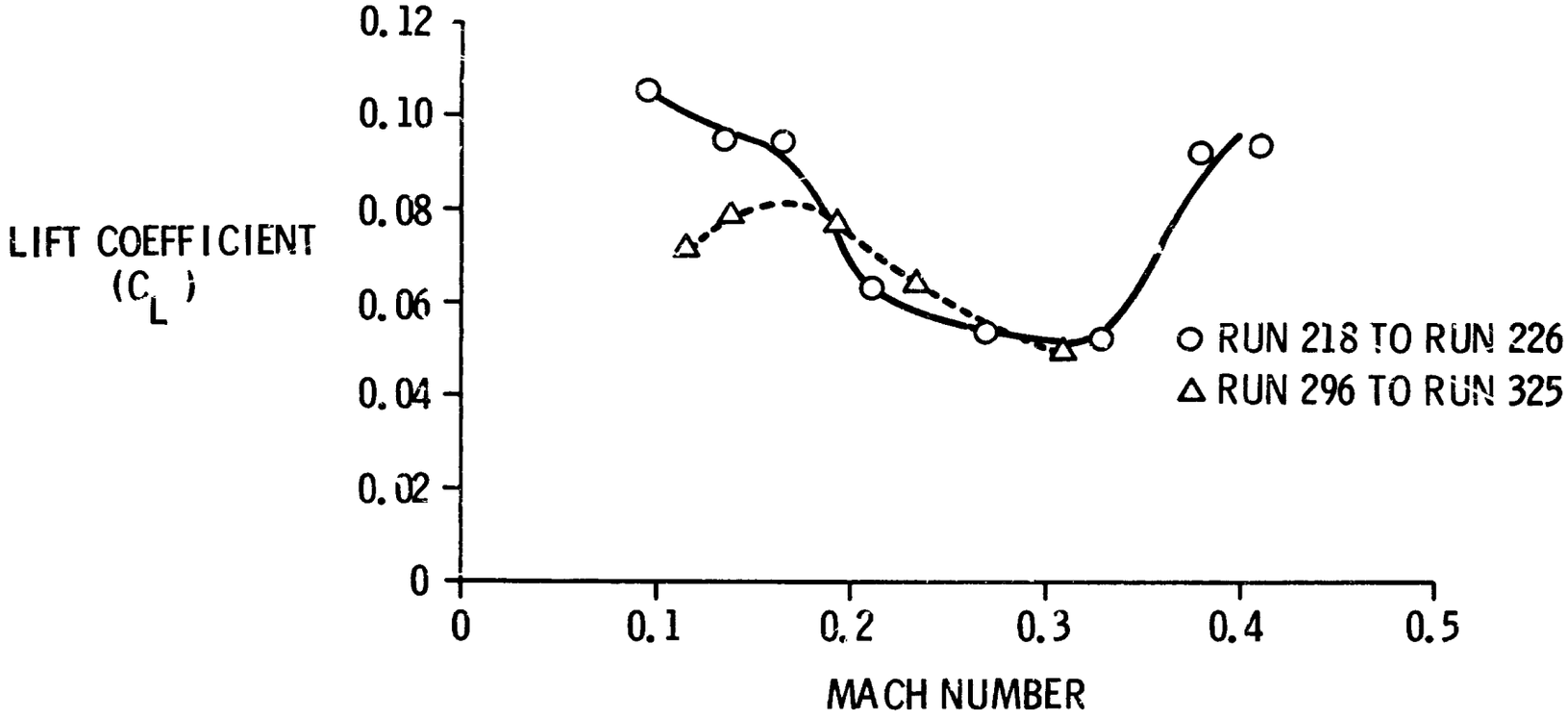

Fig. 14.

OIL FLOW PHOTOGRAPHS ILLUSTRATING MEAN SEPARATION LINE CHARACTERISTICS FOR THE BIFURCATED DATA AT CONSTANT REYNOLDS NUMBER OF 5.7×10^6

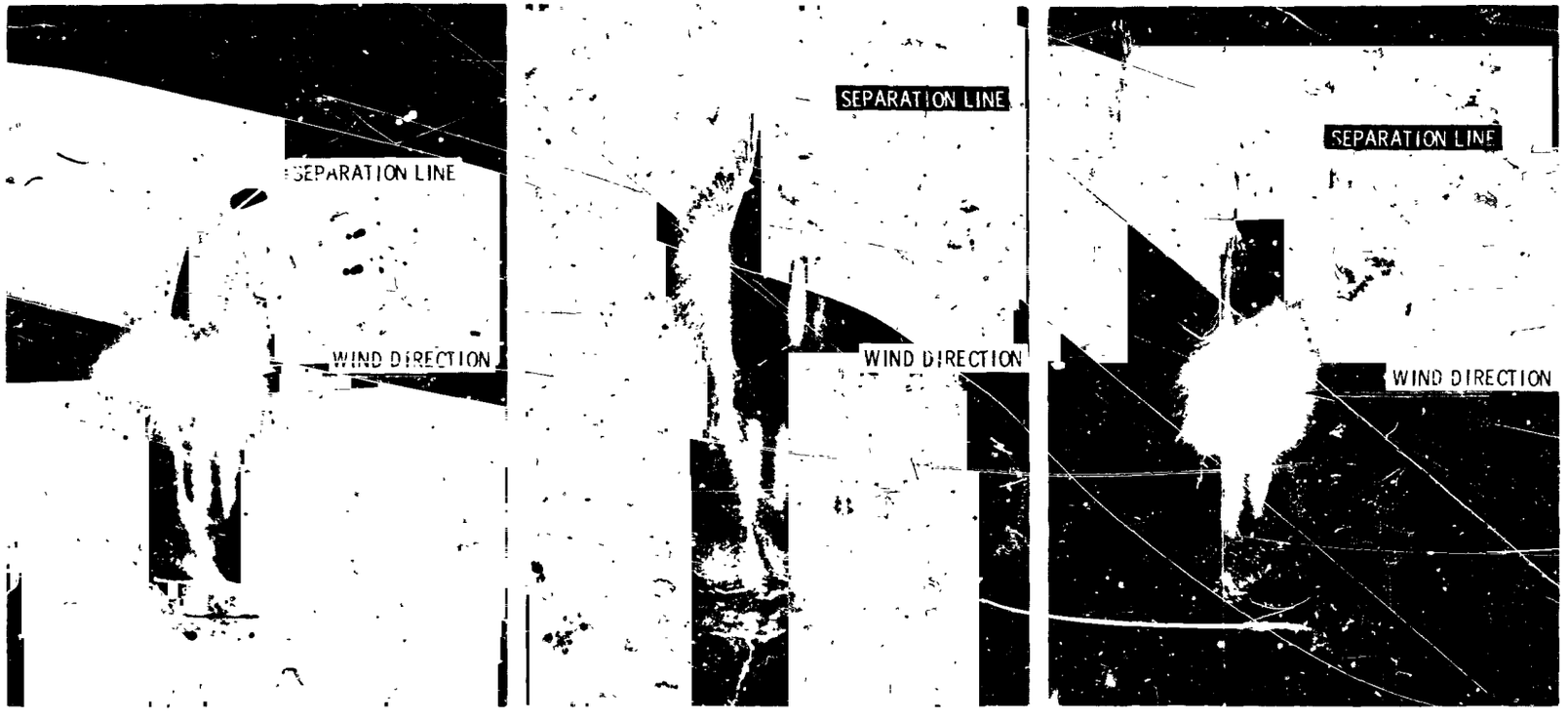

OPEN GAP-- UPPER BRANCH (a)

SEALED GAP--UPPER BRANCH (b)

OPEN GAP--LOWER BRANCH (c)

Fig. 15.

REYNOLDS NUMBER VARIATION OF UNSTEADY AERO- DYNAMIC LIFT COEFFICIENT FOR VARIOUS MACH NUMBERS, STATIONARY MODEL

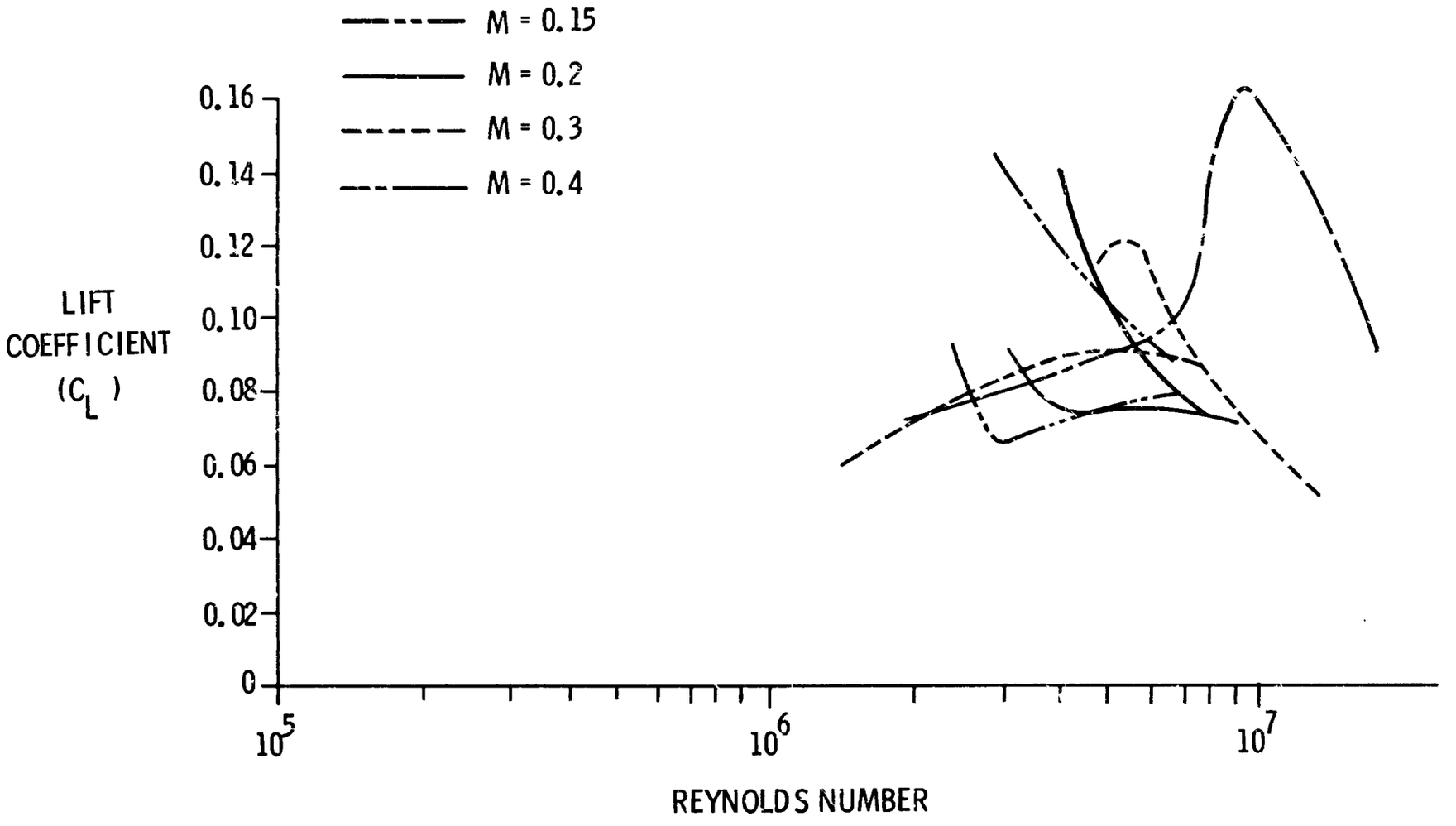

Fig. 16.

MODEL AMPLITUDE EFFECTS, RANDOM PLUS PERIODIC REYNOLDS NO. RANGE

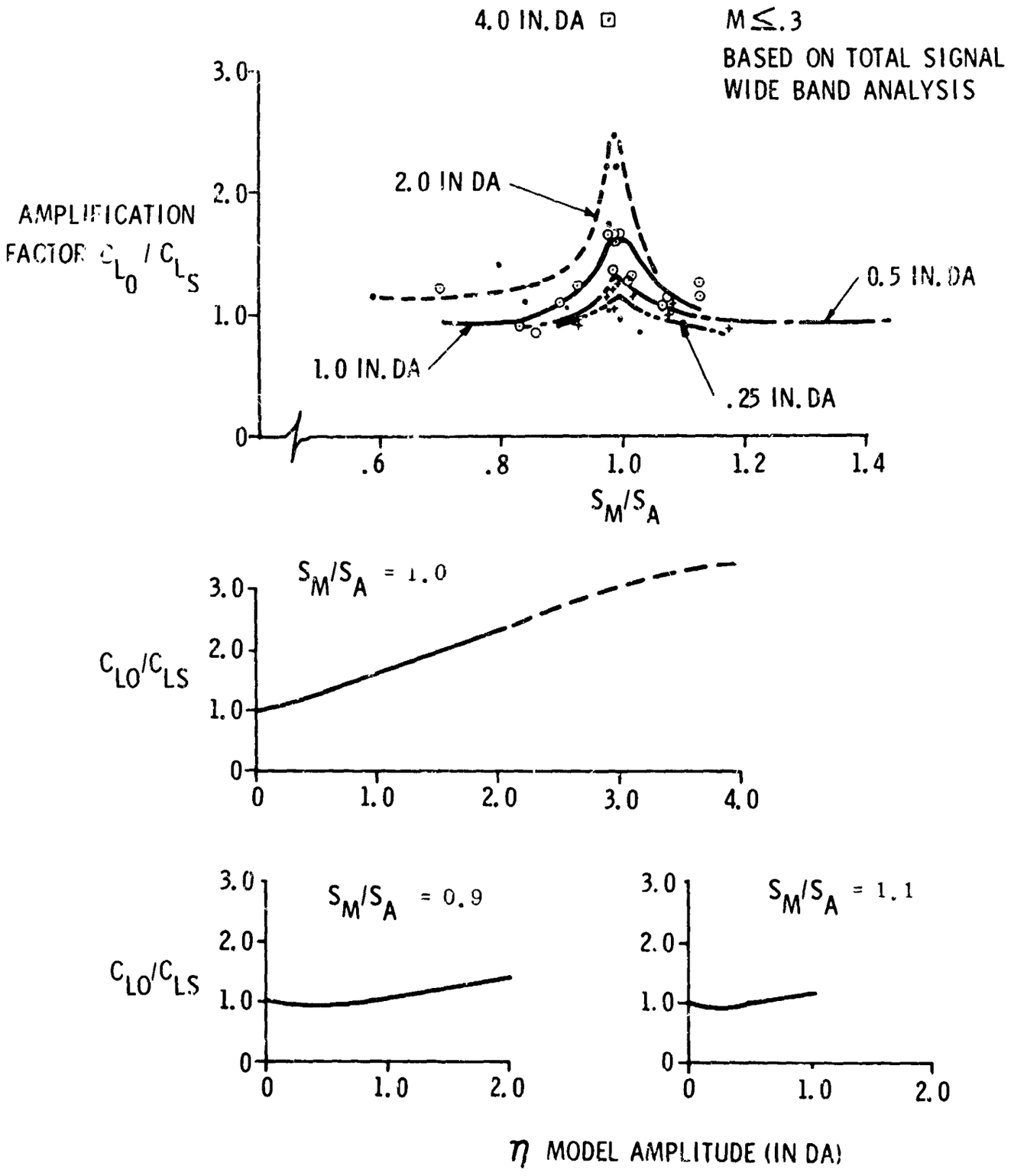

Fig. 17.

COMPONENTS OF UNSTEADY LIFT COEFFICIENT IN RANDOM PLUS PERIODIC REYNOLDS NUMBER RANGE

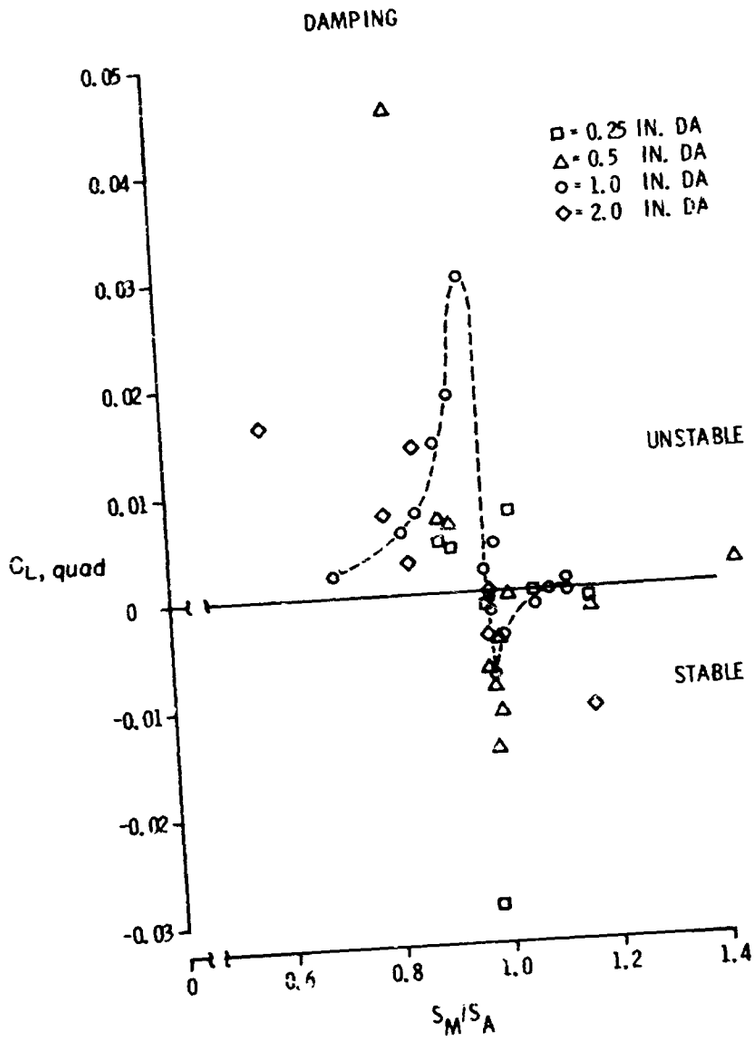

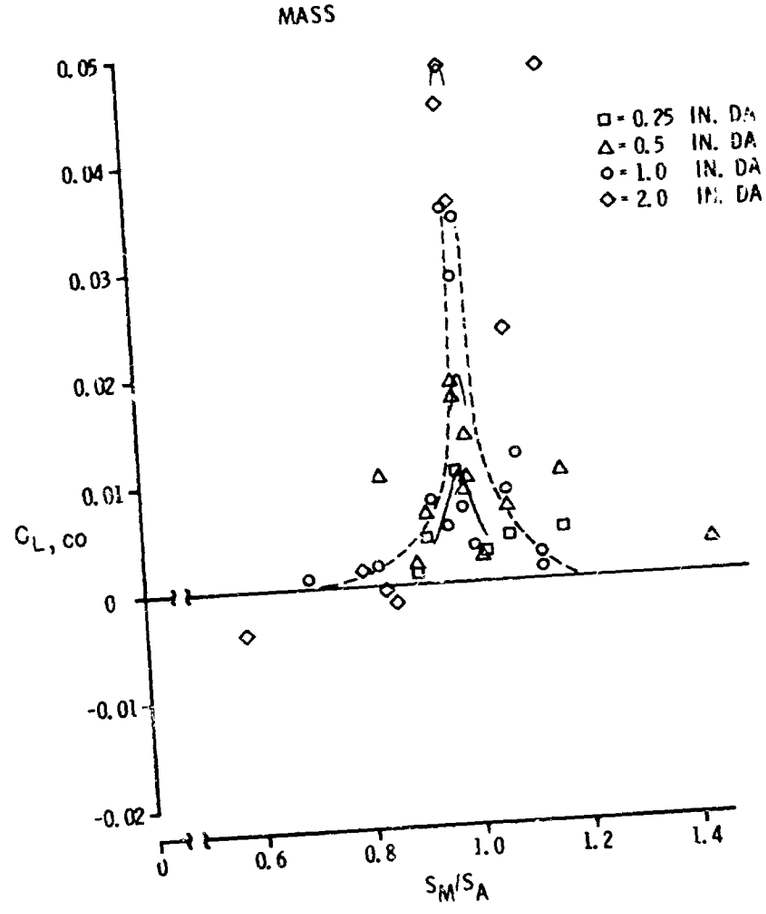

Fig. 18.

THEORY OF THE RESPONSE OF A SLENDER VERTICAL STRUCTURE TO A TURBULENT WIND WITH SHEAR‡

by

Bernard Etkin+

For presentation at NASA Conference on Wind Loads on Launch Vehicles - Langley Research Center, June 7, 8, 1966

+ Professor of Aerospace Engineering, Institute for Aerospace Studies, University of Toronto

‡ This theory was developed in 1961/62 and was used in lectures at Toronto, but has not previously been published in any form.

ABSTRACT

A theory is given for calculating the response spectra of a vertical structure exposed to a horizontal turbulent wind. The method of nodal representation is used to lead to spectra and cross-spectra of the driving forces for the different modes. The mean wind and the turbulence properties are both allowed to be functions of height to allow for wind shear. The result is in the form of double integrals for the relevant spectra, which can be evaluated readily by numerical integration when the appropriate data for the wind and the structure are available.

SYMBOLS

b	local width of structure
C_d	local drag coefficient
$f_1(x)$	Eq. (3)
$f_2(x)$	Fq. (4)
$\mathcal{F}_n(t)$	generalized force in nth mode
$F_n(x)$	shape of nth mode
$g_n(x)$, $h_n(x)$	Eq. (18)
$G(i\omega)$	transfer function
I_n	Eq. (15)
k	local additional mass coefficient
$q_n(t)$	tip deflection of nth mode
$R(\tau)$	correlation function
t	time
$u(x, t)$	horizontal wind velocity
$\bar{u}(x)$	time average of u at fixed x
$u'(x, t)$	local relative velocity
$v(x, t)$	turbulent component of u
$w(x, t)$	fluctuating part of W
$w'(x, t)$	part of w associated with the turbulence
$W(x, t)$	load on structure, force per unit length
$\bar{W}(x)$	time average of W at fixed x
x	vertical coordinate
$y(x, t)$	fluctuating part of Y
$Y(x, t)$	total deflection of structure

$\overline{Y}(x)$	time average of Y at fixed x
α, β	dummy variables of integration, denoting position on x axis
$\phi(\omega)$	spectrum function
ρ	air density
ω	circular frequency, rad/sec
ω_n	undamped natural frequency of nth mode
ζ_n	damping coefficient of nth mode

I. PRELIMINARIES

The following analysis treats that component of the motion of a vertical 'line-like' structure that results from the fluctuating drag associated with random inhomogeneous turbulence. The cross-wind motion associated with the lateral components of the turbulence is much smaller and can be treated by an essentially similar analysis. The cross-wind motion associated with vortex shedding may be of prime importance, but the spike-like nature of the driving spectrum makes the details rather different. It is not specifically dealt with here, but it could of course be handled by the same general method.

Figure 1 shows the situation. $\bar{u}(x)$ is the mean wind profile, and $v(x, t)$ is the fluctuating component in the direction of the mean wind. $\bar{Y}(x)$ is the mean deflection of the structure associated with $\bar{u}(x)$, and $y(x, t)$ is the vibrational motion associated with $v(x, t)$. The local running load on the structure is $W(x, t)$, of which $\bar{W}(x)$ is the mean, and $w(x, t)$ the fluctuating part. Thus

$$\begin{aligned} u(x,t) &= \bar{u}(x) + v(x,t) && \text{(a)} \\ W(x,t) &= \bar{W}(x) + w(x,t) && \text{(b)} \\ Y(x,t) &= \bar{Y}(x) + y(x,t) && \text{(c)} \end{aligned} \qquad (1)$$

and the 'relative wind' is

$$u'(x,t) = u(x,t) - \dot{y}(x,t) \qquad \text{(d)}$$

Assumption 1 : The local load $W(x, t)$ per unit length is given by 'strip theory', i.e.

$$W(x,t) = f_1(x)\,(u')^2 + f_2(x)\,\dot{u}' \qquad (2)$$

where

$$f_1(x) = C_d(x)\,b(x)\,\frac{\rho}{2} \qquad (3)$$

$$f_2(x) = k(x)\,b^2(x)\,\rho \qquad (4)$$

Here $b(x)$ is the width of the structure normal to the stream, $C_d(x)$ is the local steady-flow drag coefficient, and $k(x)$ is the so called 'additional mass coefficient' that gives the force associated with rate of change of the relative wind. For a flat plate of width b and a cylinder of diameter b the value of k given by ideal incompressible fluid theory is $\pi/4$. This should give a good indication of the order of magnitude of k.

The implication of equations (2) to (4), as used subsequently, is that C_d and k are themselves independent of the turbulence. It is not necessary however to assume independence of the shear of the wind, or

of end effects of the structure. If these can be calculated or measured, the appropriate values of C_d and k can be used in the formulae. The simplest assumption would be to use C_d and k appropriate to an infinitely long structure in a uniform wind. The assumption that these coefficients are independent of the turbulence implies that the lateral dimension b is small compared to the significant lateral wave-lengths of the turbulence. These in turn are determined by the natural frequencies of the structure. It is probably a good assumption for many practical cases. When it fails, the effect of reduced lateral correlation over the width of the structure could still be accounted for by a reduction in C_d and k.

II. FLUCTUATING LOAD

It follows from (2), (3), (4) and (1d) that

$$W(x,t) = f_1(x)\left[u^2 - 2u\dot{y} + \dot{y}^2\right] + f_2(x)\left[\dot{u} - \ddot{y}\right] \tag{5}$$

In order to find the fluctuating part of W, we first find its time average:

$$\overline{W}(x) = f_1(x)\left(\overline{u^2} - 2\overline{u\dot{y}} + \overline{\dot{y}^2}\right) + f_2(x)\left(\overline{\dot{u}} - \overline{\ddot{y}}\right) \tag{6}$$

Since u and y remain finite, it follows easily that $\overline{\dot{u}}$ and $\overline{\ddot{y}}$ are both zero. The mean of $u\dot{y}$ is

$$\overline{u\dot{y}} = \overline{(\bar{u} + v)\,\dot{y}} = \bar{u}\,\overline{\dot{y}} + \overline{v\dot{y}} = \overline{v\dot{y}}$$

Hence

$$\overline{W}(x) = f_1(x)\left(\overline{u^2} - 2\overline{v\dot{y}} + \overline{\dot{y}^2}\right) \tag{7}$$

On subtracting (7) from (5) we get the fluctuating load

$$w(x,t) = f_1(x)\left[(u^2 - \overline{u^2}) - 2u\dot{y} + 2\,\overline{v\dot{y}} + \dot{y}^2 - \overline{\dot{y}^2}\right] + f_2(x)\left(\dot{u} - \ddot{y}\right) \tag{8}$$

Assumption 2: Linearization

We assume that the turbulence and the unsteady motion of the structure are both small enough that the second order terms in v and $\dot{y}$ can be neglected. This is an approximation the consequences of which should be critically explored; however, in the absence of better data on the turbulence and on the coefficients C_d and k, it is probably justified. With these approximations, (8) becomes

$$w(x,t) = f_1(x)\left(2\bar{u}v - 2\,\bar{u}\,\dot{y}\right) + f_2(x)\left(\dot{v} - \ddot{y}\right) \tag{9}$$

or

$$w(x,t) = 2f_1(x)\,\bar{u}(x)\,v(x,t) + f_2(x)\,\dot{v}(x,t) - 2f_1(x)\,\bar{u}(x)\,\dot{y}(x,t) - f_2(x)\,\ddot{y}(x,t) \tag{10}$$

It should be noted that the last two terms on the r. h. s. of (10) are not dependent on the turbulence, but only on the mean wind and the motion of the structure. $f_2\ddot{y}$ is an 'aerodynamic interia' term, and $2f_1\bar{u}\dot{y}$ is the 'aerodynamic damping'. Hence they would be present in a vibration taking place in a steady laminar flow. We use this fact below in calculating the response to turbulence. The load associated with the turbulence is then

$$w'(x, t) = 2f_1(x)\,\bar{u}(x)\,v(x, t) + f_2(x)\,\dot{v}(x, t) \tag{11}$$

III. MODAL REPRESENTATION

Let the displacement of the structure be expanded in the normal modes of vibration, not in a vacuum, but in the presence of the steady non-uniform $\bar{u}(x)$. Thus the turbulence terms v and $\dot{v}$ are absent from the associated autonomous equations of motion. The displacement from the mean position is then

$$y(x, t) = \sum_{n=1}^{\infty} F_n(x)\; q_n(t) \tag{12}$$

where $F_n(x)$ are the above mode shapes and $q_n(t)$ are the generalized coordinates. The equations of motion in the absence of turbulence are then

$$\ddot{q}_n + 2\zeta_n \omega_n \dot{q}_n + \omega^2_n q_n = 0\ ,\ n = 1 \text{ to } \infty \tag{13}$$

where ζ_n is the total damping coefficient, structural and aerodynamic, and ω_n^2 is the undamped natural frequency of the nth mode. The usual methods of the theory of beam vibration must be used to find the functions $F_n(x)$ and the values of ω_n and ζ_n--this topic is not treated herein--we assume they are known.

When turbulence is present, the non-autonomous systems of equations is

$$\ddot{q}_n + 2\zeta_n \omega_n \dot{q}_n + \omega_n^2 q_n = \mathcal{F}_n(t)/I_n \tag{14}$$

where $\mathcal{F}_n$ is the generalized force associated with the turbulent input, and I_n is the generalized inertia in the nth mode

$$I_n = \int_0^{\ell} F_n^2(x)\; m'(x)\, dx \tag{15}$$

and $m'(x)$ is the mass per unit length. $\mathcal{F}_n$ is calculated from the work done δW during a virtual displacement δq_n,

$$\mathcal{F}_n = \frac{\partial(\delta W)}{\partial(\delta q_n)} \tag{16}$$

The work on each element is of course the product of the turbulent aerodynamic load and the displacement, thus

$$\delta W = \int_0^\ell w'(x,t)\ \delta y(x,t)\,dx$$

$$= \int_0^\ell w'(x,t)\ \sum_1^\infty F_n(x)\ \delta q_n(t)\,dx$$

and $$\mathcal{F}_n = \frac{\partial(\delta W)}{\partial(\delta q_n)} = \int_0^\ell w'(x,t)\ F_n(x)\,dx \qquad (17)$$

or, after substitution of (11)

$$\mathcal{F}_n(t) = \int_0^\ell g_n(x)\ v(x,t)dx + \int_0^\ell h_n(x)\ \dot{v}(x,t)\,dx \qquad (a) \qquad (18)$$

where

$$g_n(x) = 2\bar{u}(x)\ f_1(x)\ F_n(x) \qquad (b)$$

$$h_n(x) = f_2(x)\ F_n(x) \qquad (c)$$

IV. SPECTRAL ANALYSIS

Before proceeding to the next step, the relevant spectral relations should be noted. Figure 2 shows the way in which the individual modes are excited, and contribute to the total deflection y. The spectral density of y is given by the fundamental equation

$$\phi_{yy}(x,\omega) = \sum_m \sum_n F_m(x)\ G^*_m(-i\omega)\ F_n(x)\ G_n(-i\omega)\ \phi_{\mathcal{F}_m \mathcal{F}_n}(\omega) \qquad (19)$$

In this equation, $\phi_{\mathcal{F}_m \mathcal{F}_n}(\omega)$ is the cross-spectral density of $\mathcal{F}_m(t)$ and $\mathcal{F}_n(t)$; $G_n(-i\omega)$ is the transfer function relating $q_n(t)$ to $\mathcal{F}_n(t)$, and $(\ )^*$ indicates the complex conjugate. $G_n(i\omega)$ is found from the equations of motion (14) as

$$G_n(i\omega) = \frac{1}{I_n(\omega_n^2 - \omega^2 + 2i\zeta_n\omega_n\omega)} \qquad (20)$$

The spectrum function $\phi_{yy}(x,\omega)$ is the basic information needed to assess the behaviour of the structure. From it the mean square deflections and stresses can be calculated, as well as their probability distributions.

It is evident that to calculate the spectral density of y, we require all the cross-spectra and power spectra of the $\mathcal{F}$'s. In practise, it is likely that only a few of the power spectra (m = n) associated with the lower modes will be needed, and the assumption that the cross-spectra (m ≠ n) are unimportant is probably also justified. However in the interest of completeness, we treat the general case below. To obtain the general spectrum functions for the driving forces in terms of the turbulence spectra, we proceed via the correlation function, i. e.

$$\phi_{\mathcal{F}_m \mathcal{F}_n}(\omega) = \int_{-\infty}^{\infty} R_{mn}(\tau)\, e^{-i\omega\tau}\, d\tau \qquad (21)$$

where $R_{mn}(\tau) = \langle \mathcal{F}_m(t)\ \mathcal{F}_n(t+\tau) \rangle$ (22)

is the cross correlation of $\mathcal{F}_m$ and $\mathcal{F}_n$ ‡.

We now return to (18) to calculate the cross correlation. On forming the appropriate product of $\mathcal{F}$'s, and noting that the order of integration and averaging can be interchanged, we get (where α & β are dummy variables of integration, and ℓ is the height of the structure):

$$\begin{aligned} R_{mn}(\tau) = & \int_0^{\ell}\int g_m(\alpha)\, g_n(\beta) \langle v(\alpha, t).\, v(\beta, t+\tau) \rangle\, d\alpha d\beta \\ & + \int_0^{\ell}\int h_m(\alpha)\, h_n(\beta) \langle \dot{v}(\alpha, t).\, \dot{v}(\beta, t+\tau) \rangle\, d\alpha d\beta \\ & + \int_0^{\ell}\int g_m(\alpha) h_n(\beta) \langle v(\alpha, t).\, \dot{v}(\beta, t+\tau) \rangle\, d\alpha\, d\beta \\ & + \int_0^{\ell}\int h_m(\alpha) g_n(\beta) \langle \dot{v}(\alpha, t).\, v(\beta, t+\tau) \rangle\, d\alpha\, d\beta \end{aligned} \qquad (23)$$

But the mean products in these integrals are themselves cross-correlations, so that, with an obvious notation,

$$R_{mn}(\tau) = \int_0^{\ell}\int g_m(\alpha) g_n(\beta)\, R_{vv}(\alpha, \beta, \tau)\, d\alpha d\beta$$

(Eq. 24 is continued on next page)

‡ The symbol $\langle\ \rangle$ denotes an ensemble average, which in the present circumstances is equal to the time average.

$$+ \int_0^{\ell}\int h_m(\alpha)h_n(\beta)\ R_{\dot{v}\dot{v}}(\alpha,\beta,\tau)\,d\alpha\,d\beta$$

$$+ \int_0^{\ell}\int g_m(\alpha)h_n(\beta)\ R_{v\dot{v}}(\alpha,\beta,\tau)\,d\alpha\,d\beta$$

$$+ \int_0^{\ell}\int h_m(\alpha)g_n(\beta)\ R_{\dot{v}v}(\alpha,\beta,\tau)\,d\alpha\,d\beta \qquad (24)$$

As indicated in (21) we now take the Fourier transform of (24) to get the required spectrum functions. The integration with respect to τ may be performed first, so the result is

$$\phi_{\mathcal{F}_m\mathcal{F}_n}(\omega) = \int_0^{\ell}\int g_m(\alpha)g_n(\beta)\ \phi_{vv}(\alpha,\beta,\omega)\,d\alpha\,d\beta$$

$$+ \int_0^{\ell}\int h_m(\alpha)h_n(\beta)\ \phi_{\dot{v}\dot{v}}(\alpha,\beta,\omega)\,d\alpha\,d\beta$$

$$+ \int_0^{\ell}\int g_m(\alpha)h_n(\beta)\ \phi_{v\dot{v}}(\alpha,\beta,\omega)\,d\alpha\,d\beta$$

$$+ \int_0^{\ell}\int h_m(\alpha)g_n(\beta)\ \phi_{\dot{v}v}(\alpha,\beta,\omega)\,d\alpha\,d\beta \qquad (25)$$

Now the spectrum functions of the derivatives are given by

$$\phi_{\dot{v}\dot{v}} = \omega^2\,\phi_{vv} \qquad (a)$$

$$\phi_{\dot{v}v} = -i\omega\,\phi_{vv} \qquad (b) \qquad (26)$$

$$\phi_{v\dot{v}} = i\omega\,\phi_{vv} \qquad (c)$$

So the only spectrum function needed is $\phi_{vv}(\alpha,\beta,\omega)$ in order to evaluate all the terms in (25), which then becomes

$$\phi_{\mathcal{F}_m\mathcal{F}_n}(\omega) = \int_0^{\ell}\int \phi_{vv}(\alpha,\beta,\omega)\Big\{ g_m(\alpha)g_n(\beta) + \omega^2 h_m(\alpha)h_n(\beta) + i\omega\left(g_m(\alpha)h_n(\beta) - g_n(\beta)h_m(\alpha)\right)\Big\}\,d\alpha\,d\beta \qquad (27)$$

V. POWER SPECTRA

When m = n, the spectrum (27) becomes the power spectrum of v_n, and as such it must have no imaginary part. We now show that the imaginary part of $\phi_{v_n v_n}$ will indeed vanish. The cross correlation function for v is in general composed of parts that are even and odd in τ, i.e.

$$R_{vv}(\alpha, \beta, \tau) = R_1(\alpha, \beta, \tau) + R_2(\alpha, \beta, \tau) \tag{28}$$

where R_1 and R_2 are as in Fig. 3. The corresponding spectrum function is then

$$\phi_{vv}(\alpha, \beta, \omega) = \phi_1(\alpha, \beta, \omega) - i\,\phi_2(\alpha, \beta, \omega) \tag{29}$$

where, by (21)

$$\left.\begin{aligned} \phi_1 &= \int_{-\infty}^{\infty} R_1 \cos \omega\tau \; d\tau \\ \phi_2 &= \int_{-\infty}^{\infty} R_2 \sin \omega\tau \; d\tau \end{aligned}\right\} \tag{30}$$

Symmetry Properties of R_1, R_2, ϕ_1, ϕ_2

The cross-correlation of the turbulent velocity is

$$R_{vv}(\alpha, \beta, \tau) = \langle v(\alpha, t) \cdot v(\beta, t+\tau) \rangle$$

where α, β are two values of x, i.e. it is the mean product of two 'signals', the first being 'advanced' τ sec. relative to the second. Obviously, for statistically stationary processes, advancing the first signal is the same as delaying the second, so that interchanging the order is the same as changing the sign of τ, i.e.

$$R_{vv}(\alpha, \beta, \tau) = R_{vv}(\beta, \alpha, -\tau) \tag{31}$$

It follows that the even and odd parts of R have the reciprocity properties

$$\begin{aligned} R_1(\alpha, \beta, \tau) &= R_1(\beta, \alpha, \tau) \qquad \text{(a)} \\ R_2(\alpha, \beta, \tau) &= -R_2(\beta, \alpha, \tau) \qquad \text{(b)} \end{aligned} \tag{32}$$

The corresponding spectral relations are

$$\begin{aligned} \phi_1(\alpha, \beta, \omega) &= \phi_1(\beta, \alpha, \omega) \qquad \text{(a)} \\ \phi_2(\alpha, \beta, \omega) &= -\phi_2(\beta, \alpha, \omega) \qquad \text{(b)} \end{aligned} \tag{33}$$

We can now split the power spectrum integral conveniently into its real and imaginary parts, i. e.

$$\mathrm{Re}\,\phi_{f_n f_n}(\omega) = \int_0^{\ell}\int \Big\{ \phi_1(\alpha,\beta,\omega)\left[g_n(\alpha) g_n(\beta) + \omega^2 h_n(\alpha) h_n(\beta)\right] + \omega\,\phi_2(\alpha,\beta,\omega)\left[g_n(\alpha) h_n(\beta) - g_n(\beta) h_n(\alpha)\right]\Big\}\, d\alpha\, d\beta \tag{34}$$

$$\mathrm{Im}\,\phi_{f_n f_n}(\omega) = \int_0^{\ell}\int \Big\{ \omega\,\phi_1(\alpha,\beta,\omega)\left[g_n(\alpha) h_n(\beta) - g_n(\beta) h_n(\alpha)\right] - \phi_2(\alpha,\beta,\omega)\left[g_n(\alpha) g_n(\beta) + \omega^2 h_n(\alpha) h_n(\beta)\right]\Big\}\, d\alpha\, d\beta \tag{35}$$

Now consider these integrals over the α, β domain, illustrated in Fig. 4. Let the integral be evaluated by summing at pairs of elements (p, q) that are symmetric w. r. t. to the diagonal. Since (α, β) are interchanged at p and q, the following relations hold

$$\left.\begin{matrix} g_n(\alpha)\, g_n(\beta) \\ h_n(\alpha)\, h_n(\beta) \end{matrix}\right\} \text{at p} = \left\{\begin{matrix} g_n(\alpha)\ g_n(\beta) \\ h_n(\alpha)\ h_n(\beta) \end{matrix}\right. \text{at q} \tag{36}$$

These facts, together with the symmetry relations (33) for the ϕ, lead at once to the result that (35) vanishes as required and that

$$\phi_{f_n f_n}(\omega) = \text{r. h. s. (34)} \tag{37}$$

VI. REDUCTION FOR HOMOGENEOUS TURBULENCE

Equation (34) is the basic relation for calculating the power spectrum of the force driving the nth mode of vibration. The turbulence spectra ϕ_1 and ϕ_2 contained therein are seen to be functions of α and β separately. Now in homogeneous turbulence, ϕ is a function only of the separation of the two points in question, not of their individual locations, and moreover, the anti-symmetric component ϕ_2 vanishes, so that

$$\phi_{vv}(\alpha,\beta,\omega) = \phi_1(\alpha-\beta,\omega) \tag{38}$$

This property would ordinarily make the practical evaluation of the integral much simpler. Whether or not (34) can even then be integrated analytically depends very much on how complex the structure is, i. e. on the nature of the functions $C_d(x)$, $k(x)$, and $F_n(x)$. In any case, machine computation would seem entirely practical.

VII. SUMMARY

The theory given above permits the complete determination of the statistical properties of the stress and deflection of the structure from the following information.

Mean wind:	$\bar{u}(x)$
Turbulence:	$R_{vv}(\alpha, \beta, \tau)$ or $\phi_{vv}(\alpha, \beta, \omega)$
Structure Modes:	shape, $F_n(x)$ frequency, ω_n damping, ζ_n
Beam aerodynamics:	drag, $C_d(x)$ additional mass, $k(x)$

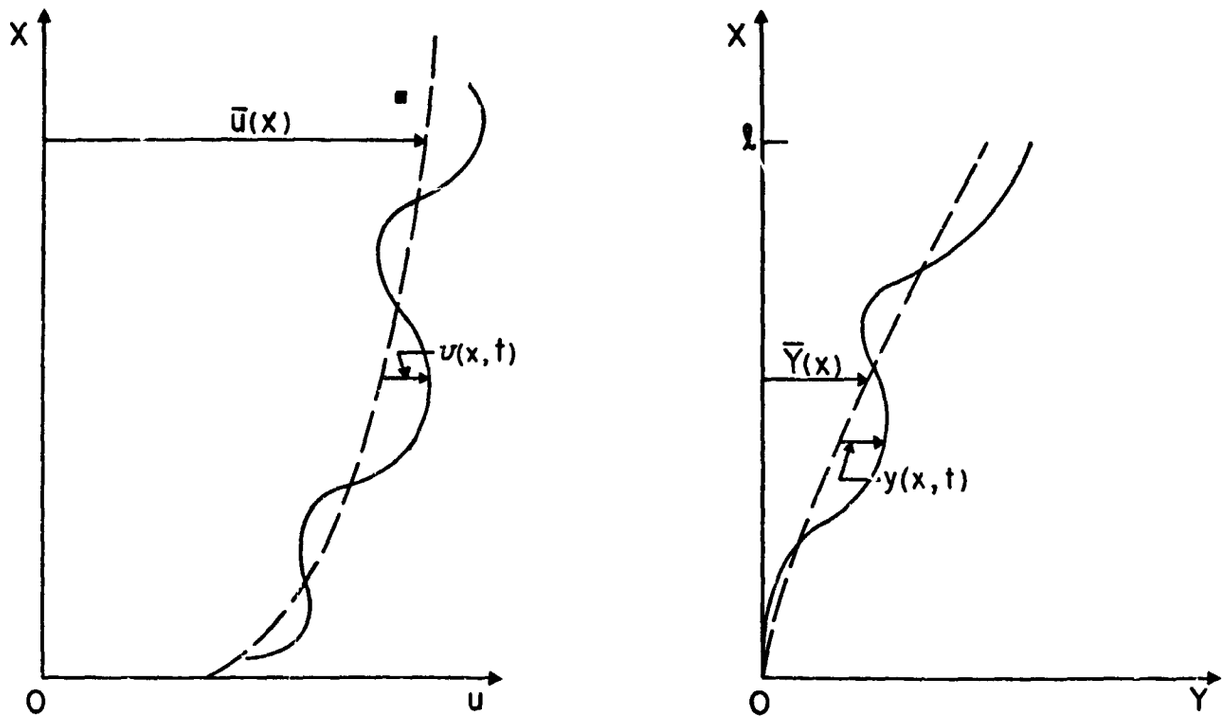

(a) Wind Profile

(b) Deflection Profile

FIG. 1

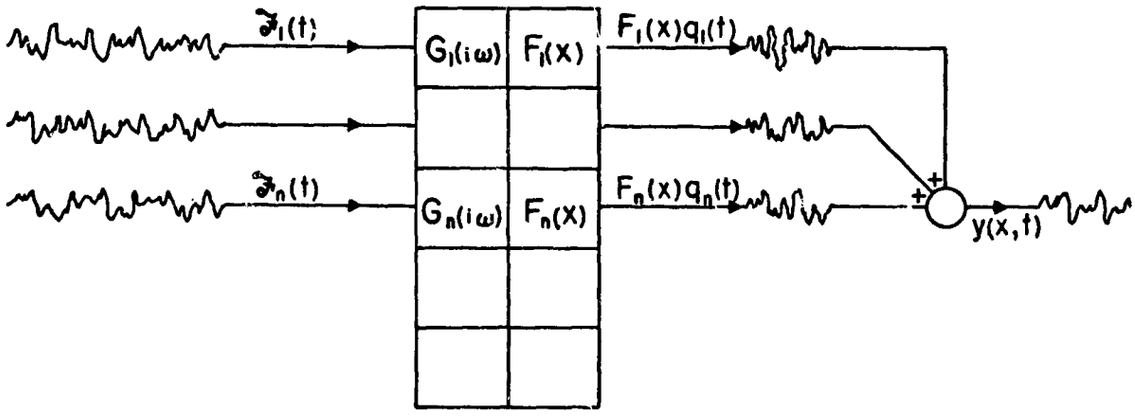

FIG. 2

Superposition of Model Responses

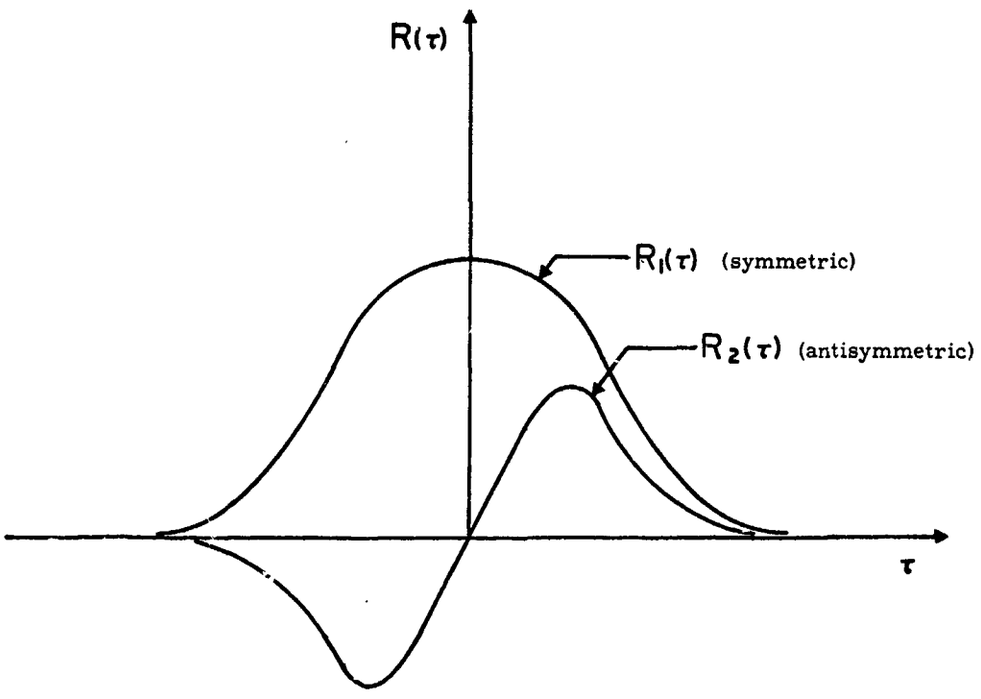

FIG. 3

Symmetric and Antisymmetric Components of R (τ)

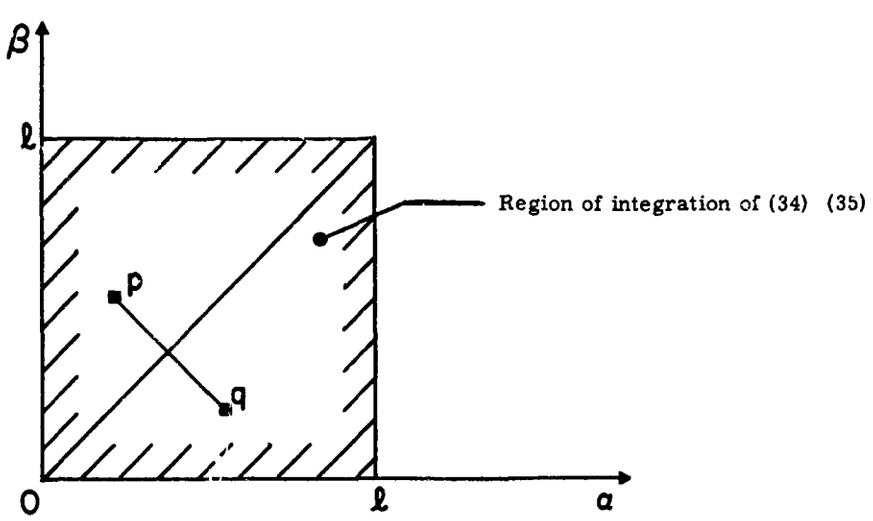

FIG. 4

Effects of Turbulence on Vortex Shedding from Circular Cylinders

by

M. Sevik

Department of Aeronautical Engineering

The Pennsylvania State University

THE EXPERIMENT

An experimental investigation is presently in progress at The Pennsylvania State University whose objective is to establish the effects of free stream turbulence on the characteristics of the time-dependent forces acting on circular cylinders.

Since this investigation is actually in progress no results can as yet be reported. This paper is, therefore, only intended to acquaint others in the field with the work presently going on at The Pennsylvania State University and to describe its background and practical importance as well as the experimental techniques which are being employed.

In the case of a rigid cylinder, the transfer function we seek to establish depends on the Reynolds number Re, on the intensity of the three space components of the turbulent velocity fluctuations $\frac{u_i}{U}$, on the ratio of a characteristic length scale of the flow to a characteristic dimension of the body L/D, on the spectral distribution of the turbulent energy ϕ, and on the ratio of the roughness of the cylinder surface e to the boundary layer thickness δ, i.e. the transfer function H depends on

$$H\left(Re, \frac{\sqrt{\overline{u_i^2}}}{U}, L/D, \phi, e/\delta\right).$$

The term "rigid" must now be more closely defined since vibrations of the test specimen will be inevitable. According to an argument by Owen[1] aeroelastic effects will be negligible if the acceleration of the fluid due to the motion of the cylinder

is very much smaller than that occuring past the boundaries of the cylinder at rest. This argument implies that

$$\frac{m\zeta}{\rho D^2} \gg \frac{U}{\omega D}$$

where m = generalized mass per unit length of cylinder

ζ = ratio of damping to critical damping

ρ = density of the medium

D = cylinder diameter

ω = frequency of oscillations.

Our experiments will cover a range of Reynolds numbers from 3×10^4 to 4×10^6. In order to achieve this range we shall utilize three cylinders, 2in, 4in and 6in diameter as well as two tunnels, namely a wind tunnel and a water tunnel.

The wind tunnel has a 48" dia test section and a maximum speed of 120 ft. sec^{-1}. The turbulence level is just under 0.3%. In this facility a range of Reynolds numbers from 3×10^4 to 5×10^5 will be covered. (Fig.1)

The water tunnel facility is in many respects a unique facility. (Fig.2) Its test section is 48in. in diameter by 14ft. long. Velocities up to 70ft sec^{-1} can be reached and the pressure in the test section can be varied from 3 to 60psia. By installing a fine mesh honeycomb in the settling section, the turbulence level can be reduced to 0.1%. In this facility a Reynolds number range from 4×10^5 to 4×10^6 can be covered.

Turbulence will be artificially introduced into the main stream by means of grids. The grids available for this purpose

all have a solidity ratio of 0.3. (Fig.3) Their mesh sizes are 2in, 4in, 6in, and 8in thus providing a mesh size to cylinder diameter ratio ranging from 4 to 1/3. During the tests the grids will each be placed at a constant multiple of their respective mesh size from the cylinder, thus producing the same intensity of turbulent fluctuations but varying length scales.

The turbulence will be varied from approximately 3% (for a length of 20M) to about 6% (for a length of 10M) although in the latter case there will be an unavoidable lack of isotropy and homogeneity in the turbulence. The test cylinders are made of brass and have a mirror finish. No variations of surface roughness are intended.

The required transfer function between the fluid flow and the forces acting on the cylinder will be measured by means of numerous pressure transducers. Two sections which can be moved relative to each other will be instrumented. The ratio of this distance to the cylinder diameter can be varied from 1/6 to 6 by means of inserts. (Fig.4)

Initially, the time-dependent pressures on a single plane of the cylinder will be measured. Twenty pressure transducers will be used for this purpose. In order to establish the instantaneous lift and drag forces the output of each transducer will be passed through a potentiometer and hence to a summing amplifier. (Fig.5) From a tape recording of the lift and drag, various periodic and random quantities will be calculated. The pressure transducers consist of Endevco type 2503 "turbulence"

gages. (Fig.6) They have a sensitivity of 120 mv/psi and accurately resolve dynamic pressures from 0.01 to 10 psi with no concurrent response static pressures. They have a linear response from 2cps to 10,000 cps with a 1,000 meg load. The maximum response to vibrations is 0.2 mv/g.

The transducers are mounted just under the exterior surface of the cylinder and are connected to the outside by means of an 0.031 in. dia. hole 0.06in long. The transfer function across such a hole is unity at least up to 500cps, which adequately covers the range of interest. Note that during the experiments transducer noise levels are established by covering the holes with tape while running the tunnel at test velocity.

ANTICIPATED BEHAVIOR

The influence of turbulence on launch vehicle loads is usually accounted for on a quasi-steady basis, i.e., the force at each instant of time is assumed to correspond to the instantaneous velocity and Reynolds number. This viewpoint is reasonable when the characteristic length of the turbulence is large compared with the vehicle diameter. In other cases the validity of this assumption is open to doubt, especially in the critical Reynolds number range.

Well-known experiments by Fage and Warsap[2] (1930) show the extreme sensitivity of the boundary layer to turbulence in the main stream in this Reynolds number range. At $R=10^5$, for instance, a turbulence level of only 2% or so changes the drag coefficient from 1.09 to 0.6 and, presumably, the characteristics of the wake as well. (Fig.7)

At other Reynolds numbers, the validity of the quasi-steady assumption may also be questioned. In some cases, the turbulence in the main stream may be so intense as to dominate the motion as, for instance deep inside the bank of tubes of a heat exchanger. Except for a general drift through the bank, the flow in this case exhibits no regular features.

However, even under less severe conditions of turbulence, the cylinder is known to be aerodynamically discriminating in its force response. The greatest influence would be expected to occur when the characteristic eddy size of the turbulence is of the same order of magnitude as the axial coherence length of eddies which naturally occur behind a cylinder in a steady stream. Some light on the problem might also be shed by Lighthill[3] (1953) who analyzed the unsteady flow over a two-dimensional arbitrary cylinder. His study is restricted to the case when the velocity very far from the cylinder is oscillating sinusoidally in magnitude, but not in direction, about a constant mean value. Only small amplitude oscillations were considered, so that non-linear interactions could be neglected.

Lighthill found that for each point along the cylinder there exists a critical frequency $\omega_0 = 0.6\ U/x$ (where x is measured along the surface from the stagnation point) such that for $\omega > \omega_0$ the oscillating motion in the boundary layer approximates "shear waves", unaffected by the mean flow. For frequencies $\omega < \omega_0$ the oscillations consist of 2 parts, one of which depends upon the instantaneous free stream velocity, the other on the acceleration.

Thus, the quasi-steady assumption implies that the frequency of oscillations is so low that the boundary layer at any instant of time will be that appropriate to the steady flow at the instantaneous value of the stream velocity. At higher frequencies, however, the redistribution of vorticity in the boundary layer will not be instantaneous. Departures from the quasi-steady state will occur at first differing only in phase and later also in amplitude. At higher frequencies still, the fluctuations of the boundary layer will resemble that appropriate to oscillating motions without a mean flow.

Although Lighthill's analysis applies to a laminar boundary layer Karlsson[4] (1958) found essentially the same behavior over a turbulent boundary layer on a flat plate, even when it was subjected to large fluctuations of the external flow.

Applying Lighthill's criterion, we find a critical L/D= 1.25, with x taken as the distance along the surface of the cylinder from the stagnation to the separation line. If L/D < 1.25 the fluctuations in the boundary layer near the separation region will resemble shear waves i.e., the steady boundary layer will be unaffected by the oscillations. These have a "depth of penetration" equal to

$$\sqrt{\frac{U}{2L\nu}}$$

which constitutes a very small fraction of the steady boundary layer thickness. Presumably the separation pattern is not affected by such waves (although we have no proof of this) and hence the

forces on the cylinder will not be affected by eddies whose size is smaller than about 1.25 D.

If L/D > 1.25, however, the entire boundary layer will be affected by the eddies and if the intensity of the turbulence is high enough, the separation pattern will be influenced.

The above-mentioned considerations--although entirely speculative at present--have been included in order to explain the choice of parameters for the experiments.

References

1. Owen, P. R., Buffeting excitation of boiler tube vibrations, Journal of Mechanical Engineering Science, Vol. 7, No. 4, Dec. 1965.

2. Fage and Warsap, A. R. C. Reports and Memoranda, No. 1283, 1930.

3. Lighthill, M. J., The response of laminar skin friction and heat transfer to fluctuations in the stream velocity, Proc. Roy. Soc. A, 224, I, 1954.

4. Karlsson, S. K. F., An unsteady turbulent boundary layer, Ph. D. Thesis, The Johns Hopkins University, 1958.

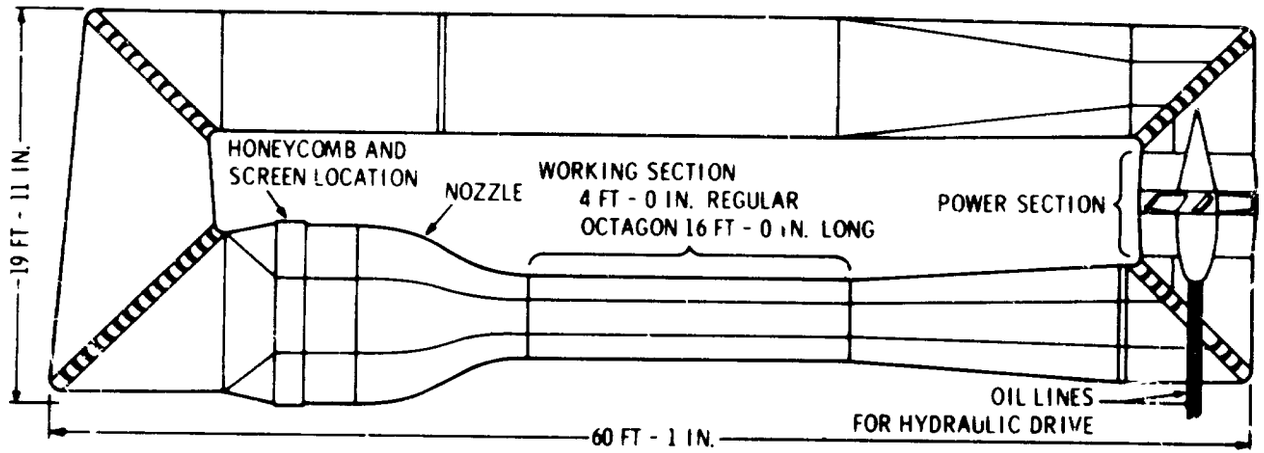

The Subsonic Wind Tunnel

FIG. 1

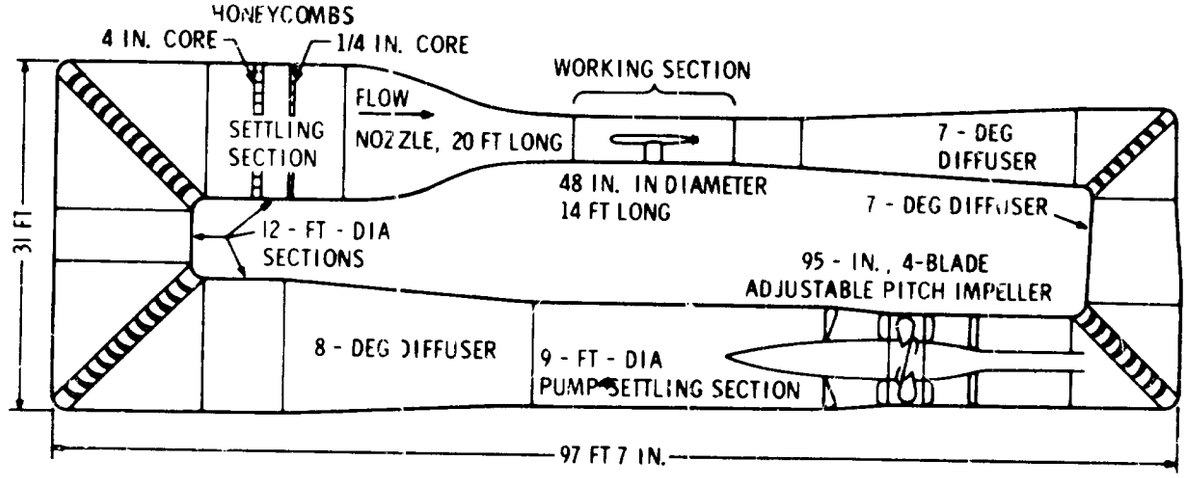

The 48-Inch Water Tunnel

FIG. 2

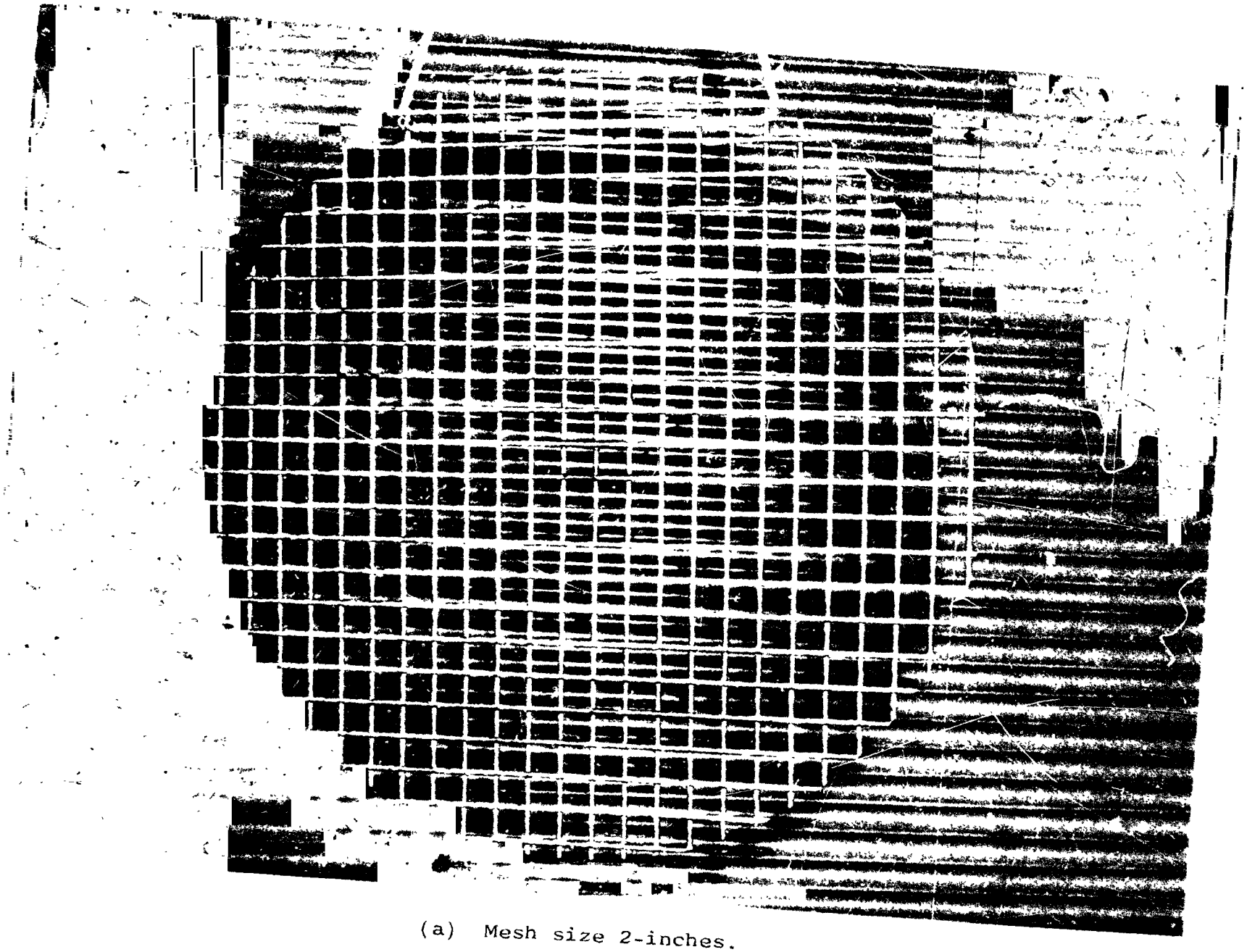

(a) Mesh size 2-inches.

Figure 3.- Turbulence grids.

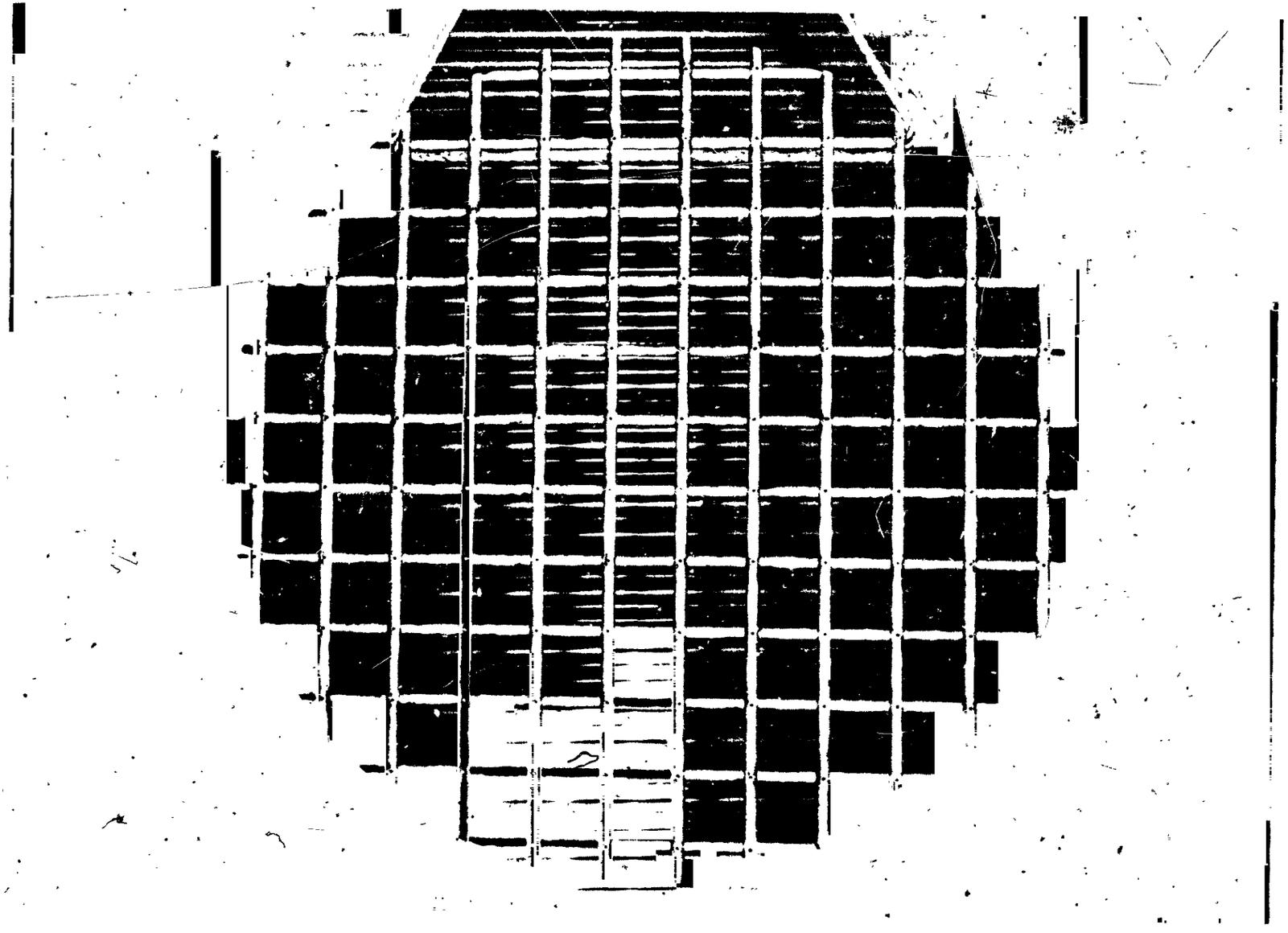

(b) Mesh size 4-inches.

Figure 3.- Continued.

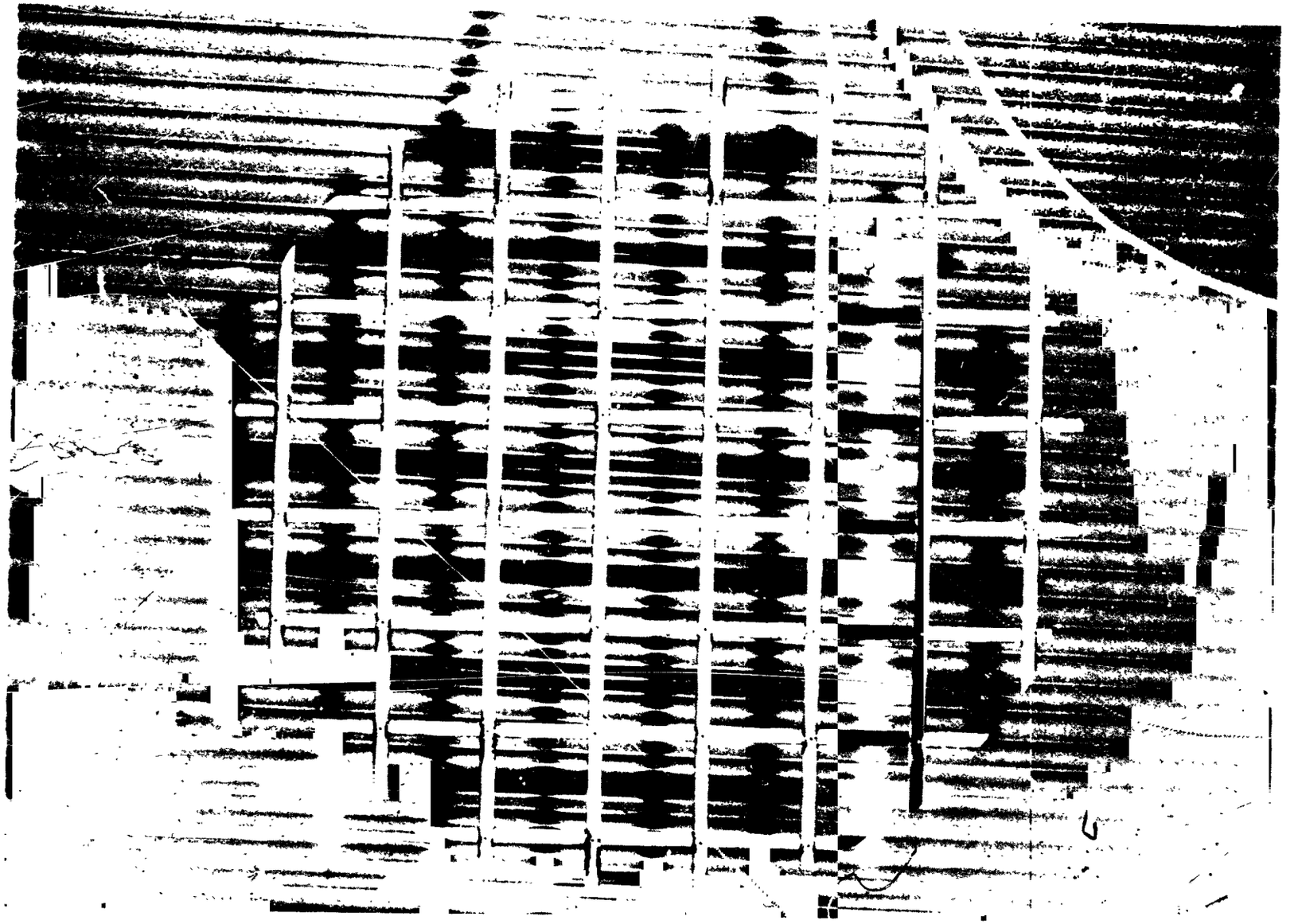

(c) Mesh size 6-inches.

Figure 3.- Continued.

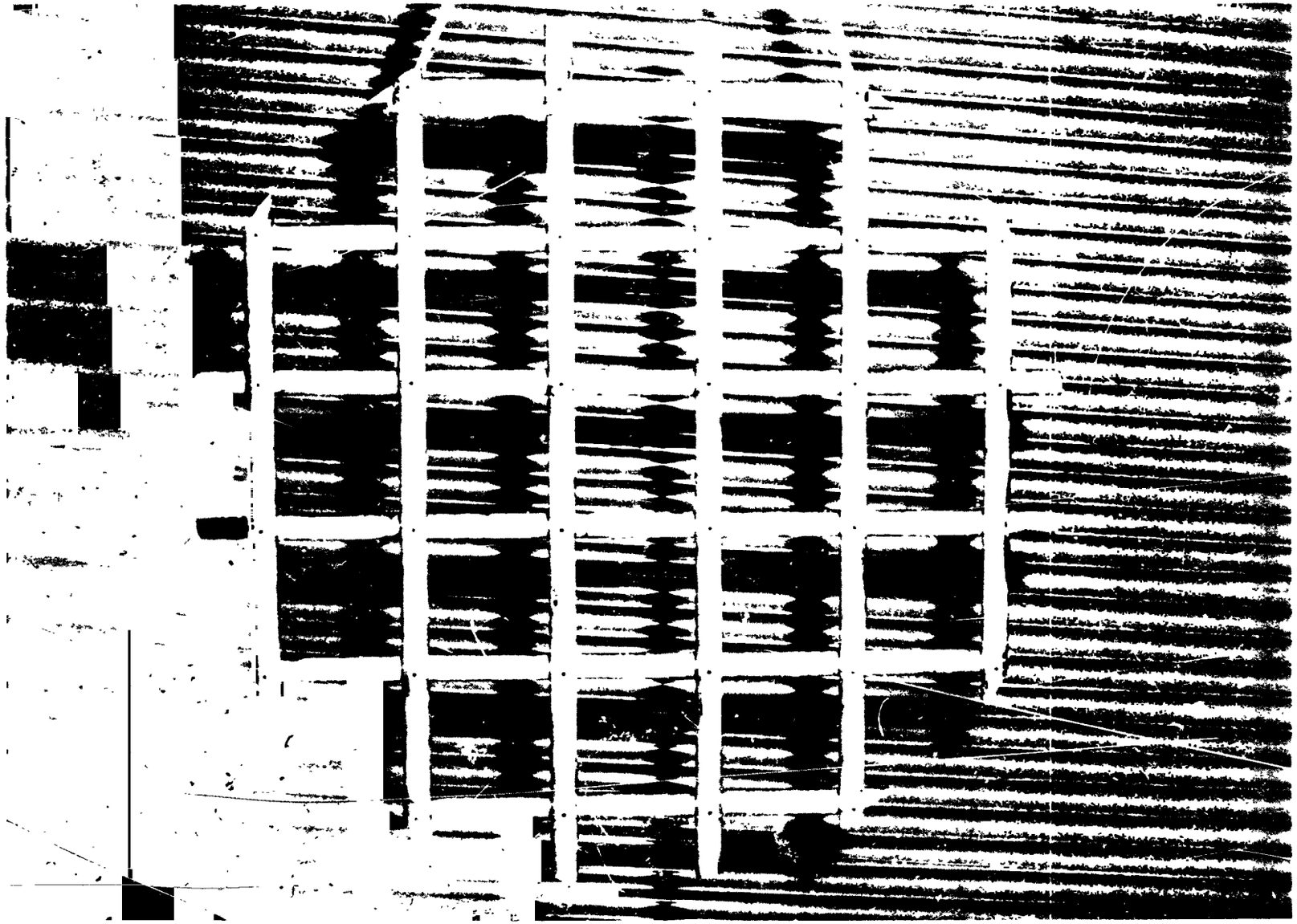

(d) Mesh size 8-inches.

Figure 3.- Concluded.

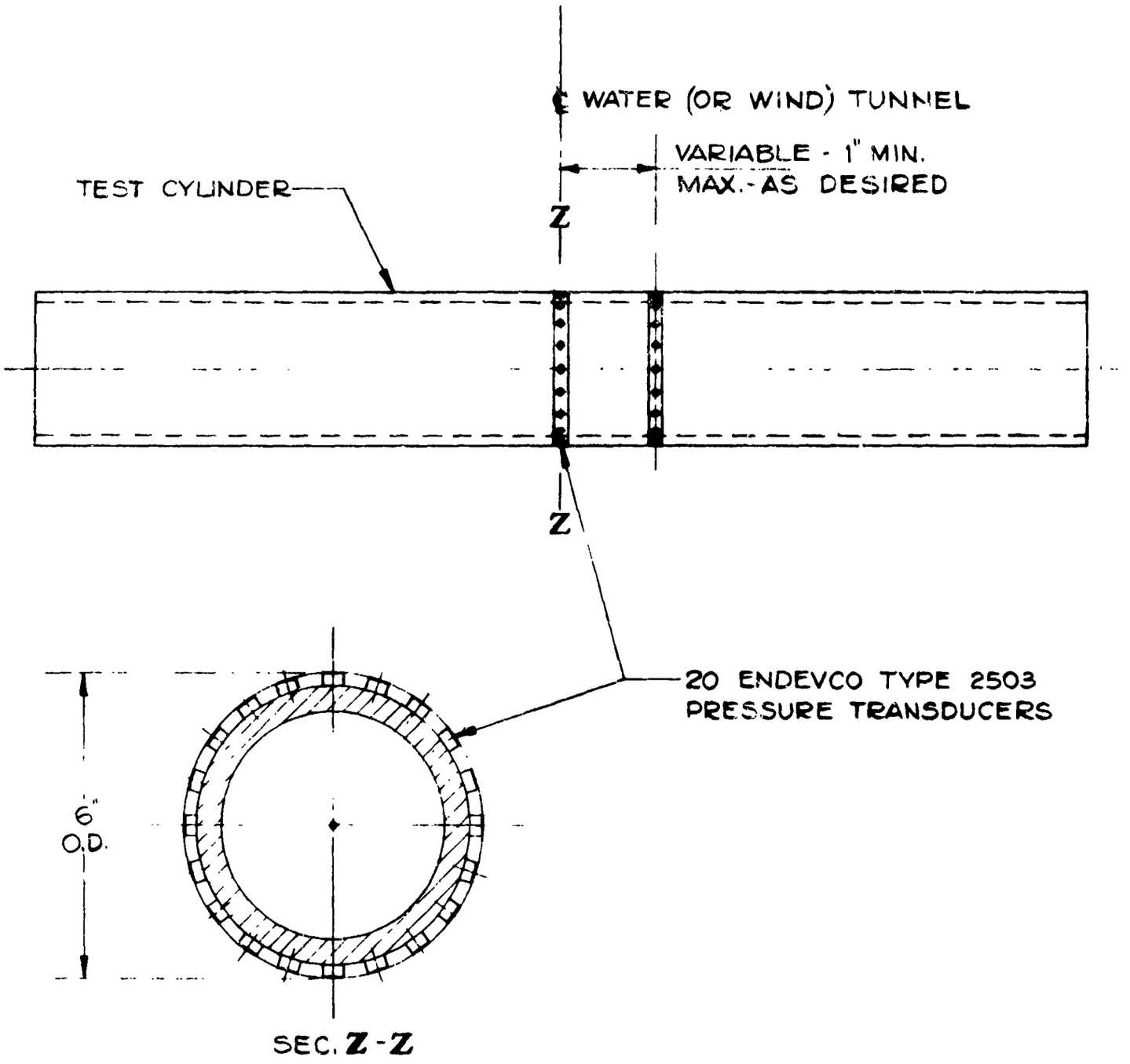

FIG 4 DETAIL OF PROPOSED TEST CYLINDER

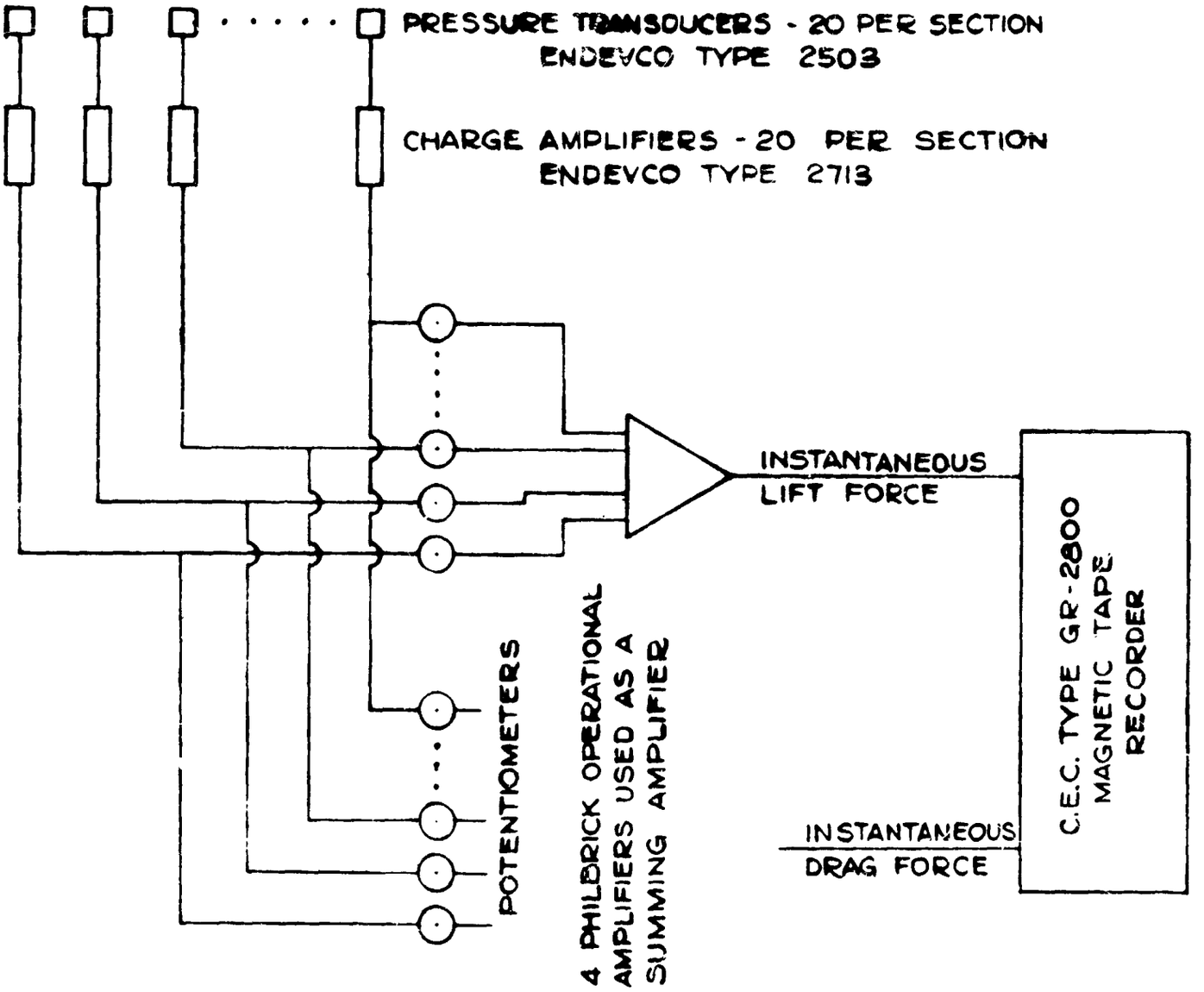

FIG 8. ELECTRICAL CIRCUITRY

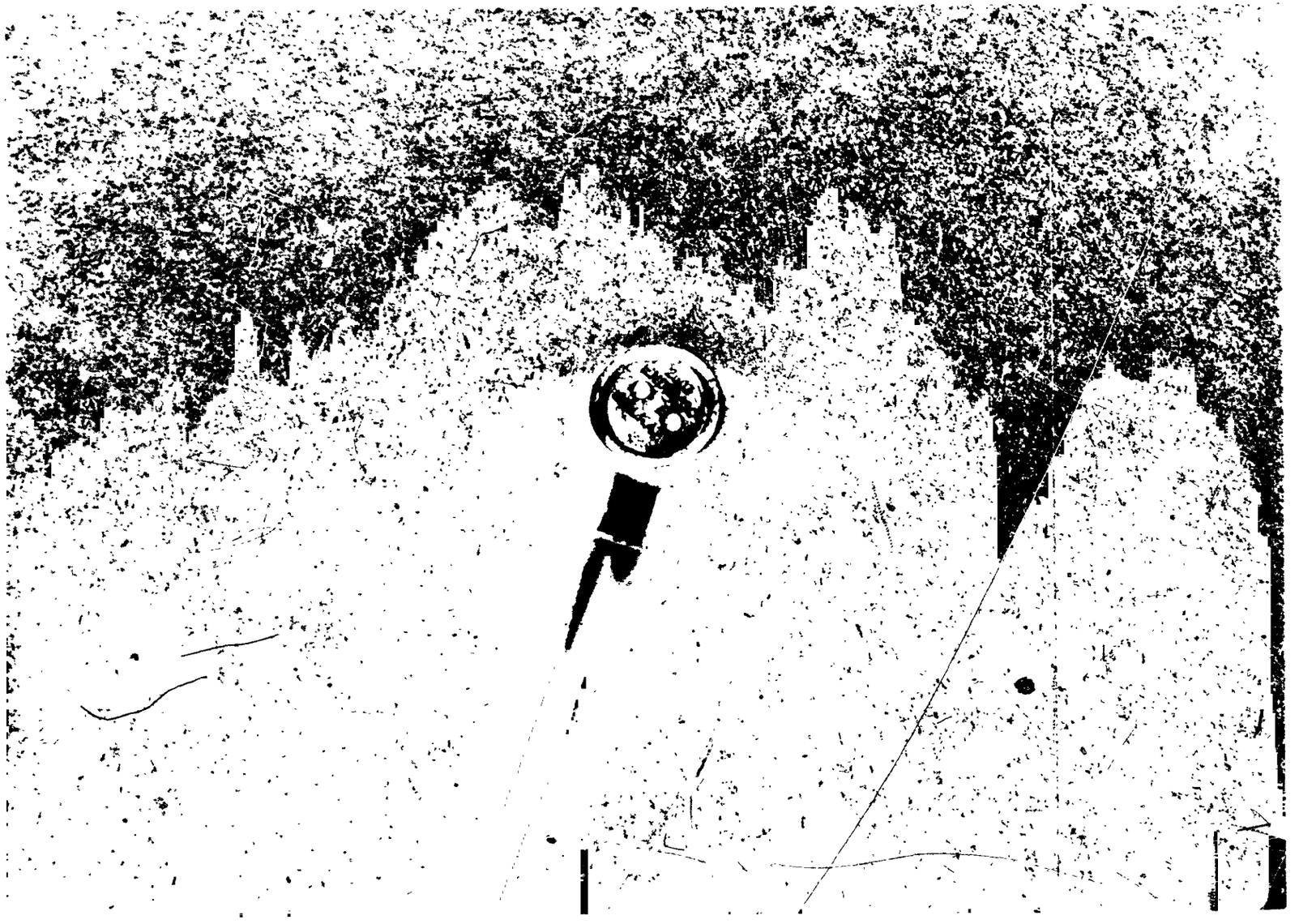

Figure 6.- Endevco type 2503 "turbulence" gages.

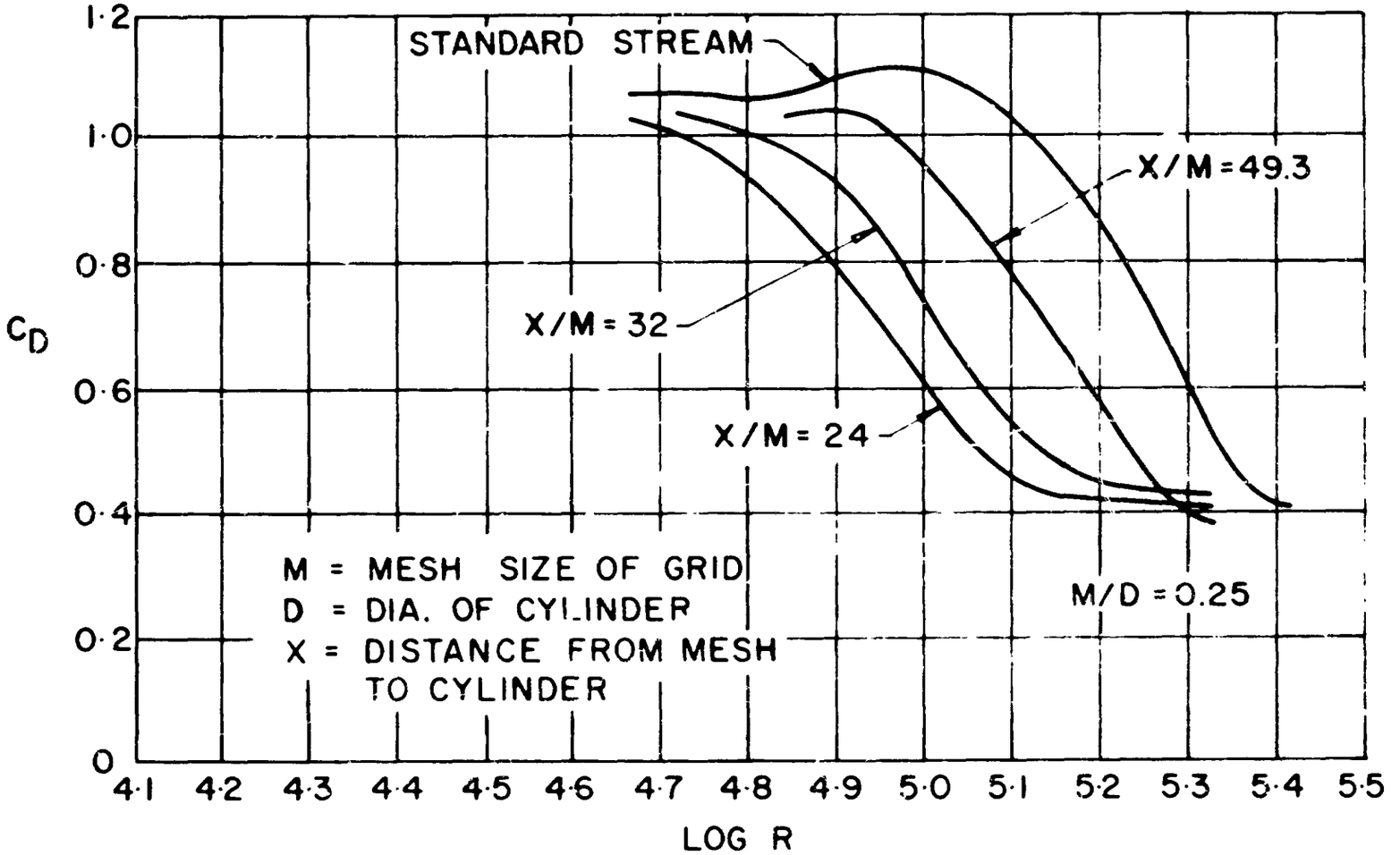

EFFECT OF TURBULENCE ON DRAG COEFFICIENT OF CIRCULAR CYLINDER

FIG. 7

IMPULSIVE AND ACCELERATED FLOW ABOUT CYLINDERS

Turgut Sarpkaya[+]

This paper presents a study of the characteristics of impulsively started steady flow and uniformly accelerated unsteady flow about circular cylinders and discusses the merits of various mathematical models and theoretical methods. In addition, the fluctuations of the lift and drag forces and the analogy between the impulsive flow over circular cylinders and the separated flow about lifting bodies are discussed and the cross-flow drag and normal force coefficients are presented.

Introduction

Periodic vortex shedding, in the flow of fluids past bluff bodies, refers to the orderly development of counter rotating vortices in the wake. Its intriguing and sometimes destructive manifestations in nature have attracted many eminent researchers. The "von Kármán vortex street" is undoubtedly the most universally recognized phraseology describing this phenomenon. It relates to Kármán's analytical solution a half century ago in which he showed that a stable arrangement of a row of counter vortices occurs for a width-to-spacing ratio of 0.281. But because the inception of separated flow occurs within the viscosity-important regions

---

[+]Professor of Mechanical Engineering, University of Nebraska, Lincoln, Neb. 68508.

of the boundary layer, complete analytical solutions to the vortex shedding problem have remained unattainable.

In recent years, the vortex shedding problem has become important to the structural design of launch vehicles. These vehicles are of long, slender construction, and are required to stand vertically on the ground for extended periods during launch preparation. The vehicles in this attitude, when subjected to ground winds, invariably exhibit vortex shedding. Critical structural loads induced by ground winds act on these vehicles under certain conditions of resonance between vehicle bending and vortex shedding frequencies. Instances of limit cycle instability involving interaction between vehicle motion and shedding forces have also been noted.

It is usually difficult and often impossible either to define the structure or the external forces with necessary accuracy to assure high confidence in calculated response particularly for man-rated vehicles, and hence it becomes necessary to rely on experimental programs guided by approximate theoretical analyses to generate the information desired for solution of immediate problems and for the refinements of analytical procedures for future analyses of similar systems.

The essential features of steady flow over bluff bodies have been studied for many years both theoretically and experimentally. Although the present state of knowledge is still unable to describe in detail some of the characteristics of steady flow, there has been in recent years, because of the problems and needs described above, considerable interest in the study of the corresponding and admittedly more complex unsteady flow problem. Apparently, there is an infinite variety of possible

unsteady motions with varying degrees of complexity, and a general theoretical or empirical solution is impracticable.

When a viscous fluid is accelerated past a stationary object, the motion which starts from rest is initially irrotational and unseparated. As the velocity increases, a wake forms and grows. The formation of the wake gives rise not only to a form drag, as would be the case if the motion were steady, but also to significant changes in the inertial forces. The velocity-dependent form drag is not the same as for steady flow of a viscous fluid, and the acceleration-dependent inertial resistance is not the same as for unseparated flow of an inviscid fluid. In other words, the drag and the inertia forces are interdependent as well as time-dependent. Although indirect, the role of viscosity is paramount in that its consequencies are separation, vortex formation and shedding, and resultant alterations of virtual mass or virtual mass-moment of inertia. The specification of these various aspects provides a basis for the correlation of theoretically predicted and observed forces.

Theoretical Models and Methods

An exact treatment of the development of steady or time-dependent flow about cylinders is considerably complicated by the occurrence of separation. Even without this complication, the basic equations present difficulties, and it is necessary, with the exception of fairly low Reynolds number flows, to employ either an approximate potential flow model or a finite-difference approximation to the partial differential equations of laminar motion together with a high-speed computer. The

use of the potential flow models is based on the premise that the periodic nature of vortex shedding, if not the circumstances leading to it, is basically independent of the Reynolds number.

The periodic vortex shedding is characteristic of cylinder cross-flow at all Reynolds numbers above 100 except for a region between approximately 100,000 and 3.5 million. The supercritical Reynolds number range of random vortex shedding is confined to this relatively narrow range. The randomness results from the fact that the point of shear layer transition from laminar to turbulent flow moves forward from the wake region toward the separation point as supercritical Reynolds numbers are approached[1]. In the supercritical range, a laminar separation may be followed by reattachment if boundary layer transition to turbulence can occur closely enough. The result is a separation bubble whose position is highly sensitive to small perturbations in local pressure. Perhaps the most profound conclusion to be drawn from these and similar observations[2, 3, 4] is that the periodic nature of vortex shedding is basically not dependent upon Reynolds number, except for secondary characteristics. For example, the subcritical Strouhal number for a circular cylinder is about 0.20 whereas at transcritical Reynolds numbers its value is 0.27[1]. The immediate consequence of the above conclusion is that the potential flow theory may be applied, with <u>proper simulation of vorticity transport</u> from the boundary layer, to the analysis of separated wake flow. Obviously, whether the various potential flow models are oversimplified to describe adequately the complex wake flow may be established only on the basis of the agreement of their results with

experimental observations of the actual flow field near the body as well as the forces acting on the body.

Lumped Vorticity Model

Edwards[5], Hill[6], and Bryson[7] proposed a flow model which seems to incorporate the main features of the flow in the simplest mathematical form. In this model, the vortex sheet is approximated by a single concentrated line vortex at the center of gravity of the vorticity. The line vortex as well as its image is connected to the body by a straight feeding sheet of vanishingly small vorticity. In addition, a condition is formulated which makes the net force on the concentrated vortex and its feeding sheet vanish. Then the force acting on the cylinder is determined by the time rate of change of the total impulse imparted to the cylinder.

The simplicity of this model is offset by its shortcomings: the calculation of the development of separated vortices requires the specification of the angular position around the body at which the feeding sheets depart and of the distance from the vortex to the body at the start of calculation. The vortices would never grow if they started with zero strength on the surface of the body. Consequently, the time origin of the theoretical drag curve is not predicted by the theory. Additional shortcomings of the model concern the couple acting on the vortex and connecting sheet and the pressure distribution around the body. Even though the net force on the vortex and connecting sheet is rendered zero, a moment acts on the combination and introduces an error

whose magnitude cannot readily be estimated. Finally, the vortex sheet introduces a pressure discontinuity on the cylinder at the point where it attaches the cylinder and gives rise to an unrealistic pressure distribution. This in turn makes difficult, if not impossible, the study of the viscous separation process.

Figure 1 shows the drag coefficient for a circular cylinder immersed in an impulsively started steady ambient flow as obtained by Bryson[7], through the use of the lumped vorticity model, and by this writer[8], experimentally. It is apparent that the lumped vorticity model fails, without further modifications, to predict accurately the drag coefficient. The applications of this method to lifting bodies of circular and elliptic cross section and additional discussions of the shortcomings of the model may be found in Refs. {9, 10, 11}. Schurr[12] recently extended Bryson's analysis to the prediction of drag on a circular cylinder immersed in a unidirectional uniform flow with constant acceleration. The initial point of separation was chosen to be θ = 35, 37.5, 40, 42.5, and 45 degrees from the rear stagnation point. The agreement between the experimental results and those predicted from the lumped vorticity model is not any better than that shown in Fig. 1 for the impulsive flow, (see Fig. 2).

Attempts to improve the lumped vorticity model leave the researchers in a state of ambivalence; better simulation of the observed characteristics of separated flow on the one hand and formidable mathematical difficulties on the other. The model suggested by Smith[13] consists of a spiraling vortex sheet of finite strength originating from the leading edge of the wing. The location of the sheet and distribution of vorticity

is numerically determined under the conditions that this sheet be everywhere force-free. This model appears to accurately describe the separated flow and also to result in an improved prediction of the pressure distribution. However, the extension of this model to more general body shapes for which there is not a convenient Kutta condition is, to say the least, a difficult undertaking and would not resolve the problem of determining an "idealized point" of separation from which the vortex sheet is supposed to emerge.

Another improvement is that adopted by Roshko[14] where the vortex feeding point is located well ahead of any separation point and the vortex strength is determined by the tangential velocity at the point selected. There is still, however, a pressure discontinuity in going across the free streamline. It is clear that, if one insists on the use of vortex sheets and at the same time wishes to eliminate the large pressure discontinuity at one point on the body, one must use several sheets with strengths proportional to the vorticity growth rate represented by each sheet. As pointed out earlier the adoption of several spiraling vortex sheets of finite strength will present insurmountable mathematical difficulties. It must be kept in mind that the object of various mathematical models, including the one to follow, is not the accurate predetermination of lift, drag and moment, which are easily measured, or the exact description of the characteristics of flow but rather a sound understanding of phenomena for the interpretation of the important effects of separation.

Method of Isolated Singularities

The vortices in the wake may be considered as columnar regions of concentrated vorticity and the feeding layers as a number of distributed small discrete vortices. Furthermore, the vortices, though not connected by a branch cut, may be assumed to grow independently with a certain rate of growth. Then the use of the generalized Blasius theorem yields the forces acting on the body in terms of the strengths, locations, and the rates of growth of vortices[15].

For the drag force, one finds*

$$D = C_{Dc}\,(s/d)\,\rho d\,\frac{U^2}{2} + C_{Mc}\,(s/d)\,\frac{\pi d^2}{4}\,\rho a \tag{1}$$

where

$$C_{Dc} = -2\sum_{k=1}^{m}\frac{\Gamma_k}{Ud}\left(\frac{v_k}{U} - \frac{v_{ki}}{U}\right) + \frac{1}{2}\sum_{k=1}^{m}\frac{q_k/d}{r_k^2/d^2}\,\frac{\partial f_k(s/d)}{\partial(s/d)} \tag{2}$$

and

$$C_{Mc} = 2 + \frac{1}{\pi}\sum_{1}^{m}\frac{q_k/d}{r_k^2/d^2}\,\frac{\Gamma_k}{Ud} \tag{3}$$

and for the lift force, one has

$$L = C_{Lc}\,(s/d)\,\rho d\,\frac{U^2}{2} + K_{Mc}\,(s/d)\,\rho\,\frac{\pi d^2}{4}\,a \tag{4}$$

where

$$C_{Lc} = 2\sum_{1}^{m}\frac{\Gamma_k}{Ud}\left(\frac{u_k}{U} + \frac{u_{ki}}{U}\right) - \sum_{1}^{m} 2\,\frac{p_{ki}}{d}\,\frac{\partial f_k(s/d)}{\partial(s/d)} \tag{5}$$

---

*Symbols are listed at the end of the paper.

and

$$K_{Mc} = -\frac{4}{\pi}\sum_{1}^{m}\frac{p_k}{d}\frac{\Gamma_k}{Ud} \qquad (6)$$

Further use of these expressions require the determination of the flux of vorticity generated in the boundary layer, the vorticity transport reduction or vorticity cancellation factor, and the location of vortices. Vorticity reduction by the creation of counter vorticity from reverse flow over the downstream portion of the cylinder becomes of primary importance particularly when the vortices become unsymmetrical. It is clear that both this method and the one discussed previously necessitate the adoption of somewhat arbitrary vorticity cancellation factors. The above analysis does, however, point out that the various drag and inertia coefficients are functions of time or the relative displacement of fluid regardless of whether the ambient flow is steady or unsteady.

Using the experimental values of Γ/Ud, q/d, r/d and dividing the feeding layer into a number of small concentrated vortices uniformly distributed along the sheet, the coefficients C_{Dc} and C_{Mc} were calculated from Eqs. (2) and (3) and the corresponding values of these coefficients for a given s/d were plotted in Fig. 3. The loop observed at the end of the curve is indicative of the variations of C_{Mc} and C_{Dc} during the shedding process. It is apparent that as the subsequent vortices are shed this loop repeats itself but not necessarily coincident with the first loop and finally encircles the average values of $C_{Mc} = 1.3$ and $C_{Dc} = 1.2$. The coefficients C_{Lc} and K_{Mc} show similar oscillations during the shedding

of vortices.

The total lift coefficient for uniformly accelerated flow, as determined directly from the measurements of lift force and from Eq. (4) is shown in Fig. 4. The ratio of the total lift and drag coefficients is shown in Fig. 5 for the purpose of understanding the build-up of the lift force as compared to the drag force. It is apparent that during the initial period of the accelerated motion the lift builds up more slowly than the drag force and gives rise to a lift deficiency. As the motion continues with uniform acceleration the lift force builds up slowly, finally reaching approximately 30% of the instantaneous total drag prevailing at that time. It is noted that there is considerable variation among various runs particularly during the shedding of subsequent vortices. Among various reasons examined the only one that at this time deserves mentioning here is the spanwise instability of line vortices.[16]

Oscillations of Lift and Drag Forces

A careful analysis of the motion pictures taken during each run (see Fig. 6) has revealed that the vortices oscillate back and forth, mainly in the direction of the ambient flow, and grow or diminish in intensity prior to their actual shedding. These oscillations cause corresponding oscillations in both the drag and lift forces. A comparison of the Eqs. (2) and (5) shows that the back and forth oscillations of the vortex affect the lift coefficient more than it does the drag coefficient since C_{Lc} depends, among other things, on u_k and u_{ki} whereas C_{Dc} depends on v_k and v_{ki}. The lift coefficient and the oscillating component

of the drag coefficient were analyzed for the 2 3/4 in. cylinder for the range of Reynolds number from 44,000 to 120,000. It was found that the rms value of the fluctuating component of the drag coefficient varied from 0.06 to 0.1 from one run to another and from one Reynolds number to another. No acceptable explanation can be offered for the large variation in rms values of $(C_{Dc}-\overline{C}_{Dc})$.

The rms values of the lift coefficient ranged from 0.65 to 0.9. The deviation of the absolute values of the peak lift coefficients from the rms values was approximately 0.2. The corresponding values for the drag coefficient, i.e. the deviation of the peak values of the drag coefficient from the rms values of the fluctuating component of the drag coefficient was approximately 0.03. It was further observed that there were definite second order fluctuations, in both the lift and drag force traces, superimposed on the larger first order oscillations. These were probably due to the interaction of the first order oscillations of the lift and drag forces.

Impulsive Flow-Lifting Body Analogy

A great deal of discussion about the normal force distribution and wake vortex characteristics of bodies of revolution and the analogy between the flow over a lifting three-dimensional body and impulsively started steady ambient flow exists in the literature.[6-9] However, the basic aerodynamic data such as that shown in Fig. 1, necessary for the evaluation of the merits of the analogy as well as those of the lumped vorticity model are scarce. The availability of the data shown in Fig. 1

made possible the evaluation of the normal force coefficient C_N, defined by $C_N = 8D/\pi\rho U^2 d^2$, shown in Fig. 7. Also shown on this figure are the comparable curves obtained from the works of Schwabe[17], Hill[6], and Bryson[7]. Within the range where a comparison is possible, the present data falls between that of Bryson and Hill.

It is apparent that, as the axial boundary layer becomes very large and undergoes a transition to turbulence, the normal force calculation based on time-dependent laminar flow analogy becomes increasingly less accurate. There are, at present, no experimental data concerning the impulsively started turbulent flow about cylinders. A series of exploratory measurements were made with a circular cylinder (d=2 3/4 in.) by attaching two tripping wires along the axis of the cylinder at ±80 deg. from the front stagnation point. The Reynolds number was about 1.2×10^5 on the average. The drag coefficients obtained in this manner are shown in Fig. 8 as a function of s/R. Despite the fact that every conceivable precaution was taken, and different methods were employed in the evaluation of the instantaneous force and velocity, the drag coefficients scattered in a wide area bounded by 0.25 in the lower limit and 0.4 in the upper limit. The force records, within the degree of accuracy afforded by the experiments, indicate that the steady-state condition is reached almost at the start of motion.

The evaluation of the normal force coefficient for slender bodies, when the flow is laminar in the front portion and turbulent in the rear, is considerably more complex than either fully laminar or fully turbulent boundary-layer cases. Obviously, there remain a number of questions that

must be answered by future studies for both the impulsively started turbulent flow and the supercritical flow about a lifting body at an angle of attack.

Symbols

a acceleration

C_{Dc} velocity-dependent drag coefficient

$\bar{C}_{Dc}$ mean drag coefficient

C_{Lc} velocity-dependent lift coefficient

C_{Mc} inertia coefficient (drag)

C_N normal force coefficient

C_{TD} total drag coefficient, $4D/\rho d^2 a$

C_{TL} total lift coefficient, $4L/\rho d^2 a$

D total drag

d diameter of cylinder

$f_k(s/d) = \Gamma_k/Ud$, circulation function

K_{Mc} inertia coefficient (lift)

L total lift

p_{ki}, q_{ki} coordinates of the k-th image vortex

p_k, q_k coordinates of the k-th real vortex

Re Reynolds number

r_k radial distance to the k-th vortex

s displacement of ambient flow

U instantaneous velocity of the ambient flow

u_{ki}, v_{ki} velocity components of the k-th image vortex

u_k, v_k velocity components of the k-th vortex

Z_{sep} distance to the point of separation (lifting body)

Γ_k circulation of the k-th vortex

ρ density of fluid

References

1. Roshko, A., "Experiments on the Flow Past a Circular Cylinder at very High Reynolds Numbers," Jour. Fluid Mechs., vol. 10, (May 1961), pp: 345-356.
2. Spitzer, R. E., "Measurements of Unsteady Pressures and Wake Fluctuations for Flow Over a Cylinder at Supercritical Reynolds Number," CIT, Pasadena, California, (1965).
3. Küchemann, D., "Report on the I.U.T.A.M. Symposium on Concentrated Vortex Motions in Fluids," Jour. Fluid Mechs., vol. 21, part 1, (1965) pp:1-20).
4. Abernathy, F. H., and Kronaur, R. E., "The Formation of Vortex Streets," Jour. Fluid. Mechs., vol. 13, (1961), pp:1-20.
5. Edwards, R. H., "Leading Edge Separation From Delta Wings," Jour. Aero. Sciences, vol. 21, (1954), p: 134.
6. Hill, J. A. F., "A Non-Linear Theory of the Lift on Slender Bodies of Revolution," NavOrd Report 5338, Proceedings U. S. Navy Symposium on Aeroballistics, (1954).
7. Bryson, A. E., "Symmetric Vortex Separation on Circular Cylinders and Cones," Jour. Appl. Mechs., Trans. ASME, (Dec. 1959), pp: 643-648.
8. Sarpkaya, T., "Separated Flow About Lifting Bodies and Impulsive Flow

About Cylinders," AIAA Jour., vol. 4, no. 3, (March 1966), pp: 414-420.

9. Schindel, L. H., "Effect of Vortex Separation on Lifting Bodies of Elliptic Cross Section," MIT Aerophysics Lab., Tech. Note 118, 1965.

10. Friberg, E. G., "Measurements of Vortex Separation, Part-I: Two-Dimensional Circular and Elliptic Bodies," MIT Aerophysics Lab. Tech. Report 114, (August 1965).

11. Friberg, E. G., "Measurement of Vortex Separation, Part-II: Three Dimensional Circular and Elliptic Bodies," MIT Aerophysics Lab. Tech. Report 115, (August 1965).

12. Schurr, G. A., "Vortex Formation and Resistance in Unsteady Flow," Ph. D. Thesis submitted to the Graduate College of the University of Nebraska, (June 1965).

13. Smith, J. H. B., "The Improved Calculation of the Mangler-Smith Model of Leading-Edge Separation from a Slender Delta Wing at Incidence," Presented at I.U.T.A.M. Symposium on Concentrated Vortex Motions, Ann Arbor, (July 1964).

14. Roshko, A., "A New Hodograph for Free-Streamline Theory," NACA Tech. Note 3168, (July 1954).

15. Sarpkaya, T., "Unsteady Flow Over Bluff Bodies," Developments in Mechanics, Proc. 8th Midwestern Mechs. Conf., Pergamon Press, (1965), pp: 45-68).

16. Humphreys, J. S., "On a Circular Cylinder in a Steady Wind at Transition Reynolds Numbers," Jour. Fluid Mechs., vol. 9, no. 4, (1960), p. 603.

17. Schwabe, M., "Über drukermittlung in der nichstationären ebenen Strömung," Ingr.-Arch. Bd. VI, 34-50 (1935). NACA TM 1039 (1943).

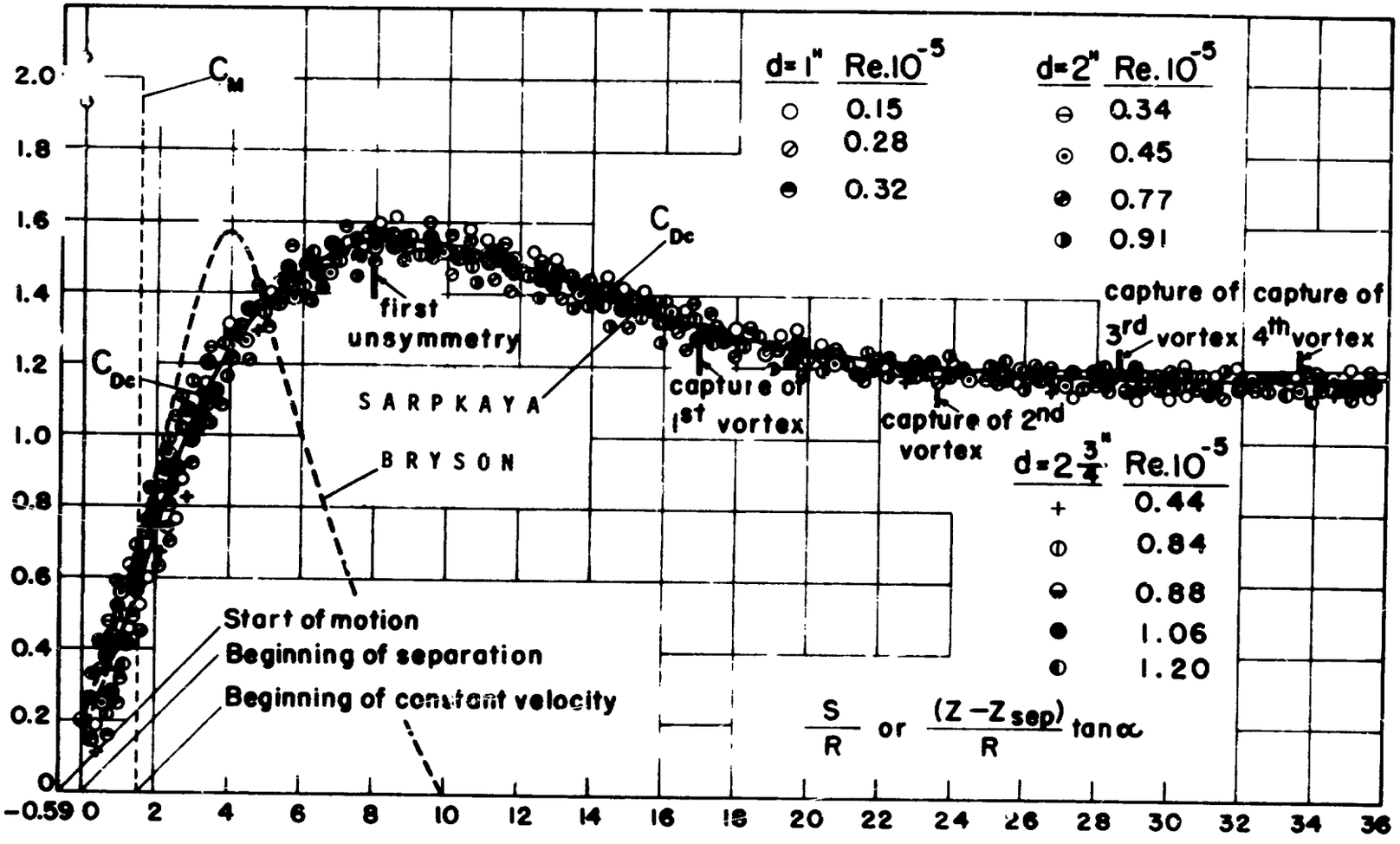

FIG. 1 DRAG COEFFICIENT FOR A CIRCULAR CYLINDER IN IMPULSIVELY STARTED LAMINAR FLOW

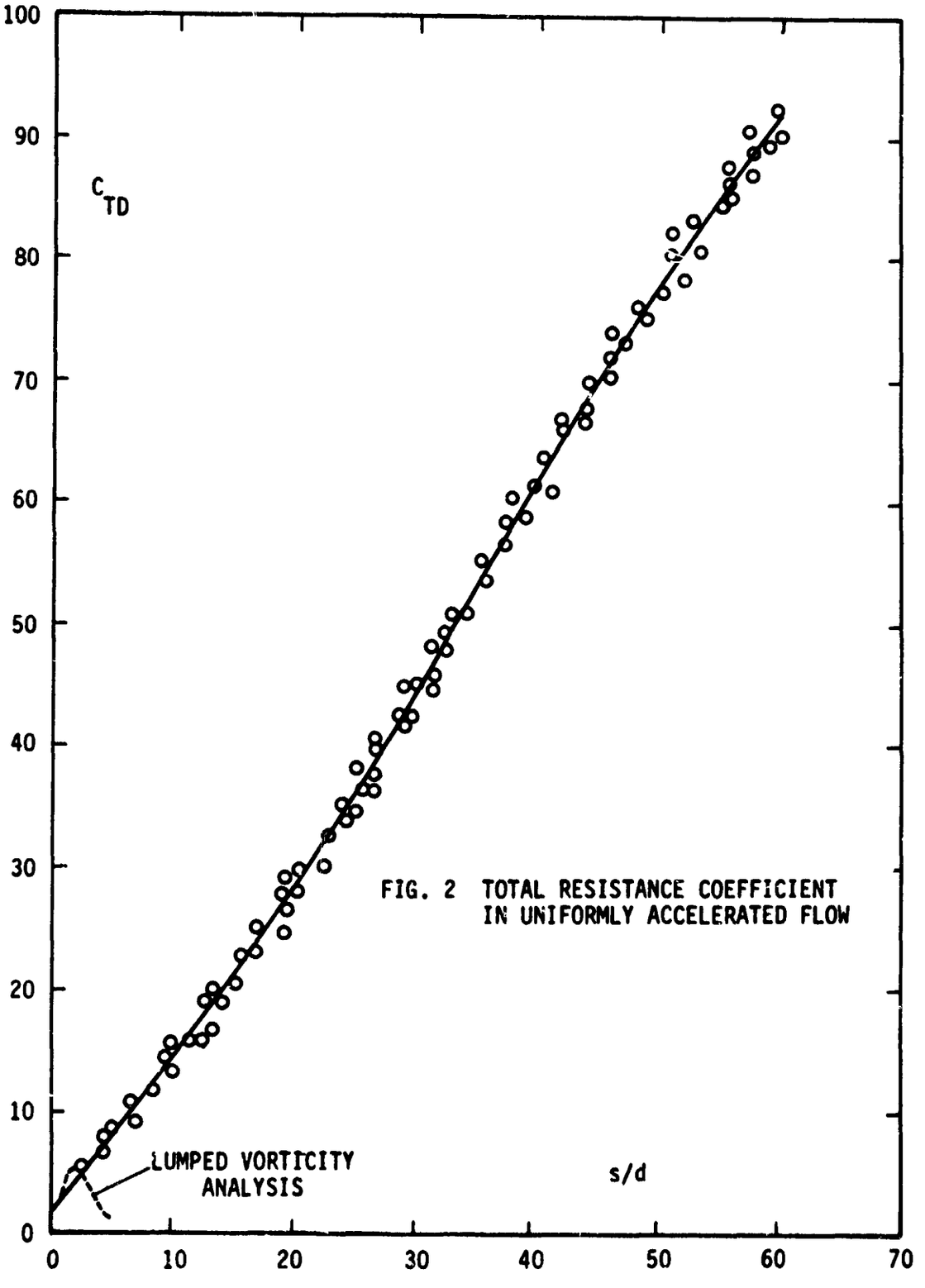

FIG. 2 TOTAL RESISTANCE COEFFICIENT IN UNIFORMLY ACCELERATED FLOW

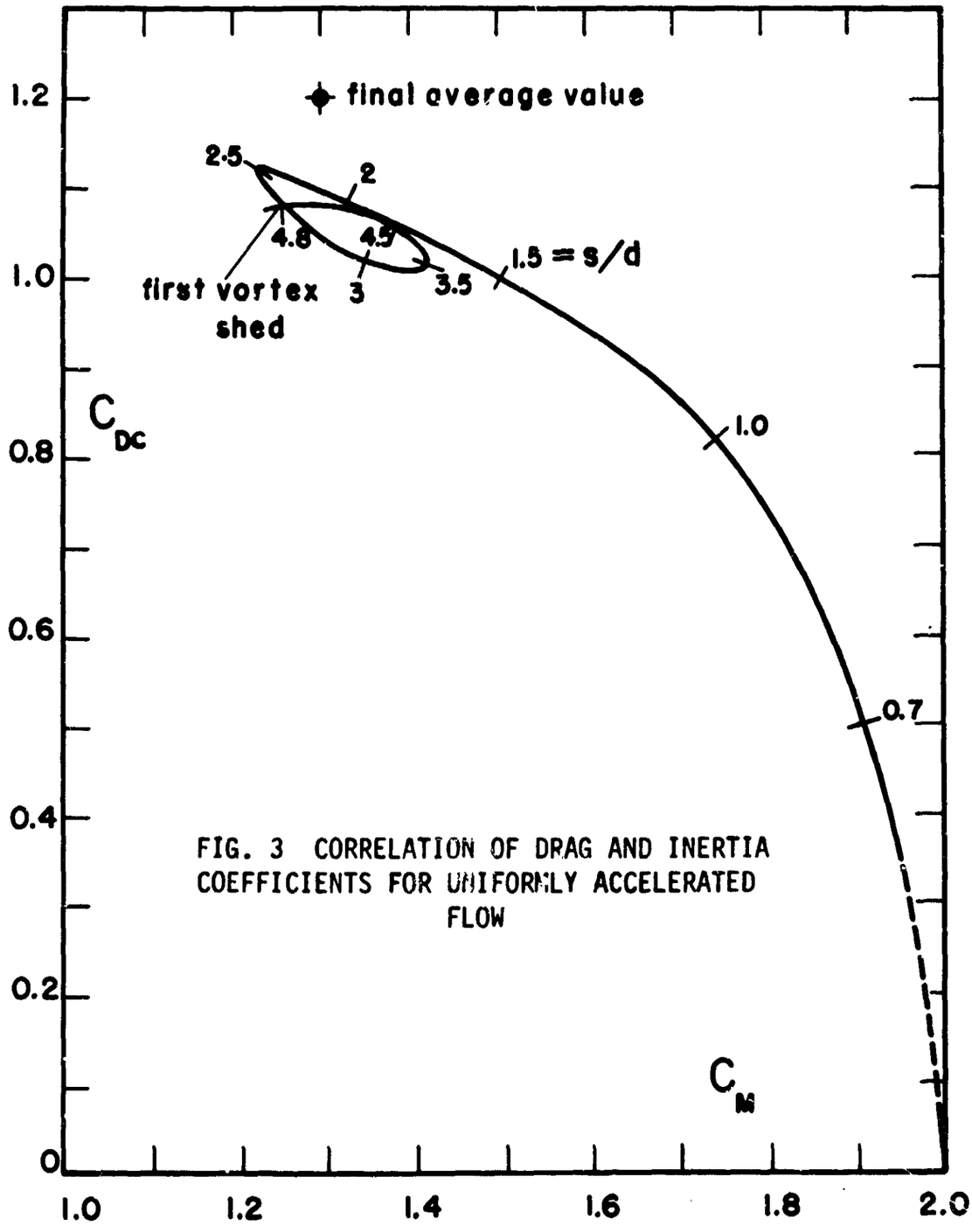

FIG. 3 CORRELATION OF DRAG AND INERTIA COEFFICIENTS FOR UNIFORMLY ACCELERATED FLOW

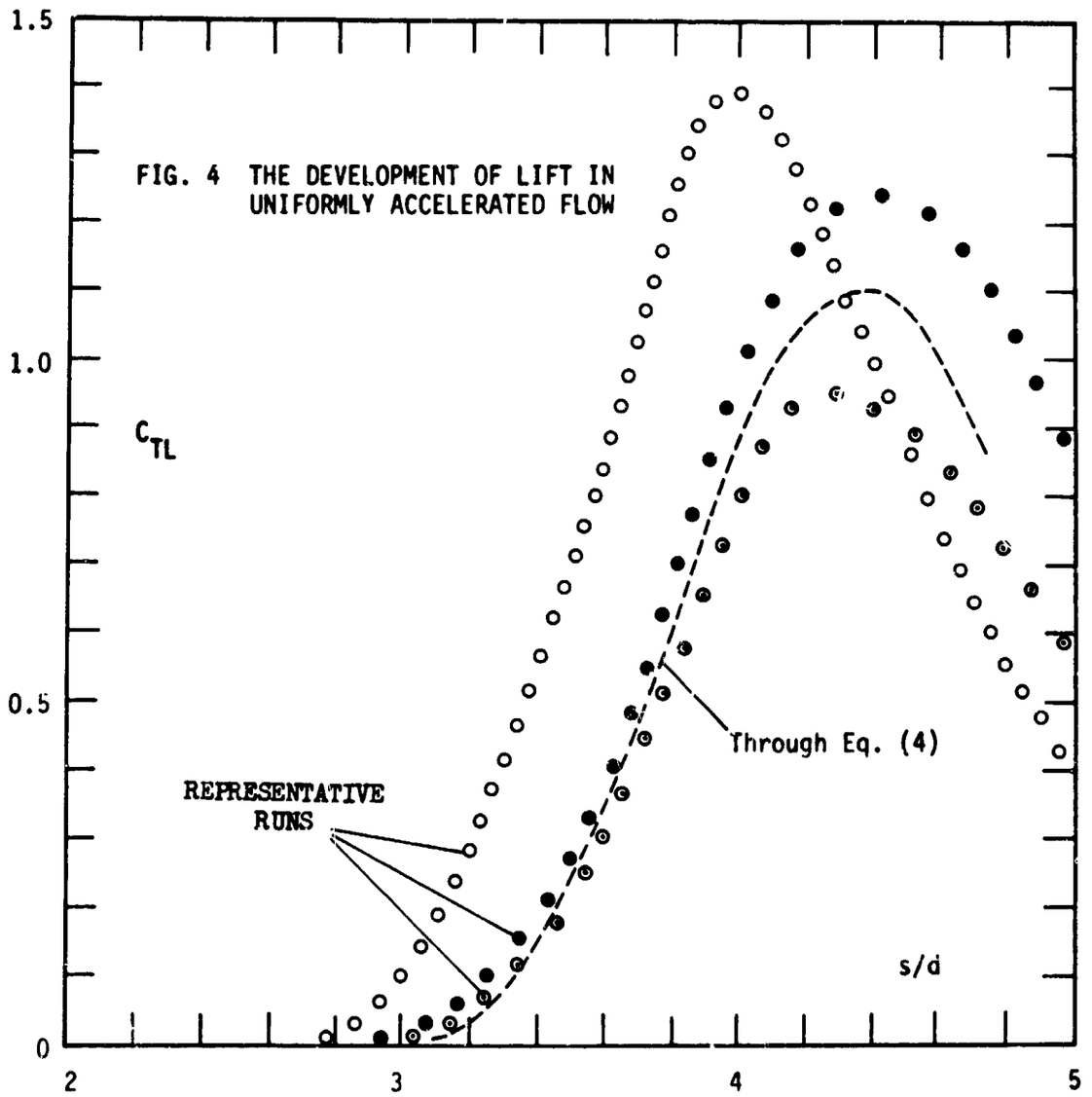

FIG. 4 THE DEVELOPMENT OF LIFT IN UNIFORMLY ACCELERATED FLOW

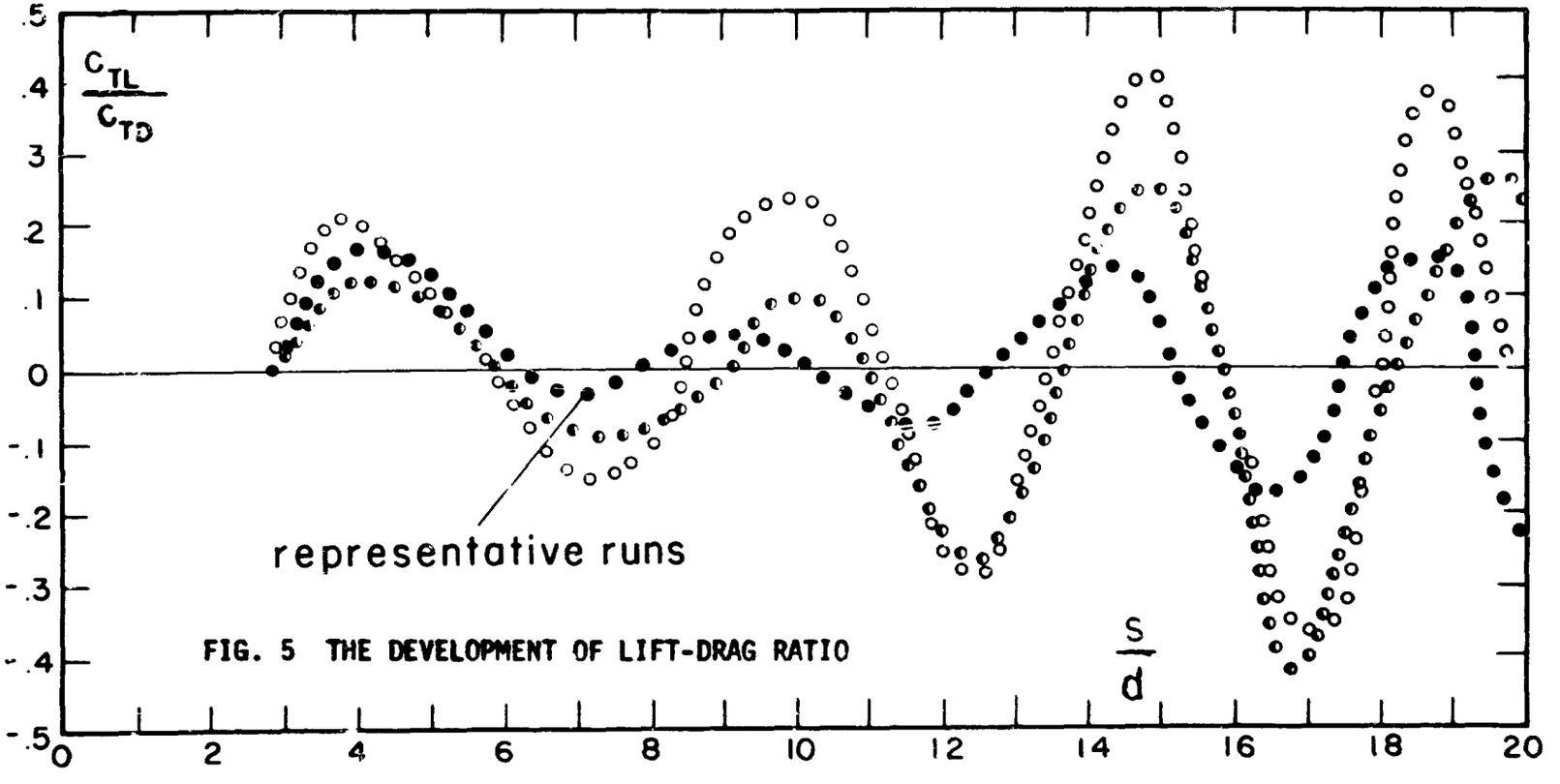

FIG. 5 THE DEVELOPMENT OF LIFT-DRAG RATIO

FIG. 6 DEVELOPMENT OF VORTICES BEHIND A CIRCULAR CYLINDER
V = 3.10 fps, d = 2 3/4 in., s/R = 8 (first frame),
$\Delta s/R = 0.71$. Frames follow from right to left.

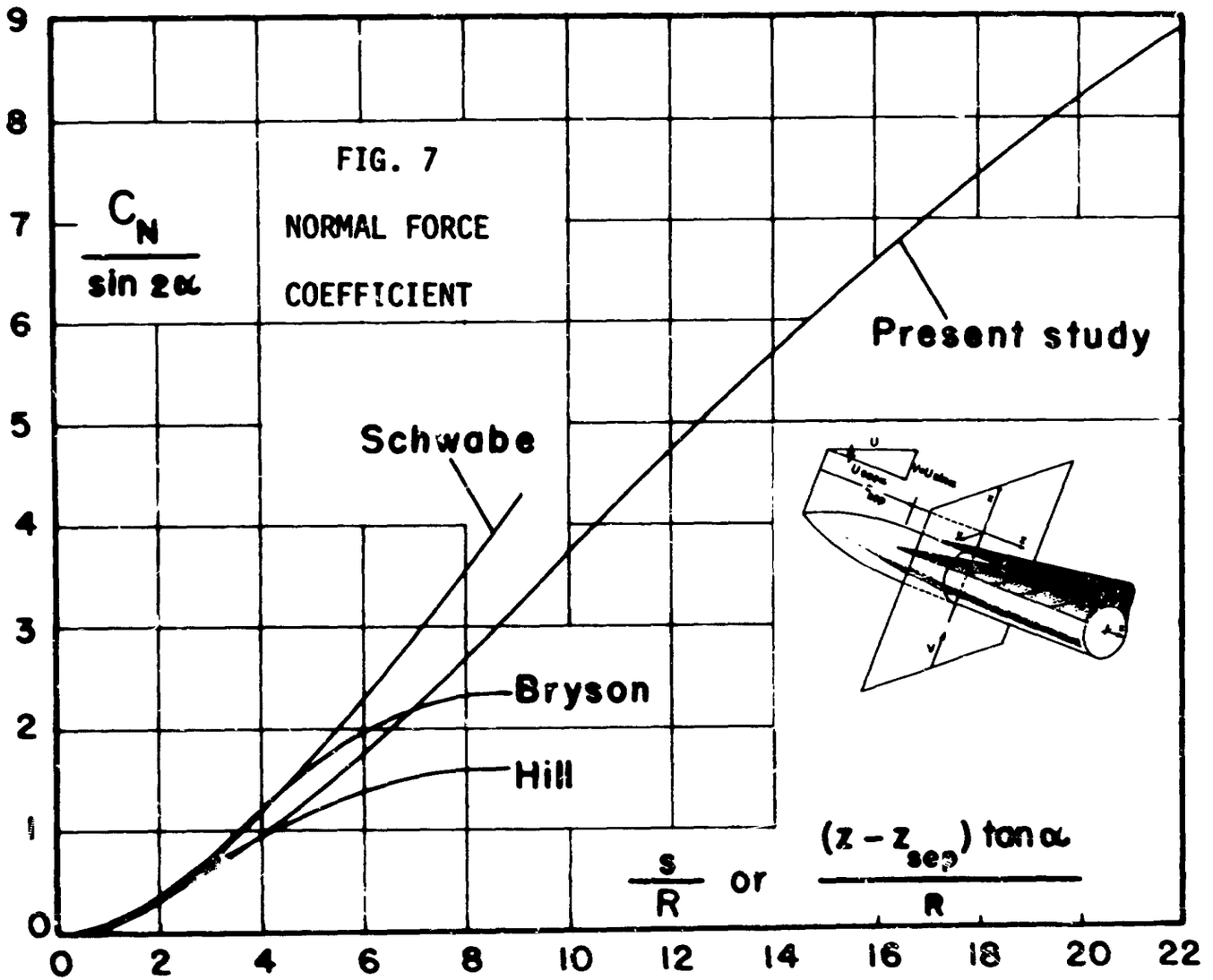
FIG. 7
NORMAL FORCE
COEFFICIENT
$\frac{C_N}{\sin 2\alpha}$
Present study
Schwabe
Bryson
Hill
$\frac{s}{R}$ or $\frac{(z - z_{sep}) \tan \alpha}{R}$
0
1
2
3
4
5
6
7
8
9
0
2
4
6
8
10
12
14
16
18
20
22

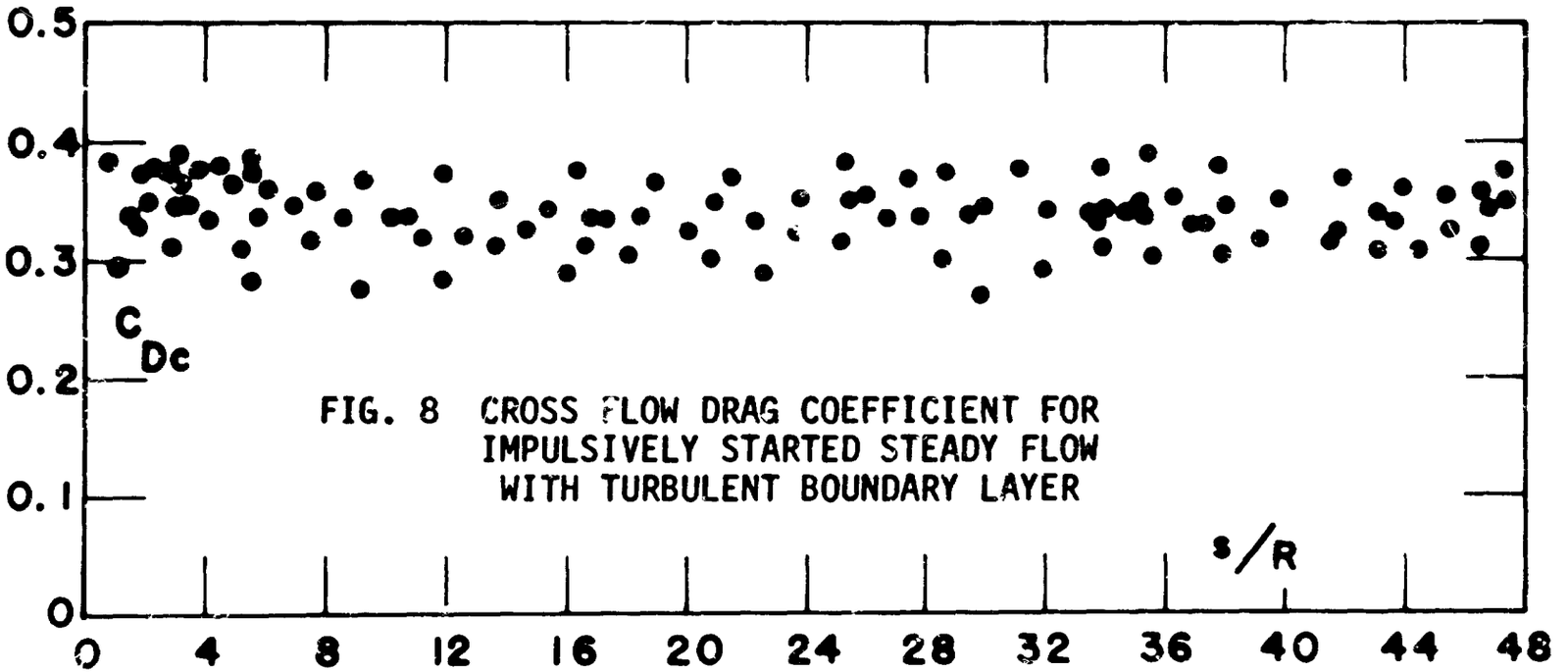

FIG. 8 CROSS FLOW DRAG COEFFICIENT FOR IMPULSIVELY STARTED STEADY FLOW WITH TURBULENT BOUNDARY LAYER

SESSION V - WHERE DO WE GO FROM HERE? - THE DESIGNER'S VIEWPOINT

Chairman: A. Gerald Rainey, NASA Langley Research Center

Panel Members: B. M. Hall, Douglas/Santa Monica
Dr. Edward Fleming, Aerospace Corporation
Wayne R. Covington, Boeing/Huntsville
C. Desmond Pengelley, Gen. Dyn. Convair/San Diego
Robert Morra, Martin/Denver
Robert M. Hunt, NASA Marshall Space Flight Center

The session commenced with opening remarks by each of the panel members.

Mr. Hall observed that from his viewpoint the work that has been accomplished in the ground wind loads problem area so far is fine, but it now needs redirection. He would encourage more basic research to gain a better understanding of the problem He considers simulation of ground wind turbulence in wind tunnels to be an unnecessary refinement. Mr. Hall was later supported by Mr. Covington who considers the lack of definition of aerodynamic forcing functions to be one of the designer's major problems. Mr. Covington pointed out that there is a lack of pressure distribution data on both models and full-scale vehicles. Both Messrs. Hall and Covington felt that certain aspects of the ground wind loads problem were not receiving due consideration. Mr. Hall cited the problem of surface wind effects on vehicles at lift-off

(vehicle drift). Mr. Covington stated that the design of both the S-IVB and S-II stages of the Saturn V are being influenced by ground wind load considerations and cautioned against using the base bending moment as the sole criterion for judging the severity of wind loads. Mr. Hall and Mr. Covington both felt that vehicles are being unduly penalized with regard to ground wind design and operating criteria because of inadequate definition of wind characteristics and their effect on vehicle loads - i.e., build-up rates, effect of exposure time, etc.

Dr. Fleming observed that another area of the ground winds problem that has not received just emphasis is that of ground support equipment. As a result of ground equipment designers not appreciating the problem of ground wind induced loads in time, Aerospace's main experience in the ground winds area has been in "fire-fighting" - that is, fixing problems in existing designs. He pointed out that of all the major launch vehicles that Aerospace has been associated with, none have had weight added to the vehicle itself because of ground wind requirements, but rather all the "fixes" have been to ground support equipment. He concluded that wind tunnel testing will continue to be a requirement for specific configurations and that projects oriented to correlation of wind-tunnel and full-scale data are of particular importance. He expressed the opinion that unless atmospheric turbulence could properly be accounted for, good correlation was unlikely.

In connection with the practical aspects of dealing with the ground wind loads problem, from the designer's viewpoint, Mr. Morra

advocated a design criteria handbook for ground wind loads that would give a basis for determining required stiffnesses, clearances, what aggravates or alleviates the problem, etc. Also, from a practical viewpoint, Mr. Morra concluded that so-called "smooth model" investigations were not apropos to reality and that effects of surface roughness, protuberances, etc., must be better defined.

In response to Mr. Morra's call for a ground wind loads criteria handbook, Mr. Hunt cited the NASA publication "Pre-Launch Ground Wind Loads" as a possible beginning for such a handbook. Mr. Hunt emphasized the need for better load prediction techniques and called for an "across-the-board" approach - neither concentrating on "basic research" or on "proof-testing." He expressed the view that we need to look at all the facets until we get a firmer "handle" on the ground wind problem. He singled out turbulence effects as one of the most important parameters.

Mr Pengelley expressed the view that much effort has been expended on the ground winds problem with the vehicle designer in mind while the problem facing the launch conductor has largely been ignored - that is, with a vehicle nearing launch time, and with wind conditions predicted to be gusting to or above limit values, the test conductor needs current information relating bending moments being experienced by the vehicle to the current wind conditions. As an example of an approach to the problem, Mr. Pengelley suggested the use of the vehicles rate gyros in the monitoring of the oscillating loads. With regard to this aspect of the ground wind problem, Mr. Pengelley emphasized the

importance of time delays in the build-up of loads due to vortices and of drag loads. He concluded that projects oriented to obtain varying velocities or gusts in wind tunnels are a step in the right direction.

Mr. Rainey expressed the view that as a wind tunnel facility operator he felt that much effort must go into improving measurement and prediction techniques. Enough evidence exists to show that refinements, such as simulation of turbulence, are needed. Mr. Rainey agreed with Dr. Fleming that more work is needed to determine the extent of the validity of wind tunnel tests with regard to ground wind loads. The session was then opened for comments or questions from the audience.

Mr Deese of Kennedy Space Center stated that he did not share Mr. Hall's views on turbulence simulation. Rather, he feels that more work needs to be invested in obtaining better meteorological data. Mr. Deese contends that as a result of inaccurate and inapplicable wind and gust data and lengthened "on-pad" times that far exceed original estimates, vehicles are being unconservatively designed. With regard to the vehicle drift problem referred to by Mr. Hall, Mr. Deese contended that vehicle drift was fairly calculable and should be well defined early in the program, although he conceded changes in the design could drastically alter the picture.

With regard to Mr. Pengelley's suggested use of the vehicle rate gyros to indicate "on-pad" oscillating loads, Mr. Ericsson of Lockheed, Sunnyvale, asked if gyros are coordinate aligned so

that the resultant wind could be obtained. Mr. Pengelley answered in the affirmative, but several in the audience objected that it was unlikely that the gyros could be used for this purpose for extended periods.

Mr. Gerus of the NASA Lewis Research Center interjected the thought that perhaps enough different types of "subtle problems" exist in the excitation of cantilever modes by ground winds to warrant the acceptance of dampers as a necessary requirement. Several objections to this philosophy were voiced from the audience.

Dr. Morkovin of Martin/Baltimore remarked that in his opinion quite accurate predictions of loads with wind are neither possible or necessary - identification of limit boundaries should be sufficient. Dr. Morkovin reminded the audience that vehicle motion could result in additional forces and that this facet would be particularly relevant to a "rough" vehicle - one having conduits, etc. - and needs further research.

Mr. Covington agreed and reiterated his view that there were several areas of basic research with regard to the ground wind loads problem that have not received due attention. Mr. Pengelley restated his concern over the launch director's dilemma and suggested that research directed toward determining load build-up time for gusting winds would be desirable.

Mr. Rainey asked for clarification of a point made in Prof. Sarpkaya's presentation regarding a change in the dynamic characteristics of the forces on a cylinder in accelerating flow

when the cylinder was equipped with tripper wires to produce a turbulent boundary layer. Prof. Sarpkaya agreed that the implication of his results were that cylinders in high Reynolds number accelerated flow with naturally turbulent boundary layers might respond in a more nearly instantaneous fashion than those with laminar boundary layers - a result which would greatly simplify the problem of predicting the response to turbulent winds.

Before the session closed, Mr. Reed of the Langley Research Center pointed out that the blowing over of the full-scale Thor vehicle used in one of Langley's ground winds investigations was due to bolts loosening in the tie-down mechanism and was not a bona fide case of vehicle failure due to ground wind loads.

LIST OF ATTENDEES

Beer, F. P.
Lehigh University

Bohne, Quentin R.
Bethel College

Boccius, Walther
Lockheed Missiles and Space Company

Buell, Donald A.
NASA - Ames Research Center

Cermak, Prof. J.
Colorado State University

Chang, Dr. Chang
Lockheed Aircraft Corporation

Child, Richard
Boeing Company

Cincotta, Joseph
Martin Company

Cooney, Thomas V.
NASA Headquarters

Covington, Wayne R.
Boeing Company

Davenport, Prof. Alan G.
University of Western Ontario

Deese, James H.
NASA - Kennedy Space Flight Center

Dave, George
Boeing Company

Ericsson, Lars-Eric
Lockheed Aircraft Corporation

Etkin, Prof. Benard
University of Toronto

Fitchl, George
NASA - Marshall Space Flight Center

Fleming, Dr. Edward R.
Aerospace Corporation

Fung, Prof. Y. C.
California Institute of Technology

Gerus, Theodore F.
NASA - Lewis Research Center

Gilstad, Douglas A.
NASA Headquarters

Hall, B. M.
Douglas Aircraft Company, Inc.

Houbolt, Dr. John C.
Aeronautical Research Association of Princeton

Hunt, Robert M.
NASA Marshall Space Flight Center

Lum, Albert J. I.
Aerospace Corporation

Lyons, J. Michael
Aerospace Corporation

Markovin, Dr. Mark V.
Martin Company

Mc Aleese, James D.
NASA - Lewis Research Center

Morra, Robert
Martin Company

Nowek, Ronald S.
Douglas Aircraft Company, Inc.

Parkinson, G. V.
University of British Columbia

Pengelley, C. Desmond
General Dynamics Corp

Peterson, Dr. Harry C.
Martin Company

Rich, Roy L.
Boeing Company

Sarpkaya, Prof. Turgut
University of Nebraska

Sawdy, David
University of Kansas

Schmidt, Dr. Louis V.
U. S. Naval Postgraduate School

Scoggins, James R.
NASA - Marshall Space Flight Center

Sevik, Maurice
Pennsylvania State University

Simon, Wayne E.
Martin Company

Smith, Orvel E.
NASA - Marshall Space Flight Center

Stahle, Clyde
Martin Company

Thomas, Dr. Richard E.
Texas A and M

Trulio, John G.
Applied Theory

Ujihara, Ben H.
North American Aviation

Vaughan, William W.
NASA - Marshall Space Flight Center

Walker, Robert W.
NASA - Marshall Space Flight Center

Whitbread, R. E.
National Physical Laboratory

Windham, John O.
NASA - Marshall Space Flight Center

Young, James C.
NASA - Marshall Space Flight Center

Zartarian, Prof. Garabed
Massachusetts Institute of Technology

NASA - Langley Research Center

Braslow, Albert L.

Catherines, John J.

Cochrane, James A.

Duberg, Dr. John E.

Duncan, Rodney L.

Farmer, Moses G.

Fedziuk, Henry A.

Foughner, Jerome T., Jr.

Garrick, I. Edward

Goble, Ross L.

Gray, Richard S.

Hanson, Perry W.

Henry, Robert M.

Jones, George W., Jr.

Leadbetter, Sumner A.

Rainey, A. Gerald

Raney, John P.

Reed, Wilmer H., III

Rhinehart, Robert

Runyan, Harry L.

Stevens, David G.

Thornton, William C.

Tolefson, Harold B.